

# HIDING IN PLAIN SIGHT

by

ADRIC RICHARD RIEDEL

Under the Direction of Todd J. Henry

## ABSTRACT

Since the first successful measurements of stellar trigonometric parallax in the 1830s, the study of nearby stars has focused on the highest proper motion stars ( $\mu > 0.18'' \text{ yr}^{-1}$ ). Those high proper motion stars have formed the backbone of the last 150 years of study of the Solar Neighborhood and the composition of the Galaxy. Statistically speaking, though, there *is* a population of stars that will have low proper motions when their space motions have been projected onto the sky. At the same time, over the last twenty years, populations of relatively young stars (less than  $\sim 100$  Myr), most of them with low proper motions, have been revealed near ( $< 100$  pc) the Sun.

This dissertation is the result of two related projects: A photometric search for nearby ( $< 25pc$ ) southern-hemisphere M dwarf stars with *low* proper motions ( $\mu < 0.18'' \text{ yr}^{-1}$ ), and a search for nearby ( $< 100pc$ ) pre-main-sequence ( $< 125 \text{ Myr}$  old) M dwarf systems. The projects rely on a variety of photometric, spectroscopic, and astrometric analyses (including parallaxes from our program) using data from telescopes at CTIO via the SMARTS Consortium and at Lowell Observatory.

Within this dissertation, I describe the identification and confirmation of 23 new nearby low proper motion M dwarf systems within 25 pc, 8 of which are within 15 pc (50% of the anticipated low-proper-motion 15 pc sample). I also report photometric, spectroscopic, and astrometric parameters and identifications for a selection of 25 known and new candidate nearby young M dwarfs, including new low-mass members of the TW Hydra,  $\beta$  Pictoris, Tucana-Horologium, Argus, and AB Doradus associations, following the methods of my [Riedel et al. \(2011\)](#) paper and its discovery of AP Col, the closest pre-main-sequence star to the Solar System. These low proper motion and nearby star discoveries are put into the context of the Solar Neighborhood as a whole by means of the new RECONS 25 pc Database, to which I have now added (including my [Riedel et al. \(2010\)](#) paper) 81 star systems (4% of the total).

INDEX WORDS: Astronomy, Astrometry, Photometry, Spectroscopy, Kinematics, Proper motion, Parallax, Nearby stars, Low-mass stars, Young stars, Pre-main-sequence stars

HIDING IN PLAIN SIGHT

by

ADRIC RICHARD RIEDEL

A Dissertation Submitted in Partial Fulfillment of the Requirements for the Degree of

Doctor of Philosophy

in the College of Arts and Sciences

Georgia State University

2012

Copyright by  
Adric R. Riedel  
2012

HIDING IN PLAIN SIGHT

by

ADRIC RICHARD RIEDEL

Committee Chair: Todd J. Henry

Committee: Russel J. White

Douglas R. Gies

Nikolaus Dietz

Inseok Song

Electronic Version Approved:

Office of Graduate Studies

College of Arts and Sciences

Georgia State University

August 2012

## DEDICATION

This thesis is dedicated to all my friends, family, and colleagues who have been instrumental in their support of me and my work over the last 28 years. I want to extend particular thanks to my parents: without their interest in science and science fiction I would never have been inspired this far; also Dr. Todd Henry, whose mentoring, advice, and scientific philosophy have incalculably shaped my last few years. I also wish to thank my fiancée, Jamie McDonald, who has been there for me in good times and bad.

## ACKNOWLEDGMENTS

Special thanks go to:

My fiancée, Jamie McDonald, without whose moral support and editorial assistance I would never have completed this thesis on time.

Noel Richardson, for help with spectroscopy and other general scientific concerns, and for help with the dissertation formatting.

John Subasavage, Serge Dieterich and Jen Winters, for thriving intellectual discussions on numerous topics.

Wei-Chun Jao, for his crazy ability to program anything, the parallax pipeline, the orbit fitting code, etc, etc.

The RECONS 25 pc Database team (Todd, Jen, Altonio, Ken, and Angelle).

Alvin Das, for his gsudiss class package.

## TABLE OF CONTENTS

|   |           |
|---|-----------|
| <b>ACKNOWLEDGMENTS</b> . . . . .  | v         |
| <b>LIST OF TABLES</b> . . . . .   | xi        |
| <b>LIST OF FIGURES</b> . . . . .  | xiii      |
| <b>LIST OF ABBREVIATIONS</b> . . . . .  | xvii      |
| <b>1 AN INTRODUCTION</b> . . . . .  | <b>1</b>  |
| <b>1.1 The Solar Neighborhood</b> . . . . .                                       | 1         |
| <i>1.1.1 History of Nearby Star discoveries</i> . . . . .                         | 3         |
| <b>1.2 The Missing Stars</b> . . . . .  | 6         |
| <i>1.2.1 Known stars without published parallaxes.</i> . . . . .                  | 7         |
| <i>1.2.2 Stars simply missed by Luyten and Giclas.</i> . . . . .                  | 7         |
| <i>1.2.3 Stars too faint for the Luyten and Giclas Surveys.</i> . . . . .         | 8         |
| <i>1.2.4 Stars moving too slowly for the Luyten and Giclas surveys.</i> . . . . . | 9         |
| <b>1.3 Hiding in Plain Sight</b> . . . . .  | 10        |
| <b>1.4 Young Stars</b> . . . . .  | 11        |
| <i>1.4.1 History</i> . . . . .  | 13        |
| <i>1.4.2 Properties</i> . . . . .   | 15        |
| <i>1.4.3 A giant mess</i> . . . . .   | 22        |
| <b>2 TECHNIQUES</b> . . . . .   | <b>25</b> |
| <b>2.1 Astrometry</b> . . . . .   | 25        |
| <i>2.1.1 The Theory Behind (Annual) Trigonometric Parallaxes</i> . . . . .        | 25        |
| <i>2.1.2 Practical Astrometric Concerns</i> . . . . .                             | 30        |
| <i>2.1.3 CTIOPI observing</i> . . . . .   | 32        |
| <i>2.1.4 Orbits</i> . . . . .   | 35        |
| <i>2.1.5 Using Astrometry</i> . . . . .   | 39        |

|            |  |           |
|------------|--|-----------|
| <b>2.2</b> | <b>Photometry</b>                          | 49        |
| 2.2.1      | <i>How we obtain photometry</i>            | 49        |
| 2.2.2      | <i>Luminosities and Colors</i>             | 51        |
| 2.2.3      | <i>X-ray Activity</i>                      | 52        |
| 2.2.4      | <i>Variability</i>                         | 54        |
| 2.2.5      | <i>Color-Magnitude relations</i>           | 58        |
| <b>2.3</b> | <b>Spectroscopy</b>                        | 64        |
| 2.3.1      | <i>Spectral Typing/Reddening</i>           | 66        |
| 2.3.2      | <i>Luminosity/Gravity</i>                  | 69        |
| 2.3.3      | <i>Activity</i>                            | 72        |
| 2.3.4      | <i>Lithium</i>                             | 73        |
| <b>2.4</b> | <b>Kinematics</b>                          | 74        |
| 2.4.1      | <i>Galactic Kinematics</i>                 | 74        |
| 2.4.2      | <i>Convergence</i>                         | 80        |
| 2.4.3      | <i>Expected proper motion distribution</i> | 84        |
| <b>2.5</b> | <b>Databases</b>                           | 89        |
| <b>3</b>   | <b>NEARBY STAR DATABASES</b>               | <b>91</b> |
| <b>3.1</b> | <b>25 pc Precursors</b>                    | 91        |
| 3.1.1      | <i>The Catalog of Nearby Stars</i>         | 92        |
| 3.1.2      | <i>NStars</i>                              | 95        |
| 3.1.3      | <i>NSted</i>                               | 96        |
| <b>3.2</b> | <b>The RECONS 25pc Database (RECX25)</b>   | 97        |
| 3.2.1      | <i>Design</i>                              | 98        |
| 3.2.2      | <i>Initial Steps</i>                       | 104       |
| 3.2.3      | <i>Current Status</i>                      | 108       |
| 3.2.4      | <i>Next Steps</i>                          | 114       |
| <b>3.3</b> | <b>The RECONS Parallax Database (RPD)</b>  | 117       |
| 3.3.1      | <i>Ground-Based and Space-Based</i>        | 119       |

|       |   |     |
|-------|---|-----|
| 3.3.2 | <i>HIPPARCOS re-reductions</i>                                    | 119 |
| 3.3.3 | <i>Problems</i>   | 121 |
| 3.4   | Young Stars Database  | 122 |
| 4     | TINYMO  | 125 |
| 4.1   | Survey Design   | 127 |
| 4.1.1 | <i>SQL query</i>  | 127 |
| 4.1.2 | <i>Photometric Distances</i>                                      | 132 |
| 4.1.3 | <i>Color cuts</i>   | 134 |
| 4.1.4 | <i>Additional photometric cuts</i>                                | 138 |
| 4.1.5 | <i>Literature Searches</i>  | 140 |
| 4.1.6 | <i>Observations</i>   | 142 |
| 4.2   | What Actually Happened, or, the Refinements of a Learning Process | 144 |
| 4.2.1 | <i>A Commentary on the Design Decisions</i>                       | 146 |
| 4.3   | TINYMO Results  | 148 |
| 5     | RESULTS   | 154 |
| 5.1   | Observations  | 154 |
| 5.1.1 | <i>CTIO 0.9m/Tek2K</i>  | 154 |
| 5.1.2 | <i>CTIO 1.5m/RCSpec</i>   | 158 |
| 5.1.3 | <i>Lowell 1.8m/De Veny</i>  | 159 |
| 5.1.4 | <i>CTIO 4.0m/RCSpec</i>   | 161 |
| 5.1.5 | <i>HST/FGS</i>  | 161 |
| 5.1.6 | <i>Literature</i>   | 162 |
| 5.2   | Riedel et al. (2010): SLOWMO Parallaxes                           | 163 |
| 5.2.1 | <i>Sample</i>   | 163 |
| 5.2.2 | <i>Results</i>  | 164 |
| 5.2.3 | <i>Systems Worthy of Note</i>                                     | 181 |
| 5.2.4 | <i>Discussion</i>   | 190 |
| 5.3   | Unpublished Nearby Low Proper Motion Stars                        | 191 |

|   |     |
|---|-----|
| 5.4 Riedel et al. (2011): AP Col                          | 201 |
| 5.4.1 <i>Observations</i>                                 | 202 |
| 5.4.2 <i>Results</i>                                      | 205 |
| 5.4.3 <i>Conclusions</i>                                  | 221 |
| 5.5 Unpublished Young Stars                               | 228 |
| 5.6 Systems Worthy of Note                                | 245 |
| 5.7 Reddened Stars  | 282 |
| 5.8 They Might Be Giants                                  | 284 |
| 6 DISCUSSION  | 288 |
| 6.1 Discoveries of Low Proper Motion Stars                | 288 |
| 6.1.1 <i>New 25pc statistics</i>                          | 288 |
| 6.1.2 <i>Where are the other low-proper-motion stars?</i> | 289 |
| 6.1.3 <i>Close passes to the Solar System</i>             | 293 |
| 6.1.4 <i>Solar Motion and Solar Siblings</i>              | 294 |
| 6.2 Discoveries of Young Stars                            | 295 |
| 6.2.1 <i>Why there were so many young stars</i>           | 298 |
| 6.2.2 <i>New 25 pc young statistics</i>                   | 299 |
| 6.2.3 <i>The (potential) impact on theory</i>             | 302 |
| 6.3 Future Directions                                     | 304 |
| 6.3.1 <i>TINYMO-North</i>                                 | 304 |
| 6.3.2 <i>Kinematic Youth Survey</i>                       | 305 |
| 6.3.3 <i>Non-population aspects</i>                       | 308 |
| REFERENCES  | 310 |
| APPENDICES  | 329 |
| A HOW ACCURATE ARE SUPERCOSMOS MAGNITUDES?                | 330 |
| A.1 Test Data   | 332 |
| A.2 Comparisons   | 333 |

|   |     |
|---|-----|
| <b>A.3 Conclusions</b> . . . . .                            | 335 |
| <b>B NEARBY LOW PROPER MOTION STARS FOUND IN TINYMO</b> . . | 337 |
| <b>C GAL_UVWXYZ</b> . . . . .                               | 345 |

## LIST OF TABLES

|            |  |     |
|------------|--|-----|
| Table 1.1  | Nearby Young Associations, Clusters and Moving Groups . . . . .                      | 15  |
| Table 2.1  | Plate photometry relations for red dwarfs (Hambly et al. 2004). . . . .              | 60  |
| Table 2.2  | CCD photometry relations for red dwarfs. (Henry et al. 2004) . . . . .               | 61  |
| Table 2.3  | CCD photometry relations for correction to absolute. . . . .                         | 61  |
| Table 2.4  | $V - K_s$ relations for Nearby Young Associations. (Riedel et al. 2011) . . . . .    | 63  |
| Table 2.5  | Nearby Young Associations . . . . .  | 75  |
| Table 2.6  | Parameters for synthetic 25 pc sample . . . . .                                      | 86  |
| Table 3.1  | Breakdown of 25 pc systems. (2012 APRIL 11) . . . . .                                | 108 |
| Table 4.1  | The TINYMO Search Cuts . . . . .   | 131 |
| Table 4.2  | The TINYMO Color Selection Regions . . . . .   | 136 |
| Table 4.3  | TINYMO Results . . . . .   | 148 |
| Table 5.1  | Astrometric Results (Riedel et al. 2010) . . . . .                                   | 166 |
| Table 5.2  | Photometric Results (Riedel et al. 2010) . . . . .                                   | 168 |
| Table 5.3  | Combined System Parallaxes (Riedel et al. 2010) . . . . .                            | 170 |
| Table 5.4  | Multiple System Parameters (Riedel et al. 2010) . . . . .                            | 171 |
| Table 5.5  | Preliminary Orbital Elements for Astrometric Binaries (Riedel et al. 2010) . . . . . | 175 |
| Table 5.6  | Comparison of Spectral Types (Riedel et al. 2010) . . . . .                          | 181 |
| Table 5.7  | Systems in this thesis . . . . .   | 192 |
| Table 5.8  | Low Proper Motion and Young Star Astrometric Results . . . . .                       | 193 |
| Table 5.9  | Low Proper Motion and Young Star Photometric Results . . . . .                       | 195 |
| Table 5.10 | Multiple star parameters . . . . .   | 200 |

|  |     |
|--|-----|
| Table 5.11 Spectroscopic Observations of AP Col (Riedel et al. 2011)           | 203 |
| Table 5.12 Vital Parameters (Riedel et al. 2011)                               | 206 |
| Table 5.13 Emission Lines in HIRES AP Col Optical Spectra (Riedel et al. 2011) | 209 |
| Table 5.14 Individual Parameters   | 229 |
| Table 5.15 Youth properties of Sample  | 233 |
| Table 5.16 New giants and supergiants in the TINYMO sample                     | 285 |
| Table 6.1 Simulated Proper Motions   | 291 |
| Table 6.2 Real Proper Motions  | 291 |
| Table 6.3 Potential Young Systems  | 296 |
| Table 6.4 Young Stars within 25pc  | 301 |
| Table B.1 X-ray bright sample  | 338 |
| Table B.2 Good sample  | 339 |
| Table B.3 Probable giants sample   | 344 |

## LIST OF FIGURES

|   |     |
|---|-----|
| Figure <a href="#">2.1 Annual parallax</a> . . . . .                          | 27  |
| Figure <a href="#">2.2 Deblending Estimation</a> . . . . .                    | 53  |
| Figure <a href="#">2.3 Relative Variability</a> . . . . .                     | 56  |
| Figure <a href="#">2.4 Relative Variability of SCR 0613-2742AB</a> . . . . .  | 57  |
| Figure <a href="#">2.5 Henry et al. (2004) photometric relation</a> . . . . . | 62  |
| Figure <a href="#">2.6 Young Star Isochrones</a> . . . . .                    | 64  |
| Figure <a href="#">2.7 Important Spectral Features</a> . . . . .              | 67  |
| Figure <a href="#">2.8 Na I Gravity indices</a> . . . . .                     | 71  |
| Figure <a href="#">2.9 Lithium EW as a function of age</a> . . . . .          | 73  |
| Figure <a href="#">2.10 Kinematics</a> . . . . .                              | 79  |
| Figure <a href="#">2.11 Simulated Proper Motion Distribution</a> . . . . .    | 88  |
| Figure <a href="#">3.1 RECONS 25pc Sky Plot</a> . . . . .                     | 109 |
| Figure <a href="#">3.2 RECONS 25pc Completion</a> . . . . .                   | 110 |
| Figure <a href="#">3.3 RECONS 25pc CMD</a> . . . . .                          | 111 |
| Figure <a href="#">3.4 RECONS 25pc Stereogram</a> . . . . .                   | 113 |
| Figure <a href="#">3.5 Young Stars Stereogram</a> . . . . .                   | 124 |
| Figure <a href="#">4.1 TINYMO Sky Map, Initial Version</a> . . . . .          | 130 |
| Figure <a href="#">4.2 TINYMO sky coverage</a> . . . . .                      | 132 |
| Figure <a href="#">4.3 TINYMO color-color diagram</a> . . . . .               | 135 |
| Figure <a href="#">4.4 TINYMO Regions</a> . . . . .                           | 137 |
| Figure <a href="#">4.5 TINYMO distance histogram</a> . . . . .                | 139 |

|             |   |     |
|-------------|---|-----|
| Figure 4.6  | TINYMO final color-color diagram                  | 149 |
| Figure 4.7  | TINYMO CCD photometry results                     | 150 |
| Figure 4.8  | TINYMO $\mu$ completeness                         | 151 |
| Figure 4.9  | Reduced Proper Motion                             | 152 |
| Figure 4.10 | Proper Motions                                    | 153 |
| Figure 5.1  | LHS 1582AB  | 173 |
| Figure 5.2  | LHS 2071AB  | 173 |
| Figure 5.3  | LHS 3739/3738AB                                   | 174 |
| Figure 5.4  | LHS 2021  | 174 |
| Figure 5.5  | LHS 4009AB  | 175 |
| Figure 5.6  | Distance Estimate Errors (Riedel et al. 2010)     | 177 |
| Figure 5.7  | Distance Estimate Comparison (Riedel et al. 2010) | 178 |
| Figure 5.8  | HR Diagram (Riedel et al. 2010)                   | 180 |
| Figure 5.9  | LHS 1630AB  | 182 |
| Figure 5.10 | LHS 1749AB  | 183 |
| Figure 5.11 | LHS 1955AB  | 184 |
| Figure 5.12 | Parallax Precision (Riedel et al. 2010)           | 189 |
| Figure 5.13 | Tangential Velocities (Riedel et al. 2010)        | 190 |
| Figure 5.14 | HR Diagram for Low Proper Motion stars            | 197 |
| Figure 5.15 | Sky Plot of Low Proper Motion stars               | 198 |
| Figure 5.16 | Low Proper Motion Distance Comparison             | 199 |
| Figure 5.17 | AP Col Optical Spectrum                           | 208 |
| Figure 5.18 | AP Col Contour (Riedel et al. 2011)               | 211 |
| Figure 5.19 | Detection Limits (Riedel et al. 2011)             | 212 |
| Figure 5.20 | AP Col with Isochrones (Riedel et al. 2011)       | 214 |

|   |     |
|---|-----|
| Figure 5.21 Lithium Comparison (Riedel et al. 2011)             | 216 |
| Figure 5.22 Gravity Comparison (Riedel et al. 2011)             | 217 |
| Figure 5.23 AP Col Variability (Riedel et al. 2011)             | 220 |
| Figure 5.24 AP Col Comparative Variability (Riedel et al. 2011) | 220 |
| Figure 5.25 AP Col UVW Plot (Riedel et al. 2011)                | 223 |
| Figure 5.26 AP Col-Argus Comparison (Riedel et al. 2011)        | 224 |
| Figure 5.27 AP Col Convergence (Riedel et al. 2011)             | 227 |
| Figure 5.28 Color-Magnitude Diagram with Isochrones             | 235 |
| Figure 5.29 Color-Magnitude Diagram with Isochrones             | 236 |
| Figure 5.30 Variability of Thesis Sample                        | 239 |
| Figure 5.31 Activity comparisons                                | 240 |
| Figure 5.32 H $\alpha$ EW                                       | 241 |
| Figure 5.33 Distance vs. X-ray luminosity                       | 242 |
| Figure 5.34 Na I Index  | 243 |
| Figure 5.35 K I EW  | 244 |
| Figure 5.36 LP 467-016AB Kinematic Traceback                    | 248 |
| Figure 5.37 GJ 2022AC variability                               | 250 |
| Figure 5.38 GJ 2022AC   | 250 |
| Figure 5.39 LP 993-116AB astrometric perturbation               | 253 |
| Figure 5.40 BD-21 01074BC astrometric perturbation              | 257 |
| Figure 5.41 BD-21 01074BC                                       | 258 |
| Figure 5.42 L 449-001AB FGS interferogram                       | 259 |
| Figure 5.43 L 449-001AB astrometric perturbation                | 260 |
| Figure 5.44 SCR 0533-4257AB astrometric perturbation            | 261 |
| Figure 5.45 SCR 0533-4257AB FGS interferogram                   | 262 |

|  |     |
|--|-----|
| Figure 5.46 SCR 0613-2742AB astrometric perturbation         | 263 |
| Figure 5.47 SCR 0613-2742AB FGS interferogram                | 264 |
| Figure 5.48 SCR 1012-3124AB                                  | 267 |
| Figure 5.49 TWA 3ABC   | 267 |
| Figure 5.50 TWA 3ABC Variability                             | 269 |
| Figure 5.51 Flares   | 270 |
| Figure 5.52 G 165-008AB Kinematic Traceback                  | 273 |
| Figure 5.53 GJ 2122AB astrometric perturbation               | 275 |
| Figure 5.54 SCR 2036-3607 Kinematic Traceback                | 277 |
| Figure 5.55 GJ 799AB variability                             | 279 |
| Figure 5.56 GJ 799AB   | 280 |
| Figure 5.57 BD-19 04371                                      | 283 |
| Figure 5.58 New Carbon Stars                                 | 287 |
| Figure 6.1 Volume completion of Thesis sample                | 289 |
| Figure 6.2 Proper Motion comparison of Thesis Sample         | 290 |
| Figure 6.3 TINYMO $\mu$ sky plot                             | 295 |
| Figure 6.4 Tangential Velocities for my thesis               | 299 |
| Figure A.1 SuperCOSMOS magnitudes                            | 333 |
| Figure A.2 SuperCOSMOS color term                            | 334 |
| Figure A.3 SuperCOSMOS colors vs Johnson-Kron-Cousins colors | 335 |
| Figure A.4 SuperCOSMOS $R_1 - R_2$                           | 336 |

## LIST OF ABBREVIATIONS

- 2MASS**            The Two-Micron All Sky Survey. A large-scale survey of the entire sky in the near-infrared.
- AU**                Astronomical Unit. Defined as the mean distance between the Earth and the Sun (although given Kepler's Second Law, the Earth spends most of its time farther than 1 AU from the Sun), 150 million km or  $1.5 \times 10^{10}$  cm. One parsec is 206265 AU. At one parsec, a projected separation of 1 AU is an angular separation of 1 arcsecond.
- BASH**             Linux command-line. I'm specifically referring to the Bourne-Again SHell (there are others, but BASH is the most common), which interprets either commands typed at a prompt or commands in a file
- CCD**              Charge-Coupled Device. A digital camera. Astronomical cameras are monochrome, more sensitive (usually 16-bit), and physically much larger than consumer digital cameras
- CMF**                Current Mass Function
- CTIOPI**            The Cerro Tololo Interamerican Observatory Parallax Investigation, a parallax and photometry program run by RECONS.
- DEC**                Declination.
- EW**                Equivalent width. The width of an infinitely sharp spectral line extending to zero flux, and the same area as the measured line (a shape-invariant measure).

|                  |   |
|------------------|---|
| <b>FGS</b>       | The Hubble Space Telescope’s Fine Guidance Sensors  |
| <b>FWHM</b>      | full-width at half-maximum  |
| <b>G</b>         | Giclas star. Prefix for stars discovered by the Giclas & Burnham surveys at Lowell from 1959-1979.  |
| <b>G1</b>        | Gliese star. Prefix applied to the stars in Gliese’s 1957 and 1969 catalogs of nearby stars. Nowadays these stars are usually known by their equivalent GJ name, i.e., G1 551=GJ 551  |
| <b>GJ</b>        | Gliese-Jahriß star. Prefix properly applied to the stars that were newly introduced in Gliese’s 1979 catalog of nearby stars. Nowadays, GJ is used for ALL stars in the Gliese-Jahreiß Catalog of Nearby Stars, including the new additions in the 1991 catalog that were never officially named. |
| <b>Gyr</b>       | Gigayear ( $10^9$ years).   |
| <b>HD</b>        | Henry Draper catalog. Prefix used for stars in early Harvard spectroscopic publications.  |
| <b>HIPPARCOS</b> | <i>HIgh Precision PARallax COLlecting Sattelite</i>   |
| <b>HIP</b>       | Prefix for stars found in the <i>HIPPARCOS</i> mission’s output catalog.  |
| <b>HST</b>       | <i>Hubble Space Telescope</i>   |
| <b>IDL</b>       | Interactive Data Language, or (more often) the proprietary interpreter for that programming language.   |
| <b>IMF</b>       | Initial Mass Function. Describes the ratio of large stars versus small  |

stars that form from a given cloud.

- IRAF** Image Reduction and Analysis Facility. A data processing suite from NOAO.
- IR** Infra-red. Colors redder than red, wavelengths longer than  $7000\text{\AA}$ . (or  $10000\text{\AA}$ , as special detectors are needed beyond  $10000\text{\AA}$ .)
- LEHPM** The Liverpool-Edinburgh High Proper Motion survey. Prefix used for stars in either of Pokorny's two papers of proper motion objects found in SuperCOSMOS.
- LHS** Luyten's Half Second. Prefix for stars in Luyten's 1976 and/or 1979 catalog of stars with proper motions higher than  $0.5'' \text{ yr}^{-1}$ . An earlier catalog was called LFT, Luyten's Five Tenths
- LSPM** Lepine-Shara Proper Motion. Covers stars in Lepin e's 2005 catalog of stars moving faster than  $0.15'' \text{ yr}^{-1}$ . Only the Northern hemisphere catalog has been officially published as of 2011, though the southern hemisphere catalog does exist.
- LSR** Local Standard of Rest. The mean rotational velocity of the Solar Neighborhood, usually measured relative to the motion of the Sun ( $\approx 20 \text{ km s}^{-1}$ ); occasionally measured as the circular rotational velocity of the Galaxy at the radius of the Sun ( $\approx 200 \text{ km s}^{-1}$ ). Alternately, a prefix for Lepine-Shara-Rich stars of high proper motion.
- LY** Light Year. The distance light travels in one (Julian) year; almost  $1 \times 10^{17} \text{ cm}$ .

|               |   |
|---------------|---|
| <b>MINIMO</b> | MINImal proper MOtion, defined as proper motion between $0.18'' \text{ yr}^{-1}$ to $0.5'' \text{ yr}^{-1}$ .   |
| <b>MOTION</b> | High proper motion sample, defined as higher than $1.0'' \text{ yr}^{-1}$ .   |
| <b>Myr</b>    | Megayear/Million years ( $10^6$ years).   |
| <b>NLTT</b>   | The New Luyten's Two Tenths. Prefix (assigned by line number) for stars in Luyten's 1979 catalog of stars with proper motions higher than $0.18'' \text{ yr}^{-1}$ , or its 1980 supplement. An earlier catalog was called LTT, Luyten's Two Tenths |
| <b>NStars</b> | The Nearby Stars project, headquartered at NASA-Ames from 1999-2003, under the supervision of Dr. Dana Backman.   |
| <b>PA</b>     | Position Angle. The angle (in degrees) of the proper motion vector.   |
| <b>pc</b>     | Parsecs. One parsec is defined as the distance to an object with an annual parallax displacement angle of one second, hence PARrallax SECond. Equivalent to 3.26 light years, 206265 AU, or $3.08 \times 10^{18}$ cm                                |
| <b>PI</b>     | Parallax value. Formally written as $\pi$ or $\varpi$ . Alternately, the Principal Investigator (e.g. person in charge) of a grant or telescope time proposal.  |
| <b>PM</b>     | Proper Motion. Formally written as $\mu$ .  |
| <b>PMI</b>    | Proper Motion, ICRS. Prefix used by Lepin , in most of his publications since $\sim 2009$ .   |
| $\mu_{ra}$    | Proper Motion, right ascension component.   |
| $\mu_{dec}$   | Proper Motion, declination component.   |
| <b>PPMXL</b>  | The latest all-sky catalog in the Positions and Proper Motions series.  |

Contains absolute ICRS positions and proper motions for 900 million stars.

- RA** Right Ascension.
- RECONS** Research Consortium On Nearby Stars
- SCR** SuperCOSMOS-RECONS. Prefix used for stars first discovered by the RECONS group, which were discovered in the SuperCOSMOS catalog.
- SED** spectral energy distribution
- SIMBAD** Stellar Database maintained by the Strabsourg Astronomical Data Center (Centre De Données, CDS) at University de Strasbourg, France. Contains basic properties and links to papers about known stars.
- SIPS** Southern Infrared Proper motion Survey. Deacon et al. 2003.
- SLOWMO** SLOW proper MOtion, defined as proper motion between  $0.5''\text{yr}^{-1}$  and  $1.0''\text{yr}^{-1}$ .
- SuperCOSMOS**
- A photographic plate digitizing machine, and the all-sky catalog it produced.
- TINYMO** TINY proper MOtion, defined as proper motion less than  $0.18''\text{yr}^{-1}$ , and the survey that found most of them
- UCAC** USNO Compiled Astrographic Catalog. A catalog of absolute proper motions for 113 million stars built from a CCD-based all-sky survey and archival photographic plate measurements. The current latest version is UCAC3, although UCAC4 (the anticipated final version) is due out in late 2012.

- USNO**                    The United States Naval Observatory.
- VizieR**                    Astronomical Catalog database server maintained by the Strasbourg  
Astronomical Data Center (Centre De Données, CDS) at University de Strasbourg,  
France.
- WDS**                    Washington Double Star catalog. A massive database maintained by  
USNO of reported visual, AO, Speckle, and Interferometric multiple star systems.
- Wo**                    Wooley star. Prefix applied to the stars in Wooley's 1970 catalog of  
nearby stars within 25 pc. An unofficial extension to the Gliese (1969) catalog since  
adopted by Jahreiß, its numbers are all above 9000. These names are very rarely used;  
even more rarely GJ is used instead. (Wo 9025= GJ 9025)
- ZAMS**                    Zero-age main sequence

# CHAPTER 1

## AN INTRODUCTION

### 1.1 The Solar Neighborhood

The Solar Neighborhood is the first place to look when studying the Galaxy we live in. Much of this has to do with the fact that nearer things are easier to study: they are brighter, the stars themselves (and the separations of companions) have larger angular sizes, and it is easiest to measure accurate trigonometric parallaxes. The best place to make a volume-limited study of stars is nearby, where the very faintest M dwarfs are easiest to see and be measured. Nearby stars are the best candidates for determining dynamical masses because binaries are resolvable at shorter orbital periods. The best place to constrain basic stellar properties is nearby, where the stars provide higher fluxes and are larger in angular size. Finally, the nearby stars are our closest neighbors in space, important on their own as the locations humanity will reach first if and when humanity develops interstellar travel.

The exact definition of the Solar Neighborhood tends to vary from observer to observer, ranging anywhere from 5 (van de Kamp 1969) to  $>100$  parsecs (pc) of the Sun (Torres et al. 2008). RECONS (the REsearch CONSortium on Nearby Stars) typically uses 10 or 25 pc. In this dissertation, I use 25 and 100 pc. One thing is common to all these definitions, however: the Solar Neighborhood is on a small enough scale that Galactic structure is not visible. The Solar Neighborhood does not reach to any Galactic arms, it is significantly smaller than the scale height of the Galactic disk (300 pc, Holmberg et al. 2009), and the positions of star systems within it are largely random. Because the Sun is in an inter-arm region, there are

very few short-lived massive stars within the Solar Neighborhood. There are no known high-mass X-ray binaries, cataclysmic variables, black holes, neutron stars, planetary nebulae, molecular clouds, star-forming regions, or other phenomena more energetic than the flares of UV Ceti stars, and interstellar reddening is generally negligible. The Solar Neighborhood thus consists mostly of low-mass, multi-Gyr old star systems, which have been stirred up so much by Galactic potential differences and encounters with other stars that they are now widely-separated from the other stars in their natal star clusters (Holmberg et al. 2009).

As has been known for years (and recently described by Aumer & Binney 2009), the space velocity dispersions of nearby disk stars follow temperature trends, with the overall W distribution (perpendicular to the plane) much smaller than the U or V motion. As one goes to cooler and cooler stars, the velocity dispersions increase, up to the Parenago Discontinuity, where they level out<sup>1</sup>. The velocity dispersions are caused by interactions with other stars and molecular clouds over the eons, pushing them to ever more inclined and eccentric orbits. There are several examples of extremely inclined and eccentric orbits within the Solar Neighborhood, in ancient stars like  $\mu$  Cas AB=GJ 53 and Kapteyn's Star=GJ 191, metal-poor subdwarfs probably around the age of the Galactic disk itself, and Barnard's Star=GJ 699, a potentially old (but otherwise normal) M dwarf on a somewhat unusual orbit perturbed by 10 Gyr of gravitational interactions with other stars. This general concept of disk heating leads to the concept of age-dating stars by their kinematics.

---

<sup>1</sup>The discontinuity happens around G0, the point at which the lifetimes of stars exceed the age of the Milky Way Galaxy (Dehnen & Binney 1998). The Parenago Discontinuity is thus due to the Galaxy not having existed long enough to have disk-heated those stars to more eccentric orbits, although a system's total mass should theoretically still determine how easily it scatters.

Our corner of the Galaxy (both inside and just outside the flexible boundaries of the Solar Neighborhood) is not *completely* devoid of structure, though. There are, for instance, famous open clusters like the Hyades and the Pleiades, both recognized in antiquity (the Pleiades were mathematically proven to be a cluster by [Michell 1767](#)), and IC 2391, supposedly seen by the Arabic astronomer Al Sufi in the 9th century<sup>2</sup>, which are all young and dense enough that they are still bound systems. Other famous examples of such clusters (several of which extend within The Solar Neighborhood) include the Ursa Major moving group, IC 2602, the “Local Association”, and myriad other clusters and superclusters studied by Olin Eggen during his career. These clusters, if sufficiently dense, appear as overdensities in a plot of UVW velocity space (though the sparsely populated and unbound local associations do not). Relevant to this dissertation, all of these young stars have very small velocity dispersions relative to the Local Standard of Rest (LSR), around  $20 \text{ km s}^{-1}$ . These space velocities usually appear as small proper motions. It is these kinematics that inform and define the majority of my thesis work.

### ***1.1.1 History of Nearby Star discoveries***

Nearby star research has specifically been a goal at least as far back as [Luyten & Shapley \(1930\)](#), who published a list of stars within 10 pc. At the time, there were 105 such systems known (55% of the expectation at the time based on constant density within the volume). The faintest star on the list was GJ 280B=Procyon B, with  $M_{vis}=13.0$ ; the current third closest star system (GJ 406=Wolf 359,  $M_V=13.5$ ) was not included at all. As of 11 APRIL

---

<sup>2</sup><http://messier.seds.org/xtra/ngc/i2391.html> retrieved 29 MAR 2012

2012, there are 261 systems (most of them quite faint) with published trigonometric parallaxes of 100 mas or more, and errors of 10 mas or less. This is 64% of the current expectation based on volume, and the faintest member is now a T dwarf (Lucas et al. 2010; Leggett et al. 2012) which is faint enough that no  $V$  magnitude has yet been measured.

The largest compendium of the overall knowledge of nearby stars (and the source of GJ names) is the Catalog of Nearby Stars (CNS) maintained by Wilhelm Gliese (with later help from Harmut Jahrei). The catalog gradually expanded from 915 systems (1094 components) within 20 pc (Gliese 1957) to 3265 systems within 25 pc in 1991 (Gliese & Jahrei 1991). Systems were identified via trigonometric, spectroscopic and photometric parallaxes. Subsequent catalogs intending to supersede CNS are the aborted NStars Database (Henry et al. 2002), with 2011 systems within 25 pc by trigonometric parallax only, the now-defunct NStED (NASA Stars and Exoplanets Database), and RECONS' own new database under construction (see § 3.2).

How do we find the nearby stars? Over the last 200 years, proper motion – the apparent motion of stars across the sky, seen over periods of years – has been used to find nearby stars. This approach has been based on the idea that stars move through space, and the closest ones should appear to move the fastest. Currently, we understand that this is due to the combination of the motions of the Sun and the star in question in their orbits around the center of the Galaxy, though this idea predates the discovery of the Galaxy and our place in it by at least 150 years (the earliest reference available seems to be William Herschel in 1783), who claims the phenomenon is well-established and credits its discovery to Sir

Edmund Halley).

This property of large proper motion has served nearby star research well from the very beginning, forming at least part of the decisions of Bessel (1838) and Henderson (1839) to observe 61 Cygni and Alpha Centauri (respectively) for parallax. This trend has continued to the present day. Nearly all nearby stars known have high proper motions, with the limit of high proper motion ( $0.5'' \text{ yr}^{-1}$ , van Maanen) or interesting proper motion ( $0.2'' \text{ yr}^{-1}$ , the Royal Greenwich Observatory) set by influential publications (van Maanen 1915; Thackeray 1917, according to Luyten) in the early part of the 20th century (Luyten 1988)<sup>3</sup>. Though Luyten does not give the reasoning behind either limit, a careful reading of Dyson (1917) suggests that Greenwich set their  $0.2'' \text{ yr}^{-1}$  limit (actually, Luyten used a lower limit of  $0.18'' \text{ yr}^{-1}$  to account for the average  $0.02'' \text{ yr}^{-1}$  differences between his relative proper motions and absolute proper motions) based on calculations that suggested only 1/8 of all nearby stars ( $<20 \text{ pc}$ ) should have lower proper motions<sup>4</sup>.

Proper motion is, of course, not an entirely foolproof method. Star systems have different intrinsic space velocities due to their particular Galactic orbits. Those Galactic orbits produce, within the Solar Neighborhood, basically random orientations. Proxima Centauri, the closest star to the Solar System, is only the 18th highest proper motion object in the New Luyten's Two Tenths Catalog (Luyten 1979b). By the same token, there is no particular

---

<sup>3</sup>The Thackeray article may predate the one to which Luyten refers, but it is the earliest reference I can find prioritizing stars with proper motions  $>0.2'' \text{ yr}^{-1}$ ; van Maanen (1915) refers to an even earlier (possibly less influential) paper by Porter (1892) as the reason for his  $>0.5'' \text{ yr}^{-1}$  limit.

<sup>4</sup>It is not, as I had naïvely assumed, the best that could be done accurately with photographic plates and blink comparators of the time. Accuracy did influence the limits set by Giclas in his surveys, where he states that larger epoch spreads between plates allowed him to impose a lower limit, ( $0.2'' \text{ yr}^{-1}$ ) on his southern survey than on his northern surveys ( $0.27'' \text{ yr}^{-1}$ ) (Giclas et al. 1979).

reason a star system could not coincidentally be heading directly towards or away from us. A good example is GJ 566, which despite a distance of 6.7 parsecs is moving at  $0.169'' \text{ yr}^{-1}$ , and would likely not have been noticed before *HIPPARCOS* if it were not a 5th magnitude G dwarf star with a K dwarf companion, and visible orbital motion.

The other obvious alternative identifier of proximity is luminosity. Thus far, only the *HIPPARCOS* mission has used this criterion in a systematic way; it observed all stars brighter than  $V=7.3$  (Perryman et al. 1997), which does incidentally demonstrate that not all objects found this way within 25 parsecs are fast moving. Given the bright magnitude limit, *HIPPARCOS* did not find all nearby stars. In fact, despite its thousand-fold improvements over *HIPPARCOS*, ESA's *Gaia* mission will not find all nearby stars either – even with a stated magnitude limit of  $V = 20$ , it will miss M dwarfs at  $M_V=21$  even within 10 pc. M dwarfs are believed to extend to  $V - K=9.5$ ,  $M_V=21$  based on stellar evolution models, though it is not yet observationally clear where the dividing line between true stars and brown dwarfs lies. As yet, no one knows how large the population of the smallest stars truly is.

## 1.2 The Missing Stars

The situation is currently thus: using an error cutoff of  $0.01''$  (10 mas), there are 51 trigonometric-parallax-verified systems within 5 parsecs<sup>5</sup>. If that is a true and useful sample, there should be 408 star systems within 10 parsecs (eight times the volume, assuming

---

<sup>5</sup>from RECONS: <http://www.chara.gsu.edu/RECONS/TOP100.posted.htm> checked 2012 JUL 15 plus the Sun, plus Leggett et al. (2012)

constant density), and 6375 systems within 25 parsecs (125 times the volume). The current tally is 261 parallax-verified systems (with 10 mas error cutoff) within 10 parsecs (RECONS 10 pc census, <http://www.recons.org/census.posted.htm> checked 2012 JUL 15) and 2089 parallax-verified systems within 25 parsecs (The RECONS database, §3.2). We are therefore missing nearly 35% of systems within 10 pc and 66% of all systems within 25 pc. The rest are hiding in plain sight.

To speak broadly, there are four general categories of where these “missing” stars may be.

### ***1.2.1 Known stars without published parallaxes.***

From many perspectives these stars are not considered ‘missing’, but as we require the unbiased accuracy of a trigonometric parallax to confirm the star is nearby, stars without parallaxes are still unconfirmed at best. The Luyten Half Second catalog (2nd ed) (Luyten 1979a), New Luyten Two Tenths catalog (Luyten 1979b), and Giclas survey papers (final entries, Giclas et al. 1979) contain over 50,000 stars and were published decades ago, most of them fainter than *HIPPARCOS* could reach. This is an area where existing parallax programs and future programs like LSST, PanSTARRS and Gaia will have a huge impact.

### ***1.2.2 Stars simply missed by Luyten and Giclas.***

Luyten’s NLTT survey objects were identified by eye from photographic plates in the far south from his earlier BPM survey (which had a limiting magnitude of  $R=16.5$ ) and machine-scanned plates from the Luyten-Palomar survey ( $R=18$ ) for more northern regions. Luyten

chose a proper motion limit of  $\mu > 0.18'' \text{ yr}^{-1}$  to make certain his catalog would contain all stars moving faster than  $0.2'' \text{ yr}^{-1}$ . Giclas's Lowell Proper Motion survey ( $R=16.5$ ) had a nominal limit of  $0.27'' \text{ yr}^{-1}$  and a goal of finding every object moving faster than  $0.30'' \text{ yr}^{-1}$ ; that proper motion limit was later reduced to  $0.20'' \text{ yr}^{-1}$  thanks to the larger epoch spread of plates in the southern hemisphere, but the survey was left unfinished in 1979 with only part of the southern hemisphere completed. Lépine & Shara (2005) estimate Luyten's completion rate within his intended bounds to be around 88%, based on internal and external criteria. Many astronomers (too many to note, though Wroblewski & Torres (1989, and subsequent), Pokorny et al. (2003), RECONS (Hambly et al. 2004, and subsequent), and Lépine et al. (2002, and subsequent) have made major contributions) have had successful programs locating such objects, particularly in the south, where Giclas was unfinished and Luyten had a higher magnitude limit than in the north.

### ***1.2.3 Stars too faint for the Luyten and Giclas Surveys.***

As mentioned earlier, Luyten and Giclas were both limited by the sensitivities and wavebands of their first or second epoch plates. The smallest stars around the M/L transition have absolute magnitudes of  $R=18$ , therefore the Luyten and Giclas surveys cannot complete a nearby star sample out to a distance of 25 pc, where such stars have  $R=20$ . More modern surveys with lower flux limits and that use infrared wavebands (for example, UKIDSS (Deacon et al. 2009), MTCN (Reid et al. 2008), SIPS (Deacon & Hambly 2007), WISE (Kirkpatrick et al. 2011) ) are better suited to detect fainter, cooler nearby stars. Given current estimates of the

Current Mass Function (CMF) and Initial Mass Function (IMF)<sup>6</sup> that are heavily skewed toward many low-mass stars, these surveys will be very profitable.

#### 1.2.4 Stars moving too slowly for the Luyten and Giclas surveys.

The limits set by Luyten (and the Royal Greenwich Observatory before him) were more out of practical than scientific reasons; small motions are harder to measure accurately<sup>7</sup>, and open up a floodgate of new objects. With the advent of modern computing capabilities, though, the flood of objects is manageable.

Many recent surveys have breached the  $0.18'' \text{ yr}^{-1}$  limit, most notably Wroblewski-Torres-Costa (Wroblewski & Torres 1989, and subsequent) ( $0.15'' \text{ yr}^{-1}$ ), the LSPM survey (Lépine & Shara 2005) ( $0.15'' \text{ yr}^{-1}$ ), the ‘Meet the Cool Neighbors’ group (Reid et al. 2007) (limit  $0.11'' \text{ yr}^{-1}$  northern hemisphere,  $0.28'' \text{ yr}^{-1}$  southern hemisphere), and Deacon (2007) ( $0.1'' \text{ yr}^{-1}$ ), (2009) ( $0.08'' \text{ yr}^{-1}$ ). Apart from the anticipated but currently unreleased<sup>8</sup> Lepine SUPERBLINK catalogs ( $0.04'' \text{ yr}^{-1}$  and up), no efforts are searching for stars with proper motions smaller than  $0.1'' \text{ yr}^{-1}$ , or down to truly zero proper motions.

---

<sup>6</sup>The mass functions describe the ratio of the number of large stars to the number of small stars, as a function of stellar mass. The IMF describes the breakdown of stars in a single star formation event; the CMF describes the current breakdown – which will be different, as successive star formation events will leave behind many long-lived low-mass stars, but only the most recent massive stars will remain. The IMF is more important to stellar evolution theory.

<sup>7</sup>Stars with high proper motions are *also* troublesome, as they are often mistaken for multiple transient objects rather than a single moving object. Some are certainly still unidentified (Henry et al. 2004; Lépine et al. 2005), though they are probably few in number.

<sup>8</sup>But see Lépine & Gaidos (2011)

### 1.3 Hiding in Plain Sight

My dissertation focuses on the discovery and characterization of new nearby stars of low proper motion. Essentially random distributions of stars within certain velocity dispersions imply that a not-insignificant fraction of stars in the Solar Neighborhood will, by chance, have space motions almost entirely in the line of sight. These stars can be relatively bright and easy to observe with small telescopes and current instrumentation – as mentioned in §1.1.1, the only survey that systematically probed down to zero proper motion was *HIPPARCOS*, which is only complete to  $V = 7.3$ .

With knowledge of the velocity dispersions of stars (Aumer & Binney 2009) and a rough idea of the current mass function (CMF) for the solar neighborhood (from RECONS), it is possible to generate a realistic approximation of the distributions and velocities of nearby stars. My Monte Carlo simulation of this distribution (described in more detail in Section 2.4.3) suggests that roughly 13.6% of stars within 25 parsecs should be moving slower than the Luyten limit of  $0.18'' \text{ yr}^{-1}$ .

There are fundamental problems with extending proper motion surveys down to zero proper motion. Even neglecting the practical limits of most of the proper motion surveys (particularly the compiled catalogs, with their uncertainties introduced by source/scanning resolution and optical defects), below a certain level, proper motions will not be indicative of proximity. Even distant background stars have some non-zero proper motion, as they too are in orbit around the Galactic center.

As such, another method is needed to identify the truly nearby stars. For this purpose, we

are using photometric distance estimates (See § 2.2.5), where two photometric magnitudes and the assumption the star is on the main sequence will give us an estimate of the distance. All-sky photometry is already available and of decent quality, and thus provides a fast way to examine samples of very low proper motion stars. One of the stellar samples that often exhibits little proper motion is young stars.

## 1.4 Young Stars

Young stars tend to be gathered into groups, which are known by a variety of terms, often used interchangeably. For the purposes of this thesis, I will be using the term “star-forming region” to refer to giant molecular clouds and all other regions still embedded in or near gas clouds, such as Orion, or  $\rho$  Ophiuchus. “Cluster” will refer to a gravitationally-bound system of young stars, like the Pleiades, IC 2391, the Hyades, or  $\eta$  Chameleontis. For unbound associations, “moving group” will refer to unbound associations old enough that M0 stars are on the main sequence, while “association” will apply to unbound associations whose M0 stars are pre-main-sequence. This distinction is a bit subjective, given remaining uncertainties in the models (Dotter et al. 2008), but for purposes of this dissertation, I will set my dividing line between the  $\sim 125$ -Myr old AB Doradus association, and the  $\sim 200$ -Myr-old Castor moving group.

As I’ve said earlier, the Solar Neighborhood (by any common definition) itself is too small to show any large-scale Galactic structure, and positions and motions within it are by and large random. The closest and most important vestige of Galactic structure is Gould’s

Belt, a large ring of gas probably connected to the nearest spiral arm. Gould's Belt is manifest as the location of (nearly) all of the nearest O and B stars; it is also where all nearby star forming regions are found: the Scorpius-Centaurus star forming region ( $\sim 100$  pc away), on the other side of the sky, Taurus-Auriga ( $\sim 150$  pc away), Perseus, and Orion OB1 ( $\sim 400$  pc away). As the closest star forming region, Sco-Cen has the most effect on the Solar Neighborhood. Though it is less dense than Orion OB1 and has correspondingly fewer high mass stars, it occupies a vast area of nearby space, and shows signs of burning like a wick as waves of star formation pass through: On one side are the open clusters IC 2391 (the Omicron Velorum cluster) and IC 2602 (the Theta Carinae Cluster, or the Southern Pleiades) with ages of somewhere between 30 and 50 Myr; on the other side of the sky is the  $\rho$  Ophiuchus star forming region (often connected to Sco-Cen), the site of current star formation and stars as young as 5 Myr old (and  $\zeta$  Oph, the nearest O star to the Solar System). Between the two ends, in formations known as Upper Centaurus Lupus, Lower Centaurus Crux, and Chameleon, are stars of intermediate ages. All of the currently known nearby stellar associations containing pre-main-sequence stars appear to originate in Scorpius-Centaurus.

Using slightly older definitions of young, there are several other nearby groups of stars as well: The Pleiades ( $\sim 125$  Myr), the Castor moving group ( $\sim 200$  Myr), the Ursa Major moving group ( $\sim 500$  Myr), and the Hyades cluster ( $\sim 650$  Myr) are all also moving with similar slightly-faster-than-LSR motions, but are likely due to other episodes of star formation.

### 1.4.1 History

For decades, all identified young stars were either several hundred million years old or hundreds of parsecs away. Of particular interest is the work done by Olin Eggen in the 1950s and 1960s (Eggen 1958, and subsequent), who noticed overdensities in spatial velocity plots of nearby stars, and defined superclusters of young stars surrounding, but related to, the nearest known clusters: the Hyades Supercluster, the Pleiades Supercluster (a name apparently interchangeable with “The Local Association”), and the IC 2602 and IC 2391 Superclusters.

On the face of it, this idea makes sense. We know most stars form in open clusters, but open clusters will gradually dissolve<sup>9</sup> through dynamical interactions with internal and external gravitational forces; there surely must be an intermediate point where a dissolving cluster is surrounded by a halo of formerly bound members. Modern studies seem to suggest Eggen may have overreached his data, finding (for instance) his Hyades supercluster composed of stars with a wide, aphysical range of ages and at improbable distances (as close as 5 pc: G 099-049), and Local Association members *everywhere*. Still, the idea was sound, and persisted.

In the 1980s, the stars TW Hydra (Rucinski & Krautter 1983, the first “isolated” T Tauri star) and  $\beta$  Pictoris (Smith & Terrile 1984) came to the attention of astronomers as IRAS sources – disk-bearing stars that were potentially young. This phenomenon was a great mystery to astronomers at the time, particularly given that parallax measurements of  $\beta$  Pic and TW Hya put them much closer than the Pleiades, and far from any star-

---

<sup>9</sup>Recent research (de Grijs et al. 2008) suggests that while most nearby open clusters have survival timescales greater than a Hubble time, the Hyades may be in the final stages of dissolution.

forming region. Something of a solution to the problem came in 1989, when de la Reza et al. (1989) located three more T Tauri stars in close spatial proximity to TW Hya and with similar kinematics. As an industry, though, young stars in the Solar Neighborhood did not take off for a few more years. While Gregorio-Hetem et al. (1992) found a fifth TW Hya member, it was not until 1999, when Webb et al. (1999) located five more members of TW Hydra, Barrado y Navascués et al. (1999) recognized the overluminous triple flare-star system AU/AT Mic as matching the space motion of  $\beta$  Pictoris, and Mamajek et al. (1999) found the nearby  $\eta$  Chameleontis cluster, that research on very nearby young stars began in earnest.

Thirteen years later, there have been several relatively nearby (within 100 pc) young (less than 125 Myr old<sup>10</sup>) groups identified, comprising associations like TW Hydra (now with over 30 members),  $\beta$  Pictoris, AB Doradus, Argus, Octans,  $\epsilon$  Chameleontis, Tucanae-Horologium, Columba and Carina, with additional older moving groups currently suspected like the Castor (Barrado y Navascués 1998) moving group at roughly 200 Myr, Ursa Major (King et al. 2003), and the putative old Wolf 630 moving group centered around GJ 644ABCD/643 (Eggen 1965; Bubar & King 2010)) at over 2 Gyr. These amalgamations of young stars, shown in Table 1.1 are sparse, not gravitationally bound, and several do not have cores. Nevertheless, they are nearby, easy-to-examine windows into the history and processes of star formation, far more accessible than the Pleiades (133 pc, Soderblom et al. 2005), and in many cases far younger.

---

<sup>10</sup>As per Fernández et al. (2008), the actual ages of these moving groups are not well determined, apart from the ones less than 20 Myr old. Relative ages, however, are likely to be correct.

Table 1.1: Nearby Young Associations, Clusters and Moving Groups

| Name           | Distance<br>(pc) | Age<br>Myr | #<br>members | ref  |
|----------------|------------------|------------|--------------|--|
| (1)            | (2)              | (3)        | (4)          | (5)  |
| $\epsilon$ Cha | 108± 9           | 6          | > 20         | <a href="#">Mamajek et al. (1999)</a> ; <a href="#">Torres et al. (2008)</a>       |
| TW Hya         | 48±13            | 8          | > 30         | <a href="#">Zuckerman &amp; Song (2004)</a> ; <a href="#">Torres et al. (2008)</a> |
| $\beta$ Pic    | 31±21            | 12         | > 50         | <a href="#">Zuckerman &amp; Song (2004)</a> ; <a href="#">Torres et al. (2008)</a> |
| Octans         | 141±34           | 20         | 15           | <a href="#">Torres et al. (2008)</a>   |
| Tuc-Hor        | 48± 7            | 30         | > 40         | <a href="#">Zuckerman &amp; Song (2004)</a> ; <a href="#">Torres et al. (2008)</a> |
| Columba        | 82±30            | 30         | > 40         | <a href="#">Torres et al. (2008)</a>   |
| Carina         | 85±35            | 30         | > 20         | <a href="#">Torres et al. (2008)</a>   |
| Argus          | 106±51           | 40         | > 60         | <a href="#">Torres et al. (2008)</a>   |
| AB Dor         | 34±26            | 125        | > 80         | <a href="#">Zuckerman &amp; Song (2004)</a> ; <a href="#">Torres et al. (2008)</a> |
| Pleiades       | 133±13           | 125        | lots         | <a href="#">Adams et al. (2001)</a> ; <a href="#">Soderblom et al. (2005)</a>      |
| Castor         | ...              | 200        | > 30         | <a href="#">Barrado y Navascues (1998)</a> ; <a href="#">Montes et al. (2001)</a>  |
| UMa            | ...              | 500        | > 60         | <a href="#">King et al. (2003)</a>   |
| Hyades         | 43±10            | 650        | lots         | <a href="#">Röser et al. (2011)</a>  |

### 1.4.2 Properties

Of course, no study of youth is complete without defining exactly what “young” itself means in the current context. Considering only the age since gravitational collapse began (as is generally done) yields a wide variety of properties and different states of formation. A, B, and O-type stars live fast and die young; thus any existing O star can only be  $\sim 10$  Myr old<sup>11</sup>, while M stars take at least 200 Myr (type M0) to settle onto the main sequence ([Dotter et al. 2008](#)). After that point, it can take periods of time longer than the current age of the Universe before the chromospheric activity of the very coldest M dwarfs drops below saturation level ([West et al. 2008](#)), and the total hydrogen-fusing lifetimes of M stars are expected to range from tens of billions to trillions of years. Thus, any given group of young stars will likely contain both massive main-sequence stars and low-mass pre-main-sequence

<sup>11</sup>Even including mass transfer, as the donor would have to be a very massive star as well.

stars, simply because of the vast disparity in the rates of stellar evolution. Here I outline several characteristics used to identify stars as young.

#### *1.4.2.1 Dynamical*

**Kinematics matched to a known cluster.** One of the most often used methods for identifying young stars, this technique exploits the idea that members of moving groups are all the result of the same formation event, picking up the location and space motion of their natal clouds.

Unfortunately, kinematics are troublesome indicators for nearby stars, and are easily contaminated by regular field stars. The nearby associations are unbound, with correspondingly large UVW velocity dispersions, and have low spatial densities (lower than open clusters like the Pleiades;  $\eta$  Cha is an exception) spread over large volumes of space. In fact, most associations spatially overlap each other, and several ( $\beta$  Pic and AB Dor in particular) are all-sky as seen from the Earth, because the Sun is embedded within them.

Our kinematic knowledge of stars has reached the point where we can take kinematics further and examine the individual motions of stars to ensure their Galactic orbits converge with the other members of the association at the time of formation – e.g., a true member of a 12 Myr old association should have an orbit that converges with all the other members around 12 Myr ago – although given that some of these clusters were probably never bound, the distance requirement to say a star “converged” is not clear, and some authorities argue that current methods of kinematic backtracking are not accurate beyond 30 Myr (Song, I. private communication 2012).

### 1.4.2.2 Physical

**Lithium features.** Lithium is easily destroyed but not readily produced by stellar thermonuclear fusion, and is thus only detected in the photospheres of objects that have not yet consumed their primordial supply of the element. This is usually interpreted as a consequence of youth, or can be used to identify brown dwarfs of masses less than  $\sim 60M_{jup}$  because their cores never reach the temperatures necessary to fuse it. Lithium depletes fastest in mid-M stars, where it is thought that the persistence of full convection throughout the star's evolution to the main sequence means that all the lithium is cycled through the core and quickly destroyed once temperatures rise high enough (Jeffries & Naylor 2001). Larger, hotter stars develop radiative cores that take longer to deplete their lithium and can trap it in their photospheres for a billion years; cooler fully-convective stars like the M4.5 type star AP Col (§5.4) have longer nuclear burning timescales. Thus, as a coeval stellar population ages, the temperature range of lithium-depleted stars widens around the mid-M stars, with a particularly sharp drop on the cooler side. The detection of lithium in a K or M-type star is therefore a strong indicator of youth.

**Low gravity features.** Certain spectral features are sensitive to the surface gravity of a star, and may therefore be used to discern giants from dwarfs. These features may be used to form age proxies for stars still contracting toward the main sequence (Hayashi 1966), at least for relative dating (e.g. Lawson et al. 2009).

To visually distinguish giants and dwarfs, the Ca II triplet is useful, although it is generally found in the middle of telluric water features. On finer scales, the Na I  $\lambda 8183/8195$  dou-

blet is particularly useful for comparative gravity studies (e.g. Lawson et al. 2009; Murphy et al. 2010; Schlieder et al. 2012b). For spectral types cooler than  $\sim M3$ , there is a marked decrease in the strength of the Na I doublet between dwarfs (strong), pre-main-sequence stars (intermediate), and giants (weak/absent).

One other measurement that can theoretically be used is the K I line at  $7699\text{\AA}$  (Shkolnik et al. 2011), part of an optical K I doublet. K I feature, like Na I, is gravity sensitive and a well-known indicator of giants and dwarfs, and unlike Na I or Ca II, K I (or at least one of the lines in its doublet) is not sitting in a major band of water absorption.

**Overluminosity.** Stars that have not yet reached the main sequence (i.e., equilibrium between gravitational collapse and radiative pressure from thermonuclear fusion) will appear overluminous compared to other stars of the same color because their photospheric surfaces are larger than main-sequence stars. Such young stars are therefore elevated relative to the main sequence on an HR diagram.

On the other hand, such overluminosity can also be due to unresolved multiplicity, which is why high angular resolution observations (e.g. Lucky imaging, Speckle interferometry, Adaptive Optics, Long Baseline Interferometry) and spectroscopy are so vitally important to young star research. Overluminosity can also be due to high metallicity, and is responsible for the nearly 2-magnitude width of the M dwarf main sequence in  $M_V$  vs  $V - K_s$  color. This makes it difficult to tell the difference between an  $[\text{Fe}/\text{H}]=+0.0$  AB Dor member and an  $[\text{Fe}/\text{H}]=+0.3$  main sequence star. The current most popular and reliable method to estimate stellar metallicity in M dwarfs uses K band Na I and Ca I spectroscopic features,

and is described in Rojas-Ayala et al. (2012).

**Chemical Abundance.** As noted by Castro et al. (1999), the Ursa Major moving group has unique barium and copper abundances. Such properties can theoretically be used to link stars of similar heritage, although not much work has been done in identifying chemical peculiarities in other associations. I suspect that this is due to a combination of factors. First is the difficulty of accurately determining chemical abundances for many classes of stars, particularly M dwarfs. Second, it is usually easier to establish membership in a young association by other means. Third, given that all nearby pre-main-sequence stars are expected to have originated in the Sco-Cen star forming region, the gas composition may be so similar that some of the younger associations are indistinguishable.

**Disks.** Accretion and protoplanetary disks are signs of the T Tauri class of pre-main-sequence stars. These disks show up as near- and mid-IR excesses. In M dwarfs, these dusty, dense disks – distinguishable from debris disks because they extend close to the star and contribute to the IR excess at hotter, bluer wavebands than  $24\ \mu\text{m}$  (Schisano et al. 2009) – are rare in stars older than 10 Myr or so (Haisch et al. 2001, 2005), making the disk around AU Mic (GJ 803,  $\beta$  Pic,  $\sim 12$  Myr) an exception to the rule. Disks are a commonly studied feature of stars embedded in star forming regions, but in the Solar Neighborhood, they should only be common in the youngest associations, TW Hya and  $\epsilon$  Cha.

#### 1.4.2.3 Activity-based parameters

There are various observable indicators of activity that can be used to identify young stars. All of them have caveats, and all of them share the weakness that the activity could also be

due to a very close interacting companion mutually tidally locking the system- thus, for any binary, it is important to correctly gauge the separation.

On the other hand, chromospheric and coronal activity is normally present in M dwarfs for longer than 650 Myr, the age of the Hyades (Zuckerman & Song 2004). Saturated activity can give upper limits on the age (West et al. 2008) dependent on spectral type (as a proxy for mass), but by M5, stars like Proxima Centauri (5 Gyr old, Porto de Mello et al. 2008) are still saturated.

**High rotation rates** Young stars are expected to rotate rapidly, with decreasing rotation as they age. Reiners et al. (2009) suggest  $v \sin i > 20 \text{ km s}^{-1}$  is a rapidly rotating M star. The only real difficulty in relying on  $v \sin i$  for a star's rotation<sup>12</sup> is that there is usually no way apart from statistical averaging to account for the star's inclination.

The effects of these high rotation rates can be seen in stellar chromospheric activity, where high rotation is believed to be responsible for the powerful magnetic dynamo responsible for the observed effects. Gyrochronology relations exist (e.g. Barnes 2003) for solar-type stars, but unfortunately, none have been developed for M dwarfs.

**H $\alpha$  in emission.** The H $\alpha$  line at 6563Å is very strong in active stars, and is caused by the magnetic field lines heating the chromosphere (Riaz et al. 2006). For the most part, H $\alpha$  emission does not correlate with any other parameters in stars with saturated magnetic activity. There are levels of H $\alpha$  emission, though, and H $\alpha$  EW stronger than  $-10$  to

---

<sup>12</sup>A better way would be to use the star's angular diameter from interferometry and trigonometric parallax to get an accurate radius, combined with a photometric rotation period, to get  $v$ , as in Desidera et al. (2011). However, all of those observations are 'expensive', and require either time-consuming or specialized instruments

$-40\text{\AA}$  (with increasing limit as temperature drops) is likely to be a sign of accretion activity (White & Basri 2003) in M dwarfs, and therefore a T Tauri accretion disk.

**Photometric variability (and flares).** Young stars were recognized for their photometric variability very early, back when they were known as “Orion-type” variables (Samus et al. 2012); they are also known to have spectacularly large and powerful white-light flares on the order of magnitudes. No less than T Tauri itself is a variable star, known for lighting up Hind’s Variable Nebula. As with all activity-related effects, the photometric variability of M dwarfs continues on in time into what are known as BY Draconis and UV Ceti variables, the “adolescent” versions of what would otherwise be considered youthful activity.

**X-ray and UV emission.** X-ray emission is again related to chromospheric activity, originating in the corona, and is quite common among young stars. Exactly how X-ray luminous the stars are for a given age is very much related to their masses.  $\beta$  Pic, a  $\sim 12$  Myr old A6V star, for example, has a much smaller X-ray luminosity than Barnard’s Star at M4.0V, even though Barnard’s Star is believed to be an intermediate-disk object, older than mean field age (Gizis 1997).<sup>13</sup>

X-ray flux (and luminosity) can be quoted directly, but is usually given relative to the bolometric luminosity of the object (or rather, the bolometric luminosity of the star assuming no X-ray emission). X-ray luminosity saturates at  $\log(L_x/L_{bol}) \approx -3$  and remains for extended periods of time, depending on the mass of the star. The main attraction of this indi-

---

<sup>13</sup>I have neglected that A6V stars are expected to have fully radiative-transfer interiors once they reach the main sequence, and M4.0V stars are expected to have fully convective-transfer interiors. The mechanisms producing magnetic activity and X-ray flux in *BOTH* these stars are currently a subject of debate among theorists.

cator is that there exists all-sky X-ray photometry, in the form of the ROSAT All-Sky Bright Source (Voges et al. 1999) and All-Sky Faint Source (Voges et al. 2000) catalogs; these catalogs are being supplemented with the GALEX NUV/FUV survey (Findeisen & Hillenbrand 2010). GALEX should be particularly useful, as its detectors are far more sensitive than ROSAT’s detectors were, even though they sample the UV part of the spectrum.

### 1.4.3 *A giant mess*

Unfortunately, the picture of nearby stellar associations is a mess. Many associations have been proposed, only to be rejected by others- Cha-Near (Zuckerman et al. 2006), Hercules-Lyra (Wichmann et al. 2003), Carina-Vela (Makarov & Urban 2000), and all of Eggen’s superclusters have all been disputed, redistributed amongst other groups, or found to be indistinct collections by other researchers.

Still other associations have been named that may not be distinct objects – Torres et al. (2008) partially combines Tucana-Horologium, Columba, and Carina into a “Great Austral Young Association” of 30 Myr old stars with semi-overlapping spatial positions they suspect may be similar, even though each group has unique UVW velocities. It is possible that these three groups are only separate because of an artifact of the iterative convergence method used by Torres, where no strong candidates in intermediate UVW velocities resulted in three areas of a single vast cloud to appear to be distinct populations.

Then there are the associations tentatively paired with clusters- AB Dor with the Pleiades, Argus with IC 2391, and the  $\epsilon$  Chameleon Cluster with the  $\eta$  Chameleon Association. With the exception of the  $\epsilon/\eta$  Cha stars, most of these clusters are apparently spread out across

hundreds of parsecs of space, which is hard to explain within the context of the typical dissolving spherical cluster model.

A specific link between the Argus association and IC 2391 provides an example. Argus is only the latest grouping presumed to be connected to IC 2391, but Torres et al. (2008) emphatically deny that any relation exists between Argus and Eggen's IC 2391 Supercluster or Makarov's Carina-Vela association; in both cases most of the stars in those supposed associations don't make Torres' Argus cut, and the ensemble kinematics are different in value and dispersion. Argus itself is composed of members with unique and overlapping kinematics and the same age ( $\sim 40$  Myr), but with members spread everywhere from the core of IC 2391 (140 pc away) to 8 pc distant (AP Col, Riedel et al. 2011), though their derived Galactic kinematics for the newest Argus candidate, AP Col, do *not* trace back to anything close to the same point in space 40 Myr ago. It may be possible that Argus was a filament of gas set off by the same impulse that formed stars in IC 2391, but it may also be that they are unrelated events, occurring at the same time from different clouds that shared the same motion- which is not, strictly speaking, impossible considering all nearby stars are coming from Sco-Cen.

Complicating this picture are resonances, an alternate way to force stars into groups. Resonances were noticed perhaps as early as Asiain et al. (1999), who attempted to break down Olin Eggen's Local Association into subgroups (of which the Pleiades were only one) using higher-precision kinematic data than Eggen had at his disposal. Famaey et al. (2005) found that Eggen's Hyades supercluster or stream was not a real entity, but likely the result

of a dynamical resonance with the Galactic bar. As for the Pleiades, [Asiain et al. \(1999\)](#), investigating components of the kinematic space of nearby stars (the “Local Association” conglomerate), noted four distinct subgroups of comoving stars in UVW space centered around the Pleiades, only one of which was similar in age. The rest of the moving groups (except Asiain’s B4, which is closest to the UVW velocities of the AB Dor association, though that may be spurious) were deemed somewhat older, with kinematics suggesting they’d emerged from a spiral arm a few Myr ago, and just happened to have similar kinematics.

The only way to link truly kindred stars may be detailed chemical analysis, such as that done by [Castro et al. \(1999\)](#), where the stars of the Ursa Major moving group were found to have distinctively unusual barium and copper abundances. [Barenfeld et al. \(2012\)](#) have found evidence that at least some of the AB Dor association is not chemically homogeneous, though they did not give any details. This implies that while the Pleiades and Hyades are most certainly real (the product of gas that collected at that resonance), AB Dor and the Hyades Stream may be collections of many generations of stars.

In my dissertation I am thus interested in finding and confirming low proper motion stars. To find the stars, confirm their proximity, and determine whether or not they are young is thus a multi-step process, which requires a number of observational and data-analysis techniques, which I will explore next.

## CHAPTER 2

### TECHNIQUES

#### 2.1 Astrometry

Measuring the positions of the stars, astrometry, is one of the most fundamental fields of astronomy. The earliest endeavors of astronomical research (after predictions of planetary orbits and solar eclipses) were the creation of vast stellar catalogs. For most purposes astrometry is a solved science – all the theoretical underpinnings were worked out centuries ago. Thanks to the *HIPPARCOS* catalog, the Two Micron All Sky Survey (2MASS), and the efforts of USNO with its stellar catalogs, stellar positions as accurate as  $0.1'' \text{ yr}^{-1}$  are commonplace, but they still leave vast areas where further astrometric information is needed.

The time-dependent positions of stars on the sky are the result of several effects that astrometric measurements must include. Stars have orbital motion around the center of the Galaxy that manifests itself as proper motion (and in some rare cases, secular acceleration) across the sky. Stars also have annual parallactic motion as a response to the Earth's orbit around the Sun. If they are in multiple systems, they have orbital motion around the system barycenter. These motions are all linked together, and understanding any of them effectively requires understanding all of them.

##### *2.1.1 The Theory Behind (Annual) Trigonometric Parallaxes*

The primary purpose of astrometry for my research thus far has been the technique of trigonometric parallax, the geometric effect that allows us to measure distances to stars,

and allows us to research scientific questions about the structure of the Galaxy and stars themselves. Trigonometric parallax is, short of radar ranging (which is obviously impractical at large distances), the most accurate method of determining the distances to objects in space, as it relies entirely on geometry.

Simply put, trigonometric parallax exploits perspective-shifting effects of living in a three-dimensional Universe. As the Earth traces out its 1 AU radius orbit around the Sun, stars in the Galaxy will seem to trace out 1 AU radius ellipses in response, shaped and diminished by where they are relative to the Earth's orbit. The sizes of those ellipses are inversely proportional to their distances. We know the shape of the Earth's orbit and the Earth's position at any given time (from the high precision JPL DE405 Solar System ephemeris), and we know the position of the star in the sky (and thus the foreshortened shape of the ellipse it will trace out), which leaves only the size of the ellipse as the unknown. The size of that tiny ellipse provides the small angle ( $\pi$ , or occasionally  $\varpi$ ) at the tip of an isosceles triangle with the (known) diameter of the Earth's orbit as the base (Figure 2.1), and the height of the triangle is then the distance to the star. Published parallaxes are usually given in units of milliarcseconds or arcseconds, convertible to distance (in parsecs, or parallax-seconds) by  $\frac{1}{\tan(\pi)}$ , which given the small angles involved is indistinguishable from  $\frac{1}{\pi}$ . These measurements are occasionally called "annual", given that it relies upon the annual motion of the Earth, to distinguish between, say, the simultaneous stereoscopic parallax of our eyes, or other less common trigonometric methods like pulsar timing parallaxes (Sandhu et al. 1997) and orbital parallaxes (Torres et al. 1997).

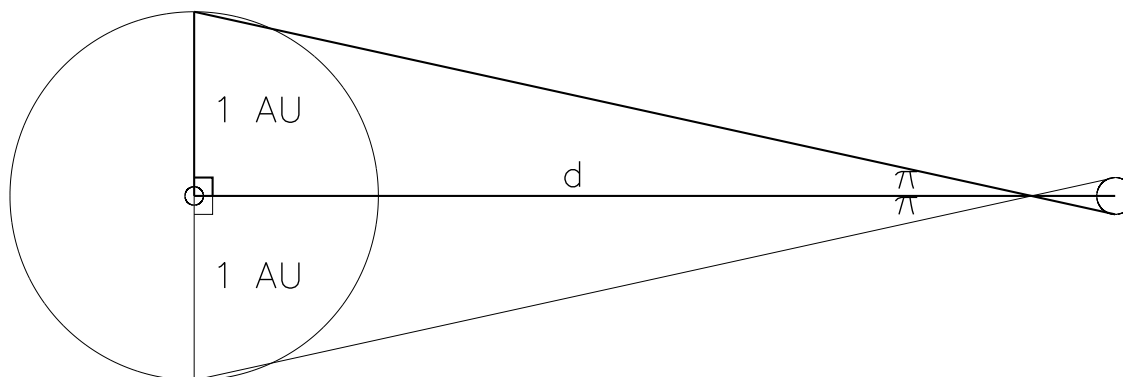


Figure 2.1: Annual Parallax: Given a measurement of the angle  $\pi$  (which is equivalently half the angular width of the parallax ellipse), the distance  $d$  to the star (in parsecs) is  $\frac{1}{\pi}$  where  $\pi$  is in arcseconds. The angular size of the ellipse in RA will always yield the true parallax; in DEC it will be foreshortened at lower ecliptic latitudes, equaling zero for a star on the ecliptic.

This basic principle was known to the ancient Greeks, at least as early as Aristarchus (Hirshfeld 2001), who correctly determined the distance to the Moon and the size of the Earth. Galileo himself attempted to see stellar parallax (Hirshfeld 2001), as this would have been yet another triumph for the Copernican and Keplerian model of the Universe. Unfortunately for Galileo, stars are extremely far away, so their parallax ellipses were far too small for his telescopes to resolve. It took almost two hundred years of technological and observational innovation before the first *successful* parallax observations were taken by Bessel and Henderson (as history records, Bessel published parallaxes to 61 Cygni A&B first in 1838, while Henderson did not publish his observations of  $\alpha$  Centauri A&B until 1839.)<sup>1</sup>

<sup>1</sup>In this way, the mantle of closest star system changed only once, from 61 Cygni to  $\alpha$  Centauri.

Measuring parallaxes is a complicated endeavor. The observed motions of stars also include their motion through space and (if multiple) orbital motion. There are also observational effects to be accounted for, such as differential color refraction – the Earth’s atmosphere acts like a prism, changing the positions of stars different amounts according to their colors and the bandpass of the waveband used, as well as the distances from zenith and azimuthal angles. Distortions within the telescope itself must be accounted for, or minimized – at least some of this can be circumvented by keeping the instrument exactly the same, although in practice that is impossible. If the astrometry is absolute (relative to some fixed time reference or celestial grid), corrections must be made for the aberration of starlight as the Earth orbits the Sun. If the astrometry is relative to other stars in the field of view, corrections must be made for the fact that the reference stars are not infinitely far away, and that their collective proper motion is not necessarily absolutely zero.

For a given star, the equations (called equations of condition) we attempt to fit are (excerpted from [Jao et al. 2005](#)):

$$X = A^n x_0 + B^n y_0 + C^n + x_0 + x_1 t + x_p(t)\pi \quad (2.1)$$

$$Y = D^n x_0 + E^n y_0 + F^n + y_0 + y_1 t + y_p(t)\pi \quad (2.2)$$

In this example,  $X$  and  $Y$  are the sky positions of a star as measured on an image, as a function of time.  $x_0$  and  $y_0$  are the measured positions of the star on a given image  $n$  (or plate, to keep the original nomenclature of the photographic plate days) taken at a known time  $t$ . The coefficients  $A$  to  $F$  account for the rotation, scaling and offset (assumed to be

telescope pointing errors) of each plate  $n$ , relative to one image picked in advance as the best (or ‘trail’ plate). Once those plate constants are applied to measurements of a set of stars, the measurements can be assumed to be free of all instrumental effects.

The proper motions are the first derivatives of position in the sky, and are represented by the free parameters  $x_1$  and  $y_1$ . They are unknowns to be solved for as a function of  $t$ . Finally, the last term deals with the parallax ellipse itself. The *shape* and *orientation* of the ellipse (represented as  $x_p$  and  $y_p$ ) are known based on the geometry of the Earth’s orbit and the position of the target star, and can be calculated beforehand as a function of  $t$ . The free parameter is  $\pi$ , the trigonometric parallax, which represents the *size* of the ellipse, solved such that  $\pi$  is the same value in both axes.

The CTIOPI pipeline, as designed by Wei-Chun Jao (Jao et al. 2005) solves these equations for every reference star and the target star simultaneously through means of an iterative least squares minimization (as recommended by van de Kamp 1981) of those equations in a matrix, with the heavy lifting carried out by the GAUSSFIT least-squares program (Jefferys et al. 1988). As there are three free parameters in each axis (e.g. the  $A$ ,  $B$ ,  $C$  plate constants, or the  $x_0 = RA, x_1 = \mu_{RA}, \pi$  motion variables) we need at least three reference stars to obtain a non-zero result for the target star, or  $\pi$  star.

These are not necessarily the only terms in the equation: Boss et al. (2009) uses additional coefficients for orbital motion (given various periods), Dittmann (private communication, 2012) used extra parameters to account for Differential Color Refraction terms; van de Kamp (1981) mentions secular acceleration (e.g.  $+x_2t^2$ ) measurable in the very near-

est stars (Proxima Cen, Barnard's Star) in addition to methods to fit an orbit; Jao et al. (2005) discusses the existence of higher order plate distortion parameters (for coma, piston, etc) and explains why CTIOPI ignores them<sup>2</sup>.

### ***2.1.2 Practical Astrometric Concerns***

The above process produces a parallax and proper motion, but the values are relative to the reference stars. Consider a field in a cluster like the Hyades: All the reference stars will probably be moving  $100 \text{ mas yr}^{-1}$  at  $110$  degrees – a net proper motion – but the mathematics of the plate solution will treat it as if it's the telescope's pointing drifting the other way,  $100 \text{ mas yr}^{-1}$  at  $290$  degrees. At the same time, all of the reference stars will trace out little ellipses of roughly  $25 \text{ mas}$ , every year; again, the plate solution will assume it's the telescope's pointing making a small counter-ellipse. If your target object were *ALSO* in the Hyades, the net parallax would most likely be  $0 \text{ mas}$  (the ellipse is no larger than that of the reference stars) and its proper motion would be  $0 \text{ mas yr}^{-1}$  (the proper motion is no larger than that of the reference stars). If the star were NOT in the Hyades (say, Aldebaran), its measured parallax would be  $25 \text{ mas}$  smaller than it should really be, and its proper motion should have an unnecessary  $100 \text{ mas yr}^{-1}$  motion at  $290$  degrees added into it. Hence, there is a correction-to-absolute term required to derive the correct  $\mu$  and  $\pi$ .

The correction takes the form of an estimate of the parallax of the reference field, which is added to the measured relative parallax – in this way, the absolute *distance* is always smaller than the measured distance. In this effort, we find photometric distances (§2.2.5) to each of

---

<sup>2</sup>Results were sufficiently accurate without them.

the reference stars used in the astrometric solution based on its measured  $VRI$  colors, and the assumption that it is a dwarf. The average of the distances of all the reference stars is taken as the mean distance to the reference field, which (converted to a parallax) is the correction from relative parallax to absolute parallax<sup>3</sup>. Corrections are on average around 1.5 mas, or 666 pc. Anomalously large corrections (nearby reference fields) are generally due to a giant among the reference stars, whose photometric distance estimate is erroneously nearby, or (in the case of a large number of stars estimated to be nearby) the field is often artificially reddened by some intervening cloud (the Galactic reddening curve is less steep than the main sequence in the M dwarf area, producing stars that are anomalously bright for their reddened colors). If the  $VRI$ -calculated average correction is over 3 mas, we use a default value of  $1.5 \pm 0.5$  mas for the correction.

We do not correct the proper motions to absolute, as the proper motions of stars at those distances are quite small. Most corrections to absolute proper motion are on the order of milliarcseconds (Luyten 1988; Lépine et al. 2005). The only check on the size of the net reference field proper motion is that we usually remove reference stars whose parallaxes are greater than 5 mas (within 200 pc), which would tend to have the highest proper motions.

---

<sup>3</sup>Other widely accepted methods include spectrophotometric distances to all of the reference stars (Benedict et al. 1999) – which require time-consuming spectroscopic observations, and using a model of the Galaxy to predict the average distance to stars of the appropriate magnitude range along that  $(l, b)$  line of sight (van Altena et al. 1995; Dupuy & Liu 2012) – which is not a good fit for CTIOPI where reference stars are chosen by hand, rather than randomly. The corrections produced by various methods are all generally similar.

### 2.1.3 CTIOPI observing

My involvement in this process has mostly been as an observer and user of a functional pipeline. CTIOPI (the Cerro Tololo Inter-american Observatory Parallax Investigation) started in 1999 as an NOAO Surveys program, and since 2003 has been under the auspices of the SMARTS Consortium. Originally, it consisted of two parallax programs, one on the CTIO 1.5m and one on the CTIO 0.9m, but the 1.5m program (Costa et al. 2005, 2006) was shut down in 2003.

CTIOPI observing takes place over (usually) whole weeks of time on the CTIO 0.9m Boller & Chivens Cassegrain reflector, with its dedicated Tek 2048 #3 CCD. Within that week, we observe (ideally) around 140 parallax targets. The rough rule of thumb is that a parallax target is to be observed five times (or for 30 total minutes of observing time, whichever is less) in a particular filter. Filters, out of CTIO's #2 Tektronix *VRI* filter set, are selected to maximize the number of available bright and spatially nearby reference stars – a star might be brightest in *V*, but if the *R* or *I* filter yields more reference stars of suitable brightness, we use that filter. Our centroids on stars, and consequently our astrometric solutions, improve with longer exposure times up to several minutes as the atmospheric distortions blur to randomness. Thus, bright red stars are often observed in *V* where the exposures take longer. Faint stars are often observed in *I* so the star is sufficiently well-exposed in 10 minutes, our adopted maximum for a single exposure.

The observations that are most important for high quality parallaxes are at the ends of the RA extensions of the parallax ellipse – found when the star transits at dawn or dusk.

Thus, the first and last hour of any given night will contain the most important observations<sup>4</sup>. RECONS nevertheless observes stars whenever they are visible, as it improves our ability to see astrometric perturbations caused by (typically) unseen companions. For proper motions, timespan is the critical factor: the longer the spread between first and last epochs, the more well-determined the proper motion is – hence the importance of the plates from the circa-1900 Astrographic Catalog (Urban et al. 1998) to modern (e.g. TYCHO-2) audiences. RECONS typically requires at least 2 years of observations and at least 30 frames in the morning and evening halves of the eclipse before publishing (with the hope that at least 20 of each are used in the final reduction), and is reaching 13 years of coverage for some long-term targets (e.g. GJ 1207).

Because RECONS uses wide-band *VRI* filters, the effective centers of the bandpasses are very different for an M star and an A star. These differences lead to Differential Color Refraction (DCR) effects, which affect the positions of stars in images, and must be corrected. To minimize DCR corrections, RECONS only observes stars as they transit the meridian – their minimum zenith distance, plus or minus 2 hours ( $\pm 30$  minutes is preferred)<sup>5</sup>. These restrictions are not always helpful, as stars at  $+30$  DEC (the northern limit) or  $-90$  DEC will always have zenith distances of at least 60 degrees. RECONS has been coordinating the CTIO 0.9m for SMARTS since 2003, which has left us in a position to maintain the optical path by changing the telescope, filters and camera as little as possible<sup>6</sup>. This minimizes

---

<sup>4</sup>For a star near an ecliptic pole, midnight is just as important, as the DEC extension of the parallax ellipse is quite large.

<sup>5</sup>Another method to reduce DCR corrections is to use filters with narrower bandpasses, but they would also require longer integration times.

<sup>6</sup>The commitment to keeping the optical path the same, as well as the exceptional stabil-

other optical distortion effects (or at least keeps them consistent).

The selection of reference stars is a key element in measuring an accurate parallax. Good reference stars are bright in the chosen filter, close in angular separation to the target, and as a group surround it on all sides. In many cases CTIOPI does not center the target in the field to bring in other reference stars that more fully surround the target. Parallax reductions use between 5 and 12 reference stars. RECONS arrived at this concept by informal experimentation, but is more formally known and mathematically defined as the geometric multiplier, and as “dependencies” (van de Kamp 1981). In practice, we must use the reference stars available, and they often fall short of the ideal.

Trigonometric parallaxes currently have limited reach. *HIPPARCOS*, with a typical 0.7 mas error, is only accurate to 10% within 150 pc. CTIOPI is typically only that accurate out to 66 pc; we usually drop stars with preliminary parallaxes beyond 100 pc. (The most accurate measurements are from long-baseline radio interferometers with sub-milliarcsecond parallaxes; no long-baseline optical interferometers currently do parallax work.) Aside from these concerns, the time required (12 visits of 30 minutes each spread out over at least two years) makes obtaining large numbers of parallaxes difficult. *HIPPARCOS*, with nearly 120,000 stars including *all* stars brighter than  $V=7.3$ , obtained parallaxes to 14 times more systems than all ground-based observatories before it combined. The biggest change to come is ESA’s Gaia mission, a follow-up to *HIPPARCOS*, which promises to measure parallaxes

---

ity of the CTIO 0.9m (constructed 1965) and its CCD (in continuous use since at least 1994, [http://www.ctio.noao.edu/ccd\\_info/ccd\\_news.html#6](http://www.ctio.noao.edu/ccd_info/ccd_news.html#6) retrieved 15 MAY 2012) and the maintenance staff at CTIO, are in no small part responsible for our results being competitive with parallaxes from newer, more powerful instruments (Dupuy & Liu 2012; Faherty et al. 2012).

for  $10^7$  stars from  $V=6$  to  $V=20$  at the 10-100 microarcsecond level, which will extend the penetration of accurate (10%) parallaxes out to kiloparsec scales (Lindgren 2007).

#### 2.1.4 *Orbits*

The third major use of astrometry, apart from parallaxes and proper motions, is the determination of orbits. This takes two very different forms: the astrometric orbit, and the visual orbit.

Visual orbits are derived from resolved observations of the two stars, either from visual observations (including Speckle Interferometry, Lucky Imaging, Adaptive Optics), or short- and long-baseline interferometry. In these cases the observers record the actual separations and positions of both stars in two dimensions. Separations and position angles can either be recorded relative to other stars in the field of view (as with parallax) or simply relative to the primary component. The product of solving for the orbit (via the Thiele-Innes method) are the actual orbital elements of a system.

An astrometric perturbation describes the orbit of the photocenter about the barycenter, not the motion of any individual component. The amplitude  $\alpha$  of an astrometric binary orbit is dependent on a number of factors:

$$\alpha \propto M_2, M_1 + M_2, a, \frac{L_1}{L_2} \quad (2.3)$$

Astrometric perturbations are therefore greater for larger luminosity differences between the components ( $\frac{L_1}{L_2}$ ), larger companion masses ( $M_2$ ), larger system masses ( $M_1 + M_2$ ), and larger semi-major axes of the orbits ( $a$ ). Note that the photocenter of an equal-mass equal-

luminosity binary will not move at all. The signal of an astrometric binary is a multivariable problem, and it is thus difficult to describe the sensitivity limits of a given program.

The CTIOPI parallax reduction pipeline fits the astrometric positions of a star to a linear proper motion and a parallax ellipse of known shape and unknown size. Any further motion caused by the orbit of a companion remains, appearing as a perturbation in the astrometric residuals (Figures 5.1, 5.2, and 5.3). The product of solving for this kind of orbit is an orbit with a semimajor axis scaled down compared to the visual orbit, and flipped 180 degrees to the real one. In a visual orbit, the moving body is the secondary component relative to the fixed primary; in an astrometric orbit, the photocenter moves, and is on the primary star's side of the barycenter.

CTIOPI's companion detection capabilities are limited by several factors. Systems are typically observed 1–4 times a year and thus the data are insensitive to periods less than a year. The program has only been running since 1999, and cannot wrap orbits with periods longer than the period of observations. CTIOPI also has a 3–6 mas nightly precision error (depending on the specifics of the reference field) that limits our sensitivity to low-amplitude binaries. Fortunately, astrometric perturbations are typically self-confirming; genuine orbital motion will show up in both the RA and DEC axes unless the orbit is nearly north-south or east-west on the sky. Nevertheless, for the three astrometric binaries in Riedel et al. (2010) (see §5.2.2.2) we reduced the three brightest reference stars in each of our astrometric perturbation fields as if they were the parallax targets, to make sure the perturbation signal was not some unnoticed systematic of the field. Infrared AO observations (currently

unpublished) later resolved two of the astrometric binaries.

To solve astrometric orbits, RECONS uses an iterative Thiel-Innes least-squares solver (Hartkopf et al. 1989) to fit the astrometric orbit, with points from nights with only a single CCD image (generally obtained for the purpose of photometry) removed. As orbital motion can bias the parallax and proper motion fits (up to, hypothetically, a one-year orbit canceling out the parallax ellipse entirely), we calculate and subtract the fitted orbit from the initial positional data and re-fit the parallax (Riedel et al. 2010). This second reduction also demonstrates the potential accuracy of the fitted orbit: the residuals with the orbit removed should be flat, to within the signal-to-noise ratio of our astrometric data, 3-6 mas per night. As a general rule, the orbit-removed proper motion and parallax are not substantially different, but the errors are far smaller. Unfortunately, it appears that we do not yet understand our errors in terms of perturbations, and our fitted astrometric orbits do not quite reproduce published orbits. Investigations are ongoing.

Obtaining a full orbit from an astrometric one can be accomplished with a single observation: The instantaneous resolved separation  $p$  between the two components at a time  $t$  can be compared to the expected astrometric separation  $\rho$  between the photocenter and the barycenter at the same time  $t$ . The ratio between  $p$  and  $\rho$  is the same as between the real semimajor axis  $a$  and the photocentric semimajor axis  $\alpha$ .

The derivation of Thiel-Innes elements (the coefficients  $A$ ,  $B$ ,  $F$  and  $G$ ) is a method of relating conventional spherical coordinates for an orbit to measured (projected) Cartesian orbital data. The Thiel-Innes elements describe the positions of a binary star as a function

of time  $t$  relative to some epoch of periastron passage  $T_0$ , and  $dx$  and  $dy$  are the differences between the predicted  $X$  and  $Y$  positions and the actual measured positions.

$$dx = XdA + YdF + P_x de - Q_x dT + Q_x(t - T_0)dT \quad (2.4)$$

$$dy = XdB + YdG + P_y de - Q_y dT + Q_y(t - T_0)dT \quad (2.5)$$

Minimizing  $dx$  and  $dy$  is an iterative process solved by recalculating several differential equations:

$$P_x = A \frac{dX}{de} + F \frac{dY}{de} \quad (2.6)$$

$$P_y = B \frac{dX}{de} + G \frac{dY}{de} \quad (2.7)$$

$$Q_x = A \frac{dX}{dM} + F \frac{dY}{dM} \quad (2.8)$$

$$Q_y = B \frac{dX}{dM} + G \frac{dY}{dM} \quad (2.9)$$

which can themselves be calculated from the “normal equations”:

$$\frac{dX}{de} = -1 - \left[ \frac{\sin^2 E}{1 - e \cos E} \right] \quad (2.10)$$

$$\frac{dY}{de} = \frac{X \sin E}{\sqrt{1 - e^2}(1 - e \cos E)} \quad (2.11)$$

$$\frac{dX}{dM} = \frac{-\sin E}{57.296(1 - e \cos E)} \quad (2.12)$$

$$\frac{dY}{dM} = \frac{\sqrt{1 - e^2} \cos E}{57.296(1 - e \cos E)} \quad (2.13)$$

where  $e$  is the orbital eccentricity,  $E$  is the eccentric anomaly calculable (iteratively) from

$$\frac{360}{P} \times (t - T_0) = E - e \sin E \quad (2.14)$$

where  $P$  is the period,  $T_0$  is the time of periastron passage, and  $t$  is the variety of times at which data are available.

At each step,  $dx$  and  $dy$  are calculated as the difference between the real orbit and a calculated orbit ( $X, Y$ ). The  $X$  ( $dA$ ,  $dF$  and  $de$ ) and  $Y$  ( $dB$ ,  $dG$ , and  $de$ ) unknowns are solved for in matrix form. Those values are added to  $A$ ,  $B$ ,  $F$ ,  $G$ , and  $e$  to produce the next step's values, which are then used to come up with new differential equations. Eventually, the answers converge on values of  $A$ ,  $B$ ,  $F$ ,  $G$  and  $e$ , which are then turned into the seven orbital elements:  $a$ ,  $i$ ,  $\omega$ ,  $\Omega$ ,  $e$ , period  $P$  (original) and  $T_0$  (original). This basic method has a constant  $P$  and  $T_0$  throughout all the operations, which is why more advanced orbital solvers sample a range of  $T_0$  and  $P$ .

### ***2.1.5 Using Astrometry***

#### *2.1.5.1 Parallax Catalogs*

The **Yale Parallax Catalog** (YPC, or more formally, the General Catalog of Trigonometric Parallaxes) is, in its fourth edition (van Altena et al. 1995), a compilation of 15994 parallax measurements for 8112 stars from various observatories, representing ground-based parallax efforts published prior to November 1995 for stars as faint as  $V = 21.5$ . YPC contains essentially every useful parallax published by a ground-based observatory (the earliest reference is actually 1900; presumably the parallaxes from the prior 60 years were of such poor/uncertain

quality that the compendium loses no accuracy), painstakingly re-weighted and corrected for systematic biases in the data, given new corrections to absolute, and combined into just over 8000 systems. YPC is often forgotten or overlooked now that the *HIPPARCOS* available, but it does contain nearly 2300 stars not observed by *HIPPARCOS* (van Altena et al. 1995). Most of those 2300 stars – like Wolf 359=GJ 406, the third closest system to us – are very nearby.

The parallaxes have a broad range of errors, but most are between 2 and 20 milliarcseconds (mas), with the average (4 mas) (van Altena et al. 1995) a distinct improvement over previous editions, made possible by the flood of new milliarcsecond-precision parallaxes from the final generation of photographic plates, and CCDs. YPC's proper motions were a somewhat lesser concern, and are of generally dubious quality, occasionally missing, and quoted without errors; they appear to not have been corrected to any particular epoch. The positions, too, are sometimes erroneous (though effort was made to bring them to epoch 1900 equinox B1900, to match the earlier editions of YPC); this is understandable given the massively heterogeneous dataset they tried to homogenize.

**HIPPARCOS** is the current gold standard for parallaxes<sup>7</sup>. Its latest reduction (van Leeuwen 2007) contains 117955 stellar parallaxes, generally with errors less than 1 mas for stars brighter than  $V = 9$ , a 14-fold increase over YPC. The faint magnitude limit of *HIPPARCOS* was  $V \sim 13$ , with a completeness limit of  $V \sim 7.3$  (Perryman et al. 1997). The *HIPPARCOS* satellite (in orbit 1989-1993) had two instruments: a photomultiplier tube pointing at a wire

---

<sup>7</sup>Notwithstanding its problem with the Pleiades (Soderblom et al. 2005), which may extend to *any* small region with correlated proper motions and parallaxes (Platais et al. 2011).

grid of known fixed spacing (the *HIPPARCOS* astrometer) and another instrument with a beamsplitter and two photomultiplier tubes (the *TYCHO* photometer). As the spacecraft spun, the astrometer measured precise timings and photometry as the pre-selected list of parallax targets appeared and disappeared behind the wire grid. Those timings, when combined with a precise model of the spacecraft orbit and orientation (down to micrometeorite impacts and passages through the South Atlantic Anomaly), were converted to absolute grid-reference positions; the resulting data were processed into absolute positions, proper motions, and parallaxes. The 1997 results were adopted as the visible-band realization of the International Coordinate Reference System (ICRS, almost identical to J2000, but linked to quasars and much more precise).

Despite a problem with the launching rocket that left the satellite in an unplanned orbit, *HIPPARCOS* greatly exceeded its general goal of 2 mas parallax average accuracy. The initial reductions published in 1997 took four years after end-of-mission to produce, and were the result of two independent reductions of the data from two consortia – FAST and NDAC. The factor-of-two improvements in the global re-reduction done single-handedly(?) by van Leeuwen (2007) (formerly of NDAC) were largely due to an improved model of the spacecraft's orbit and orientation, and ten years of improvements in computational power<sup>8</sup>.

---

<sup>8</sup>History has probably already forgotten that the catalog now on VizieR is significantly improved from the one in the 2007 book, and from the catalog initially uploaded to VizieR in 2008; reprocessing all the astrometry in 2008 took only a few months.

### 2.1.5.2 Proper Motion catalogs

There are also several important sources of proper motions, though not parallaxes. Here we describe a few catalogs important to this thesis.

The largest consideration of a proper motion catalog, apart from its accuracy, is whether or not it contains absolute proper motions. Absolute proper motions are relative to a fixed grid (usually ICRS) and are therefore accurate even when applied to stars in clusters or moving groups. The difference between relative and absolute is usually small – Lépine & Shara (2005) found the corrections to be around 10 mas, Luyten found a similar range and set his proper motion limit to  $0.18'' \text{ yr}^{-1}$  to make certain he could reach all stars with proper motions greater than  $0.2'' \text{ yr}^{-1}$  (Luyten 1988).

**TYCHO-2** (Høg et al. 2000) is the product of the other instrument on board *HIP-PARCOS*. TYCHO was nominally responsible for maintaining pointing accuracy, but also continually recorded photometry as it swept around the sky. That dataset was itself stitched into a global astrometric solution (on the same absolute ICRS reference system as the *HIP-PARCOS* catalog) of all stars brighter than  $V=12$  in two-color photometry ( $B_{TYCHO}V_{TYCHO}$ ; conversions to Johnson  $BV$  exist (Perryman et al. 1997; Bessell 2000)). The initial catalog, TYCHO-1 (Perryman et al. 1997), also contained positions, proper motions, and parallaxes for 1 million stars, but the parallaxes turned out to be rather poor quality (worse quality than YPC, with enormous systematics past 20 pc). Ultimately, the TYCHO data were co-added to produce positions, proper motions and accurate two-color photometry for 2.5 million stars brighter than  $V \approx 12$ . TYCHO-2 is considered another fundamental proper motion and po-

sitional source, and is often used by other compiled catalogs to put their astrometry on the ICRS absolute reference frame.

The **SuperCOSMOS Sky Survey** (Hambly et al. 2001a) is built from scans (from the SuperCOSMOS plate scanning machine) of Palomar Observatory Sky Survey (POSS) and Science and Engineering Research Council (SERC) sky survey plates. The survey covers the entire sky at four different epochs, deriving positions, proper motions, and (up to) four-color photometry for 1.9 billion stars. The plates were aligned by cross-matching stars out to distances of 6'' (in a spiral search pattern) between two plates – this actually provides an *upper* limit on measurable proper motions at around 0.2-0.3'' yr<sup>-1</sup> in the southern hemisphere where the epoch spreads are large; higher proper motion stars will be identified as multiple transient objects. Nigel Hambly has additional software to search for high proper motion stars within the catalog by matching transient objects. Hambly and the RECONS team have worked together to search the southern sky for proper motion stars in a series of seven papers (Hambly et al. 2004; Henry et al. 2004; Subasavage et al. 2005a,b; Finch et al. 2007; Boyd et al. 2011a,b) Other proper motion surveys using the SuperCOSMOS Database (and their own special software) include the Liverpool-Edinburgh High Proper Motion Survey (Pokorny et al. 2003), the Southern Infrared Proper Motion Survey (Deacon et al. 2005a), and Scholz & Meusinger (2002) (and subsequent).

SuperCOSMOS magnitude limits vary by field but are generally equivalent to  $B=22$ ,  $R=20$ ,  $I=19$ . 2MASS  $JHK_s$  photometry has been cross-matched to sources where available. SuperCOSMOS is *not* a source of absolute positions or proper motions, though attempts were

made to force the mean Galaxy proper motions (field by field) to zero, on fields where galaxies were available (Hambly et al. 2001c). The overall reference frame was shifted to ICRS via cross-matching with 2MASS (which is linked to TYCHO-2).

**USNO-B1** (Monet et al. 2003) uses the same plates as SuperCOSMOS with a few additional plate catalogs. Its design focused on proper motion detection and contains proper motions for *every* object possibly found on at least two plates (inclusively, thus including many spurious and duplicate entries). It contains 1 billion sources and has magnitude limits roughly similar to SuperCOSMOS. Its proper motions and positions are *not* absolute.

**PPMXL** (Roeser et al. 2010) is an attempt to put USNO-B1 on the ICRS absolute reference frame using 2MASS astrometry and the earlier PPMX catalog (which itself includes TYCHO-2, and the even earlier PPM catalog). It contains 0.9 billion sources down to the same magnitudes as USNO-B1, and also includes 2MASS photometry. Anecdotally, I have found that the PPMXL catalog contains more high proper motion stars ( $\mu > 0.5'' \text{ yr}^{-1}$ ) than any of the USNO catalogs (most of those thanks to the inclusion of earlier PPM series catalogs).

**UCAC3** (Zacharias et al. 2010) (the USNO Compiled Astrographic Catalog) primarily relies on a new CCD-based all-sky survey conducted by USNO, but its proper motions are constructed from a multitude of scanned photographic plates from different telescopes and eras, including (to the detriment of the astrometric consistency) SuperCOSMOS positional data. UCAC3 contains 1 billion sources down to 16th magnitude, and has absolute proper motions for most of them, down to  $1 \text{ mas yr}^{-1}$  accuracy, on the ICRS reference frame.

UCAC4 is expected to be released in 2012 and have a fully consistent astrometric solution better than UCAC2 or UCAC3.

The **Two Micron All-Sky Survey (2MASS)** (Cutri et al. 2003) is not a proper motion catalog at all, but I include it here as an astrometric reference because RECONS (among many other red dwarf research teams) uses it for ICRS positions (accurate to  $\sim 120$  mas, though usually 60 mas) taken between 1998-2003, and thus very close to the J2000 epoch. 2MASS is more famously the current gold-standard source of near-infrared  $JHK_s$  magnitudes, with limits of  $J=15.8$ ,  $H=15.1$ ,  $K_s=14.3$ , (Skrutskie et al. 2006), supplanting nearly all previous infrared photometric systems. 2MASS most likely contains every nearby star save a few of the hotter white dwarfs; it does not suffer from the confusion issues the UCAC and PPM catalogs have with high proper motion stars (though it does occasionally report multiple sets of  $JHK_s$  for high proper motion stars).

### 2.1.5.3 Accounting for proper motion

When your input catalog does not take into account proper motion, or you need it for a specific epoch (J2000, or today) it is necessary to slide your star forwards or backwards in time to put it at the proper location:

$$RA_{new} = RA_{old} + \left( \mu_{RA} \times (epoch_{desired} - epoch_{known}) / 3600 \times \frac{1}{\cos(DEC_{old})} \right) \quad (2.15)$$

$$DEC_{new} = DEC_{old} + (\mu_{DEC} \times (epoch_{desired} - epoch_{known}) / 3600) \quad (2.16)$$

Where *epoch* is in years,  $\mu$  is in arcsec yr<sup>-1</sup>, and the RA and DEC are in decimal degrees. This is distinct from precession of equinoxes, which amounts to uniformly rotating the entire coordinate system.

#### 2.1.5.4 Multiple Stars

One issue that often comes up with parallaxes is multiple measurements. Historically, a variety of methods have been used to deal with this:

**Assign one value as the best, and adopt it.**

**Average the parallaxes.** One example of this is the methodology of the Catalog of Nearby Stars in [Gliese & Jahreiß \(1979\)](#), who combined their reported parallaxes with a slightly uneven average of Lick and Yale parallax results, based on information from the Yale Parallax Catalog. The original *HIPPARCOS* processing was split between two consortia, FAST and NDAC. The eventual published solutions usually averaged the FAST and NDAC results.

**Combine parallaxes into a weighted mean by their errors.** This is the method used by RECONS. The equation for combining parallaxes is a standard weighted average and weighted standard deviation:

$$\pi_{mean} = \frac{\sum_i^n \frac{\pi_i}{\sigma_{\pi_i}^2}}{\sum_i^n \frac{1}{\sigma_{\pi_i}^2}}, \sigma_{\pi_{mean}} = \frac{1}{\sqrt{\sum_i^n \frac{1}{\sigma_{\pi_i}^2}}} \quad (2.17)$$

where  $\pi_i$  is the parallax of star  $i$ , and  $\sigma_{\pi_i}$  is the error on that parallax.

This formula does not take into account any discrepancy between the reported values – parallaxes of  $62 \pm 5$  mas and  $58 \pm 5$  mas will yield the same mean parallax and errors as two

measurements of  $60 \pm 5$  mas. This is valid under the assumption that both measurements were of the exact same true value, and the errors are accurately determined. The formula also assumes the parallax measurements are completely independent of each other. Nevertheless, the formula is widely used to combine measurements of binary components from the same astrometric solution, despite the fact that they have most likely been determined using the same reference stars on the same images taken with the same telescope setup.

#### 2.1.5.5 Parallax Errors and Biases

The discussion of how parallax zero points and systematic offsets were determined (per observatory, per apparent magnitude, occasionally as a function of reported error, and often broken by time period) occupies no fewer than 13 pages of the printed YPC book.

Usually, the systematics were determined by the “observatory pair” method, wherein stars published by two or more sources were compared to each other (or the mean) to chart systematic differences between the two. Within YPC, the systematics were often substantial fractions of the measured parallax – systematic errors of tens of milliarcseconds, on parallaxes that were themselves in the tens of milliarcseconds – which made them basically useless without YPC’s corrections. Jao et al. (2005) compared CTIOPI data to *HIPPARCOS* and YPC values, and determined, based on the available sample, that there was no systematic bias in our reported parallaxes and that our errors were reasonable: out of 7 calibration stars, all were within  $2\sigma$  of all other reported observations (the only error larger than  $1\sigma$  was a comparison of our Proxima value to the HST parallax of Benedict et al. 1999).

Another method of determining accuracy is the “Hertzsprung” method, whereby the size

of the negative tail (stars with negative parallaxes are assumed to be zero minus some error) is used to determine whether the error measurements are accurate. This was done by *HIPPARCOS* (van Leeuwen 2007) and taken as proof that the new errors were in fact correct. The problem with the Hertzprung method is that most parallax programs (including CTIOPI) have a.) no interest in measuring zero parallaxes, and drop such stars whenever they are encountered, and b.) intentionally avoid observing stars that might be too distant to measure. Some authors (Pourbaix & Jorissen 2000) have even based their calculations around  $\log(\pi)$  rather than  $\pi$ , so the resulting parallax cannot be negative. CTIOPI's master observing list has only five stars with negative parallaxes, all which were dropped shortly after the negative parallax was measured. They are therefore not representative of our final results, nor numerous enough to obtain useful statistics.

Beyond the accuracy of parallaxes, it is important to realize what they actually tell us. Considering that distances are calculated in a  $1/\pi$  sense, the errors are asymmetric:  $50 \pm 5$  mas corresponds to  $20 \begin{smallmatrix} +2.22 \\ -1.82 \end{smallmatrix}$  pc (although it is usually calculated as  $\frac{\sigma_\pi}{\pi} \times \frac{1}{\pi}$ , i.e.,  $\pm 2$  pc). This distinction becomes important in extreme cases, such as  $6 \pm 5$  mas. The error is not  $167 \pm 139$  pc; rather, it implies the actual position of the star is anywhere between 91 pc and 1000 pc (and in both cases consistent, to  $1.2\sigma$ , with infinite distance/zero parallax).

A less obvious effect is the Lutz-Kelker bias (Lutz & Kelker 1973) which states, simply, that within a sample of stars the reported parallaxes will be systematically too close because of volume concerns. Consider a parallax-derived distance of  $50 \pm 5$  mas (10% error): the volume exterior (between 20 and 22.22 pc) is larger than the volume interior (between

18.18 and 20 pc) by a ratio of  $\frac{(22.22-20)^3}{(20-18.18)^3} = 1.81$ . Accordingly, in a large sample of stars with measured distances of  $50 \pm 5$  mas, the average true distance will be greater than 20 pc. As Lutz and Kelker point out, the effect is highly dependent on the precision of the measurement, and somewhere between 15 and 20% parallax error, the distribution of actual distances becomes essentially indeterminate. The RECONS 25 pc database (§3.2) includes members of the solar neighborhood with  $\pi$  as small as 40 mas and errors as large as 10 mas. Thus, errors of up to 25% are possible, though the majority of systems have errors less than 4 mas (10%).

A related problem discussed in Lutz & Kelker (1973) is that setting a hard parallax lower limit to a sample (say, 40 mas=25 pc) while simultaneously ignoring parallax errors will suffer a lack of statistically relevant members. Members whose true distances put them within the sample but were measured to be too far ( $\pi$  too small) will be excluded; while a star with a larger true distance that was measured to be too close ( $\pi$  too large) will be included. Taking the Lutz-Kelker effect into account, the bias is slightly in favor of erroneous inclusion – more stars with measured  $\pi=40$  mas are actually *outside* 25 pc than inside.

## 2.2 Photometry

### 2.2.1 How we obtain photometry

Photometry is a broad-band way of determining the properties of stars by their brightnesses through several color filters. It is the first and easiest method of determining the properties of stars – one can simply look at Betelgeuse and see it is redder than Rigel – and remains

one of the most fruitful observational techniques.

RECONS regularly uses many sources of photometry. For its all-sky availability, we use SuperCOSMOS  $B_J R_1 R_2 I$  magnitudes from Hambly et al. (2001a)<sup>9</sup>. These are based on a global calibration of multiple plate sources, and are far less accurate than dedicated CCD photometry. Nevertheless, they are a readily-available all-sky source of information that requires no investment of observing time. We also routinely utilize near-infrared  $JHK_s$  photometry from 2MASS (Skrutskie et al. 2006) which is different from every other  $JHK$  system ever devised, but given the all-sky coverage of 2MASS, is now the standard.

Mostly to tap into the large body of historical work using the system, RECONS uses the Johnson-Kron-Cousins<sup>10</sup> filter system<sup>11</sup>. CTIOPI uses a rather rigorous program of standard star observations (standard stars selected from Landolt (1992) starfields) to place our stars on the  $V_J R_{KC} I_{KC}$  photometric system<sup>12</sup>. Photometry is carried out with the same instrumental setup (and during the same observing runs) as our astrometry program, but photometry is

---

<sup>9</sup>From the second reduction of the SuperCOSMOS Sky Survey, available at <http://surveys.roe.ac.uk/ssa/>

<sup>10</sup>This is the standard  $VRI$  system, usually called “Johnson-Cousins” (as preferred by Bessell, private communication 2012). We include Kron at the request of Arlo Landolt (private communication 2009); from both his summary and my reading the situation is this: Kron (Kron et al. 1957) developed an  $RI$  system of his own using different, more reliable filters than Johnson et al. (1966) used, but didn’t set his magnitude scale so that the colors of an A0V star were 0 (Cousins 1980). Cousins took Kron’s more reliable filters and came up with a different set of magnitudes and standard stars (called Cape-Kron, and later “KC” (Kron-Cape) in Cousins (1980), but eventually just Cousins) more like Johnson’s, which everyone eventually (circa 2000) gravitated to.

<sup>11</sup>Actually, the Johnson-Kron-Cousins system we use with the CTIO 0.9m, the Tek 2K CCD, and its Tek #2  $UBVRI$  filters is linked to (and defined by) Landolt (1992) standard starfields and Bessell (1990b)’s definition of the Johnson-Kron-Cousins  $UBVRI$  passbands, not the original standards of Johnson et al. (1966) or even Cousins (1980). Of course, we also occasionally use SCR 1845-6357 as a red standard, which technically makes our system different from everyone else’s, but it meshes well enough with Bessell (1990a) data that we are confident calling it Johnson-Kron-Cousins. The truly paranoid photometrist unconvinced by these minor changes will likely have to cart specific pieces of glass from telescope to telescope because every single one is different. Presumably, (s)he should also carry her/his own camera along, because each CCD has its own wavelength-dependent quantum-efficiency, and (like astrometrists) stick to one telescope, etc... but therein madness lies.

<sup>12</sup>The central wavelengths for  $V_J$ ,  $R_{KC}$ , and  $I_{KC}$  are 5475, 6425, and 8075 Å, respectively.

only attempted on photometric nights.

### 2.2.2 Luminosities and Colors

Luminosities and colors are particularly important for this dissertation because a large number of my stars are not main-sequence, and much of my analysis (§ 5) relies on colors as more reliable than spectral type. From photometric colors we can devise color-magnitude diagrams to tease out implied metallicity, luminosity class, or close multiple systems with different colored stars. From luminosities we can determine luminosity class, multiplicity, or low gravity. Published values in our papers (Winters et al. 2011, etc.) are the unweighted means<sup>13</sup> of (generally) three sets of  $VRI$  obtained on different nights, though some stars in this thesis have only one or two measurements.

Occasionally, a star is an unresolved multiple ( $M_{AB}$ ). With a  $\Delta mag$  measurement, we can deblend the magnitudes into individual component magnitudes ( $M_A, M_B$ ). The first step is to convert the magnitudes of the stars  $A$  and  $B$  to fractional fluxes  $F_A$  and  $F_B$ . We know the fractional flux  $F_B$  relative to  $F_A$  in terms of the  $\Delta mag$ :

$$F_A = 1 \tag{2.18}$$

$$F_B = 10^{\frac{\Delta mag}{-2.5}} \tag{2.19}$$

$$F_{AB} = F_A + F_B \tag{2.20}$$

---

<sup>13</sup>Our night-to-night errors are generally extremely similar for stars CTIOPI normally observes; the consequences of weighting would be minimal. This may not be true for very faint stars, where Poisson noise becomes a major factor.

Now that we have fluxes, we can calculate the differences in magnitude, and then the actual deblended magnitudes:

$$\Delta M_A = -2.5 \log_{10} \left( \frac{F_A}{F_A + F_B} \right) \quad (2.21)$$

$$\Delta M_B = -2.5 \log_{10} \left( \frac{F_B}{F_A + F_B} \right) \quad (2.22)$$

$$M_A = M_{AB} + \Delta M_A \quad (2.23)$$

$$M_B = M_{AB} + \Delta M_B \quad (2.24)$$

Plotting a binary on an HR diagram requires deblending two colors. This task is made somewhat easier by the fact that there is an approximately linear relationship between  $M_V$  and  $M_K$  throughout most of the main sequence, as seen in Figure [2.2](#). This linear relationship means that  $\Delta V \approx 2 \times \Delta K$ , independent of the actual value of  $M_V$ .

### 2.2.3 X-ray Activity

X-rays are produced in the coronae of magnetically active stars, and are thus a sign of youth. Many of the stars in this thesis have measurable X-ray flux, as this was one of the subsamples in the TINYMO survey ([§4](#)), and also my main selection criterion for young stars.

X-ray flux from the ROSAT All Sky Surveys ([Voges et al. 1999, 2000](#)) can be combined with optical photometry to obtain a ratio of X-ray luminosity ( $L_X$ ) to bolometric luminosity

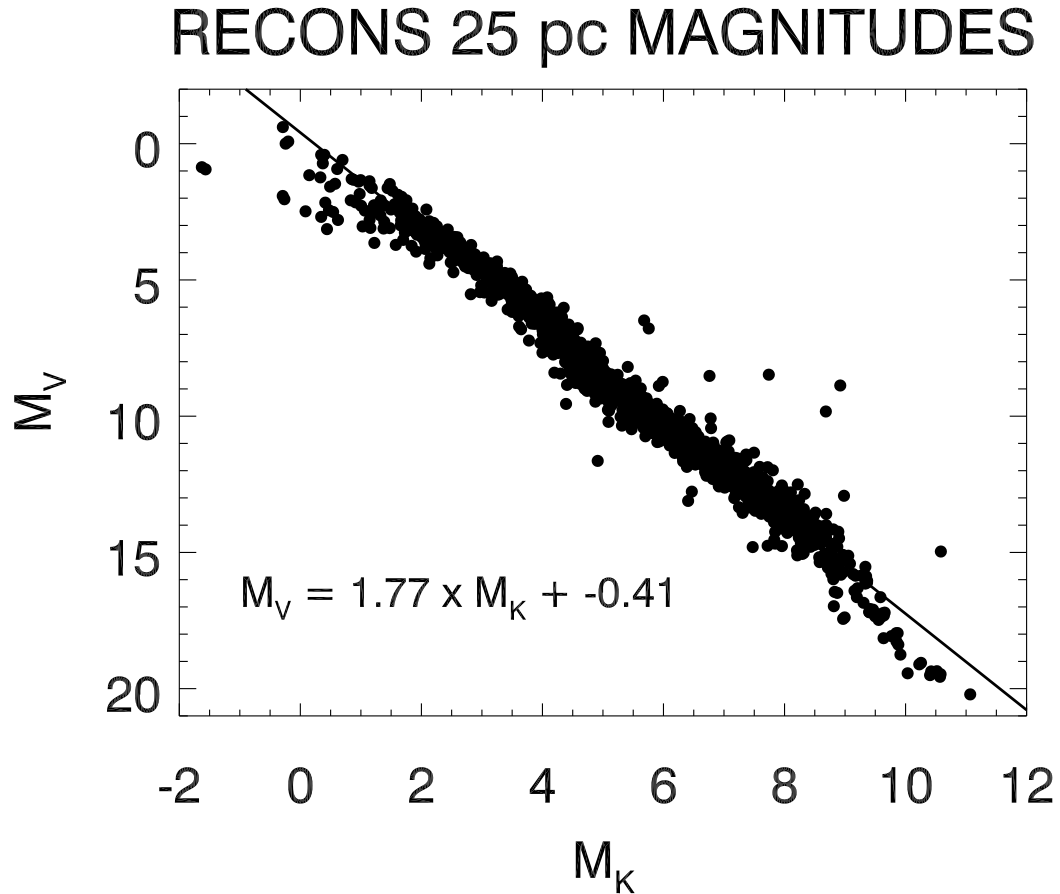


Figure 2.2: A demonstration of the roughly linear relationship between  $M_V$  and  $M_K$ , used to get deblended colors for stars that were only resolved in one waveband. Note that the given slope is representative, and not based on a clean sample.

( $L_{bol}$ ):

$$f_X = (5.30 \times hr1 + 8.31) \times 10^{-12} \times cnts \quad (2.25)$$

$$L_X = 4\pi \times (d \times 3.086 \times 10^{18})^2 \times f_X \quad (2.26)$$

$$\log \left( \frac{L_X}{L_{bol}} \right) = \log_{10}(f_X) + 4.4931 + \frac{0.26 + V + BC}{2.5} \quad (2.27)$$

where  $f_X$  is the X-ray flux,  $d$  is the distance in parsecs ( $3.086 \times 10^{18}$  is one parsec in centimeters),  $hr1$  is the ROSAT hardness ratio;  $cnts$  is the published ROSAT counts per second flux,  $V$  is Johnson  $V$ , and  $BC$  is a bolometric correction based on photometric color and interpolated from a table (e.g. Casagrande et al. 2008).

Within the M star class, X-ray emission saturates at a value of roughly  $\log(\frac{L_X}{L_{bol}}) = -3.0$ , with typical errors of  $\pm 0.5$  dex for the precision of ROSAT data and our photometry. All magnetic activity takes time to fade. It takes at least 600 Myr (the age of the Hyades) for M0V stars to not have saturated X-ray activity, and much longer for cooler stars (Zuckerman & Song 2004; West et al. 2008). Thus, though any young M star should have X-ray activity, X-ray bright M stars are not necessarily young. Of course, the magnetic fields are intrinsically tied to stellar rotation, so a slow-rotating young star (for whatever reason) will necessarily have less X-ray flux, while a tidally interacting binary of any age with forced fast rotation will have high X-ray flux.

#### 2.2.4 Variability

Variability is one of the hallmarks of the T Tauri class of stars, and is common in all kinds of young stars. This variability, like other signs of chromospheric and magnetic activity, persists for long periods of time in M dwarfs. As many of my stars appear to be young, variability is an important and readily available tool for their identification and characterization.

Variability information in this work comes from our parallax pipeline. With multiple nights of data in the filter used for parallax, we use the methods in Honeycutt (1992) to derive the nightly offsets and zero points for relative instrumental photometry (Jao et al.

2005).

The basic equation used to determine relative variability (from Jao et al. 2011) is

$$m_i^j = m_{0_i} + \delta m^j \quad (2.28)$$

where  $m_i^j$  is the instantaneous magnitude of star  $i$  on frame  $j$ ,  $m_{0_i}$  is the mean magnitude of star  $i$  over *all* frames  $j$ , and  $\delta m^j$  is the overall magnitude offset for frame  $j$  (incorporating all possible reasons for systematics: exposure time, seeing, cloud cover). The equations for each star are solved to minimize  $\delta m^j$  (the frame's global magnitude offset).

Once  $\delta m^j$  has been determined for each frame  $j$ , we hold it fixed and calculate the variability of each star ( $\sigma m_i^j$ ) relative to the mean magnitude  $m_{0_i}$  of that star:

$$\sigma m_i^j = m_i^j - m_{0_i} - \delta m^j \quad (2.29)$$

This provides a measurement of the variability  $\sigma m_i^j$  of a given star through a series of frames or, put another way,  $m_i^j - \delta m^j$  should be a magnitude corrected for global effects, centered around the mean ( $m_{0_i}$ ). Our variability is reported relative to that mean.

Analysis of the relative variability of M dwarfs (Jao et al. 2011) shows that a typical M dwarf varies by roughly 0.010 magnitudes, and statistically significantly more in  $V$  and  $R$  (0.013 mag) than  $I$  (0.008 mag). The paper also found a statistically significant difference between regular M dwarfs and their older, metal poor subdwarf cousins (variability 0.007 mag) which points to some combination of age and (possibly) metallicity influencing the amplitude of stellar variability. As seen in Figure 2.3 M dwarfs with variability higher than 0.020 mag are rare, although several are seen in the samples of stars I discuss in this thesis.

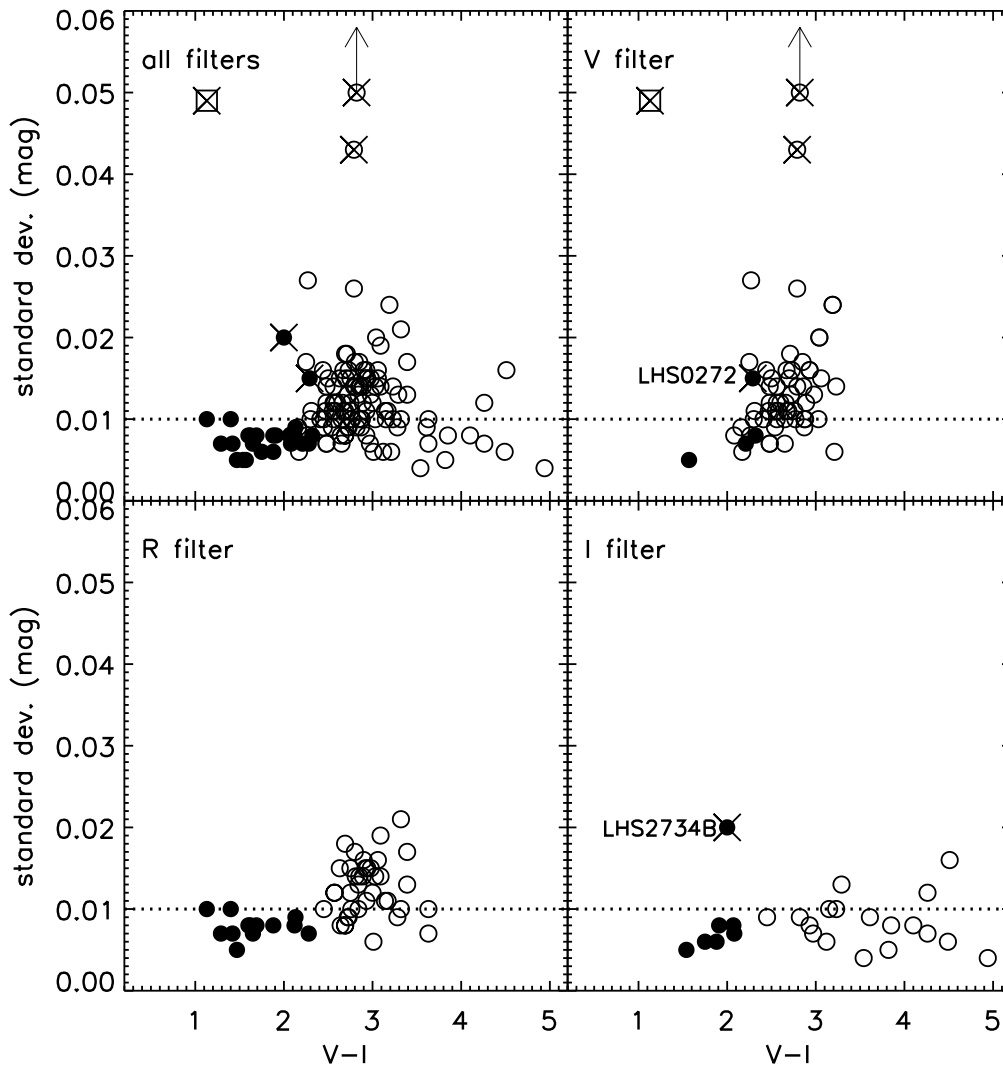


Figure 2.3: Relative Variability for stars published by RECONS, as seen in Figure 6 of Jao et al. (2011), where black points are subdwarfs, open circles are red dwarfs, and boxes and crosses are unusual stars detailed further in §5.1 of that paper. Only a few stars have more than 0.020 mag variability in any filter. Those that do are chromospherically active and presumably younger than the others. Plot from Jao et al. (2011) by Wei-Chun Jao.

One additional consideration revealed by our photometric series are long-term trends in stellar variability. Typically noticed in stars I have also identified as young, this variability manifests as a multi-year-long coherent increase or decrease in the apparent luminosity

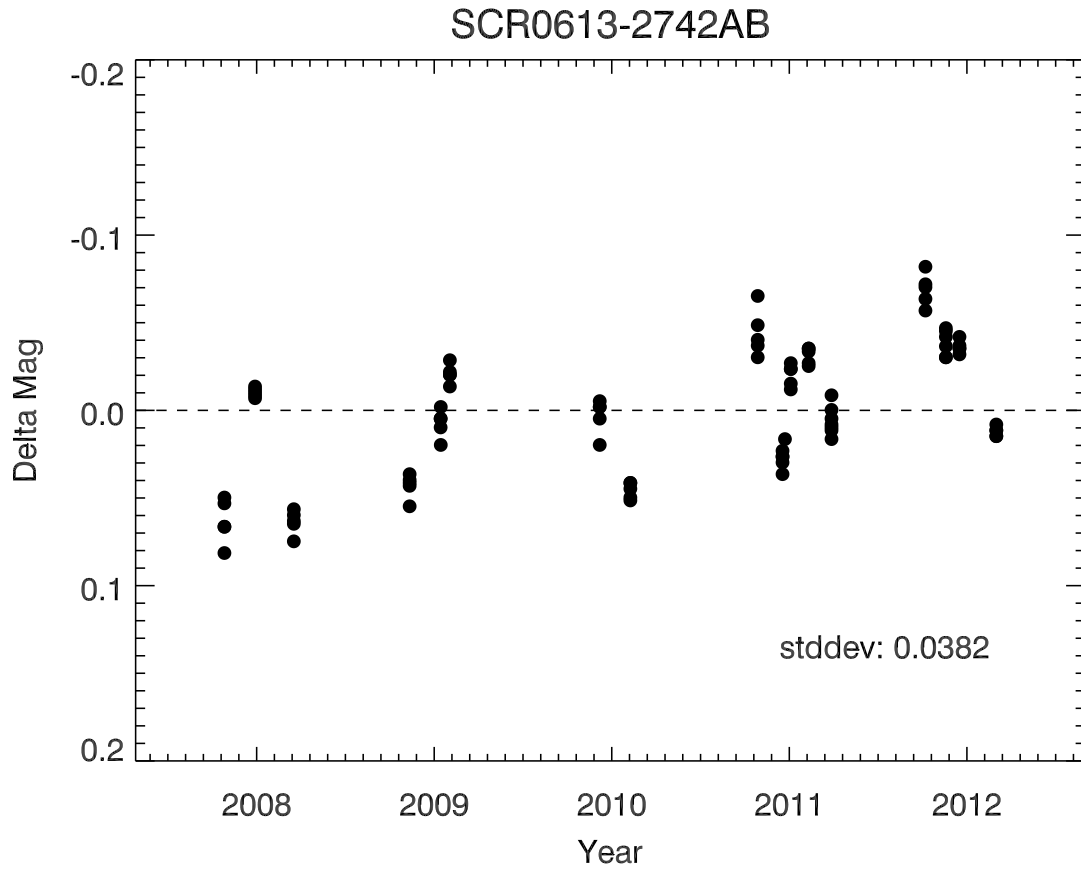


Figure 2.4: The relative variability of SCR 0613-2742AB (for instance) has a general upward trend, as if the star is getting steadily brighter. I am not certain what is causing this.

(Figure [2.4](#)). We only sample these stars for 30 minutes at a time every few months, so we cannot measure the rotational modulation of starspots, and it is highly unlikely we are seeing aliased starspot periods (although they likely do contribute to the scatter). In principle (and occasionally in practice, though I usually remove such a star from the entire reduction), the observed variations could be the result of a long-period Mira variable reference star throwing off the average variability, but the method of calculation would still identify the Mira itself as principally variable as well as noticeably increasing the variability of every star in the field

(by biasing  $\delta m^j$ ). We currently suspect that this activity is evidence of a stellar activity cycle, akin to the 11-year Solar cycle.

### ***2.2.5 Color-Magnitude relations***

Color-magnitude relations are an integral part of my thesis, used to make quick estimates of the distances to stars in the SuperCOSMOS database. RECONS, and my thesis in particular, use photometric distances extensively to determine whether it is worthwhile to commit to obtaining a parallax to a nearby star. After the fact, they can also be used as a gauge of whether or not our assumptions about the star (single, main-sequence) were correct.

The basic premise is that we can exploit the color-magnitude diagram to obtain distances to stars. Specifically, the main sequence is a roughly monotonic function: for any given color (or spectral type) there is a corresponding limited range of absolute magnitudes for a single main-sequence star.

Many variations on this theme have been used over the years. Gliese (1982) included proper motion, reasoning that higher proper motion stars were more likely subdwarfs or thick disk stars, and accordingly increased the errors on the distances. Reid et al. (1995) used a simple spectral index as a numerical proxy for spectral type. Henry et al. (2004) used 12 different color relations rather than a single color. There are also models that rely on theoretical main sequences as well as observational data (Breddels et al. 2010).

The primary appeal of color-magnitude relations is the ease of use: once the system is properly calibrated, it can take as little as one visit to get the spectroscopy or photometry necessary to make the distance estimate; with current available all-sky photometry, no addi-

tional telescope time is required at all. Compared to the two to three year timespans required to obtain a trigonometric parallax, plus the difficulty in accurately measuring parallaxes at large distances, photometric distances are fast and easy.

There are four photometric distance relations used in my thesis. All (except the last) make the critical assumption that the star is a.) on the main sequence and b.) a single star.

The first photometric distance calibration used is from Hambly et al. (2004) (Table 2.1). It uses 11 combinations of the  $SERC - J$  (roughly B-band),  $SERC - ER$  (roughly  $R_{KC}$ -band), and  $SERC - I$  ( $I_{KC}$ -band) calibrated photometry (called  $BR_2I$ ) from the SuperCOSMOS Sky Survey (Hambly et al. 2001a) and 2MASS  $JHK_s$ . Each color, treated entirely independently from the others, has a corresponding (mostly) fourth-order polynomial fit of the following form:

$$M_{K_s} = C4 \times color^4 + C3 \times color^3 + C2 \times color^2 + C1 \times color^1 + C0 \quad (2.30)$$

based on single stars with known parallaxes and photometry. The fits are only valid within certain ranges of colors typical for single main-sequence K and M dwarfs. With both  $K_s$  and up to 11 estimated values of  $M_{K_s}$ , we can produce up to 11 distances; the unweighted mean of the valid distances is the final reported distance<sup>14</sup>. The final error is the standard deviation of the valid distances (fit error), added in quadrature to a systematic error of 26% determined by running stars of known distance through the suite of relations.

---

<sup>14</sup>Improvements to this method might include: Calculating a weighted mean distance, taking the weighted mean of the distance moduli and *then* producing a distance, propagating photometric errors, and making a variable weight-map for each color combination to account for the changing height of the main sequence. These improvements can only be expected to produce minor changes in the distances, though they may reduce the systematic error.

Table 2.1: Plate photometry relations for red dwarfs (Hambly et al. 2004).

| Color         | No. Stars in Fit | Applicable Range | C4       | C3       | C2       | C1        | C0        | weight |
|---------------|------------------|------------------|----------|----------|----------|-----------|-----------|--------|
| $(B_J - I)$   | 54               | 2.48 – 6.95      | ...      | -0.06597 | +1.00958 | -3.65843  | +9.49477  | 0.74   |
| $(B_J - J)$   | 54               | 3.53 – 9.51      | +0.01720 | -0.44789 | +4.18392 | -15.61513 | +25.69047 | 0.62   |
| $(B_J - H)$   | 54               | 4.15 – 10.22     | +0.01736 | -0.49708 | +5.13558 | -21.71069 | +37.74852 | 0.64   |
| $(B_J - K_s)$ | 54               | 4.38 – 10.69     | +0.01385 | -0.41706 | +4.52981 | -20.08433 | +36.70961 | 0.63   |
| $(R_2 - I)$   | 54               | 0.67 – 4.08      | ...      | ...      | +0.07403 | +1.16691  | +4.59375  | 0.76   |
| $(R_2 - J)$   | 55               | 1.08 – 6.43      | +0.03685 | -0.53287 | +2.68760 | -4.56720  | +8.21182  | 0.70   |
| $(R_2 - H)$   | 55               | 1.68 – 7.49      | +0.02066 | -0.37082 | +2.36926 | -5.37494  | +9.74196  | 0.72   |
| $(R_2 - K_s)$ | 55               | 1.92 – 8.15      | +0.01260 | -0.25196 | +1.78947 | -4.36444  | +9.10891  | 0.71   |
| $(I - J)$     | 55               | 0.04 – 3.65      | ...      | -0.19062 | +1.13456 | -0.07582  | +6.05024  | 1.00   |
| $(I - H)$     | 55               | 0.61 – 4.71      | ...      | -0.17978 | +1.40873 | -1.58307  | +6.60017  | 1.03   |
| $(I - K_s)$   | 55               | 0.91 – 5.37      | ...      | -0.16765 | +1.47110 | -2.23929  | +7.04432  | 0.99   |

The second, from Henry et al. (2004), is similar to the Hambly et al. (2004) relations except in that it utilizes  $VRIJHK_s$  photometry. Out of the 15 possible color combinations, 12 are fit with fourth-order polynomials (ignoring errors on the parallax and photometry of the input stars). These fits ( $M_{K_s}$  vs.  $V - K_s$  demonstrated in Figure 2.5) provide up to 12 different estimates of  $M_K$ , again valid within only specific ranges of color common to single main-sequence K and M dwarfs. As in Hambly et al. (2004), the distance is the unweighted mean of all valid distance relations, and the error is the standard deviation of those distances added in quadrature to a systematic error. In this case, however, the systematic error is 15.25%, because our Johnson-Kron-Cousins  $VRI$  photometry is more precise than SuperCOSMOS  $BR_2I$ .

The third set of photometric distance relations used employs a more restricted set of  $VRI$  relations to estimate the distances to reference stars. They are again polynomial coefficients, this time solving for  $M_V$ :

$$M_V = C5 \times color^5 + C4 \times color^4 + C3 \times color^3 + C2 \times color^2 + C1 \times color^1 + C0 \quad (2.31)$$

These relations are used to determine the astrometric corrections to absolute parallax (Table

Table 2.2: CCD photometry relations for red dwarfs. (Henry et al. 2004)

| Color       | No. Stars in Fit | Applicable Range | C4        | C3         | C2         | C1         | C0         | weight |
|-------------|------------------|------------------|-----------|------------|------------|------------|------------|--------|
| $(V - R)$   | 125              | 0.53 – 2.40      | + 2.79703 | – 17.48617 | + 36.67711 | – 25.90589 | + 9.96960  | 0.40   |
| $(V - I)$   | 134              | 0.88 – 4.81      | + 0.02853 | – 0.49504  | + 2.64479  | – 3.51296  | + 5.62135  | 0.40   |
| $(V - J)$   | 130              | 2.51 – 8.00      | + 0.02447 | – 0.52310  | + 3.91317  | – 10.94674 | + 15.31851 | 0.39   |
| $(V - H)$   | 115              | 3.59 – 8.69      | + 0.03207 | – 0.77797  | + 6.74382  | – 23.61879 | + 34.23360 | 0.42   |
| $(V - K_s)$ | 134              | 2.24 – 9.27      | + 0.00959 | – 0.23953  | + 2.05071  | – 5.98231  | + 9.77683  | 0.42   |
| $(R - I)$   | 126              | 0.43 – 2.42      | – 1.08390 | + 5.68997  | – 9.78999  | + 9.22596  | + 1.54462  | 0.41   |
| $(R - J)$   | 123              | 1.64 – 5.66      | + 0.07380 | – 1.15011  | + 6.26647  | – 12.52051 | + 13.44932 | 0.41   |
| $(R - H)$   | 108              | 2.68 – 6.36      | + 0.10427 | – 1.91432  | + 12.58352 | – 33.56316 | + 36.76955 | 0.45   |
| $(R - K_s)$ | 126              | 1.63 – 6.97      | + 0.01785 | – 0.37226  | + 2.59680  | – 5.75029  | + 8.19804  | 0.45   |
| $(I - J)$   | 135              | 0.88 – 3.36      | + 0.58092 | – 4.69507  | + 12.35365 | – 9.20851  | + 6.22309  | 0.45   |
| $(I - H)$   | 120              | 1.67 – 4.23      | + 0.14094 | – 1.31052  | + 3.12906  | + 2.68748  | – 2.62035  | 0.54   |
| $(I - K_s)$ | 139              | 1.07 – 4.83      | + 0.19771 | – 2.44679  | + 10.18426 | – 14.30638 | + 10.38741 | 0.52   |

<sup>a</sup> “No. Stars in Fit” column combines RECONS and Very Red samples

2.3, Jao et al. 2005). They are the only relations that apply to stars bluer than K, and they have not yet been published in a paper.

Table 2.3: CCD photometry relations for correction to absolute.

| Color     | C5          | C4         | C3        | C2        | C1        | C0        |
|-----------|-------------|------------|-----------|-----------|-----------|-----------|
| $(V - R)$ | +2.745919   | –16.24443  | +32.56145 | –26.25209 | +16.33187 | +1.082261 |
| $(V - I)$ | +0.01340408 | –0.2351777 | +1.392817 | –3.566166 | +7.521329 | +1.007786 |
| $(R - I)$ | –0.7647815  | +3.344504  | –2.50887  | –5.577088 | +13.90569 | +1.005736 |

The fourth set of photometric distance relations used in my thesis is from Riedel et al. (2011). These relations are fifth order polynomials (solving for  $M_V$  as in the  $VRI$  set) to single stars with trigonometric parallaxes<sup>15</sup> that are known members of nearby young associations.

The input data for the stars came from my young stars database, described in §3.4. To produce empirical isochrones (Table 2.4) for nearby associations, the dataset had to be cleaned. Multiples, suspected multiples, and obvious outliers (generally noted as such in the

<sup>15</sup>While adding kinematic distances (as seen Zuckerman & Song 2004, Torres et al. 2008, and Table 6.4 for stars without *HIPPARCOS* parallaxes) would increase the number of points used in the fits, there are very few known young M dwarfs in these associations to begin with.

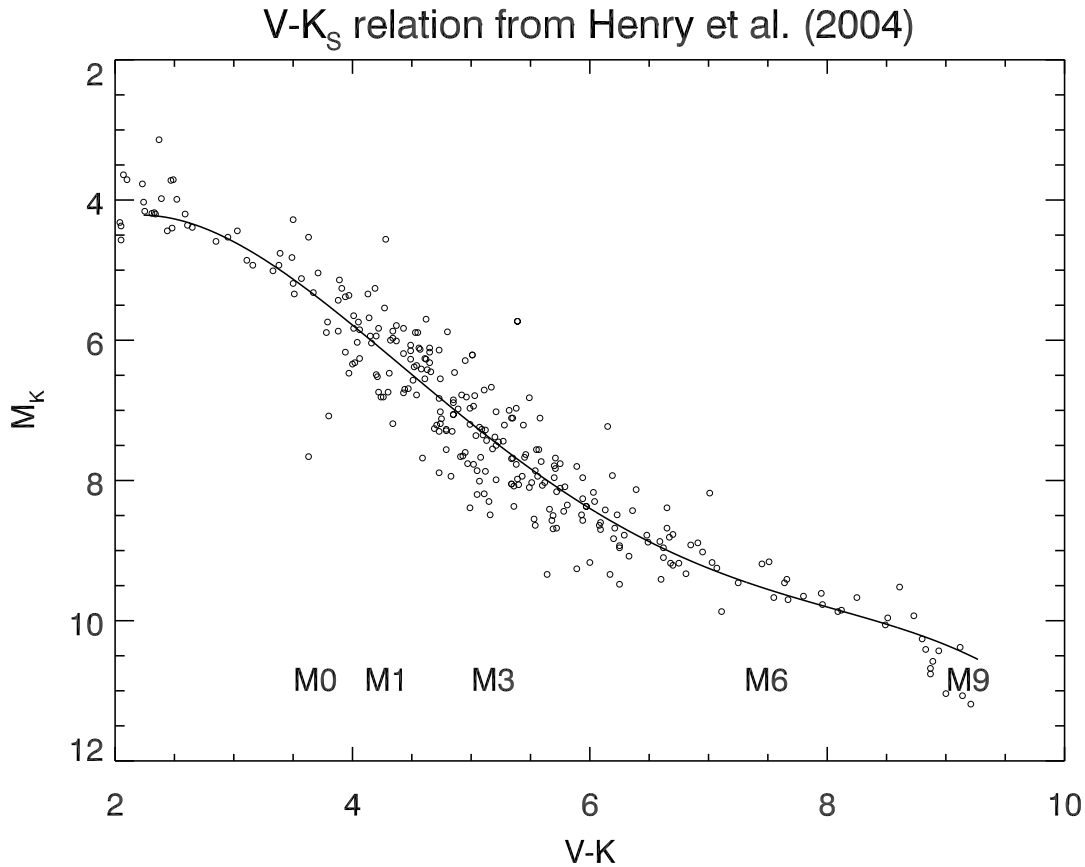


Figure 2.5: The  $V - K_s$  photometric distance relation from Henry et al. (2004) over its valid range, plotted on top of the 10 pc sample (Henry et al. 2006).

*HIPPARCOS* catalog, Zuckerman & Song (2004), or Torres et al. (2008)) were removed from the subsets of young stars with parallaxes. Isochrones were then fit to this assumed-single main sequence in the form of fifth-order polynomials without, as before, regard to errors on any of the photometry or parallaxes. Only one color combination,  $V - K_s$  was used; as in the other distance relations, only certain ranges of  $V - K_s$  color were valid.

Figure 2.6 shows AP Col, the nearest (8.4 pc) pre-main-sequence star as described in Riedel et al. (2011) (§5.4), and the other members of the RECONS 10 pc sample (stars in

Table 2.4:  $V - K_s$  relations for Nearby Young Associations. (Riedel et al. 2011)

| Association    | No. stars in fit | $V - K_s$ range | C5       | C4      | C3      | C2      | C1       | C0      |
|----------------|------------------|-----------------|----------|---------|---------|---------|----------|---------|
| $\beta$ Pic    | 32               | 0.0 – 6.3       | +0.00370 | -0.0550 | +0.2978 | -0.6631 | +2.1789  | +1.6265 |
| TW Hya         | 16               | 0.0 – 8.3       | -0.00485 | +0.0915 | -0.5648 | +1.2706 | +0.8992  | +1.4555 |
| AB Dor         | 41               | 1.2 – 5.1       | +0.00845 | -0.1949 | +1.6629 | -6.5304 | +13.6063 | -5.7448 |
| Tuc-Hor        | 31               | -0.6 – 3.9      | +0.02960 | -0.2199 | +0.4269 | -0.0707 | +1.8747  | +1.3926 |
| $\epsilon$ Cha | 10               | -0.3 – 6.6      | -0.01376 | +0.2256 | -1.2254 | +2.2331 | +1.2320  | +0.4050 |

systems with parallaxes greater than 100 mas and errors less than 10 mas, (Henry et al. 2006).

Known young stars with trigonometric parallaxes are also shown on the graph, along with error bars based on their parallactic and photometric errors (AP Col’s errors are smaller than the plotted symbol), and polynomial fits to three of the associations. As the fifth-order polynomials are highly sensitive to the colors of their most extreme members, I have not plotted them past the reddest young star in each association. The  $\epsilon$  Cha isochrone relies on too few points to be reliable, and there are no quality Tuc-Hor members cooler than M1 (the single point near AU Mic appears to be a binary). The reddest object in the  $\beta$  Pic isochrone is TWA 22AB, originally misclassified as a TW Hya member, with a parallax reported by (Teixeira et al. 2009). Only the TW Hya association extends redder than the plot in Figure 2.6; its reddest member with a parallax is the brown dwarf TWA 27 ( $V - K_s=8.25$ ,  $M_V=16.60$ ), with parallaxes in (Gizis et al. 2007), (Biller & Close 2007) and (Ducourant et al. 2008).

The isochrones were not used for predictive power in (Riedel et al. 2011), but to identify the apparent age of AP Col as being somewhere between the ages of the  $\beta$  Pic ( $\sim 12$  Myr) and AB Dor ( $\sim 125$ ) Myr associations, though in principle they could also be used to predict distances.

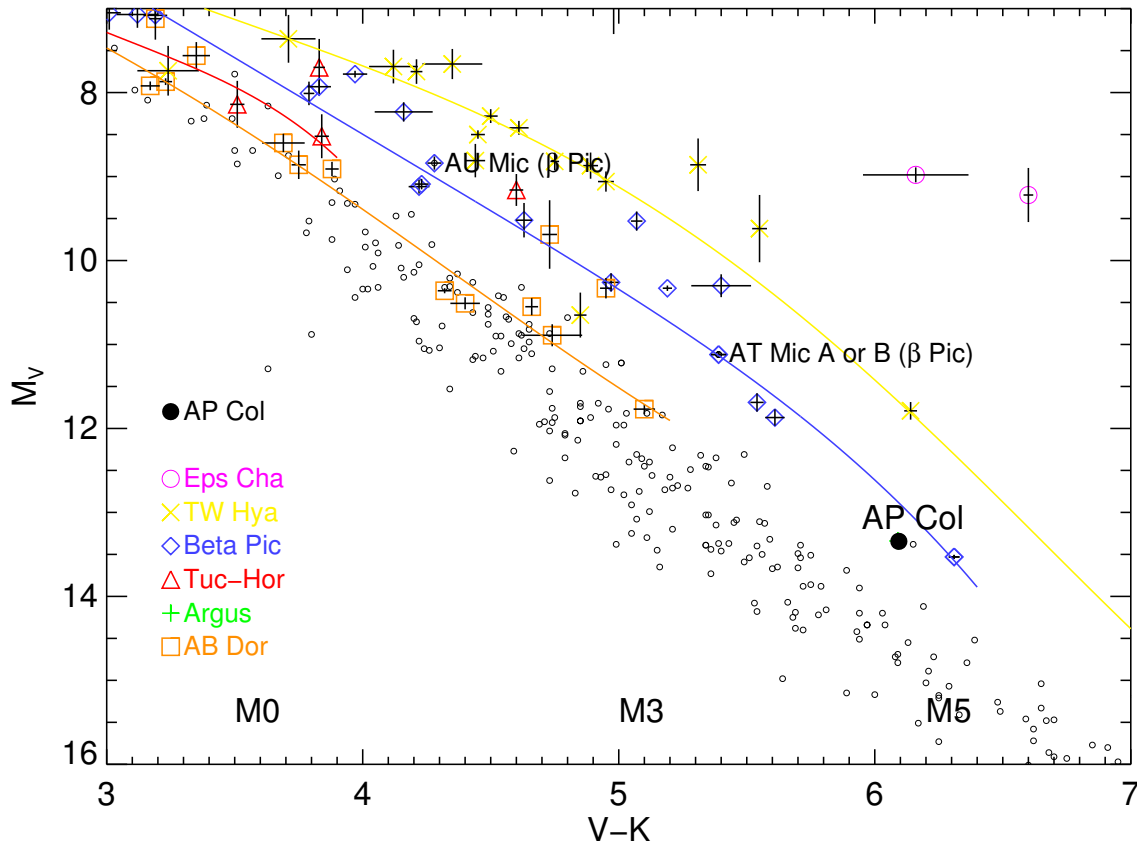


Figure 2.6: A few of the young star isochrones from [Riedel et al. \(2011\)](#), overplotted on the RECONS 10 pc sample (small circles). Each association is color and shape-coded. All young stars with known parallaxes are plotted with accompanying errors, though all stars were not included in the fits (multiples, mistaken memberships, etc.). The isochrones are (top to bottom) TW Hya,  $\beta$  Pic, Tuc-Hor, and AB Dor. The  $\epsilon$  Cha isochrone is not plotted because the fit (to 10 stars) is too poor. The 10 pc object just redder than AP Col is the unusual star GJ 896B=EQ Peg B, see [5.4.3](#).

### 2.3 Spectroscopy

My interest in spectroscopy involved measurements of six important spectral features, shown in [Figure 2.7](#) and listed below (locations taken from [Kirkpatrick et al. 1991](#)):

**H $\alpha$  (6563Å)** Visible in K and hot M stars, gradually decreasing in strength. In emission (negative EW), it is a sign of chromospheric activity; most (but not all, West et al. 2008) stars below M5.0V are still in emission. Above a certain level, it is indicative of ongoing accretion.

**Li I (6708Å)** A close doublet, visible only in young stars that have not yet fused their entire primordial lithium supply, brown dwarfs that never reach lithium fusing temperatures, or post-AGB stars with unusual r-process elements.

**K I (7665Å, 7699Å)** visible only in dwarfs and subdwarfs, blended with atmospheric A band due to O<sub>2</sub> and TiO. Comparing the atmospheric extinction of the Hinkle et al. (2003) atmospheric spectrum convolved to the resolution of our CTIO 1.5m RCSpec spectra reveals that only the K I 7699Å line is affected by less than 4% atmospheric absorption. Chromospheric emission can fill in the line cores (Reid & Hawley 1999), so the K I EW is a function of (increasing) surface gravity, (decreasing) temperature, and (decreasing) activity. At the spectral resolution of the CTIO 1.5m, we cannot resolve any emission features in this line, and none of our dwarf stars are sufficiently active for the emission to overwhelm the intrinsic absorption.

**The ‘Seesaw’ (7750Å–8150Å)** Visible and consistently changing in K and hot to mid M stars. This is a relatively clear continuum region, and as such is responsive to temperature, and corresponds roughly to the blackbody peak of the K9 and M0 stars. With properly flux-calibrated spectra (we use a selection of A-type and white dwarf spectral standards observed on the same night) we find that in K stars, the linear slope of the seesaw region is negative

(trending downwards toward longer  $\lambda$ ); in M stars, the slope is positive (trending upwards). The RECONS spectral typing system was set such that the slope of the seesaw is 0 for the spectrum of a flux-calibrated M0.0V star, which is close to where it already was.

**Na I (8183Å, 8195Å)** is found in all cool star spectra, but strongest in dwarfs. At our resolution and signal to noise, the Na I feature all but disappears in giants. Like the K I EW, the Na I EW is a function of (increasing) surface gravity, (decreasing) temperature, and (decreasing) activity. None of the stars observed at the CTIO 1.5m were sufficiently active to register a negative EW (emission).

**Ca II (8498Å, 8542Å, 8662Å)** Visible in all stars, strongest in cool K and hot M stars. Contamination and noise make these spectral line features difficult to measure at our resolution and noise levels. This triplet is both temperature and gravity-sensitive; in stars cooler than M2.5 it shows up almost exclusively in giants. Like K I (above), emission can fill in the line cores, leading to lower apparent EWs. Ca II EWs are a function of (decreasing) surface gravity, (decreasing) temperature, and (decreasing) activity.

### *2.3.1 Spectral Typing/Reddening*

Spectral typing, first and foremost, provides a representation of the effective temperatures of stars, which allows them to be placed on the classic H-R diagram. This is the traditional purpose and intent of spectral classification; to offer a few discrete labels into which is condensed a great deal of information about the gross properties of stars.

Spectral classification was started in the latter half of the nineteenth century, and eventually settled on letters for different types of stars. First, Fleming's A-Q letters corresponded

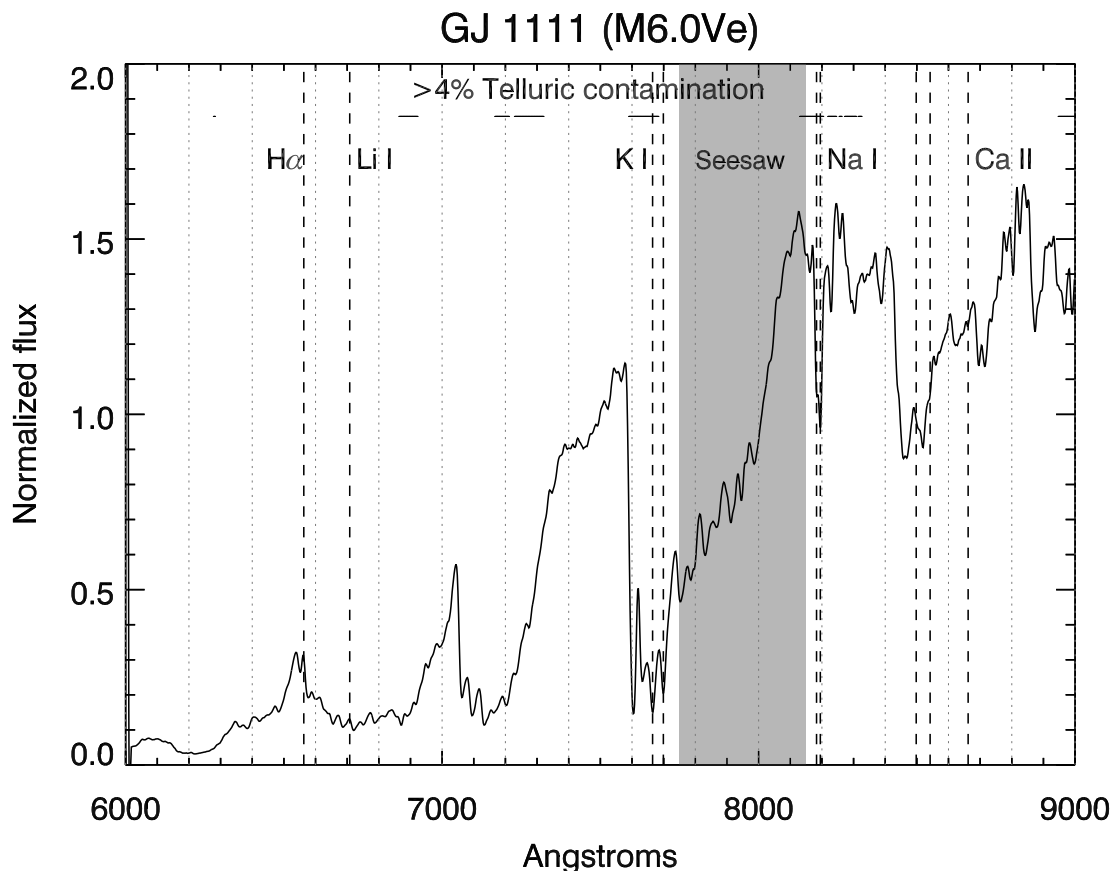


Figure 2.7: Important activity and luminosity features relevant to my thesis work, as seen on an M6.0Ve standard, which was artificially normalized to 1.0 at 7500Å.

to the complexity of the spectrum (Pickering 1890), then the more familiar O, B, A, F, G, K, M system was arranged by temperature (Cannon & Pickering 1901), and finally the more modern formation with luminosity classes (Morgan et al. 1943, hereafter the MK system). Boeshaar (1976), Kirkpatrick et al. (1991) and Henry et al. (2002) have made modifications to classify the large number of M stars that were too faint and red to be seen in 1943, while Kirkpatrick et al. (1999), Martín (2000) and Cushing et al. (2011) added L, T and Y designations for brown dwarfs. In all cases, M dwarfs are principally identifiable by the

appearance of broad molecular absorption bands in the spectrum – titanium oxide (TiO), and vanadium oxide (VO) in cooler M dwarfs.

Spectral typing is still commonly used to identify the types of stars, though it has its downfalls. It artificially subdivides the main sequence into discrete aphysical boxes. Using the exact same terminology, it has been implemented in so many subtly different ways that large discrepancies exist in published spectral types<sup>16</sup> and re-using spectral types is a dubious prospect without considering the lineage of a particular measurement. Even free of those inconsistencies, the MK system does not keep track of metallicity effects<sup>17</sup>, composition, magnetic fields, or a variety of other second-order parameters that define the physical parameters of stars. Of course, at the time spectral typing was first devised, few of those parameters were understood or recognized.

Still, RECONS has a history of working with spectral typing in the red part of the spectrum (Kirkpatrick et al. 1991; Henry et al. 1994) and automated spectral typing codes including ALLSTAR (Henry et al. 2002) and, more recently, MATCHSTAR, which I developed and use to measure my results<sup>18</sup>. In the process of attempting to redefine the M and

<sup>16</sup>An exhaustive, if not exhausting, selection of information on the major spectral standards as they have evolved over time has been collected by Eric Mamajek here: <http://www.pas.rochester.edu/~emamajek/spt/>

<sup>17</sup>apart from the VI luminosity class for subdwarfs, as in Kapteyn’s Star=G1 191=M1p VI in Keenan’s final catalog, <http://cassini.mps.ohio-state.edu/MKCool/mkcat.txt>

<sup>18</sup>MATCHSTAR, an IDL routine, uses matches to a library of standard spectra to produce spectral types. It nulls out telluric features (based on the Hinkle et al. 2003 sky transmission map) and H $\alpha$  emission, regrids spectra to 1Å bins between 6000-9000Å (nulling out portions not covered by the input spectrum), smooths them to a uniform resolution with Gaussian convolution, and normalizes them to 1 at 7500Å. Actual spectral typing is done by dividing the input spectrum by our similarly processed library of standards (a currently unpublished set of 40 stars in 29 spectral types spanning K0V to K9V in whole types and M0.0V to M9.0V in half-types, developed by myself, Todd Henry, and Thom Beaulieu) and taking the spectral type of the best match (lowest standard deviation) as the winner. MATCHSTAR also measures the H $\alpha$  EW (§2.3.3), Na I index, and K I EW (§2.3.2) (prior to removing telluric+H $\alpha$ ) and is thus capable of reporting emission-line stars and luminosity classes, as seen in §5.3 and §5.8. MATCHSTAR will be published if and when the list of standards is finalized.

K spectral sequences for an as-yet unpublished paper, we settled upon a key feature called the seesaw (defined above) for our spectral determinations.

Familiarity with M dwarf spectral typing did allow me to identify several reddened stars found in the TINYMO sample (Chapter 4). They had colors appropriate for M dwarfs and a corresponding positively-sloped seesaw region, but no titanium oxide features. In many cases these stars turned out to be in the direction of the Upper Scorpius star-forming region and associated star forming regions (§5.7). Those regions are at least 100 pc away; all such stars were removed from our parallax program.

### 2.3.2 *Luminosity/Gravity*

My main functional interest in spectra was the ability to distinguish between M giants and M dwarfs in the TINYMO survey (Chapter 4), and later between M dwarfs and pre-main-sequence stars. In red spectra (6000Å – 9000Å) there are three useful spectroscopic features that distinguish dwarfs from giants. Ca II is strong in giants and weak in dwarfs; Na I and K I are weak in giants and strong in dwarfs<sup>19</sup>. The Ca II triplet is almost completely absent in mid-M dwarfs, but prominent in M giants, which makes it an easy diagnostic to use in luminosity classifying.

The Na I index is particularly useful for determining the relative surface gravities of mid and cool M dwarfs (Schlieder et al. 2012b). As defined in Lyo et al. (2004), the index value is formed by the ratio of the average flux in two 24 Å wide bands: one on the doublet and

---

<sup>19</sup>The general pattern, based on Allers et al. (2007), is that Na I, K I, and Ca I are strong in dwarfs; Na II, K II, and Ca II are strong in giants.

one on the immediately adjacent pseudo-continuum (Figure 2.8).

$$NaI_{index} = \frac{F_{8148-8172}}{F_{8176-8200}} \quad (2.32)$$

The Na I doublet EW (and index) increases as the stellar temperature decreases, or as surface gravity increases. Empirically, an index of 1.03 or less indicates a giant, and intermediate index values between dwarfs (which increase to lower temperatures) and giants (which remain flat at 1.03) indicate a low-surface-gravity pre-main-sequence star. Unfortunately, giants and dwarfs overlap at colors bluer than  $V - K_s = 5$ . Alkali metal lines such as Na I can also be affected by stellar activity, where emission fills in the absorption line cores, leading to lower EWs (Reid & Hawley 1999). Slesnick et al. (2006b) notes that the Na I doublet can be affected by telluric absorption over the region 8161–8282 Å, leading to artificially low Na I index values for stars observed at large airmasses.

Measuring the equivalent width of K I 7699Å (Shkolnik et al. 2011) shows that it is equivalent to Na I for use in classifying relative surface gravities, and according to Hinkle et al. (2003) it is *not* contaminated by telluric O<sub>2</sub> absorption. As with the Na I index, the EW values for giants and dwarfs overlap at colors bluer than  $V - K_s = 5$ .

When it comes to dwarf stars, three effects conspire to place a star above the main sequence: multiplicity, youth, and higher metallicity. At first glance, these methods of identifying surface gravity (Na I, K I) should neatly separate out those effects from youth.

Multiplicity should have no effect on the Na I index or K I EW (the brighter component should dominate, except in the case of an equal-luminosity binary where the strengths are equal anyway); youth should *decrease* the strength of the EW or index as the surface gravity

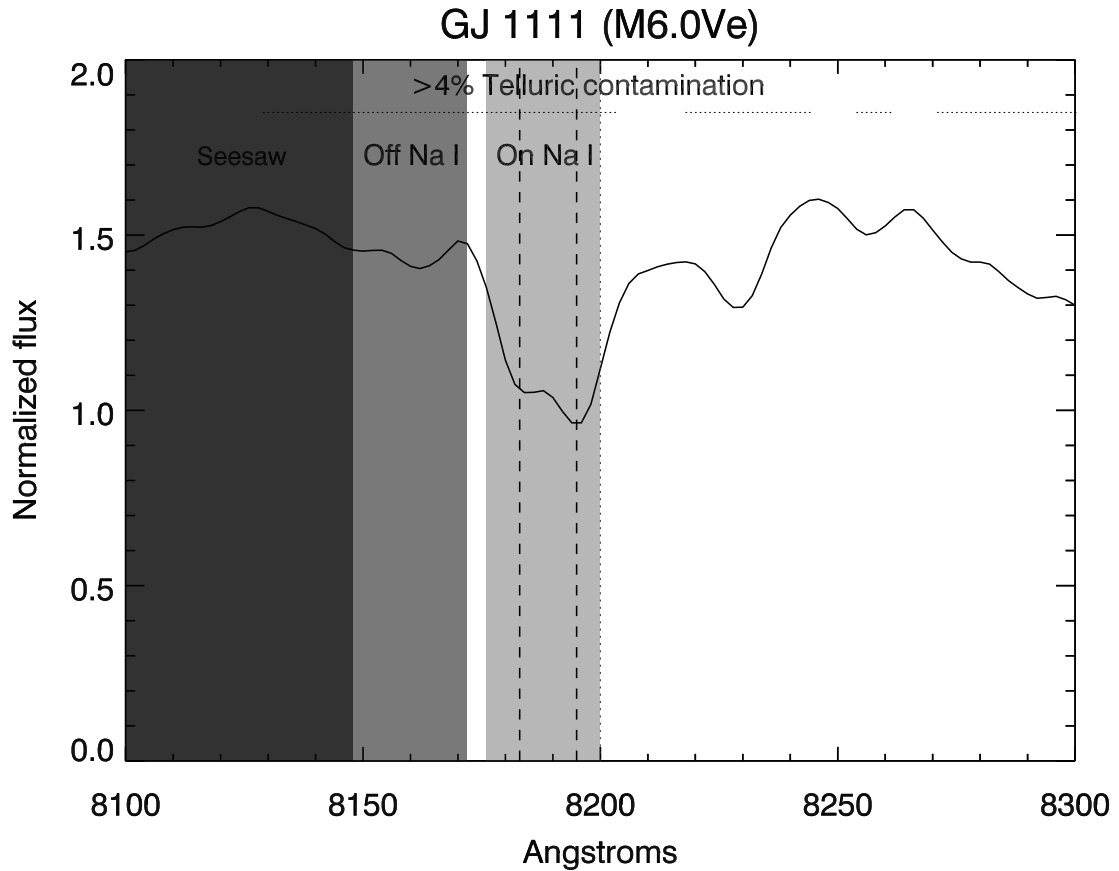


Figure 2.8: Bands used in the Na I gravity indices from Lyo et al. (2004), also used in Riedel et al. (2011). That the Na I-on band does not include the complete red end of the Na I line wing is an unfortunate side-effect of using the Lyo indices.

is lower.

Metallicity is somewhat troubling. Low-metallicity subdwarfs should certainly have weaker lines due to the decreased availability of alkali metals in their atmospheres, but these plot *below* the main sequence and will not be mistaken for pre-main-sequence stars. However, as noted by Shkolnik et al. (2009), high metallicity stars of a given mass and bolometric luminosity will masquerade as stars of lower temperature *and* lower surface gravity

(the additional metals increase the opacity of the stellar atmosphere and therefore put the effective photosphere farther from the center of the star), and will thus appear above the main sequence. It is not clear from the sources in Shkolnik et al. (2009) if the increased abundance of metals offsets this effect – Shkolnik et al. (2009) used TiO and CaH molecular features, and apparently found atomic K I significantly less sensitive to metallicity; this may extend to our atomic Na I features as well. In any case, this region of the Galaxy lacks stars with sufficiently high  $[\text{Fe}/\text{H}]$  to masquerade as an M dwarf in Tuc-Hor, which limits the potential confusion.

### 2.3.3 Activity

Chromospheric activity can be detected in several ways – various spectral lines such as  $\text{H}\alpha$  (6563Å) in emission, the so-called Mount Wilson Index (measured in the near-UV Calcium H and K lines, Gray et al. 2003), NUV or X-ray emission. For my thesis, only red spectra were employed, so all activity features came from  $\text{H}\alpha$  EWs and the ROSAT All-Sky Surveys (Voges et al. 1999, 2000).

The EW of  $\text{H}\alpha$  appears in emission in all M stars with chromospheric activity. M stars live so long (M0V stars for an estimated 50 Gyr, M9V stars for perhaps trillions of years) and evolve so slowly that the youthful activity stretches out into an extended adolescence, forming the starspotted BY Draconis and flaring UV Ceti type stars. According to West et al. (2008), a statistical analysis of SDSS data suggests that M stars take at least 800 Myr (M0V) to as long as 8 Gyr (M7V) to cease magnetic activity. Interestingly,  $\text{H}\alpha$  flux does saturate, but does not correlate well with X-ray emission (Riaz et al. 2006; West & Basri 2009) implying

that H $\alpha$  features in emission are generated by different means (corona vs. chromosphere). According to White & Basri (2003), emission levels above 10 $\text{\AA}$  (K7-M2.5), 20 $\text{\AA}$  (M2.5-M5.5), 40 $\text{\AA}$  (M6.5 and later) are signs of classical T Tauri stars (with accretion disks).

### 2.3.4 Lithium

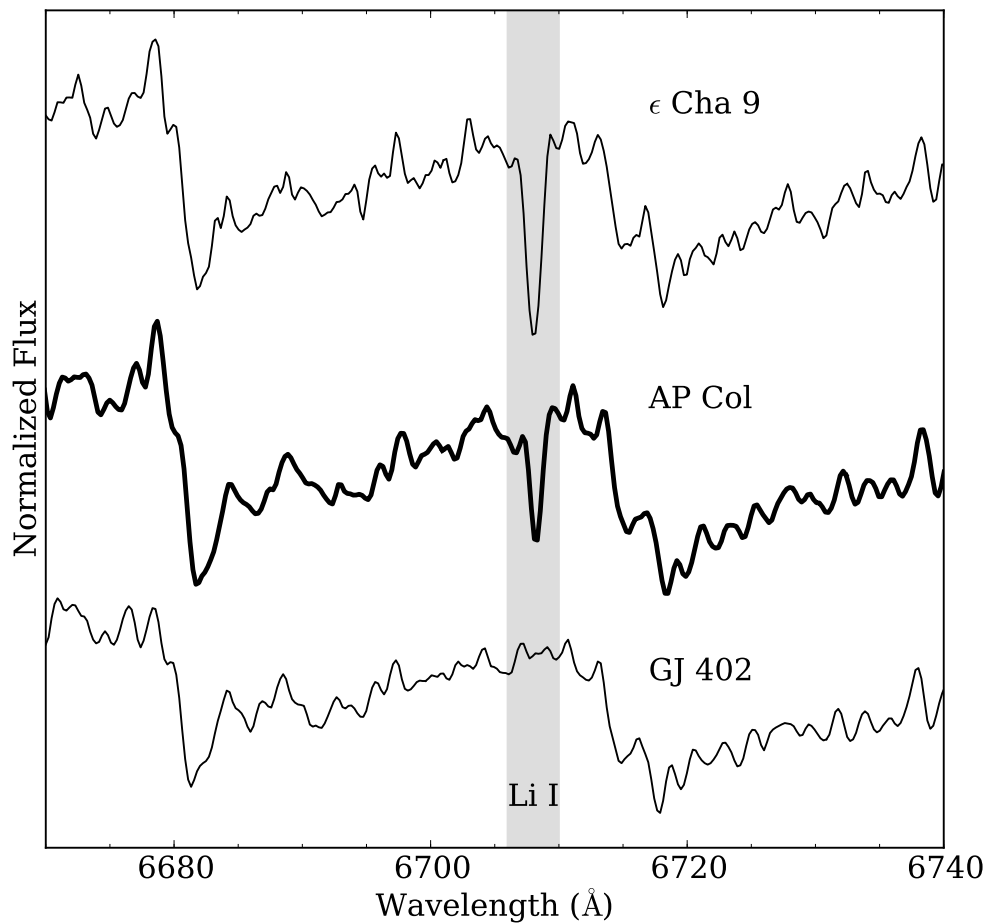


Figure 2.9: The spectra of three stars of similar spectral types but varying ages ( $\epsilon$  Cha 9, 6 Myr ; AP Col, 40 Myr; GJ 402, field age) around the lithium 6708 $\text{\AA}$  doublet feature. Lithium is very quickly fused and removed from the atmospheres of low mass stars, making it a marker of youth. (Riedel et al. 2011, plot by Simon Murphy.)

The lithium 6708 $\text{\AA}$  doublet is extremely important for age-dating of stars. The depen-

dence of lithium burning efficiency on stellar age (see Figure 2.9) and temperature leads to the concept of a lithium depletion boundary (LDB), where only a small change in stellar mass and temperature can lead to the appearance or disappearance of the Li I  $\lambda 6708$  feature (Song et al. 2002). For instance, at the age of the  $\beta$  Pic association ( $\sim 12$  Myr), the cool edge of the LDB lies at spectral type M4.5 (Song et al. 2002; Torres et al. 2003), while at the age of the Pleiades ( $\sim 100$ -130 Myr) it has shifted to M6.5 (Stauffer et al. 1998; Barrado y Navascués et al. 2004). While Yee & Jensen (2010), Song et al. (2002) and others have noted that lithium depletion ages are systematically larger than those derived by isochrone fitting or kinematic expansion ages, relative age ranks are not affected. It is, however, dangerous to take lithium EW as a foolproof age indicator. Baraffe & Chabrier (2010) have identified a mechanism whereby lithium might suddenly become depleted during a fast accretion event. Ultimately, this means that if all other parameters of youth point to a particular age or membership, lithium cannot single-handedly rule it out.

## 2.4 Kinematics

### 2.4.1 Galactic Kinematics

Galactic kinematics are used to identify potential memberships in comoving stellar associations, and to derive rough disk-heating ages for stars. They are usually dealt with as Cartesian coordinates centered on the Sun, defined as XYZ positions in parsecs, and UVW velocity vectors in kilometers per second. These kinematic coordinates are distinct from normal Galactic  $(l, b, \pi)$  coordinates, and require spherical geometric transforms to calculate.

There is a matter of dispute concerning the orientation of the axes: All sources define the V (and Y) unit vectors in the direction of Galactic motion, and the W (and Z) unit vectors in the direction of the North Galactic Pole, but there is disagreement in the U (X) direction. Most sources, including Johnson & Soderblom (1987), Zuckerman & Song (2004) and Torres et al. (2008), define the U/X vector as pointing toward the Galactic center so as to make the coordinate system right-handed. A few others, most notably including NASA’s IDL GAL\_UVW.pro routine<sup>20</sup>, define U/X as pointing away from Galactic center, presumably for physical reasons.

The primary utility of rendering kinematics in this fashion is that it is easy to identify unusual clustering or groups of stars in a more easily manipulatable format. Even partial solutions (for instance, Asiain et al. 1999 used only UV kinematics for most of their analysis) can yield useful information about a system. Indeed, as research into moving groups has continued, more accurate kinematic information has teased out smaller and smaller substructures in the local velocity field. Our best information about current nearby moving groups is summarized in Table 2.5, in right-handed UVWXYZ space.

Table 2.5: Nearby Young Associations

| Name                        | U                  | $\sigma_U$         | V                  | $\sigma_V$         | W                  | $\sigma_W$         | min X | max X | min Y | max Y | min Z | max Z | Age              |
|-----------------------------|--------------------|--------------------|--------------------|--------------------|--------------------|--------------------|-------|-------|-------|-------|-------|-------|------------------|
| (1)                         | km s <sup>-1</sup> | pc    | pc    | pc    | pc    | pc    | pc    | Myr              |
| (1)                         | (2)                | (3)                | (4)                | (5)                | (6)                | (7)                | (8)   | (9)   | (10)  | (11)  | (12)  | (13)  | (14)             |
| $\epsilon$ Cha <sup>b</sup> | -11.0              | 1.2                | -19.9              | 1.2                | -10.4              | 1.6                | 34    | 60    | -105  | -78   | -44   | -12   | 6 <sup>a</sup>   |
| TW Hya                      | -10.5              | 0.9                | -18.0              | 1.5                | -4.9               | 0.9                | 2     | 34    | -61   | -26   | 10    | 27    | 8 <sup>a</sup>   |
| $\beta$ Pic                 | -10.1              | 2.1                | -15.9              | 0.8                | -9.2               | 1.0                | -32   | 76    | -33   | 21    | -29   | -1    | 12 <sup>a</sup>  |
| Octans                      | -14.5              | 0.9                | -3.6               | 1.6                | -11.2              | 1.4                | -79   | 142   | -138  | -60   | -85   | -38   | 20               |
| Tuc-Hor                     | -9.9               | 1.5                | -20.9              | 0.8                | -1.4               | 0.9                | -61   | 43    | -47   | -4    | -44   | -30   | 30               |
| Columba                     | -13.2              | 1.3                | -21.8              | 0.8                | -5.9               | 1.2                | -106  | 9     | -168  | 1     | -99   | 6     | 30               |
| Carina                      | -10.2              | 0.4                | -23.0              | 0.8                | -4.4               | 1.5                | -2    | 33    | -154  | -39   | -33   | 5     | 30               |
| Argus                       | -22.0              | 0.3                | -14.4              | 1.3                | -5.0               | 1.3                | -55   | 64    | -154  | -6    | -67   | 8     | 50               |
| AB Dor                      | -6.8               | 1.3                | -27.2              | 1.2                | -13.3              | 1.6                | -94   | 73    | -131  | 58    | -66   | 23    | 125 <sup>c</sup> |
| Pleiades <sup>d</sup>       | -6.6               | 0.4                | -27.6              | 0.3                | -14.5              | 0.3                | -134  | -108  | 14    | 40    | -66   | -40   | 125 <sup>c</sup> |
| Castor <sup>e</sup>         | -10.7              | 3.5                | -8.0               | 2.4                | -9.7               | 3.0                | ...   | ...   | ...   | ...   | ...   | ...   | 200              |

*Continued on next page*

<sup>20</sup>[http://idlastro.gsfc.nasa.gov/ftp/pro/astro/gal\\_uvw.pro](http://idlastro.gsfc.nasa.gov/ftp/pro/astro/gal_uvw.pro)

Table 2.5 – *Continued from previous page*

| Name                | U                  | $\sigma_U$         | V                  | $\sigma_V$         | W                  | $\sigma_W$         | min X | max X | min Y | max Y | min Z | max Z | Age |
|---------------------|--------------------|--------------------|--------------------|--------------------|--------------------|--------------------|-------|-------|-------|-------|-------|-------|-----|
| (1)                 | km s <sup>-1</sup> | pc    | pc    | pc    | pc    | pc    | pc    | Myr |
| UMa <sup>f</sup>    | 14.56              | 2.28               | 2.81               | 1.75               | -8.37              | 3.42               | ...   | ...   | ...   | ...   | ...   | ...   | 500 |
| Hyades <sup>g</sup> | -41.1              | 2.0                | -19.2              | 2.0                | -1.4               | 2.0                | -53   | -33   | -9.3  | 10.7  | -27.3 | 7.3   | 650 |

<sup>a</sup>Only these ages are known with any degree of certainty or corroboration.

<sup>b</sup>All data (unless otherwise specified) from [Torres et al. \(2008\)](#).

<sup>c</sup>Age from [Luhman et al. \(2005\)](#)

<sup>d</sup>Dimensions [Soderblom et al. \(2005\)](#), 13 pc tidal radius [Adams et al. \(2001\)](#)

<sup>e</sup>[Barrado y Navascues \(1998\)](#)

<sup>f</sup>[King et al. \(2003\)](#)

<sup>g</sup>[Röser et al. \(2011\)](#)

The primary source for the geometric transforms is [Johnson & Soderblom \(1987\)](#), which lays out the calculations needed for computing UVW velocities and their associated errors. [Johnson & Soderblom \(1987\)](#) do not include the calculation of XYZ space positions or their associated errors, but they can be calculated as well. The full suite of equations, with errors, starts with the rotation matrix between the J2000 equinox and Galactic coordinates ( $[t]$ ).

$$t = \begin{bmatrix} -0.0548755604 & -0.8734370902 & -0.4838350155 \\ +0.4941094279 & -0.4448296300 & +0.7469822445 \\ -0.8676661490 & -0.1980763734 & +0.4559837762 \end{bmatrix} \quad (2.33)$$

With  $[t]$ , we can transform the star's position in RA, DEC, and  $\pi$  into right-handed Cartesian coordinates.

$$|pos| = |t| \begin{bmatrix} \cos(DEC) \times \cos(RA) \\ \cos(DEC) \times \sin(RA) \\ \sin(DEC) \end{bmatrix} \quad (2.34)$$

$$\begin{bmatrix} X \\ Y \\ Z \end{bmatrix} = \frac{1}{\pi} \times [pos] \quad (2.35)$$

Normally, we would break  $[pos]$  down into normal spherical  $(l, b)$  coordinates, but here we use them and  $\pi$  to get XYZ Cartesian Galactic coordinates.

Calculating the errors ( $\sigma_{XYZ}$ ) on the XYZ cartesian positions requires the derivative of the above operation:

$$\begin{bmatrix} \sigma_X^2 \\ \sigma_Y^2 \\ \sigma_Z^2 \end{bmatrix} = \frac{\sigma_\pi^2}{\pi^4} [pos^2] + \frac{1}{\pi^2} [t^2] \begin{bmatrix} (\cos(DEC) \times -\sin(RA) \times \sigma_{RA})^2 + (-\sin(DEC) \cos(RA) \times \sigma_{DEC})^2 \\ (\cos(DEC) \cos(RA) \times \sigma_{RA})^2 + (-\sin(DEC) \sin(RA) \times \sigma_{DEC})^2 \\ (\cos(DEC) \times \sigma_{DEC})^2 \end{bmatrix} \quad (2.36)$$

where  $[pos^2]$  is every element of  $[pos]$ , squared; the same for  $[t^2]$ .

The calculation of the UVW velocities and their errors are as given in Johnson & Soderblom (1987), and require additional matrices. For a given proper motion and radial velocity, the UVW space velocities will be different depending on where the star is in the sky. We must therefore account for the star's position ( $[a]$ ) as well:

$$a = \begin{bmatrix} \cos(RA) \cos(DEC) & -\sin(RA) & -\cos(RA) \sin(DEC) \\ \sin(RA) \cos(DEC) & \cos(RA) & -\sin(RA) \cos(DEC) \\ \sin(DEC) & 0 & \cos(DEC) \end{bmatrix} \quad (2.37)$$

$$|b| = |t||a| \quad (2.38)$$

$$k = 4.74047 \quad (2.39)$$

$[b]$  now incorporates both the necessary rotation to account for the star's sky position ( $[a]$ ) and the transform from equatorial J2000 coordinates to Galactic coordinates ( $[t]$ ). The scalar  $k$  is the transformation from  $\text{AU yr}^{-1}$  to  $\text{km s}^{-1}$  we need to transform our proper motions

(in AU yr<sup>-1</sup>) into km s<sup>-1</sup>, as in the formula  $V_{tan} = 4.74\mu\frac{1}{\pi}$ .

$$\begin{bmatrix} U \\ V \\ W \end{bmatrix} = [b] \begin{bmatrix} RV \\ \frac{k \times \mu_{RA}}{\pi} \\ \frac{k \times \mu_{DEC}}{\pi} \end{bmatrix} \quad (2.40)$$

The calculation of the errors on the velocities ( $\sigma_{UVW}$ ) is analogous to the calculation for the positions.  $[b^2]$  is every element of  $[b]$ , squared.

$$\begin{bmatrix} \sigma_U \\ \sigma_V \\ \sigma_W \end{bmatrix} = [b^2] \begin{bmatrix} \sigma_{R.V.}^2 \\ \frac{k^2}{\pi} (\sigma_{\mu_{RA}}^2 + (\frac{\mu_{RA}\sigma_{\pi}}{\pi})^2) \\ \frac{k^2}{\pi} (\sigma_{\mu_{DEC}}^2 + (\frac{\mu_{DEC}\sigma_{\pi}}{\pi})^2) \end{bmatrix} + 2\mu_{RA}\mu_{DEC}k^2\frac{\sigma_{\pi}}{\pi^4} \begin{bmatrix} b_{12} \times b_{13} \\ b_{22} \times b_{23} \\ b_{32} \times b_{33} \end{bmatrix} \quad (2.41)$$

I have made a modified GAL\_UVW.pro file called GAL\_UVWXYZ.pro (§C), which includes the above calculations for XYZ and errors, using the right-handed (U toward Galactic center) coordinates. This program has formed the basis of my kinematic investigations. I have compared my results to a different version of the same code that uses Monte Carlo to calculate errors, and find both versions to be equivalent (though the Monte Carlo version is substantially slower).

Because RECONS does not observe stars for radial velocity, most of my sample members have no radial velocity measurements. For this purpose, I generate a range of radial velocities  $V_r$  from  $-500$  to  $+500$  km s<sup>-1</sup> in increments of  $V_{tan}$  (to match the precisions of our astrometric data), and the GAL\_UVWXYZ routine is run for each possible radial velocity. This produces a line in 3-D space of potential UVW velocities (Figure 2.10) consistent with our other observations (RA, DEC,  $\pi$ ,  $\mu_{RA}$ ,  $\mu_{DEC}$ ). While these kinematics cannot prove membership in any given kinematic association, they can demonstrate that an association is incompatible

with available observations. Beyond this, the program is designed to calculate the best-fit radial velocity (lowest velocity-space “separation”) for any given star, to aid in detections.

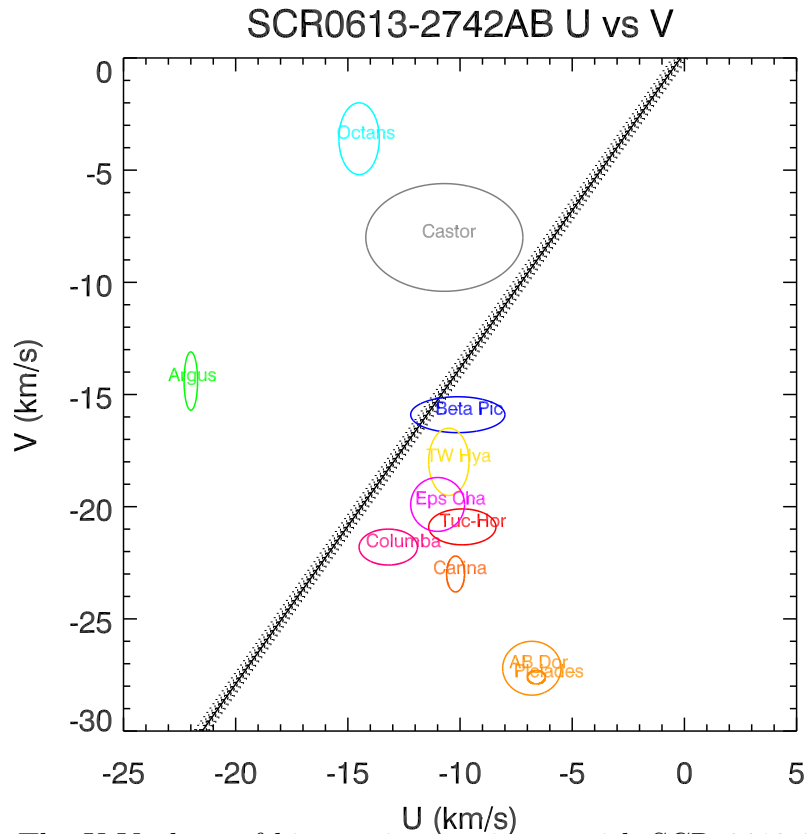


Figure 2.10: The U-V plane of kinematics consistent with SCR 0613-2742AB. Because we have no radial velocity, we can only draw a line through 3-dimensional space; it apparently intersects here with the  $\beta$  Pic association (best-fit is  $0.8\sigma$  from the mean  $\beta$  Pic UVW, with a radial velocity of  $21.4 \text{ km s}^{-1}$ ). In actual fact, it also comes within  $1.7\sigma$  of the Castor moving group as well (with a radial velocity of  $13.9 \text{ km s}^{-1}$ ), but its deblended luminosity demonstrates it is too young to be a Castor member. It is therefore more likely (though *not* certain) to be a  $\beta$  Pic member.

This approach can also be used to treat parallax *and* radial velocity as variables, though in this case – cutting a plane through 6-D space – more spurious matches will be made. In this example, the estimated best-fit distance to a particular cluster would have to put the star on the correct isochrone for that cluster. For example, a kinematic match to the 6 Myr

old  $\epsilon$  Cha association that put the system on the main sequence would be a bad match.

### *2.4.2 Convergence*

As kinematic data improve, it becomes possible to analyze stars *within* their associations, which can form a powerful check on the consistency of an association. For instance, the positions of members of an association of 12 Myr old stars should converge 12 Myr ago, at least to within a distance that would put all of them within their natal clouds. By the same token, an association that does *not* converge in this way points to either an unphysical group, an incorrect age, or some mistaken assumptions about input parameters.

Because tracing the convergence is a difficult problem, this is typically addressed via Monte Carlo simulations. Inputs are varied randomly between  $1\text{-}\sigma$ ,  $2\text{-}\sigma$  and  $3\text{-}\sigma$  limits, and these are taken to describe the likelihood of convergence at a given time in the past. Next, I discuss two methods I have used to evaluate association ages and memberships.

#### *2.4.2.1 Linear backtracking*

This is the easiest method. Given UVW velocities and positions for both the star in question and the mean values of the association stars (Table [2.5](#)), the difference between the star and

the mean location of the association ( $d$ ) can be found at time  $t$ .

$$\begin{aligned} \tau &= \frac{31557600}{3.08568025e13} \\ d(t) &= (((X_{star} - U_{star} \times t \times \tau) - (X_{assoc.} - U_{assoc.} \times t \times \tau))^2 \\ &+ ((Y_{star} - V_{star} \times t \times \tau) - (Y_{assoc.} - V_{assoc.} \times t \times \tau))^2 \\ &+ ((Z_{star} - W_{star} \times t \times \tau) - (Z_{assoc.} - W_{assoc.} \times t \times \tau))^2)^{0.5} \end{aligned} \tag{2.42}$$

where  $\tau$  is the conversion factor between  $\text{km s}^{-1}$  and  $\text{pc yr}^{-1}$ .

#### 2.4.2.2 Galactic Potential

Linear backtracking only works for a few million years. For a better, more useful approximation, we need to use a full Galactic potential. My kinematics code for this instance is derived from a Galactic Structure homework problem, using the cylindrically symmetric [Dehnen & Binney \(1998\)](#) Galactic potential model #2 and cylindrical  $r$ ,  $\phi$ ,  $z$  coordinates centered on the Galactic center. The calculations are carried out for star and association independently, and then compared.

We start by defining the position and motion of an object in the Galaxy in a cylindrical Galaxy-centered coordinate system. We know where they are (in  $(l, b, \pi)$  space) relative to the Sun, which we assume to be at Galactic coordinates  $R_{\odot}=8$  kpc,  $Z_{\odot}=0.02$  kpc,  $\phi_{\odot}=0$ . Our Cartesian  $U$  and  $W$  space velocities are already (or are close enough to) the correct values for  $\delta r$  and  $\delta z$ , so we use them directly (apart from converting them to  $\text{kpc/Myr}$ , to match the Dehnen & Binney potential grid).  $\delta\phi$  is composed of  $V$  and the local standard of rest (LSR) at the location of the star, which we interpolate out of the Dehnen & Binney

potential grid. It also must be converted to an angular measurement.

$$r_{sun} = 8.000(kpc) \quad (2.43)$$

$$z_{sun} = 0.02(kpc) \quad (2.44)$$

$$r = \sqrt{(r_{sun} - (\pi \times \cos(b)) \times \cos(l))^2 + ((\pi * \cos(b)) \times \sin(l))^2} \quad (2.45)$$

$$\delta r = U \div 977.7753 \quad (2.46)$$

$$\phi = asin\left(\frac{\pi \times \cos(b) \times \sin(l)}{r}\right) \quad (2.47)$$

$$lsr = \sqrt{r \times (INTERPOLATE(dpdr, rgrid, zgrid))} \quad (2.48)$$

$$\delta\phi = \frac{LSR + V \div 977.7753}{r} \quad (2.49)$$

$$z = z_{sun} + \pi \times \sin(b) \quad (2.50)$$

$$\delta z = W \div 977.7753 \quad (2.51)$$

At each timestep  $t$  (in Myr), the potentials  $\delta p \delta r$  and  $\delta p \delta z$  are pulled from the Dehnen & Binney model at the current  $r, \phi, z$  location. Those values go into calculating the following

differential equations (where  $L$  is angular momentum):

$$L = r^2 + \delta\phi \quad (2.52)$$

$$\delta r = \delta r \quad (2.53)$$

$$\delta^2 r = -dpdr_1 + \frac{L^2}{r^3} \quad (2.54)$$

$$\delta\phi = \frac{L}{r^2} \quad (2.55)$$

$$\delta^2\phi = \frac{-2L\delta r}{r^3} \quad (2.56)$$

$$\delta z = \delta z \quad (2.57)$$

$$\delta^2 z = -dpdz_1 \quad (2.58)$$

as the inputs of Runge-Kutta integration. The integration then proceeds to the next timestep  $t$  with  $r_{new} = r_{old} + \delta r$ ,  $z_{new} = z_{old} + \delta z$ , and  $\phi_{new} = \phi_{old} + \delta\phi$ .

These calculations are carried out for the star and the mean association motion, and then separations are obtained from the resulting paths:

$$sep^2 = (r_{star1}(t) \times \cos(\phi_{star1}(t)) - r_{star2}(t) \times \cos(\phi_{star2}(t)))^2 \quad (2.59)$$

$$+ (r_{star1}(t) \times \sin(\phi_{star1}(t)) - r_{star2}(t) \times \sin(\phi_{star2}(t)))^2 \quad (2.60)$$

$$+ (z_{star1}(t) - z_{star2}(t))^2 \quad (2.61)$$

### 2.4.3 *Expected proper motion distribution*

In discussing the TINYMO search for nearby low-proper-motion stars (Chapter 4), it is useful to define your expectations of the parameter space, i.e., the number of stars expected within 25 pc with various proper motions. To do this, I constructed a Monte Carlo simulation of stars within 25 pc, which was then compared to (initially) the NStars Database and (more recently) the RECONS Database.

The key observable I was interested in was the proper motions of the stars, and specifically the fraction of stars that could be expected to move slower than  $0.18'' \text{ yr}^{-1}$ . This problem is not analytic, and must be simulated numerically.

The first problem is the distribution of star systems. As can be seen in CNS, NStars and the RECONS Databases, the distribution of K stars (and hotter) within 25 pc is essentially uniform (see Figure 3.2). No Galactic disk or arm effects are visible; the positions are random and uniform. We can therefore surmise that *all* nearby stars are uniformly distributed, and the apparent lack of M stars as distance increases is entirely an observational effect, due to those stars' low luminosities. Accordingly, we take the density of systems within 5 pc (51 stars, or  $0.09 \text{ systems pc}^{-3}$ ) as correct, and scale it up to find 6375 stars within 25 pc.

Next, some accounting of the velocity dispersions of star systems must be made. These vary noticeably by spectral type. As the primaries get hotter, their dispersion relative to the local standard of rest shrinks, most likely a product of their age – a very hot star will by definition not have lived long, and will still be tracing a Galactic orbit similar to the cloud from which it formed. Therefore, we need two different pieces of information: velocities as a

function of spectral type, and number density as a function of spectral type.

The kinematics (as a function of spectral type) came from Aumer & Binney (2009), who determine kinematics primarily from the Geneva-Copenhagen survey of solar type stars, and includes the revised astrometry from van Leeuwen (2007). Aumer & Binney (2009, Figures 3&4) determine the velocity dispersions for main-sequence stars from  $B - V = -0.2$  to  $B - V = +0.9$  – redder than that, we are apparently saved by the Parenago Discontinuity: redder than  $B - V = 0.6$  (a G star), the velocity dispersions stop increasing (although Aumer & Binney (2009) have few data points to substantiate this claim, and M dwarfs should have lower masses and be more easily moved by gravitational encounters<sup>21</sup>). Additional kinematics for subdwarfs and white dwarfs were sourced from Gizis (1997) and Mihalas & Binney (1981), respectively<sup>22</sup>. The frequency of various types of stellar primary were taken from the RECONS 10 pc statistics<sup>23</sup> on the 261 known systems within 10 pc of the Solar System, with the assumption that our census of A, F, G and K stars is complete within 10 pc, that white dwarfs (20/261) and subdwarfs (3/261) are only proportionally complete, and the remainder of the 408 expected stars by volume are M dwarfs and brown dwarfs. I also included the assumption of 1/6375 B star (Regulus) within 25 pc.

---

<sup>21</sup>This is also overly simplistic. The mass of the *system* should determine how much it is perturbed by encounters, not just the mass of the primary. For instance, the GJ 644ABCD/643 quintuple system has a mass comparable to the Solar System, despite having an M3V primary.

<sup>22</sup>Neither giants nor young stars were included in this analysis. Giants, at least, are so uncommon that there are none within 10 pc (though there certainly are some within 25 pc); young stars are a more complicated question.

<sup>23</sup><http://www.chara.gsu.edu/RECONS/census.posted.htm> checked 2012 JUL 15. The RECONS 25 pc Database (§3.2) currently lacks the spectral type information necessary to derive these kinds of statistics.

Table 2.6: Parameters for synthetic 25 pc sample

| $V - K_s$ | Fraction | $\sigma U$<br>km s <sup>-1</sup> | $\sigma V$<br>km s <sup>-1</sup> | $\sigma W$<br>km s <sup>-1</sup> | Note   |
|-----------|----------|----------------------------------|----------------------------------|----------------------------------|--|
| -1        | 0.0000   | 8                                | 8                                | 5                                | B systems (Regulus= 1/6375)                                |
| 0         | 0.00016  | 14                               | 9                                | 4.5                              | A systems (4/408)  |
| 1         | 0.0098   | 22                               | 14                               | 10                               | F systems (6/408)  |
| 2         | 0.0245   | 38                               | 26                               | 20                               | G systems (20/408)   |
| 3         | 0.0735   | 37                               | 26                               | 19                               | K systems (44/408)   |
| 3.8       | 0.1814   | 37                               | 26                               | 19                               | M0-3 systems   |
| 5         | 0.3500   | 37                               | 26                               | 19                               | M3-5 systems   |
| 6         | 0.5000   | 37                               | 26                               | 19                               | M5-7 systems   |
| 8         | 0.7200   | 37                               | 26                               | 19                               | M7-9.5 systems   |
| 10        | 0.8100   | 37                               | 26                               | 19                               | L,T systems  |
| 20        | 0.91186  | 37                               | 26                               | 19                               | Transition <sup>a</sup>                                    |
| -1        | 0.91187  | 177                              | 100                              | 82                               | Subdwarfs ( <a href="#">Gizis 1997</a> )                   |
| 20        | 0.92336  | 177                              | 100                              | 82                               | Transition <sup>a</sup>                                    |
| -1        | 0.92337  | 50                               | 30                               | 20                               | White dwarfs ( <a href="#">Mihalas &amp; Binney 1981</a> ) |
| 0         | 0.9500   | 50                               | 30                               | 20                               | White dwarfs   |
| 2.7       | 1.0000   | 50                               | 30                               | 20                               | White dwarfs   |

<sup>a</sup>These are not real; they are a computational necessity included to separate the “sequences” and prevent interpolation from making many oddly-distributed stars.

To model the proper motion distribution, a table (Table [2.6](#)) was made listing the  $V - K_s$  colors of the spectral types listed in the RECONS statistics, corresponding UVW dispersions for that color/spectral type, and a cumulative fraction of stars more massive than that spectral type (bent slightly to account for the 5% white dwarf and 0.5% subdwarf populations; we suspect those dispersions, which are from different older sources, are not as accurate). Using a random number generator, a “spectral type” was chosen. I then interpolated into Table [2.6](#) to obtain an associated  $V - K_s$  color and velocity dispersions for that “spectral type”. Uniformly-distributed randomized XYZ positions (within 25 pc, but otherwise completely random) and uniformly-distributed UVW velocities were calculated within the appropriate dispersions. To these I added the effect of Strömberg’s asymmetric drift equa-

tion ( $\langle V \rangle = \frac{U^2}{k}, k = 74 \pm 5$  Aumer & Binney (2009)), and subtracted the UVW velocity of the Sun relative to the local standard of rest, as sourced from Schönrich et al. (2010): (U=11.10, V=12.24, W=7.25 km s<sup>-1</sup>). The UVW and XYZ positions were then used to calculate proper motions.

The result is a table of  $N$  objects randomly distributed within a 25 pc radius, with a semi-realistic distribution of spectral types and space velocities. For a sufficiently large  $N$  (here, 10,000,000), I can generate the expected distribution of stars, which can be compared to a list of observed stars.

As can be seen in Figure 2.11, the RECONS 25 pc database is fairly complete for stars with proper motions higher than 1''yr<sup>-1</sup>, and staggeringly incomplete for proper motions around 0.2''yr<sup>-1</sup>. Overall, 13.6% of all stars within 25 pc should be moving at speeds slower than 0.18'' yr<sup>-1</sup>; this is in line with other estimates (Reid et al. 2007 find 11%).

There are multiple potential improvements to this process. The relationships between frequency,  $V - K_s$  color and UVW velocities are all very granular and ad-hoc. There has been no accounting for vertex deviation; all velocities are chosen within a velocity ellipse aligned to the UVW axes. The distribution is also very sensitive to the LSR velocity: using the more traditional Aumer & Binney (2009) solar motion values (U=9.96, V=5.25, W=7.07 km s<sup>-1</sup>), 14.9% of all nearby stars were found moving less than 0.18'' yr<sup>-1</sup>. This dataset purposefully does not reproduce young stars, either. While we know of two definite pre-main-sequence systems within 10 pc (AU/AT Mic, Barrado y Navascues (1998) and AP Col, Riedel et al. (2011)), both with space velocities of roughly 20 km s<sup>-1</sup>, they do not define

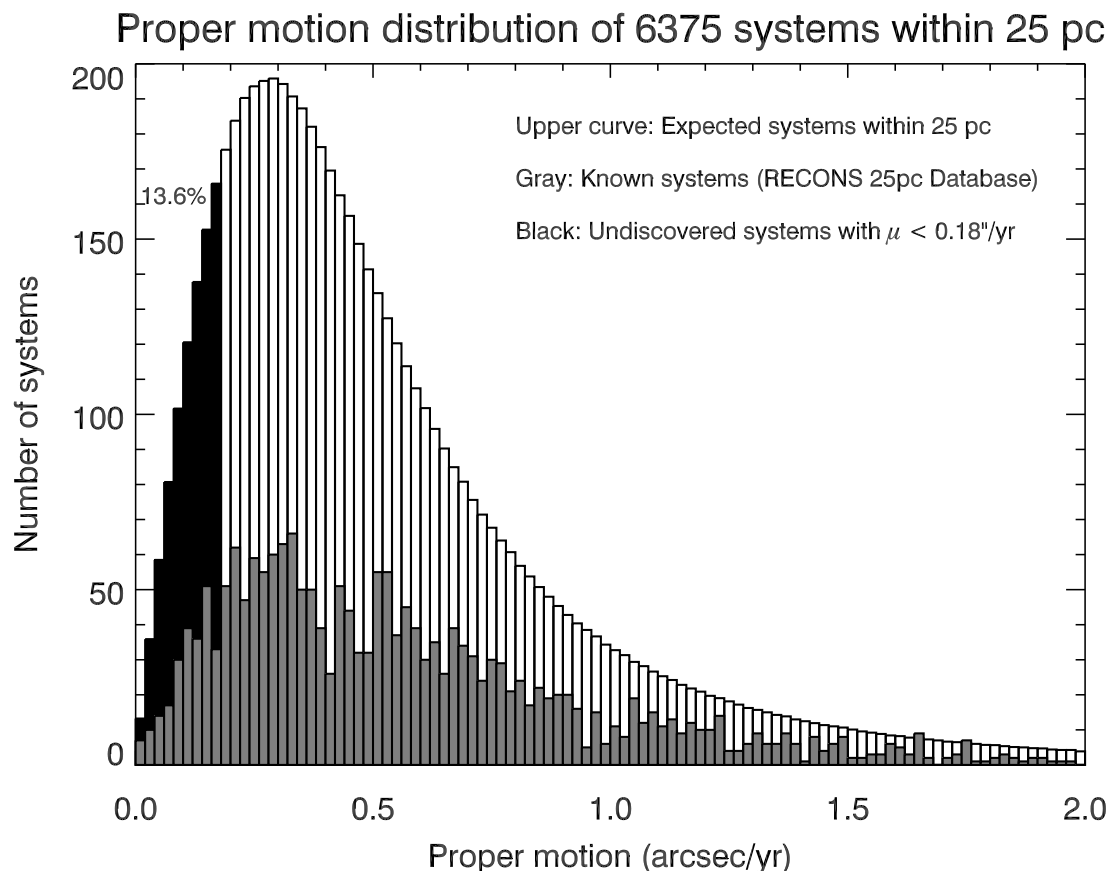


Figure 2.11: Shown here is a simulated proper motion distribution using [Aumer & Binney \(2009\)](#), [Gizis \(1997\)](#) and [Mihalas & Binney \(1981\)](#) velocity distributions, and a CMF from RECONS data. The top black and white plotted histogram is the distribution assuming 51 systems within 5 pc is the uniform number density of systems, with systems moving slower than  $0.18''\text{yr}^{-1}$  in black; the gray curve represents actual proper motions from the RECONS 25 pc Database (See [3.2](#)).

the entirety of that kinematic population. There are, for instance, indistinguishably main-sequence members of the Ursa Major Moving Group nearby (GJ 229AB, GJ 216AB, GJ 447, GJ 566, etc. [King et al. 2003](#)), as well as Castor (Vega, Fomalhaut); all of these have similarly small space velocities (otherwise Eggen would not have noticed them as overdensities in a velocity plot). However, in the case of Vega and Fomalhaut, their low space velocities are

already accounted for by being A-type main sequence stars; *all* A-type main sequence stars are by necessity fairly young objects.

To correctly account for stellar youth (and as a better way to handle subdwarfs), one would have to generate and add together multiple waves of star formation (from a template IMF, scaled by total formation event mass and accounting for multiplicity), each with its own age, density, and age-dependent space velocity dispersions. Only the youngest would contain B stars (although the very youngest may not be dense enough to produce even A-type stars); all would produce A, F, G, K and M stars. This kind of simulation (which requires an accurate template IMF) is being done (Aumer & Binney 2009; Just & Jahreiß 2010), but is a substantial research project in and of itself.

## 2.5 Databases

RECONS relies heavily on empirical data for testing our relationships, as does my thesis work. This reliance led to the construction of three stellar databases. I have been heavily involved in their construction, and use them extensively in the analysis of my thesis. They are described in much greater detail in Chapter 3.

The first, the RECONS 25 pc Database (§3.2), is a major RECONS effort that encompasses a large number of other researchers, and aims to build a successor to the Catalog of Nearby Stars (Gliese & Jahreiß 1991). It will play a large role in multiple PhD and undergraduate thesis projects.

The second, the RECONS Parallax Database (§3.3), is an attempt to locate all the

trigonometric parallaxes (apart from *HIPPARCOS*) published since the monumental Yale Parallax Catalog van Altena et al. (1995, §2.1.5.1). Its sole purpose (at the moment) is to improve the contents of the RECONS 25 pc Database.

Finally, I used many of the same techniques and experience from the construction of the RECONS 25 pc Database, as well as the RPD itself, to build a sample of young stars. This database was used to provide context for my youthful discoveries (Riedel et al. 2011, §5.4, and §5.5). Thus far its most notable use has been in the empirical young association isochrones (§2.2.5) though I hope to expand it for other uses.

## CHAPTER 3

### NEARBY STAR DATABASES

To fully understand the importance of nearby star discoveries requires some manner of statistical comparison to known nearby stars, and for that there is no better sample than the Solar Neighborhood itself. Placing my many young discoveries in §5.5 into context requires a comparison with samples of main-sequence stars and young stars.

The benefit of a dedicated, carefully vetted database over a large catch-all database like SIMBAD is the individual attention given. SIMBAD gives a few parameters (RA, DEC,  $\mu$ ,  $\pi$ , *BVRIJHK*) of varying quality and source. Only a few of those are searchable, and the rest of the data is hidden behind an enormous and comprehensive series of links to published literature. A dedicated database can cut out large amounts of work for someone interested in a reliable sample of nearby stars by providing reliable numbers and figures in one place.

#### 3.1 25 pc Precursors

The motivating reasons for a 25 pc database are largely statistical, with many applications. Studies of the IMF (via the CMF) need some idea of what to predict – the faintest stars are easiest to see nearby, so the most complete sample (statistically) will be nearby stars. Researchers with some new and novel kind of star need to be able to quantify just how unusual it is. Researchers wishing to calibrate the distance ladder or other stellar relations will need good data to do so – again found within regions close enough to measure with parallaxes. One other argument, now more valid than it has perhaps ever been in history, is that finding *nearby* exoplanets is exceedingly important if we are to ever visit or colonize

one. By the same token, the study of nearby stars for their affect on our Solar System – by close passes – is extremely important.

Cutting out such small samples is not without its drawbacks. Within 25 pc there may be only  $\sim 6000$  systems, none of them O-type and only one B-type star (Regulus). With the scale height of the Galaxy measured around 300 pc, and its diameter at least 30,000 pc, a 25 pc spherical volume will contain fewer than  $1 \times 10^{-7}$  of the constituents of the Galaxy, no information about the spiral arm structure, and minimal indication of the scale height of the Galaxy. Of course, in bygone ages when parallaxes were only accurate to tens of milliarcseconds, even measuring 25 pc (40 mas) was pushing the limits of accurate measurements.

### ***3.1.1 The Catalog of Nearby Stars***

The sample most commonly in use today is the Catalog of Nearby Stars, Third Edition (preliminary) by Wilhelm Gliese and Harmut Jahreiß (1991) (hereafter CNS3p). It is the source of the Gl and GJ prefixes attached to many nearby stars. It was not the first such list, but it has been the most successful, starting with the first edition of 915 systems within 20 pc in 1957, eventually expanded over the years to 22 pc (Gliese 1969) and then 25 pc (Gliese & Jahreiß 1991), with additional contributions out to 25 pc by Woolley et al. (1970).

The 1991 preliminary catalog included 3803 entries for objects, 1388 of them unnamed by Gliese, Jahreiß or Weilen. Later, the Centre de Donnes in Strasbourg invented GJ numbers exceeding 3000<sup>1</sup>. Thanks to the ubiquity of the SIMBAD and VizieR databases, these

---

<sup>1</sup>Gliese names are notoriously baroque, which probably comes with 40 years of evolution. Unfortunately, this makes it difficult to figure out at a glance how many systems there are in the catalog.

have become de-facto standard ways to refer to these stars. For their parts, Gliese and Jahreiß recommended using other names- generally Luyten's. As Gliese died in 1993 and the available data changed considerably (the release of YPC in 1995 and the *HIPPARCOS* results in 1997), a final version of the Third Edition has never been published. There is, however, an online version of CNS hosted by the Astronomisches Rechen-Institut Heidelberg (ARI), which I refer to as ARICNS<sup>2</sup>.

The Catalog of Nearby Stars, in all versions, included stars with photometric and spectroscopic distance estimates, as well as a variety of parallax errors (with some judicious care; Gliese (1969) notes that he excluded several known members of the Pleiades whose low quality mean parallaxes erroneously put them within 22 pc). With the exception of the occasional astrometric or spectroscopic binary, The Catalog of Nearby Stars is a one-object-per-line table, with systems identified by Gliese name and component ID. Systems

---

The 1957 catalog lists 915 systems in increasing B1950 right ascension order, with A and B designating components. In the 1969 second edition, Gliese used decimal points to insert more systems (Gl 87.1AB are between Gl 87 and Gl 88 in B1950 right ascension, and unrelated to either). The new systems in the 1979 update have GJ prefixes and restart their numbering at 1001 (stars with reliable parallaxes) or 2000 (stars without reliable parallaxes). "GJ" has largely supplanted "Gl" for all CNS stars.

1,388 entries in CNS3p are marked NN (no name); by 1997, common usage (and CDS Strasbourg) settled on renumbering all the new stars by line - all GJ 3000+ names are artificial, and each refers to a *star*, not a system. Note that the original system did not work out so well: famous multiples with different names include Gl 49/51; Gl 264/Gl 264.1AB; Gl 559AB/Gl 551= $\alpha$  Cen AB and Proxima; Gl 643/644ABCD; Gl 799AB/803=AU Mic/AT Mic; Gl 879/881=Fomalhaut and TW PsA.

<sup>2</sup>Jahreiß & Weilen, <http://www.ari.uni-heidelberg.de/datenbanken/aricns/> checked 2012 JUL 15. Jahreiß claims (in the 2001 NStars workshop) the final CNS3 was released in 1991, and CNS4 was released in 1997 with 3134 components to 2679 systems; ARICNS seems to have over 5800 entries and is therefore probably CNS4+working sample. This is borne out by the difficulty of using it: ARICNS exists as 5800 separate HTML files accessible by a set of index pages that divide the stars up in different ways, and some relevant information like Giclas and Ross names only exist on their respective index pages. ARICNS also introduces *five* new prefixes, all going by system and starting over from 1 each time: N1 (2055 systems), N2 (111 systems), NV (215 systems), N3 (10 systems), and NH (215 systems). N1 contains all 1388 no-name stars from CNS3p and may have been the final CNS3 additions; it's not clear what the rest are, and all of the stellar samples named via the new prefixes contain large numbers of stars not even remotely close to being within 25 pc.

are included based on a trigonometric parallax, photometric parallax, and/or spectroscopic parallax larger than 39 mas (25.6 pc) to increase the likelihood that all stars within 25 pc (40 mas) have been included. There is also one entry for the Sun, which contains an apparent and absolute  $V$  magnitude and a few colors.

CNS3p contains B1950 positions, two parallaxes (the trigonometric parallax where available, and the catalog's adopted parallax, which is always the trigonometric parallax when the error is less than 14%, otherwise a photometric or spectroscopic one), proper motions and position angles, radial velocities, spectral types (a mix of MK system, original HD catalog classifications, and estimates by Luyten),  $V$  magnitudes and an assortment of colors ( $B - V$ ,  $U - B$ ,  $R - I$ ) on the Johnson-Kron system, computed UVW space velocities (with U toward the Galactic center), an assortment of names (HD, Durchmusterung, Giclas, LHS, other) and brief remarks. ARICNS additionally contains positions in J2000 E2000 and B1900 E1900 epochs and equinoxes, proper motion broken into RA and DEC, and *HIPPARCOS* data in the form of names and unformatted table entries from [Perryman et al. \(1997\)](#).

Only the parallaxes are quoted with errors, though most important data are accompanied by a remarks column that pertains to quality or, occasionally, source; the photometry column also contains a specification for joint magnitudes. There are no references to source publications for any of the data except as may be included in the remarks. Information about multiple systems is relegated to the remarks as well; generally the separation and position angle (or orbital period) is given in the B component's note, while the alternate name and delta magnitude is given in A component's note.

### 3.1.2 NStars

The NStars project (1998-2001 or 2006) was a NASA Ames Research Center project (lead by Dana Backman and including Todd Henry) allied to the now-defunct Terrestrial Planet Finder and Space Interferometer mission (SIM) working groups. It was meant to provide the target stars for the SIM/TPF survey of nearby stars, with the intent to find planets. It differed from CNS in several key ways. Its data quality requirements were higher: no photometric or spectroscopic parallaxes, only stars with good trigonometric parallaxes were to be considered, and only high quality data from those stars were to be considered. It was also a working group dedicated to conducting new research to fill in the database – resulting in publications of *new* data on nearby stars such as Gray et al. (2003), Lépine & Shara (2005) and Jao et al. (2005). It is also responsible for CTIOPI's focus on nearby stars in the southern sky.

The NStars Database was ultimately a strict one-object-per-line list of 2633 entries for 2028 systems by a count of my 2009 extraction. The last published account is 2011 systems given in Henry et al. (2002), or 1832 systems if the more stringent <10 mas error limit of the RECONS 25 pc Database is applied. NStars presented J2000, E2000 coordinates for all resolved objects, proper motions and position angles to the milliarcsecond, incomplete Johnson-Kron-Cousins photometry and spectroscopy for most star systems, a wide variety of names, and parallaxes (within 25 parsecs, greater than 40 mas). The initial plans, though unrealized, were going to include radial velocities, *vsini*, abundances, asteroseismology, photometric variability, X-ray detections, orbital elements, a wide variety of thermal

and sub-mm photometry, and actual spectra for each object searchable in the SQL database (Backman et al. 2001), along with finder charts.

Unfortunately, NASA funding dried up in 2001 and the database part of NStars was moved to Northern Arizona University, where it was available online<sup>3</sup>. The last major addition was a compiled table of UBVRI values from Justin Cantrell, which was never actually incorporated into the database. Most troublingly, somewhere between 2001 and 2009, the fields in the actual NStars database (as extracted by me in March 2009) were truncated to two decimal places, rendering much of the information useless.

NStars got little professional use (one of the very few is NEXXUS2<sup>4</sup>, itself unpublished). NStars lives on in both Neil Reid's work (i.e. Reid et al. 2007, though limited to 20 pc) and in the amateur community (thanks to Jerry Blackwell and the Near-By Stars Observatory), where one enthusiast, Ken Slatten, has begun providing his own list of corrections and additions NStars to interested parties, including NEXXUS2 (and the RECONS 25 pc Database).

### 3.1.3 NSted

The NASA Stellar and Exoplanet Database (NSted) was set up by the Michelson Science Center/IPAC after NStars ended, and largely focused on the Exoplanet Database part of their mandate. One of the most important datasets on the stellar side was the Stauffer et al. (2010) catalog of accurate coordinates for all CNS stars. Unfortunately, NSted only ever included the Perryman et al. (1997) *HIPPARCOS* catalog parallaxes, and thus had only 1549

<sup>3</sup>[http://nstars.nau.edu/nau\\_nstars/index.htm](http://nstars.nau.edu/nau_nstars/index.htm) (site now defunct)

<sup>4</sup><http://www.hs.uni-hamburg.de/DE/For/Gal/Xgroup/nexxus/index.html> checked 2012 JUL 15

systems within 25 pc, making it an inferior source to NStars or CNS itself for population studies, despite occasionally being used for such. In December 2011, NSted became the NASA Exoplanet Archive, dropping the stellar portion entirely.

### 3.2 The RECONS 25pc Database (RECX25)

The RECONS 25 pc Database (internally, RECX25<sup>5</sup> or RECons eXtended to 25pc) grew out of a number of events in the RECONS group. CTIOPI had originally started as a parallax observational campaign to provide NStars with new targets, and despite its success, the astronomical community continues to use the Catalog of Nearby Stars, now 20 years out of date. Todd Henry is still maintaining an exhaustive list of all stars within 10 pc, something that actually predated the NStars effort (Backman et al. 2001). Most RECONS students' thesis samples involved stellar samples out to at least 25 pc, beyond the 10 pc outer limit. Not only does my thesis extend out beyond 25 pc, I spent 2009 attempting to rejuvenate the NStars database for a Planetary Sciences class project and this thesis work. Aside from adding in the UBVRI table and Gray et al. (2003, 2006) spectral types, I had done massive cleanup of some of the more confusing aspects of NStars, but making it all trustworthy again is an enormous task. Accordingly, when Todd Henry, John Subasavage, and Wei-Chun Jao met with Deepak Raghavan to work on modernizing our internal databases, their prototypes were also made with the thought of a publicly available 25 parsec database in mind.

---

<sup>5</sup>and only internally; the name RECX has been taken by “ROSAT  $\eta$  Chameleon X-ray source” stars (Mamajek et al. 1999), of which there are 19.

### 3.2.1 Design

RECX25 is intended to contain basic astrophysical information on every component of every star system ever reported to be within 25 pc of the Sun by trigonometric parallax, divided into three categories of quality:

- **VETTED:** Systems with weighted mean parallaxes greater than 40 mas (within 25 pc) and with weighted mean errors less than 10 mas. The error cutoff is not based on a fractional error because the reliability (though not necessarily usefulness) of a parallax is best described in terms of the actual observable angular measurement.
- **FLIMSY:** Systems with mean parallaxes greater than 40 mas but errors larger than 10 mas, which (as explained above) we deem to be unreliable. Some are genuinely nearby stars, many are not.
- **BOOTED:** Systems with mean parallaxes less than 40 mas, that were at least once reported to be greater than 40 mas. This is largely for posterity, so researchers can still find systems that were once considered 25 pc objects.

At this writing, like the 10 pc sample curated by Todd Henry, RECX25 is a one-entry-per-object flat text file, with columns for data. The concept here is that, apart from parallaxes, only one best value will be used.

At the moment RECX25 keeps track of the following:

- Coordinates

Sexagesimal Guide coordinates (best source, usually [van Leeuwen 2007](#))

Decimal 2MASS ICRS coordinates and epoch (Julian Date) (Skrutskie et al. 2006)

Proper Motions and Position Angles (best source, usually van Leeuwen 2007)

Parallaxes (separated for bookkeeping purposes):

Weighed Mean Parallax and source key

individual parallaxes: YPC (van Altena et al. 1995), HIP97 (Perryman et al. 1997)<sup>6</sup>, vLe07 (van Leeuwen 2007), *HIPPARCOS* re-reductions (see § 3.3.2), RECONS/CTIOPI, Other (see §3.3.1)

- Photometry

Guide  $V$

SuperCOSMOS  $B_J R_1 R_2 I$

Johnson  $UBV$

Kron-Cousins  $RI$

2MASS  $JHK_s$

- Spectroscopy

Spectral Type

- Multiplicity

Real Component ID

Number of Components

---

<sup>6</sup>for posterity only; values from the new reduction by van Leeuwen uniformly supercede the original

Hierarchical Key

Separation and Position Angle

Delta Magnitude with filter

- Names

Preferred Name

GJ, LHS, HIP, YPC, variable, HD, Durchmusterung (BD/CD/CPD), 2MASS, other

- Notes (not in the main table)

References are given explicitly for most data values. The only data for which we currently record multiple values are the parallaxes; the table currently supports up to 20 values. Parallaxes from any member of the system are applied to all members of the system<sup>7</sup>, and combined to form weighted mean system parallaxes. Care has been taken to make certain that datasets do not count more than once, as that would unfairly bias the results. For instance, RECONS has occasionally re-published parallaxes if the solution changes noticeably (e.g. GJ 633 in Riedel et al. 2010). The reduction in the older paper is flagged as obsolete and not included in the weighted mean, as that would unfairly bias the parallax toward the RECONS data. In the same way, the original *HIPPARCOS* parallaxes in Perryman et al. (1997) are included in the table, but they are uniformly superceded by the new van Leeuwen (2007) values.

---

<sup>7</sup>Currently, the only multiple system we do *not* combine into a single weighted system mean parallax is  $\alpha$  Centauri: Proxima Centauri ( $768.85 \pm 0.29$  mas) is  $17\sigma$  closer than  $\alpha$  Centauri AB ( $747.23 \pm 1.17$  mas). Gaia will almost certainly resolve more systems.

Proper motion and position angle are taken from the source of the parallax (HIP, RECONS, YPC, other), LSPM (Lépine & Shara 2005), or UCAC2 (Zacharias et al. 2004) (in that general order). Proper motions for companions are assumed to be the same unless we have specific astrometry (from parallax sources) that says otherwise. Although there are multiple sources of proper motions, we will *not* be combining them as we do parallaxes; most proper motion catalogs are built from similar sources (e.g. *HIPPARCOS*, Palomar Optical Sky Survey (POSS) and Science and Engineering and Research Council (SERC) plates), and are thus not actually unique. Eventually it is hoped that we will standardize on UCAC4 for anything not in *HIPPARCOS*, and have the entire database in the ICRS reference frame. Accurate coordinates (and their precise epoch in Julian Date) are taken from 2MASS (Skrutskie et al. 2006). Eventually the goal will be to process each star to Epoch 2000, ICRS Equinox using this 2MASS position and a good proper motion.

*UBVRI* photometry is currently either unfiltered white  $Hpmag$  (a proxy for  $V$ ) from *HIPPARCOS*, some kind of  $V$  from YPC or *UBVRI* from a clear hierarchy of trusted sources starting with Bessell (1990a), various papers by Weis (1993, 1996) (which use the Kron-system  $RI$ ), our own photometry, and papers by Koen and Kilkenny (e.g. Koen et al. 2002).

Right now, each star is indexed by its own rough coordinates and given at least one preferred name, generally the Gliese number or a Luyten name (L, LP, or LHS). The guide coordinates, rough magnitude, and preferred name are all usable placeholder of unknown provenance and uncertain quality, useful until we obtain better values (particularly in the

case of brown dwarfs and other stars not in the 2MASS catalog).

The Notes section is not part of the main table, but is a separate text file named with the HHMM+DDMM coordinates of the system; detailed notes and the notes in ARICNS will be included as needed. Already, several paragraphs of information have been laid out for the more complicated systems. This unrestricted method both reduces the clutter of the main database, and frees up the files for more useful details.

The Sun is included, as it was in CNS3p, ARICNS and NStars; this time it has a “parallax” of 206265” (1 AU) to allow proper calculations of absolute magnitudes and space positions; there are also entries for each planet in the Solar System.

### 3.2.1.1 Multiples

Multiple star systems present additional organizational difficulties. To start with, there are several common ways of naming their components. Although the more pedantic may care, common usage has validated the idea of extending existing names- there is no LHS 1749B in Luyten (1979a), but it is the accepted name for the companion to LHS 1749 as of Jao et al. (2003). RECX25 extends names in the same fashion. As for the method of assigning letters to primaries and companions, there are multiple different schemes on the subject. RECX25 (and RECONS) use the following<sup>8</sup>:

---

<sup>8</sup>The IAU and WDS ([http://ad.usno.navy.mil/wds/wmc/wmc\\_post191.html](http://ad.usno.navy.mil/wds/wmc/wmc_post191.html) checked 2012 JUL 15.) recommend **Hierarchical Order**, as used by (for example) Raghavan et al. (2010). If a currently-known companion is split into two, the name is split between the two stars (Aa, Ab), going by  $V$  magnitude brightness. If a new companion is found at a resolved separation from the first, it gets a new letter (B). With the example of the GJ 644 system, GJ 644 A=Aa, GJ 644 B=Ab1, GJ 644 D=Ab2, GJ 643=B, GJ 644 C=C.

The benefits are a sense of the system’s structure, and no ambiguity between resolved and unresolved components (it would be clear whether observations of GJ 644 B refer to GJ 644 B (Ab1) itself, or the combination (Ab) before it was split into B and D). Unfortunately, it comes with serious organizational problems: It can take up to  $n - 1$  letters to distinguish between  $n$  components. The names themselves offer

**Johnson  $V$  magnitude** (Where available). Component ID is purely a function of Johnson  $V$  magnitude in descending order. This does *not* always correspond to the component letter given by someone else- GJ 644C is the faintest component of the GJ 644/643 quintuple system, and is thus the E component by our reckoning. A slight variant would use bolometric luminosity, but given the way blackbody radiation works, the differences would be minor.

**Discovery Order.** WDS and CNS traditionally add letters by order of discovery. In this instance, GJ 644 C was the third component of GJ 644 discovered, and is the C component even though the later D component is brighter. When a new component is resolved, the brighter component assumes the original letter, and the fainter component takes a new letter. Stars that already had names are not renamed when they are discovered to be in a bound system (i.e., GJ 643). Exoplanets use this system, and the RECX25 database uses it when the  $V$  magnitudes of companions are not known.

RECX25 (and the RECONS 10 pc list) use another column that reports the number of components in the system- the primary is given a number, all other components get zeros. For instance,  $\alpha$  Centauri A is listed as '3', while  $\alpha$  Centauri B and Proxima Centauri are both listed with '0'. This enables a quick sort of the table to find out how many system primaries there are, and the multiplicity of each. Meanwhile, in a nod to hierarchical arrangement of the system, separations and delta magnitudes are given for the various components:  $\alpha$  Cen A and

---

no easy way to distinguish between stars and barycenters (Aa is a real star, Ab is a spectroscopic binary containing the stars Ab1 and Ab2) no indication that Aa is a real star and Ab is only a barycenter. The lowercase letters can be confused with planets (WDS recommends treating planets no differently from stars, but this has not caught on - perhaps forcing letters would solve this (AAA, ABA, ABB, BAA, CAA) but this is not the system advocated by the IAU). One-object-per-line tables are not conducive to separately storing information that applies to an unresolved multiple anyway.

B list the A-B separation; Proxima Centauri lists the A-C separation and delta magnitudes (relative to A). Brown dwarfs, white dwarfs, and stars are considered components, planets are counted separately.

Coordinates and magnitudes are contingent on a resolved multiple. As the resolution limit of 2MASS is roughly  $3''$ , stars with smaller separations are generally unresolved (although individual *UBVRI* photometry may be resolved). In the unresolved case, the coordinates and magnitudes are applied to the more luminous of the pair (magnitudes are given a “J” to denote their joint, convolved status); the secondary is given “no data” entries in those fields. In the future, multiples may be deblended where adequate information exists, but this has not been done yet.

### ***3.2.2 Initial Steps***

In August 2010, RECONS began from scratch, but with the experience of NStars and a far greater understanding of how to construct the database of nearby stars, brown dwarfs, and planets. Like NStars, we started with the Yale Parallax Catalog (van Altena et al. 1995), as the vast majority of nearby stars can be found there. To this we added the *HIPPARCOS* catalog. Where NStars folded in the original *HIPPARCOS* reduction, RECONS began with the new van Leeuwen (2007) *HIPPARCOS* re-reduction. RECONS also has the benefit of all our published parallaxes (Jao et al. 2005; Costa et al. 2005, etc.) which added a sizable amount of systems.

Angelle Tanner and I independently cross-matched YPC and the new *HIPPARCOS*, her by automation and I by hand (later, I also did an automatic cross-match). The first step

was to merge the YPC and re-reduced HIPPARCOS catalogs, as they contain  $\sim 90\%$  of the currently known systems. Accordingly, the initial work involved extracting and formatting the lists to be identical; sorting the lists together, and sifting them manually in GNU *emacs*. If a match was discovered, I merged the lines, overwriting YPC information with HIPPARCOS information; the only information from YPC that survives a match is the list of names (including YPC ID) and the YPC parallax.

This task was made difficult by errors in YPC (which was, again, attempting to homogenize an enormously heterogeneous dataset); sometimes coordinates for stars were off by arc-minutes, and occasional typos in the names or coordinates made it worse. There were additional difficulties matching up the correct set of components to each other, which often required paying attention to the  $V$  magnitude, proper motion, or other sources of information about the stars. While there was no hard limit (this being a by-hand sort), the rough parameters used were: match to within  $\pm 30''$  in either RA or DEC;  $V$  within 0.2 mag, proper motion to within  $0.1'' \text{ yr}^{-1}$ , position angle to within  $10^\circ$ . Leniency was granted in the more obvious cases, under the assumption that, for example, there would not be more than one  $4^{\text{th}}$  magnitude star moving at  $2'' \text{ yr}^{-1}$  within a few arcminutes, and so on. Companions often appeared as discrepancies in  $V$  magnitudes (or multiple matches in the same catalog). The sorting and final list production was done by October 2010.

The nagging issue here, however, is that one cannot simply download a list of all stars within 25 pc in both catalogs and match them up. Some stars do appear in the other catalog, but not within 25 pc. For instance, YPC and the original *HIPPARCOS* (Perryman et al.

[1997] put Mizar and Alcor within 25 pc; the new *HIPPARCOS* (van Leeuwen [2007]) does not<sup>9</sup>. The second phase of the sort involved running the entire list of coordinates from the first phase through the VizieR versions of YPC and *HIPPARCOS* to find parallax matches *not* within 25pc to stars within 25pc. This was finally completed in November 2010.

The resulting list had good parallaxes, but lacked companions, and lacked stars added by more recent trigonometric parallaxes. All RECONS parallaxes (for new and existing entries) were quickly added to this final table, along with white dwarf systems from the DENSE project<sup>10</sup>. Jen Winters added the RECONS Parallax Database (see §[3.3]) in stages, starting with trigonometric parallaxes published between November 1995-January 2000, then 2000-2005, and finally 2005-2011. Angelle Tanner folded in a table of values from [Stauffer et al. (2010)] that provided accurate coordinates and GJ names for all systems in any public version of the Catalog of Nearby Stars, as well as additional companions.

At this point, the table was separated out into the three quality sections (VETTED, FLIMSY, BOOTED), plus an additional “confusing” section for entries that proved particularly challenging.

2MASS data (astrometry and photometry) was blindly (closest-entry) extracted from VizieR for the entire sample, and Justin Cantrell’s 2006 NStars photometry list was folded in (creating companions where photometry existed for them). I extracted the list of known verified planets from the Exoplanet Data Explorer<sup>11</sup>, a more thoroughly vetted list than Jean

---

<sup>9</sup>With a weighted mean parallax of  $39.90 \pm 0.13$  mas, it is still possible they are within 25 pc, though new measurements to settle the question will be difficult. There are few remaining instruments capable of measuring parallaxes for stars that bright.

<sup>10</sup>Subasavage, J.P. <http://www.denseproject.com>

<sup>11</sup><http://exoplanets.org/> checked 2012 JUL 15.

Schneider’s Extrasolar Planets Encyclopædia<sup>12</sup>. Finally, I downloaded all 5835 HTML pages that form ARICNS and extracted all the information I could with UNIX ‘grep’ statements; the resulting table and its notes formed a starting point for adding still more well-known companions – these are referred to in the database as CNS98.

Eventually, in June 2011, Ken Slatten was invited to GSU, and work began cross-comparing our extensive list of systems and companions with his database. The hour-by-hour folding in of companions identified in that search continues (largely by Jen Winters).

The confusing entries were eventually resolved by comparison to multiple catalogs, appeal to Occam’s Razor, and eventually the intervention of Ken Slatten, who resolved the last 7 problem cases. They usually resulted from multiple pieces of erroneous or contradictory information between two catalogs (switching the members of a binary by position and name, but not magnitude) or just plain misleading (e.g. the dozen proposed companions to Capella, of which only four are physically linked: Capella A=Aa, B=Ab=P, H, and L.) Another large chunk were members of the Pleiades and Hyades with erroneous parallaxes that put them within 25 pc, and terribly large errors that made them potentially match *many* members of the Pleiades and Hyades (all of which had similar proper motion vectors). The Pleiades and Hyades members were resolved by assuming more realistic distances of 133 and 38 pc (respectively) for the erroneous entry, and throwing out all “companions” with separations larger than 63,000 AU ( $\sim 1$  ly). The erroneously high-parallax entries were themselves kept, though, in the FLIMSY and BOOTED sections.

---

<sup>12</sup><http://exoplanet.eu/> checked 2012 JUL 15.

### 3.2.3 Current Status

There are currently believed to be 51 star systems within 5 pc of the Sun, comprising the Sun, 49 other systems with a stellar primary, and one system (UGPS J072227.51-054031.2, Leggett et al. 2012) composed of a single brown dwarf. This corresponds to a volume density of  $0.0974$  systems  $\text{pc}^{-3}$ . If this density is constant within a spherical volume with radius 25 pc, we expect 6375 systems.

The 51 star systems within 5 pc of the Sun contain 73 stellar, white dwarf, and brown dwarf companions in 5 triple systems, 12 binaries, and 34 single star systems (a 33.3% multiplicity fraction). The 51 star systems also contain 15 planets in 5 systems (9.8% planetary systems). We should expect similar multiplicity fractions within 25 pc if the 5 pc sample is large enough to be representative.

As of 2012 APRIL 11, RECX25 contains 3592 components in 2744 systems that have at some point been considered to be within 25 pc by a trigonometric parallax of any quality.

Within the VETTED sample (weighted mean parallax greater than or equal to 40 mas; error less than 10 mas), there are only 2872 components in 2089 systems<sup>13</sup>. As can be seen in Table 3.1 (and to a lesser extent in Figure 3.1), there is a substantial Declination bias in the distribution of nearby stars favoring the northern hemisphere, with no corresponding bias in Right Ascension.

Table 3.1: Breakdown of 25 pc systems. (2012 APRIL 11)

|            | 0-6h | 6-12h | 12-18h | 18h-0h | ALL |
|------------|------|-------|--------|--------|-----|
| +30 to +90 | 123  | 155   | 142    | 145    | 565 |

*Continued on next page*

<sup>13</sup>As of 2012 JULY 15, the VETTED sample contains 2971 components in 2124 systems.

Table 3.1 – *Continued from previous page*

|            | 0-6h | 6-12h | 12-18h | 18h-0h | ALL  |
|------------|------|-------|--------|--------|------|
| +00 to +30 | 139  | 140   | 154    | 136    | 569  |
| -30 to +00 | 144  | 111   | 135    | 110    | 500  |
| -90 to -30 | 125  | 100   | 98     | 132    | 455  |
| ALL        | 531  | 506   | 529    | 523    | 2089 |

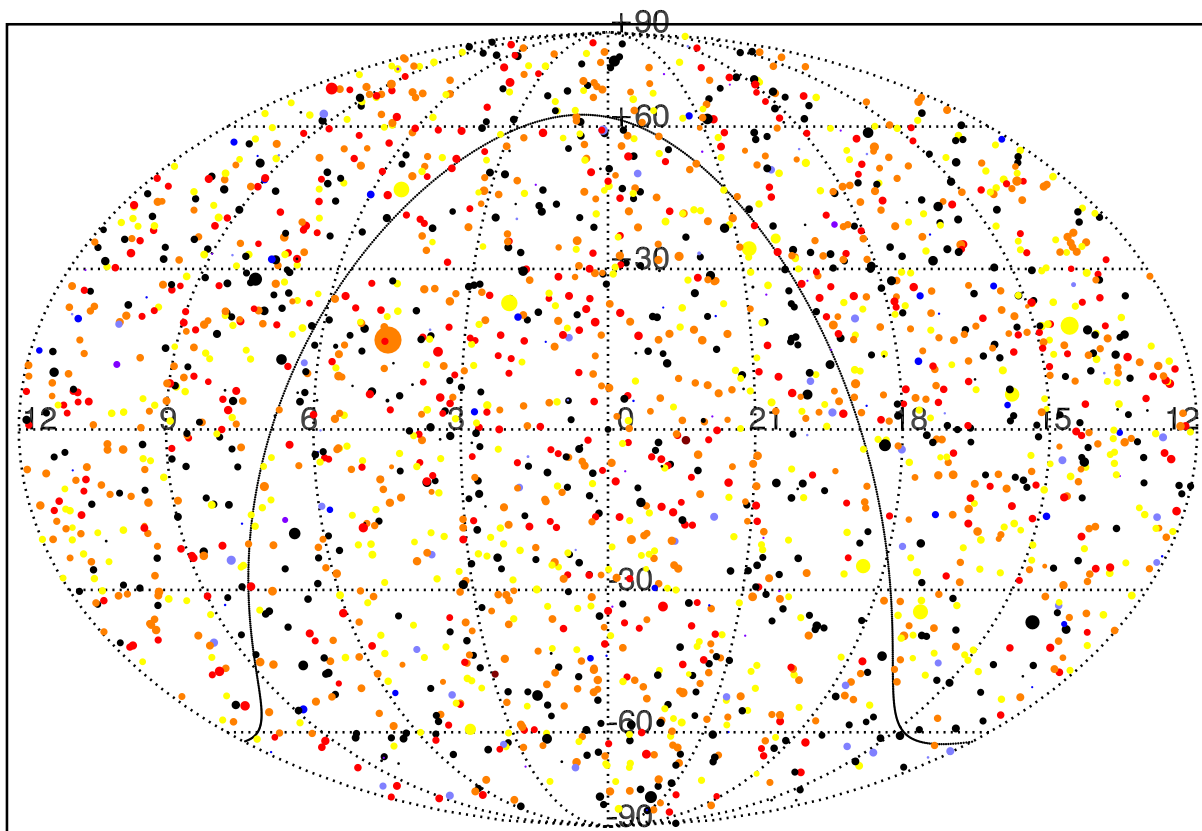


Figure 3.1: Mollweide equal-area projection of the RECONS 25 pc sample (2012 APRIL 11) with points approximately colored by spectral type of the primary (although G stars are black), and sized by evolutionary status of the primary. The black line is the Galactic plane. The point at RA=4h30, DEC+18 is the evolved star GJ 171.1 A= $\alpha$  Tau=Aldebaran. Only primaries with good  $V$  and  $K$  magnitudes (2028) are plotted.

An analysis of RECX25 in the depth dimension (Figure [3.2](#)) demonstrates that while the

number of systems within a given distance  $d$  should scale as  $d^3$  (thick line), the actual known values fall well short of that. At 10 pc, we expect 408 systems; at 15 pc, 1376; at 20 pc, 3262; at 25 pc, 6375. We are only complete within perhaps 6.3 pc (expected: 102 systems; known: 91; poisson error ( $\sqrt{102}$ ):  $\pm \approx 10$ ).

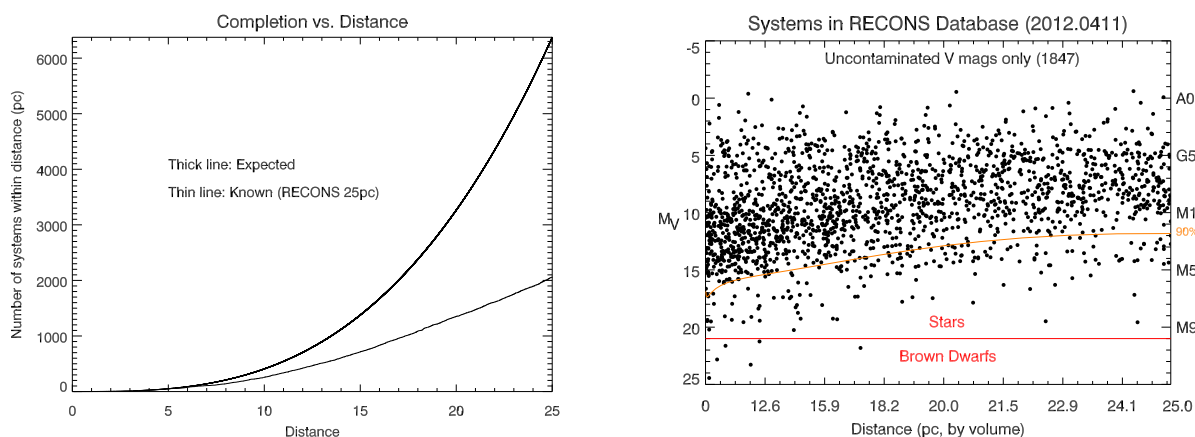


Figure 3.2: On the left, a traditional plot of the number density of stars within a given distance, which (under an assumption of equal volume) should follow a relation of  $n \propto d^3$  (thick line, fixed at 5 pc). The actual number of known systems (thin line) in the RECONS 25 pc sample (2012 APRIL 11) shows that we are potentially complete out to 6.3 pc, but no further.

So what are the missing stars? On the right, we plot distance (as  $d^3$ , for constant volume elements) versus  $M_V$  magnitude. Brighter than  $M_V=9$ , the density of stars is constant out to 25 pc, implying that constant stellar density (assumed throughout this dissertation) is correct, and that we are complete down to M0V. Below that threshold, we are massively incomplete at even the closest distances – there should be no gradient. 90% of all stars lie above the orange line, which would be flat if all stars within 25 pc had been identified.

Among the 2089 systems, 557 are multiple (461 binaries, 77 triples, 15 quadruples, 3 quintuplets [GJ 2069, GJ 564.1= $\alpha$  Lib<sup>14</sup>, GJ 644/643], and 1 sextuplet [GJ 278= $\alpha$  Gem=Castor])

<sup>14</sup>Zubenelgenubi= $\alpha$  Lib (GJ 564.1AB/GJ 563.4AB/KT Lib) is an intriguing system; Caballero (2010) argues the G-type star KT Lib is physically bound (and not merely another member of the Castor moving group) despite being at least 1 pc away. This may seem unreasonable, but given the probable combined mass of the other four members – which include at least one F-type and one A-type star – Caballero (2010) argue that the binding energy is higher than several other known binaries.

and 1532 are single. Given the general incompleteness of our companion searches, the multiplicity fraction of 26.7% (noticeably lower than the multiplicity fraction of the 5 pc subsample) should be considered a lower limit.

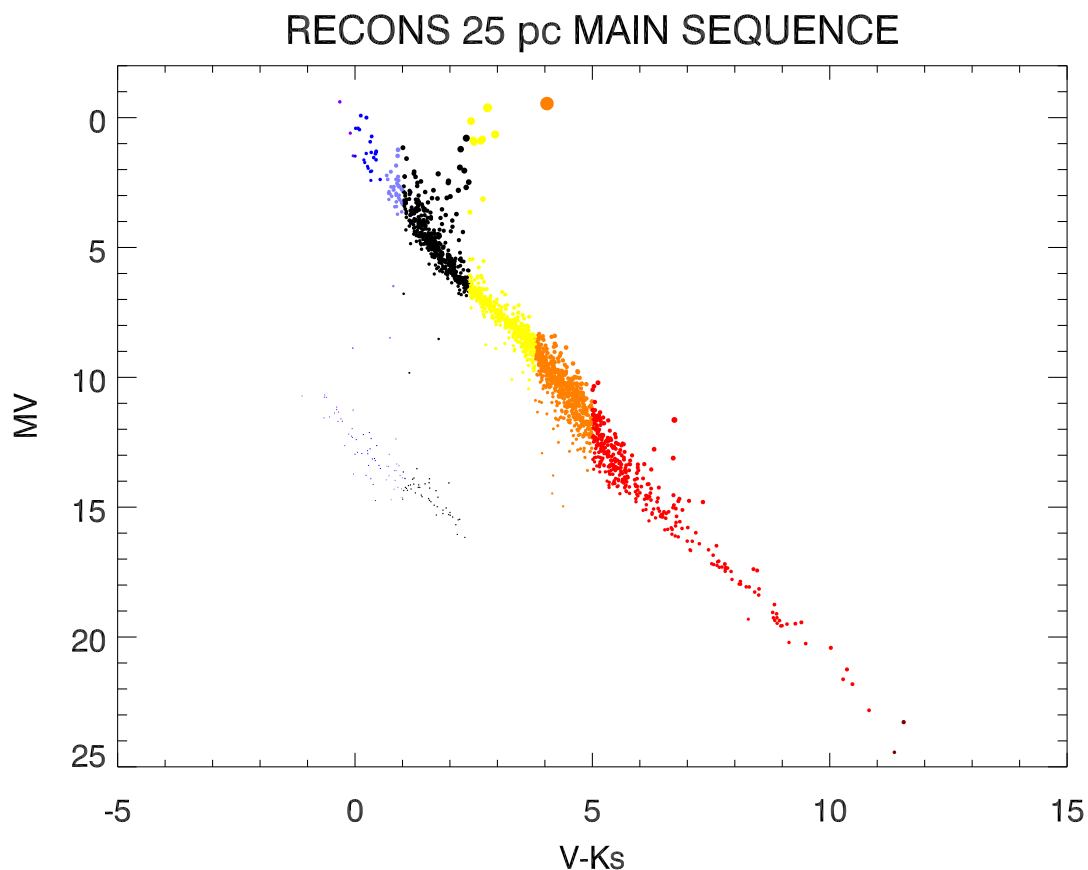


Figure 3.3: Color-Magnitude diagram for the RECONS 25 pc sample primaries (2012 APRIL 11) with points approximately colored by spectral type (although G stars are black), and sized by evolutionary status. Only primaries with good  $V$  and  $K$  magnitudes (2028) are plotted. Some unrecognized unresolved binaries undoubtedly remain.

Among these systems, there are 106 planets in 70 planetary systems (3.4% planetary fraction, far lower than the 5 pc sample); one eight-planet system (the Sun), one five-planet system (55 Cnc= $\rho$  Cnc=GJ 324), three four-planet systems (GJ 876, GJ 691, GJ 581),

five three-planet systems, six two-planet systems, and the remaining 54 systems only have one planet. Of these, the overwhelming majority have been detected with radial velocity searches; only GJ 1214 b (transit), Fomalhaut b (optical detection, possibly not real), and the planets in our Solar System were found by other means.

The most evolved star in the database is GJ 171.1 A= $\alpha$  Tau=Aldebaran (Figure 3.3), a K5III giant. The least evolved stars are TWA 22AB (Teixeira et al. 2009), twin M5Ve probable members of the 12 Myr old  $\beta$  Pic association. The bluest object with accurate photometry is WD0644+375 ( $V - K = -1.12$ ). The reddest object with accurate  $V$  photometry is DEN0255-4700 ( $V - K = +11.36$ ). The most massive object is  $\alpha$  Leo=Regulus A (B7V, Gies et al. 2008). The least massive object is Mercury. The most complex systems are the Sun (9 objects: 1 star, 8 planets) and 55 Cnc (7 objects: 2 stars, 5 planets).

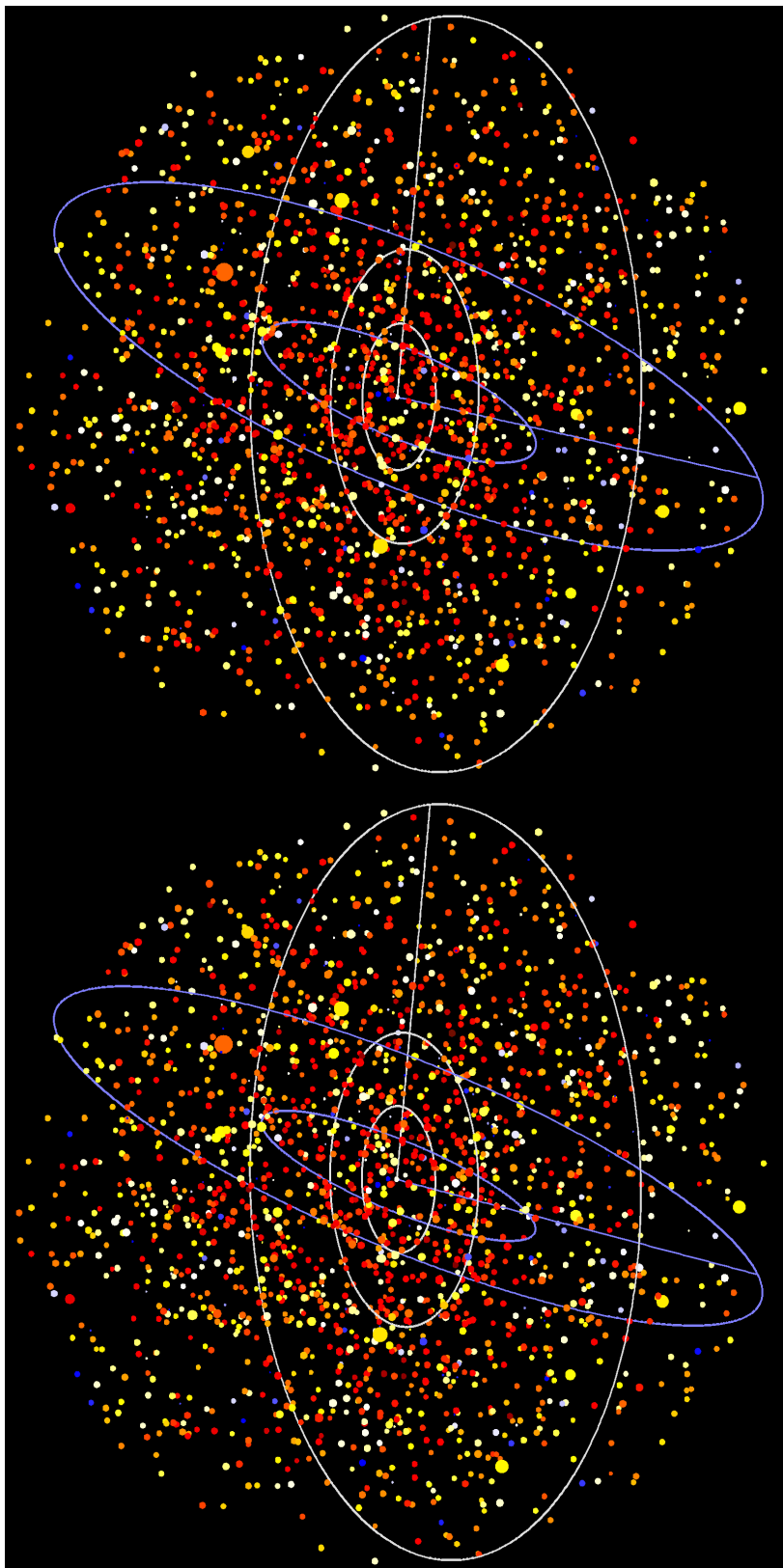


Figure 3.4: Cross-eyed 3D stereogram of the 25 pc sample, looking toward the Sun along a line of sight from RA=18h40m, DEC=+30d00m. Points are colored by spectral type and sized by luminosity class. The white circles are the celestial equator at 5, 10 and 25 pc, the blue line is the vernal equinox (RA 0h, DEC 0d). The blue circles are the Galactic plane at 10 and 25 pc, the blue line points toward the Galactic center. The red and yellow stars just “below” the Sun along the Galactic center line are GJ 699=Barnard’s Star and GJ 559= $\alpha$  Cen, respectively. One may also notice that the center of the plot is redder than the edges, again suggesting that most of the missing stars at greater distances are M dwarfs.

Most stars in the sample qualified before *HIPPARCOS*: 1152 systems (55.1%) have accurate (i.e., less than 10 mas error) parallaxes contributed by YPC. *HIPPARCOS* contributed the first accurate measurements for a further 648 systems (31.0%), while RECONS has contributed the first accurate parallaxes for more systems (149, 7.1%) than all other sources combined (136, 6.5%, including all *HIPPARCOS re-reductions*). The final four systems include the Sun, and three systems whose weighted mean error alone puts them within our sample, but no individual measurement does.

The highest relative parallax error (and highest absolute error) in the 25 pc list is HIP 63028, whose parallax of  $41.33 \pm 10.00$  mas gives it an error of 24.2%, or  $24.2 \pm 5.9$  pc. It is probably not within 25 pc both considering the Lutz-Kelker bias (§2.1.5.5), and the suspiciously large error for an *HIPPARCOS* parallax. The smallest parallax error (not counting the Sun) is GJ 144= $\epsilon$  Eri,  $311.22 \pm 0.09$  mas (which implies we know its location to within 192 AU); although the smallest absolute error is GJ 551=Proxima Cen, ( $768.85 \pm 0.29$  mas), whose location we supposedly know to within 101 AU. Whether either of those values are actually accurate is a matter of debate.

### 3.2.4 Next Steps

RECX25 is eventually planned to be an openly available relational SQL database (and officially renamed The RECONS Database), much the same as NStars was supposed to be; for the moment it is proprietary and very much unfinished. Some discussion has been made as to what properties could be calculated on the fly from the available data, and thus not actually stored in the database- the most obvious being the weighted mean parallaxes,

coordinates in other combinations of epoch and equinox, and photometric colors.

The database has already been designed (by John Subasavage, Wei-Chun Jao, Todd Henry, and Deepak Raghavan), and is separated into multiple tables by type of information. One advantage of using a relational database is the reduction of empty entries. Right now, there are 20 parallax slots for every star; at most 6 are actually used. The parallax table in the eventual database will eventually only record system ID/parallax pairs: if there are six reported parallaxes for a particular system, six entries in the parallax table will have that system's ID. In the same way, if only *VRI* information for a star exists, there will be only three entries in the photometry table, one for each filter. This enables more complicated after-the-fact processing, such as including multiple *VRI* filter datasets separated by reference, and selecting among them.

We will continue to gather astrometry and new members as parallax programs (including CTIOPI) publish more targets. Right now, proper motions (without accompanying errors) are a mix of RECONS (relative), YPC (relative), parallax papers (relative), PPMXL (absolute), UCAC2 (absolute), and HIPPARCOS (absolute). Eventually, we hope to replace them with all absolute proper motions (with errors), probably from UCAC4 and *HIPPARCOS*. Once Gaia releases results, its astrometry will likely supercede everything else in the database.

RECX25 photometry is currently incomplete and heterogeneous. It will be replaced with correct and correctly transformed photometry from our hierarchy of trusted sources (e.g. Bessell 1990a; Weis 1993; Jao et al. 2005; Koen et al. 2002). We will probably also

add photometry from other useful sources (the APASS survey with its all-sky Johnson  $BV$  and SDSS  $g'r'i'$  photometry; SDSS for higher-quality  $u'g'r'i'z'$ ; TYCHO-2 for Johnson  $BV$  photometry after the appropriate transformations). Eventually, LSST and Gaia photometry will provide further deep photometry to incorporate.

As yet, very little spectroscopic information has been added to the database, though we currently have a place to put spectral types. As with photometry, we have a trusted hierarchy of spectral type sources, including Richard Gray’s NStars publications (Gray et al. 2001, 2003, 2006), RECONS spectral types from Kirkpatrick et al. (1991); Henry et al. (1994, 2002), and the Michigan Spectral Survey catalogs (Reid et al. 1995; Hawley et al. 1996; Gizis et al. 2002). Conversations with interested parties suggest that the database should eventually include a wider variety of spectroscopically derived parameters (metallicities, temperatures, rotational velocities, radial velocities...) but these are far from settled.

Even though we have a “preferred name” column, we will need some sort of internal designation apart from line number to link stars into systems. History suggests that, even though we have a “preferred name” from elsewhere, researchers using the RECX25 database will simply use our catalog names whether we want them to or not<sup>15</sup>. Like RE-

---

<sup>15</sup>To quote Willem Luyten in his introduction to the second edition of the LHS catalog (Luyten 1979a): “The question of the proper designation of each entry is always a vexing one. Whenever possible, I have used *BD* and *CoD* reference numbers as I can see no point in coining new, and usually quite meaningless new “discovery” designations for stars contained in these two catalogues. Such practice leads to utter confusion... It seems quite certain – given the present prevalence of plagiarism – that many of the most interesting stars I have found in the Bruce and Palomar Surveys will be usurped, annexed and plagiarized... Such piracy is not only grossly unethical, it creates unnecessary confusion as well since it clutters up the literature with totally superfluous, and usually completely meaningless numbers... Against that day I have entered in the last column the original discoverer’s notation of *BD* and *CoD* stars such that at least then, future astronomers may realize who did the work, and who were the plagiarizers and astronomical shoplifters.”

It is perhaps worth noting that Luyten did not number the stars in his New Luyten Two Tenths catalog (Luyten 1979b) (or LHS 6000+ in Luyten 1979a), but someone else “helpfully” did it for him. Luyten’s 10+ other names, few of which he apparently intended anyone to use, clutter SIMBAD to this day.

CONS and NStars, RECX25 will have HHMM+DDMM system names based on the coordinates of the system primary (coordinates are the most fundamental and reproducible way to identify stars) in ICRS E2000 coordinates –  $\alpha$  Cen will be REC1439-6050, and Proxima will be REC1439-6050C, notwithstanding that its actual RA and DEC are 14h 29m –62d40m. Other historical names have not been thoroughly researched, but in addition to our currently-complete HIP, Gliese (courtesy of [Stauffer et al. 2010](#)), YPC and 2MASS identifiers, we intend to have a wide variety of other historical names (Luyten, Giclas, SCR, Lepine, Bayer/Flamsteed/Gould)

Ultimately, while one can envision a future researcher simply pulling data from the *HIP-PARCOS* and Gaia catalogs and calling it complete, the extra care I mentioned at the beginning still applies. The fact that the Catalog of Nearby Stars is still a frequently used research sample, 20 years after its release and 15 years after the release of the *HIPPARCOS* catalog, speaks volumes about the value of a properly-curated sample of stars (and their additional material).

### 3.3 The RECONS Parallax Database (RPD)

The Yale Parallax Catalog ([van Altena et al. 1995](#)) contains the sum-total of all annual trigonometric parallaxes reported in scientific literature, as of November 1995. *HIPPARCOS* has another  $\sim 1500$  relevant parallaxes. Trigonometric parallaxes continue to be reported, however, and the only way to get the best set of stars within 25 pc is to track down all of the publications.

Where YPC made a massive effort to remove systematic errors and re-weight parallax solutions, the RPD makes no attempt to correct the parallaxes or errors of various programs. The values published in papers are simply taken as-is, despite our reservations about some papers and authors – several do not correct parallaxes to absolute, several others do not say if they did or not. Ultimately, most recent parallax programs have published so few stars that corrections on the level of what YPC did would be impossible. Not counting *HIPPARCOS* re-reductions, 1071 stars have been measured in the past 16 years in 178 papers; most are single-star papers, while RECONS alone accounts for 279 of the parallaxes published with only 9 papers, and the largest paper, Riedel et al. (2010)<sup>16</sup>, with 67 parallaxes to 64 star systems (see § 5.2).

The RECONS Parallax Database properly exists in three parts: A list of all papers known to contain trigonometric parallaxes, with a check of whether they've been added to our tables; a table of all ground- and space-based parallaxes; and a table of *HIPPARCOS* re-reductions. The actual table of ground- and space-based parallaxes is rather informal, as we have only systematically collected information for stars within 25 pc. The table of *HIPPARCOS* re-reductions, on the other hand, is fairly complete. Inasmuch as the RPD only exists to feed the RECONS Database with new parallax data, its value and existence as an independent project are questionable. The RPD may never be published formally, though the list of known papers is already online<sup>17</sup>.

<sup>16</sup>Recently exceeded by Faherty et al. (2012), 70 parallaxes.

<sup>17</sup><http://www.chara.gsu.edu/RECONS/RPD.references.posted> checked 2012 JUL 15.

### 3.3.1 *Ground-Based and Space-Based*

This category essentially contains every parallax published using either a ground-based optical/infrared observatory, long-baseline radio interferometry, or Hubble Space Telescope parallaxes, mostly done with the Fine Guidance Sensors (HST-FGS), though several papers have used the Wide Field/Planetary Camera 2 (HST-WFPC2) or even the Advanced Camera for Surveys (HST-ACS). This section of the RPD was originally designed and curated by Jennifer Winters, though others (including myself) have added to it as well.

The list of papers contains many notable entries: the final publications of the Yale parallax program (Weis et al. 1999); the final McCormick Observatory (Virginia) parallaxes (Ianna et al. 1996); the (possibly) last publications from Allegheny Observatory (Gatewood & Coban 2009); the last (at least thus far) photographic plate-based parallax (Deacon et al. 2005b). Contained within the list are the first VLBI parallaxes Bradshaw et al. (1997) (which are typically accurate to  $10 \mu\text{as}$ ), and all HST parallaxes.

Other notable entries include Gatewood et al. (2001) and Gatewood (2005), both of which include ground-based *and* space-based parallax measurements, and Lucas et al. (2010), the only instance I'm aware of where two CCD-based sources of astrometry were combined in a parallax solution.

### 3.3.2 *HIPPARCOS re-reductions*

This category does not include the van Leeuwen (2007) re-reductions, as those were done from scratch. Rather, this category concerns the massive number of publications that have re-

analyzed Hipparcos Intermediate Data (HID) (van Leeuwen & Evans 1998) to obtain better parallaxes. These intermediate data evidently already have the raw transit scans reduced to absolute sky positions on the ICRS grid, but with no other processing done.

*HIPPARCOS* re-reductions generally fall into two categories: Stars with incorrect positions in the *HIPPARCOS* input catalog (if the star did not pass through the center of the astrometer's grid, the automated reduction pipelines had problems), and multiple star systems (where the orbital motion was often incorrectly modeled into the parallax or proper motion). The most famous *HIPPARCOS* re-reduction (and the only one used by the NStars team) was Söderhjelm (1999), who combined Hipparcos Intermediate Data with TYCHO-2 data and speckle measurements to re-calculate parallaxes to 205 nearby binary systems.

He was not, however, the only one. There were 240 systems with improved results included in the notes to the original *HIPPARCOS* catalog (Perryman et al. 1997). Many authors have published papers re-reducing *HIPPARCOS* data with constraints of known orbits (or, in Guillermo Torres's case, solving the entire 3D orbit, parallax, systemic radial velocity and proper motion at once, Torres & Ribas 2002).

Originally, I divided the papers into groups based on which of a short series of authors had worked on them (Dimitri Pourbaix, François Mignard, Valeri Makarov, and Guillermo Torres are on most re-reduction papers), with the intent to discern whose re-engineered solutions were more accurate, and which (if any) should be preferred over van Leeuwen (2007). Eventually, it was decided that more recent papers should supercede older papers, and *all* instances of individual attention and extra data should supercede the global solutions in

van Leeuwen (2007). In any event, van Leeuwen (2007) released new Hipparcos Intermediate Data, which have already been used in a paper by Ramm et al. (2009).

### 3.3.3 Problems

Not all papers can be smoothly incorporated into the RPD or RECX25.

Several *HIPPARCOS* re-reductions claim to have re-evaluated all the astrometry but do not publish the new values, or at worst only publish deltas between the old and new values—this is especially bad for Sozzetti & Desidera (2010), whose deltas are apparently relative to the original *HIPPARCOS* reduction and Intermediate Data, but did not explicitly say so.

Several other papers (Ianna et al. 1996; Bartlett et al. 2009; Khrutskaya et al. 2010) only published relative parallaxes. Ianna and Khrutskaya do include corrections to absolute, the absolute parallaxes need to be calculated explicitly.

Superseded values are occasionally tricky to deal with. Martinache et al. (2009) re-reduced the parallax data from Pravdo et al. (2004) (by reading values off a graph!) and thus supersedes Pravdo et al. (2004) despite no involvement from any of the authors of Pravdo et al. (2004). Tinney (1996) updates parallaxes from Tinney (1993) which were included in YPC; in those cases YPC has been made obsolete, and we assume Tinney (1996) has none of the systematics YPC corrected for. Ianna et al. (1996) is particularly difficult, as it updates McCormick observatory results for many stars that were already included in YPC as the mean of many observations, and thus supersedes only *part* of the published YPC value. It is unlikely that we will go back to the original YPC data (in Volume II) and re-run their mean parallaxes.

Most of the other confusing cases are statistical, orbital, microlensing (stereoscopic) or pulsar timing parallaxes, though Boden et al. (2006) still manages to confuse by deriving an orbital parallax using re-reduced *HIPPARCOS* data.

### 3.4 Young Stars Database

In order to have context for my young stars in Riedel et al. (2011) (§5.4) and §5.5, I have developed a smaller database of my own, using many of the methods and techniques I learned from the construction of the 25 pc database, as well as the parallaxes in the RPD.

The primary sources for the entries in my young stars database are Zuckerman & Song (2004) and Torres et al. (2008), with trigonometric parallaxes<sup>18</sup> sourced from *HIPPARCOS*, YPC, TW Hya parallaxes from Weinberger et al. (2011) and the RPD. Where no parallax was available, I use the estimated distances in the original source papers. Like the RECONS 25 pc Database, it is a one-object-per-line flat text database.

The young stars list (Figure 3.5) was originally designed to provide comparisons for my isochrone fits (§2.2.5) and kinematic analysis in Riedel et al. (2011). The database is thus driven toward the purpose of young star analysis, and is more specific but less comprehensive than the 25 pc Database. It tracks proper motions split into RA and DEC, space for radial velocities, *vsini* values, variability, X-ray data from ROSAT, and an entry for which association a given star belongs to. Every measured item (except variability)

---

<sup>18</sup>Unlike the generally kinematic distances in Zuckerman & Song (2004) and Torres et al. (2008), trigonometric parallaxes are insensitive to any accidental mis-identifications with associations. While adding kinematic distances to high-confidence members *would* improve the number of points used in the fits, there are very few known young M dwarfs in these associations.

has accompanying error, and all astrometric data are quoted in milliarcseconds rather than arcseconds. To save time in construction, the majority of my proper motions and  $BVJHK$  photometry are sourced from ASCC (Kharchenko 2001), a TYCHO-2 based catalog with additional entries from PPM (Roeser & Bastian 1988; Bastian & Röser 1993; Röser et al. 1994) and CMC11 (Copenhagen University Observatory et al. 1999), with 2MASS  $JHK$  provided via cross-match, and Johnson  $BV$  via transformations from Tycho  $B_{TYCHO}V_{TYCHO}$ . I have filled in additional data on members from 2MASS and RECONS where possible.

I anticipate expanding the database to include other useful comparative values, like  $H\alpha$  EW, lithium EW, activity parameters, and Na I gravity measures (§2.3); thus far all of my analysis has come from other sources.

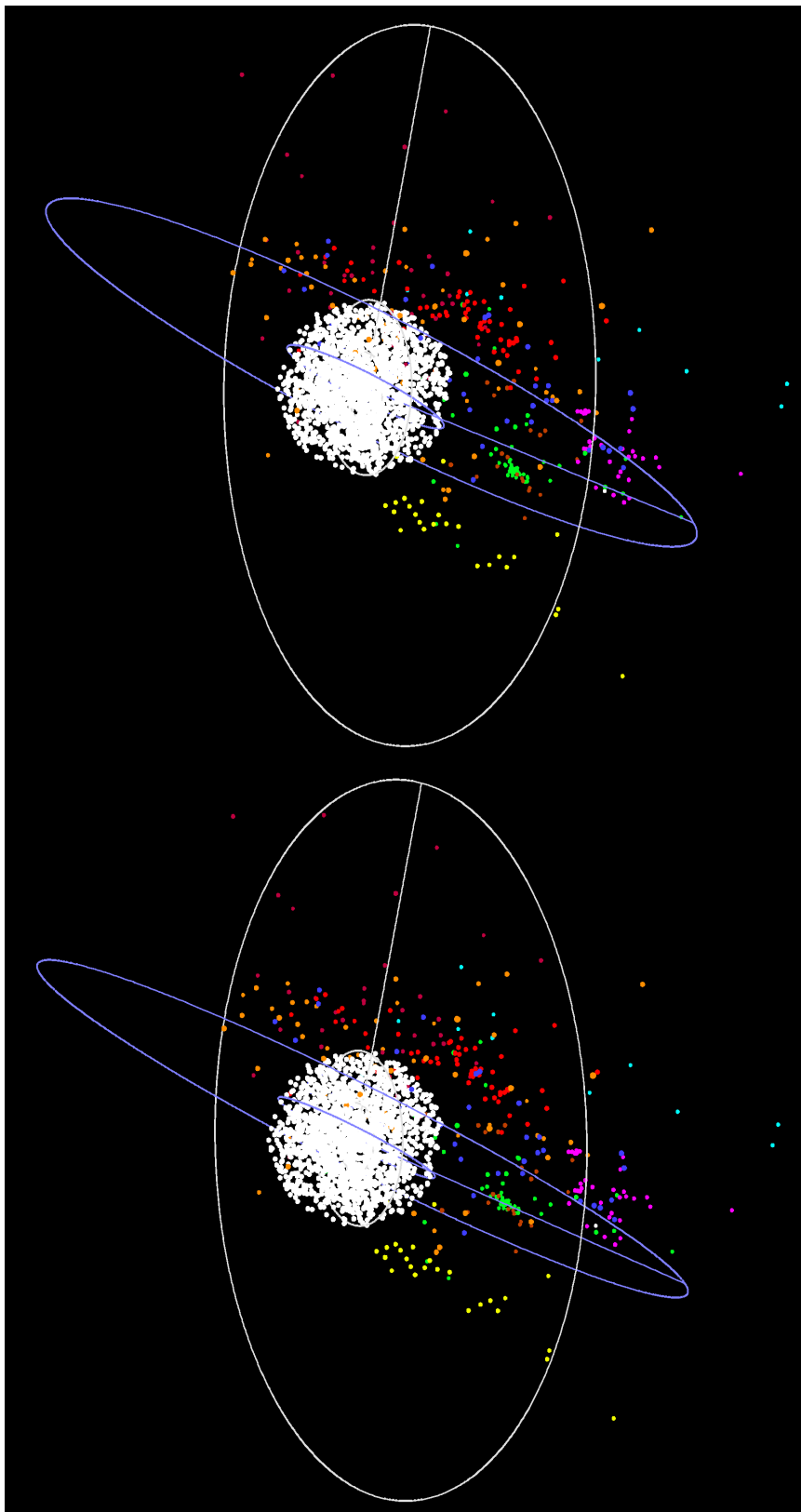


Figure 3.5: Cross-eyed 3D stereogram of nearby ( $\sim 100$  pc) young stars from Zuckerman & Song (2004) and Torres et al. (2008), as viewed along a line of sight from RA=19h20m, DEC=+30d00m. The white central ball is the RECX25 database (Figure 3.4), for scale and density comparison. The white circles are the equatorial plane at 25 and 100 pc, the blue line is toward RA=00h00m, DEC=+00d00m. The blue circles are the Galactic plane at 25 and 100 pc, the blue line is toward the Galactic center. Note how all the associations lie in sheets parallel to the Galactic plane. Points are coded by association:  $\epsilon/\eta$  Cha (6 Myr) is pink, TW Hydra (8 Myr) is yellow,  $\beta$  Pictoris (12 Myr) is blue, Octans (20 Myr) is blue. Tucanae-Horologium (30 Myr) is red, Columba (30 Myr) is purplish-red, Carina (30 Myr) is orangish-red, Argus/IC 2391 (40 Myr) is green, AB Doradus (125 Myr) is orange.

## CHAPTER 4

### TINYMO

The bulk of the discoveries in my thesis discussed in Chapter 5, both young and low-proper-motion, came from a novel search known as TINYMO (TINY proper MOtions) designed to specifically go after low-proper motion stars, which have never been studied as a population.

We expect such stars should exist, because there is no particular reason a star could not have a space motion vector pointing toward us. Simulations using realistic velocity dispersions (Figure 2.11, see also §2.4.3) suggest the number of stars with low proper motions within 25 pc may account for as much as 13.6% (nearly 1 in 7) of the total. These low proper motion stars are therefore a small but significant portion of the stars a complete 25 pc sample (the RECONS Database) should expect to include. Given that very few surveys have gone below the limit of “interesting” proper motion,  $0.18'' \text{ yr}^{-1}$  (set, effectively, by the New Luyten’s Two Tenths catalog (Luyten 1979b), though Luyten attributes it to the Royal Greenwich Observatory, who set the limit based on the likelihood that such slow-moving stars would *not* be a significant fraction of nearby stars), these stars have most likely never been recognized as nearby.

Using traditional proper motion search techniques to search for low proper motion stars runs into two rather serious problems. One, there is a finite limit to how well proper motions may be measured from any given source. Two, even distant background objects are moving at some level; even an accurate tiny proper motion (below a certain level) is useless as an indicator of proximity.

One method of finding nearby low proper motion stars is to throw out proximity criteria altogether and get parallaxes to every single star in the sky. *HIPPARCOS* observed every star in the sky brighter than  $V=7.3$ . ESA's followup to that mission, Gaia, is expected to observe every star in the sky from  $V=6$  to  $V=20$ , obtaining parallaxes to billions of stars in the process. These will most certainly be effective, but the time and effort expended is enormous.

Instead, we chose to use an alternative method of identifying potential nearby stars: the photometric distance estimate. RECONS has developed several photometric distance estimates (§2.2.5), and has been successfully relying upon them for years.

In particular, RECONS has been using the SuperCOSMOS Database (Hambly et al. 2001a) as a means for discovering new nearby stars (all designated SCR, or SuperCOSMOS-RECONS) for years, producing nine papers to date (Hambly et al. 2004; Henry et al. 2004; Subasavage et al. 2005a,b; Finch et al. 2007; Boyd et al. 2011a,b). As explained in §2.1.5.1, SuperCOSMOS has positions, proper motions, and up to 4-color photometry for 1.9 billion stars in up 4 epoch spanning 1949-2001, covering the entire sky to a depth of  $B=22, R_2=20, I=19$ , and is publicly available for searches via SQL query. As an astrometric source, we have found its proper motions accurate to  $0.02'' \text{ yr}^{-1}$ , and position angles accurate to  $3.9^\circ$  (Finch et al. 2007), as compared to *HIPPARCOS*. As a photometric source, we have found its colors accurate to 0.07 mag (Hambly et al. 2001b), and its resultant photometric distance estimates accurate to 26%.

Accordingly, the TINYMO search was conducted using the SuperCOSMOS Sky Survey

(Hambly et al. 2001a) to search for truly motionless stars in the southern hemisphere. This time, rather than relying on proper motions for identifying nearby stars, the empirical SuperCOSMOS  $BR_2I$  and 2MASS  $JHK_s$  plate photometry relations in (Hambly et al. 2004) were used to obtain distance estimates to these targets, with the intent to select stars within 25 pc. Color-color cuts were then used to refine the sample of potential 25 pc objects, and the best results were kept for confirmation using low-resolution spectroscopy, our more accurate CCD photometry and CCD photometric relations (§2.2.5), and (in the best cases) CTIOPI astrometry.

## 4.1 Survey Design

### 4.1.1 SQL query

RECONS has been using SuperCOSMOS as our primary sky catalog utilizing a special output catalog produced by Nigel Hambly to get around the fact that the generic catalog processing (as with many compiled sky catalogs) generally assumed stars have zero proper motion, and only looked within  $6''$  for matches (Hambly et al. 2001a) across plates. Stars with proper motions larger than  $0.2'' \text{ yr}^{-1}$  on a set of plates with an epoch spread of  $\sim 30$  years will move more than  $6''$ , and won't get crossmatched to their other appearances. The main SuperCOSMOS catalog thus contains multiple disconnected entries for high proper motion objects, a small price to pay – perhaps a hundred thousand badly-matched objects out of nearly two billion.

For the purposes of TINYMO, the main catalog is sufficient, provided we limit ourselves

to sources identified on all four plates. The variable epoch spreads between the plates result in a variable upper limit for proper motions that is above  $0.18'' \text{ yr}^{-1}$ , except in regions northward of  $-18 \text{ DEC}$ , where far older POSS-I E red plates were used. In those areas, the reliable upper limit is at least  $0.12'' \text{ yr}^{-1}$ .

The TINYMO survey was done in two pieces, the first (between 20h and 08h) by Dr. Henry in October 2007; the second (between 08h and 20h) by myself in May 2009. In both cases, the SuperCOSMOS Science Archive<sup>1</sup> was searched via SQL query for objects in the southern sky that:

**Appeared on all four plates.** This sets an upper proper motion limit as described above, as well as limits on color – the star could not be so red it did not appear in the  $B_J$  plate. This cuts out a number of cool and faint stars. This also cut out a small region of sky (roughly RA 16:00 to 16:20, DEC  $-10$  to  $-15$ ) where there is no  $R_1$  plate.

**Appeared to be single stellar sources by ellipticity and other quality parameters.** This cut out a large number of extragalactic and spurious sources.

**Are brighter than  $R_2 = 16.5$ .** The  $R_2$  magnitude limit allows for detection of stars with  $B_J=21$  and  $B_J - R_2$  colors as red as 6 (a brown dwarf), and matches the Giclas surveys (Giclas et al. 1979) as well as previous RECONS proper motion surveys.

**Were detected in 2MASS within  $5''$  of the weighted mean plate position.** The mean plate position recorded by SuperCOSMOS is weighted by the positional accuracy of each of the detections; the epoch of this effective plate position is usually around 1985 (Hambly, N.C. private communication, 2010), while the mean epoch of 2MASS is around

---

<sup>1</sup><http://surveys.roe.ac.uk/ssa/> checked 2012 JUL 15.

2000. Thus, any star moving less than  $5''$  in 15 years ( $\mu < 0.333'' \text{ yr}^{-1}$ ) will be matched to its 2MASS entry. The more stringent limit is thus the 4-plate-detection requirement, although requiring 2MASS entries does limit us to the 470 million targets in the 2MASS point source catalog [Cutri et al. \(2003\)](#).

**Are in the southern hemisphere, more than 10 degrees from the Galactic plane and 20 degrees from the Galactic center.** This removes the enormously reddened and crowded fields in the center of the Galaxy. In the second half of the TINYMO search we had to go back and eliminate three other small areas (RA 15:00 to 16:00, DEC +00 to  $-30$ ; RA 15:00 to 16:00, DEC  $-30$  to  $-60$ ; RA 17:00 to 18:00, DEC +00 to  $-30$ ) around the North Galactic Spur just outside the bulge that contained as many potential nearby stars as the rest of the sample combined (see [Figure 4.1](#) and [Figure 4.2](#)). We did not, however, remove the Large and Small Magellanic clouds. Cutting out these areas of the sky (and the one removed by the missing  $R_1$  plate) reduces the area covered by TINYMO to 16214 square degrees, or 39.3% of the sky.

The limit of 2MASS is effectively  $JHK \approx 15$ . SuperCOSMOS goes to  $B_J = 21$ , and we have set our magnitude cutoff at  $R_2 = 16.5$ , which roughly means our faintest  $V$  (assuming the average of  $B_J$  and  $R_2$  is  $v$ ) is  $v=18.75$ . The limiting magnitudes for M dwarfs are all set by the  $R_2$  filter. For an M0V star (see [Appendix A](#)) ( $M_{B_J} = 10$ ,  $B_J - R_2 = 2.3$ ,  $B_J - K = 4.5$ ) corresponding to our cutoff at  $R_2 = 16.5$  are  $B_J = 18.8$ ,  $R_2 = 16.5$ , and  $K = 14.3$ . This implies a limiting distance of 630 pc. For an M9.0V star ( $M_{B_J} = 20.4$ ,  $B_J - R_2 = 3$ ,  $B_J - K = 10.2$ ) the magnitude limit is  $B_J = 19.5$ ,  $R_2 = 16.5$ , and  $K = 9.3$ ,

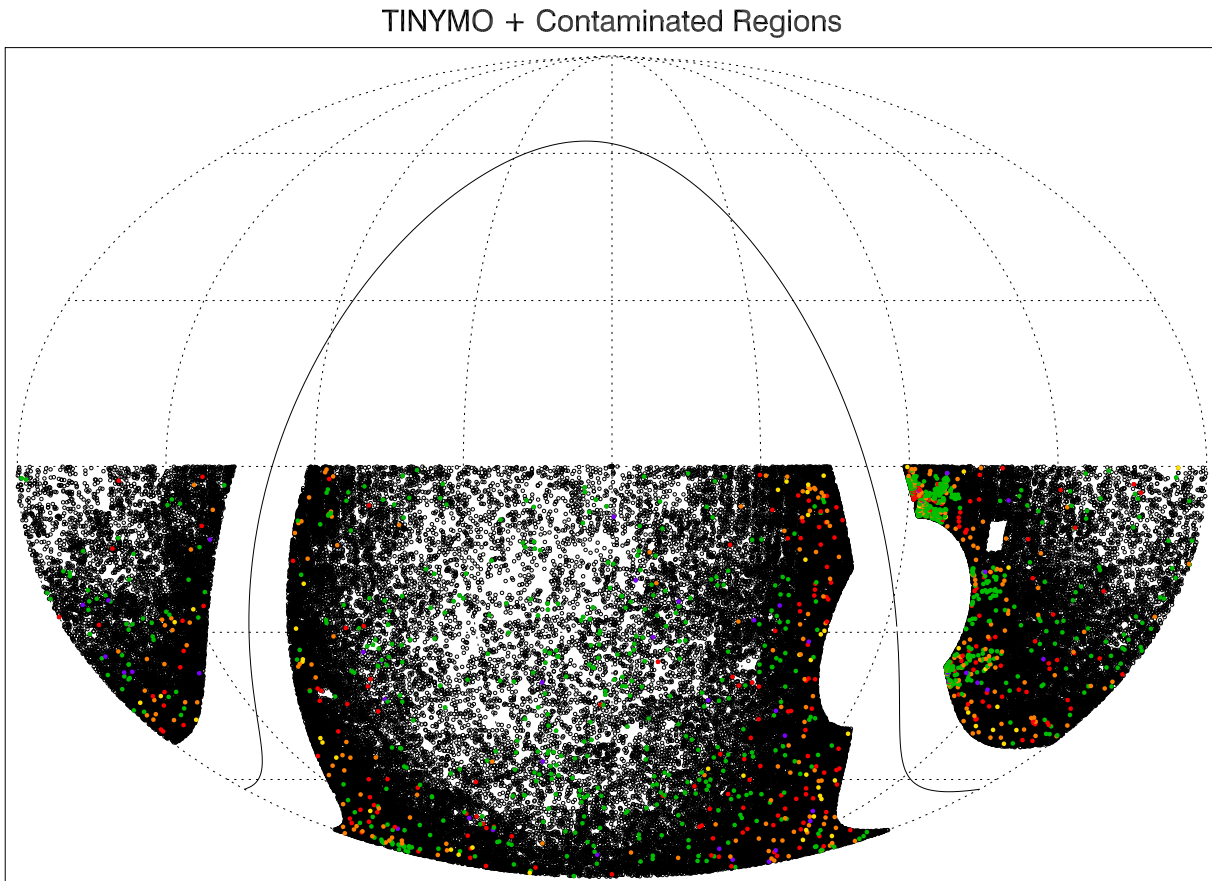


Figure 4.1: Mollweide equal-area projection of the TINYMO survey extraction centered on RA=0h,DEC=0d, with a  $10^\circ$  band around the Galactic equator and a  $20^\circ$  region around the Galactic Center removed. The colored points (green, yellow, orange, and red) are stars selected by later phases of the survey processing, demonstrating the crowded areas around the Galactic bulge that were later removed. Also visible is the 25 square degree area without  $R_1$  plate data.

which implies a limiting distance of 6.6 pc. Within 25 pc (distance modulus 1.99) we should be able to detect every M dwarf bluer than  $B_J - R_2 = 2.6$  (M7V).

Ultimately, the search picked up just short of 14 million stars in the covered 16000 square degree region seen in Figure [4.2](#).

```

SELECT
  s.objID,t.pts_key,s.ra,s.dec,muacosd,sigmaacosd,mud,sigmud,scormagB,scorma
  gR1,scormagR2,scormagI,j_m,j_msigcom,h_m,h_msigcom,k_m,k_msigcom
FROM   Source AS s WITH (INDEX(0)),
       CrossNeighbours2MASSPSC AS x,
       TWOMASS..twomass_psc AS t
WHERE
  s.ra BETWEEN 0.0 AND 2.0 AND s.dec BETWEEN 0 AND -30.0
  and Nplates=4 AND sCorMagR2 < 16.5 AND chi2 < 3.0 AND
  prfstatB BETWEEN -3.0 AND +3.0 AND
  prfstatR1 BETWEEN -3.0 AND +3.0 AND
  prfstatR2 BETWEEN -3.0 AND +3.0 AND
  prfstatI BETWEEN -3.0 AND +3.0 AND
  ellipB < 0.2 AND
  ellipR1 < 0.2 AND
  ellipR2 < 0.2 AND
  ellipI < 0.2 AND
  qualB < 128 AND
  qualR1 < 128 AND
  qualR2 < 128 AND
  qualI < 128 AND
  s.objID=x.ssaID AND t.pts_key=x.pscID AND distanceMins < 5.0/60.0
order by s.objID

```

Code 1: The SQL query. Carried out in chunks 2h RA by 30° DEC.

Table 4.1: The TINYMO Search Cuts

| Step | Sift  | Number      |
|------|---|-------------|
| 0    | Stars in SuperCOSMOS  | 1.9 billion |
| 1    | Stars meeting quality, plate detection, and sky coverage criteria | 14 million  |
| 2    | ... within 25 pc by plate distance                                | 88586       |
| 3    | ... within color regions  | 1077        |
| 4    | ... and remnants of the original color regions                    | 1154        |
| 5    | ... plus by-eye companion detections                              | 1215        |
| 6    | ... that are not confirmed giants or outside regions              | 788         |

### 4.1.2 Photometric Distances

The next phase of the search for low proper motion, nearby stars, was photometric distance estimates following the fourth-order polynomial fits to the main sequence developed in [Hambly et al. \(2004\)](#). As explained in [§2.2.5](#), this method produces up to 11 distance estimates by color, but is only calibrated for a range of colors consistent with known K and M

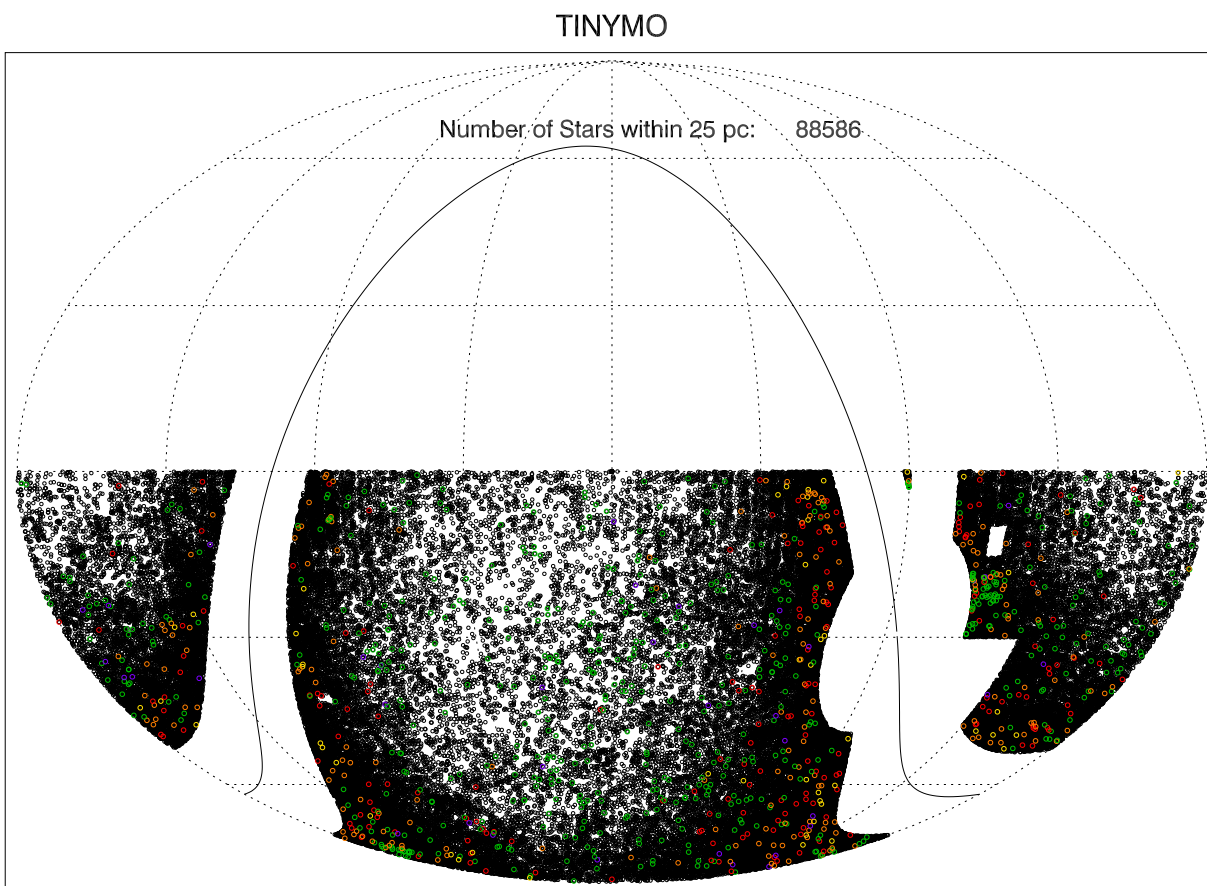


Figure 4.2: Mollweide equal-area projection of the TINYMO survey sky coverage, centered on RA=0h,DEC=0d. The colored points (green, yellow, orange, and red) are stars selected by later phases of the survey processing. Total sky coverage is 16,000 square degrees, or 39.3% of the total sky.

dwarfs, and with the assumption that they are single main-sequence stars. This cuts out any portion of the main sequence for which the plate relations are not valid. As *HIPPARCOS* can reasonably be expected to have observed all hotter stars within 25 pc with its  $V=7.3$  completion limit, it is a reasonable tradeoff. Of the 14 million point sources from the first step, slightly less than 89000 (see Figure 4.2, Table 4.1) were estimated to be within 25 pc by those relations.

As there are only roughly 6000 systems expected within 25 pc (§3.2), the 89000 figure suggests massive contamination. In particular, apart from subdwarfs and (theoretically) stars with unresolved white dwarf companions, contaminants with the colors of main-sequence stars are much brighter. They will have scattered *into* the sample, given a magnitude-limited survey such as ours. The most common culprits are giants, particularly Mira Ceti variables and AGB stars, whose red colors can look very much like M dwarfs (Figure 4.3). To this we can also add carbon stars, distant objects reddened by the ISM or a molecular cloud, multiple stars, young stars and AGN (SIMBAD has listed one object, the nearby (16 pc) star SCR 2036-3607, as a possible AGN, although that definition was retracted recently).

K and M giants and supergiants have broad-band photometric colors similar to dwarfs. There are, among *BRIJHK* color combinations, two particular colors in which M dwarfs are distinguishable from red giants:  $J - H$  and  $J - K$ . In these colors (and only these), mid-M dwarfs are bluer than mid-M giants. This property does not appear in any other combination of colors, including  $H - K$ , but it shows up when  $J - H$  or  $J - K$  is plotted against any other color. I hypothesize that there are gravity-sensitive absorption features in

all three bands: the  $J$  band feature decreases in strength as gravity increases, and the  $H$  and  $K$  band features both increase in strength as gravity increases. Allers et al. (2007) identifies a number of potentially gravity-sensitive features: VO and TiO weaken with increasing gravity (and are predominantly found in the  $J$  band); FeH (which dominates in  $H$ ), CO (which dominates in  $K$ ), K I, and Na I all strengthen with increasing gravity. This would explain why dwarfs are bluer in  $J - H$  and  $J - K$  (increased  $J$  flux, decreased  $H$  or  $K$  flux) and yet there is no effect on  $H - K$  (correlated loss of flux). I am not certain why this does not appear in any other color ( $R$  and  $I$  are also dominated by TiO); it may have to do with the rate at which the band strengths change.

As RECONS normally uses  $V - K$  color to distinguish photometric spectral types, we generated a simulated  $V$  by taking the average of the SuperCOSMOS  $B_J$  and  $R2$  plates, which is hereafter referred to as  $v$ . Plotting the  $J - K$  versus  $v - K$  combination of colors (Figure 4.3) demonstrates the lower concave locus where M dwarfs are distinguishable from M giants entirely by photometric colors.

#### 4.1.3 Color cuts

The final decision in our large-scale sort was the choice of color-color selection regions to enclose as much of the dwarf branch as possible. This task was hampered by the variable position of the giant branch in  $v - K$  color in different parts of the sky (SuperCOSMOS Sky Survey data was downloaded and sorted in pieces), most likely due to various degrees of interstellar reddening (see Figure 4.4). After many iterations, we selected four boxes (Table 4.2): One containing the most obvious batch of dwarf stars, another containing the end of

the main sequence where brown dwarf stars are located past  $J - K_s = 1.2$ , and one catching all stars with  $v - K_s > 10$ , as such ultra-red objects are extremely unusual and would have to be extremely close (or bright) if they really were visible in the SuperCOSMOS  $B_J$  plates. A fourth region was drawn around an unusual scatter of points with  $J - K_s > 4$  and small  $v - K_s$ , in every case these turned out to be giants with incorrect 2MASS cross-matches – the

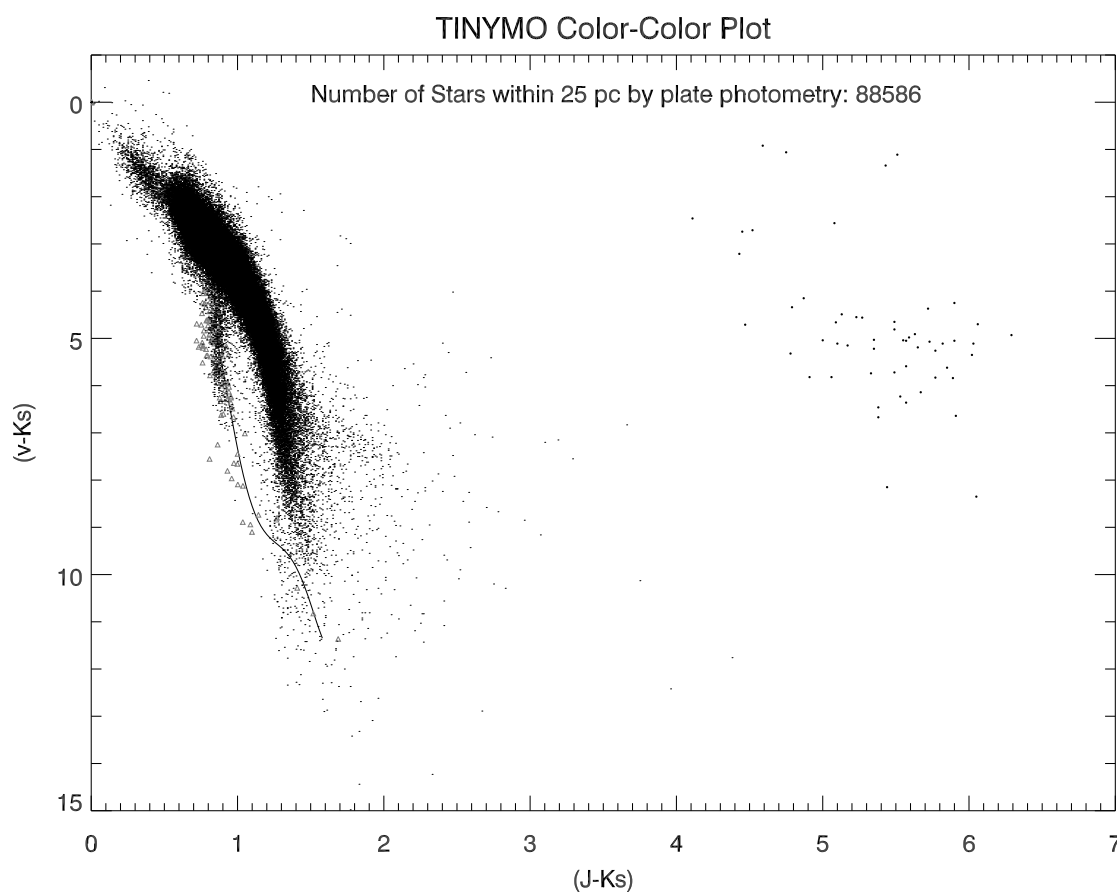


Figure 4.3: The nearly 89000 targets found to be within 25 pc by plate photometric distance relations, plotted as  $J - K$  vs  $v - K$ . The curve is a fifth-order fit to the main sequence (as determined by the 10 pc sample with real measured  $V - K$ , plotted as gray triangles). The cluster of points beyond  $J - K=4$  were later revealed to be bad cross-matches to spurious 2MASS entries.

optical counterparts of the 2MASS hits are likely too faint to have actually appeared in the SuperCOSMOS plates. The result was a reduction of 88586 candidates to 1077 promising nearby objects (Table 4.1), although given some slightly different boxes initially used to extract the first half of the search (see §4.2), the actual number of stars extracted from both pieces of the search was 1154 objects.

Table 4.2: The TINYMO Color Selection Regions

| Vertices |         |         |                 |
|----------|---------|---------|-----------------|
| Box      | $J - K$ | $v - K$ | Purpose         |
| 1        | 0.7     | 4.5     | Main Sequence   |
|          | 0.95    | 4.5     |                 |
|          | 1.2     | 8.0     |                 |
|          | 1.2     | 10.0    |                 |
|          | 0.7     | 10.0    |                 |
| 2        | 1.2     | 8.0     | Brown dwarfs    |
|          | 1.6     | 10.0    |                 |
|          | 1.2     | 10.0    |                 |
| 3        | 0.0     | 10.0    | Very red dwarfs |
|          | 7.0     | 10.0    |                 |
|          | 7.0     | 15.0    |                 |
|          | 0.0     | 15.0    |                 |
| 4        | 4.0     | 0.0     | “Flyers”        |
|          | 7.0     | 0.0     |                 |
|          | 7.0     | 9.0     |                 |
|          | 4.0     | 9.0     |                 |

The exact blue  $v - K$  color cutoff to choose was not obvious. Many of the downloaded chunks – 2 hours of RA (30 degrees) in width and 30 degrees in DEC each – show the possibility of distinguishing red dwarfs with colors as blue as  $v - K=4$  from the giant branch, while others clearly overlap with the giants at colors redder than  $v - K=5$ . Assuming the photometry is accurate to better than half a magnitude, this not surprisingly implies that reddening values (which mostly affect  $v$ ) are very different across the sky. This is possibly

supported by the giants being reddest in the north Galactic spur regions that were removed.

Ultimately, the limit was set uniformly at  $v - K = 4.5$ .

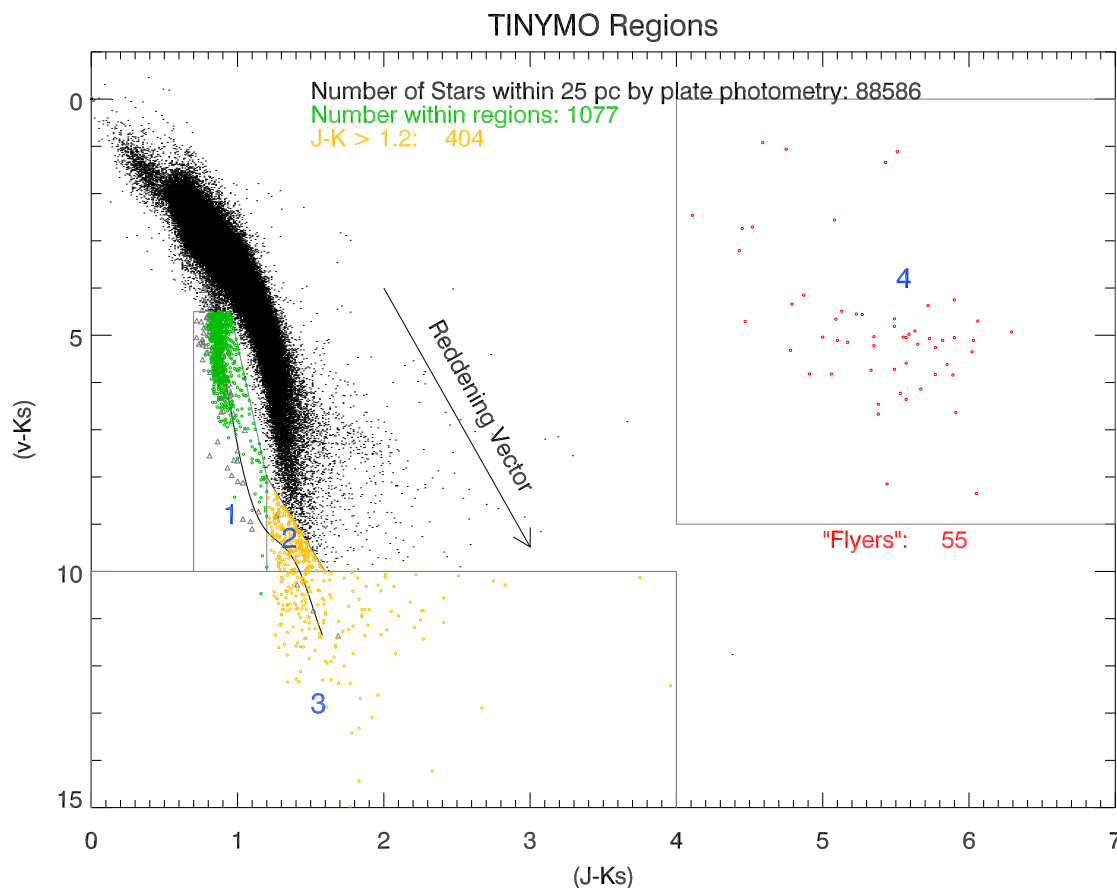


Figure 4.4: Using the color-color regions shown on this  $J - K$  vs  $v - K$  diagram, we separate giants from dwarfs and potential other overlap regions. The curve is a fifth-order fit to the main sequence (as determined by the 10 pc sample, plotted as gray triangles). The cluster of points beyond  $J - K = 4$  (“flyers”) were later revealed to be accidental cross-matches to spurious 2MASS entries. The appropriate interstellar reddening vector from [Fitzpatrick \(1999\)](#) (Table 2, assuming  $v, J, K_s = \text{Johnson } V, J, K$ ) is also shown.

#### 4.1.4 Additional photometric cuts

There is still a lot of giant contamination remaining in the sample of 1154 candidates, particularly where the locus of dwarfs intersects with giants in region 2, around  $J - K = 1.2$ . These objects are potentially nearby brown dwarfs, but the contamination issues are severe, and all were flagged as potential giants. In an effort to distinguish the most likely nearby stars in the sample, we turned to the plate relations themselves to distinguish between dwarfs and giants. The 11 plate relations were calibrated to main sequence stars within specific ranges; if a few of the star's colors are unusual, it is less likely to be a main sequence star. We therefore flagged all objects with fewer than 9 valid distance relations (out of 11 total).

In addition, all objects whose  $R_1$  and  $R_2$  colors differed by more than 1 magnitude were also flagged as probable giants. Even allowing for differences in the photographic emulsions and filters used in the  $R_1$  and  $R_2$  surveys and the precision of the photometric data (see Appendix [A](#)), variability of more than one magnitude suggests a real and large change in magnitude. These changes are most common for Mira variables, which are always giants.

These are admittedly imperfect methods: low-amplitude Mira variables or Miras caught at two similar points in their lightcurve will not be flagged by their  $R_1 - R_2$  magnitudes, while stars with bad  $R_1$  or  $R_2$  photometry will be unfairly excluded. Requiring 9 valid plate relations may have also removed real dwarfs with colors beyond the limits of the [Hambly et al. \(2004\)](#) relations. However, nothing convinces like careful followup: in practice, all but one of the remaining stars in this group (with 9 or more valid relations) turned out to be giants when examined with low-resolution spectroscopy ([§4.1.6](#)). The one potential nearby

star is SCR 1931-1757 (19:31:39.88 -17:57:36.0,  $\mu = 0.028$   $P.A. = 188.2^\circ$ ), a spectroscopically confirmed M2.0Ve star with all 11 valid plate relations and  $R_1 - R_2 = -3.03$  (SuperCOSMOS colors are apparently wrong); its predicted distance was too far (17.67 pc by the average of 12 CCD distance estimates) to deserve further followup (§4.1.6).

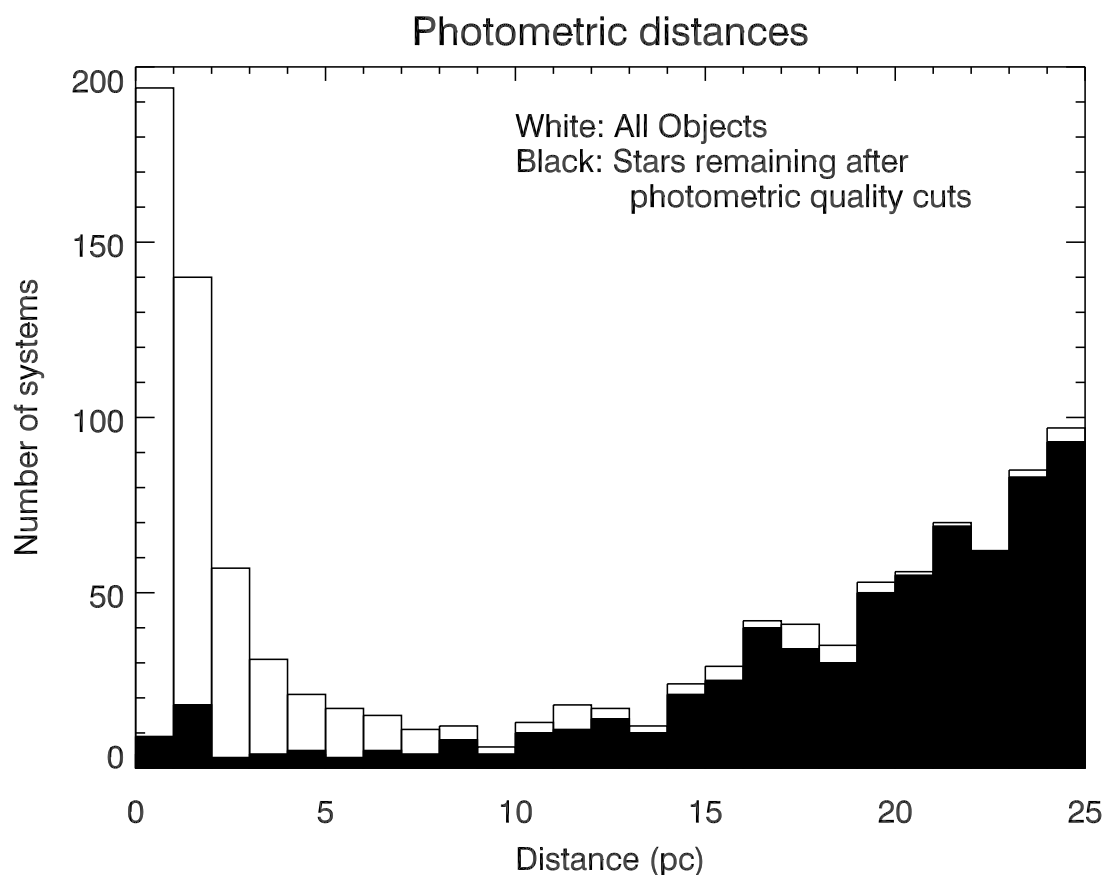


Figure 4.5: Photometric distances for (white) the entire sample of 1215 (including later additions found by eye) objects and (black) the X-ray bright and normal samples. The trend of photometric distances is clearly bimodal, although applying our additional photometric cuts has weeded out an immense number of fake nearby stars (all giants).

Plotting a histogram of plate distance estimates (Figure 4.5) shows that the original sample was bimodal, with peaks at 25 pc and 1 pc. The photometric cuts remove most of

the stars with predicted distances less than 2 pc. Given the expected rarity of stars at those distances, all stars with estimated distances within 2 pc were put on hold until a spectrum was taken, reducing the candidate list to 748. Unfortunately, all the potential stars within 2 pc were spectroscopically revealed to be giants.

#### 4.1.5 Literature Searches

There are useful bodies of work in the literature that can be used to further characterize the remaining stars of interest. Apart from SIMBAD<sup>2</sup> and its admirable but unreliable attempt to contain everything<sup>3</sup>, The General Catalog of Variable Stars (Samus et al. 2012, in VizieR as b/GCVS) maintains a list of all known variable stars and can be used to identify Mira variables, Carbon stars, and other semi-regular and irregular giant stars. The Catalog of Galactic Carbon Stars (Alksnis et al. 2001) also furnished some Carbon star identifications. Finally, the entire list was run through the VizieR versions of the LSPM (Lépine & Shara 2005) and NLTT (Luyten 1979b) catalogs.

On the advice of Inseok Song, we mined the ROSAT (Voges et al. 1999, 2000) catalog for cross-matches to our objects, as giants are not generally expected to be strong X-ray emitters. Stars that had X-ray detections (eventually rigorously defined as a source within 25'' of the optical source, with less than 25% error on the count rate, the 90% limit from Voges et al. 1999) were prioritized for photometry, spectroscopy, and astrometry. It was later discovered that most of these X-ray bright objects were found earlier by Riaz et al. (2006);

<sup>2</sup><http://simbad.u-strasbg.fr/simbad/sim-fbasic> checked 2012 JUL 15.

<sup>3</sup>SIMBAD, as a living database, changed several times during the course of the project. Several stars remarked as being *near* named Mira variables were later listed *as* those Mira variables.

apart from identifying them as X-ray bright M dwarfs and taking a spectrum for spectral typing, very little had been done.

Out of the 88 X-ray bright targets, the first half of the search (20h-08h RA) contains 59 (67%) stars, while the second half (08h-20h RA) contains the remaining 29 (33%). This can be entirely accounted for by the fractional sky area covered: the second half of the sky contains all of the Galactic Bulge region (removed), most of the Galactic Plane, *and* the regions removed or missing for other reasons. The first half of the search covered 9637 square degrees (59.4%), while the second half covered only 6577 square degrees (40.6%). The remainder of the difference can be interpreted as small number statistics.

At this stage, the 1154 remaining color-selected objects were blinked<sup>4</sup> using SuperCOSMOS scans with a SIMBAD overlay loaded into the Aladin Skyview Applet. Each was individually examined to check if they were a.) real objects, b.) moving (if possible), c.) matched to the proper 2MASS point (mistakes in the 2MASS identification account for the open circled points now lying outside the color-color boxes in Figure 4.6), and d.) previously known objects. At this stage, several proper motion objects (usually companions) were non-exhaustively identified by eye to bring the total candidate list to 1215 objects, with proper motions ranging from  $0.000'' \text{ yr}^{-1}$  to  $0.444'' \text{ yr}^{-1}$ . The highest proper motion from the search itself was  $0.397'' \text{ yr}^{-1}$ . In practice, the limit of the proper motion I could visibly distinguish on the Southern Hemisphere plates was around  $0.08'' \text{ yr}^{-1}$ .

---

<sup>4</sup>Aladin allows the user to create an animation that flips, or blinks, between any number of images. We load SuperCOSMOS  $B$ ,  $R_2$  and  $I$  images to see our stars move.

#### 4.1.6 Observations

The list was then divided up into five subsamples to comprise the final TINYMO sample:

1. Good targets with X-rays
2. Good targets
3. Probable giants ( $J - K > 1.2, |R_1 - R_2| > 1$ )
4. Known giants (from SIMBAD, the General Catalog of Variable Stars (Samus et al. 2012, GCVS), and the Catalog of Galactic Carbon Stars (Alksnis et al. 2001, CGCS))
5. Discarded objects (objects not within 25 pc or not within the color-selection boxes.

These were generally found by eye, in the original set of color boxes only, or “flyers”).

Without the collection of more data, very little further could be done. It was decided to follow up all low proper motion ( $<0.18'' \text{ yr}^{-1}$ ) candidates within 15 pc that had not been identified as giants in the literature (Regions 1,2, and 3 [if they had more than 9 valid plate relations] of Figure 4.4). This cut the number of stars for followup down to 115 objects of which 50 were predicted to be within 2 pc.

For the 115 stars of interest, we first obtained low resolution spectroscopy. Along with 10 spectra of interesting targets obtained by a collaborator at the CTIO 4m in 2008 (§4.2), a program was conducted from 2009-2011 on the CTIO 1.5m using the same 32/I grating setup (5994-9600Å) as earlier RECONS spectroscopy efforts in 2003-2006. Classification was done by eye using the techniques from Henry et al. (2002), Kirkpatrick et al. (1991), Boeshaar

(1976), and Keenan & McNeil (1976), which solely focused on identifying dwarfs and giants by Na I, Ca II and K I line features. Many additional giants were weeded out this way, and two carbon stars were identified.

CCD-based *VRI* photometry was obtained for all targets that were spectroscopically confirmed to not be giants, plus the extra 55 X-ray bright targets. All photometry for this project was collected at the CTIO 0.9m, and reduced in the same manner as all RECONS photometry since Jao et al. (2003). CCD-based photometric distances were calculated from this following the principles of Henry et al. (2004) (see also § 2.2.5).

As X-rays were supposed to be an excellent indicator of dwarfs (and turned out to be an excellent indicator of young stars), we did attempt to obtain photometry for all X-ray bright targets within 25 pc (i.e., all of them). That added an extra 55 photometry targets, several of which were then added to the astrometry program when their CCD photometric distance estimate put them within 15 pc (at which point it was retroactively added to the spectroscopy program). A few additional targets of interest (usually astrometric targets already being observed for parallax) were added to this list, bringing it to 187 total targets.

Astrometry observations commenced on any target with both spectroscopy indicating it was a dwarf and CCD photometric distance estimates that placed it within 15 pc. Most targets were added to the program between 2007 and 2009; the last target to be added was SCR 1942-2045 in late 2010. Every target formally included in CTIOPI's TINYMO and YOUNG! samples under my direction has enough data for at least a preliminary reduction, and all are described in Chapter 5.

One additional opportunity occurred in 2008 when the Hubble Space Telescope’s data bus broke. As a result, the only available instrument was the Fine Guidance Sensors (FGS), which communicate via the telemetry subsystems. GSU became an enormous beneficiary of this incident, and I included my entire X-ray bright sample (at the time, 66 targets) in the massive 300-target observing list. Roughly half of the list was observed, and results are mentioned where appropriate (see §5.6).

## 4.2 What Actually Happened, or, the Refinements of a Learning Process

What has been described thus far is the final state of affairs. As my thesis was a learning process, the procedures and survey itself evolved between 2007 and 2010.

As briefly mentioned in §4.1.4, the first half of the southern sky (extracted by Dr. Henry) was extracted using a different set of color-color selection boxes that came very close to the giant locus at the blue end of the M dwarf sequence. While this was eventually changed to the current set of boxes, the targets that were now excluded remain in an “outside the boxes” section of the master list (note the small group of open points around (1.0,4.5) in Figure 4.6). The second half of the search (done by myself in 2009) used the final set of color-color selection boxes the entire way through.

Originally, my thesis dealt with all of the stars found in the TINYMO survey, as a result many higher proper motion objects within 15 pc were also within my purview. This definition changed in 2010 to include only stars with proper motions less than  $0.18'' \text{ yr}^{-1}$ ; the higher proper motion targets (because nearby stars are *always* of interest to RECONS) were

donated to other research samples<sup>5</sup>; it is because of work on those other samples that Table 4.3 includes so many results for those objects. In return, I gained claim over several CTIOPI astrometry targets *not* found in the TINYMO search that were nevertheless moving slower than  $0.18'' \text{ yr}^{-1}$ . In general, these objects are hotter spectral types than M2 (removed by color cut), cooler than M6 (removed by the merger with the giant branch), outside the spatial range of the southern hemisphere we searched, or beyond 15 pc by CCD photometric distance estimate. Some are harder to explain, though; they may have been thrown out by ellipticity, quality, or the 4-plate-detection requirements in the first stage of the SuperCOSMOS search.

By the same token, the 15 pc distance limit was settled upon in 2009. Prior to this, all the stars in the first half of the search with plate distances less than 12.5 pc had been added to the parallax observing list, while the intention was to get photometry for *all* of the “X-ray” and “good” samples (which would have placed an inordinate drain on our photometry program). Thus, when the distance limits were imposed, several stars with plate distances greater than 15 pc had nevertheless been observed for CCD photometry, and found to have CCD distances within 15 pc, and were added to the program. This biased the sample toward stars from the first half of the TINYMO search, and is partially responsible for our interest in getting photometry for *all* the X-ray bright targets.

Several promising targets were added directly to the photometry and parallax observing lists in 2007 and 2009. These targets were typically (but not always) X-ray bright and had predicted distances close to 10 pc. Spectroscopy was only started in 2009, and was not used to keep targets off the observing programs until 2010. Fortunately, there were only a handful

---

<sup>5</sup>Several of the stars were young, and were added to my YOUNG! sample.

of cases where giants were accidentally observed for parallax. Only two – SCR 0747-5412 and SCR 0833-6107 – were observed for long enough to attempt a parallax reduction; the rest were kicked off after one or two observing sessions. This caused a problem for the photometry program when the Mira variables turned out to vary greatly from run to run, and initially caused our photometrists to throw out entire nights<sup>6</sup> of good data.

The spectroscopic goals changed over the course of the project. Several stars that did not meet our later 15 pc/9 plate distances criteria – including both our Carbon stars (§5.8) – were observed in the early days of our spectroscopy program. Several known giants were intentionally observed to provide comparisons. 10 targets were observed by Stella Kafka on the CTIO 4m in February 2008, prior to our commitment to do spectroscopy ourselves. Those spectra are higher resolution than later CTIO 1.5m spectra, and cover 4900Å– 8050Å, omitting both Na I and Ca II features we normally used to identify spectra.

Finally, the X-ray sample was originally defined by SIMBAD rather than VizieR’s ROSAT All-Sky survey catalogs; in this way my X-ray bright sample originally included several targets that either had high X-ray error or were too far from an X-ray source to ultimately qualify as a detection. This original list, from the first half of the search, was the one sent to HST in 2008.

#### ***4.2.1 A Commentary on the Design Decisions***

Some time has passed since the initial survey was done; and in that light there are changes that would be made if the survey were attempted now:

---

<sup>6</sup>I’m sorry, Jen.

- The initial survey relies greatly on the epoch spreads of the individual plates to set its upper limit. This information was in the SuperCOSMOS output but was never checked to make sure the survey would reasonably contain all stars with proper motions as large as  $0.18'' \text{ yr}^{-1}$ - this could be done with an age-map to pinpoint areas of larger epoch spreads. Nigel Hambly has more recently provided an extra sift of the database for the obvious case of the region between 0 DEC and  $-20$  DEC where older POSS-I  $R_1$  plates were used, to complete proper motions up to  $0.18'' \text{ yr}^{-1}$ . This extra list – EXTRMO – was never added to the thesis.
- If a single color was erroneous, up to 5 color relations could have been wrong. Using this logic, Finch et al. (2007) and Boyd et al. (2011a) both accepted objects with as few as 6 matching color relations, rather than the 9 I selected here. Given that the only colors in five relations were  $B_J$  and  $R_2$ , the most useful way to do this would be to determine if the failed color relations all involve one specific filter.
- The regions of sky around the North Galactic Spur were probably *not* too contaminated to deal with.
- The X-ray error cutoff (25%) was chosen arbitrarily.
- I did not take proper motion into account when searching literature sources that listed no proper motion themselves. With the General Catalog of Variable Stars (GCVS Samus et al. 2012), and the Catalog of Galactic Carbon Stars (CGCS Alksnis et al. 2001), no epoch of observations were included, so no proper motion sliding could be

done. The ROSAT All-Sky catalogs were built from observations taken in 1990 and 1991; fortunately, sliding stars to epoch 1991 made no change in the X-ray detections (not that it should have, the fastest-moving object in the TINYMO survey ( $0.444'' \text{ yr}^{-1}$ ) only moved  $4''$  in 9 years).

### 4.3 TINYMO Results

Figure 4.6 shows the final state of the TINYMO sample, with its five categories and an indication of which stars have been measured with CCD photometry (filled circles). Figure 4.7 shows those photometry targets plotted with their actual  $V - K$  colors, which displaces them vertically from where they appeared in Figure 4.6. It is apparent from Figure 4.7 that not all of our “good” (green) targets are actually dwarfs; some of them now lie in the giant locus (which is still drawn with  $v - K$  color). This is unsurprising, as our “good” sample is comprised of the survivors of our various sifts; they are stars that are thus far unremarkable.

Table 4.3: TINYMO Results

|                          | Subsample 1 <sup>a,b</sup> | Subsample 2 <sup>c</sup> | Subsample 3 <sup>d</sup> | Subsample 4 <sup>e</sup> | Total   | Subsample 5 <sup>f</sup> |
|--------------------------|----------------------------|--------------------------|--------------------------|--------------------------|---------|--------------------------|
| Within 25 pc (by $\pi$ ) | 7/ 4                       | 7/ 15                    | 0/ 0/ 0                  | 0/ 0                     | 14/ 19  | 0/ 0                     |
| Within 2 pc (by phot)    | 0/ 0                       | 12/ 0                    | 152/ 38/ 0               | 160/ 0                   | 329/ 0  | 2/ 0                     |
| Found by eye             | 4/ 2                       | 7/ 5                     | 1/ 0/ 0                  | 0/ 0                     | 11/ 7   | 37/ 10                   |
| Giant                    | 0/ 0                       | 22/ 0                    | 53/ 51/ 0                | 223/ 0                   | 298/ 0  | 21/ 0                    |
| All                      | 68/ 20                     | 396/168                  | 221/ 53/ 0               | 223/ 0                   | 908/188 | 109/ 10                  |

<sup>a</sup>Each box is broken up into low  $\mu$ /high  $\mu$

<sup>b</sup>X-ray bright sample.

<sup>c</sup>Good sample.

<sup>d</sup>Potential Giants. These boxes are broken up into low  $\mu$ /low  $\mu$  and  $> 9$  plate relations/high  $\mu$

<sup>e</sup>Known Giants.

<sup>f</sup>Objects not within regions or 25 pc.

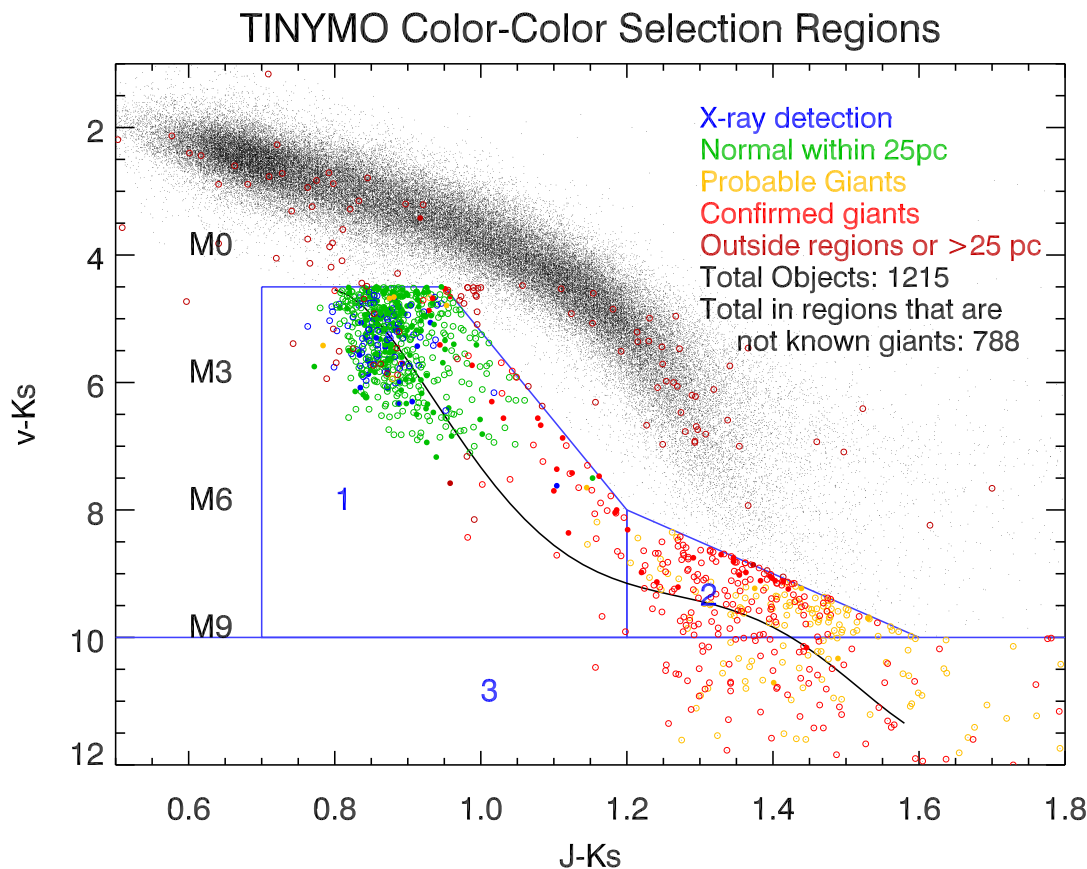


Figure 4.6: The TINYMO sample, showing all known X-ray bright, “good”, probable giants, known giants, and discarded objects. Open circles have only plate photometry, filled circles have CCD photometry (though all are plotted here by plate photometry). A small cluster of points around  $J - K = 1.0, v - K = 4.5$  remains from the original set of color-color boxes (§ 4.2). The rest of the points outside the regions were found by eye or “flyers”.

Table 4.3 lists the results of the TINYMO survey, broken into low proper motion/high proper motion in every area. There are (in total) 14 low proper motion stars in TINYMO known to have distances within 25 pc (all described in § 5.3); the 19 high proper motion stars were observed for other reasons § 4.2). A table of the 444 potentially nearby low proper motion stars can be found in Appendix B.

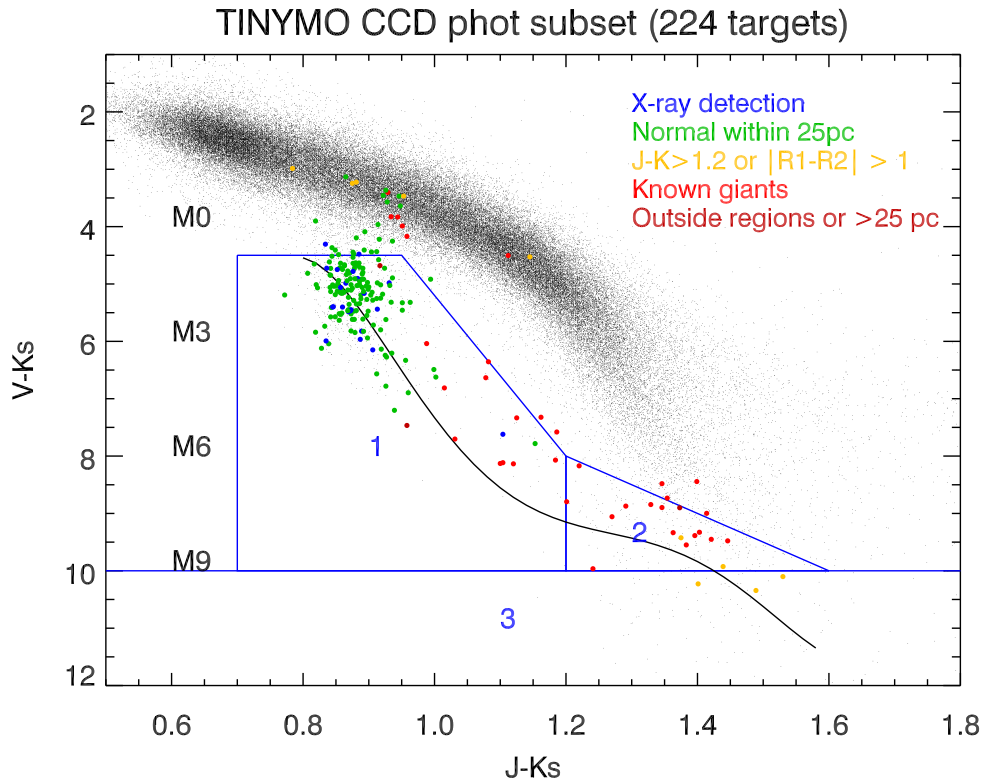


Figure 4.7: The final state of the TINYMO sample’s subset of stars observed for CCD photometry (the filled circles in Figure 4.6). There has been some vertical shifting due to the differences between our simulated  $v$  and Johnson  $V$ . 148 of the stars with CCD photometry are low proper motion ( $<0.18'' \text{ yr}^{-1}$ ), the remaining 76 stars are high proper motion stars observed for other reasons (other CTIOPI targets recovered by TINYMO). Note that the black points are still being drawn in  $v - K$  color.

TINYMO is very incomplete in terms of proper motions (Figure 4.8), but this is not surprising as TINYMO is not a proper motion survey, and is probing the range of proper motions more common for giants. By the same token, we cannot make use of reduced proper motion diagrams. Reduced proper motion diagrams (Figure 4.9) operate under the assumption that lower proper motion objects are farther away; we are specifically looking for nearby stars that move like distant giants.

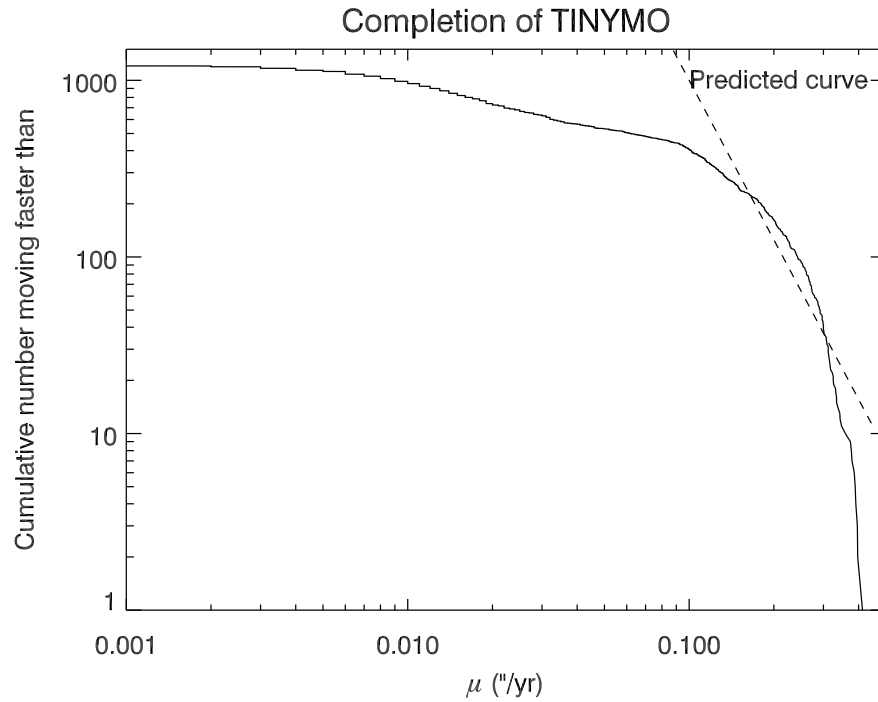


Figure 4.8: A diagram of the completeness of stars, as in Figure 1 of [Lépine et al. \(2005\)](#). The  $\mu^{-3}$  curve follows from the assumption that the number density of stars goes as  $n \propto d^3$ , and proper motion goes as  $\mu \propto d^{-1}$ .

Finally, TINYMO offers a rough idea of the point at which a proper motion search (even if the proper motions are accurate) will be overwhelmed by giants. This limit (seen in Figure [4.10](#)) appears to be around  $0.035'' \text{ yr}^{-1}$ , which is not coincidentally near the lower limit of Lépine's SUPERBLINK surveys,  $0.04'' \text{ yr}^{-1}$ .

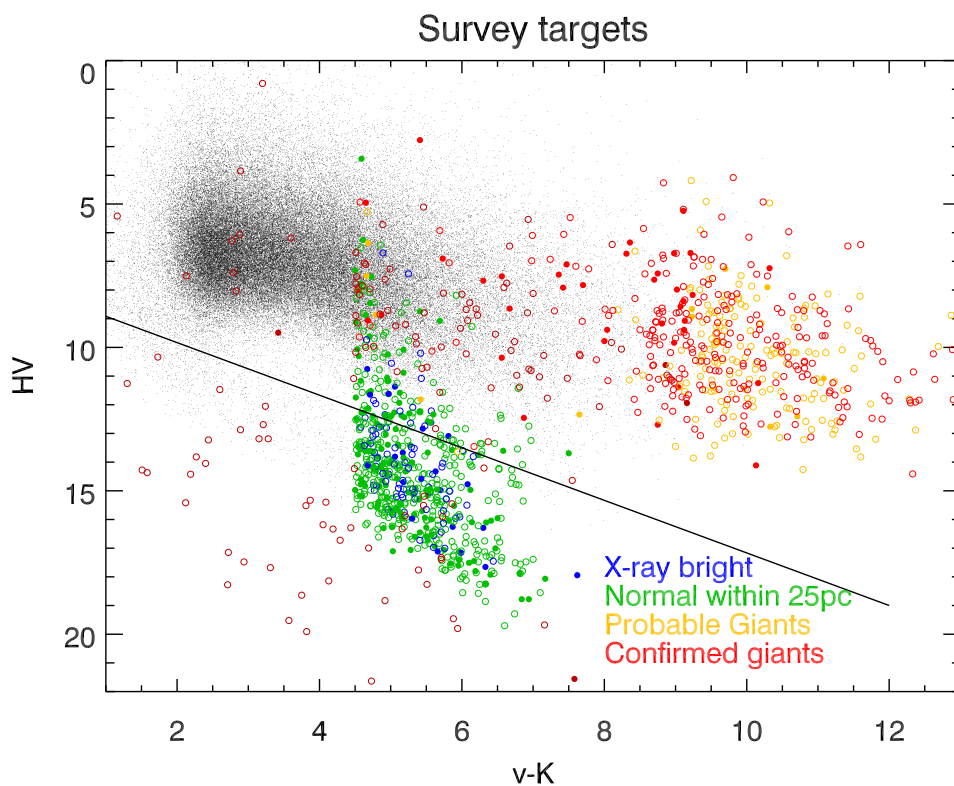


Figure 4.9: Reduced Proper Motion diagram for the TINYMO sample. Reduced Proper Motion is  $HV - v = 5 \log\left(\frac{1}{\mu}\right) - 5$  (i.e.,  $\mu$  replaces  $\pi$  in the distance modulus equation). As can be seen above, there are clearly two locii, one (top) for giants, and one (bottom) for dwarfs; while most of the green/blue “good” sample of stars obeys those trends, there are clearly green/blue “good” stars in the giant locus.

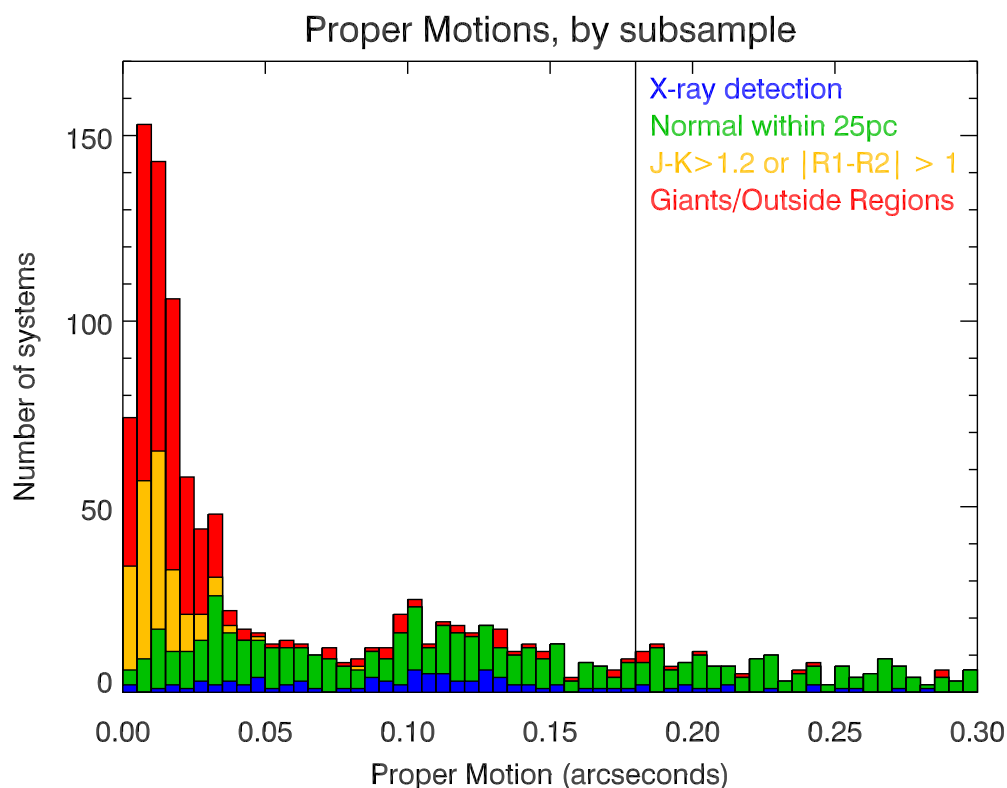


Figure 4.10: Proper motions of the TINYMO sample, in  $0.005'' \text{ yr}^{-1}$  bins. Using my subsamples as a proxy for the type of star, we see that below  $0.035'' \text{ yr}^{-1}$ , the sample is dominated by the red and yellow (giants and suspected giants, respectively), while above that, it is dominated by X-ray bright and regular stars. The vertical line is at  $0.18'' \text{ yr}^{-1}$ .

## CHAPTER 5

### RESULTS

#### 5.1 Observations

##### 5.1.1 CTIO 0.9m/Tek2K

All astrometric and photometric observations were carried out at the CTIO 0.9m telescope<sup>1</sup>, initially (1999-2003) under the aegis of the NOAO (National Optical Astronomy Observatory) Surveys Program, and later (2003-present) via the SMARTS (Small and Moderate Aperture Research Telescope System) Consortium. The astrometric and photometric observations presented in this thesis were obtained utilizing the center  $1024 \times 1024$  pixels of the 0.9m telescope's Tek  $2048 \times 2046$  CCD, and CTIO's  $V_J$ ,  $R_{KC}$ , and  $I_{KC}$ <sup>2</sup> (hereafter without subscripts) filters. I have been on four observing runs at CTIO.

Astrometric observations are typically series of five frames in a single filter, taken in sequence, with no dithering between frames. The total time on a target is not to exceed 15 minutes per exposure or generally 30 minutes for the set – thus, some target sequences only have two to four frames taken. It has been found that more than five frames does not provide significantly better centroiding; this point of diminishing returns was determined in tests done by Charlie Finch.

At a minimum, it takes at least 3 nights spanning at least 1 year of coverage to get a preliminary parallax result, though it takes at least 2 years and six nights before the errors are reliable. Most published stars have been observed for 12-20 nights over more than 3

---

<sup>1</sup><http://www.chara.gsu.edu/~thenry/SMARTS/index.htm> checked 2012 JUL 15.

<sup>2</sup>The central wavelengths for  $V_J$ ,  $R_{KC}$ , and  $I_{KC}$  are 5475, 6425, and 8075 Å, respectively.

years. RECONS uses three guidelines to determine if a parallax is publishable.

1. To ensure good coverage of the parallax ellipse, there is an informal limit of 30 frames each in the ‘morning’ and ‘evening’ halves of the ellipse with a goal of having 20 usable frames each. Unusable frames have poor tracking, seeing  $>2.5''$ , high background counts (moonlight or twilight), or saturated target stars.
2. The system must be followed for about two years to accurately decouple the star’s motion into parallax and proper motion.
3. The system is expected to have a parallax error less than 3 mas before publishing, which corresponds to 3% error at 10 pc, and 10% error at 33 pc.

As of April 2012, the CTIOPI 0.9m program has published 216 parallaxes for 204 stars in 173 star systems, out of over 600 current and former observing targets. They have a typical parallax error of roughly 1.5 mas, which is twice the average *HIPPARCOS* parallax error, but far better than the *HIPPARCOS* errors for stars at the faint magnitudes of objects CTIOPI observes.

Each night photometry is attempted,  $\sim 20$  stars (of a variety of colors; at least two of which should be red stars) are observed three times each at a range of airmasses between 1 and 2 to obtain the color-dependent atmospheric extinction curves for that night. Fortunately, the requirements for 20 stars are satisfied by Landolt fields<sup>3</sup> containing up to 7 standard stars.

Photometry is extracted using (usually)  $7''$  synthetic apertures in IRAF’s PHOT package,

---

<sup>3</sup>According to Mike Bessell (private communication, 2012), Landolt’s initial Johnson-Kron-Cousins *U* and *B* filters (and corresponding results) were too blue (*U*) and too narrow (*B*), but this does not affect RECONS because we do not typically obtain *U* or *B* band photometry.

using a pipeline designed by Wei-Chun Jao and typically operated by Jennifer Winters. The extinction curves of the standards are then used to produce calibrated photometry accurate to 0.03 magnitudes (Winters et al. 2011).

Four significant instrumental events in the course of the CTIOPI program have affected the results in this thesis:

- In February 2005, the Tektronix #2  $V$  filter (hereafter “old  $V$ ” or  $oV$ ) used by CTIOPI cracked and was replaced by the almost-photometrically identical (transmission properties and bandwidth) Tektronix #1  $V$  filter (hereafter “new  $V$ ” or  $nV$ ). With four years of  $nV$  data, we are able to make some comparisons between the two:

As reported in Subasavage et al. (2009), the  $nV$  filter is photometrically consistent with the  $oV$  filter to within reported CTIOPI accuracies (0.03 mag, Henry et al. 2004; Winters et al. 2011), although we find our  $V$  filter photometry is only accurate to 0.05 mag in this dataset.

Also as reported in Subasavage et al. (2009), some  $nV$  filter data cause a few-mas offset in the RA axis astrometric residuals. This is endemic to the  $nV$  filter itself and is not the result of changing filters; recent data taken with the  $oV$  filter show no such behavior in the residuals when added to older data. Parallax results using only  $nV$  filter data are slightly but non-systematically displaced relative to results using only  $oV$  data, which were found to be consistent with YPC and *Hipparcos* parallaxes in Jao et al. (2005). Part of the error appears to depend on the filter itself, the rest appears to depend on coverage: tests were only conducted on stars with large datasets

before and after the  $V$  filter replacement. Those stars tend to have better coverage of the parallax ellipse in  $oV$  (earlier) than in  $nV$  (later, when their parallaxes were well determined and they became lower priority targets). Even so, the  $nV$  parallax is usually within  $2\text{-}\sigma$  of the  $oV$  measurement, and mixed  $V$  parallaxes are always within  $2\text{-}\sigma$ . All parallaxes in this paper using  $nV$  filter data are noted in Table [5.1](#). Puzzlingly, several stellar fields indicated *no* adverse effects on the astrometry when reducing data with and without recent data in the  $oV$  filter. At the moment the exact cause is not clear, but apparently selecting reference stars closer to the target on the CCD reduces the effect, suggesting this is caused by a localized distortion effect through the  $nV$  filter.

- In April 2005, the Telescope Control System (TCS) on the 0.9m was completely replaced and refurbished, yielding improved pointing and tracking. No astrometric effects have been detected in datasets spanning the TCS upgrade.
- On 7 March 2009, a power outage damaged the gain = 1 circuitry for the CCD, and CTIOPI began using gain = 2. The differences between the two gains are purely electrical, and tests confirm that the switch does not affect our astrometry, as expected.
- In July 2009 (during one of my observing runs), the  $oV$  filter was returned to service. Tests showed the hairline crack near the edge does not affect data acquired on the central quarter of the CCD as used in CTIOPI.

### 5.1.2 CTIO 1.5m/RCSpec

Most of the spectroscopy (all of it long-slit, single object) for this thesis was collected on the CTIO 1.5m telescope with the Ritchie-Crétchien spectrograph<sup>4</sup> and the standard SMARTS 32/Ia first-order grating setting (15.13° tilt, 5994Å–9600Å, R=500, OG570 blocking filter), and a 2'' slit to maximize the stellar flux. The RC spectrograph uses a relatively old 1200x800 Loral CCD with few bad lines and no backthinning, which makes it less prone to fringing in the red end of the spectrum. Two distinct epochs of observations were conducted, from 2003-2006 for the spectral typing thesis work of Thom Beaulieu; and from 2009-2011 specifically for the TINYMO survey targets. The regular operation was one Neon-Argon (NeAr) lamp exposure for wavelength solution, followed by two exposures of the target object, with one flux standard taken per night.

From 2003-2006, observing was done in person on nine user runs, intermingled with blue spectra. They were taken with the 9/I first-order grating setting and BG38 order blocking filter, for John Subasavage's white dwarf program.

From 2009-2011, observing was done in SMARTS queue mode. At the time, the 32/Ia setting was no longer a common setup, so for the most part TINYMO data were collected in large chunks of nights. The flux standard was chosen by the queue manager, Dr. Fred Walter, from a small subset of stars, all of which are in IRAF's standard *onedstds* directory. Spectra were reduced using standard IRAF *onedspec*, *ccdred* and *ctioslit* packages.

---

<sup>4</sup>Interestingly, the CTIO RCspec was a clone of the Kitt Peak White spectrograph – <http://www.ctio.noao.edu/spectrographs/60spec/manual/node1.html> checked 15 JULY 2012, see next section.

### 5.1.3 Lowell 1.8m/De Veny

Additional spectroscopy was gathered at Lowell Observatory's Perkins 1.8m telescope with the DeVeney spectrograph<sup>5</sup> and its 400 g/mm grating tilted at 17 degrees, with the OG570 blocking filter, for coverage from 5800-9200Å at a spectral resolution of roughly R=1500. Spectra were obtained on five runs throughout 2009 and 2010, all carried out by me. Owing to the observatory's northern latitude, only targets north of -36 DEC were observed from Lowell.

The process of obtaining spectra changed considerably over the course of the project, partly owing to the fact that the DeVeney was not regularly used and rarely in the red end of the spectral range. Every night, one flux standard (one of the ones available in IRAF's standard *onedstds* directory) was observed for spectral calibration. For the first run (2009 FEB), only one spectrum was taken of each target, with Neon-Argon calibration lamp spectra taken at four different times throughout the night. Subsequent runs (2009 MAY and 2009 DEC) included lamps taken after each exposure and a large catalog of flatfields, and finally (2010 MAR and 2010 MAY) flat lamps were taken after every exposure. Spectra were reduced using standard IRAF *onedspec*, *ccdred* and *kpnoslit* packages.

At the time of the observations, the DeVeney was outfitted with a blue-sensitive back-thinned 2200x515 CCD, which had enormous (> 50%) 2-dimensional fringing problems at wavelengths longer than 7500Å, which combined with instrument flexure, makes data reduc-

---

<sup>5</sup>Also interestingly, the DeVeney spectrograph is the Kitt Peak White spectrograph, on indefinite loan and separately upgraded by Lowell.

tion difficult, and adequate removal of the fringes apparently impossible.

Based on observations collected in 2009 FEB, it was clear that the telescope had a 2-dimensional fringe pattern. Such fringe patterns can be removed by flat-fielding the spectrum with a flat containing the same set of patterns. As the data could not be properly flat-fielded, it was apparent the fringe pattern changed during the night. Initially, it was hoped that creating fringe maps at many different positions and then using the closest one to the actual observations would help, but it turned out that the fringes are not repeatable, and change over periods of seconds – subtracting a series of consecutive flatfields showed that the shifts are frequent and sudden: Flats 1 and 2 matched perfectly, but Flat 3 (taken 10 seconds later) matched neither of the other two (but removed the most fringing from the associated object spectrum!). This may explain why brighter stars had less obvious fringes than fainter stars: their spectra were shorter and thus more likely to match the flatfield preceding them, while fainter stars had several fringe patterns superimposed on their spectra.

Solving this problem is apparently beyond current techniques. Separating the fringes from the flatfield and then recombining them at different subpixel offsets made no noticeable difference in the results. Filtering out a specific frequency of noise failed as the frequency of the interference fringes changes with wavelength, and the titanium oxide bands in M dwarf spectra are quasi-periodic in this region. The most technologically-advanced method, using wavelet transforms to generate a multi-frequency fringemap, only work if the fringe pattern is stable (Rojo & Harrington 2006).

Ultimately, observations at Lowell were discontinued in light of the difficult behavior of

the instrument, and the 2009 DEC data were never reduced, with focus shifting to CTIO. Fortunately, the resulting spectra from the DeVeney were of sufficient quality to distinguish gravity indicators, i.e. dwarfs vs giants/supergiants and the results of the MATCHSTAR auto-typing code suggest the spectra are accurate to within  $\pm 1$  subtype of the values from CTIO spectra.

It has recently come to my attention (Shkolnik, private communication 2011) that Lowell now has a new fringe-reducing CCD to replace that chip, but it may not yet have been installed.

#### ***5.1.4 CTIO 4.0m/RCSpec***

On 18 SEPTEMBER 2008 and 19 SEPTEMBER 2008, Stella Kafka observed ten objects for us with the CTIO 4.0m RCSpec, using the KPGLF-1 grating (632 g/mm) and an unknown blocking filter. The spectra are higher resolution than our CTIO 1.5m spectra (1.90Å), and cover 4900Å– 8050Å. These spectra do not have the Na I doublet or Ca II triplet used for gravity detection, but do contain H $\alpha$  and the K I doublet. For a few stars (most notably SCR 0613-2742, §5.6) this is the only spectrum available.

#### ***5.1.5 HST/FGS***

The stars in my X-ray sample (as of 2008, with only half the southern sky searched) were added to GSU’s large Cycle 16B proposal, “Binaries at the Extremes of the H-R Diagram”. Of the input sample of 66 stars, 42 were actually observed before Servicing Mission 4 and the resumption of normal HST observations.

A large fraction of the observed stars turned out to be resolved binaries, far more than the rest of the red dwarf samples. Multiple stars are brighter and more likely to scatter into my sample. TINYMO, the result of a photometric selection, is thus biased toward multiplicity.

The HST/FGS results are unfortunately not an accurate representation or cross-section of the TINYMO sample. In 2008, I had not yet done the second half of the sky (8h-20h RA), I had not yet rigorously defined X-ray luminosity spatial or sensitivity cutoffs, and my sample of interest still included stars found in the TINYMO survey that were higher proper motion. The only three complete reductions that have been done thus far are courtesy of Ed Nelan, in support of a follow-up FGS proposal for three binary systems.

### 5.1.6 Literature

The primary sources of additional information on these stars were found via SIMBAD<sup>6</sup>. Later, I branched out to include specific searches in the most useful General Catalog of Variable Stars (Samus et al. 2012, and continually updated in VizieR<sup>7</sup> as b/GCVS), the General Catalog of Galactic Carbon Stars (Alksnis et al. 2001), the ROSAT All-Sky Survey (Voges et al. 1999, 2000), the LSPM catalog (Lépine et al. 2005), and the New Luyten's Two Tenths catalog (Luyten 1979b). Notable sources (found via SIMBAD) included Beuzit et al. (2004), Bergfors et al. (2010), Delfosse et al. (1999), Gizis et al. (2002), Hawley et al. (1996), Reid et al. (1995), Riaz et al. (2006), and Shkolnik et al. (2009).

<sup>6</sup><http://simbad.u-strasbg.fr/simbad/sim-fbasic> checked 15 JUL 2012.

<sup>7</sup><http://vizier.u-strasbg.fr/viz-bin/VizieR> checked 15 JUL 2012.

## 5.2 Riedel et al. (2010): SLOWMO Parallaxes

Riedel et al. (2010) reported trigonometric parallaxes for our “SLOWMO” sample of stars, defined as systems with  $\mu$  between  $0.5'' \text{ yr}^{-1}$  and  $1.0'' \text{ yr}^{-1}$ . As the fifth paper of results from RECONS’ CTIOPI program, it furthered our goal of completing the census of the Solar Neighborhood within 25 pc, and formed the largest ground-based parallax paper since van Altena et al. (1995).

Riedel et al. (2010) contains 67 new trigonometric parallax measurements of 64 systems. Of the 64 systems, 56 are within 25 pc of the Sun (2.6% of the current total number of systems, 2089), and all are south of  $\text{DEC} = +30$ . In addition to the parallaxes, it provides new measurements of proper motions, Johnson-Kron-Cousins *VRI* photometry, variability, spectral types, and astrometric measurements of multiple systems. This sample builds upon our previous efforts that also revealed systems within 25 pc, including stars with  $\mu > 1.0'' \text{ yr}^{-1}$  (Jao et al. 2005) (our MOTION sample), red dwarfs within 10 pc (Henry et al. 2006), and white dwarfs within 25 pc (Subasavage et al. 2009) from the CTIOPI 0.9m program, and mixed samples from our 1.5m program (Costa et al. 2005, 2006).

### 5.2.1 Sample

The 64 systems discussed in Riedel et al. (2010) are listed in Tables 5.1 (astrometric results) and 5.2 (photometric results). They were selected for the CTIOPI program for a variety of reasons: either their high proper motions made them targets for M. Brown’s masters thesis on SLOWMO systems, their estimated distances suggested they might be

within 10 parsecs, or they had YPC parallaxes with large errors that placed the system within 10 parsecs. The systems themselves are all from Luyten (1979a) (Luyten Half Second, Second Edition), Luyten (1957) (Luyten’s Two Tenths), Wroblewski & Torres (1991), Wroblewski & Torres (1994), Scholz et al. (2000), and a private communications with R-D. Scholz for APMPM J2127-3844. Most of them were investigated for companions in Jao et al. (2003). All of the systems have proper motions of 0.5 to 1.0'' yr<sup>-1</sup>, have red dwarf primaries with  $V = 10.35$  to 19.17 and have spectral types M1.0V to M6.0V. Seven of the systems presented here have known or suspected companions; we confirm six of them and present individual parallax measurements for components of three. We have also discovered evidence of multiplicity for a further three systems and suspect additional components in five more systems; thus 14% (9 out of 64) of our systems are confirmed multiple, and an additional 9% (5 out of 64) are suspected multiples. This suggests a multiplicity fraction of 21.9%.

## 5.2.2 Results

### 5.2.2.1 Astrometry — Parallaxes and Proper Motions

Parallaxes and proper motions of 64 stellar systems are given in Table 5.1, as presented in Riedel et al. (2010). Nine of the systems have multiple parallax measurements, from YPC, our CTIOPI 1.5m program (Costa et al. (2005, 2006), Smart et al. (2010) or multiple components published in Riedel et al. (2010)<sup>8</sup>. For these cases, weighted average system parallaxes are presented in Table 5.3.

<sup>8</sup>The parallax of LHS 1050=GJ 12 in Smart et al. (2010) was not noticed at the time of the publication of Riedel et al. (2010) but has been included here.

All parallax data were analyzed with the custom IRAF/IDL pipeline used in CTIOPI publications since 2005, using an iterative Gaussfit program described in Jao et al. (2005). Starting in 2007, the reduction methodology was changed by the implementation of a new SExtractor centroiding algorithm, described in Subasavage et al. (2009).

As always, CTIOPI parallaxes must meet several criteria before they are deemed fit to publish. First, as outlined in 5.1.1, to ensure good coverage of the parallax ellipse, there is an informal limit of 30 frames each in the ‘morning’ and ‘evening’ halves of the ellipse with a goal of having 20 usable frames each; the number of frames used in the final reductions ranged from 45 (LHS 2899) to 137 (LHS 1630AB). Second, the system must be followed for about two years to decouple the star’s motion into parallax and proper motion; the coverage varies from 1.99 years (LHS 2335) to 10.15 years (LHS 4009AB). Third, CTIOPI targets are expected to have parallax errors less than 3 mas before publishing. The smallest parallax error is 0.63 mas (GJ 1157) and the largest is 2.57 mas (LHS 1050 and LHS 2122), while the median error on these parallaxes is 1.37 mas.

Prior to the publication of Riedel et al. (2010), CTIOPI re-observed a few systems (e.g. LHS 1561, LHS 3909, and LHS 3443) after a multi-year hiatus to improve proper motion precisions and possibly reveal long-period perturbations (see §5.2.2.3). The extra observations had minor effects on the derived parallaxes. Only the suspected and confirmed astrometric multiples are still on the program; all results in this section are identical to those in Riedel et al. (2010).

Table 5.1: Astrometric Results (Riedel et al. 2010)

| Name<br>(1)      | R.A.<br>(2) | Decl.<br>(3) | Filter<br>(4) | $N_{\text{sea}}^b$<br>(5) | $N_{\text{frm}}$<br>(6) | Coverage <sup>b</sup><br>(7) | Years <sup>b</sup><br>(8) | $N_{\text{ref}}$<br>(9) | $\pi_{\text{rel}}$<br>(mas)<br>(10) | $\pi_{\text{corr}}$<br>(mas)<br>(11) | $\pi_{\text{abs}}$<br>(mas)<br>(12) | $\mu$<br>(mas yr <sup>-1</sup> )<br>(13) | P.A.<br>(deg)<br>(14) | $V_{\text{tan}}$<br>(km s <sup>-1</sup> )<br>(15) | Notes<br>(16)    |
|------------------|-------------|--------------|---------------|---------------------------|-------------------------|------------------------------|---------------------------|-------------------------|-------------------------------------|--------------------------------------|-------------------------------------|--|-----------------------|---|------------------|
| LHS 1050         | 00 15 49.25 | +13 33 22.3  | V             | 7s                        | 60                      | 1999.71–2009.75              | 10.03                     | 7                       | 84.46±2.56                          | 1.39±0.22                            | 85.85±2.57                          | 699.2±0.5                                | 061.7±0.08            | 38.6  | c                |
| LHS 1351         | 02 11 18.06 | -63 13 41.0  | V             | 3c+                       | 68                      | 2000.58–2004.97              | 4.40                      | 5                       | 70.62±1.64                          | 0.91±0.09                            | 71.53±1.64                          | 704.6±1.3                                | 243.2±0.18            | 50.7  | c                |
| LHS 1358         | 02 12 54.63 | +00 00 16.8  | R             | 5s                        | 58                      | 1999.71–2003.86              | 4.15                      | 5                       | 64.09±2.07                          | 1.18±0.13                            | 65.27±2.07                          | 558.3±1.3                                | 086.1±0.20            | 40.5  | c                |
| LHS 1491         | 03 04 04.49 | -20 22 43.0  | V             | 5s                        | 70                      | 1999.71–2005.00              | 5.29                      | 9                       | 66.30±1.24                          | 0.96±0.16                            | 67.28±1.25                          | 685.4±0.7                                | 135.2±0.12            | 48.3  | c                |
| LHS 1582AB       | 03 43 22.08 | -09 33 50.9  | R             | 9s                        | 70                      | 2000.87–2009.63              | 8.76                      | 6                       | 45.50±1.43                          | 1.99±0.28                            | 47.49±1.46                          | 506.2±0.5                                | 052.3±0.10            | 50.5  | c,d              |
| LHS 1630AB       | 04 07 20.50 | -24 29 13.7  | V             | 10s                       | 137                     | 1999.71–2009.03              | 9.32                      | 5                       | 54.44±1.04                          | 1.74±0.20                            | 56.18±1.06                          | 683.1±0.4                                | 163.7±0.05            | 57.6  | c,e              |
| LHS 1748         | 05 15 46.72 | -31 17 45.3  | V             | 5c                        | 58                      | 2000.88–2005.14              | 4.26                      | 9                       | 41.70±1.40                          | 1.42±0.05                            | 43.18±1.40                          | 551.6±1.1                                | 062.6±0.22            | 60.6  | c                |
| LHS 1749A        | 05 16 00.39 | -72 14 12.6  | V             | 5s                        | 91                      | 2000.88–2005.05              | 4.17                      | 6                       | 44.93±1.46                          | 1.21±0.08                            | 46.14±1.46                          | 814.2±1.1                                | 356.4±0.12            | 83.6  | c                |
| LHS 1767         | 05 31 04.33 | -30 11 44.8  | R             | 5c                        | 57                      | 2003.96–2007.99              | 4.03                      | 10                      | 64.53±1.51                          | 0.73±0.05                            | 65.26±1.51                          | 580.1±1.1                                | 143.8±0.22            | 42.1  | e                |
| LHS 1778         | 05 37 39.77 | -61 54 43.8  | R             | 5s+                       | 68                      | 1999.91–2003.77              | 3.86                      | 10                      | 60.53±0.89                          | 1.49±0.09                            | 62.02±0.89                          | 502.9±0.9                                | 015.8±0.19            | 38.4  | c                |
| APMPM J0544-4108 | 05 43 46.56 | -41 08 08.4  | V             | 5c                        | 76                      | 2000.14–2005.05              | 4.91                      | 8                       | 47.63±0.78                          | 0.78±0.08                            | 48.41±0.78                          | 601.4±0.4                                | 165.6±0.07            | 58.9  | c                |
| LHS 1807         | 06 02 22.62 | -20 19 44.2  | R             | 4c+                       | 66                      | 2000.88–2007.83              | 6.95                      | 6                       | 70.02±1.57                          | 0.98±0.14                            | 71.00±1.58                          | 558.3±1.3                                | 355.7±0.19            | 37.3  | c                |
| GJ 1088          | 06 10 52.89 | -43 24 17.8  | V             | 5s                        | 51                      | 2000.88–2005.06              | 4.18                      | 6                       | 85.44±1.27                          | 1.59±0.19                            | 87.03±1.28                          | 745.5±0.8                                | 010.6±0.11            | 40.6  | c                |
| LHS 1932         | 07 36 12.03 | -51 55 21.3  | V             | 3c                        | 93                      | 2000.88–2003.14              | 2.26                      | 9                       | 60.91±0.98                          | 1.01±0.09                            | 61.92±0.98                          | 595.1±1.2                                | 042.8±0.22            | 45.6  | c                |
| LHS 1955A        | 07 54 54.80 | -29 20 56.4  | R             | 5c                        | 83                      | 2000.94–2009.32              | 8.38                      | 10                      | 72.76±1.09                          | 1.60±0.29                            | 74.36±1.13                          | 596.6±0.5                                | 146.8±0.09            | 38.0  | c                |
| LHS 2010         | 08 27 11.83 | -44 59 21.1  | V             | 4c                        | 85                      | 2001.14–2004.18              | 3.03                      | 9                       | 71.33±1.27                          | 1.47±0.30                            | 72.80±1.30                          | 537.0±1.2                                | 343.1±0.22            | 35.0  | c                |
| LHS 2021         | 08 30 32.57 | +09 47 15.5  | V             | 6s+                       | 54                      | 2003.94–2009.24              | 5.30                      | 8                       | 62.06±1.14                          | 1.61±0.18                            | 63.67±1.15                          | 667.2±0.6                                | 226.6±0.10            | 49.7  | c                |
| LHS 2071AB       | 08 55 20.25 | -23 52 15.0  | R             | 7s                        | 69                      | 2000.07–2009.30              | 9.23                      | 11                      | 66.16±1.25                          | 0.65±0.08                            | 66.81±1.25                          | 591.5±0.3                                | 276.5±0.06            | 42.0  | c,d              |
| LHS 2106         | 09 07 02.75 | -22 08 50.1  | R             | 5s                        | 56                      | 2000.06–2006.04              | 5.97                      | 7                       | 65.12±1.16                          | 1.11±0.06                            | 66.23±1.16                          | 505.7±0.4                                | 215.4±0.08            | 36.2  | c                |
| LHS 2122         | 09 16 25.99 | -62 04 16.0  | R             | 6s+                       | 64                      | 2001.15–2009.04              | 7.89                      | 9                       | 56.42±2.57                          | 2.17±0.15                            | 58.59±2.57                          | 933.8±0.9                                | 313.3±0.10            | 75.5  | c                |
| LHS 5156         | 09 42 49.60 | -63 37 56.1  | V             | 4s+                       | 60                      | 2005.97–2009.32              | 3.35                      | 9                       | 94.42±1.17                          | 0.73±0.07                            | 95.15±1.17                          | 516.6±0.9                                | 084.5±0.15            | 25.7  | c,f              |
| WT 244           | 09 44 23.73 | -73 58 38.3  | V             | 7s+                       | 64                      | 1999.92–2008.00              | 8.08                      | 12                      | 42.05±1.48                          | 1.25±0.23                            | 43.30±1.50                          | 517.6±0.5                                | 258.1±0.08            | 56.7  | c                |
| LHS 2328         | 10 55 34.47 | -09 21 25.9  | R             | 8s                        | 66                      | 2001.15–2009.25              | 8.10                      | 9                       | 53.03±1.47                          | 0.81±0.08                            | 53.84±1.47                          | 516.2±0.5                                | 330.9±0.10            | 45.4  | c                |
| LHS 2335         | 10 58 35.10 | -31 08 38.4  | V             | 3c                        | 56                      | 2001.14–2005.14              | 1.99                      | 8                       | 49.58±1.54                          | 0.97±0.20                            | 50.55±1.55                          | 571.7±3.0                                | 260.9±0.49            | 53.6  | c                |
| LHS 2401         | 11 23 57.31 | -18 21 48.6  | V             | 5s                        | 70                      | 2001.15–2009.14              | 3.99                      | 5                       | 51.74±2.50                          | 2.73±0.17                            | 54.47±2.51                          | 576.4±1.4                                | 266.6±0.22            | 50.2  | c                |
| GJ 1147          | 11 38 24.95 | -41 22 32.5  | R             | 5s+                       | 64                      | 2001.15–2009.04              | 7.89                      | 10                      | 65.13±1.08                          | 0.95±0.09                            | 66.08±1.08                          | 942.4±0.7                                | 274.0±0.06            | 67.6  | c                |
| GJ 438           | 11 43 19.82 | -51 50 25.9  | R             | 6s+                       | 92                      | 2000.06–2009.32              | 9.26                      | 6                       | 89.13±2.03                          | 2.57±0.30                            | 91.70±2.05                          | 857.0±0.9                                | 129.9±0.12            | 44.3  | c,e              |
| LHS 2520         | 12 10 05.59 | -15 04 16.9  | V             | 4s                        | 56                      | 2000.07–2004.43              | 4.37                      | 7                       | 77.11±2.40                          | 0.82±0.17                            | 77.93±2.41                          | 718.6±1.6                                | 183.5±0.18            | 43.7  | c                |
| GJ 1157          | 12 23 01.43 | -46 37 08.4  | V             | 5s                        | 61                      | 2001.14–2005.14              | 3.99                      | 7                       | 61.00±0.61                          | 1.42±0.16                            | 62.42±0.63                          | 819.5±0.5                                | 245.0±0.06            | 62.2  | c                |
| LHS 2567         | 12 29 54.19 | -05 27 28.4  | R             | 7s                        | 58                      | 2000.07–2009.03              | 8.96                      | 7                       | 45.54±1.83                          | 1.26±0.07                            | 46.80±1.83                          | 611.1±0.6                                | 241.0±0.11            | 61.9  | c,A              |
| LHS 2568         | 12 29 54.66 | -05 27 20.6  | R             | 7s                        | 58                      | 2000.07–2009.03              | 8.96                      | 7                       | 47.29±1.81                          | 1.26±0.07                            | 48.55±1.81                          | 597.8±0.6                                | 241.5±0.11            | 58.4  | c,B              |
| LHS 2718         | 13 20 03.86 | -35 24 44.1  | R             | 5s                        | 62                      | 2001.15–2005.14              | 3.99                      | 11                      | 72.05±0.78                          | 0.99±0.11                            | 73.04±0.79                          | 961.6±0.6                                | 241.1±0.07            | 62.4  | c                |
| LHS 2729         | 13 23 38.02 | -25 54 45.1  | R             | 5s                        | 56                      | 2001.15–2005.09              | 3.94                      | 12                      | 70.32±1.52                          | 1.16±0.14                            | 71.48±1.53                          | 633.9±1.3                                | 249.8±0.21            | 42.0  | c                |
| LHS 2836         | 13 59 10.45 | -19 50 03.4  | V             | 3c+                       | 108                     | 2000.14–2004.18              | 4.04                      | 8                       | 91.23±0.86                          | 1.64±0.23                            | 92.86±0.89                          | 573.4±1.0                                | 252.0±0.17            | 29.3  | c                |
| LHS 2899         | 14 21 15.12 | -01 07 19.7  | V             | 5s                        | 45                      | 2000.14–2005.14              | 4.99                      | 8                       | 74.00±2.15                          | 0.66±0.05                            | 74.66±2.15                          | 643.5±1.4                                | 164.4±0.21            | 40.9  | c,gA             |
| LHS 3001         | 14 56 27.16 | +17 55 00.0  | V             | 5s                        | 78                      | 2000.58–2009.25              | 8.67                      | 9                       | 56.36±1.34                          | 0.81±0.07                            | 57.17±1.34                          | 982.4±0.8                                | 301.2±0.09            | 81.5  | c                |
| LHS 3002         | 14 56 27.79 | +17 55 08.9  | V             | 5s                        | 78                      | 2000.58–2009.25              | 8.67                      | 9                       | 54.89±1.35                          | 0.81±0.07                            | 55.64±1.35                          | 987.8±0.8                                | 301.5±0.09            | 84.2  | c                |
| LHS 3167         | 16 13 05.93 | -70 09 08.0  | R             | 6s                        | 85                      | 2000.57–2009.32              | 8.75                      | 10                      | 58.22±0.93                          | 2.03±0.21                            | 60.25±0.95                          | 607.1±0.5                                | 202.1±0.08            | 47.8  | c                |
| LHS 3169         | 16 14 21.93 | -28 30 36.7  | V             | 5s                        | 53                      | 2000.58–2004.45              | 3.87                      | 10                      | 52.03±1.45                          | 1.40±0.17                            | 53.43±1.46                          | 523.9±1.0                                | 230.8±0.22            | 46.5  | c                |
| LHS 3197         | 16 26 48.12 | -17 23 34.3  | R             | 4c+                       | 51                      | 2000.23–2006.37              | 6.14                      | 9                       | 53.53±1.27                          | 1.50±0.50                            | 55.03±1.36                          | 522.2±1.0                                | 219.0±0.22            | 45.0  | c,h              |
| LHS 3218         | 16 35 24.64 | -27 18 54.7  | R             | 6s                        | 77                      | 2000.23–2009.32              | 9.09                      | 8                       | 51.31±0.74                          | 2.57±0.23                            | 53.88±0.77                          | 889.0±0.3                                | 180.7±0.03            | 78.2  | c                |
| GJ 633           | 16 40 45.26 | -45 59 59.3  | V             | 7s+                       | 100                     | 1999.64–2007.44              | 7.80                      | 10                      | 56.88±1.05                          | 2.59±0.56                            | 59.47±1.19                          | 527.2±0.4                                | 137.4±0.09            | 42.0  | c,e              |
| LHS 3295         | 17 29 27.34 | -80 08 57.4  | V             | 5s                        | 68                      | 2000.57–2004.25              | 3.68                      | 8                       | 78.20±1.79                          | 1.75±0.33                            | 79.95±1.82                          | 701.7±1.5                                | 312.8±0.25            | 41.6  | c                |
| WT 562           | 18 26 19.80 | -65 47 41.1  | V             | 4c+                       | 80                      | 2000.58–2005.64              | 5.06                      | 7                       | 57.53±0.90                          | 0.90±0.07                            | 58.43±0.90                          | 610.8±1.1                                | 180.9±0.15            | 49.6  | c                |
| LHS 3413         | 18 49 51.21 | -57 26 48.6  | R             | 5s                        | 69                      | 2000.57–2009.32              | 8.75                      | 9                       | 81.13±2.01                          | 1.08±0.08                            | 82.21±2.01                          | 675.7±0.8                                | 254.9±0.12            | 39.0  | c                |
| LHS 3443         | 19 13 07.96 | -39 01 53.8  | V             | 5s                        | 69                      | 2000.58–2009.75              | 9.17                      | 8                       | 47.44±1.14                          | 1.13±0.10                            | 48.57±1.14                          | 509.2±0.5                                | 118.3±0.10            | 49.7  | c                |
| LHS 3583         | 20 46 37.08 | -81 43 13.7  | V             | 8s                        | 68                      | 2000.58–2009.32              | 8.75                      | 9                       | 93.12±2.37                          | 1.60±0.21                            | 94.72±2.38                          | 704.6±1.0                                | 135.0±0.15            | 38.3  | c                |
| APMPM J2127-3844 | 21 27 04.58 | -38 44 50.8  | R             | 4s                        | 58                      | 1999.62–2004.73              | 5.11                      | 8                       | 48.70±1.38                          | 0.49±0.03                            | 49.25±1.38                          | 897.2±0.8                                | 144.6±0.10            | 86.3  | c                |
| WT 795           | 21 36 25.30 | -44 01 00.2  | R             | 4c+                       | 74                      | 2000.41–2004.44              | 4.03                      | 5                       | 68.84±0.69                          | 0.69±0.12                            | 69.53±0.70                          | 827.0±0.6                                | 144.4±0.08            | 56.4  | c                |
| LHS 3719         | 21 49 25.91 | -63 06 51.9  | V             | 4s+                       | 70                      | 2000.58–2003.69              | 3.11                      | 10                      | 59.05±1.37                          | 1.23±0.08                            | 60.28±1.37                          | 537.2±1.2                                | 032.2±0.24            | 42.2  | c                |
| LHS 3738AB       | 21 58 49.13 | -32 26 25.5  | R             | 9s                        | 113                     | 1999.64–2009.65              | 10.01                     | 10                      | 49.60±1.14                          | 1.27±0.07                            | 50.87±1.14                          | 537.3±0.5                                | 228.8±0.08            | 50.1  | BC <sup>cd</sup> |
| LHS 3739         | 21 58 50.19 | -32 28 17.8  | R             | 9s                        | 113                     | 1999.64–2009.65              | 10.01                     | 10                      | 49.70±1.05                          | 1.27±0.07                            | 50.97±1.05                          | 535.5±0.3                                | 229.2±0.07            | 49.8  | A <sup>e</sup>   |
| WT 870           | 22 06 40.68 | -44 58 07.4  | R             | 3c+                       | 70                      | 2000.41–2005.90              | 5.48                      | 7                       | 55.41±1.13                          | 1.10±0.05                            | 56.51±1.13                          | 736.3±0.7                                | 219.6±0.11            | 61.8  | c                |
| LHS 3909         | 23 12 11.30 | -14 06 11.9  | R             | 3c+                       | 55                      | 2000.58–2007.55              | 6.97                      | 6                       | 53.41±2.00                          | 1.49±0.05                            | 54.90±2.00                          | 716.3±1.7                                | 196.0±0.24            | 61.8  | c                |
| LHS 3925         | 23 17 50.33 | -48 18 20.2  | R             | 4c                        | 62                      | 2000.58–2005.80              | 5.23                      | 10                      | 45.38±1.17                          | 1.47±0.08                            | 46.85±1.17                          | 755.5±0.6                                | 157.5±0.08            | 76.4  | c                |
| LHS 4009AB       | 23 45 31.26 | -16 10 20.1  | R             | 6s                        | 83                      | 1999.62–2009.78              | 10.15                     | 7                       | 79.38±1.37                          | 0.59±0.03                            | 79.97±1.37                          | 690.7±0.4                                | 216.9±0.07            | 40.9  | c                |
| LHS 4016         | 23 48 36.06 | -27 39 38.9  | V             | 6s                        | 68                      | 2000.87–2009.75              | 8.87                      | 6                       | 40.75±1.54                          | 0.50±0.19                            | 41.25±1.55                          | 595.3±0.4                                | 246.2±0.08            | 68.5  | c                |

Continued on next page

Table 5.1 – Continued from previous page

| Name<br>(1)  | R.A.<br>(2) | Decl.<br>(3) | Filter<br>(4) | $N_{sea}^b$<br>(5) | $N_{frm}^b$<br>(6) | Coverage <sup>b</sup><br>(7) | Years <sup>b</sup><br>(8) | $N_{ref}^b$<br>(9) | $\pi_{rel}$<br>(mas)<br>(10) | $\pi_{corr}$<br>(mas)<br>(11) | $\pi_{abs}$<br>(mas)<br>(12) | $\mu$<br>(mas yr <sup>-1</sup> )<br>(13) | P.A.<br>(deg)<br>(14) | $V_{tan}$<br>(km s <sup>-1</sup> )<br>(15) | Notes<br>(16) |
|--------------|-------------|--------------|---------------|--------------------|--------------------|------------------------------|---------------------------|--------------------|------------------------------|-------------------------------|------------------------------|--|-----------------------|--|---------------|
| LHS 4021     | 23 50 31.64 | -09 33 32.6  | V             | 4s+                | 60                 | 2000.71–2004.89              | 4.18                      | 6                  | 61.48±1.70                   | 0.93±0.04                     | 62.41±1.70                   | 758.1±1.4                                | 121.7±0.20            | 57.6                                       | <sup>c</sup>  |
| LHS 4058     | 23 59 51.38 | -34 06 42.5  | V             | 5s+                | 59                 | 2000.41–2006.87              | 6.45                      | 7                  | 61.15±1.98                   | 1.99±0.38                     | 63.14±2.02                   | 939.0±1.2                                | 132.8±0.15            | 70.5                                       | <sup>c</sup>  |
| Beyond 25 pc |             |              |               |                    |                    |                              |                           |                    |                              |                               |                              |  |                       |  |               |
| LHS 1561     | 03 34 39.63 | -04 50 33.3  | V             | 6c                 | 61                 | 2000.07–2009.99              | 9.93                      | 9                  | 33.19±1.72                   | 1.01±0.11                     | 34.20±1.72                   | 513.0±0.7                                | 126.6±0.16            | 71.1                                       | <sup>c</sup>  |
| LHS 1656     | 04 18 51.03 | -57 14 01.1  | I             | 5c+                | 51                 | 2003.95–2009.74              | 5.78                      | 8                  | 38.16±1.94                   | 1.25±0.08                     | 39.41±1.94                   | 814.5±1.3                                | 022.1±0.16            | 98.0                                       |               |
| LTT 5066     | 13 13 29.63 | -32 27 05.3  | R             | 6s+                | 69                 | 2000.14–2009.32              | 9.18                      | 8                  | 20.61±0.92                   | 0.98±0.04                     | 21.59±0.92                   | 575.9±0.4                                | 267.6±0.05            | 126.4                                      | <sup>c</sup>  |
| LHS 3080     | 15 31 54.17 | +28 51 09.7  | R             | 6c                 | 66                 | 2000.58–2009.57              | 8.99                      | 9                  | 34.73±1.85                   | 0.79±0.06                     | 35.52±1.85                   | 538.8±0.7                                | 274.4±0.11            | 71.9                                       |               |
| LHS 3147     | 16 02 23.57 | -25 05 57.3  | R             | 5s+                | 72                 | 2001.21–2009.31              | 8.10                      | 8                  | 37.19±1.35                   | 1.99±0.22                     | 39.18±1.37                   | 666.3±0.6                                | 202.3±0.09            | 80.6                                       |               |
| GJ 762       | 19 34 36.48 | -62 50 38.6  | V             | 4c                 | 74                 | 2000.58–2003.30              | 2.72                      | 10                 | 37.20±1.34                   | 1.52±0.10                     | 38.72±1.34                   | 510.7±1.5                                | 227.2±0.34            | 62.5                                       |               |
| LHS 3484     | 19 47 04.49 | -71 05 33.1  | R             | 7s                 | 65                 | 2000.58–2009.32              | 8.75                      | 8                  | 37.51±1.51                   | 2.14±0.15                     | 39.65±1.52                   | 649.8±0.6                                | 172.9±0.09            | 77.7                                       |               |
| LHS 3836     | 22 38 02.92 | -65 50 08.8  | R             | 5s                 | 61                 | 1999.62–2004.45              | 4.82                      | 7                  | 35.90±1.32                   | 0.52±0.02                     | 36.42±1.32                   | 693.9±1.0                                | 118.9±0.17            | 90.3                                       |               |

<sup>a</sup>Coordinates are epoch and equinox 2000.0; each target's coordinates were extracted from 2MASS and then transformed to epoch 2000.0 using the proper motions and position angles listed here.

<sup>b</sup>'Coverage' and 'Years' run from the first to last data point; ' $N_{sea}$ ' counts observing semesters where a dataset was taken, and denotes if coverage was 'c'ontinuous (more than one night of data in all seasons) or 's'cattered. Coverage extended by a single frame is denoted with a + in the  $N_{sea}$  column.  $N_{frm}$  is number of frames,  $N_{ref}$  is the number of reference stars. System has notes in §5.2.3.

<sup>d</sup>The astrometric perturbation was removed from the final parallax fit.

<sup>e</sup>Astrometric results use new  $V$  filter data.

<sup>f</sup>Astrometric results use new  $V$  filter data *only*.

<sup>g</sup>Coordinates were wrong in Riedel et al. (2010).

<sup>h</sup>Generic correction to absolute adopted; field is reddened by a nebula.

Table 5.2: Photometric Results (Riedel et al. 2010)

| Name<br>(1)      | Alternate<br>Name<br>(2) | $V_J$<br>(3) | $R_{KC}$<br>(4) | $I_{KC}$<br>(5) | No. of abs.<br>nights<br>(6) | $\pi$<br>filter <sup>a</sup><br>(7) | $\sigma$<br>(mag) <sup>b</sup><br>(8) | No. of rel.<br>Nights <sup>b</sup><br>(9) | No. of rel.<br>Frames <sup>b</sup><br>(10) | $J$<br>(11) | $H$<br>(12) | $K_s$<br>(13) | spectral<br>type<br>(14) | ref<br>(15)        | phot<br>distance<br>(16) | No. of<br>Relations<br>(17) | notes<br>(18) |
|------------------|--------------------------|--------------|-----------------|-----------------|------------------------------|-------------------------------------|---------------------------------------|---|--|-------------|-------------|---------------|--------------------------|--------------------|--------------------------|-----------------------------|---------------|
| LHS 1050         | GJ 12                    | 12.62        | 11.46           | 10.04           | 3                            | V                                   | .011                                  | 12  | 60   | 8.62        | 8.07        | 7.81          | M3.0V                    | .....              | 15.17±2.37               | 12                          |               |
| LHS 1351         | L 125-51                 | 12.23        | 11.15           | 9.82            | 2                            | V                                   | .010                                  | 12  | 68   | 8.54        | 7.98        | 7.73          | M2.5V                    | Haw96 <sup>c</sup> | 18.04±2.81               | 12                          |               |
| LHS 1358         | G 159-46                 | 13.58        | 12.31           | 10.66           | 2                            | R                                   | .015                                  | 11  | 58   | 9.06        | 8.52        | 8.17          | M4.0V                    | Rei95 <sup>d</sup> | 12.54±1.94               | 12                          |               |
| LHS 1491         | LP 771-77                | 12.84        | 11.65           | 10.13           | 2                            | V                                   | .018                                  | 15  | 70   | 8.63        | 8.02        | 7.75          | M3.5V                    | Rei95              | 12.42±1.95               | 12                          |               |
| LHS 1582AB       | G 160-19                 | 14.69        | 13.33           | 11.60           | 4                            | R                                   | .019                                  | 19  | 70   | 9.80        | 9.18        | 8.85          | M4.5VJ                   | Rei95              | 13.27±2.25               | 12                          |               |
| LHS 1630AB       | LP 833-42                | 12.38        | 11.22           | 9.68            | 4                            | R                                   | .015                                  | 22  | 137  | 8.24        | 7.68        | 7.44          | M3.5VJ                   | .....              | 11.72±1.84               | 12                          | a             |
| LHS 1748         | L 521-2                  | 12.08        | 11.06           | 9.83            | 2                            | V                                   | .017                                  | 11  | 58   | 8.59        | 7.99        | 7.73          | M2.5V                    | Haw96              | 19.91±3.13               | 12                          |               |
| LHS 1749A        | L 57-44                  | 11.74        | 10.70           | 9.47            | 2                            | V                                   | .028                                  | 16  | 91   | 8.21        | 7.62        | 7.36          | M2.0V                    | Haw96              | 16.44±2.58               | 12                          |               |
| LHS 1767         | LP 892-51                | 13.11        | 11.93           | 10.45           | 2                            | V                                   | .012                                  | 13  | 57   | 9.05        | 8.49        | 8.19          | M3.0V                    | .....              | 17.31±2.72               | 12                          | a             |
| WT 178           | LP 178                   | 14.81        | 13.47           | 11.77           | 3                            | R                                   | .014                                  | 16  | 68   | 10.14       | 9.53        | 9.23          | M4.5V                    | Rei07 <sup>e</sup> | 18.41±2.86               | 12                          |               |
| APMPM J0544-4108 |                          | 14.12        | 12.85           | 11.25           | 2                            | V                                   | .010                                  | 17  | 76   | 9.74        | 9.16        | 8.87          | M3.5V                    | .....              | 19.08±3.01               | 12                          |               |
| LHS 1807         | LP 779-10                | 13.26        | 12.10           | 10.62           | 2                            | R                                   | .008                                  | 12  | 66   | 9.22        | 8.67        | 8.37          | M3.0V                    | Kir95 <sup>f</sup> | 19.12±2.98               | 12                          |               |
| GJ 1088          | LHS 1831                 | 12.28        | 11.11           | 9.61            | 2                            | V                                   | .016                                  | 13  | 51   | 8.17        | 7.58        | 7.31          | M3.5V                    | .....              | 11.02±1.69               | 12                          |               |
| LHS 1932         | L 240-16                 | 12.48        | 11.36           | 9.92            | 2                            | V                                   | .010                                  | 16  | 93   | 8.55        | 8.04        | 7.76          | M3.5V                    | Haw96              | 15.84±2.52               | 12                          |               |
| LHS 1955AB       | L 601-78                 | 12.79        | 11.52           | 9.89            | 2                            | R                                   | .011                                  | 13  | 83   | 8.31        | 7.69        | 7.35          | M4.0VJ                   | Rei95              | 8.56±1.35                | 12                          |               |
| LHS 2010         | L 387-102                | 11.86        | 10.70           | 9.19            | 3                            | V                                   | .011                                  | 14  | 85   | 7.75        | 7.15        | 6.87          | M3.5V                    | Haw96              | 8.91±1.37                | 12                          |               |
| LHS 2021         | LP 485-17                | 19.21        | 16.94           | 14.66           | 3                            | J                                   | .016                                  | 15  | 54   | 11.89       | 11.17       | 10.76         | M6.0V                    | .....              | 14.42±2.26               | 12                          |               |
| LHS 2071AB       | LP 844-28                | 13.88        | 12.55           | 10.82           | 3                            | R                                   | .016                                  | 16  | 69   | 9.11        | 8.54        | 8.20          | M4.0VJ                   | .....              | 10.77±1.66               | 12                          |               |
| LHS 2106         | LP 845-23                | 14.21        | 12.87           | 11.13           | 3                            | R                                   | .014                                  | 12  | 56   | 9.53        | 9.00        | 8.65          | M4.5V                    | Rei95              | 14.47±2.42               | 12                          |               |
| LHS 2122         | L 140-119                | 12.57        | 11.43           | 9.94            | 2                            | R                                   | .015                                  | 14  | 64   | 8.47        | 7.83        | 7.55          | M3.5V                    | Haw96              | 11.86±2.00               | 12                          |               |
| LHS 5156         | L 140-289                | 13.30        | 11.98           | 10.28           | 4                            | V                                   | .010                                  | 14  | 60   | 8.62        | 8.10        | 7.77          | M4.5V                    | .....              | 9.62±1.50                | 12                          | a             |
| WT 244           | L 15-17                  | 15.17        | 13.80           | 12.02           | 3                            | J                                   | .010                                  | 14  | 64   | 10.23       | 9.71        | 9.38          | M4.5V                    | .....              | 17.13±2.66               | 12                          |               |
| LHS 2328         | G 163-23                 | 13.55        | 12.37           | 10.86           | 2                            | V                                   | .020                                  | 15  | 66   | 9.42        | 8.87        | 8.61          | M3.5V                    | Rei95              | 20.27±3.16               | 12                          |               |
| LHS 2335         | LP 905-36                | 11.93        | 10.90           | 9.63            | 2                            | V                                   | .010                                  | 9   | 56   | 8.36        | 7.76        | 7.47          | M2.5V                    | Haw96              | 16.62±2.68               | 12                          |               |
| LHS 2401         | L 755-53                 | 13.10        | 11.97           | 10.54           | 3                            | V                                   | .014                                  | 12  | 70   | 9.17        | 8.59        | 8.32          | M3.0V                    | Rei95              | 19.89±3.06               | 12                          |               |
| GJ 1147          | LHS 2435                 | 13.72        | 12.49           | 10.91           | 3                            | V                                   | .014                                  | 14  | 64   | 9.44        | 8.86        | 8.54          | M3.0V                    | Haw96              | 17.40±2.73               | 12                          |               |
| GJ 438           | LHS 2447                 | 10.35        | 9.36            | 8.27            | 4                            | V                                   | .008                                  | 14  | 92   | 7.14        | 6.58        | 6.32          | M1.0V                    | .....              | 12.63±1.98               | 12                          | a             |
| LHS 2520         | LP 734-32                | 12.09        | 10.88           | 9.30            | 3                            | V                                   | .014                                  | 10  | 56   | 7.77        | 7.14        | 6.86          | M3.5V                    | Rei95              | 7.59±1.20                | 12                          |               |
| GJ 1157          | LHS 2552                 | 13.59        | 12.35           | 10.71           | 2                            | V                                   | .015                                  | 13  | 61   | 9.17        | 8.63        | 8.36          | M4.0V                    | Haw96              | 14.98±2.37               | 12                          |               |
| LHS 2567         | G 13-44A                 | 13.08        | 11.87           | 10.33           | 3                            | R                                   | .015                                  | 12  | 58   | 8.82        | 8.27        | 7.96          | M3.5V                    | Rei95              | 13.55±2.09               | 12                          | A             |
| LHS 2568         | G 13-44B                 | 14.21        | 12.96           | 11.37           | 3                            | R                                   | .013                                  | 12  | 58   | 9.79        | 9.24        | 8.92          | M3.5V                    | Rei95              | 18.99±2.94               | 12                          | B             |
| LHS 2718         | L 473-1                  | 12.84        | 11.70           | 10.24           | 3                            | V                                   | .012                                  | 9   | 62   | 8.63        | 8.25        | 7.98          | M3.0V                    | Haw96              | 16.04±2.46               | 12                          |               |
| LHS 2729         | L 617-35                 | 12.89        | 11.68           | 10.14           | 2                            | R                                   | .012                                  | 12  | 56   | 8.66        | 8.07        | 7.78          | M3.5V                    | Rei95              | 12.59±1.94               | 12                          |               |
| LHS 2836         | L 763-63                 | 12.88        | 11.60           | 9.90            | 3                            | V                                   | .013                                  | 22  | 108  | 8.33        | 7.76        | 7.44          | M4.0V                    | .....              | 8.86±1.39                | 12                          |               |
| LHS 2899         | G 124-27                 | 13.12        | 11.92           | 10.39           | 3                            | V                                   | .016                                  | 12  | 45   | 8.95        | 8.39        | 8.09          | M3.5V                    | Rei95              | 15.40±2.41               | 12                          | A             |
| LHS 3001         | LP 441-33                | 15.81        | 14.35           | 12.52           | 2                            | J                                   | .013                                  | 17  | 78   | 10.74       | 10.15       | 9.85          | M4.5V                    | Rei95              | 19.74±3.12               | 12                          | B             |
| LHS 3002         | LP 441-34                | 18.68        | 16.65           | 14.42           | 2                            | R                                   | .012                                  | 14  | 78   | 11.98       | 11.30       | 10.92         | M6.0V                    | Rei95              | 17.47±2.72               | 12                          |               |
| LHS 3167         | L 74-208                 | 13.71        | 12.45           | 10.82           | 3                            | R                                   | .014                                  | 17  | 85   | 9.26        | 8.74        | 8.39          | M4.0V                    | .....              | 14.73±2.30               | 12                          |               |
| LHS 3169         | L 626-41                 | 12.95        | 11.80           | 10.29           | 2                            | V                                   | .011                                  | 10  | 53   | 8.92        | 8.36        | 8.11          | M3.5V                    | Rei95              | 17.31±2.82               | 12                          |               |
| LHS 3197         | LP 805-10                | 14.30        | 12.93           | 11.16           | 2                            | R                                   | .011                                  | 14  | 51   | 9.55        | 9.00        | 8.68          | M4.5V                    | .....              | 14.13±2.43               | 12                          |               |
| LHS 3218         | LP 862-184               | 14.18        | 12.93           | 11.28           | 2                            | R                                   | .016                                  | 18  | 77   | 9.78        | 9.27        | 9.00          | M4.0V                    | Rei95              | 20.86±3.67               | 12                          |               |
| GJ 633           | LHS 3233                 | 12.67        | 11.56           | 10.20           | 5                            | V                                   | .011                                  | 20  | 100  | 8.89        | 8.31        | 8.05          | M2.5V                    | .....              | 19.47±3.03               | 12                          | a             |
| LHS 3295         | L 21-3                   | 12.18        | 11.02           | 9.53            | 2                            | V                                   | .007                                  | 14  | 68   | 8.09        | 7.52        | 7.30          | M3.0V                    | .....              | 11.32±1.75               | 12                          |               |
| WT 562           | L 165-102                | 15.36        | 13.93           | 12.13           | 3                            | J                                   | .010                                  | 18  | 80   | 10.35       | 9.81        | 9.45          | M4.5V                    | .....              | 16.96±2.65               | 12                          |               |
| LHS 3413         | LP 207-41                | 12.68        | 11.44           | 9.88            | 3                            | R                                   | .017                                  | 13  | 69   | 8.32        | 7.70        | 7.46          | M3.5V                    | Haw96              | 9.85±1.56                | 12                          |               |
| LHS 3443         | L 491-42                 | 12.39        | 11.27           | 9.85            | 3                            | V                                   | .009                                  | 14  | 69   | 8.47        | 7.92        | 7.66          | M2.0V                    | Haw96              | 14.98±2.30               | 12                          |               |
| LHS 3583         | L 23-30                  | 11.50        | 10.39           | 9.02            | 3                            | V                                   | .014                                  | 14  | 68   | 7.69        | 7.12        | 6.83          | M2.5V                    | Haw96              | 10.83±1.69               | 12                          | a             |
| APMPM J2127-3844 |                          | 14.60        | 13.31           | 11.66           | 2                            | R                                   | .015                                  | 12  | 58   | 10.03       | 9.56        | 9.28          | M4.0V                    | .....              | 21.41±3.53               | 12                          |               |
| WT 795           | L 4-15                   | 12.80        | 11.08           | 9.83            | 3                            | V                                   | .015                                  | 17  | 74   | 9.46        | 8.83        | 8.53          | M4.0V                    | .....              | 13.11±2.05               | 12                          |               |
| LHS 3719         | L 165-102                | 12.56        | 11.45           | 10.08           | 2                            | V                                   | .012                                  | 14  | 70   | 8.74        | 8.12        | 7.89          | M2.0V                    | Haw96              | 17.23±2.69               | 12                          | BC            |
| LHS 3738AB       | LP 930-69                | 15.78        | 14.29           | 12.46           | 3                            | R                                   | .010                                  | 24  | 113  | 10.65       | 10.09       | 9.76          | M4.5VJ                   | Haw96              | 18.50±2.96               | 12                          |               |
| LHS 3739         | LP 930-70                | 14.72        | 13.45           | 11.88           | 3                            | R                                   | .010                                  | 24  | 113  | 10.39       | 9.83        | 9.56          | M3.5V                    | Haw96              | 27.56±4.50               | 12                          | A             |
| WT 870           | L 4-43                   | 14.43        | 13.10           | 11.40           | 2                            | R                                   | .015                                  | 15  | 70   | 9.76        | 9.18        | 8.89          | M4.0V                    | .....              | 15.99±2.47               | 12                          |               |
| LHS 3909         | LP 762-3                 | 12.97        | 11.82           | 10.40           | 2                            | R                                   | .012                                  | 12  | 55   | 9.06        | 8.48        | 8.22          | M3.0V                    | Rei95              | 19.45±3.09               | 12                          |               |
| LHS 3925         | L 359-91                 | 13.61        | 12.44           | 10.92           | 2                            | R                                   | .008                                  | 12  | 62   | 9.53        | 8.97        | 8.71          | M3.5V                    | Haw96              | 21.89±3.53               | 12                          |               |
| LHS 4009AB       | G 273-130                | 14.38        | 12.90           | 10.99           | 3                            | R                                   | .017                                  | 17  | 83   | 9.21        | 8.61        | 8.31          | M4.5VJ                   | .....              | 9.21±1.51                | 12                          |               |
| LHS 4016         | G 275-106                | 12.34        | 11.24           | 9.90            | 2                            | V                                   | .016                                  | 16  | 68   | 8.58        | 8.02        | 7.74          | M2.5V                    | Rei95              | 17.20±2.67               | 12                          |               |
| LHS 4021         | G 273-147                | 13.44        | 12.19           | 10.59           | 2                            | V                                   | .017                                  | 15  | 60   | 8.94        | 8.39        | 8.04          | M4.0V                    | Rei95              | 11.84±1.95               | 12                          |               |
| LHS 4058         | G 267-11                 | 12.84        | 11.64           | 10.08           | 2                            | V                                   | .011                                  | 16  | 59   | 8.59        | 7.98        | 7.74          | M3.5V                    | .....              | 12.24±1.89               | 12                          | a             |

Continued on next page

Table 5.2 – Continued from previous page

| Name<br>(1) | Alternate<br>Name<br>(2) | $V_J$<br>(3) | $R_{KC}$<br>(4) | $I_{KC}$<br>(5) | No. of abs.<br>nights<br>(6) | $\pi$<br>filter <sup>a</sup><br>(7) | $\sigma$<br>(mag) <sup>b</sup><br>(8) | No. of rel.<br>Nights <sup>b</sup><br>(9) | No. of rel.<br>Frames <sup>b</sup><br>(10) | $J$<br>(11) | $H$<br>(12) | $K_s$<br>(13) | spectral<br>type<br>(14) | ref<br>(15) | phot<br>distance<br>(16) | No. of<br>Relations<br>(17) | notes<br>(18) |
|-------------|--------------------------|--------------|-----------------|-----------------|------------------------------|-------------------------------------|---------------------------------------|---|--|-------------|-------------|---------------|--------------------------|-------------|--------------------------|-----------------------------|---------------|
| LHS 1561    | G 77-64                  | 13.07        | 11.84           | 10.30           | 4                            | V                                   | .010                                  | Beyond 25 pc                              | 61   | 8.83        | 8.27        | 7.93          | M3.5V                    | Rei95       | 13.49±2.14               | 12                          |               |
| LHS 1656    | L 178-47                 | 13.29        | 12.18           | 10.84           | 2                            | I                                   | .009                                  | 13  | 51   | 9.52        | 8.94        | 8.65          | M2.5V                    | .....       | 25.68±4.03               | 12                          |               |
| LTT 5066    | LHS 2698                 | 14.21        | 13.14           | 11.76           | 2                            | R                                   | .010                                  | 16  | 69   | 10.48       | 9.96        | 9.70          | M3.0V                    | .....       | 44.38±7.27               | 12                          |               |
| LHS 3080    | G 167-47                 | 14.32        | 13.01           | 11.32           | 2                            | R                                   | .012                                  | 17  | 66   | 9.67        | 9.11        | 8.82          | M4.0V                    | .....       | 15.73±3.41               | 12                          |               |
| LHS 3147    | LP 861-12                | 13.20        | 12.09           | 10.63           | 2                            | R                                   | .012                                  | 18  | 72   | 9.28        | 8.69        | 8.41          | M3.5V                    | Rei95       | 20.74±3.23               | 12                          |               |
| GJ 762      | LHS 3471                 | 12.09        | 11.07           | 9.83            | 2                            | V                                   | .008                                  | 13  | 74   | 8.59        | 8.00        | 7.77          | M2.5V                    | Haw96       | 20.36±3.14               | 12                          |               |
| LHS 3484    | L 79-24                  | 13.88        | 12.70           | 11.19           | 2                            | R                                   | .008                                  | 14  | 65   | 9.79        | 9.22        | 8.98          | M3.5V                    | Haw96       | 24.66±3.94               | 12                          |               |
| LHS 3836    | L 119-44                 | 14.34        | 13.14           | 11.61           | 2                            | R                                   | .009                                  | 11  | 61   | 10.18       | 9.67        | 9.41          | M3.5V                    | .....       | 29.54±5.00               | 12                          |               |

<sup>a</sup> Astrometric results and relative photometry use  $\sigma V$  and  $mV$  filter data.

<sup>b</sup> Absolute Photometry has been transformed to Johnson-Kron-Cousins using comparisons to photometric standard stars. Relative photometry is calculated in instrumental magnitudes, relative to the reference stars, on our astrometric frames.

<sup>c</sup> Hawley et al. (1996)

<sup>d</sup> Reid et al. (1995)

<sup>e</sup> Reid et al. (2007) (luminosity class inferred from the paper, where giants were simply discarded)

<sup>f</sup> Kirkpatrick et al. (1995)

Table 5.3: Combined System Parallaxes (Riedel et al. 2010)

| Name<br>(1) | $\pi$<br>(mas)<br>(2) | source<br>(3) | Name<br>(4) | $\pi$<br>(mas)<br>(5) | source<br>(6)                       | Weighted $\pi$<br>(mas)<br>(7) |
|-------------|-----------------------|---------------|-------------|-----------------------|-------------------------------------|--------------------------------|
| LHS 1050    | 85.85±2.57            | this work     | LHS 1050    | 86.60±13.40           | YPC                                 |                                |
|             |                       |               | LHS 1050    | 87.40±3.40            | <a href="#">Smart et al. (2010)</a> | 86.42±2.03                     |
| LHS 1749A   | 46.14±1.46            | this work     | LHS 1749A   | 45.36±5.08            | <a href="#">Costa et al. (2006)</a> | 46.08±1.40                     |
| LHS 2021    | 63.67±1.15            | this work     | LHS 2021    | 59.81±4.52            | <a href="#">Costa et al. (2006)</a> | 63.44±1.11                     |
| GJ 438      | 91.70±2.05            | this work     | GJ 438      | 118.90±15.00          | YPC                                 | 92.20±2.03                     |
| LHS 2567    | 46.80±1.83            | this work     | LHS 2568    | 48.55±1.81            | this work                           | 47.68±1.29                     |
| LHS 3001    | 57.17±1.34            | this work     | LHS 3002    | 55.64±1.35            | this work                           | 56.41±0.95                     |
| GJ 633      | 59.47±1.19            | this work     | GJ 633      | 104.00±13.70          | YPC                                 | 59.80±1.19                     |
| LHS 3739    | 50.97±1.05            | this work     | LHS 3738AB  | 50.87±1.14            | this work                           | 50.92±0.77                     |
| GJ 762      | 38.72±1.34            | this work     | GJ 762      | 60.30±14.90           | YPC                                 | 38.89±1.33                     |

### 5.2.2.2 Astrometry — Multiples

There are 14 apparent multiples in this sample. LHS 1630AB, LHS 1749AB, LHS 1955AB, LHS 2567/2568, LHS 3001/3002, LHS 3739/3738, and LHS 4009AB were all known prior to [Riedel et al. \(2010\)](#). LHS 1582AB, LHS 2071AB, and LHS 3738AB are new astrometric multiples first published in [Riedel et al. \(2010\)](#). We suspected LHS 1561, LHS 2520, LHS 2567, LHS 3080, and LHS 4016 (and see [Shkolnik et al. 2010](#)) of being unresolved binaries based on their locations on color-magnitude diagrams.

We have resolved orbital motion above the  $3\text{-}\sigma$  level (angular motion or changes in separation) for five of the previously known multiple systems (LHS 1749AB, LHS 1955AB, LHS 2567/2568, LHS 3001/3002, LHS 3739/3738), as described in [Table 5.4](#). Apart from LHS 1955AB, all values published in [Table 5.4](#) are derived from at least three frames on the nights listed. Semimajor axes of photocentric orbits are noted with  $\alpha$ .

*Continued on next page*

Table 5.4 – *Continued from previous page*

| Binary Name | UT Date | Sep. (mas) | P.A. (deg) | Period (years) | $\Delta$ (mag) | Notes |
|-------------|---------|------------|------------|----------------|----------------|-------|
| (1)         | (2)     | (3)        | (4)        | (5)            | (6)            | (7)   |

Table 5.4: Multiple System Parameters (Riedel et al. 2010)

| Binary Name | UT Date     | Sep. (mas)    | P.A. (deg) | Period (years) | $\Delta$ (mag)      | Notes                                    |
|-------------|-------------|---------------|------------|----------------|---------------------|--|
| (1)         | (2)         | (3)           | (4)        | (5)            | (6)                 | (7)                                      |
| LHS 1582AB  | -           | 18.4±2.8      | -          | 6.4±0.3        | -                   | photocentric $\alpha$                    |
| LHS 1630AB  | -           | -             | -          | >9             | -                   | (never resolved)                         |
| LHS 1749AB  | 2002 JAN 31 | 2847.8±28.5   | 138.2±0.30 | >4             | $\Delta V \sim 2.8$ |  |
|             | 2004 DEC 28 | 2853.8±10.9   | 140.0±0.19 |                |                     |  |
| LHS 1955AB  | 2001 JAN 18 | 808.1±31.8    | 103.9±4.40 | $\sim 80$      | $\Delta R \sim 0.5$ |  |
|             | 2009 APR 28 | 948.8:        | 66.5:      |                |                     | based on one frame                       |
| LHS 2071AB  | -           | 21.2±4.0      | -          | 16.5±2.8       |                     | photocentric $\alpha$ ; period uncertain |
| LHS 2567/8  | 2000 JAN 27 | 7938.2± 3.6   | 61.3±0.03  | >9             | $\Delta V = 1.14$   |  |
|             | 2009 JAN 13 | 8062.2± 1.7   | 61.4±0.03  |                |                     |  |
| LHS 3001/2  | 2000 JUL 30 | 12676.9± 7.3  | 45.4±0.02  | >9             | $\Delta V = 2.96$   |  |
|             | 2009 MAR 31 | 12702.6± 4.7  | 46.1±0.02  |                |                     |  |
| LHS 3739/8  | 1999 OCT 26 | 113215.6±31.4 | 353.7±0.01 | >10            | $\Delta V = 1.06$   | (wide)                                   |
|             | 2009 AUG 27 | 113115.6±25.1 | 354.3±0.01 |                |                     |  |
| LHS 3738AB  | -           | 26.5±1.8      | -          | 5.9±0.2        |                     | photocentric $\alpha$ (close)            |
| LHS 4009AB  | -           | -             | -          | -              | -                   | (never resolved)                         |

The components of LHS 1630AB, LHS 1749AB and LHS 1955AB are close enough that their point spread functions (PSFs) overlap, but all are at least elongated, providing evidence of two stars in the systems. In the case of LHS 1630AB the B component was never fully resolved, but it does appear as an elongation to the PSF. LHS 1749AB was only resolved in 15 frames from four nights. LHS 1955AB was only resolved in seven frames from five nights using restricted centroiding parameters that enabled the separation of blended sources; the two frames from the earliest night and the one frame from the latest night are used to derive the results in Table 5.4.

Errors presented in Table 5.4 include both measurement and systematic errors. The systematic errors were computed from the nights of data measured for Table 5.4, with the

exception of the three frames used for LHS 1955AB. All frames from a single visit (one night of observations on one system) were compared to the 2MASS All-Sky Point Source Catalog using *imwcs*<sup>9</sup>; the standard deviations of the plate scales and rotations per-visit were then averaged across all visits to get a more representative error. Systematics for the CTIO 0.9m on those frames give a 0.015% error in the plate scale (and therefore separations), and a 0.0083° error in the rotation (and therefore position angles). In all cases, the measurement errors dominate the systematic errors.

### 5.2.2.3 Astrometry — New astrometric multiples ( $sep \ll 1''$ )

Three of the systems discussed in Riedel et al. (2010) — LHS 1582AB, LHS 2071AB, and LHS 3738AB — have been found to be previously undetected astrometric binaries, as shown in Figures 5.1, 5.2, and 5.3, respectively. For comparison, three additional stars — LHS 2021, LHS 3739 and LHS 4009AB — are shown in Figures 5.4, 5.3 and 5.5. LHS 2021 and LHS 3739 appear to be single stars while LHS 4009AB is a known close binary that exhibits no perturbation in CTIOPI data to date. CTIOPI re-observed LHS 4009AB several years after the parallax was finished to search for a long-term perturbation; none was found. All five systems are discussed in detail in §5.2.3.

Photocentric orbital elements for the three new astrometric binaries were computed from the astrometric residuals using an iterative Thiele-Innes least-squares solver (Hartkopf et al. 1989) and are given in Table 5.5. Points from nights with only a single CCD image (generally obtained for the purpose of photometry) were removed. The orbits should be considered

---

<sup>9</sup>A World Coordinate System setting program from the WCSTools library, <http://td-www.harvard.edu/software/wcstools/> checked 15 JUL 2012

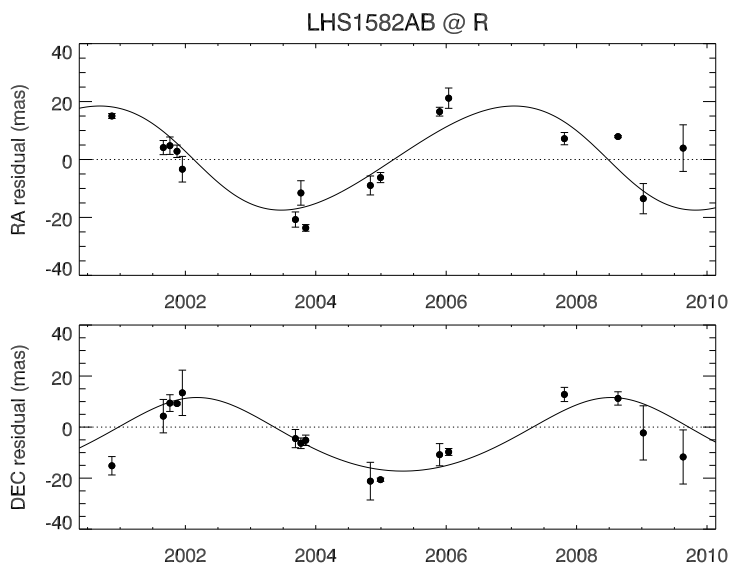


Figure 5.1: Plots of the nightly means of our astrometric residuals in RA and DEC for LHS 1582AB after solving for parallax and proper motion. A perturbation with a  $\sim 6$  year period is evident, and the resultant orbital fit (Table 5.5) is plotted on this graph. Two nights with only a single CCD image each (obtained for photometry) are not shown or used in the orbital solution.

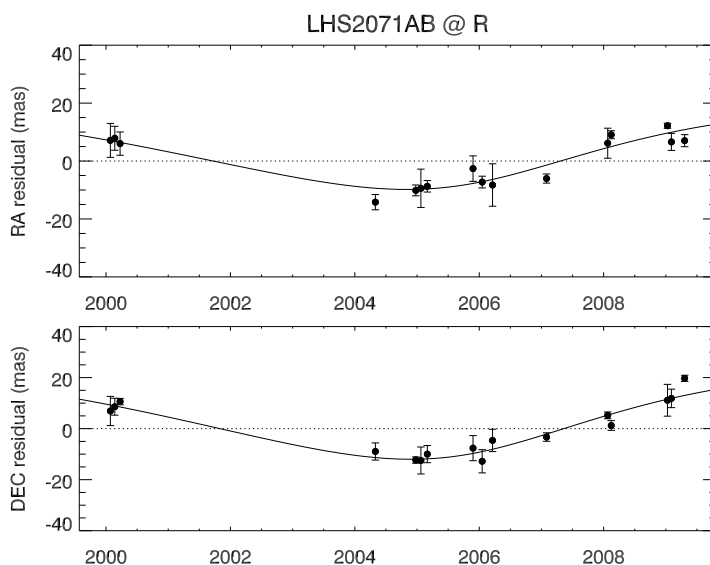


Figure 5.2: Plots of the nightly means of our astrometric residuals in RA and DEC for LHS 2071AB after solving for parallax and proper motion. A perturbation is evident, but the orbit has not wrapped in our data so the plotted orbital fit (Table 5.5) is poorly determined.

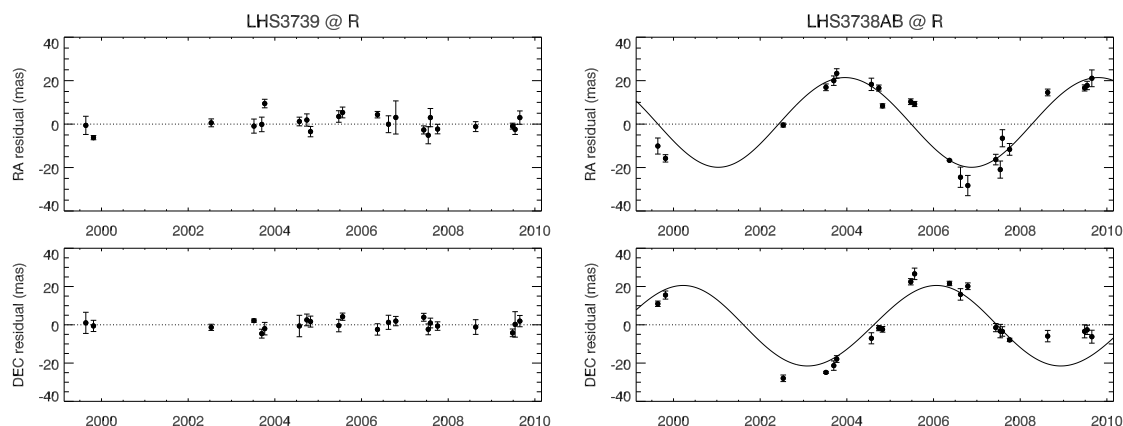


Figure 5.3: Plots of the nightly means of our astrometric residuals in RA and DEC for LHS 3739 (left) and LHS 3738AB (right) after solving for parallax and proper motion. LHS 3738AB clearly shows a perturbation with a period of  $\sim 6$  years whose orbital fit (Table 5.5) is overplotted; using the same CCD frames and reference stars the residuals for LHS 3739 remain flat. Two nights with only a single CCD image each (obtained for photometry) are not shown or used in the orbital solution.

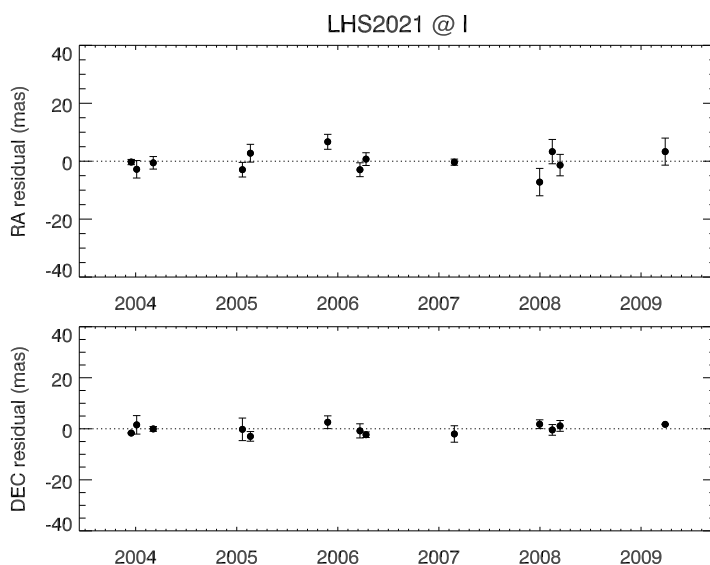


Figure 5.4: Plots of the nightly means of our astrometric residuals in RA and DEC for LHS 2021 after solving for parallax and proper motion. This star appears to a single main-sequence M dwarf. Two nights with only a single CCD image each (obtained for photometry) are not shown.

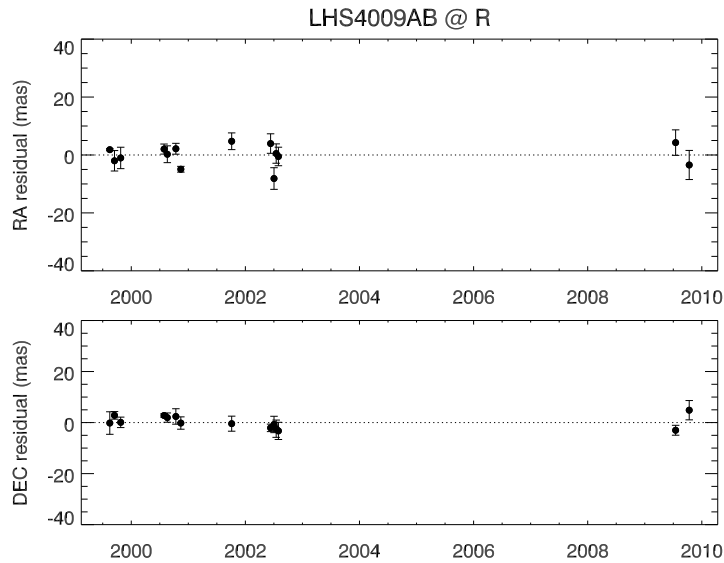


Figure 5.5: Plots of the nightly means of our astrometric residuals in RA and DEC for LHS 4009AB after solving for parallax and proper motion. There is no perturbation evident. The two components discovered in Montagnier et al. (2006) with separation  $0.07''$  have a magnitude difference of only  $\Delta K=0.1$  and an orbital period  $\sim 3$  years. We see no evidence of duplicity in the data. One night with only a single CCD image (obtained for photometry) is not shown.

preliminary, as our astrometric datasets do not have sufficient time coverage to publish definitive orbits, particularly in the case of LHS 2071AB for which the orbit is not complete, even two years after the publication of Riedel et al. (2010). LHS 2071AB and LHS 3738AB have now both been resolved through followup work, as discussed in §5.2.3.

Table 5.5: Preliminary Orbital Elements for Astrometric Binaries (Riedel et al. 2010)

| Name       | $P$<br>(years)   | $\alpha^a$<br>(arcsec) | $i$<br>(deg)     | Long. Nodes $\Omega$<br>(deg) | $T$<br>(year)    | $e$             | Long. Periastron $\omega$<br>(deg) |
|------------|------------------|------------------------|------------------|-------------------------------|------------------|-----------------|------------------------------------|
| (1)        | (2)              | (3)                    | (4)              | (5)                           | (6)              | (7)             | (8)                                |
| LHS 1582AB | $6.4 \pm 0.2$    | $0.018 \pm 0.003$      | $140.8 \pm 14.1$ | $279.7 \pm 24.0$              | $2002.2 \pm 0.3$ | $0.19 \pm 0.06$ | $258.4 \pm 23.0$                   |
| LHS 2071AB | $16.4 \pm 2.8^b$ | $0.021 \pm 0.004$      | $090.9 \pm 2.6$  | $219.1 \pm 3.6$               | $2005.9 \pm 1.0$ | $0.31 \pm 0.12$ | $33.2 \pm 26.23$                   |
| LHS 3738AB | $5.8 \pm 0.2$    | $0.027 \pm 0.002$      | $118.9 \pm 5.16$ | $315.9 \pm 5.5$               | $2006.9 \pm 1.3$ | $0.04 \pm 0.04$ | $26.7 \pm 82.7$                    |

<sup>a</sup>Photocentric semimajor axis

<sup>b</sup>Highly uncertain

The parallaxes for those systems published in Table 5.1 were computed from data where the photocentric orbit was removed. The orbital position of the photocenter was calculated and subtracted from the actual measured position of the photocenter at each data point, including those from nights with only a single CCD image. The parallax was then re-reduced based on this new dataset.

To check for systematics within the field we have reduced the three brightest reference stars in each of our astrometric perturbation fields as if they were the parallax target. In only one case did a reference star showed a perturbation of any kind; that reference was removed from the reduction of LHS 2071AB.

#### 5.2.2.4 Photometry — Variability

Although many M dwarfs are minutely variable (§2.2.4), none of the stars in Riedel et al. (2010) were found to vary by more than 2% in the frame series available (Column 8 of Table 5.2), which is standard for M dwarfs (Jao et al. 2011). The single exception is LHS 1749AB at 0.028 mag. In this case, the variability is likely due to the B component at a separation of 3" falling within the relative photometry aperture, and variations in seeing affecting the extracted fluxes in the standard 7" aperture.

#### 5.2.2.5 Photometry — Distance Estimates

For purposes of initial target selection as well as for additional analysis once trigonometric distances are determined, Riedel et al. (2010) used CTIOPI's *VRI* photometry combined with 2MASS *JHK* photometry to calculate the photometric distances listed in Table 5.2

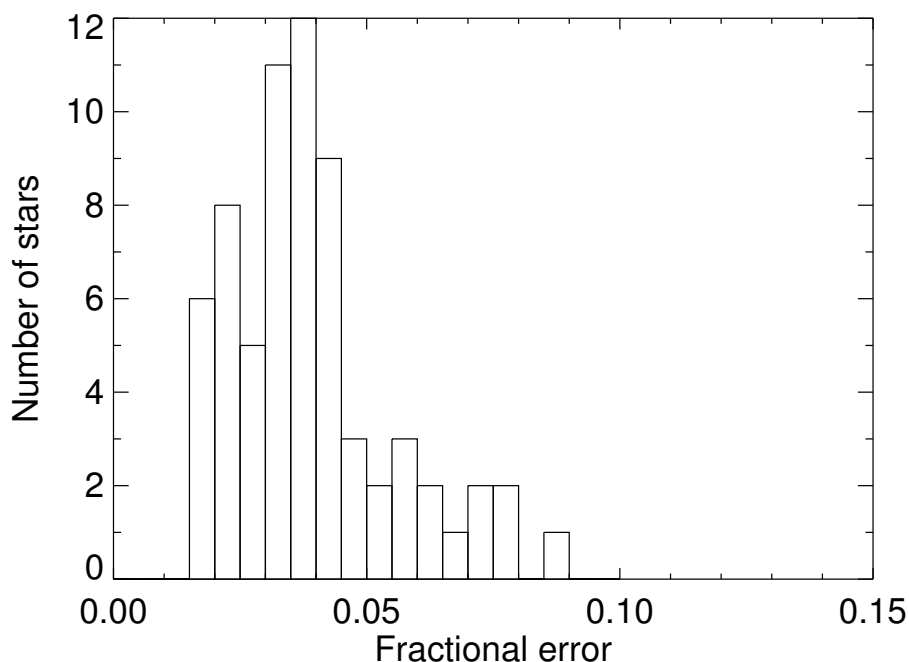


Figure 5.6: The internal photometry distance errors are shown without the 15.3% external systematic error. The average error is 3.9%, indicating that the distance estimates are remarkably consistent for this sample.

(Columns 16 and 17) based on the relations in Henry et al. (2004) (also described in more detail in §2.2.5). The quoted photometric distances have internal errors (which represent the spread in the up to 12 separate distances from the color relations) below 10%. The distribution of internal errors is shown in Figure 5.6; the average error is 3.9%, which is much smaller than the external errors (15.3%). The errors listed for the photometric distances given in Table 5.2 include both internal and external errors.

Because the fits used for the photometric distance estimates are derived using main sequence stars, the estimates are only accurate when the objects are single, main-sequence, M dwarfs. For the most part, these systems are indeed single, and 54 of the 67 stars (84%)

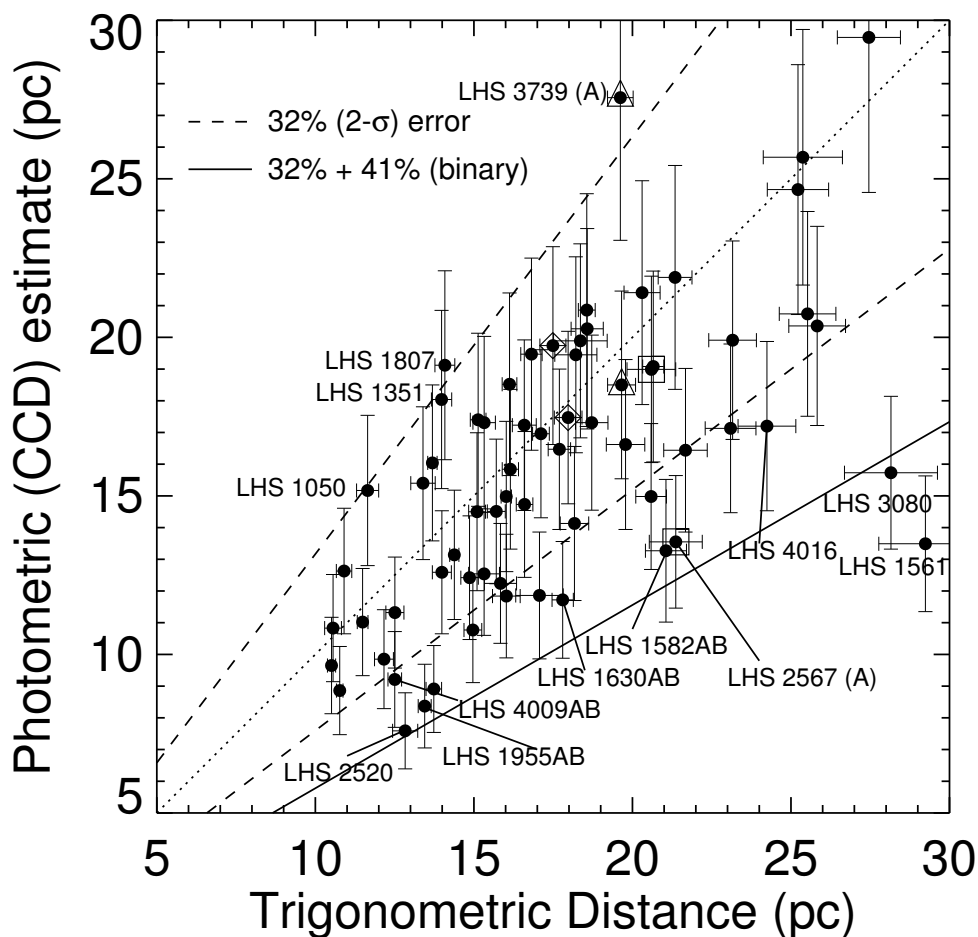


Figure 5.7: Photometric distance estimates compared to trigonometric parallax distances, identical distances are plotted with a dotted line. Dashed lines display the average  $2\text{-}\sigma$  error of our photometric distance estimates. Beyond the solid line, even an equal-luminosity binary cannot fully account for the mismatch between trigonometric and photometric distance estimates. LHS 2567/2568 are plotted with squares, LHS 3001 (the nearer one by trigonometric parallax)/3002 with diamonds, and LHS 3739/3738AB with triangles. LTT 5066 at 46 pc is not plotted.

fall within the  $2\text{-}\sigma$  range when their combined internal and external errors are considered, as shown in Figure 5.7. Stars above the  $2\text{-}\sigma$  line in Figure 5.7 are likely to be underluminous subdwarfs, while those below the  $2\text{-}\sigma$  line are presumably overluminous multiples or young stars. There are no subdwarfs in this sample (although LHS 1050, LHS 1807, and LHS 3739/3738AB may be slightly metal-poor), but there are several known close multiples with combined photometry, either previously known (LHS 1630AB, LHS 1955AB, LHS 4009AB), or discovered by us (LHS 1582AB, LHS 2071AB, LHS 3738AB). There is considerable scatter in  $M_V$  along the main sequence, visible in Figure 5.8 with up to two full magnitudes of spread for early to mid M dwarfs. An equal magnitude binary will have a distance estimated to be 41% closer via photometry than is determined trigonometrically, but given the spread in  $M_V$  in the main sequence, only further work will confirm or refute the multiplicity of suspected targets.

#### 5.2.2.6 Spectral Typing

Spectral types for the stars in Riedel et al. (2010) are given in Table 5.2 and come from five sources that can be arranged into two broad groups. One group is from RECONS spectroscopy, detailed in Kirkpatrick et al. (1991), Henry et al. (1994), and Henry et al. (2002). RECONS spectroscopy was used to determine the spectral types of all stars not taken from literature, and by Kirkpatrick et al. (1995) to classify LHS 1807.

The remaining spectral types are from the Palomar/Michigan State University Nearby Star Spectroscopic Survey (PMSU) (Reid et al. 1995; Hawley et al. 1996) and related paper Reid et al. (2007), all of which use the same weighted spectral indices method linked to

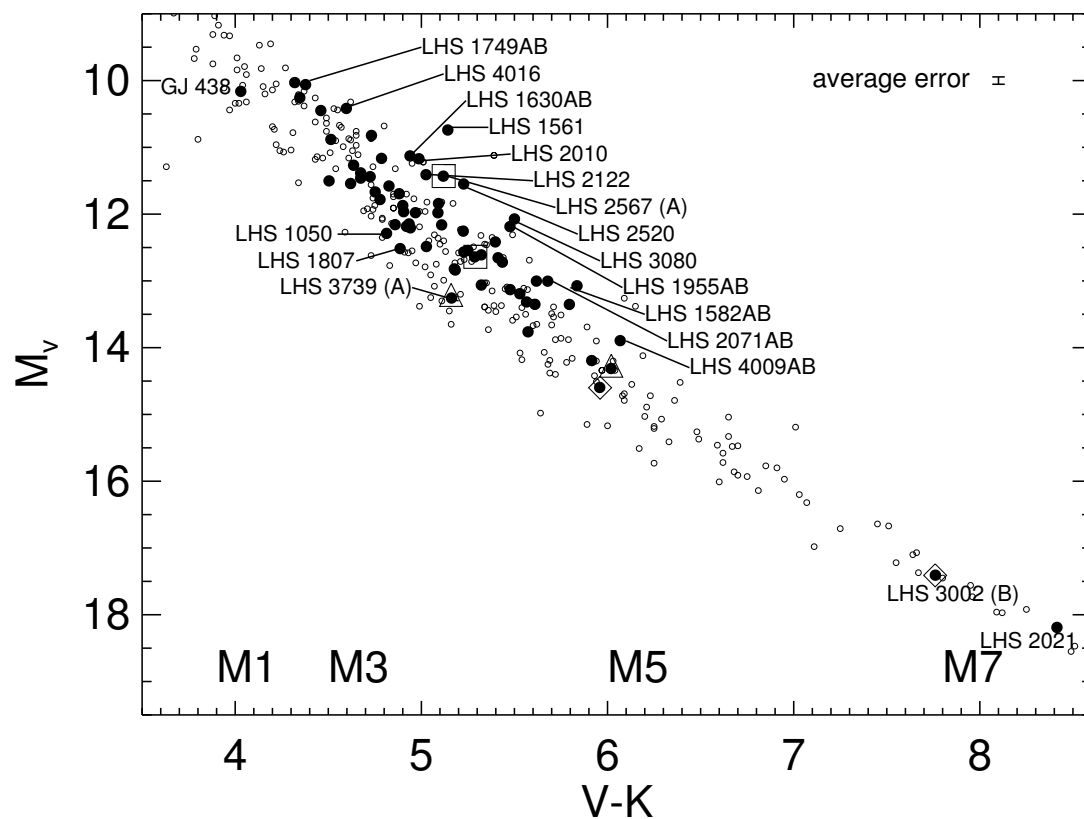


Figure 5.8: All 67 system components with parallaxes reported here are plotted as large solid points on an observational HR diagram. Small points represent stars in the RECONS 10 pc sample. LHS 2567/2568 are enclosed with squares, LHS 3001/3002 with diamonds, and LHS 3739/3738AB with triangles.

the spectral standards in Kirkpatrick et al. (1991). Where RECONS classifications were done over a range of 6000–9000Å with an effective resolution of 5.7–8.6Å depending on the setup (§5.1.2), the PMSU program used 6200–7500Å with resolution 1.8Å. In practice the RECONS results differ from PMSU results only occasionally and never more than half a subtype (see Table 5.6 for a comparison).

Table 5.6: Comparison of Spectral Types (Riedel et al. 2010)

| Name      | SpType<br>RECONS | SpType<br>PMSU | Ref <sup>a</sup> |
|-----------|------------------|----------------|------------------|
| (1)       | (2)              | (3)            | (4)              |
| LHS1050   | M3.0V            | M3.0           | 1                |
| LHS1630AB | M3.5VJ           | M3.5           | 2                |
| LHS1767   | M3.0V            | M3.5           | 2                |
| LHS2071AB | M4.0VJ           | M4             | 2                |
| LHS2836   | M4.0V            | M4             | 2                |
| LHS3197   | M4.5V            | M4.5           | 2                |
| LHS3295   | M3.0V            | M3.5           | 2                |
| LHS4009AB | M4.5VJ           | M5             | 2                |
| LHS4058   | M3.5V            | M3.0           | 2                |
| LHS3080   | M4.0V            | M4.5           | 1                |
| LHS3836   | M3.5V            | M3.5           | 2                |

<sup>a</sup> 1.) Reid et al. (1995) 2.) Hawley et al. (1996)

### 5.2.3 Systems Worthy of Note

**LHS 1050:** A  $1.3\text{-}\sigma$  underluminous single-star system ( $11.7\pm 0.3$  pc trig/ $15.2\pm 2.4$  pc phot dist) that still appears to be on the main sequence as shown in Figure 5.8. The YPC distance  $11.5\pm 1.8$  pc is consistent with our distance,  $11.7\pm 0.3$  pc, as is the distance from Smart et al. (2010),  $11.4\pm 0.4$  pc. Weighted mean parallaxes are given in Table 5.3.

**LHS 1561:** The most overluminous system in the sample, it has a  $4.4\text{-}\sigma$  distance mismatch ( $29.2\pm 1.5$  pc trig/ $13.5\pm 2.1$  pc phot dist, see Figure 5.7), and is noticeably elevated above the main sequence in Figure 5.8. We see no astrometric perturbation; it may be a multiple CTIOPI is not sensitive to or a pre-main-sequence object. The parallax has not ‘stabilized’: additional data continue to change the answer by more than  $1\text{-}\sigma$ , which is often a sign of unresolved orbital motion.

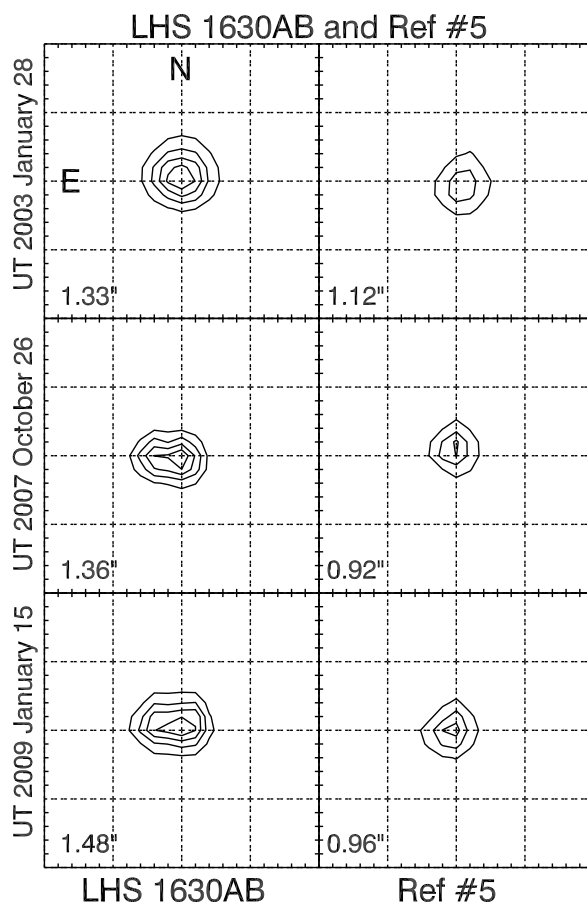


Figure 5.9: Contour plots of LHS 1630AB (left) and example single star Ref #5 (right, contours exaggerated 20 times) on three different nights in the  $I$  filter. LHS 1630B was first reported by Beuzit et al. (2004) at separation  $0.61''$ , angle  $72$  deg in 2002. Grid markings are 5 pixels ( $2.05''$ ), FWHM values for the PSFs are given in the lower left of each panel.

**LHS 1582AB:** A new astrometric binary with a 6.4 yr period and an 18 mas photocentric semi-major axis (see Figure 5.1). It has a  $2.7\text{-}\sigma$  distance mismatch ( $21.1\pm 0.7$  pc/ $13.3\pm 2.3$  pc phot dist, see Figure 5.7) and is elevated above the main sequence in Figure 5.8. A preliminary orbit is given in Table 5.5; the orbital motion was removed from the data before fitting the final parallax.

**LHS 1630AB:** We confirm the Adaptive Optics companion reported in Beuzit et al.

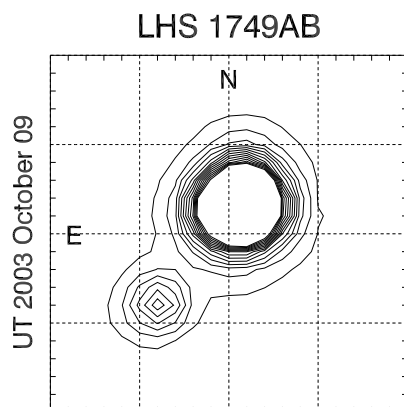


Figure 5.10: Contour plot of LHS 1749AB in the  $V$  filter on 2003 October 09. The B component is obvious in the image but difficult to separate cleanly on most frames. The four years of available data suggest slight orbital motion. Grid markings are 5 pixels ( $2.05''$ ).

(2004) seen on 18 September 2002 with a separation of  $0.61''$  at a position angle of  $72$  deg.

The B component is visible in  $I$  band photometry frames as of 2007, as shown in Figure 5.9. The system has a  $2.8\text{-}\sigma$  distance mismatch ( $17.8\pm 0.3$  pc trig/ $11.7\pm 1.8$  pc phot dist) and is elevated above the main sequence as seen in Figure 5.8, but we see no astrometric perturbation.

**LHS 1749AB:** A close visual binary discovered by Jao et al. (2003) with a separation of  $2.9''$  at a position angle of  $140$  deg (see Table 5.4). The parallax in Table 5.1 was calculated for the A component only, and that distance ( $21.7\pm 0.7$  pc) is consistent with  $22.0\pm 2.5$  pc reported by the CTIOPI 1.5m program (Costa et al. 2006). A weighted mean parallax for the system is given in Table 5.3.

The B component is  $\sim 2.8$  mag fainter in  $V$  than A, as shown in Figure 5.10. LHS 1749B is separable from A on 15 parallax frames; the resulting relative parallax result is  $43.17\pm 4.33$

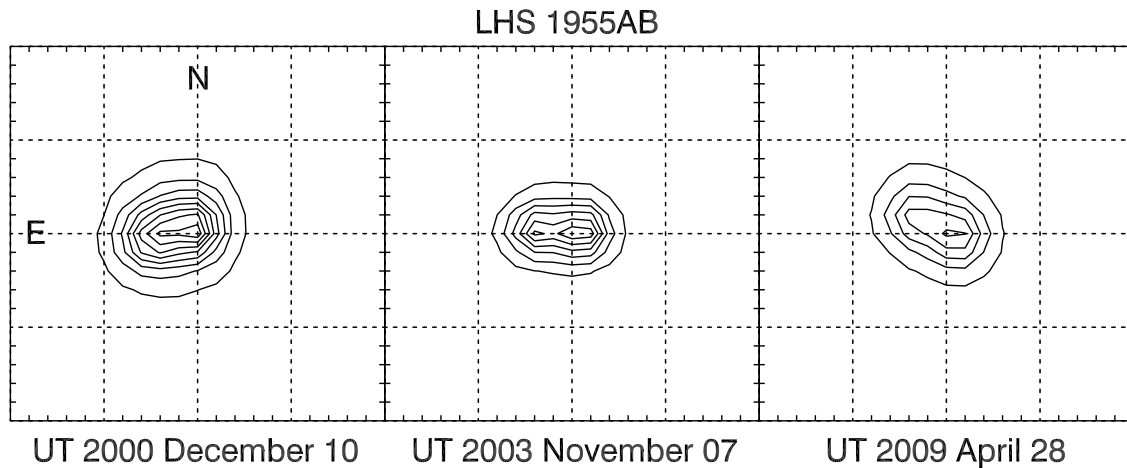


Figure 5.11: Contour plots of LHS 1955AB for three nights in the  $R$  filter. LHS 1955B is occasionally visible as a saddle point or even a peak (middle frame). The motion seen here suggests an  $\sim 80$  yr orbit. Grid markings are 5 pixels ( $2.05''$ ).

mas ( $23.2 \pm 2.3$  pc) which is of poor quality but consistent with other measurements. Possible (if weak) evidence for orbital motion is shown in Table [5.4](#).

**LHS 1807:** A  $1.5\text{-}\sigma$  underluminous system ( $14.1 \pm 0.3$  pc trig/ $19.1 \pm 3.0$  pc phot dist), but still evidently a main sequence star (see Figure [5.8](#)).

**LHS 1955AB:** A close visual binary listed in [Luyten \(1979a\)](#) with a  $0.8''$  separation at an angle of  $290$  deg. Our astrometric reduction uses relaxed ellipticity constraints (we normally remove frames from the reduction when the target star has an ellipticity of  $0.2$ , but in this case we kept up to  $e=0.6$ ) to keep frames where B extends the PSF of A. The B component is within the photometric aperture and causes the  $3.1\text{-}\sigma$  overluminosity ( $13.5 \pm 0.2$  pc trig/ $8.6 \pm 1.4$  pc phot dist) and the elevation above the main sequence seen in Figure [5.8](#). We detect no astrometric perturbation of A over the period the system was observed despite the motion of the B component.

LHS 1955B is  $\sim 0.5$  magnitudes fainter in  $R$  than A, and separable from A on only seven frames over five nights using special SExtractor settings. Using those frames, we can obtain a relative parallax for B:  $73.65 \pm 19.58$  mas ( $13.6 \pm 3.6$  pc), consistent with the relative parallax of A in Table 5.1,  $72.76 \pm 1.09$  mas ( $13.7 \pm 0.2$  pc). Considerable orbital motion can be seen in Figure 5.11 and Table 5.4 suggesting  $P \sim 80$  yr. All results for B are questionable due to severe PSF contamination.

**LHS 2010:** This system has a  $3.0\text{-}\sigma$  distance mismatch ( $13.7 \pm 0.3$  pc trig/ $8.9 \pm 1.4$  pc phot dist) and is elevated above the main sequence in Figure 5.8. We see no astrometric perturbation, but it may be a multiple to which CTIOPI is not sensitive.

**LHS 2021:** Is the lowest luminosity star in our sample:  $V = 19.17$ ,  $M_V = 18.2$ , spectral type M6.0V (despite unusually red colors), which can be seen in the lower right of Figure 5.8. The distance I find ( $15.7 \pm 0.3$  pc) is consistent with the  $16.7 \pm 1.3$  pc distance reported by the CTIOPI 1.5m program in Costa et al. (2006). A weighted mean system parallax is given in Table 5.3. Observations of this system are plotted as an example of single-star astrometric residuals in Figure 5.4.

**LHS 2071AB:** A new astrometric binary with  $P > 9$  years and a 21 mas photocentric semi-major axis (see Figure 5.2). The unseen companion is causing a  $2.2\text{-}\sigma$  overluminosity ( $15.0 \pm 0.3$  pc trig/ $10.8 \pm 1.7$  pc phot dist, see Figure 5.7) and a noticeable elevation above the main sequence in Figure 5.8. The system has been resolved with adaptive optics on Gemini North; further results will follow in a later paper (Dieterich et al., in prep). An orbit consistent with our current dataset is given in Table 5.5 but is unreliable, as evidenced by

the  $90^\circ$  inclination, a classic indicator of a poor orbital fit. The orbital motion was removed from the data before fitting the final parallax.

**LHS 5156:** The final parallax is entirely based on  $nV$  filter data due to insufficient  $oV$  coverage. Our reduction does not show the characteristic  $nV$  wobble (§5.1.1) in the residuals, but it may be inaccurate by more than  $1\text{-}\sigma$ .

**GJ 438:** The hottest and most luminous star in the sample, as can be seen in Figure 5.8. The YPC distance ( $8.4\pm 1.1$  pc) is inconsistent with our distance,  $10.9\pm 0.3$  pc. This system is not in the RECONS 10 parsec sample. A weighted mean parallax to this system is given in Table 5.3.

**LHS 2520:** The third-most overluminous system in this sample; it has a  $3.2\text{-}\sigma$  distance mismatch ( $12.8\pm 0.4$  pc trig/ $7.6\pm 1.2$  pc phot dist, see Figure 5.7) and is elevated above the main sequence as shown in Figure 5.8. We detect no astrometric perturbation; it may be a multiple to which CTIOPI is not sensitive (§2.1.4).

**LHS 2567/2568:** A visual binary with a separation of  $8.0''$  at a position angle of  $61$  deg (see Table 5.4). The A component (LHS 2567) has a  $2.7\text{-}\sigma$  distance mismatch ( $21.4\pm 0.8$  pc trig/ $13.6\pm 2.1$  pc phot dist, see Figure 5.7) while the B component (LHS 2568) distance matches to  $0.4\text{-}\sigma$  ( $20.6\pm 0.8$  pc trig/ $19.0\pm 2.9$  pc phot dist). LHS 2567 shows no astrometric perturbation, but given that it should be the same age and metallicity as LHS 2568, it is potentially an unresolved binary much like LHS 4009AB, below. The proper motions of A and B are discrepant by  $11.1\text{-}\sigma$  due to orbital motion presented in Table 5.4. A weighted system parallax is given in Table 5.3.

**LHS 3001/3002:** A visual binary with a separation of  $12.7''$  at a position angle of  $43.9$  deg (see Table 5.4). The B component (LHS 3002) is the second-coolest star in this sample, as shown in Figure 5.8. The proper motions of A and B are discrepant by  $4.8\text{-}\sigma$  due to orbital motion presented in Table 5.4. A weighted system parallax is given in Table 5.3.

**LHS 3080:** The second-most overluminous system in this sample. It has a  $3.2\text{-}\sigma$  distance mismatch system ( $28.2\pm 1.5$  pc trig/ $15.7\pm 2.4$  pc phot dist, see Figure 5.7) and is elevated above the main sequence as shown in Figure 5.8. We detect no astrometric perturbation; it may be a multiple to which CTIOPI is not sensitive (§2.1.4).

**LHS 3197:** We have used an average correction to absolute parallax ( $1.50\pm 0.50$  mas) for this system because the calculated correction ( $3.44$  mas) was abnormally large. This is likely due to artificial reddening of the reference stars, caused by the molecular cloud LDN 1781 (Lynds 1962), which (if circular) has radius  $37'$  and a center only  $22'$  away at a position angle of  $43$  deg.

**GJ 633:** The published YPC distance ( $9.6\pm 1.3$  pc) is inconsistent with our distance,  $16.8\pm 0.3$  pc, which supersedes the  $22.5\text{ pc}\pm 0.9$  pc distance published by us in Henry et al. (2006). Improvements in centroiding discussed in §5.2.2.1 now reliably distinguish GJ 633 from a point source  $7''$  away that contaminated the previous result. The system is still not in the RECONS 10 parsec sample. A weighted mean system parallax (this new result and YPC) is given in Table 5.3.

**WT 562:** Unrelated to the system SCR 1826-6542 (Finch et al. 2007),  $5.8'$  away. WT 562 has  $\mu = 0.611''\text{yr}^{-1}$  at  $180.9$  deg while SCR 1826-6542 has  $\mu = 0.311''\text{yr}^{-1}$  at  $178.9$  deg.

Early results also suggest SCR 1826-6542 is several parsecs closer than WT 562.

**LHS 3739/3738AB:** A hierarchical triple system consisting of a new astrometric binary, LHS 3738AB, which is itself the B component of a known visual binary with LHS 3739. The system is the most underluminous in our sample. Using identical reference fields and frames (see Figure 5.3), LHS 3739 has no sign of a perturbation and is  $1.6\text{-}\sigma$  *underluminous* ( $19.6\pm 0.4$  pc trig/ $27.6\pm 4.5$  pc phot dist, see Figure 5.7) while the light of the components of LHS 3738AB combine to give only a  $0.3\text{-}\sigma$  ( $19.7\pm 0.4$  pc trig/ $18.5\pm 3.0$  pc phot dist) difference from expectations. Even so, LHS 3739 (and therefore LHS 3738 A and B) seems to be main-sequence in Figure 5.8

The LHS 3739/LHS 3738AB visual binary has a separation of  $113.1''$  at a position angle of  $95.7$  deg, and has proper motions discrepant by  $2.3\text{-}\sigma$ . This orbital motion is detected and presented in Table 5.4. A weighted system parallax is given in Table 5.3

The LHS 3738AB new astrometric binary has a 5.8 year period and a 27 mas photocentric semi-major axis (see Figure 5.3), and has been resolved by Gemini North. A preliminary orbit is given in Table 5.5 and was removed from the data before fitting the final parallax. Further results will be published in a later paper.

**LHS 4009AB:** We do not confirm the companion from Montagnier et al. (2006) resolved with adaptive optics on 14 October 2005 with a separation of  $0.07''$  at a position angle of  $250$  deg, and  $\Delta K = 0.15$  in what Montagnier et al. (2006) claim is a three year orbit. The system has a  $1.9\text{-}\sigma$  distance mismatch ( $12.5\pm 0.2$  pc trig/ $9.2\pm 1.5$  pc phot dist) and is elevated above the main sequence, (see Figure 5.8) but we detect no astrometric perturbation (see

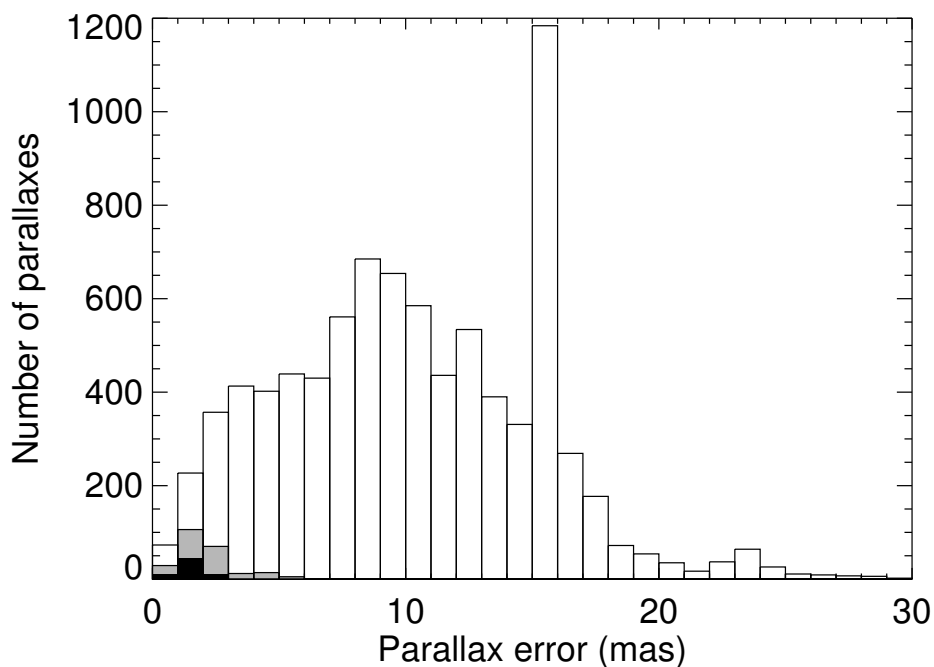


Figure 5.12: Parallax errors for systems in [Riedel et al. \(2010\)](#) (black), and prior CTIOPI parallax papers (gray) are shown versus previous ground-based parallaxes from YPC (white, extends off this graph). Our improved precision is due to our CCD-based astrometry while the bulk of previous work was done with photographic plates. A few systems in this paper are also in YPC (see [Table 5.3](#)). The enormous spike at 15 mas is a result of the methods used in YPC to assign errors to parallaxes published without error.

Figure [5.5](#)), probably because the system components are nearly equal luminosity in  $R$ .

**LHS 4016:** The system has a  $2.0\text{-}\sigma$  distance mismatch ( $24.2 \pm 0.9$  pc trig/ $17.2 \pm 2.7$  pc phot dist, see [Figure 5.7](#)) and is elevated above the main sequence as shown in [Figure 5.8](#).

There are possible signs of an astrometric perturbation, but a gap from 2005 to 2009 when the  $oV$  filter was not used prevents any definite determination. Shortly prior to the publication of [Riedel et al. \(2010\)](#), [Shkolnik et al. \(2010\)](#) published it as a short-period SB1.

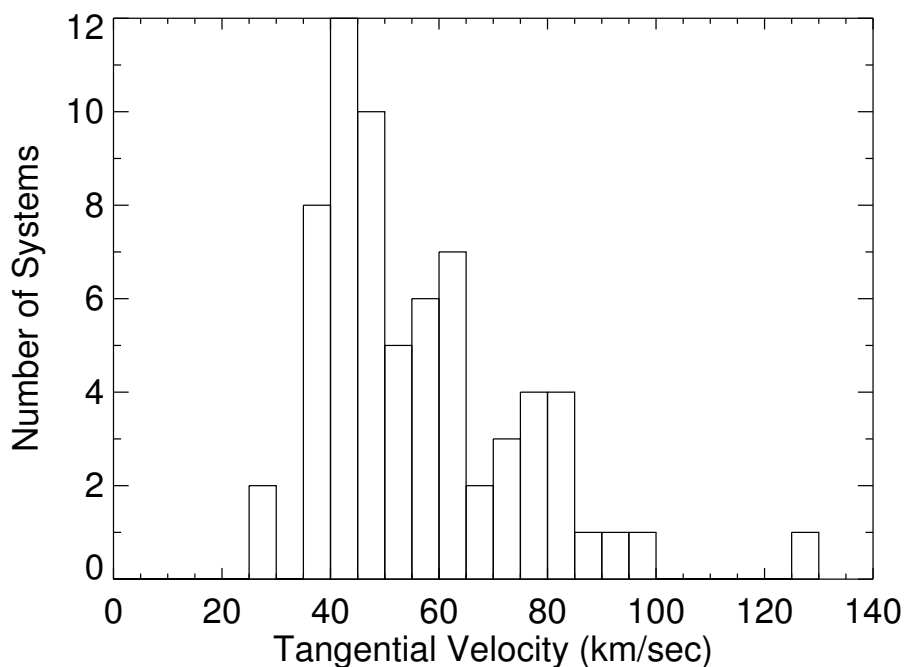


Figure 5.13: Tangential velocity distribution for the systems in Riedel et al. (2010). The fastest moving star is also the most distant, LTT 5066.

#### 5.2.4 Discussion

As shown in Figure 5.12, CTIOPI’s parallax errors compare favorably to the errors from other ground-based parallax efforts, as summarized in YPC. The increased accuracy can be attributed to CTIOPI’s use of CCD images for astrometry, while most of the YPC parallaxes were measured from photographic plates.

In Figure 5.13 we plot the distribution of tangential velocities listed in Column 15 of Table 5.1. Most of the stars have  $v_{tan} = 25$  to  $100$  km sec<sup>-1</sup>, as expected for disk red dwarfs (Mihalas & Binney 1981). The single star with  $v_{tan} = 126$  km sec<sup>-1</sup> is LTT 5066, which at 46 pc is the furthest star discussed in this paper; by photometry and spectroscopy

it is a dwarf, not a subdwarf. Our sample is kinematically biased, requiring stars to have  $0.5'' \leq \mu \leq 1.0'' \text{ yr}^{-1}$ . As such, the nearest star, LHS 5156, must have a tangential velocity between 25 and 50 km sec<sup>-1</sup>, while our farthest star, LTT 5066, would not meet our proper motion criterion if it were moving any slower than 110 km sec<sup>-1</sup>.

The 56 systems within 25 pc described in Riedel et al. (2010) constitute 2.7% of all systems now confirmed by parallax to be in the 25 pc sample (5.7% of systems in the southern hemisphere), according to the statistics from the RECONS 25 pc Database (§3.2). As of 11 APRIL 2012, the entire CTIOPI program has added 149 new systems (a 7.1% increase) to the all-sky 25 pc sample.

### 5.3 Unpublished Nearby Low Proper Motion Stars

*As there is overlap between the low proper motion sample and the young stars sample, all stars will be listed together in the results tables.*

What I describe here are two stellar samples with significant overlap: (a) low proper motion objects from TINYMO and other sources already on the CTIOPI parallax program, and (b) stars with saturated X-rays ( $\log\left(\frac{L_X}{L_{bol}}\right)$  from the upcoming Riedel et al. (2012, in prep) paper. Together, this sample includes 113 objects in 84 systems (see Table 5.14), of which 10 systems (14 stars) have already been published. The stars have been divided into four groups, comprising stars that are:

- Nearby low proper motion (less than  $0.18'' \text{ yr}^{-1}$ ) stars
- Young low proper motion stars

- Other apparently young stars ( $\log\left(\frac{L_x}{L_{bol}}\right) > -3.5$ , as per Riedel et al. (in prep)<sup>10</sup>
- Previously published stars from the CTIOPI program with saturated X-rays, which I intend to include in the analysis in Riedel et al. (2012, in prep).

Thus, the stars I consider low proper motion are in samples 1 and 2; the stars I consider young are in samples 2, 3, and 4.

The astrometric results are given in Table 5.8, where every resolved object has astrometric results (with the exception of GJ 2022AC, see §5.6) as calculated from CTIOPI data. Photometric results are provided in Table 5.9 for all objects in the sample, save two with no *VRI* photometry (both L dwarfs), and two close companions (SIP 1110-3731B, GJ 799B) resolved by neither our photometric pipeline nor 2MASS. All objects in the Tables are in the same order.

Table 5.7: Systems in this thesis

|   | # systems | # objects <sup>a</sup> |
|---|-----------|------------------------|
| Low $\mu$ ( $\leq 0.18'' \text{ yr}^{-1}$ ) | 21        | 23                     |
| Low $\mu$ and Young                         | 28        | 40                     |
| Young                                       | 25        | 36                     |
| Previously published                        | 10        | 14                     |
| All Low $\mu$                               | 50        | 65                     |
| All Young                                   | 63        | 90                     |
| Total                                       | 84        | 113                    |

<sup>a</sup>We use “object” as several components are probably unresolved binaries.

<sup>10</sup>The known  $\beta$  Pic member TX PsA=GJ 871.1B=LP 984-092 is on the CTIOPI observing program, but there is no ROSAT X-ray detection for the star within  $25''$ . The primary, WW PsA(=GJ 871.1A=LP 984-091), *does* meet my criteria but was not observed by CTIOPI. Our parallax agrees with the existing *HIP-PARCOS* parallax for WW PsA; both put the system within 25 pc of the Sun.

Table 5.8: Low Proper Motion and Young Star Astrometric Results

| Name<br>(1)                 | R.A.<br>(2) | Decl.<br>(3) | Filt<br>(4) | $N_{scab}$<br>(5) | $N_{frm}$<br>(6) | Coverage <sup>b</sup><br>(7) | Years <sup>b</sup><br>(8) | $N_{ref}$<br>(9) | $\pi_{rel}$<br>(mas)<br>(10) | $\pi_{corr}$<br>(mas)<br>(11) | $\pi_{abs}$<br>(mas)<br>(12) | $\mu$<br>(mas yr <sup>-1</sup> )<br>(13) | P.A.<br>(deg)<br>(14) | $V_{tan}$<br>(km s <sup>-1</sup> )<br>(15) | Notes<br>(16) |
|-----------------------------|-------------|--------------|-------------|-------------------|------------------|------------------------------|---------------------------|------------------|------------------------------|-------------------------------|------------------------------|--|-----------------------|--|---------------|
| Low Proper Motion           |             |              |             |                   |                  |                              |                           |                  |                              |                               |                              |  |                       |  |               |
| NLT00372                    | 00 08 51.79 | +20 49 07.9  | V           | 11s               | 97               | 1999.71-2011.89              | 12.18                     | 7                | 10.50±1.44                   | 1.16±0.07                     | 11.66±1.44                   | 147.8±0.3                                | 121.1±0.23            | 60.1                                       | cg            |
| SCR0128-1458                | 01 28 39.52 | -14 58 04.2  | V           | 3s                | 19               | 2009.93-2011.77              | 1.85                      | 6                | 67.47±4.63                   | 1.50±0.50                     | 68.97±4.66                   | 84.0±5.6                                 | 220.6±7.63            | 5.6  | dh            |
| SCR0143-0602                | 01 43 45.13 | -06 02 40.1  | V           | 3s                | 21               | 2009.74-2011.96              | 2.22                      | 8                | 51.19±2.29                   | 0.93±0.14                     | 52.12±2.29                   | 51.3±3.4                                 | 109.6±6.71            | 4.7  | dg            |
| L1703-019                   | 02 00 38.31 | -55 58 04.8  | V           | 5s                | 57               | 2007.81-2011.96              | 4.15                      | 7                | 121.59±2.70                  | 0.34±0.18                     | 121.93±2.71                  | 124.8±1.7                                | 122.8±1.55            | 4.9  | cdg           |
| 2MA0314-0450                | 03 14 40.11 | -04 50 31.8  | I           | 2c                | 10               | 2010.75-2011.73              | 0.99                      | 6                | 30.59±2.19                   | 0.81±0.10                     | 31.40±2.19                   | 137.2±5.5                                | 220.8±4.57            | 20.7                                       | dc            |
| 2MA0429-3123                | 04 29 18.43 | -31 23 56.7  | R           | 4s                | 63               | 2003.95-2010.73              | 3.78                      | 11               | 64.59±1.50                   | 0.23±0.05                     | 64.82±1.40                   | 129.8±0.6                                | 38.6±0.53             | 9.5  | cdg           |
| 2MA0451-3402                | 04 51 00.94 | -34 02 14.9  | I           | 4s                | 18               | 2008.86-2012.10              | 6.24                      | 10               | 47.21±1.50                   | ...                           | ...                          | 163.4±1.1                                | 34.8±0.78             | 16.4                                       | ede           |
| HD271076                    | 05 10 09.70 | -72 36 27.8  | V           | 3c                | 28               | 2009.75-2011.74              | 2.01                      | 5                | 44.94±2.55                   | 1.44±0.29                     | 46.38±2.57                   | 132.9±3.9                                | 82.9±2.62             | 13.6                                       | d             |
| SCR0533-4257AB              | 05 33 28.03 | -42 57 20.5  | R           | 5c                | 78               | 2007.81-2012.10              | 4.29                      | 6                | 98.37±1.69                   | 0.98±0.17                     | 99.35±1.70                   | 35.5±1.4                                 | 330.7±4.28            | 1.7  | cdg           |
| LP780-032                   | 06 39 37.41 | -21 01 33.3  | V           | 3c                | 52               | 2009.93-2012.27              | 2.34                      | 13               | 63.22±0.79                   | 1.17±0.11                     | 64.39±0.80                   | 177.8±1.1                                | 294.8±0.66            | 13.1                                       | d             |
| 2MA0936-2610                | 09 36 57.83 | -26 10 11.2  | V           | 3c                | 31               | 2010.16-2012.20              | 2.04                      | 9                | 49.11±2.48                   | 1.01±0.15                     | 50.12±2.48                   | 45.5±2.2                                 | 138.8±5.41            | 4.3  | d             |
| SDR1214-2345                | 12 14 08.67 | -23 45 17.0  | V           | 3c                | 39               | 2010.16-2012.20              | 2.04                      | 11               | 92.38±2.24                   | 0.66±0.10                     | 93.04±2.24                   | 98.6±2.9                                 | 32.6±3.30             | 5.0  | d             |
| SDS1416-1348                | 14 16 24.08 | +13 48 26.3  | I           | 3c                | 20               | 2010.40-2012.17              | 1.77                      | 10               | 110.02±2.10                  | ...                           | ...                          | 167.7±3.9                                | 35.5±2.58             | 7.2  | cdg           |
| 2MA1507-2000                | 15 07 27.81 | -20 00 43.3  | I           | 6c                | 73               | 2004.45-2009.57              | 5.12                      | 6                | 41.84±0.62                   | 0.89±0.12                     | 42.73±0.63                   | 129.3±0.5                                | 121.9±0.44            | 14.3                                       | cdg           |
| GJ2122AB                    | 16 45 16.97 | -38 48 33.3  | V           | 12c               | 164              | 2000.58-2012.25              | 11.68                     | 7                | 73.37±1.64                   | 1.50±0.50                     | 74.87±1.71                   | 59.4±0.5                                 | 208.2±0.90            | 3.6  | cdg           |
| 2MA1705-0516                | 17 05 48.33 | -05 16 46.6  | I           | 3c                | 16               | 2009.32-2011.50              | 2.17                      | 12               | 45.83±2.10                   | ...                           | ...                          | 161.9±2.8                                | 133.4±1.97            | 16.7                                       | cdg           |
| DEN1756-4805                | 17 56 56.20 | -48 05 09.7  | I           | 3s                | 13               | 2009.32-2011.53              | 2.21                      | 12               | 50.25±2.05                   | ...                           | ...                          | 91.4±2.4                                 | 66.0±2.85             | 8.6  | cdg           |
| SCR1942-2045                | 19 42 12.82 | -20 45 48.0  | R           | 2c                | 32               | 2010.66-2011.77              | 1.12                      | 10               | 61.52±1.61                   | 0.88±0.16                     | 62.40±1.62                   | 147.4±3.8                                | 182.6±2.20            | 11.2                                       | cdg           |
| SCR2036-3607                | 20 36 08.30 | -36 07 11.5  | V           | 3s                | 48               | 2009.62-2011.74              | 2.12                      | 7                | 60.22±1.44                   | 1.46±0.48                     | 61.68±1.52                   | 51.7±1.9                                 | 6.7±3.31              | 4.0  | cdg           |
| SCR2049-4012                | 20 49 09.94 | -40 12 06.3  | R           | 5s                | 61               | 2007.82-2011.71              | 3.89                      | 9                | 106.71±1.58                  | 0.75±0.04                     | 107.46±1.58                  | 64.6±1.4                                 | 293.9±2.31            | 2.8  | cdg           |
| 2MA2057-0252                | 20 57 54.09 | -02 52 30.3  | I           | 2c                | 18               | 2010.50-2011.77              | 1.28                      | 14               | 65.14±1.85                   | ...                           | ...                          | 93.1±3.5                                 | 180.5±...             | 6.8  | cdg           |
| Low Proper Motion and Young |             |              |             |                   |                  |                              |                           |                  |                              |                               |                              |  |                       |  |               |
| SCR0017-6645                | 00 17 23.53 | -66 45 12.5  | V           | 3s                | 29               | 2009.75-2011.89              | 2.14                      | 9                | 23.96±2.01                   | 0.90±0.10                     | 24.86±2.01                   | 95.1±3.3                                 | 103.6±3.47            | 18.1                                       | cdg           |
| GJ2006A                     | 00 27 50.24 | -32 33 06.1  | V           | 9s                | 69               | 2000.57-2010.82              | 10.25                     | 7                | 29.49±2.50                   | 0.65±0.11                     | 30.14±2.50                   | 115.0±0.6                                | 109.6±0.55            | 18.1                                       | cdg           |
| SCR00103B                   | 00 27 50.36 | -32 33 23.9  | V           | 9s                | 69               | 2000.57-2010.82              | 10.25                     | 7                | 31.13±2.47                   | 0.65±0.11                     | 31.78±2.47                   | 115.8±0.6                                | 108.6±0.53            | 17.3                                       | cdg           |
| SCR0103-5515                | 01 03 35.63 | -55 15 56.2  | R           | 5s                | 39               | 2007.82-2011.89              | 4.07                      | 7                | 20.68±1.70                   | 0.41±0.07                     | 21.09±1.70                   | 90.7±1.5                                 | 116.2±1.85            | 20.4                                       | cdg           |
| 2MA0123-6921                | 01 23 11.27 | -69 21 38.0  | I           | 4s                | 19               | 2008.70-2011.89              | 3.19                      | 10               | 22.95±2.68                   | 0.78±0.07                     | 23.73±2.68                   | 86.5±2.1                                 | 106.9±2.52            | 17.3                                       | cdg           |
| BAR161-012                  | 01 35 13.94 | -07 12 51.8  | R           | 3s                | 26               | 2009.94-2011.77              | 1.84                      | 7                | 26.43±2.30                   | 1.56±0.14                     | 27.99±2.32                   | 99.0±3.5                                 | 110.7±3.71            | 16.8                                       | d             |
| SIP152-6329                 | 01 52 55.35 | -63 29 30.2  | R           | 5s                | 26               | 2007.82-2011.77              | 3.96                      | 7                | 28.47±1.70                   | 1.37±0.14                     | 29.84±1.71                   | 126.1±1.1                                | 95.0±0.78             | 20.0                                       | d             |
| SCR0222-6022                | 02 22 44.17 | -60 22 47.6  | V           | 3s                | 22               | 2009.75-2011.74              | 1.99                      | 10               | 34.47±2.41                   | 0.89±0.11                     | 35.36±2.41                   | 131.7±4.4                                | 98.5±3.12             | 17.7                                       | cdg           |
| 2MA2336-5203                | 02 36 51.71 | -52 03 03.7  | V           | 3c                | 27               | 2009.92-2011.78              | 1.85                      | 6                | 25.90±1.83                   | 1.90±0.25                     | 27.80±1.85                   | 85.9±3.0                                 | 96.6±3.24             | 14.6                                       | c             |
| 2MA0254-5108A               | 02 54 33.17 | -51 08 31.4  | V           | 3c                | 29               | 2009.92-2011.78              | 1.85                      | 7                | 24.78±2.49                   | 1.95±0.24                     | 26.73±2.50                   | 92.2±3.7                                 | 101.2±3.96            | 16.4                                       | c             |
| 2MA0254-5108B               | 02 54 34.77 | -51 08 28.8  | V           | 3c                | 29               | 2009.92-2011.78              | 1.85                      | 7                | 16.93±3.18                   | 1.95±0.24                     | 18.88±3.19                   | 102.3±4.5                                | 94.5±4.04             | 25.7                                       | c             |
| SCR0336-2619                | 03 36 31.46 | -26 19 57.9  | I           | 5s                | 30               | 2007.82-2011.73              | 3.91                      | 10               | 23.28±1.92                   | 0.64±0.06                     | 23.92±1.92                   | 73.6±1.5                                 | 106.5±2.12            | 14.6                                       | cdg           |
| RX0413-0139                 | 04 13 26.64 | -01 39 21.2  | V           | 3s                | 18               | 2009.94-2012.10              | 2.16                      | 10               | 35.53±2.48                   | 0.74±0.17                     | 36.27±2.49                   | 130.6±4.3                                | 91.8±2.76             | 17.1                                       | cdg           |
| LP476-207ABC                | 05 01 58.81 | +09 58 58.8  | V           | 5s                | 64               | 2000.06-2005.06              | 5.00                      | 8                | 39.52±2.11                   | 1.15±0.20                     | 40.67±2.12                   | 106.4±1.4                                | 165.4±1.31            | 12.4                                       | c             |
| BD-21-01074BC               | 05 06 49.47 | -21 35 03.8  | V           | 7s                | 95               | 1999.81-2012.16              | 12.35                     | 5                | 48.51±1.62                   | 2.02±0.12                     | 50.53±1.62                   | 50.7±0.4                                 | 151.4±0.84            | 4.8  | c             |
| BD-21-01074A                | 05 06 49.92 | -21 35 09.2  | V           | 4c                | 49               | 2000.06-2012.16              | 12.10                     | 5                | 52.54±2.16                   | 2.02±0.12                     | 54.56±2.16                   | 51.3±0.5                                 | 111.1±1.06            | 4.5  | c             |
| SCR0529-3239                | 05 29 44.69 | -32 39 14.2  | R           | 3c                | 49               | 2008.85-2011.96              | 3.10                      | 7                | 41.13±1.72                   | ...                           | ...                          | 25.3±1.7                                 | 87.3±5.64             | 2.9  | cdg           |
| SCR0613-2742AB              | 06 13 13.31 | -27 42 05.5  | V           | 5c                | 89               | 2007.82-2012.17              | 4.35                      | 6                | 32.62±0.95                   | 1.68±0.17                     | 34.30±0.97                   | 10.7±0.7                                 | 244.9±6.95            | 1.5  | cdg           |
| SCR0757-7114                | 07 57 32.55 | -71 14 53.8  | V           | 3c                | 41               | 2009.92-2011.96              | 2.04                      | 10               | 44.17±1.96                   | 1.08±0.12                     | 45.25±1.96                   | 104.1±2.5                                | 90.5±1.94             | 10.9                                       | cdg           |
| SCR1012-3124AB              | 10 12 09.08 | -31 24 45.2  | V           | 3c                | 59               | 2010.01-2012.27              | 2.26                      | 9                | 17.52±1.74                   | 1.02±0.12                     | 18.54±1.74                   | 70.5±1.9                                 | 258.0±2.61            | 18.0                                       | cdg           |
| SIP1110-3731AC              | 11 10 27.88 | -37 31 52.0  | V           | 4c                | 35               | 2009.32-2012.25              | 2.93                      | 12               | 22.18±3.09                   | 0.96±0.09                     | 23.14±3.09                   | 82.0±3.3                                 | 268.1±3.33            | 16.8                                       | cdg           |
| SIP1110-3731B               | 11 10 27.88 | -37 31 52.0  | V           | 4c                | 33               | 2009.32-2012.25              | 2.93                      | 12               | 79.84±4.02                   | 0.96±0.09                     | 28.80±4.02                   | 116.3±4.0                                | 251.1±3.50            | 19.1                                       | cdg           |
| RX1132-2651A                | 11 32 41.17 | -26 52 09.0  | V           | 5s                | 65               | 2000.14-2011.16              | 11.02                     | 6                | 19.80±1.44                   | 1.32±0.12                     | 21.22±1.44                   | 75.3±0.3                                 | 253.9±0.42            | 16.8                                       | c             |
| RX1132-2651B                | 11 32 41.25 | -26 51 55.9  | V           | 5s                | 65               | 2000.14-2011.16              | 11.02                     | 6                | 20.01±1.40                   | 1.32±0.12                     | 21.33±1.41                   | 76.6±0.3                                 | 251.9±0.41            | 17.0                                       | c             |
| STEPHO164                   | 12 06 22.15 | -13 14 56.1  | V           | 3c                | 21               | 2010.20-2011.44              | 1.96                      | 5                | 22.29±5.70                   | 0.58±0.15                     | 22.87±5.70                   | 123.3±6.4                                | 129.6±5.98            | 25.5                                       | d             |
| DEN1306-6723                | 13 06 56.56 | -77 23 09.5  | V           | 2c                | 40               | 2010.16-2012.16              | 1.28                      | 7                | 6.54±1.37                    | 2.73±0.33                     | 9.27±1.41                    | 16.8±2.7                                 | 265.0±14.27           | 8.6  | cdg           |
| SCR1425-4113                | 14 25 29.13 | -41 13 32.4  | V           | 3c                | 53               | 2010.16-2012.26              | 2.10                      | 11               | 14.64±0.97                   | 0.56±0.13                     | 15.20±0.98                   | 60.7±1.5                                 | 224.1±2.85            | 18.9                                       | cdg           |
| SCR1609-2222                | 16 09 20.63 | -22 22 05.7  | I           | 2c                | 32               | 2010.39-2011.64              | 1.25                      | 12               | 6.65±3.12                    | 1.62±0.08                     | 7.47±3.12                    | 35.4±6.9                                 | 184.5±...             | 22.5                                       | d             |
| SIP1809-7613                | 18 09 06.94 | -76 13 23.9  | I           | 2c                | 26               | 2010.40-2011.61              | 1.21                      | 10               | 36.19±3.96                   | 1.69±0.21                     | 37.88±3.97                   | 141.8±5.0                                | 176.4±3.11            | 17.7                                       | d             |
| SCR1816-5844                | 18 16 12.37 | -58 44 05.6  | V           | 2c                | 24               | 2010.50-2011.74              | 1.24                      | 11               | 32.48±2.03                   | 0.86±0.15                     | 33.34±2.04                   | 139.1±4.2                                | 173.9±2.70            | 19.8                                       | d             |

Continued on next page

Table 5.8 – Continued from previous page

| Name<br>(1)                   | R.A.<br>(2) | Decl.<br>(3) | Filt<br>(4) | N <sub>sec</sub> <sup>b</sup><br>(5) | N <sub>fr</sub> <sup>m</sup><br>(6) | Coverage <sup>b</sup><br>(7) | Years <sup>b</sup><br>(8) | N <sub>ref</sub> <sup>c</sup><br>(9) | π <sub>rel</sub><br>(mas)<br>(10) | π <sub>corr</sub><br>(mas)<br>(11) | π <sub>abs</sub><br>(mas)<br>(12) | μ<br>(mas yr <sup>-1</sup> )<br>(13) | P.A.<br>(deg)<br>(14) | V <sub>tan</sub><br>(km s <sup>-1</sup> )<br>(15) | Notes<br>(16)       |
|-------------------------------|-------------|--------------|-------------|--------------------------------------|-------------------------------------|------------------------------|---------------------------|--------------------------------------|-----------------------------------|------------------------------------|-----------------------------------|--------------------------------------|-----------------------|---|---------------------|
| SCR2010-2801AB                | 20 10 00.03 | -28 01 41.2  | R           | 4s                                   | 57                                  | 2008.71-2011.62              | 2.91                      | 10                                   | 19.86±1.32                        | 0.99±0.12                          | 20.85±1.33                        | 74.9±1.2                             | 147.5±1.73            | 17.0  | cd                  |
| SCR2033-2556                  | 20 33 37.59 | -25 56 52.1  | R           | 4s                                   | 39                                  | 2008.71-2011.77              | 3.06                      | 11                                   | 23.63±1.84                        | 0.89±0.26                          | 24.52±1.86                        | 87.9±1.8                             | 141.4±2.31            | 17.0  | cd                  |
| BD-13-06424                   | 23 32 30.87 | -12 15 51.4  | V           | 2s                                   | 16                                  | 2010.73-2011.77              | 1.03                      | 6                                    | 37.89±5.88                        | 0.63±0.05                          | 38.52±5.88                        | 169.0±18.9                           | 107.9±11.50           | 20.8  | c                   |
| Young                         |             |              |             |                                      |                                     |                              |                           |                                      |                                   |                                    |                                   |                                      |                       |   |                     |
| G131-026AB                    | 00 08 53.92 | +20 50 25.4  | V           | 11s                                  | 97                                  | 1999.71-2011.89              | 12.18                     | 7                                    | 52.97±1.35                        | 1.16±0.17                          | 54.13±1.35                        | 251.2±0.3                            | 194.4±0.11            | 22.0  | j                   |
| LP467-016AB                   | 01 11 25.41 | +15 26 21.6  | R           | 8s                                   | 79                                  | 1999.71-2009.57              | 9.86                      | 7                                    | 44.88±1.77                        | 0.91±0.16                          | 45.79±1.78                        | 222.9±0.6                            | 122.7±0.29            | 23.1  | c                   |
| GJ2022AC                      | 01 24 27.69 | -33 55 08.8  | R           | 7s                                   | 66                                  | 1999.62-2011.53              | 11.91                     | 7                                    | 38.40±2.13                        | 0.40±0.07                          | 38.80±2.13                        | 206.0±0.7                            | 127.5±0.36            | 25.2  | c                   |
| LP993-115                     | 02 45 10.71 | -43 44 32.4  | R           | 7s                                   | 60                                  | 1999.62-2011.97              | 12.35                     | 10                                   | 88.09±2.13                        | 1.52±0.10                          | 89.61±2.13                        | 387.0±0.6                            | 175.4±0.12            | 20.5  | cg                  |
| LP993-116AB                   | 02 45 14.32 | -43 44 10.6  | V           | 7s                                   | 60                                  | 1999.62-2011.97              | 12.35                     | 10                                   | 86.00±2.29                        | 1.52±0.10                          | 87.52±2.29                        | 363.2±0.6                            | 174.3±0.14            | 19.7  | cg                  |
| G007-034                      | 04 17 18.52 | +08 49 22.1  | R           | 6s                                   | 72                                  | 1999.64-2007.83              | 8.19                      | 9                                    | 71.98±1.26                        | 1.29±0.19                          | 73.27±1.27                        | 395.2±0.7                            | 161.2±0.17            | 25.6  | c                   |
| G039-029AB                    | 04 38 12.59 | +28 13 00.0  | V           | 5s                                   | 70                                  | 2000.88-2005.06              | 4.18                      | 8                                    | 76.01±2.00                        | 2.60±0.40                          | 78.61±2.04                        | 403.2±1.8                            | 103.0±0.42            | 24.3  | c                   |
| LP655-048                     | 04 40 23.28 | -05 30 08.1  | I           | 9s                                   | 93                                  | 2003.95-2011.97              | 8.02                      | 7                                    | 101.42±0.74                       | 1.32±0.08                          | 102.74±0.74                       | 359.5±0.2                            | 69.2±0.07             | 16.6  | g                   |
| LP776-025                     | 04 52 24.42 | -16 49 22.2  | V           | 3c                                   | 47                                  | 2005.89-2008.12              | 2.24                      | 7                                    | 68.33±1.70                        | 1.07±0.09                          | 69.40±1.70                        | 245.0±2.2                            | 151.3±1.00            | 16.7  | g                   |
| L449-001AB                    | 05 17 22.91 | -35 21 54.7  | V           | 5c                                   | 76                                  | 2007.81-2012.10              | 4.29                      | 7                                    | 84.81±1.34                        | 0.78±0.12                          | 85.59±1.35                        | 273.7±1.0                            | 233.3±0.42            | 15.2  | cdeg                |
| L034-026                      | 07 49 12.71 | -76 42 06.6  | V           | 7s                                   | 88                                  | 2006.21-2012.19              | 5.97                      | 6                                    | 92.15±1.98                        | 1.50±0.50                          | 93.65±2.04                        | 224.6±1.0                            | 206.6±0.49            | 11.2  | cg                  |
| G161-071                      | 09 44 54.18 | -12 20 54.4  | V           | 8s                                   | 75                                  | 2003.94-2010.98              | 7.04                      | 8                                    | 69.96±1.36                        | 1.77±0.10                          | 71.73±1.36                        | 326.2±0.6                            | 277.5±0.17            | 21.6  | cg                  |
| SCR1157-0149                  | 11 57 45.55 | -01 49 02.6  | I           | 7s                                   | 65                                  | 2004.18-2011.11              | 6.93                      | 8                                    | 48.90±1.00                        | 1.19±0.13                          | 50.09±1.01                        | 459.3±0.5                            | 118.6±0.11            | 43.5  | c                   |
| G165-008AB                    | 13 31 46.62 | +29 16 36.6  | R           | 10s                                  | 181                                 | 2000.14-2009.25              | 9.11                      | 5                                    | 53.56±2.36                        | 1.95±0.31                          | 55.51±2.38                        | 260.1±1.1                            | 237.1±0.46            | 22.2  | c                   |
| LHS2880                       | 14 13 04.86 | -12 01 26.8  | R           | 6s                                   | 82                                  | 2004.58-2009.49              | 4.91                      | 8                                    | 30.88±1.35                        | 1.45±0.13                          | 32.33±1.36                        | 711.3±0.9                            | 237.0±0.15            | 104.3   | c                   |
| GJ1224                        | 18 07 32.85 | -15 57 47.0  | I           | 9s                                   | 181                                 | 2003.52-2011.55              | 8.03                      | 6                                    | 125.51±0.90                       | 1.50±0.50                          | 127.01±1.03                       | 702.3±0.4                            | 241.1±0.06            | 25.8  | h                   |
| G141-029                      | 18 42 44.99 | +13 54 17.1  | I           | 6c                                   | 77                                  | 2003.52-2010.61              | 7.09                      | 7                                    | 88.35±2.36                        | 1.50±0.50                          | 89.85±2.41                        | 359.1±1.3                            | 354.7±0.32            | 18.3  | h                   |
| LP870-065                     | 20 04 30.79 | -23 42 02.4  | R           | 7s                                   | 68                                  | 2004.57-2010.50              | 5.92                      | 6                                    | 53.79±1.59                        | 1.21±0.15                          | 55.00±1.60                        | 357.0±0.8                            | 160.9±0.23            | 30.8  | h                   |
| ZMA2009-0113                  | 20 09 18.24 | -01 13 38.2  | I           | 6s                                   | 56                                  | 2004.73-2009.62              | 4.88                      | 8                                    | 91.58±1.74                        | 2.02±0.11                          | 93.00±1.74                        | 370.5±1.2                            | 187.7±0.30            | 18.8  | c                   |
| LEHPM2-0783                   | 20 19 49.82 | -58 16 43.0  | I           | 4c                                   | 58                                  | 2006.37-2009.63              | 3.26                      | 9                                    | 61.24±1.02                        | 0.69±0.09                          | 61.93±1.02                        | 331.4±0.8                            | 185.4±0.22            | 25.4  | c                   |
| L755-019                      | 20 28 43.63 | -11 28 30.8  | R           | 5s                                   | 55                                  | 2007.82-2011.73              | 3.91                      | 6                                    | 53.11±1.92                        | 1.03±0.09                          | 54.14±1.92                        | 184.1±1.4                            | 119.9±0.81            | 16.1  | cd                  |
| GJ0799B                       | 20 41 51.14 | -32 26 07.8  | V           | 8s                                   | 136                                 | 2003.52-2011.73              | 8.21                      | 7                                    | 99.70±1.69                        | 2.72±0.14                          | 102.42±1.70                       | 434.4±0.6                            | 137.3±0.17            | 20.1  | cg                  |
| GJ0799A                       | 20 41 51.14 | -32 26 07.8  | V           | 8s                                   | 136                                 | 2003.52-2011.73              | 8.21                      | 7                                    | 99.28±1.84                        | 2.72±0.14                          | 102.00±1.85                       | 446.8±0.7                            | 149.2±0.17            | 20.8  | cg                  |
| LP756-003                     | 20 46 43.64 | -11 48 13.3  | R           | 3c                                   | 25                                  | 2004.58-2006.37              | 1.79                      | 10                                   | 56.07±4.37                        | 1.43±0.12                          | 57.50±4.37                        | 348.9±5.1                            | 102.0±1.55            | 28.8  | g                   |
| LHS3799                       | 22 23 07.00 | -17 36 26.1  | V           | 8s                                   | 106                                 | 2003.52-2011.77              | 8.25                      | 6                                    | 137.87±2.03                       | 0.80±0.21                          | 138.67±2.04                       | 769.0±0.5                            | 157.7±0.07            | 26.3  | g                   |
| LP932-083                     | 22 49 08.41 | -28 51 20.1  | V           | 8s                                   | 62                                  | 2004.58-2011.50              | 6.92                      | 9                                    | 26.36±2.20                        | ...                                | ...                               | 286.6±0.8                            | 217.0±0.33            | 51.5  | g                   |
| GJ1284AB                      | 23 30 13.45 | -20 23 27.4  | V           | 8s                                   | 95                                  | 2003.51-2011.51              | 8.00                      | 5                                    | 66.35±2.27                        | 1.55±0.29                          | 67.90±2.29                        | 363.5±0.9                            | 121.1±0.27            | 25.4  | cdg                 |
| Previously Published Examples |             |              |             |                                      |                                     |                              |                           |                                      |                                   |                                    |                                   |                                      |                       |   |                     |
| LHS1302                       | 01 51 04.09 | -06 07 05.1  | R           | 12s                                  | 178                                 | 1999.71-2011.78              | 12.06                     | 6                                    | 95.64±0.95                        | 0.64±0.06                          | 96.28±0.95                        | 597.0±0.3                            | 116.0±0.05            | 29.4  | Hen06               |
| LHS1358                       | 02 12 54.63 | +00 00 16.8  | R           | 5s                                   | 58                                  | 1999.71-2003.86              | 4.15                      | 5                                    | 64.09±2.07                        | 1.18±0.13                          | 65.27±2.07                        | 558.3±1.3                            | 86.1±0.20             | 40.5  | Rie10               |
| G099-049                      | 06 00 03.52 | +02 42 23.6  | V           | 13s                                  | 364                                 | 1999.91-2011.97              | 12.07                     | 4                                    | 191.14±0.96                       | 1.50±0.50                          | 192.64±1.08                       | 307.6±0.3                            | 97.1±0.10             | 7.5   | Hen06 <sup>b</sup>  |
| APCOL                         | 06 04 52.16 | -34 33 36.0  | V           | 8c                                   | 183                                 | 2004.74-2011.97              | 7.22                      | 14                                   | 117.45±0.93                       | 0.96±0.10                          | 118.41±0.94                       | 342.0±0.4                            | 4.5±0.11              | 13.7  | Rie11 <sup>g</sup>  |
| G041-014ABC                   | 08 58 56.33 | +08 28 26.0  | V           | 13s                                  | 203                                 | 1999.97-2011.96              | 11.98                     | 5                                    | 146.09±1.61                       | 1.73±0.16                          | 147.78±1.62                       | 503.2±0.4                            | 130.4±0.09            | 16.1  | Hen06 <sup>g</sup>  |
| ZMA1207-3932AB                | 12 07 33.46 | -39 32 54.0  | I           | 3c                                   | 56                                  | 2005.41-2007.56              | 2.15                      | 7                                    | 18.80±0.93                        | 0.58±0.05                          | 19.38±0.93                        | 68.0±1.4                             | 250.7±2.14            | 16.6  | Giz07 <sup>c</sup>  |
| LHS2729                       | 13 23 38.02 | -25 54 45.1  | R           | 5s                                   | 56                                  | 2000.15-2005.09              | 3.94                      | 12                                   | 70.32±1.52                        | 1.16±0.14                          | 71.48±1.53                        | 633.9±1.3                            | 249.8±0.21            | 42.0  | Rie10               |
| LHS2836                       | 13 59 10.42 | -19 50 03.6  | V           | 5s                                   | 119                                 | 2000.14-2012.25              | 12.11                     | 7                                    | 91.30±0.76                        | 1.82±0.27                          | 93.12±0.81                        | 574.6±0.2                            | 251.6±0.04            | 29.2  | Rie10 <sup>g</sup>  |
| GJ1207                        | 16 57 05.73 | -04 20 56.3  | V           | 13s                                  | 226                                 | 1999.62-2011.55              | 11.92                     | 9                                    | 111.81±0.87                       | 0.75±0.18                          | 112.56±0.89                       | 606.7±0.3                            | 127.0±0.05            | 25.6  | Hen06 <sup>cg</sup> |
| LHS4016AB                     | 23 48 36.06 | -27 39 38.9  | V           | 8s                                   | 97                                  | 2000.87-2011.74              | 10.87                     | 6                                    | 40.79±1.48                        | 0.50±0.19                          | 41.29±1.49                        | 595.1±0.3                            | 245.5±0.06            | 68.3  | Rie10 <sup>c</sup>  |

<sup>a</sup>Coordinates are epoch and equinox 2000.0; each target's coordinates were extracted from 2MASS and then transformed to epoch 2000.0 using the proper motions and position angles listed here.  
<sup>b</sup>'Coverage' and 'Years' run from the first to last data point; 'N<sub>sec</sub>' counts observing semesters where a dataset was taken, and denotes if coverage was 'c'ontinuous (more than one night of data in all seasons) or 's'cattered. Coverage extended by a single frame is denoted with a + in the N<sub>sec</sub> column.  
<sup>c</sup>System has notes in §5.6.  
<sup>d</sup>System is from the TINYMO survey (Chapter 4).  
<sup>e</sup>The astrometric perturbation was removed from the final parallax fit.  
<sup>f</sup>No independent astrometry.  
<sup>g</sup>Astrometric results calculated with  $\sigma V$  and  $nV$  filter data.  
<sup>h</sup>Generic correction to absolute adopted; field is reddened by a nebula.

Table 5.9: Low Proper Motion and Young Star Photometric Results

| Name<br>(1)                 | Alternate<br>Name<br>(2) | $V_J$<br>(3) | $R_{KC}$<br>(4) | $I_{KC}$<br>(5) | # abs.<br>nights <sup>a</sup><br>(6) | $\pi$<br>filter<br>(7) | $\sigma$<br>(mag)<br>(8) | # rel.<br>Nights<br>(9) | #<br>Fr.<br>(10) | 2MASS<br>$J$<br>(11) | 2MASS<br>$H$<br>(12) | 2MASS<br>$K$<br>(13) | spectral<br>type <sup>b</sup><br>(14) | ref<br>(15) | phot<br>dist.<br>(16) | #<br>Rel.<br>(17) | notes<br>(18) |
|-----------------------------|--------------------------|--------------|-----------------|-----------------|--------------------------------------|------------------------|--------------------------|-------------------------|------------------|----------------------|----------------------|----------------------|---------------------------------------|-------------|-----------------------|-------------------|---------------|
| Low Proper Motion           |                          |              |                 |                 |                                      |                        |                          |                         |                  |                      |                      |                      |                                       |             |                       |                   |               |
| NLTU00372                   |                          | 15.87±0.04   | 14.66±0.03      | 13.12±0.05      | 3                                    | V                      | 0.0137                   | 21                      | 97               | 11.636±0.021         | 10.999±0.032         | 10.716±0.022         | M4.5V                                 | Ref95       | 47.39                 | 12                |               |
| SCR0128-1458                |                          | 13.60±0.03   | 12.33±0.02      | 10.25±0.01      | 3                                    | V                      | 0.0104                   | 3                       | 19               | 9.088±0.023          | 8.555±0.039          | 8.198±0.029          | M3.0Ve                                | 1           | 12.77                 | 12                |               |
| SCR0143-0602                | RBS 237                  | 13.01±0.02   | 11.80±0.02      | 10.67±0.01      | 2                                    | V                      | 0.0187                   | 4                       | 21               | 8.770±0.023          | 8.174±0.034          | 7.912±0.018          | M4.0Ve                                | 1           | 13.33                 | 12                |               |
| LI73-019                    |                          | 11.90±0.02   | 10.70±0.03      | 9.15±0.02       | 3                                    | I                      | 0.0207                   | 11                      | 57               | 7.625±0.021          | 7.088±0.038          | 6.773±0.020          | M2.0Ve                                | 1           | 7.78                  | 12                |               |
| 2MA0314-0450                |                          | 19.87±0.05   | 17.62±0.02      | 15.24±0.02      | 2                                    | I                      | 0.0047                   | 3                       | 10               | 12.640±0.024         | 12.003±0.025         | 11.602±0.025         | M7.5V                                 | Crn03       | 21.91                 | 12                |               |
| 2MA0429-3123                |                          | 17.39±0.05   | 15.50±0.01      | 13.32±0.03      | 3                                    | R                      | 0.0183                   | 14                      | 63               | 10.874±0.024         | 10.211±0.024         | 9.770±0.022          | M5.5Ve                                | 1           | 10.56                 | 12                |               |
| 2MA0451-3402                |                          | 22.11±0.05   | 19.38±0.02      | 16.84±0.02      | 2                                    | R                      | 0.0478                   | 8                       | 18               | 13.541±0.023         | 12.826±0.023         | 12.294±0.026         | M9.0Ve                                | 1           | 24.14                 | 5                 |               |
| HD271076                    |                          | 11.36±0.02   | 10.34±0.01      | 9.12±0.01       | 2                                    | V                      | 0.0109                   | 5                       | 28               | 7.888±0.027          | 7.317±0.033          | 7.054±0.016          | M2.0V                                 | 1           | 14.94                 | 12                |               |
| SCR0533-4257AB              | RBS 661                  | 12.58±0.04   | 11.27±0.03      | 9.59±0.03       | 3                                    | R                      | 0.0109                   | 16                      | 78               | 7.997±0.027          | 7.402±0.027          | 7.116±0.026          | M4.0Ve                                | 1           | 7.41                  | 12                | c             |
| LP780-032                   |                          | 12.77±0.02   | 11.56±0.02      | 10.00±0.02      | 2                                    | V                      | 0.0094                   | 10                      | 52               | 8.507±0.024          | 7.912±0.027          | 7.650±0.016          | M4.0V                                 | Sch05       | 11.63                 | 12                |               |
| 2MA0936-2610                |                          | 13.10        | 11.86           | 10.31           | 1                                    | V                      | 0.0092                   | 6                       | 31               | 8.860±0.029          | 8.278±0.053          | 7.955±0.018          | M4.0Ve                                | 1           | 13.65                 | 12                |               |
| SCR1214-2345                |                          | 13.97        | 12.58           | 10.80           | 1                                    | V                      | 0.0116                   | 8                       | 39               | 9.067±0.022          | 8.564±0.047          | 8.234±0.025          | M4.0Ve                                | 1           | 10.56                 | 12                |               |
| SDS1416+1348                |                          | 18.82±0.09   | 16.40±0.03      | 16.74±0.02      | S                                    | I                      | 0.0180                   | 6                       | 20               | 13.148±0.025         | 12.456±0.028         | 12.114±0.023         | L5.0V                                 | Sch10       | 14.35                 | 12                |               |
| 2MA1507-2000                |                          | 9.67±0.03    | 8.72±0.02       | 7.69±0.02       | 2                                    | V                      | 0.0089                   | 16                      | 73               | 11.713±0.023         | 11.045±0.022         | 10.661±0.021         | M7.5                                  | Crn03       | 14.35                 | 12                |               |
| GJ2122AB                    |                          | ...          | ...             | ...             | 2                                    | V                      | 0.0138                   | 31                      | 164              | 6.570±0.019          | 5.944±0.029          | 5.720±0.026          | M1.0V                                 | 1           | 9.86                  | 12                | c             |
| 2MA1705-0516                |                          | 21.88±0.06   | 19.12±0.02      | 16.65±0.02      | S                                    | I                      | 0.0409                   | 6                       | 16               | 13.309±0.030         | 12.552±0.024         | 12.032±0.021         | L0.5                                  | Ref06       | ...                   | ...               |               |
| DEN1756-4805                |                          | 14.33±0.05   | 12.98±0.02      | 11.25±0.01      | 2                                    | R                      | 0.0110                   | 5                       | 13               | 13.409±0.022         | 12.709±0.023         | 12.190±0.021         | L0±1                                  | Pha08       | 23.60                 | 4                 |               |
| SCR1942-2045                |                          | 11.66±0.03   | 10.59±0.01      | 9.27±0.02       | 2                                    | V                      | 0.0140                   | 6                       | 32               | 8.958±0.024          | 8.026±0.022          | 7.756±0.023          | M4.0Ve                                | 1           | 14.62                 | 12                |               |
| SCR2036-3607                | RBS1687                  | 11.66±0.03   | 10.59±0.01      | 9.27±0.02       | 2                                    | R                      | 0.0164                   | 8                       | 48               | 8.026±0.023          | 7.418±0.033          | 7.172±0.020          | M2.5Ve                                | 1           | 14.18                 | 12                |               |
| SCR2049-4012                |                          | 13.53±0.02   | 12.12±0.03      | 10.31±0.03      | 3                                    | R                      | 0.0142                   | 12                      | 61               | 8.596±0.030          | 8.018±0.027          | 7.704±0.023          | M4.5Ve                                | 1           | 7.93                  | 12                |               |
| 2MA2057-0252                |                          | 21.67±0.05   | 18.82±0.01      | 16.50±0.02      | S                                    | I                      | 0.0134                   | 6                       | 18               | 13.121±0.024         | 12.268±0.024         | 11.724±0.025         | L1.5                                  | Crn03       | 18.00                 | 5                 |               |
| Low Proper Motion and Young |                          |              |                 |                 |                                      |                        |                          |                         |                  |                      |                      |                      |                                       |             |                       |                   |               |
| SCR0017-6645                | RBS 38                   | 12.45±0.02   | 11.37±0.01      | 10.00±0.01      | 2                                    | V                      | 0.0308                   | 6                       | 29               | 8.563±0.021          | 7.928±0.042          | 7.703±0.021          | M2.5Ve                                | 1           | 14.82                 | 12                |               |
| RJ2006A                     | RBS 67                   | 12.95±0.02   | 11.79±0.03      | 10.29±0.02      | 3                                    | V                      | 0.0774                   | 17                      | 69               | 8.882±0.032          | 8.236±0.038          | 8.012±0.033          | M3.5Ve                                | 1           | 17.08                 | 12                |               |
| GJ2006B                     | RBS 67                   | 13.25±0.03   | 12.04±0.02      | 10.48±0.02      | 4                                    | V                      | 0.0362                   | 17                      | 69               | 8.973±0.027          | 8.390±0.034          | 8.116±0.027          | M3.5Ve                                | 1           | 14.29                 | 12                |               |
| SCR0103-5515                |                          | 15.48±0.03   | 14.00±0.02      | 12.07±0.02      | 2                                    | R                      | 0.0145                   | 9                       | 39               | 10.162±0.023         | 9.580±0.025          | 9.237±0.022          | M4.5Ve                                | 1           | 12.86                 | 12                |               |
| 2MA0123-6921                |                          | 19.12±0.19   | 17.22±0.03      | 14.91±0.02      | 2                                    | I                      | 0.0106                   | 5                       | 19               | 12.320±0.023         | 11.711±0.025         | 11.323±0.026         | M8.0V                                 | Sch07       | 20.42                 | 12                |               |
| BAR161-012                  |                          | 13.42±0.01   | 12.19±0.02      | 10.57±0.01      | 2                                    | R                      | 0.0791                   | 5                       | 26               | 8.964±0.021          | 8.387±0.027          | 8.078±0.033          | M3.0Ve                                | 1           | 12.34                 | 12                |               |
| SIP152-6329                 |                          | 15.41±0.04   | 13.93±0.02      | 12.01±0.01      | 2                                    | R                      | 0.0148                   | 5                       | 26               | 10.167±0.024         | 9.604±0.024          | 9.261±0.021          | M4.5Ve                                | 1           | 13.69                 | 12                |               |
| SCR022-6022                 | RBS 309                  | 13.36±0.05   | 12.12±0.03      | 10.52±0.03      | 3                                    | V                      | 0.0259                   | 5                       | 22               | 8.990±0.021          | 8.390±0.042          | 8.102±0.031          | M3.5Ve                                | 1           | 13.25                 | 12                |               |
| 2MA0236-5203                | RBS 332                  | 12.06±0.02   | 11.02±0.01      | 9.75±0.02       | 2                                    | V                      | 0.0297                   | 6                       | 27               | 8.420±0.023          | 7.755±0.023          | 7.501±0.027          | M2.5Ve                                | 1           | 15.61                 | 12                |               |
| 2MA0254-5108A               |                          | 12.08±0.03   | 11.06±0.03      | 9.87±0.02       | 3                                    | V                      | 0.0293                   | 6                       | 29               | 8.608±0.027          | 8.074±0.035          | 7.782±0.033          | M1.5Ve                                | 1           | 21.39                 | 12                |               |
| 2MA0254-5108B               |                          | 17.55±0.09   | 15.96±0.12      | 13.91±0.03      | 2                                    | V                      | 0.0329                   | 6                       | 29               | 12.074±0.024         | 11.492±0.022         | 11.188±0.019         | M5.0Ve                                | 1           | 30.44                 | 12                |               |
| SCR0336-2619                |                          | 16.33±0.03   | 14.76±0.01      | 12.72±0.01      | 2                                    | I                      | 0.0100                   | 7                       | 30               | 10.675±0.023         | 10.134±0.024         | 9.763±0.021          | M1.5Ve                                | 1           | 14.19                 | 12                |               |
| RX0413-0139                 |                          | 13.96±0.02   | 12.66±0.01      | 10.98±0.01      | 2                                    | V                      | 0.0363                   | 5                       | 18               | 9.375±0.024          | 8.761±0.027          | 8.504±0.021          | M1.5Ve                                | 1           | 13.94                 | 12                |               |
| LP476-207ABC                |                          | 11.53±0.07   | 10.33±0.04      | 8.74±0.04       | 2                                    | V                      | 0.0205                   | 13                      | 64               | 7.212±0.023          | 6.657±0.029          | 6.370±0.021          | M3.0VeJ                               | 1           | 6.28                  | 12                | c             |
| BD-21-0107ABC               |                          | 11.08±0.05   | 9.92±0.05       | 8.45±0.04       | 4                                    | V                      | 0.0455                   | 16                      | 95               | 7.003±0.020          | 6.392±0.018          | 6.114±0.021          | M3.0VeJ                               | 1           | 6.37                  | 12                | c             |
| BD-21-01074A                |                          | 10.41±0.02   | 9.40±0.02       | 8.25±0.02       | 3                                    | V                      | 0.0428                   | 10                      | 49               | 7.046±0.021          | 6.391±0.049          | 6.117±0.017          | M1.5Ve                                | 1           | 9.91                  | 12                |               |
| SCR0529-3239                |                          | 13.79        | 12.50           | 10.80           | 1                                    | R                      | 0.0131                   | 11                      | 49               | 9.215±0.026          | 8.609±0.042          | 8.316±0.027          | M4.0Ve                                | 1           | 12.83                 | 12                |               |
| SCR0613-2742AB              |                          | 12.30±0.03   | 11.10±0.03      | 9.55±0.02       | 4                                    | V                      | 0.0382                   | 17                      | 89               | 8.002±0.034          | 7.432±0.071          | 7.145±0.024          | M4.0Ve                                | 1           | 8.98                  | 12                | c             |
| SCR0757-7114                |                          | 12.46±0.02   | 11.29±0.02      | 9.79±0.02       | 2                                    | V                      | 0.0071                   | 7                       | 41               | 8.319±0.023          | 7.745±0.038          | 7.423±0.021          | M3.5V                                 | 1           | 11.24                 | 12                |               |
| SCR1012-3124AB              |                          | 13.51±0.02   | 12.20±0.01      | 10.51±0.03      | 2                                    | V                      | 0.0154                   | 11                      | 59               | 8.848±0.018          | 8.262±0.046          | 7.993±0.031          | M4.0Ve                                | 1           | 10.56                 | 12                | c             |
| SIP1110-3731AC              | TWA 3A                   | 12.06±0.03   | 10.82±0.02      | 9.20±0.02       | 2                                    | V                      | 0.1127                   | 9                       | 35               | 7.651±0.019          | 7.041±0.027          | 6.774±0.020          | M4.0VeJ                               | 1           | 6.99                  | 12                | c             |
| SIP1110-3731B               | TWA 3B                   | ...          | ...             | ...             | 2                                    | V                      | 0.2219                   | 9                       | 33               | ...                  | ...                  | ...                  | ...                                   | ...         | ...                   | ...               | d             |
| RX1132-2651B                | TWA 8B                   | 15.20±0.08   | 13.68±0.03      | 11.75±0.04      | 2                                    | V                      | 0.1240                   | 11                      | 65               | 9.837±0.024          | 9.276±0.022          | 9.012±0.025          | M5.0Ve                                | 1           | 11.68                 | 12                |               |
| RX1132-2651A                | TWA 8A                   | 12.23±0.08   | 11.16±0.04      | 9.80±0.04       | 2                                    | V                      | 0.0780                   | 11                      | 65               | 8.337±0.024          | 7.663±0.042          | 7.430±0.017          | M4.0Ve                                | 1           | 12.71                 | 12                |               |
| STEPH0164                   |                          | 12.73        | 11.57           | 10.10           | 1                                    | V                      | 0.0145                   | 5                       | 20               | 8.702±0.026          | 8.070±0.040          | 7.813±0.029          | M3.5Ve                                | 1           | 14.41                 | 12                |               |
| DEN1306-7723                |                          | 17.58        | 15.64           | 13.51           | 1                                    | V                      | 0.0126                   | 9                       | 40               | 10.951±0.023         | 10.225±0.025         | 9.798±0.025          | M4.5Ve                                | 1           | 10.44                 | 12                |               |
| SCR1425-4113                |                          | 12.64        | 11.60           | 10.13           | 1                                    | V                      | 0.0770                   | 10                      | 53               | 8.546±0.026          | 7.910±0.034          | 7.614±0.021          | M2.5Ve                                | 1           | 12.09                 | 12                |               |
| SCR1609-2222                |                          | 15.99        | 14.41           | 12.49           | 1                                    | I                      | 0.0091                   | 6                       | 32               | 10.498±0.028         | 9.842±0.027          | 9.499±0.021          | M4.5Ve                                | 1           | 13.15                 | 12                |               |
| SIP1809-7613                |                          | 15.11±0.03   | 13.62±0.02      | 11.71±0.03      | 2                                    | I                      | 0.0069                   | 5                       | 26               | 9.817±0.021          | 9.275±0.021          | 8.989±0.021          | M4.5Ve                                | 1           | 11.97                 | 12                |               |
| SCR1816-5844                |                          | 12.90        | 11.71           | 10.14           | 1                                    | R                      | 0.0736                   | 6                       | 24               | 8.599±0.024          | 7.964±0.059          | 7.699±0.016          | M3.5Ve                                | 1           | 11.25                 | 12                | c             |
| SCR2010-2801AB              |                          | 12.98±0.03   | 11.78±0.02      | 10.20±0.02      | 3                                    | R                      | 0.0115                   | 11                      | 57               | 8.651±0.023          | 8.014±0.047          | 7.733±0.027          | M4.0Ve                                | 1           | 11.18                 | 12                | c             |
| SCR2033-2556                |                          | 14.87±0.02   | 13.44±0.02      | 11.57±0.01      | 2                                    | R                      | 0.0185                   | 9                       | 39               | 9.712±0.024          | 9.146±0.022          | 8.877±0.019          | M4.5Ve                                | 1           | 12.04                 | 12                |               |
| BD-13-06424                 | RBS2020                  | 10.50±0.03   | 9.56±0.03       | 8.58±0.03       | 2                                    | V                      | 0.0314                   | 3                       | 16               | 7.450±0.021          | 6.769±0.040          | 6.569±0.018          | M4.5Ve                                | 1           | 14.60                 | 12                |               |
| G131-026AB                  |                          | 13.52±0.06   | 12.19±0.04      | 10.50±0.04      | 3                                    | R                      | 0.0179                   | 21                      | 97               | 8.870±0.027          | 8.264±0.031          | 8.010±0.024          | M4.0Ve                                | 1           | 10.74                 | 12                | c             |
| LP467-016AB                 |                          | 14.46±0.05   | 12.95±0.01      | 11.03±0.02      | 2                                    | R                      | 0.0192                   | 15                      | 79               | 9.082±0.026          | 8.512±0.036          | 8.208±0.033          | M4.5Ve                                | 1           | 7.88                  | 12                | c             |

Continued on next page

Table 5.9 – Continued from previous page

| Name<br>(1)          | Alternate<br>Name<br>(2) | $V_I$<br>(3) | $R_{KC}$<br>(4) | $I_{KC}$<br>(5) | $\pi$<br>filter<br>(7) | $\sigma$<br>(mag)<br>(8) | # nights <sup>a</sup><br>(6) | # rel.<br>nights<br>(9) | # Fr.<br>(10) | 2MASS<br>$J$<br>(11) | 2MASS<br>$H$<br>(12) | 2MASS<br>$K$<br>(13) | spectral<br>type <sup>b</sup><br>(14) | ref<br>(15) | phot<br>dist.<br>(16) | #<br>Rel.<br>notes<br>(17)<br>(18) |
|----------------------|--------------------------|--------------|-----------------|-----------------|------------------------|--------------------------|------------------------------|-------------------------|---------------|----------------------|----------------------|----------------------|---------------------------------------|-------------|-----------------------|------------------------------------|
| GJ2022AC             | RBS 195                  | 13.56±0.04   | 12.26±0.01      | 10.62±0.05      | R                      | 0.0156                   | 3                            | 16                      | 66            | 9.203±0.036          | 8.659±0.046          | 8.240±0.031          | M4.0VeJ                               | 1           | 14.78                 | 12                                 |
| GJ2022B              |                          | 15.50±0.06   | 14.09±0.02      | 12.33±0.06      | R                      | 0.0156                   | 3                            | 16                      | 66            | 10.555±0.024         | 10.009±0.024         | 9.682±0.021          | M4.5Ve                                | 1           | 19.65                 | 12                                 |
| LP993-115            |                          | 12.38±0.08   | 11.17±0.03      | 9.61±0.03       | V                      | 0.0228                   | 3                            | 13                      | 60            | 8.141±0.021          | 7.553±0.024          | 7.270±0.024          | M3.5Ve                                | 1           | 9.94                  | 12                                 |
| LP993-116AB          | RBS 353                  | 12.69±0.06   | 11.37±0.02      | 9.67±0.02       | V                      | 0.0140                   | 3                            | 13                      | 60            | 8.059±0.024          | 7.525±0.042          | 7.196±0.024          | M4.0Ve                                | 1           | 7.62                  | 12                                 |
| G007-034             |                          | 13.84±0.02   | 12.50±0.01      | 10.75±0.01      | R                      | 0.0240                   | 3                            | 15                      | 72            | 9.030±0.026          | 8.483±0.029          | 8.182±0.020          | M4.0Ve                                | 1           | 10.65                 | 12                                 |
| G039-029AB           |                          | 12.56±0.05   | 11.31±0.01      | 9.70±0.02       | R                      | 0.0150                   | 3                            | 13                      | 70            | 8.173±0.018          | 7.616±0.018          | 7.326±0.021          | M4.0Ve                                | 1           | 9.40                  | 12                                 |
| LP655-048            |                          | 17.81±0.04   | 15.72±0.03      | 13.36±0.05      | I                      | 0.0130                   | 3                            | 19                      | 93            | 10.658±0.024         | 9.986±0.021          | 9.545±0.019          | M6.5Ve                                | 1           | 8.43                  | 12                                 |
| RBS 596              |                          | 11.63±0.02   | 10.53±0.03      | 9.12±0.02       | V                      | 0.0156                   | 3                            | 9                       | 47            | 7.740±0.021          | 7.146±0.031          | 6.891±0.027          | M3.0Ve                                | 1           | 10.44                 | 12                                 |
| LP449-001AB          |                          | 11.69±0.01   | 10.48±0.02      | 8.91±0.01       | V                      | 0.0223                   | 3                            | 15                      | 76            | 7.400±0.026          | 6.854±0.049          | 6.558±0.020          | M3.5Ve                                | 1           | 7.01                  | 12                                 |
| L034-026             |                          | 11.31±0.03   | 10.19±0.03      | 8.79±0.03       | V                      | 0.0184                   | 3                            | 17                      | 85            | 8.406±0.021          | 7.862±0.031          | 7.579±0.018          | M3.0Ve                                | 1           | 9.16                  | 12                                 |
| GJ161-071            |                          | 13.76±0.02   | 12.26±0.02      | 10.36±0.02      | V                      | 0.0399                   | 3                            | 11                      | 77            | 8.496±0.024          | 7.919±0.024          | 7.601±0.018          | M4.5Ve                                | 1           | 6.31                  | 12                                 |
| SCR1157-0149         |                          | 15.99±0.04   | 14.54±0.03      | 12.68±0.04      | I                      | 0.0113                   | 2                            | 13                      | 65            | 10.905±0.022         | 10.354±0.024         | 10.024±0.019         | M4.5Ve                                | 1           | 21.39                 | 12                                 |
| L165-008AB           | RBS1280                  | 12.02±0.09   | 10.77±0.05      | 9.15±0.07       | R                      | 0.0180                   | 3                            | 32                      | 181           | 7.561±0.024          | 7.002±0.023          | 6.720±0.018          | M4.0VeJ                               | 1           | 6.73                  | 12                                 |
| LHS2880              | GJ0540.2                 | 13.89±0.03   | 12.52±0.03      | 10.79±0.03      | R                      | 0.0140                   | 3                            | 15                      | 82            | 9.040±0.032          | 8.453±0.040          | 8.163±0.029          | M4.5Ve                                | 1           | 10.16                 | 12                                 |
| GJ1224               |                          | 13.48±0.04   | 12.08±0.02      | 10.31±0.03      | I                      | 0.0100                   | 2                            | 24                      | 181           | 8.639±0.024          | 8.085±0.044          | 7.827±0.027          | M4.0Ve                                | 1           | 9.11                  | 12                                 |
| GJ141-029            |                          | 12.86±0.04   | 11.58±0.04      | 9.95±0.04       | I                      | 0.0120                   | 3                            | 16                      | 77            | 8.361±0.018          | 7.813±0.038          | 7.551±0.021          | M4.0Ve                                | 1           | 9.78                  | 12                                 |
| LP870-065            |                          | 13.02±0.03   | 11.75±0.02      | 10.09±0.03      | R                      | 0.0133                   | 3                            | 18                      | 68            | 8.559±0.027          | 8.012±0.049          | 7.701±0.029          | M4.0Ve                                | 1           | 10.71                 | 12                                 |
| 2MA2009-0113         |                          | 14.47±0.05   | 12.98±0.03      | 11.16±0.03      | I                      | 0.0137                   | 3                            | 11                      | 56            | 9.403±0.026          | 8.832±0.025          | 8.512±0.023          | M4.5Ve                                | 1           | 10.81                 | 12                                 |
| LEHPM2-0783          |                          | 17.17±0.04   | 15.28±0.04      | 13.03±0.02      | I                      | 0.0250                   | 3                            | 11                      | 58            | 10.664±0.022         | 10.104±0.025         | 9.715±0.023          | M6.5Ve                                | 1           | 10.57                 | 12                                 |
| L755-019             |                          | 12.47±0.02   | 11.31±0.01      | 9.81±0.02       | R                      | 0.0164                   | 3                            | 11                      | 55            | 8.394±0.027          | 7.759±0.029          | 7.496±0.031          | M3.0Ve                                | 1           | 12.01                 | 12                                 |
| GJ0799A              | RBS1692                  | 10.36±0.03   | 9.08±0.03       | 7.40±0.03       | V                      | 0.0566                   | 3                            | 19                      | 136           | 5.807±0.026          | 5.201±0.046          | 4.944±0.042          | M4.0VeJ                               | 1           | 2.77                  | 12                                 |
| GJ0799B              |                          | ...          | ...             | ...             | V                      | 0.0502                   | 2                            | 19                      | 136           | ...                  | ...                  | ...                  | ...                                   | ...         | ...                   | ...                                |
| LP756-003            |                          | 13.80±0.08   | 12.52±0.06      | 10.88±0.05      | R                      | 0.0205                   | 2                            | 7                       | 25            | 9.349±0.027          | 8.728±0.034          | 8.435±0.021          | M4.0Ve                                | 1           | 14.62                 | 12                                 |
| LHS3799              |                          | 13.30±0.03   | 11.88±0.03      | 10.05±0.03      | V                      | 0.0138                   | 3                            | 17                      | 106           | 8.242±0.027          | 7.638±0.047          | 7.319±0.018          | M4.5Ve                                | 1           | 6.06                  | 12                                 |
| LP932-083            |                          | 13.94±0.06   | 12.67±0.05      | 10.98±0.03      | V                      | 0.0435                   | 3                            | 15                      | 62            | 9.342±0.020          | 8.780±0.051          | 8.474±0.021          | M4.0Ve                                | 1           | 13.71                 | 12                                 |
| GJ1284AB             | RBS2013                  | 11.14±0.04   | 10.02±0.04      | 8.59±0.04       | V                      | 0.0270                   | 3                            | 20                      | 95            | 7.200±0.019          | 6.608±0.042          | 6.329±0.026          | M3.0Ve                                | 1           | 7.78                  | 12                                 |
| Previously Published |                          |              |                 |                 |                        |                          |                              |                         |               |                      |                      |                      |                                       |             |                       |                                    |
| LHS1302              |                          | 14.49±0.05   | 13.00±0.02      | 11.16±0.03      | R                      | 0.0205                   | 5                            | 31                      | 178           | 9.413±0.021          | 8.841±0.021          | 8.552±0.022          | M4.5Ve                                | 1           | 11.04                 | 12                                 |
| LHS1358              |                          | 13.58±0.03   | 12.31±0.03      | 10.66±0.02      | R                      | 0.0147                   | 2                            | 11                      | 58            | 9.055±0.030          | 8.518±0.026          | 8.168±0.021          | M4.0V                                 | Ref95       | 12.54                 | 12                                 |
| G099-049             |                          | 11.31±0.05   | 10.04±0.04      | 8.43±0.03       | V                      | 0.0120                   | 5                            | 54                      | 364           | 6.905±0.020          | 6.308±0.022          | 6.042±0.022          | M3.5Ve                                | 1           | 5.09                  | 12                                 |
| APCOL                | LP939-44                 | 12.96±0.02   | 11.49±0.02      | 9.60±0.02       | V                      | 0.0175                   | 4                            | 30                      | 183           | 7.742±0.027          | 7.183±0.018          | 6.866±0.021          | M4.5Ve                                | 1           | 4.62                  | 12                                 |
| G041-014ABC          | RBS 732                  | 10.92±0.04   | 9.67±0.02       | 8.05±0.02       | V                      | 0.0128                   | 3                            | 29                      | 203           | 6.507±0.018          | 5.966±0.033          | 5.688±0.016          | M3.5VeJ                               | 1           | 4.39                  | 12                                 |
| 2MA1207-3932AB       | TWA 27AB                 | 19.95±0.20   | 17.99±0.07      | 15.92±0.05      | I                      | 0.0168                   | 5                            | 14                      | 56            | 12.995±0.026         | 12.388±0.027         | 11.945±0.026         | M3.5VeJ                               | 1           | 26.99                 | 12                                 |
| LHS2729              |                          | 12.89±0.06   | 11.68±0.03      | 10.14±0.02      | R                      | 0.0117                   | 3                            | 8                       | 56            | 8.664±0.025          | 8.066±0.055          | 7.781±0.031          | M3.5Ve                                | 1           | 12.59                 | 12                                 |
| LHS2836              |                          | 12.88±0.04   | 11.60±0.02      | 9.90±0.03       | V                      | 0.0111                   | 2                            | 23                      | 119           | 8.334±0.037          | 7.761±0.061          | 7.445±0.026          | M4.0Ve                                | 1           | 8.86                  | 12                                 |
| GJ1207               |                          | 12.25±0.04   | 10.99±0.05      | 9.43±0.05       | V                      | 0.1989                   | 5                            | 42                      | 226           | 7.971±0.023          | 7.442±0.080          | 7.120±0.021          | M3.5Ve                                | 1           | 9.36                  | 12                                 |
| LHS4016AB            |                          | 12.34±0.04   | 11.25±0.03      | 9.90±0.02       | V                      | 0.0124                   | 3                            | 22                      | 97            | 8.584±0.029          | 8.023±0.049          | 7.743±0.022          | M2.5VeJ                               | 1           | 17.18                 | 12                                 |

<sup>a</sup>S=SOAR photometry (from Sergio Dieterich)  
<sup>b</sup>“\*” denotes spectral types from this work.  
<sup>c</sup>Joint photometry.  
<sup>d</sup>No independent photometry.

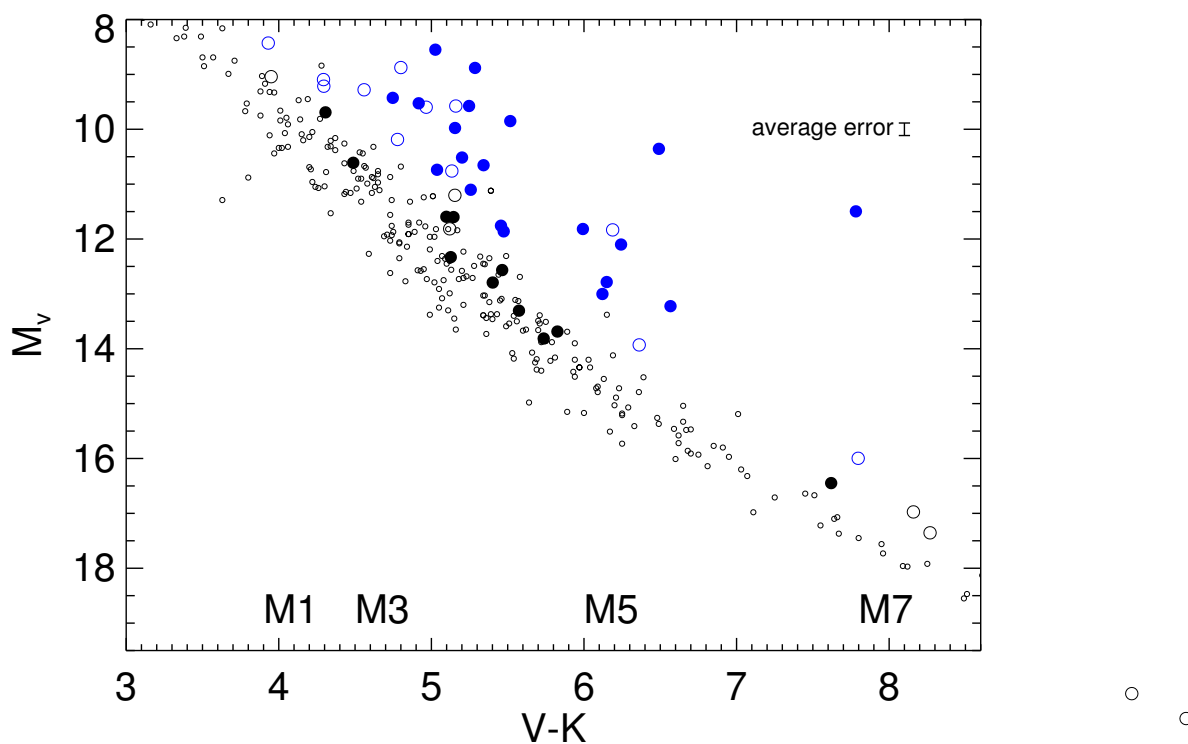


Figure 5.14: HR diagram of low proper motion stars. Black stars are probably main sequence stars, blue stars are probably young; filled circles are stars from the TINYMO survey (Chapter 4). The small open circles are the RECONS 10pc sample.

We have 55 parallax results for members of 50 star systems with proper motions less than  $0.18'' \text{ yr}^{-1}$  from both the TINYMO search and targets already on the CTIOPI program for other reasons. Of these, 23 systems are within 25 pc, and 21 more are between 25 and 50 pc, with the remaining 11 beyond 50 pc. They are plotted on a color-magnitude diagram in Figure 5.14, and on the sky with transverse motion vectors in Figure 5.15. One, 2MA1207-3932AB (better known as TWA 27), has already had its CTIOPI parallax published (Gizis et al. 2007); another, LP 476-207ABC, already has a (poor quality) *HIP-PARCOS* parallax that puts it outside 25 pc; our new result places it at  $24.9 \pm 1.3$  pc.

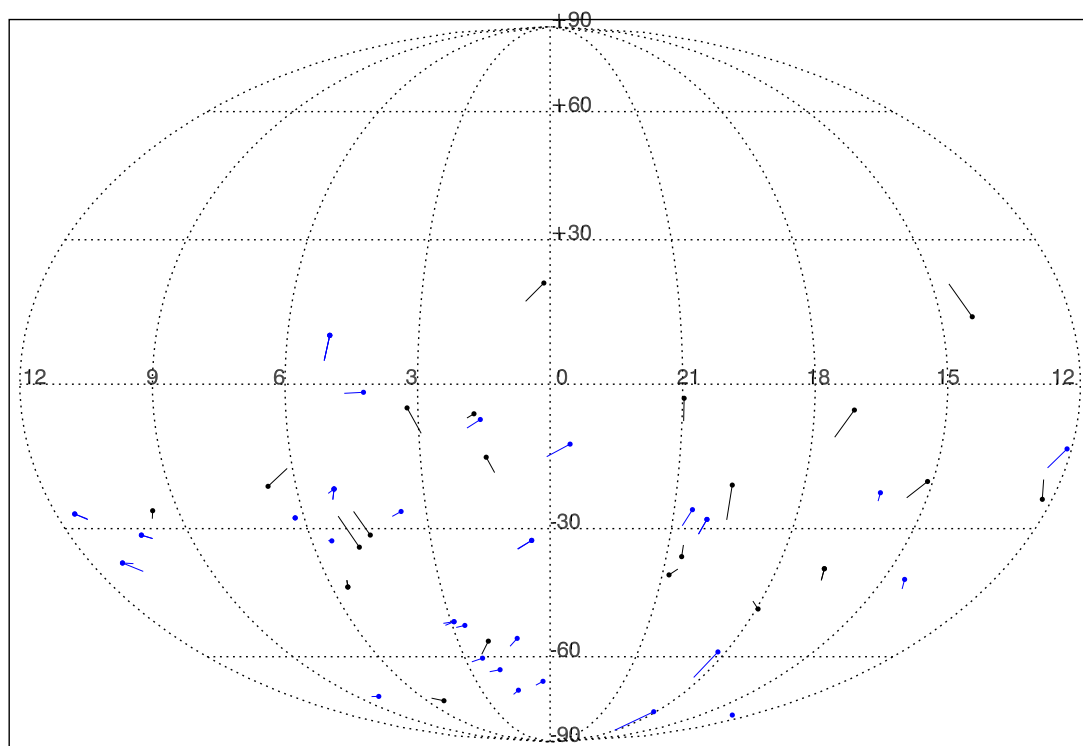


Figure 5.15: Mollweide projection of the low proper motion stars, showing their proper motion vectors (scaled up by a factor of 180,000). Blue points are also probably young. Points with two motion vectors have two components.

As can be seen in Figure 5.14 the vast majority of stars are either multiple or young, lying above (in some cases, well above) the main sequence. This is also borne out by Figure 5.16, which shows the discrepancy between CCD photometric distance estimates and their trigonometric parallaxes. Nearly the entire sample observed has  $H\alpha$  emission (noted by “e” in the spectral types of Table 5.9) in low-resolution spectroscopy, also suggesting chromospheric activity from either (relative) youth or close companions.

At least some of this is an observational bias in the sample toward objects with substantial X-ray flux as measured in the ROSAT All-Sky surveys (Voges et al. 1999, 2000); early on

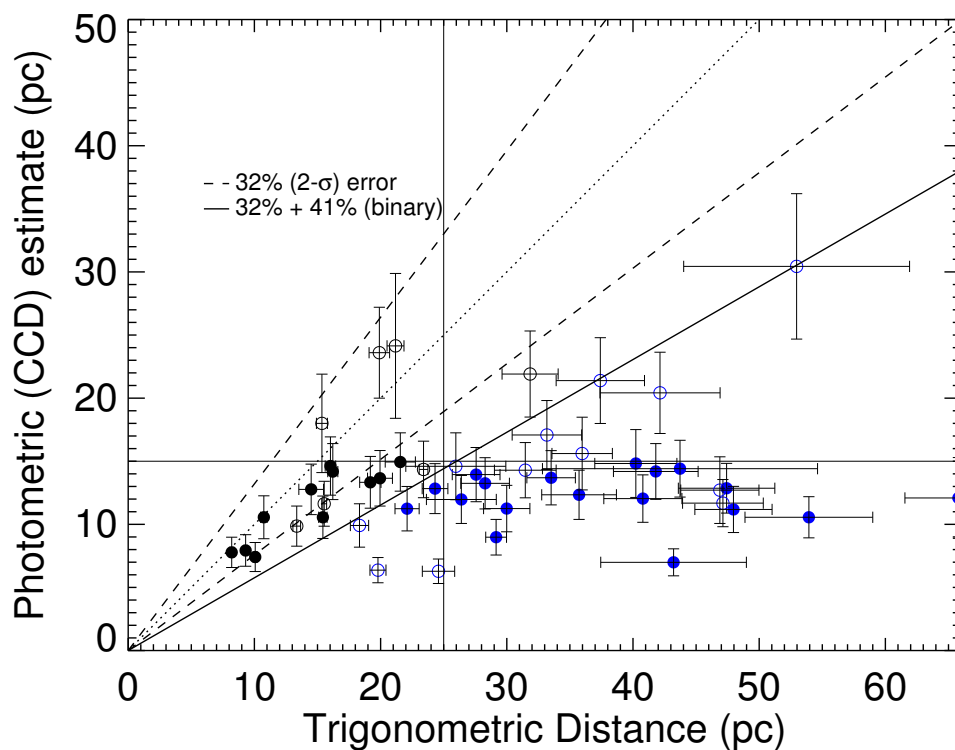


Figure 5.16: Comparison of CCD photometry-based distance estimates and trigonometric parallaxes. Black points are probable main sequence stars, Blue points are probably young; filled circles are from the TINYMO survey (Chapter 4).

it was discovered that nearly every object with an IRAS detection was a giant, and nearly everything with an X-ray detection was a genuine nearby star with a chance of being young. As described in Chapter 4, when we prioritized those X-ray bright stars, we biased the sample toward apparent youth.

At least some of this is also the result of multiplicity – multiple stars will appear brighter (and therefore have closer photometric distance estimates) than a single star of the same color, and scatter into the sample. A large number of stars in my thesis sample are known to be multiple, their properties are summarized in Table 5.10.

Table 5.10: Multiple star parameters

| Primary Name (1)  | Secondary Name (2) | Separation (arcsec) (3) | Position Angle (°) (4) | Ref (5)                             | $\Delta mag$ (6) | Filter (7)            | Ref (8)                  | Period (years) (9) | Ref (10)               | Note <sup>c</sup> (11) |
|-------------------|--------------------|-------------------------|------------------------|-------------------------------------|------------------|-----------------------|--------------------------|--------------------|------------------------|------------------------|
| Low Proper Motion |                    |                         |                        |                                     |                  |                       |                          |                    |                        |                        |
| G 131-026 A       | G 131-026 B        | 0.111                   | 169.9                  | Beuzit et al. (2004)                | 0.46             | MKO K <sub>s</sub>    | Beuzit et al. (2004)     | ~4                 | Beuzit et al. (2004)   | AO                     |
| GJ 2006 A         | GJ 2006 B          | 17.9                    | 4.9                    | (this work)                         | 0.46             | Johnson V             | (this work)              | ...                | ...                    | VB                     |
| LP 467-016 A      | LP 467-016 B       | 0.409                   | 147.2                  | Beuzit et al. (2004)                | 0.69             | MKO K <sub>s</sub>    | Beuzit et al. (2004)     | ...                | ...                    | AO                     |
| GJ 2022 AC        | GJ 2022 B          | 37.2                    | 78.8                   | (this work) <sup>b</sup>            | 1.94             | Johnson V             | (this work) <sup>b</sup> | ...                | ...                    | VB                     |
| GJ 2022 A         | GJ 2022 C          | 1.8                     | 224.4                  | (this work)                         | 0.08             | Johnson V             | (this work)              | ...                | ...                    | VB                     |
| LP 993-115        | LP 993-116 AB      | 44.8                    | 60.9                   | (this work) <sup>b</sup>            | 0.31             | Johnson V             | (this work) <sup>b</sup> | ...                | ...                    | VB                     |
| LP 993-116 A      | LP 993-116 B       | 0.257                   | 214.6                  | Bergfors et al. (2010)              | 1.12             | SDSS z'               | Bergfors et al. (2010)   | ...                | ...                    | LJ, PB                 |
| 2MA 0254-5108 A   | 2MA 0254-5108 B    | 15.3                    | 80.2                   | (this work)                         | 4.72             | Johnson V             | (this work)              | ...                | ...                    | VB?                    |
| G 039-029 A       | G 039-029 B        | 0.87                    | 300.6                  | Daemgen et al. (2007)               | 0.37             | Altair K <sub>s</sub> | Daemgen et al. (2007)    | ...                | ...                    | AO                     |
| LP 476-207 AC     | LP 476-207 B       | 1.0                     | 165                    | Henry et al. (1997)                 | 1.03             | CIT K                 | Henry et al. (1997)      | ...                | ...                    | SP                     |
| LP 476-207 A      | LP 476-207 C       | ...                     | ...                    | ...                                 | ...              | ...                   | ...                      | 12 days            | Delfosse et al. (1999) | SB                     |
| BD-21 01074 A     | BD-21 01074 BC     | 8.3                     | 229.3                  | (this work) <sup>b</sup>            | 0.67             | Johnson V             | (this work) <sup>b</sup> | ...                | ...                    | VB                     |
| BD-21 01074 B     | BD-21 01074 C      | 0.8                     | 321                    | WDS                                 | 1.19             | ?                     | WDS                      | ...                | ...                    | VB, PB                 |
| L 449-001 A       | L 449-001 B        | 0.046                   | ...                    | (this work)                         | 1.0              | FGS F583W             | (this work)              | ~2.5               | (this work)            | FGS, PB                |
| SCR 0533-4257 A   | SCR 0533-4257 B    | 0.056                   | ...                    | (this work)                         | 0.7              | FGS F583W             | (this work)              | ~2                 | (this work)            | FGS, PB                |
| SCR 0613-2742 A   | SCR 0613-2742 B    | 0.093                   | ...                    | (this work)                         | 0.6              | FGS F583W             | (this work)              | >4                 | (this work)            | FGS, PB                |
| G 041-014 AC      | G 041-014 B        | 0.62                    | ...                    | Delfosse et al. (1999) <sup>b</sup> | 0.5              | MKO K                 | Delfosse et al. (1999)   | ~10                | Delfosse et al. (1999) | AO                     |
| G 041-014 A       | G 041-014 C        | ...                     | ...                    | ...                                 | ...              | ...                   | ...                      | 7.6 days           | Delfosse et al. (1999) | SB                     |
| SCR 1012-3124 A   | SCR 1012-3124 B    | 1.00                    | 270                    | (this work) <sup>c</sup>            | 0.03             | Johnson V             | (this work) <sup>c</sup> | ...                | ...                    | VB                     |
| SIP 1110-3731 AC  | SIP 1110-3731 B    | 1.16                    | 210.2                  | (this work) <sup>b</sup>            | 0.27             | Johnson V             | (this work) <sup>b</sup> | ...                | ...                    | VB                     |
| SIP 1110-3731 A   | SIP 1110-3731 C    | ...                     | ...                    | ...                                 | ...              | ...                   | ...                      | ...                | Webb et al. (1999)     | SB                     |
| RX 1132-2651 A    | RX 1132-2651 B     | 13.1                    | 184.7                  | (this work)                         | 2.97             | Johnson V             | (this work)              | ...                | ...                    | VB                     |
| 2MA 1207-3239 A   | 2MA 1207-3239 B    | 0.778                   | 125.8                  | Chauvin et al. (2004)               | 4.98             | 2MASS K <sub>s</sub>  | Chauvin et al. (2004)    | ...                | ...                    | AO                     |
| 2MASS J1306-7723  | DEN 1306-7723      | 32.1                    | 184.6                  | (this work)                         | 1.19             | Johnson V             | (this work)              | ...                | ...                    | VB                     |
| G 165-008 A       | G 165-008 B        | 0.17                    | 253.3                  | Beuzit et al. (2004)                | 0.16             | MKO K <sub>s</sub>    | Beuzit et al. (2004)     | ...                | ...                    | AO                     |
| GJ 2122 A         | GJ 2122 B          | 0.59                    | 255.4                  | Heintz (1987)                       | 2.0              | ?                     | Heintz (1987)            | ...                | ...                    | VB, PB                 |
| SCR 2010-2801 A   | SCR 2010-2801 B    | 0.61                    | 280.4                  | Bergfors et al. (2010)              | 0.75             | SDSS z'               | Bergfors et al. (2010)   | ...                | ...                    | LJ                     |
| GJ 0799 A         | GJ 0799 B          | 2.3                     | 156                    | (this work)                         | 0.04             | Johnson V             | (this work)              | ...                | ...                    | VB                     |
| GJ 0803           | GJ 0799 A          | 4681.0                  | 212.4                  | (this work) <sup>b</sup>            | 1.71             | Johnson V             | (this work) <sup>b</sup> | ...                | ...                    | VB                     |
| LTT 9210          | LP 932-083         | 217.3                   | 69.2                   | (this work)                         | 1.39             | 2MASS K <sub>s</sub>  | (this work)              | ...                | ...                    | VB                     |
| GJ 1284 A         | GJ 1284 B          | ...                     | ...                    | ...                                 | ...              | ...                   | ...                      | ...                | Torres et al. (2006)   | SB                     |
| LHS 4016 A        | LHS 4016 B         | ...                     | ...                    | ...                                 | ...              | ...                   | ...                      | <20 days           | Shkolnik et al. (2010) | SB                     |

<sup>a</sup>VB= Visual Binary, AO= Resolved by AO, LJ= Resolved by Lucky Imaging, SP= Resolved by Speckle Interferometry, FGS= Resolved by FGS Interferometry.

SB= Spectroscopic Binary, PB= Astrometric Perturbation

<sup>b</sup>Relative to unresolved components.

<sup>c</sup>Estimate from PSF peaks.

#### 5.4 Riedel et al. (2011): AP Col

In Riedel et al. (2011) we presented the results of a multi-technique investigation of the M4.5Ve flare star AP Col, in which we discovered it to be the nearest pre-main-sequence star. The investigation included astrometric data from the CTIO 0.9m, from which we derive a proper motion of  $342.0 \pm 0.5$  mas yr<sup>-1</sup>, a trigonometric parallax of  $119.21 \pm 0.98$  mas ( $8.39 \pm 0.07$  pc), and photometry and photometric variability at optical wavelengths. We also provided spectroscopic data, including radial velocity ( $22.4 \pm 0.3$  km s<sup>-1</sup>), lithium Equivalent Width (EW) ( $0.28 \pm 0.02 \text{ \AA}$ ), H $\alpha$  EW ( $-6.0$  to  $-35 \text{ \AA}$ ), vsini ( $11 \pm 1$  km s<sup>-1</sup>), and gravity indicators from the Siding Spring 2.3-m WiFeS, Lick 3-m Hamilton echelle, and Keck-I HIRES echelle spectrographs. The combined observations demonstrate that AP Col is the closer of only two known systems within 10 pc of the Sun younger than 100 Myr. Given its space motion and apparent age of 12-50 Myr, AP Col is likely a member of the recently proposed  $\sim 40$  Myr old Argus/IC 2391 association. Results are collected in Table 5.12.

The X-ray active M dwarf AP Col (=LP 949-015, LTT 2449, SIPS J0604-3433, 2MASS J06045215-3433360) was identified as a UV-Ceti type flare star as early as 1995 (Ball & Bromage 1995), whereupon it was given its variable star designation. It was studied by Scholz et al. (2005) as one of three active M dwarfs detected within a predicted distance of 8 pc, and again by Riaz et al. (2006), where the star's potential youth and proximity was again noted. It was also targeted for Lucky Imaging by Bergfors et al. (2010), and for Speckle Imaging with the USNO Specklecam on the CTIO 4-m by Mason & Hartkopf (2011, private communication). RECONS' searches for nearby stars in the southern sky (Henry et al. 2006) also identified

this star as a potential solar neighbor, and it was put on the CTIOPI target list in 2004. As described in [Riedel et al. \(2011\)](#), the star was more recently investigated at the Lick, Keck, and Siding Spring Observatories.

In conjunction with the new data presented in [Riedel et al. \(2011\)](#), we first demonstrated that the observed characteristics of AP Col are signs of a youthful age of less than 100 Myr, and not caused by interactions with a close companion. We then argued that its age and kinematics match those of the Argus association defined by [Torres et al. \(2008\)](#).

### **5.4.1 Observations**

#### *5.4.1.1 Astrometry and Photometry*

The 158 *V* filter observations of AP Col used in our astrometric and relative photometry sequences were obtained on 27 nights between September 2004 and March 2011. Additional details of the observing protocols for the astrometry and photometry programs can be found in §2.1, §2.2, [Jao et al. \(2005\)](#) and [Winters et al. \(2011\)](#). The same setup was used to obtain four nights of *VRI* photometry, interleaved with standard star observations from [Graham \(1982\)](#), [Landolt \(1992\)](#), and [Landolt \(2007\)](#) at various airmasses.

#### *5.4.1.2 Spectroscopy*

##### 5.4.1.2.1 CTIO 1.5-m RCspec

To measure a spectral type, AP Col was observed on the CTIO 1.5-m on UT 14 March 2004 using the 32/I grating setup (6000-9600Å, R=500). The resulting spectrum was reduced using standard IRAF procedures and then classified as M4.5Ve using the ALLSTAR code

Table 5.11: Spectroscopic Observations of AP Col (Riedel et al. 2011)

| UT Date     | Instrument | Setup                      | Coverage<br>Å | Resolving <sup>a</sup><br>Power | S/N | $\lambda$ of S/N <sup>b</sup><br>Å | H $\alpha$ EW<br>Å | Li $\lambda$ 6708 EW<br>Å | RV <sup>c</sup><br>km s <sup>-1</sup> | $vsini$<br>km s <sup>-1</sup> |
|-------------|------------|----------------------------|---------------|---------------------------------|-----|------------------------------------|--------------------|---------------------------|---------------------------------------|-------------------------------|
| (1)         | (2)        | (3)                        | (4)           | (5)                             | (6) | (7)                                | (8)                | (9)                       | (10)                                  | (11)                          |
| 08 Jan 2011 | WiFeS      | R7000/RT480 <sup>d</sup>   | 5500-7000     | 7,000                           | 30  | 6300                               | -7.5 $\pm$ 1.0     | 0.25 $\pm$ 0.1            | 21.3 $\pm$ 1.0                        | ...                           |
| 08 Jan 2011 | WiFeS      | R7000/RT480                | 5500-7000     | 7,000                           | 25  | 6300                               | -8.0 $\pm$ 1.0     | 0.25 $\pm$ 0.1            | 24.1 $\pm$ 0.8                        | ...                           |
| 25 Jan 2011 | Hamilton   | 800 $\mu$ m slit, Dewar #6 | 3850-8850     | 40,000                          | 25  | 6700                               | -35 $\pm$ 3        | 0.19 $\pm$ 0.03           | 23 $\pm$ 1                            | ...                           |
| 25 Jan 2011 | WiFeS      | B/R3000/RT560 <sup>d</sup> | 3400-9650     | 3,000                           | 60  | 7400                               | -28 $\pm$ 3        | ...                       | ...                                   | ...                           |
| 25 Jan 2011 | WiFeS      | B/R3000/RT560              | 3400-9650     | 3,000                           | 60  | 7400                               | -26 $\pm$ 3        | ...                       | ...                                   | ...                           |
| 25 Jan 2011 | WiFeS      | B/R3000/RT560              | 3400-9650     | 3,000                           | 60  | 7400                               | -35 $\pm$ 3        | ...                       | ...                                   | ...                           |
| 26 Jan 2011 | WiFeS      | B/R3000/RT560              | 3400-9650     | 3,000                           | 60  | 7400                               | -12 $\pm$ 3        | ...                       | ...                                   | ...                           |
| 11 Feb 2011 | WiFeS      | R7000/RT480                | 5500-7000     | 7,000                           | 30  | 6300                               | -13.5 $\pm$ 1.0    | 0.25 $\pm$ 0.05           | 21.5 $\pm$ 0.9                        | ...                           |
| 24 Feb 2011 | WiFeS      | R7000/RT480                | 5500-7000     | 7,000                           | 25  | 6300                               | -7.5 $\pm$ 1.0     | 0.3 $\pm$ 0.05            | 20.0 $\pm$ 0.8                        | ...                           |
| 16 Mar 2011 | WiFeS      | R7000/RT480                | 5500-7000     | 7,000                           | 35  | 6300                               | -12.1 $\pm$ 1.0    | 0.25 $\pm$ 0.1            | 24.1 $\pm$ 1.0                        | ...                           |
| 17 Mar 2011 | WiFeS      | R7000/RT480                | 5500-7000     | 7,000                           | 40  | 6300                               | -6.5 $\pm$ 1.0     | 0.25 $\pm$ 0.05           | 23.2 $\pm$ 1.0                        | ...                           |
| 17 Mar 2011 | WiFeS      | R7000/RT480                | 5500-7000     | 7,000                           | 50  | 6300                               | -6.0 $\pm$ 1.0     | 0.3 $\pm$ 0.05            | 22.5 $\pm$ 1.1                        | ...                           |
| 17 Mar 2011 | HIRES      | Red Collimator             | 3580-7950     | 50,000                          | 20  | 6700                               | -7.3 $\pm$ 0.5     | 0.37 $\pm$ 0.03           | 22.3 $\pm$ 0.3                        | 11 $\pm$ 1                    |

<sup>a</sup> Resolving Power is measured from the FWHM of single arclines in our comparison spectra.

<sup>b</sup> Wavelength where S/N measurement is made in the spectrum.

<sup>c</sup> RV errors for WiFeS are internal errors with reference to the standards. The approximate error per epoch is 2 km s<sup>-1</sup>.

<sup>d</sup> RT480 and RT560 are dichroics for the beam splitter.

(Henry et al. 2002), which compares it to spectral standards on the Kirkpatrick et al. (1991)

system.

#### 5.4.1.2.2 SSO 2.3-m WiFeS IFU

To measure a preliminary radial velocity, H $\alpha$ , and Li I  $\lambda$ 6708 line strengths, AP Col was observed several times during 2011 January – March with the Wide Field Spectrograph (WiFeS) on the Australian National University 2.3-m at Siding Spring Observatory. WiFeS (Dopita et al. 2007, 2010) is a new dual-beam image slicing integral field spectrograph that provides a nominal 25''  $\times$  38'' field-of-view with 0.5'' pixels to two gratings and camera assemblies simultaneously using a beam splitter, one ‘beam’ optimized for red spectra, the other for blue. AP Col was observed in single-beam mode with the R7000 grating, yielding a resolving power of  $R \simeq 7000$  and wavelength coverage of 5500–7000Å. Following Murphy (2012), we used WiFeS in single-star mode with twice the spatial binning (1'' spatial pixels) and optimally extracted and combined the 5 image slices (effectively a 5'' diameter aperture

around the object) that contain the majority of the stellar flux.

WiFeS has a measured radial velocity precision capability of  $\sim 2 \text{ km s}^{-1}$  per epoch at this resolution and signal-to-noise (Table 5.11 Murphy 2012). We therefore observed AP Col seven times on different nights to improve the mean velocity and check for changes in H $\alpha$  emission line strength. These observations motivated further high-resolution observations with the Lick Hamilton Echelle and Keck HIRES Echelle, discussed in the next sections.

In addition to the *R*7000 observations, AP Col was observed on 25–26 January 2011 with the *B*3000 and *R*3000 gratings in dual-beam mode, yielding a resolving power of  $R \simeq 3000$  and wavelength coverage from 3400–9560Å. The spectra from each beam were independently flux-calibrated and corrected for telluric features, and combined into a single spectrum. Details about the WiFeS observations are presented in Table 5.11.

#### 5.4.1.2.3 Lick Shane 3-m Hamilton Echelle

Contemporaneous with the low-resolution WiFeS spectra, additional measurements of radial velocity, H $\alpha$ , and Li I  $\lambda$ 6708 EW were obtained at the Lick Observatory Shane 3-m telescope with the Hamilton echelle spectrograph (Vogt 1987), which is located at the telescope’s Coudé focus. The spectra covering 3800–8850Å at  $R=40,000$  were bias-subtracted, flat-fielded, extracted, and wavelength calibrated with ThAr arclamp spectra. Further details on data reduction for the Hamilton echelle with IRAF tasks are outlined in detail in Lick Technical Report No. 74<sup>11</sup>.

Details about the observations are presented in Table 5.11. We note that AP Col, at DEC

---

<sup>11</sup><http://astronomy.nmsu.edu/cwc/Software/irafman/manual.html> checked 15 JUL 2012

−34, is at the southern limit of what can reasonably be observed from Lick Observatory; the average airmass during observations was 3.3.

#### 5.4.1.2.4 Keck I 10-m HIRES Echelle

More precise measurements of radial velocity and *vsini* were obtained on the Keck-I 10-m telescope on Mauna Kea using the HIRES echelle spectrograph (Vogt et al. 1994). The spectra covering 3580–7900 Å at R=50,000 were reduced with standard IRAF echelle reduction tasks: data are bias-subtracted, then flat-fielded with “wide-decker” flats (flats taken with twice the decker height of the science data). Data are extracted and then wavelength-calibrated with ThAr arc spectra. Observational parameters are given in Table 5.11. The iodine cell was in the light path during the observations of AP Col; as a result, strong iodine absorption features are present from ~5000-6000 Å.

Archival HIRES observations of the M4.5V star GJ 83.1 were retrieved from the Keck Observatory Archive<sup>12</sup> for use in radial velocity cross-correlation. GJ 83.1 has a radial velocity known to be stable to <100 m s<sup>−1</sup> (Nidever et al. 2002). The archival observations from UT 10 Aug 2009 (PI Haghighipour) were performed with an identical instrument setup.

### 5.4.2 Results

#### 5.4.2.1 Astrometry and Photometry

Based on the *VRI* photometry from CTIOPI, *JHK<sub>s</sub>* photometry from 2MASS (Cutri et al. 2003) (Table 5.12), and the photometric distance relations from Henry et al. (2004) (see also

<sup>12</sup><http://www2.keck.hawaii.edu/koa/public/koa.php> checked 2012 JUL 15.

Table 5.12: Vital Parameters (Riedel et al. 2011)

| AP Col  |                                     |
|---|-------------------------------------|
| $\pi_{rel}$ (mas)                                 | $118.26 \pm 0.97$                   |
| $\pi_{corr}$ (mas)                                | $0.95 \pm 0.11$                     |
| $\pi_{abs}$ (mas)                                 | $119.21 \pm 0.98$                   |
| Distance (pc)                                     | $8.39 \pm 0.07$                     |
| $\mu_{\alpha} \cos \delta, \mu_{\delta}$ (mas/yr) | $(27.33, 340.92) \pm (0.35)$        |
| $\mu$ (mas/yr)                                    | $342.0 \pm 0.5$                     |
| P.A. (deg)  | $004.6 \pm 0.13$                    |
| $V_{tan}$ (km s <sup>-1</sup> )                   | $13.60 \pm 0.11$                    |
| Photometric                                       |                                     |
| $V_J$   | $12.96 \pm 0.01$                    |
| $R_{KC}$  | $11.49 \pm 0.02$                    |
| $I_{KC}$  | $9.60 \pm 0.01$                     |
| $J_{2MASS}$                                       | $7.74 \pm 0.03$                     |
| $H_{2MASS}$                                       | $7.18 \pm 0.02$                     |
| $K_{s2MASS}$                                      | $6.87 \pm 0.02$                     |
| $M_V$   | 13.34                               |
| $V_J - K_{s2MASS}$                                | 6.09                                |
| $L_x/L_{bol}$                                     | $-2.95 \pm 0.16$                    |
| $\log(L_x)$                                       | $28.49 \pm 17\%$                    |
| Variability (mag)                                 | 0.017 ( $V_J$ )                     |
| Spectroscopic                                     |                                     |
| Spectral Type                                     | M4.5e <sup>a</sup>                  |
| Li I $\lambda 6708$ EW (Å)                        | $0.28 \pm 0.02$                     |
| H $\alpha$ EW (Å)                                 | $-9.1 \pm 5.2$ [variable -6 to -35] |
| $V_{rad}$ (km s <sup>-1</sup> )                   | $+22.4 \pm 0.3$                     |
| $v \sin i$ (km s <sup>-1</sup> )                  | $11 \pm 1$                          |
| Derived Quantities                                |                                     |
| X (pc)  | $-3.72 \pm 0.04$                    |
| Y (pc)  | $-6.70 \pm 0.08$                    |
| Z (pc)  | $-3.41 \pm 0.04$                    |
| U (km s <sup>-1</sup> )                           | $-21.98 \pm 0.17$                   |
| V (km s <sup>-1</sup> )                           | $-13.58 \pm 0.24$                   |
| W (km s <sup>-1</sup> )                           | $-4.45 \pm 0.13$                    |
| Isochronal Age (Myr)                              | 12–125                              |
| Na I (gravity) Age (Myr)                          | 12–100                              |
| Li I Age (Myr)                                    | 12–50                               |

<sup>a</sup> Measured type is M4.5Ve, but AP Col is not a main sequence star.

§2.2.5), we estimated a main-sequence photometric distance of  $4.6 \pm 0.7$  pc. This is consistent with the spectrophotometric distance estimates from Scholz et al. (2005) (6.1 pc, M5.0e) and Riaz et al. (2006) (4 pc, M5 + H $\alpha$ ).

The astrometric solution for AP Col was calculated using 14 reference stars on 158  $V$ -band frames taken over 6.48 years, from September 2004 – March 2011. The resulting absolute trigonometric parallax (calculated using the pipeline from Jao et al. 2005) is  $119.21 \pm 0.98$  mas ( $8.39 \pm 0.07$  pc), and the relative proper motion is  $342.0 \pm 0.5$  mas yr<sup>-1</sup> at  $4.6 \pm 0.1$  degrees ( $(\mu_{\alpha} \cos \delta, \mu_{\delta}) = (27.33, 340.92) \pm (0.35)$  mas yr<sup>-1</sup>), corresponding to a tangential velocity of

$13.60 \pm 0.11 \text{ km s}^{-1}$ ; more details are given in Table 5.12. The trigonometric distance therefore differs from the photometric distance estimate by  $5\text{-}\sigma$ , putting AP Col  $\sim 1.5$  mag in  $M_V$  above the main sequence. This can be caused by youth and/or unresolved multiplicity (see Figure 5.20 and §5.4.2.3).

The issue with the  $V$  filters (described in § 5.1.1) produces a  $\sim 20$  mas false astrometric signal in the R.A. data. An alternative parallax reduction was carried out using only the data from the other, preferred  $V$  filter and was found to agree with the adopted reduction using all data. We are thus convinced that our parallax and proper motion are accurate, but our ability to detect the presence of companions in our astrometric residuals is thus limited.

#### 5.4.2.2 Spectroscopy

Based on our CTIO spectrum (Figure 5.17), AP Col is an M4.5e<sup>13</sup> (accurate to half a subtype) star with substantial  $H\alpha$  emission (Table 5.12). This is confirmed with our WiFeS  $B/R3000$  spectra, from which we derive a spectral type of M4.5-M5 based on various spectral indices and spectrophotometry.

Each of the Hamilton and WiFeS  $R7000$  spectra have been cross-correlated with spectra of stars with known radial velocities to derive AP Col's radial velocity and to search for radial velocity variability between epochs. The Hamilton and WiFeS  $R7000$  spectra yield radial velocity measurements for AP Col with precisions of roughly  $1 \text{ km s}^{-1}$  and  $2 \text{ km s}^{-1}$ , respectively. Thanks to the use of the iodine absorption cell, we are able to obtain the best precision and accuracy on the HIRES radial velocity measurement (see Table 5.11), and it

---

<sup>13</sup>AP Col is not a main sequence star.

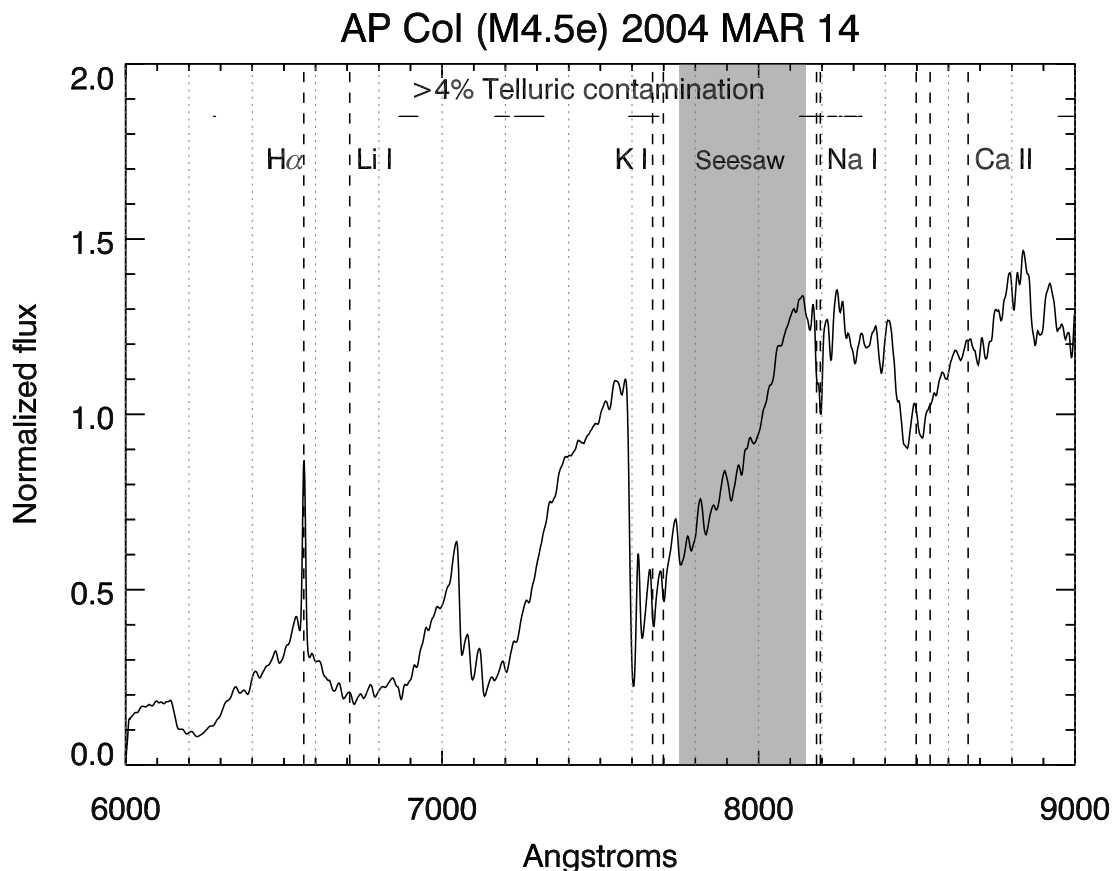


Figure 5.17: The red/optical spectrum (6000–9000Å) of AP Col, taken on the CTIO 1.5m RCSpec with the 32/I standard grating setting on 2004 MAR 14. The star has clear H $\alpha$  emission, weak Na I and K I, and no Ca II features; Li is not visible at this low spectral resolution. This figure was not included in Riedel et al. (2011).

is most responsible for the resulting weighted mean radial velocity (Table 5.12).

AP Col’s radial velocity appears stable to  $1.3 \text{ km s}^{-1}$  over 68 days, based on all 9 measurements (Table 5.11). Assuming it is in fact stable, the weighted mean radial velocity is  $+22.4 \pm 0.3 \text{ km s}^{-1}$ . Our result is consistent with, but much more precise than, the RV reported by Scholz et al. (2005), ( $V_{rad} = +67 \pm 30 \text{ km s}^{-1}$ ).

AP Col is a known flare star, as reported in Ball & Bromage (1995), and we detected

strong  $H\alpha$  and numerous other emission lines in its optical spectra (listed in Table 5.13). Indeed, the Lick and WiFeS  $R3000$  data show AP Col in the midst of an energetic outburst ( $H\alpha$  EW  $\approx 35\text{\AA}$ ). This outburst will be discussed in detail in a future publication led by Carl Melis.

Table 5.13: Emission Lines in HIRES AP Col Optical Spectra (Riedel et al. 2011)

| Spectral Feature  | Rest Wavelength<br>( $\text{\AA}$ in air) | EW<br>( $\text{\AA}$ ) |
|-------------------|---|------------------------|
| $H\alpha$         | 6562.852                                  | $-7.3\pm 0.5$          |
| Na D <sub>1</sub> | 5895.924                                  | $-0.4\pm 0.1^a$        |
| Na D <sub>2</sub> | 5889.951                                  | $-1.1\pm 0.1^a$        |
| He I              | 5875.621                                  | $-0.8\pm 0.1^a$        |
| $H\beta$          | 4861.350                                  | $-8\pm 1$              |
| He I              | 4471.480                                  | $-0.3\pm 0.1$          |
| $H\gamma$         | 4340.472                                  | $-6\pm 1$              |
| $H\delta$         | 4101.734                                  | $-5\pm 1$              |
| $H\epsilon$       | 3970.075                                  | $-4\pm 1$              |
| Ca II H           | 3968.470                                  | $-10\pm 2$             |
| Ca II K           | 3933.660                                  | $-13\pm 3$             |
| H8                | 3889.064                                  | $-5\pm 2$              |
| H9                | 3835.397                                  | $-4\pm 2^b$            |
| H10               | 3797.909                                  | $-0.7\pm 0.2^b$        |

<sup>a</sup> Line contaminated by iodine absorption.

<sup>b</sup> Continuum around line not significantly detected.

#### 5.4.2.3 Multiplicity

As determined in §5.4.2.1, AP Col lies  $\sim 1.5$  magnitudes in  $M_V$  above the main sequence for a star of spectral type M4.5. Overluminosity in an M dwarf can be attributed to at least one of three things: 1) multiplicity (where the brightness of the star is actually the combination of two or more stars); 2) youth (where the star is still gravitationally contracting onto the main sequence), and/or 3) high metallicity (where the star is not brighter, but redder than

a typical main sequence star of the same mass and luminosity, much as subdwarfs are bluer than corresponding main-sequence stars).

Given that AP Col lies well above even the high-metallicity envelope of stars within 10 pc (Figure 5.20), we can reasonably discard the last option. Multiplicity can conspire to make a system appear up to 41% closer as an equal-luminosity binary, or 73% closer as an equal-luminosity trinary. The measured discrepancy, 81%, cannot thus be explained by an equal luminosity binary, even when the full  $2\sigma$  systematic error on the photometric distance – 30% (Henry et al. 2004) – is assumed. However, if the multiple system is close enough, the stars can tidally interact and force synchronous rotation, which can maintain fast rotational velocities and cause chromospheric activity until the system is far older than what is considered ‘young’.

To address the potential multiplicity of AP Col, we work our way inwards. Wide surveys of AP Col on SuperCOSMOS plate scans (Hambly et al. 2001a) reveal no wide companions to the star within  $15'$  and brighter than  $SERC(J) = 21$ ,  $SERC(I) = 19$ ; within that range only the star 2MASS J06052273-3429245 has noticeable proper motion,  $(-62.38, -119.63) \pm (7.02, 9.95)$  mas yr $^{-1}$  measured by the SuperCOSMOS Sky Survey (Hambly et al. 2001a), but this proper motion is not similar to AP Col. 2MASS  $JHK_s$  images show no genuine companions down to  $\sim 3''$ ; the apparent close companions in the 2MASS database are actually ‘glints’, detector artifacts from internal reflections in the camera<sup>14</sup>.

The highest resolution seeing-limited image of AP Col from the CTIOPI frames (FWHM  $0.94''$ , taken on UT 11 NOV 2008, Figure 5.18) shows no signs of companions to AP Col down

<sup>14</sup><http://www.ipac.caltech.edu/2mass/releases/allsky/doc/sec4.7.html> checked 2012 JUL 15

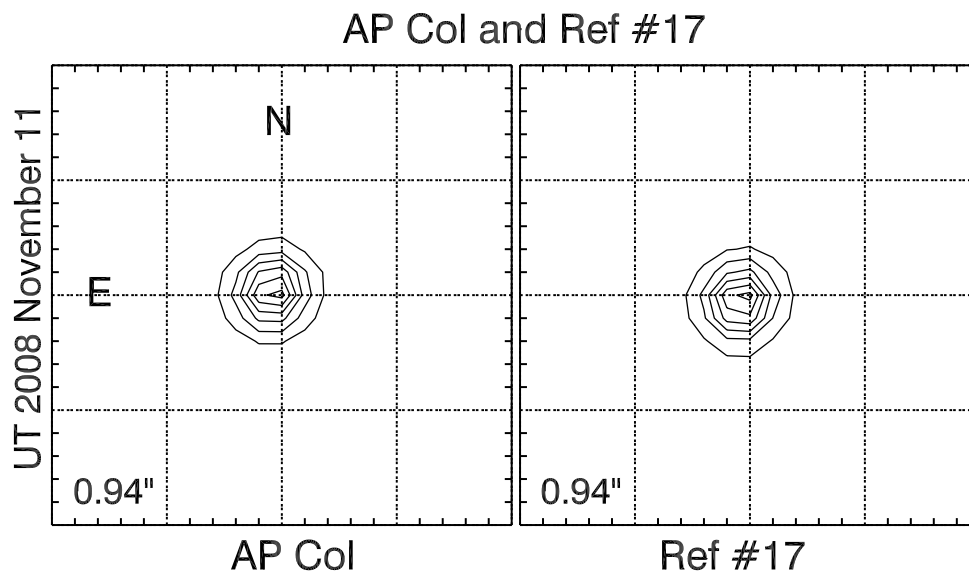


Figure 5.18: The field immediately surrounding AP Col and the closest reference star, in  $V$  from the CTIO 0.9m, on a night with good seeing (FWHM=0.94"). There is no sign of a companion to AP Col down to  $\Delta V=5$  mag, or any visible difference between the PSF of AP Col and Reference Star #17.

to separations of 0.9" and  $\Delta V=5$ , nor any sign of elongation from an unresolved companion;

other images in all three filters show nothing to approximately that limit as well<sup>15</sup>.

Bergfors et al. (2010) lucky-imaged 124 M dwarfs from the Riaz et al. (2006) sample, including AP Col. Their images, taken in early November 2008, detected no companions to AP Col at angular separations between 0.1"–6.0", and a magnitude difference of  $\Delta z' \leq 2$  mag at the smallest separations. Independently, Mason & Hartkopf (2011, private communication) observed AP Col in early March 2006 with the USNO Specklecam on the CTIO 4-m and also obtained a null result, with  $\Delta vis \leq 3$  at a separation of 0.05"–1.0".

Further constraints using our CTIO astrometric data are problematic due to the issue

<sup>15</sup>CTIOPI exposes target stars to roughly the same ADU limit regardless of filter; the limits in  $\Delta V$ ,  $\Delta R$  and  $\Delta I$  are thus roughly identical.

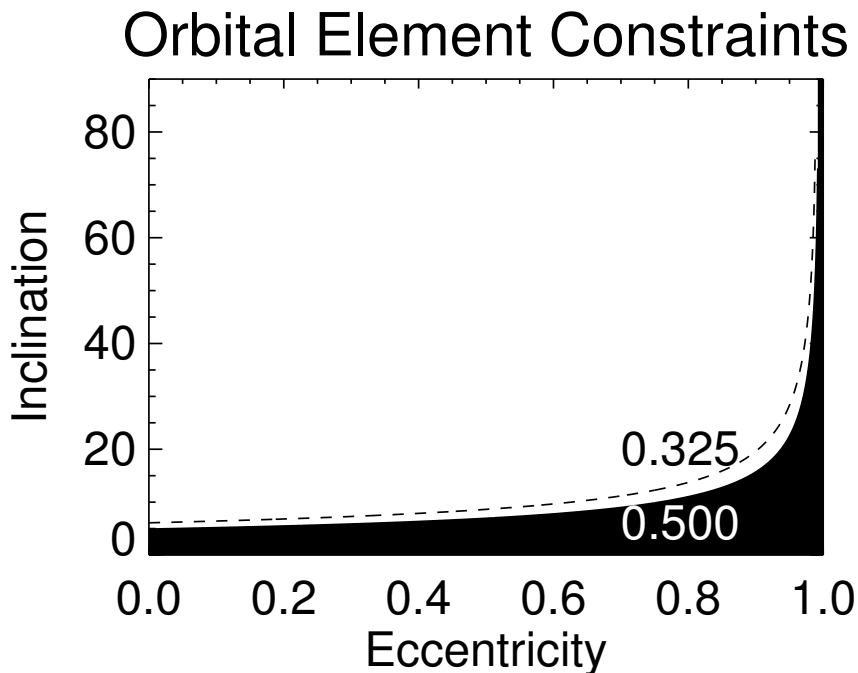


Figure 5.19: Companion detection limits, given the null results of our companion search down to  $0.05''$  separations, radial velocities stable to  $1.3 \text{ km s}^{-1}$  over 68 days, and assuming a maximum separation of 0.42 AU corresponding to  $0.05''$  at 8.4 pc. Below the dashed line, a  $0.075M_{\odot}$  brown dwarf ( $M_{tot} = 0.325M_{\odot}$ ) could be hidden; within the filled region, two M4.5V stars ( $M_{tot} = 0.5M_{\odot}$ , the most likely scenario to explain the overluminosity) could be hidden. Such eccentricities and inclinations are unlikely, and we conclude that AP Col is a single star.

with the  $V$  filters mentioned in §5.4.2.1. While we see no evidence for a companion in the astrometric residuals, we can only constrain the possible multiplicity of AP Col to objects that would produce a photocentric shift smaller than 20 mas in right ascension or 6 mas in declination.

These visual limits, particularly the Lucky and Speckle imaging, set strict limits on the size of a companion's orbit. Henry et al. (1999) suggests an M4.5V main sequence star has a mass of roughly  $0.25 M_{\odot}$ ; to best explain the overluminosity requires twin  $0.25 M_{\odot}$  stars<sup>16</sup>.

<sup>16</sup>As mentioned earlier, additional components would better provide the additional flux, but would neces-

With those masses, the longest period circular orbit that could be hidden within  $0.05''$  ( $0.42$  AU) is  $0.38$  years ( $139$  days), for which the full velocity amplitude would be  $33 \text{ km s}^{-1}$ . We have already established that the radial velocity of AP Col is stable to within  $1.3 \text{ km s}^{-1}$  over the  $9$  epochs and  $68$  days of RV observations ( $\sim \frac{1}{2}$  of the maximum orbital period) with cadences as short as  $1$  day; this significantly limits the inclinations and eccentricities in which a companion could remain undetected, as shown in Figure [5.19](#). Low inclinations can particularly be ruled out given that we have measured the *vsini* rotational velocity as  $11 \pm 1 \text{ km s}^{-1}$ , which would translate to nearly  $300 \text{ km s}^{-1}$  (near break-up speed) if the star's rotational axis were sufficiently inclined (Figure [5.19](#)) to hide a low-eccentricity orbit. We are thus convinced that AP Col has no stellar-mass companions; substellar companions may still be present but cannot explain AP Col's elevation above the main sequence. We conclude that the activity and overluminosity we see in AP Col are intrinsic to the star itself (and that it is *not* necessarily a main sequence star with a mass of  $0.25 M_{\odot}$ ), and not the result of a stellar companion.

#### 5.4.2.4 Youth

##### 5.4.2.4.1 Isochronal age

To properly compare AP Col to other known young stars without relying on theoretical models requires accurate data. To this end, I compiled a list of young stars (see §[3.4](#) for more details) with the best available data, and attempted to fit the non-multiple high-confidence members of various associations with fifth-degree polynomials (see §[2.2.5](#)).

---

sitate a higher system mass and larger velocity variations.

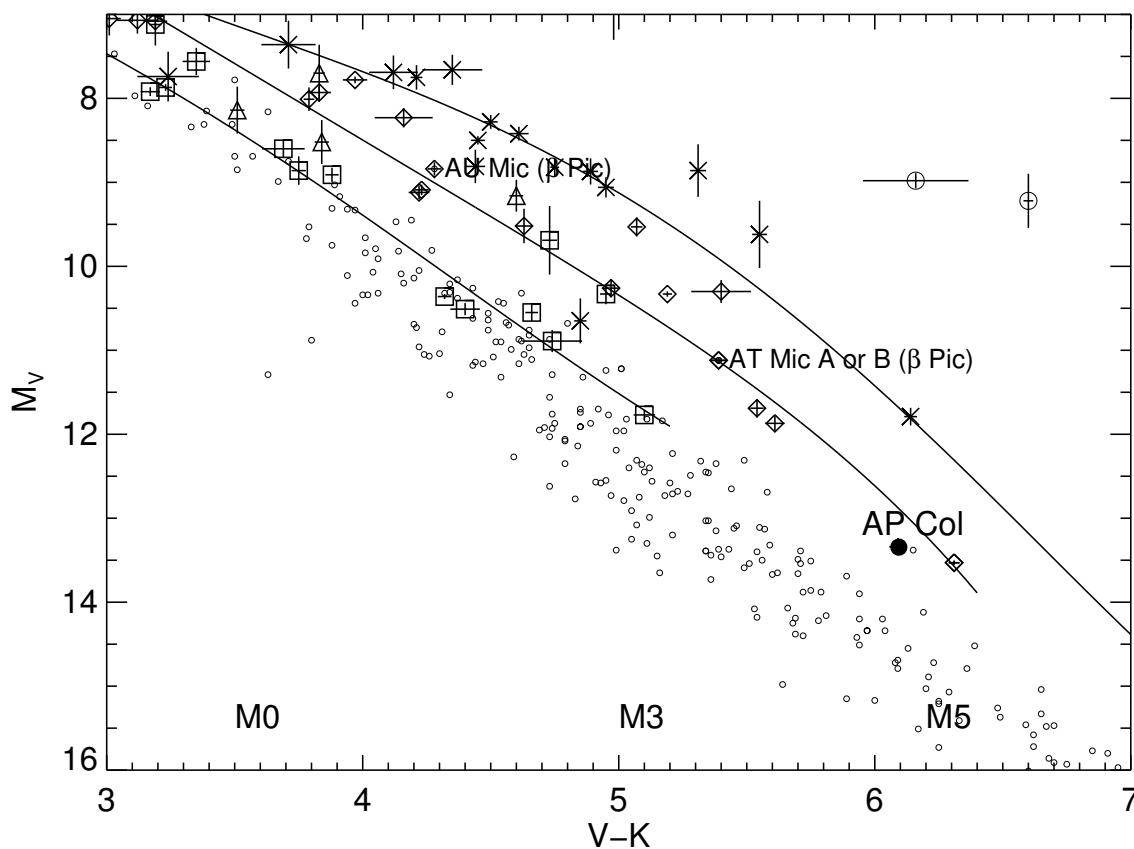


Figure 5.20: AP Col (filled circle) plotted relative to the RECONS 10 pc sample (the elevated 10 pc object near AP Col is EQ Peg B, see the text), with error bars smaller than the plotted symbol. Also plotted are members of nearby young associations from [Zuckerman & Song \(2004\)](#) and [Torres et al. \(2008\)](#):  $\epsilon$  Cha (large open circles), TW Hya (Xs),  $\beta$  Pic (diamonds), Tuc-Hor (triangles), and AB Dor (squares). Fifth order fits ([§2.2.5](#)) are plotted for (top to bottom) TW Hya,  $\beta$  Pic, and AB Dor. No attempt has been made to split any unresolved binaries among the associations other than the AT Mic A&B and TWA 22 A&B systems, which both provide overlapping points. AP Col appears to be older than (but consistent with),  $\beta$  Pic (12 Myr); and younger than (but consistent with) AB Dor (125 Myr), although at such red colors and low temperatures, none of the association memberships or isochrone fits are well defined.

As can be seen in Figure 5.20, AP Col is clearly older than members of the  $\epsilon$  Cha cluster ( $\sim 6$  Myr), TW Hya ( $\sim 8$  Myr), and consistent with but likely older than  $\beta$  Pic ( $\sim 12$  Myr). There are no comparably red AB Dor or Tuc-Hor members with known parallaxes; despite this, the position of AB Dor at the high-metallicity upper envelope of the main sequence suggests that AP Col is younger than the  $\sim 125$  Myr AB Dor association.

#### 5.4.2.4.2 Lithium

The Li I  $\lambda 6708$  equivalent width of AP Col is  $0.28 \pm 0.02 \text{ \AA}$ , the weighted mean of all our high resolution spectral measurements.

We plot in Figure 5.21 the lithium measurements for AP Col, several of the young stellar associations in the solar vicinity from da Silva et al. (2009), and the young cluster IC 2391 from Barrado y Navascués et al. (2004). The  $\beta$  Pic Lithium Depletion Boundary (LDB, §2.3.4) at M4.5 (dashed line) is clearly visible as the discontinuity in equivalent width for upward triangle points around 3300 K, while the IC 2391 LDB at  $\sim M5$  (3200K) is shown as a dotted line. AP Col lies between the two boundaries at  $T_{\text{eff}} \simeq 3250$  K (based on  $V - I$  color and the conversion of Kenyon & Hartmann 1995), implying an age between  $\beta$  Pic ( $\sim 12$  Myr) and IC 2391 ( $50 \pm 5$  Myr lithium depletion age, Barrado y Navascués et al. 2004), though consistent with either.

#### 5.4.2.4.3 Low-gravity features

Figure 5.22 shows the Na I doublet  $\lambda 8200$  index for AP Col compared to the mean trends of other young associations in Lawson et al. (2009). To match the resolution used in that

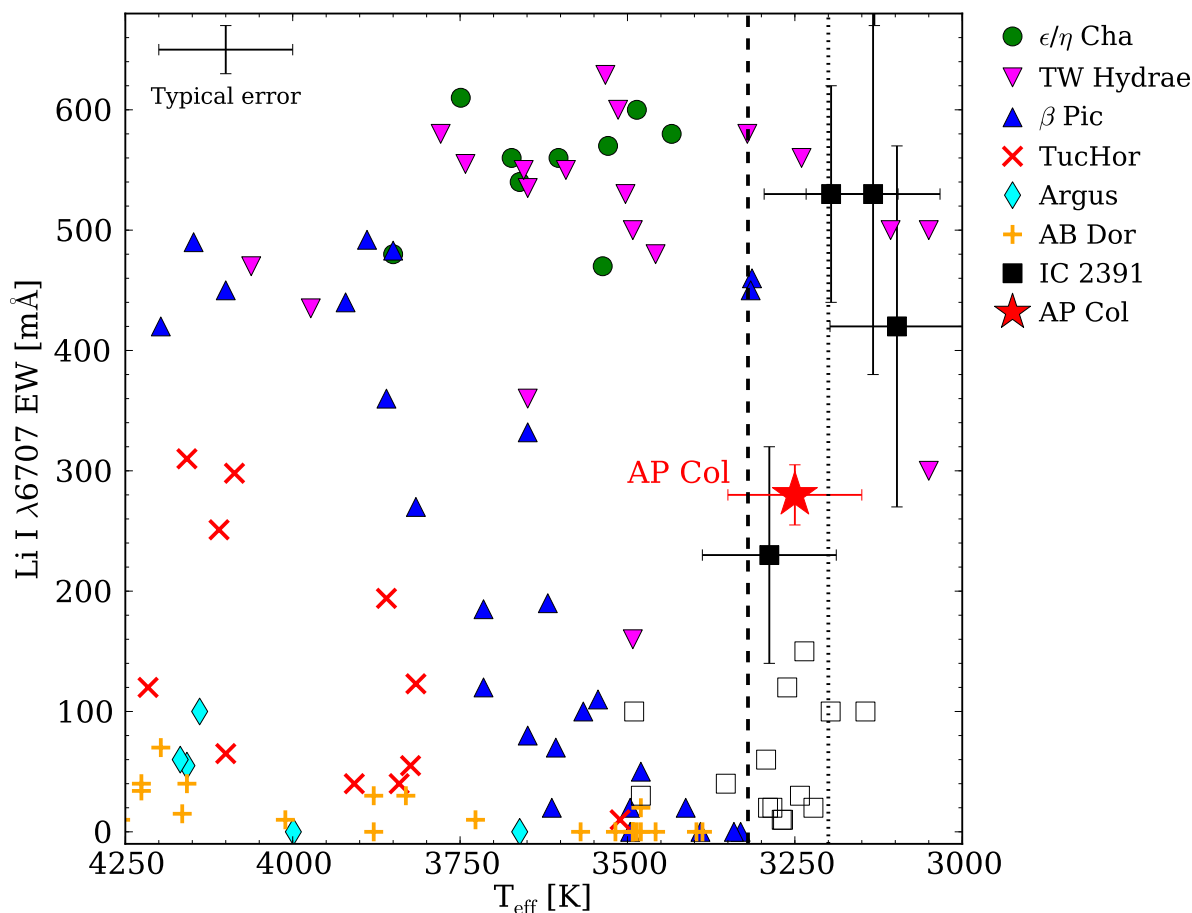


Figure 5.21: Li I  $\lambda 6708$  absorption for AP Col (filled star) relative to the young local association members measured by [da Silva et al. \(2009\)](#) ( $\epsilon/\eta$  Cha,  $\sim 6$  Myr; TW Hya,  $\sim 10$  Myr;  $\beta$  Pic,  $\sim 12$  Myr; Tucana-Horologium,  $\sim 30$  Myr; Argus,  $\sim 40$  Myr; AB Dor,  $\sim 125$  Myr). For consistency all temperatures were calculated from  $V - I$  color and the transformation of [Kenyon & Hartmann \(1995\)](#). Lower main sequence members of IC 2391 with  $V - I$  colors from [Barrado y Navascués et al. \(2004\)](#) are also plotted (filled squares, open squares denote upper limits). The decreasing trend in  $EW$  with decreasing temperature in the older groups is readily apparent, as are the effects of lithium depletion with age. AP Col is moderately lithium-depleted compared to the younger groups and lies between the  $\beta$  Pic Lithium Depletion Boundary (LDB, dashed line defined by the two systems at  $\sim 3300$  K,  $EW_{\text{LiI}} \approx 450$  mÅ) and the IC 2391 LDB (approximated by the dotted line). This constrains the age of AP Col to between that of  $\beta$  Pic (12 Myr) and IC 2391 ( $50 \pm 5$  Myr [Barrado y Navascués et al. 2004](#)). Plot in [Riedel et al. \(2011\)](#) by Simon Murphy.

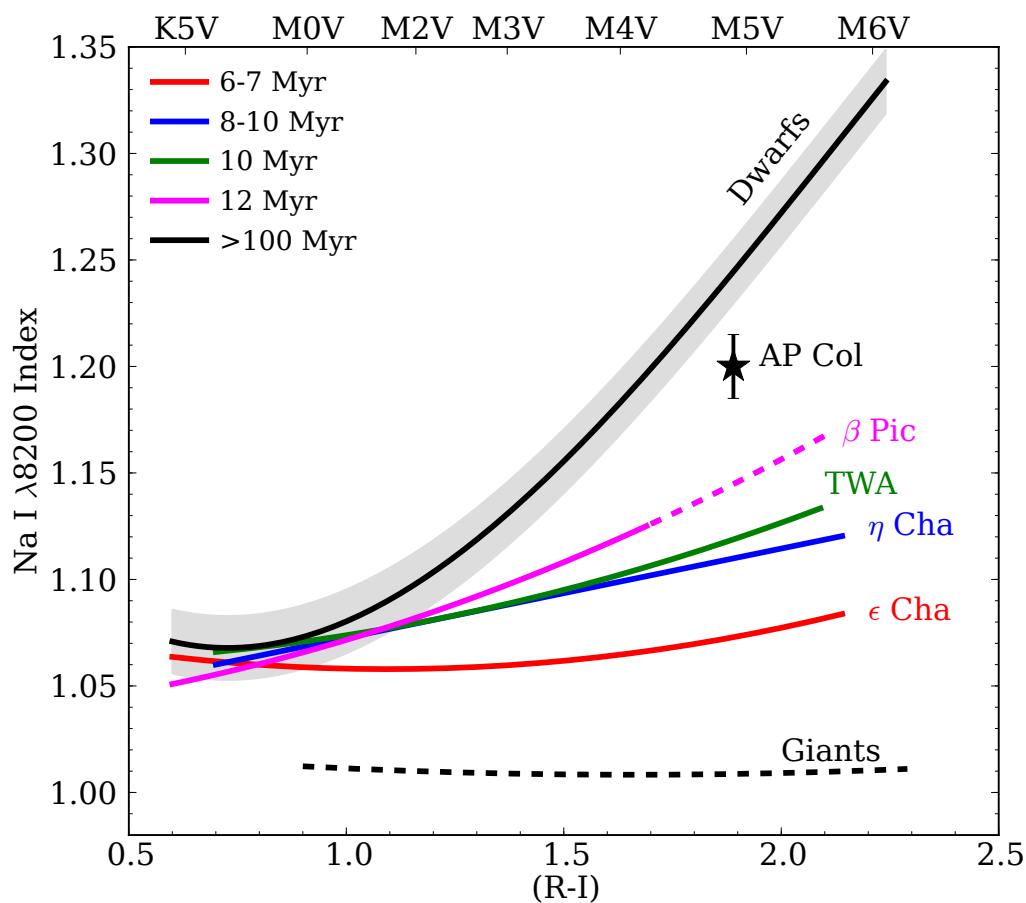


Figure 5.22: Na I index trends for various young, local associations from [Lawson et al. \(2009\)](#). The shaded band represents the variation around the mean dwarf trend seen in [Lyo et al. \(2004\)](#). The value for AP Col has been derived from our WiFeS R3000 spectra, smoothed to the approximate resolution of the [Lawson et al.](#) data. The error bar shows the variation observed between the four exposures. AP Col has an intermediate gravity, suggestive of an age between 12–100 Myr. Plot in [Riedel et al. \(2011\)](#) by Simon Murphy.

study, we have smoothed and resampled the WiFeS  $R3000$  data to  $R \sim 900$  and the same wavelength scale used by [Lawson et al. \(2009\)](#). Although close to the dwarf locus, AP Col nevertheless lies at intermediate gravities between  $\beta$  Pic and field dwarfs; we can again constrain the age to greater than that of  $\beta$  Pic and less than the Pleiades, whose M-type

members have gravity features indistinguishable from field stars (Slesnick et al. 2006a).

Alkali metal lines such as the Na I doublet can also be affected by stellar activity, where emission fills in the absorption line cores, leading to lower EWs (Reid & Hawley 1999). Our WiFeS observations of AP Col span a factor of three in  $H\alpha$  EW, but no correlation between that activity indicator and our Na I doublet EW measurements could be found. Slesnick et al. (2006b) notes that the Na I  $\lambda 8183/8195$  doublet can be affected by telluric absorption over the region 8161–8282 Å, leading to artificially low Na I index values for stars observed at large airmasses. Our WiFeS  $R3000$  spectra were observed at  $\sec(z) \simeq 1$ ; nevertheless we have checked the telluric correction of the spectra and find no excess that could affect the index measurements. We conclude that the location of AP Col’s point in Figure 5.22 is correct.

#### 5.4.2.4.4 $v \sin i$

From the Keck-I HIRES spectra, we measure a  $v \sin i = 11 \pm 1 \text{ km s}^{-1}$ , indicating that AP Col is not necessarily a rapidly rotating star. Because it is not in a binary system, this spin is not due to tidal synchronization with a companion; it is a remnant of the star’s formation.

While gyrochronology relations exist (e.g. Mamajek 2009) for solar-type stars, no reliable relations have been developed for M dwarfs, nor stars with saturated X-ray emission such as AP Col. Gyrochronology cannot (yet) be used to estimate an age for AP Col.

#### 5.4.2.4.5 Activity: X-ray emission, H $\alpha$ emission, flares, and photometric variability

AP Col is cross-identified as the ROSAT All Sky Survey object 1RXS J060452.1-343331, and has  $\log(L_x/L_{bol})=-2.95\pm 0.16$  and  $\log(L_x)=28.49$  (17% error). These values match Riaz et al. (2006) and agree with the range of X-ray variability published by Scholz et al. (2005),  $\log(L_x/L_{bol})=-3$  to  $-4$ .

As seen in Table 5.11 during our spectroscopic observations the H $\alpha$  EW of AP Col varied from  $-6\text{\AA}$  in apparent quiescence, to  $-35\text{\AA}$  during the strong flare on 2011 Jan 25, with an average EW of  $-9.1\pm 5.2\text{\AA}$ , in agreement with the  $-12.1\text{\AA}$  single epoch measurement published by Riaz et al. (2006).

AP Col is a known UV Ceti flare star, and Ball & Bromage (1995) observed 5 flares over 9 hours of *U*-band observations, the largest of which was 2.5 magnitudes above background. A 12-hour X-ray flare was also measured by ROSAT and presented by Scholz et al. (2005); during this event AP Col increased in X-ray luminosity by roughly an order of magnitude and slowly dropped back to normal levels. We have also measured an extremely energetic white-light flare in Lick Hamilton Echelle data taken 25 January 2011, which will be presented in a future publication by Carl Melis.

Finally, we have measured the relative photometric variability of AP Col using the *V* filter data from the CTIOPI astrometric frames. The standard deviation of the variability is 1.7%, (Figure 5.23). As shown in Figure 5.24, this is typical when compared to field M dwarfs observed during CTIOPI (Jao et al. 2011). The 158 CTIOPI astrometry frames constitute a total observing time of 14715 seconds over 27 nights (4 hours, with a median time of 450

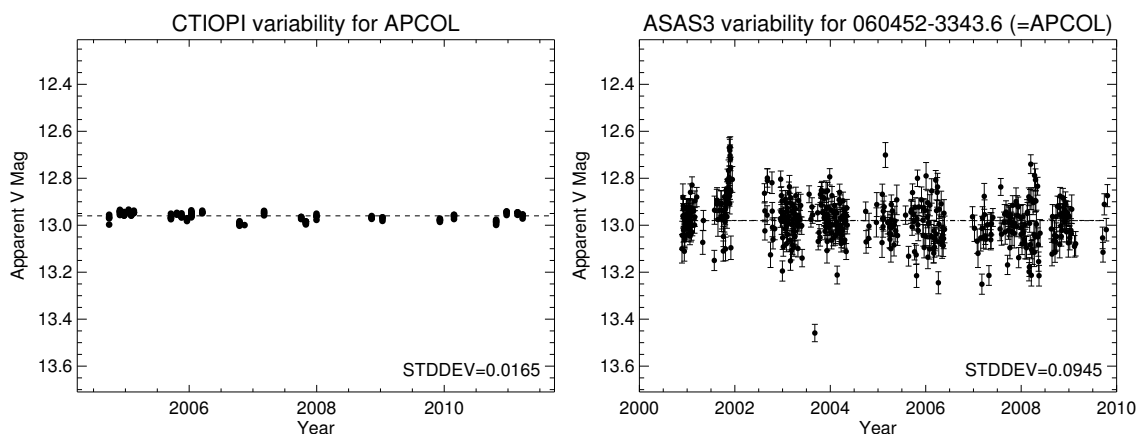


Figure 5.23: AP Col relative photometric variability in the  $V$  filter observations from CTIOPI (left) and ASAS (right). ASAS has lower photometric accuracy than CTIOPI relative photometry. Neither time series shows convincing variability or flares.

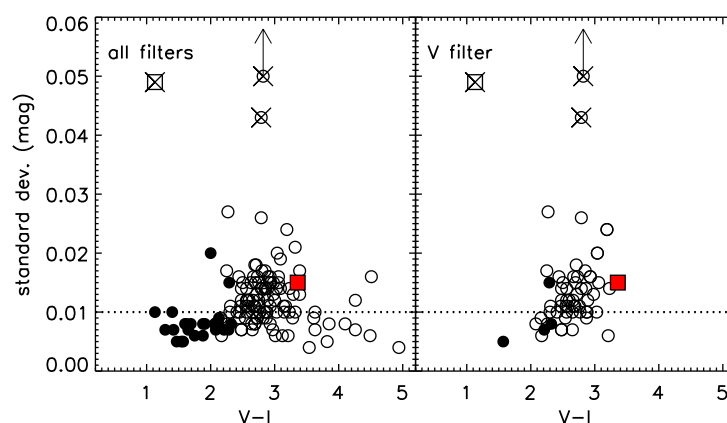


Figure 5.24: AP Col (filled square) relative variability as compared to other stars studied during CTIOPI (Jao et al. 2011, X and boxed objects are from that paper). Apart from being somewhat redder than other stars observed in the  $V$  filter, AP Col is unremarkable. Plot in Riedel et al. (2011) by Wei-Chun Jao.

seconds in five observations per night) spanning 6.48 years. We additionally checked the ASAS3 database (Pojmanski 1997) for photometry on AP Col, and find no evidence of large flares ( $>0.5$  mag) in their dataset (see Figure 5.23) either. We report our own variability in Table 5.12, as our 0.91-m telescope aperture lends itself to better photometry than the 8-cm

ASAS telescopes.

#### 5.4.2.4.6 IR detection

IRAS and WISE photometry from the preliminary data release show no obvious signs of infrared excess around AP Col. This is not unexpected if AP Col is older than  $\sim 10$  Myr, as suggested by our other age indicators.

### 5.4.3 Conclusions

The balance of the age indicators place AP Col somewhere between the ages of  $\beta$  Pic and IC 2391, or  $\sim 12$  Myr to  $\sim 50$  Myr following Torres et al. (2008) and Barrado y Navascués et al. (2004). To give the discovery of AP Col context, we compare it to the other 255 stellar systems known within 10 pc as of January 1, 2011 (Henry et al. 2006, and updates at *www.recons.org*). As shown in the color-magnitude diagram of Figure 5.20, AP Col is one of only a few red dwarfs noticeably elevated above the main sequence, with a location of  $M_V = 13.34$ ,  $V - K = 6.09$ .

Three of the elevated points within 10 pc are in one system, comprised of AU Mic, AT Mic A, and AT Mic B (9.9 pc; note that the AT Mic A+B point is actually the overlap of two similar points — the two stars have virtually identical  $V$  and  $K$  magnitudes). This triple is one of the prototypical members of the  $\beta$  Pic association (Barrado y Navascués et al. 1999) with an age of  $\sim 12$  Myr, and is remarkable as the youngest of the 256 systems known within 10 pc.

The elevated point near AP Col in Figure 5.20 represents GJ 896 B (6.3 pc), otherwise

known as EQ Peg B, at  $M_V = 13.38$ ,  $V - K = 6.15$ . Both EQ Peg A and B are known to flare, have H $\alpha$  in emission, and emit X-rays (Robrate et al. 2004). Both components have also been reported to have companions (Delfosse et al. 1999), but a private communication from the first author of that study indicated that neither spectroscopic companion was confirmed. Thus, we are left with a mystery: the EQ Peg system exhibits some indicators of youth and neither component is known to be multiple, but the A component at  $M_V = 11.24$ ,  $V - K = 4.95$ , is not significantly elevated above the main sequence, while the B component is. (Nakajima & Morino (2012) suggest it to be a member of the Cha-Near association (Zuckerman & Song 2004), whose existence has been disputed by Torres et al. (2008))

Another potentially young star within 10 pc is GJ 393 (7.1 pc), which Torres et al. (2008) report as a member of AB Dor. However, the star has weak X-ray and NUV emission (Rodriguez et al. 2011), no H $\alpha$  emission, and slow rotation ( $v \sin i < 3 \text{ km s}^{-1}$ , Rodriguez et al. 2011), all more typical of older stars. We suspect it is a high metallicity field star with space velocities coincidentally similar to AB Dor, and note that the AB Dor isochrone happens to lie along the high-metallicity envelope of the main sequence (Figure 5.20). López-Santiago et al. (2009) also report GJ 393 as a main sequence interloper to AB Dor.

Ultimately, the statuses of GJ 393 and GJ 896 AB are still uncertain. AP Col is now the closest pre-main-sequence star, at only 8.4 pc from the Sun.

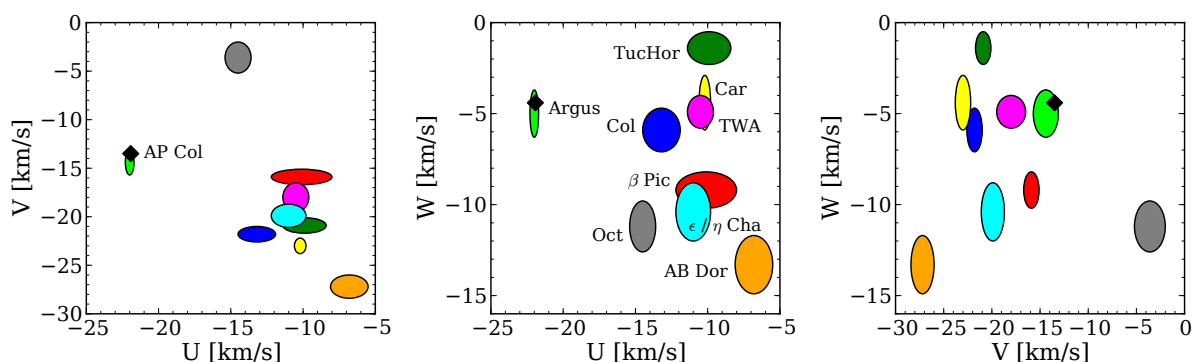


Figure 5.25: AP Col (diamond) plotted in  $UVW$  phase space relative to the associations in Torres et al. (2008). Ellipses show the velocity dispersions of the various groups. Error bars (within the diamond) reflect the accuracy of our measurements. The space motion of AP Col is consistent only with the Argus association. Plot in Riedel et al. (2011) by Simon Murphy.

#### 5.4.3.1 Argus / IC 2391 membership

One additional point of great interest is that the kinematics of AP Col are an excellent match for the  $\sim 40$  Myr old Argus association defined in Torres et al. (2003) and updated in Torres et al. (2008). Combining the radial velocity with the CTIOPI parallax and proper motion data allows us to calculate the  $UVWXYZ$  phase-space positions for AP Col. These are  $(X, Y, Z) = (-3.72, -6.70, -3.41) \pm (0.04, 0.08, 0.04)$  pc and  $(U, V, W) = (-21.98, -13.58, -4.45) \pm (0.17, 0.24, 0.13)$  km s $^{-1}$ . This places AP Col only 1.0 km s $^{-1}$  from the mean velocity of the Argus Association,  $(U, V, W) = (-22.0, -14.4, -5.0) \pm (0.3, 1.3, 1.3)$  km s $^{-1}$  (Torres et al. 2008). As seen in Figure 5.25, Argus is the only possible match for AP Col among the nine nearest known associations, given its observed kinematics. In Figure 5.26 we plot the phase space location of AP Col relative to other proposed Argus members from Torres et al. (2008), Desidera et al. (2011), and Zuckerman et al. (2011). In addition

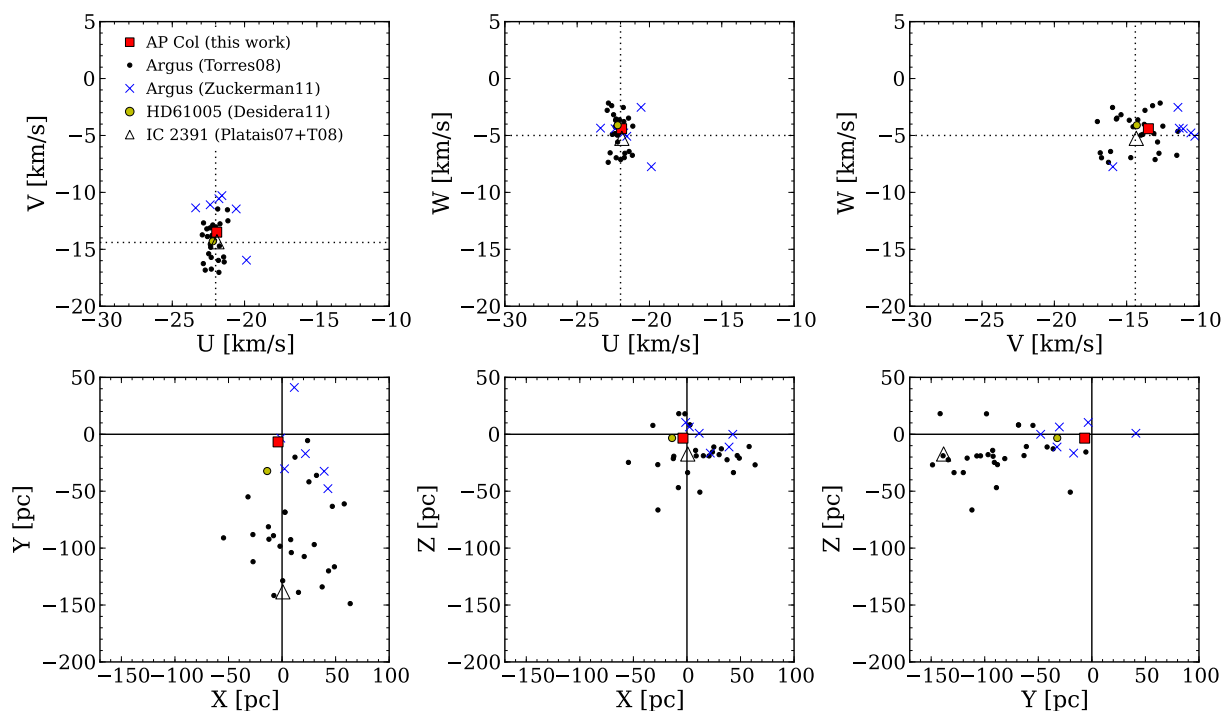


Figure 5.26: AP Col (filled square) plotted in  $UVWXYZ$  phase space relative to the Argus Association as defined by Torres et al. (2008) (small points). Recent new members found by Desidera et al. (2011) (HD 61005, large circle) and Zuckerman et al. (2011) (Xs) are also plotted. As shown by Torres et al. (2008), the young open cluster IC 2391 (open triangle, data from Platais et al. (2007); Torres et al. (2008)) appears to be kinematically and spatially associated with Argus as well as having a similar age (see text). Plot in Riedel et al. (2011) by Simon Murphy.

to congruent kinematics, AP Col occupies a region of  $XYZ$  space on the outskirts of known members. Argus is likely much larger than the volume traced by known members, and new members continue to be identified. At an age of  $\sim 40$  Myr, Argus also has an isochronal age in the middle of the range expected from our gamut of age indicators.

Although suggestive, kinematics alone are insufficient to argue membership. Unfortunately, there are no previously known M-type Argus members to which we can directly compare AP Col. However, the apparent link between Argus and the young open cluster

IC 2391 can provide some insight and reduce the range of possible ages for AP Col.

IC 2391 has similar kinematics (including its “special U velocity”,  $-22 \text{ km s}^{-1}$  Torres et al. 2008, see Figure 5.26), spatial location<sup>17</sup> (Figure 5.26), and a similar age to Argus (Torres et al. 2008; Makarov & Urban 2000). As such, the field members of Argus may be ‘evaporated’ members of IC 2391 stripped free by internal and external interactions with other stars, or distant products of the same filament of gas that eventually became IC 2391. Argus is projected to extend over a huge volume of space, reaching from the center of IC 2391 (distance  $\sim 139 \pm 7 \text{ pc}$ , Torres et al. 2008) to as close as 11 pc (Zuckerman et al. 2011), and, with the discovery and characterization of AP Col, perhaps even 8.4 pc.

Along with their kinematics and spatial positions, the lithium distributions and color-magnitude diagrams of Argus and IC 2391 show good agreement for the solar-type members of the Torres et al. (2008) sample. As already discussed, Figure 5.21 shows the Barrado y Navascués et al. (2004) IC 2391 members that define the LDB (approximated by the dotted line) at around M5 and an age of  $50 \pm 5 \text{ Myr}$ , subject to the inaccuracies of lithium dating (Yee & Jensen 2010; Song et al. 2002). The position of AP Col in this diagram is consistent with an age similar to that of IC 2391. In fact, the star appears to lie on the LDB, a position supported by the exact agreement of its  $(R - I)$  color and that derived for the LDB by Barrado y Navascués et al. (2004).

In a wider context, da Silva et al. (2009) found that Argus members have a level of

---

<sup>17</sup>IC 2391’s location is shown as derived from thirteen Torres et al. (2008) members (drawn from the list of Platais et al. 2007) with Hipparcos astrometry. The Torres et al. (2008) distance, 139.5 pc, gives the best kinematic agreement between Argus and IC 2391 but differs from the Platais et al. 2007 best-fit main sequence distance of 156 pc. The mean Hipparcos distance is between those two values, at 146 pc.

lithium depletion between that of the  $\sim 30$  Myr old Tuc-Hor and the  $\sim 70$  Myr old AB Dor associations. This is consistent with the lithium age for IC 2391 above, and our putative age range for AP Col. Thus, given its appropriate kinematics and age, we claim that AP Col, at 8.4 pc, is a likely member of the  $\sim 40$  Myr old Argus association.

One curious piece of evidence contradicts this scenario: if AP Col is an ‘evaporated’ member of Argus/IC 2391, it should converge on the mean location of IC 2391, roughly 40 Myr ago. Using both linear (Murphy et al. 2010) and epicycle (Makarov et al. 2004) approximations to Galactic dynamics to retrace its motion, we find that AP Col does not converge with IC 2391 until (at the very earliest) 80 Myr ago (Figure 5.27). This result suggests that either the approximations are insufficient for a 40 Myr traceback, AP Col (and potentially Argus) have been kinematically perturbed since formation (as the evaporated outer envelope of IC 2391), or AP Col (and potentially Argus) formed elsewhere at roughly the same time as IC 2391.

While the evaporation and perturbation scenario can explain our failure to trace AP Col back to IC 2391, it does not explain why, post-interaction(s), the velocity of AP Col is still so close to that of Argus/IC 2391. We instead speculate, like Desidera et al. (2011), that Argus is actually the product of gas *surrounding* what became IC 2391, thrust into star formation within a few million years of the cluster, perhaps triggered by supernovae in IC 2391. A similar relationship was suggested by Luhman et al. (2005) and Ortega et al. (2007) in connecting AB Dor with the Pleiades.

In any case, the physicality of Argus is beyond the purpose of this study of AP Col; our

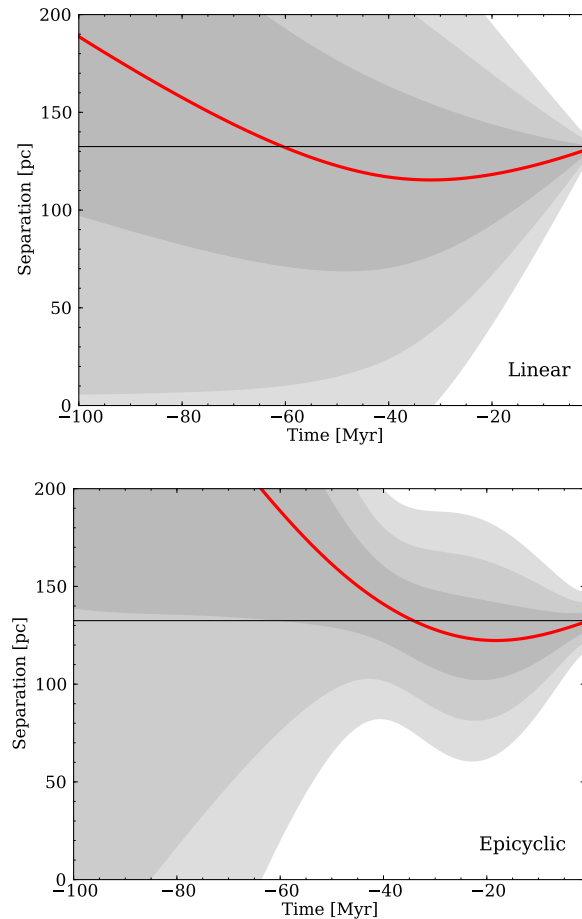


Figure 5.27: The separation between AP Col and the mean IC 2391 location (solid line) as a function of time, with their current separation ( $\sim 130$  pc) on the right hand side. Each plot shows the result of 1000 Monte Carlo simulations of the linear/ballistic (top) and epicyclic (bottom) approximations to Galactic dynamics, using the observed uncertainties in the observed AP Col and IC 2391 space motions. The shaded regions show 1 (darkest), 2 and  $3\sigma$  (lightest) confidence intervals around the mean trend. If AP Col were a member of IC 2391, the separation of AP Col and IC 2391 should go to zero when they were both born ( $\sim 40$ – $50$  Myr ago); they do not reasonably converge at the  $\sim 2\sigma$  level until  $\sim 80$  Myr ago. This implies either interactions have modified the observed velocities, or that AP Col did not form near the core of IC 2391. Plots in [Riedel et al. \(2011\)](#) by Simon Murphy.

main conclusion is that, as defined in [Torres et al. \(2008\)](#), AP Col is a member of the Argus association, and is now its closest member. With a presumed age of  $\sim 40$  Myr as part of the Argus association, AP Col is thus the second youngest member of the immediate solar neighborhood, forming during the Eocene epoch on Earth, and at 8.4 pc, the closest star with an age less than 100 Myr.

## 5.5 Unpublished Young Stars

My goal with this thesis is to determine the youth and potential association memberships of the variety of nearby stars I have found. I have already published one result from this attempt, the analysis of AP Col ([§5.4](#)). Thanks to TINYMO and various other objects on the CTIOPI program, I have the 84 other star systems to analyze with these techniques.

Table [5.14](#) lists the positions (Columns 2 and 3), weighted mean parallaxes (Columns 4 and 5), proper motions (Columns 6 and 7), radial velocities (Columns 8 and 9), deblended  $V$  and  $K$  magnitudes (Columns 10 and 11), and X-ray detections (Columns 12 and 13) used to reach the conclusions in Table [5.15](#) and the various other plots in this section.

Table 5.14: Individual Parameters

| Name<br>(1)                 | RA<br>(2)   | J2000<br>DEC<br>(3) | Weighted<br>$\pi$ (mas)<br>(4) | $\mu_{RA} \cos \delta^{DEC}$<br>(mas yr <sup>-1</sup> )<br>(6) | $\mu_{DEC}$<br>(mas yr <sup>-1</sup> )<br>(7) | RV<br>(km s <sup>-1</sup> )<br>(8) | RV<br>ref<br>(9) | Johnson <sup>b</sup><br>V<br>(10) | 2MASS <sup>b</sup><br>K<br>(11) | ROSAT<br>cnts s <sup>-1</sup><br>(12) | hr1<br>(13) |
|-----------------------------|-------------|---------------------|--------------------------------|--|---|------------------------------------|------------------|-----------------------------------|---------------------------------|---------------------------------------|-------------|
| Low Proper Motion           |             |                     |                                |  |   |                                    |                  |                                   |                                 |                                       |             |
| NJ1700372                   | 00 08 51.79 | +20 49 07.9         | 11.66±1.44                     | 126.58±2.22  | -76.26±0.22                                   |                                    |                  | 15.87 ±0.04                       | 10.716 ±0.022                   |                                       |             |
| SCR0128-1458                | 01 28 39.53 | -14 58 04.2         | 68.97±4.66                     | -54.67±4.23  | -63.72±3.67                                   | 11.0 ± 3.9                         | RAVE             | 13.60 ±0.03                       | 8.198 ±0.029                    | 4.12e-02±1.22e-02                     | -0.52       |
| SCR0143-0602                | 01 43 45.13 | -06 02 40.1         | 52.12±2.29                     | 48.30±2.41   | -17.20±2.33                                   |                                    |                  | 13.01 ±0.02                       | 7.912 ±0.018                    | 2.78e-01±2.80e-02                     | -0.38       |
| L173-019                    | 02 00 38.31 | -55 58 04.8         | 121.93±2.71                    | 104.88±1.23  | 67.62±1.22                                    |                                    |                  | 11.90 ±0.02                       | 6.773 ±0.020                    |                                       |             |
| 2MA0314-0450                | 03 14 40.11 | -04 50 31.8         | 31.40±2.19                     | -89.63±3.97  | -103.90±3.79                                  |                                    |                  | 19.87 ±0.05                       | 11.602 ±0.025                   |                                       |             |
| 2MA0429-3123                | 04 29 18.43 | -31 23 56.7         | 64.82±1.40                     | 81.01±0.42   | 101.47±0.42                                   |                                    |                  | 17.39 ±0.05                       | 9.770 ±0.022                    | 3.58e-02±1.30e-02                     | 0.40        |
| 2MA0451-3402                | 04 51 00.94 | -34 02 14.9         | 47.21±1.50                     | 93.15±0.80   | 134.27±0.81                                   |                                    |                  | 22.11 ±0.05                       | 12.294 ±0.026                   |                                       |             |
| HD271076                    | 05 10 09.70 | -72 36 27.9         | 46.38±2.57                     | 131.84±2.81  | 16.39±2.71                                    |                                    |                  | 11.36 ±0.02                       | 7.054 ±0.016                    | 1.37e-02±6.01e-03                     | 0.15        |
| SCR0533-4257A               | 05 33 28.03 | -42 57 20.5         | 99.35±1.70                     | -17.41±0.98  | 30.98±0.97                                    |                                    |                  | 13.04D±0.04                       | 7.708D±0.026                    | 2.52e-01±2.94e-02J                    | -0.03       |
| SCR0533-4257B               | 05 33 28.03 | -42 57 20.5         | 99.35±1.70                     | -17.41±0.98  | 30.98±0.97                                    |                                    |                  | 13.04D±0.04                       | 8.058D±0.026                    |                                       |             |
| LP780-032                   | 06 39 37.41 | -21 01 33.3         | 64.39±0.80                     | 161.42±0.77  | 74.64±0.77                                    |                                    |                  | 12.77 ±0.02                       | 7.650 ±0.016                    |                                       |             |
| 2MA0936-2610                | 09 36 57.83 | -26 10 11.2         | 50.12±2.48                     | 29.95±1.51   | -34.20±1.54                                   |                                    |                  | 13.10 ±0.01                       | 7.955 ±0.018                    | 8.75e-02±1.64e-02                     | 0.09        |
| SCR1214-2345                | 12 14 08.67 | -23 45 17.1         | 93.04±2.24                     | 53.18±2.04   | 83.06±2.09                                    |                                    |                  | 13.97 ±0.01                       | 8.234 ±0.025                    | 1.32e-01±2.58e-02                     | -0.24       |
| SDS1416+1348                | 14 16 24.09 | +13 48 26.3         | 110.02±2.10                    | 97.46±2.59   | 136.49±2.89                                   |                                    |                  | 12.114 ±0.023                     | 12.114 ±0.023                   |                                       |             |
| 2MA1507-2000                | 15 07 27.81 | -20 00 43.3         | 42.73±0.63                     | 109.77±0.36  | -68.36±0.36                                   |                                    |                  | 18.82 ±0.09                       | 10.661 ±0.021                   |                                       |             |
| GJ2122A                     | 16 45 16.97 | -38 48 33.3         | 74.82±1.70                     | -28.10±0.34  | -52.32±0.34                                   | -20.3 ±                            | Tor06            | 10.42G±0.03                       | 6.473G±0.026                    | 9.76e-02±2.04e-02J                    | -0.56       |
| GJ2122B                     | 16 45 16.97 | -38 48 33.3         | 74.82±1.70                     | -28.10±0.34  | -52.32±0.34                                   | -20.3 ±                            | Tor06            | 10.42G±0.03                       | 6.473G±0.026                    |                                       |             |
| 2MA1705-0516                | 17 05 48.35 | -05 16 46.3         | 45.83±2.10                     | 117.59±1.97  | -111.27±1.97                                  |                                    |                  | 21.88 ±0.06                       | 12.190 ±0.021                   |                                       |             |
| DMEN1756-4805               | 17 56 56.20 | -48 05 09.7         | 50.25±2.05                     | 83.54±1.73   | 37.18±1.72                                    |                                    |                  | 14.33 ±0.05                       | 8.756 ±0.023                    | 1.03e-01±2.10e-02                     | -0.16       |
| SCR1942-2045                | 19 42 12.82 | -20 45 48.0         | 62.40±1.62                     | -6.71±2.71   | -147.22±2.71                                  | 18.2 ±                             | Tor06            | 11.66 ±0.03                       | 7.172 ±0.020                    | 4.30e-01±4.13e-02                     | -0.09       |
| SCR2036-3607                | 20 36 08.30 | -36 07 11.5         | 61.68±1.52                     | 6.07±1.34  | 51.39±1.34                                    |                                    |                  | 13.53 ±0.02                       | 7.704 ±0.023                    |                                       |             |
| SCR2049-4012                | 20 49 09.94 | -40 12 06.3         | 107.46±1.58                    | -59.02±0.99  | 26.20±0.98                                    |                                    |                  | 21.67 ±0.05                       | 11.724 ±0.025                   |                                       |             |
| 2MA2057-0252                | 20 57 54.09 | -02 52 30.4         | 65.14±1.85                     | -0.76±2.41   | -93.12±2.48                                   |                                    |                  |                                   |                                 |                                       |             |
| Low Proper Motion and Young |             |                     |                                |  |   |                                    |                  |                                   |                                 |                                       |             |
| SCR0017-6645                | 00 17 23.53 | -66 45 12.5         | 24.86±2.01                     | 92.41±2.23   | -22.29±2.43                                   |                                    |                  | 12.45 ±0.02                       | 7.703 ±0.021                    | 2.13e-01±3.20e-02                     | -0.08       |
| GJ2006A                     | 00 27 50.24 | -32 33 06.2         | 30.97±1.76                     | 108.36±0.43  | -38.57±0.43                                   |                                    |                  | 12.79 ±0.01                       | 8.112 ±0.033                    | 3.50e-01±3.43e-02J                    | -0.19       |
| GJ2006B                     | 00 27 50.24 | -32 33 06.2         | 30.97±1.76                     | 108.36±0.43  | -38.57±0.43                                   |                                    |                  | 13.25 ±0.03                       | 8.116 ±0.027                    |                                       |             |
| SCR0103-5515                | 01 03 35.64 | -55 15 56.2         | 21.09±1.70                     | 81.78±1.09   | -40.02±1.09                                   |                                    |                  | 15.48 ±0.03                       | 9.237 ±0.022                    |                                       |             |
| 2MA0123-6921                | 01 23 11.27 | -69 21 38.0         | 23.73±2.68                     | 82.78±1.37   | -25.19±1.57                                   |                                    |                  | 19.12 ±0.19                       | 11.323 ±0.026                   |                                       |             |
| BAR161-021                  | 01 35 13.94 | -07 12 51.8         | 27.99±2.32                     | 92.61±2.45   | -34.98±2.50                                   |                                    |                  | 13.42 ±0.01                       | 8.078 ±0.033                    | 1.78e-01±2.25e-02                     | -0.28       |
| SIP0152-6329                | 01 52 55.35 | -63 29 30.2         | 29.84±1.71                     | 125.64±0.80  | 11.01±0.79                                    |                                    |                  | 15.41 ±0.04                       | 9.261 ±0.021                    | 2.11e-02±8.71e-03                     | -0.73       |
| SCR0222-6022                | 02 22 44.17 | -60 22 47.7         | 35.36±2.41                     | 130.26±3.04  | -19.52±3.17                                   |                                    |                  | 13.36 ±0.05                       | 8.102 ±0.031                    | 3.57e-01±4.23e-02                     | -0.01       |
| 2MA0236-5103                | 02 36 51.71 | -52 03 03.7         | 27.80±1.85                     | 85.29±2.25   | -9.93±2.21                                    | 16.0 ± 0.1                         | Tor06            | 12.06 ±0.02                       | 7.501 ±0.027                    | 3.32e-01±2.84e-02                     | -0.05       |
| 2MA0254-5108A               | 02 54 33.31 | -51 08 31.4         | 23.74±1.97                     | 90.48±2.42   | -17.83±2.76                                   |                                    |                  | 12.08 ±0.03                       | 7.785 ±0.033                    | 1.22e-01±2.21e-02J                    | -0.01       |
| 2MA0254-5108B               | 02 54 34.77 | -51 08 28.8         | 23.74±1.92                     | 101.95±2.93  | -8.04±3.38                                    |                                    |                  | 17.55 ±0.09                       | 11.188 ±0.019                   |                                       |             |
| SCR0336-2619                | 03 36 31.46 | -26 19 57.9         | 23.92±1.92                     | 70.53±1.08   | -20.94±1.10                                   |                                    |                  | 16.33 ±0.03                       | 9.763 ±0.021                    |                                       |             |
| RX0413-0139                 | 04 13 26.64 | -01 39 21.2         | 36.27±2.49                     | 130.54±3.06  | -4.20±3.05                                    |                                    |                  | 13.96 ±0.02                       | 8.504 ±0.021                    | 9.77e-02±2.01e-02                     | 0.01        |
| LP476-207A                  | 05 01 58.81 | +09 58 58.8         | 40.18±2.07                     | 26.88±0.99   | -102.91±1.02                                  | 14.7 ± 3.7                         | Giz02            | 11.79D±0.07                       | 7.001D±0.021                    | 6.61e-01±5.98e-02J                    | -0.34       |
| LP476-207B                  | 05 01 58.81 | +09 58 58.8         | 40.18±2.07                     | 26.88±0.99   | -102.91±1.02                                  | 14.7 ± 3.7                         | Giz02            | 13.52G±0.07                       | 7.663G±0.021                    |                                       |             |
| LP476-207C                  | 05 01 58.81 | +09 58 58.8         | 40.18±2.07                     | 26.88±0.99   | -102.91±1.02                                  | 14.7 ± 3.7                         | Giz02            | 14.79G±0.07                       | 8.506G±0.021                    |                                       |             |
| BD-21-01074B                | 05 06 49.47 | -21 35 03.9         | 51.98±1.30                     | 24.25±0.28   | -44.50±0.27                                   | 23.7 ± 1.7                         | Giz02            | 11.39D±0.05                       | 6.609D±0.021                    |                                       |             |
| BD-21-01074C                | 05 06 49.47 | -21 35 03.9         | 51.98±1.30                     | 24.25±0.28   | -44.50±0.27                                   | 23.7 ± 1.7                         | Giz02            | 12.58D±0.05                       | 7.204D±0.021                    |                                       |             |
| BD-21-01074A                | 05 06 49.92 | -21 35 09.2         | 51.98±1.30                     | 47.89±0.36   | -18.45±0.37                                   | 21.2 ± 0.9                         | Giz02            | 10.41 ±0.02                       | 6.117 ±0.017                    | 1.15e+00±9.91e-02J                    | -0.15       |
| SCR0529-3239                | 05 29 44.69 | -32 39 14.2         | 41.13±1.72                     | 25.31±1.25   | 1.20±1.19                                     |                                    |                  | 13.79 ±0.02                       | 8.316 ±0.027                    | 1.00e-01±1.63e-02                     | -0.21       |
| SCR0613-2742A               | 06 13 13.31 | -27 42 05.5         | 34.30±0.97                     | -9.66±0.49   | -4.52±0.49                                    |                                    |                  | 12.79D±0.03                       | 7.758D±0.024                    | 4.27e-01±2.63e-02J                    | -0.21       |
| SCR0613-2742B               | 06 13 13.31 | -27 42 05.5         | 34.30±0.97                     | -9.66±0.49   | -4.52±0.49                                    |                                    |                  | 13.39D±0.03                       | 8.058D±0.024                    |                                       |             |
| SCR0757-7114                | 07 57 32.55 | -71 14 53.8         | 45.25±1.96                     | 104.05±1.73  | -0.89±1.75                                    |                                    |                  | 12.46 ±0.02                       | 7.423 ±0.021                    |                                       |             |
| SCR1012-3124A               | 10 12 09.09 | -31 24 45.2         | 18.54±1.74                     | -68.98±1.35  | -14.72±1.36                                   |                                    |                  | 14.25D±0.02                       | 8.738D±0.031                    |                                       |             |
| SCR1012-3124B               | 10 12 09.09 | -31 24 45.2         | 18.54±1.74                     | -68.98±1.35  | -14.72±1.36                                   |                                    |                  | 14.28D±0.02                       | 8.752D±0.031                    |                                       |             |
| SIP1110-3731A <sup>c</sup>  | 11 10 27.88 | -37 31 52.7         | 25.24±2.45                     | -81.91±2.31  | -2.73±2.31                                    | 15.6 ± 0.2                         | Tor06            | 13.50G±0.03                       | 8.218G±0.020                    | 2.78e-01±3.15e-02J                    | -0.01       |
| SIP1110-3731B <sup>c</sup>  | 11 10 27.88 | -37 31 52.7         | 25.24±2.45                     | -81.91±2.31  | -2.73±2.31                                    | 15.6 ± 0.2                         | Tor06            | 13.50G±0.03                       | 8.218G±0.020                    |                                       |             |
| SIP1110-3731C <sup>c</sup>  | 11 10 27.88 | -37 31 52.9         | 25.24±2.45                     | -110.07±2.80   | -37.65±2.80                                   | 15.5 ± 1.8                         | Tor06            | 12.88D±0.03                       | 7.596D±0.020                    |                                       |             |
| RX1132-2651B                | 11 32 41.16 | -26 52 09.0         | 21.28±1.01                     | 72.40±0.22   | -20.86±0.22                                   | 8.93 ± 0.27                        | Shk11            | 15.20 ±0.08                       | 9.012 ±0.025                    | 3.20e-01±3.53e-02J                    | 0.03        |
| RX1132-2651A                | 11 32 41.25 | -26 51 55.9         | 21.28±1.01                     | -72.63±4.22  | -24.26±4.22                                   | 8.34 ± 0.48                        | Shk11            | 12.23 ±0.08                       | 7.813 ±0.017                    | 1.30e-01±2.13e-02                     | -0.13       |
| STEPH0164                   | 12 06 22.16 | -13 14 56.1         | 22.87±5.70                     | 94.93±4.27   | -78.61±4.83                                   | -8.1 ± 2.6                         | RAVE             | 12.73 ±0.02                       | 7.813 ±0.029                    |                                       |             |
| DEN1306-7723                | 13 06 56.56 | -77 23 09.5         | 9.27±1.41                      | -16.75±1.93  | -1.47±1.92                                    |                                    |                  | 17.58 ±0.02                       | 9.798 ±0.025                    |                                       |             |
| SCR1425-4113                | 14 25 29.13 | -41 13 32.4         | 15.20±0.98                     | -42.19±1.07  | -43.59±1.07                                   |                                    |                  | 12.64 ±0.01                       | 7.614 ±0.021                    |                                       |             |
| SCR1609-2222                | 16 09 20.63 | -22 22 05.7         | 7.47±3.12                      | -2.75±1.99   | -35.32±4.79                                   |                                    |                  | 15.99 ±0.02                       | 9.499 ±0.021                    |                                       |             |
| SIP1809-7613                | 18 09 06.95 | -76 13 23.9         | 37.88±3.97                     | 8.93±3.63  | -141.56±3.49                                  |                                    |                  | 15.11 ±0.03                       | 8.989 ±0.021                    |                                       |             |
| SCR1816-5844                | 18 16 12.37 | -58 44 05.6         | 33.34±2.04                     | 14.73±2.98   | -138.29±3.01                                  |                                    |                  | 12.90 ±0.02                       | 7.699 ±0.016                    |                                       |             |
| SCR2010-2801A               | 20 10 00.04 | -28 01 41.2         | 20.85±1.33                     | 40.28±0.79   | -63.20±0.86                                   |                                    |                  | 13.30C±0.03                       | 8.222C±0.027                    | 1.92e-01±2.97e-02J                    | -0.15       |

Continued on next page

Table 5.14 – Continued from previous page

| Name<br>(1)   | RA<br>(2)   | J2000<br>DEC<br>(3) | Weighted<br>$\pi$ (mas)<br>(4) | $\pi^a$<br>ref(s)<br>(5) | $\mu_{RA} \cos \delta_{DEC}$<br>(mas yr $^{-1}$ )<br>(6) | $\mu_{DEC}$<br>(mas yr $^{-1}$ )<br>(7) | RV<br>(km s $^{-1}$ )<br>(8) | RV<br>ref<br>(9) | Johnson $^b$<br>V<br>(10) | 2MASS $^b$<br>K<br>(11) | ROSAT<br>counts s $^{-1}$<br>(12) | hr1<br>(13) |
|---|-------------|---------------------|--------------------------------|--------------------------|--|---|------------------------------|------------------|---------------------------|-------------------------|-----------------------------------|-------------|
| SCR2010-2801B   | 20 10 00.04 | -28 01 41.2         | 20.85 $\pm$ 1.33               | R 1                      | 40.28 $\pm$ 0.79   | -63.20 $\pm$ 0.86                       |                              |                  | 14.50G $\pm$ 0.03         | 8.827G $\pm$ 0.027      |                                   |             |
| SCR2033-2556  | 20 33 37.59 | -25 56 52.2         | 24.52 $\pm$ 1.86               | R 1                      | 54.85 $\pm$ 1.26   | -68.69 $\pm$ 1.26                       |                              |                  | 14.87 $\pm$ 0.02          | 8.877 $\pm$ 0.019       | 4.65e-02 $\pm$ 1.73e-02           | -0.02       |
| BD-13-06424   | 23 32 30.87 | -12 15 51.4         | 38.52 $\pm$ 5.88               | R 1                      | 160.88 $\pm$ 13.17                                       | -51.84 $\pm$ 13.59                      | 1.8 $\pm$ 0.7                | Tor06            | 10.50 $\pm$ 0.03          | 6.569 $\pm$ 0.018       | 6.20e-01 $\pm$ 4.82e-02           | -0.10       |
| G131-026A   | 00 08 53.92 | +20 50 25.4         | 54.13 $\pm$ 1.35               | R 1                      | -62.65 $\pm$ 0.21  | -243.25 $\pm$ 0.21                      |                              |                  | 13.94D $\pm$ 0.06         | 8.580D $\pm$ 0.024      | 8.99e-02 $\pm$ 2.11e-02J          | -0.28       |
| G131-026B   | 00 08 53.92 | +20 50 25.4         | 54.13 $\pm$ 1.35               | R 1                      | -62.65 $\pm$ 0.21  | -243.25 $\pm$ 0.21                      |                              |                  | 14.75D $\pm$ 0.06         | 8.982D $\pm$ 0.024      |                                   |             |
| LP467-016A  | 01 11 25.41 | +15 26 21.6         | 45.79 $\pm$ 1.78               | R 1                      | 187.65 $\pm$ 0.41  | -120.34 $\pm$ 0.41                      | 4.0 $\pm$ 0.1                | Mon01            | 14.50G $\pm$ 0.05         | 8.662D $\pm$ 0.033      | 9.36e-02 $\pm$ 1.82e-02J          | -0.08       |
| LP467-016B  | 01 11 25.41 | +15 26 21.6         | 45.79 $\pm$ 1.78               | R 1                      | 187.65 $\pm$ 0.41  | -120.34 $\pm$ 0.41                      | 2.6 $\pm$ 1.1                | Giz02            | 16.11D $\pm$ 0.05         | 9.359D $\pm$ 0.033      |                                   |             |
| GJ2022C $^c$  | 01 24 27.65 | +33 55 09.7         | 38.80 $\pm$ 2.13               | R 1                      | 160.68 $\pm$ 0.86  | -120.08 $\pm$ 0.90                      |                              |                  | 14.35D $\pm$ 0.04         | 9.009D $\pm$ 0.031      |                                   |             |
| GJ2022A $^c$  | 01 24 27.76 | +33 55 08.3         | 38.80 $\pm$ 2.13               | R 1                      | 169.22 $\pm$ 0.92  | -125.27 $\pm$ 0.95                      |                              |                  | 14.28D $\pm$ 0.04         | 8.977D $\pm$ 0.031      | 2.08e-01 $\pm$ 2.84e-02J          | -0.14       |
| GJ2022B   | 01 24 30.62 | +33 55 01.6         | 38.80 $\pm$ 2.13               | R 1                      | 163.43 $\pm$ 0.46  | -125.35 $\pm$ 0.46                      |                              |                  | 15.50 $\pm$ 0.06          | 9.682 $\pm$ 0.021       |                                   |             |
| LP993-115   | 02 45 10.71 | +43 44 32.4         | 88.64 $\pm$ 1.56               | RR 2                     | 31.04 $\pm$ 0.37   | -385.80 $\pm$ 0.44                      |                              |                  | 12.38 $\pm$ 0.08          | 7.270 $\pm$ 0.024       |                                   |             |
| LP993-116A  | 02 45 14.32 | +43 44 10.6         | 88.64 $\pm$ 1.56               | RR 2                     | 36.14 $\pm$ 0.40   | -361.41 $\pm$ 0.48                      |                              |                  | 12.93G $\pm$ 0.06         | 7.637G $\pm$ 0.024      | 2.33e-01 $\pm$ 3.57e-02J          | -0.41       |
| LP993-116B  | 02 45 14.32 | +43 44 10.6         | 88.64 $\pm$ 1.56               | RR 2                     | 36.14 $\pm$ 0.40   | -361.41 $\pm$ 0.48                      |                              |                  | 14.43G $\pm$ 0.06         | 8.387G $\pm$ 0.024      |                                   |             |
| G007-029A   | 04 17 18.52 | +08 49 22.1         | 73.27 $\pm$ 1.27               | R 1                      | 127.45 $\pm$ 0.46  | -374.10 $\pm$ 0.46                      |                              |                  | 13.84 $\pm$ 0.02          | 8.182 $\pm$ 0.020       | 1.21e-01 $\pm$ 2.34e-02           | -0.34       |
| G039-029A   | 04 38 12.59 | +28 13 00.0         | 78.61 $\pm$ 2.04               | R 1                      | 392.84 $\pm$ 1.28  | -90.98 $\pm$ 1.22                       | 27.6 $\pm$ 1.6               | Giz02            | 12.97D $\pm$ 0.05         | 7.889D $\pm$ 0.021      | 3.10e-01 $\pm$ 2.82e-02J          | -0.19       |
| G039-029B   | 04 38 12.59 | +28 13 00.0         | 78.61 $\pm$ 2.04               | R 1                      | 392.84 $\pm$ 1.28  | -90.98 $\pm$ 1.22                       | 27.6 $\pm$ 1.6               | Giz02            | 13.81D $\pm$ 0.05         | 8.309D $\pm$ 0.021      |                                   |             |
| LP655-048   | 04 40 23.28 | +05 30 08.1         | 102.74 $\pm$ 0.74              | R 1                      | 336.12 $\pm$ 0.16  | 127.49 $\pm$ 0.17                       |                              |                  | 17.81 $\pm$ 0.04          | 9.545 $\pm$ 0.019       | 5.46e-02 $\pm$ 1.24e-02           | -0.28       |
| LP776-025   | 04 52 24.42 | +16 49 22.2         | 69.40 $\pm$ 1.70               | R 1                      | 117.65 $\pm$ 1.57  | -214.90 $\pm$ 1.57                      |                              |                  | 11.63 $\pm$ 0.02          | 6.891 $\pm$ 0.027       | 4.31e-01 $\pm$ 3.46e-02           | -0.22       |
| L449-001A   | 05 17 22.91 | +35 21 54.7         | 85.59 $\pm$ 1.35               | R 1                      | -219.47 $\pm$ 0.71                                       | -163.62 $\pm$ 0.71                      |                              |                  | 12.03D $\pm$ 0.01         | 7.070D $\pm$ 0.020      | 6.08e-01 $\pm$ 6.28e-02J          | -0.18       |
| L449-001B   | 05 17 22.91 | +35 21 54.7         | 85.59 $\pm$ 1.35               | R 1                      | -219.47 $\pm$ 0.71                                       | -163.62 $\pm$ 0.71                      |                              |                  | 13.13D $\pm$ 0.01         | 7.620D $\pm$ 0.020      |                                   |             |
| L034-026  | 07 49 12.71 | +76 42 06.6         | 93.65 $\pm$ 2.04               | R 1                      | -100.72 $\pm$ 0.70                                       | -200.75 $\pm$ 0.72                      | 0.9 $\pm$                    | Tor06            | 11.31 $\pm$ 0.03          | 6.579 $\pm$ 0.018       | 5.94e-01 $\pm$ 7.01e-02           | -0.22       |
| G161-071  | 09 44 54.18 | +12 20 54.4         | 71.73 $\pm$ 1.36               | R 1                      | -321.97 $\pm$ 0.42                                       | 40.93 $\pm$ 0.42                        |                              |                  | 13.76 $\pm$ 0.02          | 7.601 $\pm$ 0.018       | 2.82e-01 $\pm$ 2.70e-02           | -0.15       |
| SCR1157-0149  | 11 57 45.55 | +01 49 02.6         | 50.09 $\pm$ 1.01               | R 1                      | 403.22 $\pm$ 0.33  | -220.04 $\pm$ 0.33                      |                              |                  | 15.99 $\pm$ 0.04          | 10.024 $\pm$ 0.019      | 2.21e-02 $\pm$ 1.00e-02           | -0.09       |
| G165-008A   | 13 31 46.63 | +29 16 36.5         | 55.51 $\pm$ 2.38               | R 1                      | -218.43 $\pm$ 0.75                                       | -141.20 $\pm$ 0.76                      | -7.5 $\pm$ 6.5               | Giz02            | 12.62D $\pm$ 0.09         | 7.396D $\pm$ 0.018      | 4.10e-01 $\pm$ 3.23e-02J          | -0.32       |
| G165-008B   | 13 31 46.63 | +29 16 36.5         | 55.51 $\pm$ 2.38               | R 1                      | -218.43 $\pm$ 0.75                                       | -141.20 $\pm$ 0.76                      | -7.5 $\pm$ 6.5               | Giz02            | 12.94D $\pm$ 0.09         | 7.566D $\pm$ 0.018      |                                   |             |
| LHS2880   | 14 13 04.87 | +12 01 26.8         | 32.33 $\pm$ 1.36               | R 1                      | -596.71 $\pm$ 0.65                                       | -387.12 $\pm$ 0.65                      | -164.6 $\pm$ 0.6             | RAVE             | 13.89 $\pm$ 0.03          | 8.163 $\pm$ 0.029       | 1.99e-01 $\pm$ 2.94e-02           | -0.17       |
| G11224  | 18 07 32.85 | +15 57 47.0         | 127.41 $\pm$ 0.99              | Y R 2                    | -614.68 $\pm$ 0.27                                       | -339.80 $\pm$ 0.27                      | -34.8 $\pm$ 1.7              | Giz02            | 13.48 $\pm$ 0.04          | 8.227 $\pm$ 0.027       | 2.11e-01 $\pm$ 2.91e-02           | -0.45       |
| G141-029  | 18 42 44.99 | +13 54 17.1         | 90.00 $\pm$ 2.36               | Y R 2                    | -33.17 $\pm$ 0.92  | 357.55 $\pm$ 0.92                       | -33.2 $\pm$                  | Giz02            | 12.86 $\pm$ 0.04          | 7.551 $\pm$ 0.021       | 1.32e-01 $\pm$ 1.78e-02           | -0.15       |
| LP876-065   | 20 04 30.79 | +23 42 02.4         | 55.00 $\pm$ 1.60               | R 1                      | 117.07 $\pm$ 0.56  | -337.26 $\pm$ 0.53                      |                              |                  | 13.02 $\pm$ 0.03          | 7.701 $\pm$ 0.029       | 2.57e-01 $\pm$ 3.03e-02           | -0.37       |
| ZMA2009-0113  | 20 09 18.24 | +01 13 38.2         | 93.60 $\pm$ 1.74               | R 1                      | 49.49 $\pm$ 0.86   | -367.18 $\pm$ 0.88                      |                              |                  | 14.47 $\pm$ 0.05          | 8.512 $\pm$ 0.023       | 5.25e-02 $\pm$ 1.26e-02           | -0.28       |
| LEHPM2-0783   | 20 19 49.82 | +58 16 43.0         | 61.93 $\pm$ 1.02               | R 1                      | -31.30 $\pm$ 0.59  | -329.95 $\pm$ 0.59                      |                              |                  | 17.17 $\pm$ 0.04          | 9.715 $\pm$ 0.023       | 1.21e-01 $\pm$ 3.45e-02           | 0.44        |
| L755-019  | 20 28 43.62 | +11 28 30.8         | 54.14 $\pm$ 1.92               | R 1                      | 159.65 $\pm$ 0.99  | -91.71 $\pm$ 0.93                       |                              |                  | 12.47 $\pm$ 0.02          | 7.496 $\pm$ 0.031       | 1.94e-01 $\pm$ 3.19e-02           | -0.44       |
| GJ0799A (N) $^c$  | 20 41 51.17 | +32 26 07.0         | 101.46 $\pm$ 0.78              | YYVVR 6                  | 294.69 $\pm$ 0.45  | -319.20 $\pm$ 0.44                      | -3.7 $\pm$ 3.0               | Mon01            | 11.09D $\pm$ 0.02         | 5.687D $\pm$ 0.042      | 3.91e+00 $\pm$ 1.20e-01J          | -0.19       |
| GJ0799B (S) $^c$  | 20 41 51.23 | +32 26 09.5         | 101.46 $\pm$ 0.78              | YYVVR 6                  | 228.55 $\pm$ 0.49  | -393.86 $\pm$ 0.48                      | -2.7 $\pm$ 3.0               | Mon01            | 11.13D $\pm$ 0.02         | 5.706D $\pm$ 0.042      |                                   |             |
| LP756-003   | 20 46 43.64 | +11 48 13.3         | 57.50 $\pm$ 4.37               | R 1                      | 341.32 $\pm$ 2.83  | -72.41 $\pm$ 4.23                       |                              |                  | 13.80 $\pm$ 0.08          | 8.435 $\pm$ 0.021       | 1.33e-01 $\pm$ 2.05e-02           | -0.11       |
| LHS3799   | 22 23 07.00 | +17 36 26.1         | 138.04 $\pm$ 1.88              | Y R 2                    | 294.78 $\pm$ 0.38  | -710.89 $\pm$ 0.41                      | -2.1 $\pm$ 1.1               | Giz02            | 13.30 $\pm$ 0.03          | 7.319 $\pm$ 0.018       | 1.58e-01 $\pm$ 2.62e-02           | -0.05       |
| LP932-083   | 22 49 08.41 | +28 51 20.1         | 25.63 $\pm$ 1.55               | V R 2                    | -172.56 $\pm$ 0.59                                       | -228.82 $\pm$ 0.59                      |                              |                  | 13.94 $\pm$ 0.06          | 8.474 $\pm$ 0.021       |                                   |             |
| GJ1284A   | 23 30 13.45 | +20 23 27.4         | 65.79 $\pm$ 1.86               | V R 2                    | 311.29 $\pm$ 0.62  | -187.77 $\pm$ 0.62                      | -5.7 $\pm$                   | Tor06            | 11.89G $\pm$ 0.04         | 7.082G $\pm$ 0.026      | 5.00e-01 $\pm$ 4.27e-02J          | -0.19       |
| GJ1284B   | 23 30 13.45 | +20 23 27.4         | 65.79 $\pm$ 1.86               | V R 2                    | 311.23 $\pm$ 0.62  | -187.77 $\pm$ 0.62                      | -5.7 $\pm$                   | Tor06            | 11.89G $\pm$ 0.04         | 7.082G $\pm$ 0.026      |                                   |             |
| LHS1302   | 01 51 04.09 | +06 07 05.1         | 96.28 $\pm$ 0.95               | R 1                      | 536.68 $\pm$ 0.19  | -261.47 $\pm$ 0.19                      |                              |                  | 14.49 $\pm$ 0.05          | 8.552 $\pm$ 0.022       | 5.01e-02 $\pm$ 1.78e-02           | -0.36       |
| LHS1358   | 02 12 54.63 | +00 00 16.8         | 65.27 $\pm$ 2.07               | R 1                      | 557.05 $\pm$ 0.86  | 37.50 $\pm$ 0.93                        |                              |                  | 13.58 $\pm$ 0.03          | 8.168 $\pm$ 0.021       | 8.48e-02 $\pm$ 1.90e-02           | -0.24       |
| G099-049  | 06 00 03.52 | +02 42 23.6         | 192.57 $\pm$ 1.07              | Y R 2                    | 311.13 $\pm$ 0.49  | -42.02 $\pm$ 0.49                       | 28.7 $\pm$ 0.7               | Giz02            | 11.31 $\pm$ 0.05          | 6.042 $\pm$ 0.023       | 4.04e-01 $\pm$ 4.47e-02           | -0.20       |
| AP Col  | 06 04 52.16 | +34 33 36.0         | 118.41 $\pm$ 0.94              | R 1                      | 26.58 $\pm$ 0.29   | 341.00 $\pm$ 0.29                       | 22.4 $\pm$ 0.3               | Rie11            | 12.96 $\pm$ 0.02          | 6.866 $\pm$ 0.021       | 4.28e-01 $\pm$ 5.01e-02           | 0.06        |
| G041-014A   | 08 58 56.33 | +08 28 26.0         | 147.78 $\pm$ 1.62              | R 1                      | 383.05 $\pm$ 0.29  | -326.27 $\pm$ 0.29                      | -6.4 $\pm$ 19.0              | Giz02            | 11.66G $\pm$ 0.04         | 6.745G $\pm$ 0.016      | 1.53e+00 $\pm$ 1.19e-01J          | -0.12       |
| G041-014B   | 08 58 56.33 | +08 28 26.0         | 147.78 $\pm$ 1.62              | R 1                      | 383.05 $\pm$ 0.29  | -326.27 $\pm$ 0.29                      | -6.4 $\pm$ 19.0              | Giz02            | 12.62G $\pm$ 0.04         | 7.258G $\pm$ 0.016      |                                   |             |
| G041-014C   | 08 58 56.33 | +08 28 26.0         | 147.78 $\pm$ 1.62              | R 1                      | 383.05 $\pm$ 0.29  | -326.27 $\pm$ 0.29                      | -6.4 $\pm$ 19.0              | Giz02            | 12.28D $\pm$ 0.04         | 6.719D $\pm$ 0.016      |                                   |             |
| TWA027  | 12 07 33.46 | +39 32 54.0         | 19.07 $\pm$ 0.36               | BDR 3                    | -64.14 $\pm$ 0.97  | -22.44 $\pm$ 1.00                       | 11.2 $\pm$ 2.0               | Moh03            | 19.95 $\pm$ 0.20          | 11.945 $\pm$ 0.026      |                                   |             |
| LHS2729   | 13 23 38.02 | +25 54 45.1         | 71.48 $\pm$ 1.53               | R 1                      | -594.97 $\pm$ 0.92                                       | -218.64 $\pm$ 0.92                      |                              |                  | 12.89 $\pm$ 0.06          | 7.781 $\pm$ 0.031       | 1.37e-01 $\pm$ 2.38e-02           | -0.30       |
| LHS2836   | 13 59 10.42 | +19 50 03.6         | 93.12 $\pm$ 0.81               | R 1                      | -545.26 $\pm$ 0.15                                       | -181.27 $\pm$ 0.15                      | -15.8 $\pm$                  | Giz02            | 12.88 $\pm$ 0.03          | 7.445 $\pm$ 0.026       | 1.95e-01 $\pm$ 2.73e-02           | -0.33       |
| GJ1207  | 16 57 05.73 | +04 20 56.3         | 112.53 $\pm$ 0.89              | Y R 2                    | 484.84 $\pm$ 0.18  | -364.79 $\pm$ 0.18                      | -4.2 $\pm$ 1.6               | Giz02            | 12.25 $\pm$ 0.04          | 7.120 $\pm$ 0.021       | 3.74e-01 $\pm$ 4.30e-02           | -0.46       |
| LHS4016A  | 23 48 36.06 | +27 39 38.9         | 41.29 $\pm$ 1.49               | R 1                      | -544.73 $\pm$ 0.30                                       | -240.21 $\pm$ 0.30                      | 25.3 $\pm$ 0.55              | Shk10            | 13.09G $\pm$ 0.04         | 8.450G $\pm$ 0.022      | 1.87e-01 $\pm$ 2.69e-02J          | -0.32       |
| LHS4016B  | 23 48 36.06 | +27 39 38.9         | 41.29 $\pm$ 1.49               | R 1                      | -544.73 $\pm$ 0.30                                       | -240.21 $\pm$ 0.30                      | 25.3 $\pm$ 0.55              | Shk10            | 13.09G $\pm$ 0.04         | 8.450G $\pm$ 0.022      |                                   |             |
| Parallax SourceKex: R=RECONS, V=van Leeuwen (2007), Y=van Altena et al. (1995), F=Fabricius & Makarov (2000), B=Billier & Close (2007), D=Ducourant et al. (2008) |             |                     |                                |                          |  |   |                              |                  |                           |                         |                                   |             |

Number of parallaxes in mean also listed

 $^b$ D=Deblended using published  $\Delta mag$  (See §2.2.2); G=Guess (SB2 assumed to be  $\Delta mag = 0$ ) $^c$ Coordinates calculated from our astrometric solution, not 2MASS.

There are six broad ways I can determine youth with my current dataset:

1. Overluminosity, as seen on a color-absolute magnitude diagram (§2.2.5), made possible with an accurate parallax
2. Relative photometric variability (§2.2.4) from our astrometric pipeline
3. X-ray luminosity (§2.2.3) from ROSAT
4. H $\alpha$  strength (§2.3.3) from our spectra
5. Gravity features (§2.3.2) from our spectra
6. Space Motion match to known young association (§2.4.1)

I have applied all of these methods to the systems in my samples, and the results are collected in Table 5.15. Because there is no single smoking gun for youth – and none of my available parameters are particularly strong on their own (I cannot measure the Lithium  $\lambda 6708\text{\AA}$  EW)– I have collected as many as I can: Overluminosity (Columns 2-4, from parallaxes in Table 5.14), Variability (Column 5), X-ray luminosity (Columns 6 and 7), H $\alpha$  EW (Column 8), the Na I index (Column 9) and K I EW (Column 10), and possible matches to known young associations and moving groups (Column 11) along with the expected RV (Column 12) for that match. I have followed the example of Shkolnik et al. (2009) and summarized all the parameters into a key (Column 13) as follows:

O=overluminous (more than 71% farther than distance estimate), o=(between 30% and 71%, possibly only a binary and 2- $\sigma$  distance error). V=variability greater than 0.05 mag,

v=variability greater than 0.02 mag. X=  $L_x/L_{bol} > 3.5$  (saturated), x=unsaturated X-rays. H=H $\alpha$  emission stronger than  $-10\text{\AA}$ , h=H $\alpha$  emission stronger than  $-5\text{\AA}$ . N=Na I index indicates lower gravity than main sequence star. K=K I EW indicates lower gravity than main sequence star. A=kinematics allow membership in a known association, a=association is old enough (AB Dor, Castor, Ursa Major) that the star should not be overluminous and could also be a high-metallicity main sequence star. Dashes indicate missing required data; everywhere else a blank means a null result.

Table 5.15: Youth properties of Sample

| Name<br>(1)                 | $M_V$<br>(2) | $V - K$<br>(3) | Dist. Est.<br>error (%)<br>(4) | rel.<br>var.<br>(5) | $L_X/L_{bol}$<br>(6) | $L_X$<br>(7) | EW<br>(8) | $H\alpha^b$<br>index<br>(9) | EW<br>(10) | Association<br>match <sup>e</sup><br>(11) | Exp <sup>d</sup> /RV<br>(12) | Youth<br>Key <sup>g</sup><br>(13) | Notes<br>(14) |
|-----------------------------|--------------|----------------|--------------------------------|---------------------|----------------------|--------------|-----------|-----------------------------|------------|---|------------------------------|-----------------------------------|---------------|
| Low Proper Motion           |              |                |                                |                     |                      |              |           |                             |            |   |                              |                                   |               |
| NLT00372                    | 11.20        | 5.15           | 81                             | 0.014               | -3.63                | 27.74        | ...       | ...                         | ...        | UrsaMaj                                   | 2                            | O                                 | a             |
| SCR0128-1458                | 12.79        | 5.40           | 14                             | 0.010               | -2.88                | 28.89        | -3.5      | 1.22                        | 2.2        | Castor                                    | 11                           | o                                 | a             |
| SCR0143-0602                | 11.60        | 5.10           | 44                             | 0.019               | -3.9                 | 1.20         | 1.8       | 1.8                         | 1.1        | UrsaMaj                                   | 16                           | o                                 | a             |
| L173-019                    | 12.33        | 5.13           | 5                              | 0.021               | -2.67                | 28.03        | -24.8     | 1.33                        | 4.1        | [Argus]                                   | 17                           | o                                 | a             |
| 2MA0314-0450                | 17.35        | 8.27           | 45                             | 0.005               | -4.44                | 27.84        | 0.2       | 1.11                        | 0.8        | Castor                                    | 14                           | o                                 | a             |
| 2MA0429-3123                | 16.45        | 7.62           | 46                             | 0.018               | -3.12                | 28.40        | -4.6      | 1.26                        | 2.2        | [Castor]                                  | 17                           | o                                 | a             |
| 2MA0451-3402                | 20.48        | 9.82           | -12                            | 0.048               | -3.21                | 28.56        | -2.4      | 1.26                        | 2.5        | ...                                       | ...                          | ...                               | b             |
| HD271076                    | 9.69         | 4.31           | 44                             | 0.011               | -3.00                | 28.11        | -7.4      | 1.35                        | 3.6        | ...                                       | ...                          | ...                               | ...           |
| SCR0533-4257AB              | 12.57        | 5.46           | 36                             | 0.011               | -4.37                | 28.05        | 0.3       | 1.08                        | 0.8        | UrsaMaj                                   | 6                            | o                                 | a             |
| LP780-032                   | 11.81        | 5.12           | 34                             | 0.009               | -2.89                | 28.37        | -5.4      | 1.24                        | 2.5        | UrsaMaj                                   | 9                            | o                                 | a             |
| 2MA0936-2610                | 11.60        | 5.15           | 46                             | 0.009               | -2.94                | 29.03        | -3.2      | 1.13                        | 0.9        | UrsaMaj !                                 | 14                           | X                                 | a             |
| SCR1214-2345                | 13.81        | 5.74           | 2                              | 0.012               | -3.00                | 28.11        | -7.4      | 1.35                        | 3.6        | UrsaMaj                                   | 14                           | X                                 | a             |
| SDS1416+1348                | ...          | ...            | ...                            | 0.018               | ...                  | ...          | ...       | ...                         | ...        | ...                                       | ...                          | ...                               | ...           |
| 2MA1507-2000                | 16.97        | 8.16           | 63                             | 0.010               | -4.37                | 28.05        | 0.3       | 1.08                        | 0.8        | UrsaMaj                                   | 6                            | o                                 | a             |
| GJ2122AB                    | 9.04         | 3.95           | 36                             | 0.014               | -2.89                | 28.37        | -5.4      | 1.24                        | 2.5        | UrsaMaj                                   | 9                            | o                                 | a             |
| 2MA1705-0516                | ...          | ...            | ...                            | 0.041               | -2.94                | 29.03        | -3.2      | 1.13                        | 0.9        | UrsaMaj                                   | 14                           | X                                 | a             |
| DEN1756-4805                | 20.29        | 9.59           | -16                            | 0.011               | -2.94                | 29.03        | -3.2      | 1.13                        | 0.9        | UrsaMaj !                                 | 14                           | X                                 | a             |
| SCR1942-2045                | 13.31        | 5.57           | 10                             | 0.014               | -3.00                | 28.11        | -7.4      | 1.35                        | 3.6        | ...                                       | ...                          | ...                               | ...           |
| SCR2036-3607                | 10.61        | 4.49           | 14                             | 0.016               | -3.00                | 28.11        | -7.4      | 1.35                        | 3.6        | ...                                       | ...                          | ...                               | ...           |
| SCR2049-4012                | 13.69        | 5.83           | 17                             | 0.014               | -3.00                | 28.11        | -7.4      | 1.35                        | 3.6        | ...                                       | ...                          | ...                               | ...           |
| 2MA2057-0252                | 20.74        | 9.95           | -15                            | 0.013               | ...                  | ...          | ...       | ...                         | ...        | ...                                       | ...                          | ...                               | ...           |
| Low Proper Motion and Young |              |                |                                |                     |                      |              |           |                             |            |   |                              |                                   |               |
| SCR0017-6645                | 9.43         | 4.75           | 171                            | 0.031               | -3.01                | 29.51        | -4.8      | 1.11                        | -0.7       | BetaPic                                   | 12                           | O                                 | K A           |
| GJ2006A                     | 10.24        | 4.78           | 94                             | 0.077               | -2.69                | 29.50        | -5.6      | 1.13                        | 0.6        | BetaPic                                   | 9                            | O                                 | K A           |
| GJ2006B                     | 10.70        | 5.13           | 120                            | 0.036               | -2.63                | 29.50        | -10.0     | 1.15                        | 1.1        | BetaPic                                   | 9                            | O                                 | K A           |
| SCR0103-5515                | 12.10        | 6.24           | 269                            | 0.015               | -2.63                | 29.50        | -14.5     | 1.25                        | 3.0        | [TWHydra]                                 | 9                            | O                                 | K A           |
| 2MA0123-6921                | 16.00        | 7.80           | 106                            | 0.011               | -2.96                | 29.27        | -10.5     | 1.15                        | 1.4        | [TWHydra]                                 | 9                            | O                                 | K A           |
| BAR161-012                  | 10.66        | 5.34           | 190                            | 0.079               | -3.55                | 28.10        | -9.7      | 1.19                        | 2.5        | BetaPic                                   | 7                            | O                                 | K A           |
| SIP0152-6329                | 12.78        | 6.15           | 145                            | 0.015               | -2.97                | 29.58        | -10.2     | 1.25                        | 2.5        | [TWHydra]                                 | 16                           | O                                 | K A           |
| SCR0222-6022                | 11.10        | 5.26           | 113                            | 0.026               | -2.97                | 29.58        | -10.5     | 1.18                        | 1.1        | Argus                                     | 23                           | O                                 | K A           |
| 2MA0236-5203                | 9.28         | 4.56           | 130                            | 0.030               | -2.91                | 29.62        | -5.5      | 1.09                        | 0.5        | [ABDor]                                   | 27                           | O                                 | K A           |
| 2MA0254-5108A               | 9.21         | 4.30           | 75                             | 0.029               | -3.23                | 29.23        | -2.1      | 1.09                        | 0.7        | Tuc-Hor                                   | 13                           | O                                 | K A           |
| 2MA0254-5108B               | 13.93        | 6.36           | 74                             | 0.033               | -1.75                | 29.53        | ...       | ...                         | ...        | Tuc-Hor                                   | 10                           | O                                 | K A           |
| SCR0336-2619                | 13.22        | 6.57           | 195                            | 0.010               | -2.97                | 28.87        | -10.2     | 1.25                        | 2.5        | [TWHydra]                                 | 16                           | O                                 | K A           |
| RX0413-0139                 | 11.76        | 5.46           | 98                             | 0.036               | -3.11                | 29.49        | -8.9      | 1.14                        | 1.1        | Argus                                     | 23                           | O                                 | K A           |
| LP476-207ABC                | 9.55         | 5.16           | 292                            | 0.021               | -2.92                | 29.58        | -5.2      | 1.13                        | 0.8        | BetaPic !                                 | 17                           | O                                 | K A           |
| BD-21-01074BC               | 9.66         | 4.97           | 211                            | 0.046               | -2.92                | 29.58        | -5.2      | 1.13                        | 0.8        | BetaPic !                                 | 20                           | O                                 | K A           |
| BD-21-01074A                | 8.99         | 4.29           | 85                             | 0.043               | -2.97                | 29.58        | -2.0      | 1.10                        | 0.7        | BetaPic !                                 | 22                           | O                                 | K A           |
| SCR0529-3239                | 11.86        | 5.47           | 90                             | 0.013               | -3.09                | 28.71        | -6.0      | 1.18                        | 1.5        | BetaPic                                   | 21                           | O                                 | K A           |
| SCR0613-2742AB              | 9.98         | 5.16           | 225                            | 0.038               | -2.95                | 29.49        | -6.0      | 1.17                        | 0.7        | BetaPic                                   | 21                           | O                                 | K A           |
| SCR0757-7114                | 10.74        | 5.04           | 97                             | 0.007               | -3.21                | 29.63        | -9.2      | 1.10                        | 0.5        | TWHydra                                   | 18                           | O                                 | K A           |
| SCR1012-3124AB              | 9.85         | 5.52           | 411                            | 0.015               | -3.21                | 29.63        | -9.2      | 1.10                        | 0.5        | TWHydra                                   | 18                           | O                                 | K A           |
| SIP1110-3731AC              | 9.07         | 5.29           | 518                            | 0.113               | ...                  | ...          | ...       | ...                         | ...        | TWHydra                                   | 12                           | O                                 | K A           |
| SIP1110-3731B               | ...          | ...            | ...                            | 0.222               | ...                  | ...          | ...       | ...                         | ...        | TWHydra !                                 | 15                           | O                                 | K A           |
| RX1132-2651B                | 11.84        | 6.19           | 304                            | 0.124               | -2.19                | 29.86        | -13.8     | 1.14                        | 1.5        | TWHydra !                                 | 9                            | O                                 | K A           |
| RX1132-2651A                | 8.87         | 4.80           | 269                            | 0.078               | -2.91                | 29.86        | -9.2      | 1.12                        | 0.5        | TWHydra !                                 | 10                           | O                                 | K A           |
| STEPH0164                   | 9.53         | 4.92           | 203                            | 0.015               | -3.19                | 29.36        | -4.2      | 1.05                        | 1.4        | [UrsaMaj]                                 | -3                           | O                                 | K A           |
| DEN1306-7723                | 12.42        | 7.78           | 1478                           | 0.010               | -18.4                | 1.05         | 1.0       | 1.0                         | 1.0        | [Castor]                                  | 6                            | O                                 | K A           |
| SCR1425-4113                | 8.55         | 5.03           | 444                            | 0.077               | -7.0                 | 1.08         | 0.6       | 1.08                        | 0.6        | TWHydra                                   | 1                            | O                                 | K A           |
| SCR1609-2222                | 10.36        | 6.49           | 918                            | 0.009               | -14.4                | 1.12         | 0.7       | 1.12                        | 0.7        | [EpsCha]                                  | -1                           | O                                 | K A           |
| SIP1809-7613                | 13.00        | 6.12           | 121                            | 0.007               | -8.3                 | 1.17         | 2.0       | 1.17                        | 2.0        | BetaPic                                   | 9                            | O                                 | K A           |
| SCR1816-5844                | 10.51        | 5.20           | 167                            | 0.074               | -6.5                 | 1.15         | 1.1       | 1.15                        | 1.1        | BetaPic                                   | 1                            | O                                 | K A           |
| SCR2010-2801AB              | 9.58         | 5.25           | 329                            | 0.012               | -3.03                | 29.60        | -9.8      | 1.15                        | 1.1        | [BetaPic]                                 | -8                           | O                                 | K A           |
| SCR2033-2556                | 11.82        | 5.99           | 239                            | 0.019               | -3.10                | 28.88        | -12.6     | 1.18                        | 2.0        | [BetaPic]                                 | -7                           | O                                 | K A           |
| BD-13-06424                 | 8.43         | 3.93           | 78                             | 0.031               | -3.06                | 29.59        | ...       | ...                         | ...        | BetaPic !                                 | 2                            | O                                 | K A           |

Young  
Continued on next page

Table 5.15 – Continued from previous page

| Name<br>(1)          | $M_V$<br>(2) | $V - K$<br>(3) | Dist. Est.<br>error (%)<br>(4) | rel.<br>var. $L_X/L_{bol}$<br>(5) | $L_X/L_{bol}$<br>(6) | $L_X$<br>(7) | EW<br>(8) | Na I<br>index<br>(9) | K I<br>index<br>(10) | EW<br>(10) | Association<br>match <sup>e</sup><br>(11) | Exp <sup>d</sup> /<br>RV<br>(12) | Youth<br>Key <sup>g</sup><br>(13) | Notes<br>(14) |
|----------------------|--------------|----------------|--------------------------------|-----------------------------------|----------------------|--------------|-----------|----------------------|----------------------|------------|---|----------------------------------|-----------------------------------|---------------|
| G131-026AB           | 12.19        | 5.51           | 72                             | 0.018                             | -3.28                | 28.38        | -3.5      | 1.25                 | 2.2                  | 2.2        |   | O                                | X                                 |               |
| LP467-016AB          | 12.76        | 6.25           | 177                            | 0.019                             | -3.08                | 28.62        | -9.9      | 1.19                 | 2.5                  | BetaPic!   |   | 4                                | O                                 | X h N K A d   |
| GJ2022AC             | 11.50        | 5.32           | 74                             | 0.016                             | -2.78                | 29.10        | -9.4      | 1.23                 | 2.1                  | ABDor      |   | 18                               | O                                 | X h a a       |
| GJ2022B              | 13.44        | 5.82           | 31                             | 0.016                             | -6.3                 | 1.24         | -6.3      | 1.24                 | 2.4                  | ABDor      |   | 18                               | o                                 | h a           |
| LP993-115            | 12.12        | 5.11           | 12                             | 0.023                             | -1.6                 | 1.19         | -1.6      | 1.19                 | 1.5                  |            |   |                                  | v                                 |               |
| LP993-116AB          | 12.43        | 5.49           | 50                             | 0.014                             | -3.24                | 28.32        | -7.7      | 1.25                 | 2.2                  |            |   |                                  | o                                 | X h h N K a   |
| G007-034             | 13.16        | 5.66           | 28                             | 0.024                             | -3.09                | 28.24        | -8.4      | 1.19                 | 2.0                  | ABDor      |   | 14                               | o                                 | X X H         |
| G039-029AB           | 12.04        | 5.23           | 35                             | 0.015                             | -3.00                | 28.64        | -4.7      | 1.19                 | 2.1                  |            |   |                                  | o                                 | X X H         |
| LP655-048            | 17.87        | 8.26           | 16                             | 0.013                             | -2.72                | 27.60        | -17.8     | 1.35                 | 5.0                  |            |   |                                  | o                                 | X X H         |
| LP776-025            | 10.84        | 4.74           | 38                             | 0.016                             | -3.08                | 28.86        | -4.9      | 1.16                 | 0.9                  | ABDor      |   | 25                               | o                                 | X X a a d     |
| L449-001AB           | 11.35        | 5.13           | 67                             | 0.022                             | -3.02                | 28.86        | -5.9      | 1.21                 | 1.6                  | UrsaMa]    |   | 0                                | o                                 | v X h a       |
| L034-026             | 11.17        | 4.73           | 17                             | 0.018                             | -3.07                | 28.77        | -4.9      | 1.18                 | 1.0                  | UrsaMa]    |   | 6                                | o                                 | v X a a       |
| G161-071             | 13.04        | 6.16           | 121                            | 0.040                             | -2.85                | 28.71        | -24.4     | 1.22                 | 2.4                  | [Argus]    |   | 15                               | O                                 | v X H N K A b |
| SCR1157-0149         | 14.49        | 5.97           | -7                             | 0.011                             | -2.99                | 27.91        | -4.2      | 1.32                 | 3.0                  |            |   |                                  | O                                 | v X X K A c   |
| G165-008AB           | 10.74        | 5.30           | 168                            | 0.018                             | -3.16                | 29.02        | -7.3      | 1.17                 | 1.3                  | [Tuc-Hor]  |   | -5                               | O                                 | X h N K A     |
| LHS2880              | 11.44        | 5.73           | 204                            | 0.014                             | -2.82                | 29.13        | -8.4      | 1.19                 | 1.6                  |            |   |                                  | O                                 | X h N K       |
| GJ1224               | 14.01        | 5.65           | -14                            | 0.010                             | -3.03                | 27.96        | -4.3      | 1.26                 | 3.1                  |            |   |                                  | X                                 |               |
| G141-029             | 12.63        | 5.31           | 14                             | 0.012                             | -3.27                | 28.17        | -4.7      | 1.22                 | 2.0                  | [Hyades]   |   | -43                              | X                                 | X a a         |
| LP870-065            | 11.72        | 5.32           | 70                             | 0.013                             | -2.98                | 28.90        | -7.8      | 1.24                 | 2.1                  | [ABDor]    |   | -8                               | o                                 | X h a a       |
| SCR2009-0113         | 14.33        | 5.96           | -1                             | 0.014                             | -3.31                | 27.65        | -5.5      | 1.28                 | 3.3                  |            |   |                                  | o                                 | X h h         |
| LEHPM2-0783          | 16.13        | 7.45           | 53                             | 0.025                             | -2.20                | 28.57        | -26.6     | 1.34                 | 5.6                  |            |   |                                  | o                                 | v X H         |
| L755-019             | 11.14        | 4.97           | 54                             | 0.016                             | -3.25                | 28.68        | -5.0      | 1.17                 | 1.1                  | Argus      |   | -22                              | o                                 | X h A         |
| GJ0799A              | 10.39        | 5.42           | 254                            | 0.057                             | -2.85                | 29.52        | -10.8     | 1.16                 | 1.5                  | BetaPic!   |   | -7                               | O                                 | V X H N K A d |
| GJ0799B              | ...          | ...            | ...                            | 0.050                             | -2.85                | 29.52        | ...       | ...                  | ...                  | BetaPic!   |   | -4                               | V                                 | X - A d       |
| LP756-003            | 12.60        | 5.36           | 19                             | ...                               | -2.89                | 28.57        | -5.8      | 1.25                 | 2.0                  | [Hyades]   |   | -36                              | -                                 | X h a         |
| LHS799               | 14.00        | 5.98           | 19                             | 0.014                             | -3.20                | 27.91        | -3.8      | 1.31                 | 2.9                  |            |   |                                  | -                                 | X h h         |
| LP932-083            | 10.98        | 5.47           | 177                            | 0.044                             | -3.20                | 27.91        | -8.3      | 1.21                 | 1.6                  |            |   |                                  | O                                 | v h N K       |
| GJ1284AB             | 10.23        | 4.81           | 89                             | 0.027                             | -3.23                | 29.00        | -3.7      | 1.17                 | 1.0                  | [Columba]  |   | -3                               | O                                 | v X A         |
| Previously Published |              |                |                                |                                   |                      |              |           |                      |                      |            |   |                                  |                                   |               |
| LHS1302              | 14.41        | 5.94           | -6                             | 0.021                             | -3.32                | 27.58        | -3.6      | 1.27                 | 3.1                  |            |   |                                  | v                                 | X             |
| LHS1358              | 12.65        | 5.41           | 22                             | 0.015                             | -3.23                | 28.22        | ...       | ...                  | ...                  | [Hyades]   |   | 21                               | X                                 | - a           |
| G099-049             | 12.73        | 5.27           | 2                              | 0.012                             | -3.40                | 27.98        | -4.6      | 1.22                 | 2.1                  | [Hyades]   |   | 45                               | X                                 | - a           |
| APCOL                | 13.33        | 6.09           | 83                             | 0.018                             | -2.92                | 28.49        | -18.4     | 1.17                 | 2.2                  | Argus!     |   | 23                               | O                                 | X H N K A d   |
| G041-014ABC          | 11.77        | 5.23           | 54                             | 0.013                             | -2.94                | 28.81        | -4.0      | 1.22                 | 2.0                  |            |   |                                  | o                                 | X a a         |
| 2MA1207-3932A        | 16.35        | 8.01           | 91                             | 0.017                             | ...                  | ...          | ...       | ...                  | ...                  | TWHydra!   |   | 8                                | O                                 | - - A d       |
| LHS2729              | 12.16        | 5.11           | 11                             | 0.012                             | -3.21                | 28.33        | -3.4      | 1.16                 | 1.7                  |            |   |                                  | X                                 | X             |
| LHS2836              | 12.73        | 5.43           | 22                             | 0.011                             | -3.22                | 28.25        | -3.7      | 1.22                 | 2.0                  |            |   |                                  | X                                 | X             |
| GJ1207               | 12.51        | 5.13           | -5                             | 0.199                             | -3.11                | 28.30        | -4.9      | 1.17                 | 1.3                  |            |   |                                  | V                                 | X             |
| LHS4016AB            | 10.42        | 4.60           | 41                             | 0.012                             | -3.14                | 28.94        | -2.1      | 1.14                 | 1.0                  |            |   |                                  | o                                 | X X           |

<sup>a</sup>Untrustworthy  $\pi$ .<sup>b</sup>Might be member if unresolved multiple, otherwise not a member.<sup>c</sup>Wrong region of the sky.<sup>d</sup>Known member of association.<sup>e</sup>Most likely match (if many) given; brackets denote implausible matches; ! notes a published RV is consistent with membership.<sup>f</sup>Best-fit RV if the object is a member of the association.<sup>g</sup>See text for explanation of key.<sup>h</sup>H $\alpha$  EW and K I EW are (by rough estimate) only good to 0.2A.

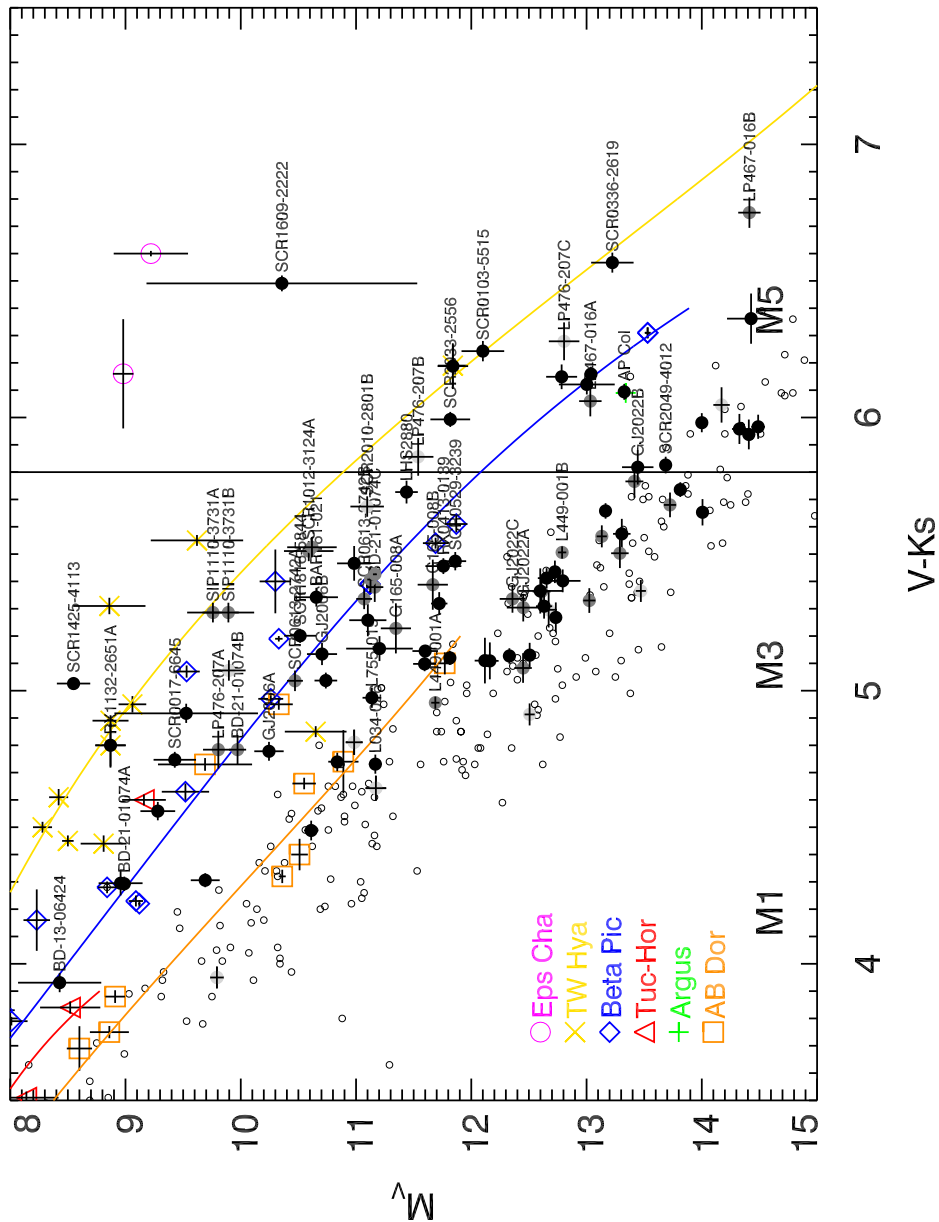


Figure 5.28: A color-magnitude diagram showing (with Figure 5.29) all of the stars from this sample, split according to Table 5.14 and displayed with the young association members and isochrones from Riedel et al. (2011), and (as small circles) the RECONS 10 pc sample. Black points are resolved stars, dark gray points are debledended, and light gray points have only guesses as to the debledending. The vertical line at  $V - K_s = 5.8$  is roughly the location of the transition to full convection.



All of the stars in my sample meet at least one of the youth criteria, even if they were merely included as low proper motion stars, and a large number are potential kinematic matches to known nearby young associations and moving groups – this is at least partially due to my five-element solutions, which leave radial velocity unconstrained. Very few stars had radial velocities from literature sources. Most stars with one potential kinematic match (defined as passing within  $3\sigma$  of the velocity ellipse as defined in Table 2.5;  $3\sigma$  was needed to pick up all of the known members of young associations) actually had several potential matches, and in Table 5.15 I have listed the most likely match based on color-magnitude position (Figures 5.28 and 5.29).

At least part of this enormous bounty of young stars is real – Figure 5.28 demonstrates that, even when deblended according to available information (and the assumptions that  $\Delta V = 2 \times \Delta K$ , and  $\Delta FGS = \Delta V$ ; see §2.2.2), many of my stars are well-elevated above the main sequence and are therefore likely young. One curious effect explored in some detail in the system notes (§5.6) is that a large number of potential kinematic matches to the  $\beta$  Pic association lie *above* the isochrone line from Riedel et al. (2011) – see SCR 0017-6645, SCR 2010-2801AB, SCR 1816-5844, BAR 161-012, LP 476-207BC, SCR 2033-2556. This may be no accident; it may simply be that the isochrone from Riedel et al. (2011) does not actually follow the  $\beta$  Pic isochrone. However, this will cause problems with known  $\beta$  Pic members and the supposed  $\beta$  Pic members that lie on or below the current line (e.g. GJ 2006AB, SCR 0529-3239) as I doubt the  $\beta$  Pic isochrone has as much width as the main

sequence<sup>18</sup> – it should be no wider than the errors<sup>19</sup> on the parallaxes. It is also possible (though currently untested) that I have discovered another association entirely with an age between  $\beta$  Pic and TW Hya.

In addition, as shown in Figure 5.29, several very cool M dwarfs (e.g. 2MA 1507-2000, 2MA 0314-0450, 2MA 2057-0252, DEN 1756-4805) are prospective members of Ursa Major, yet are overluminous. Given that it may take up to 1 billion years (Dotter et al. 2008) for such low mass stars to reach the main sequence, they may be genuinely pre-main-sequence members of Ursa Major, though without radial velocity, lithium EW, or chemical abundance measurements, it is hard to confirm membership.

The relative variability measurements for my stars demonstrate that they are markedly different from all other subsets of stars previously published by CTIOPI. In Figure 5.30, plotted as in Jao et al. (2011), a large number of young stars are *much* more variable than the average M dwarf. These are almost exclusively bright stars observed in the  $V$  band.

On the other hand, there are demonstrably no strong correlations between the various signs of chromospheric activity – see Figure 5.31. I also note that in a plot of  $V - K_s$  vs  $H\alpha$ , (Figure 5.32) none of these stars qualify as Classical T Tauri stars by the White & Basri (2003) metric.

One thing I can demonstrate is that lack of X-ray detection is not a serious strike against youth past a distance of 45 pc, see Figure 5.33. The only detections beyond 45 pc are some of

<sup>18</sup>Although debris disks (GJ 803=AU Mic) are possible and would spread the  $\beta$  Pic sequence on the HR diagram, they shouldn't be that common.

<sup>19</sup>Addendum added after defense: At Cool Stars 17, Baraffe reported that fast accretion events could artificially age stars by several million years, which would be a noticeable effect at young ages like that of the  $\beta$  Pic association.

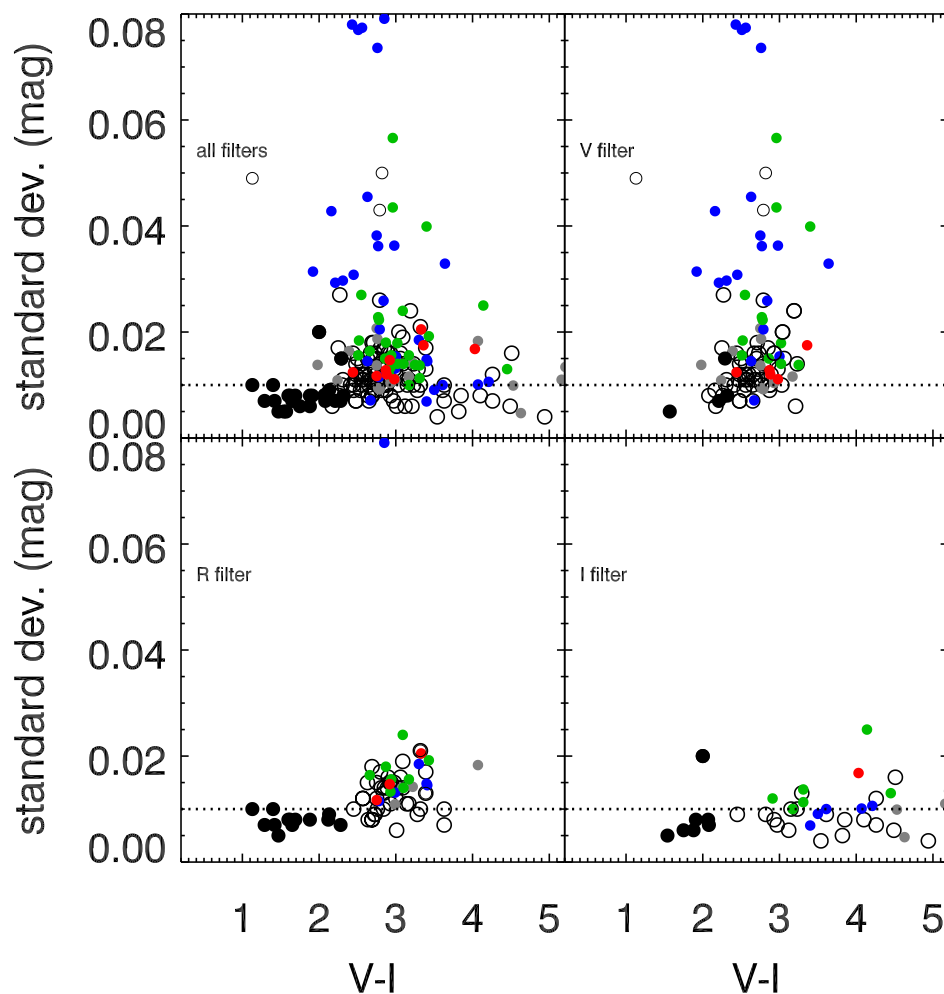


Figure 5.30: A plot of the relative variability of the stars in this thesis, compared to previously published CTIOPI stars (black open/closed points), as in Jao et al. (2011). Gray points are normal low-proper-motion stars, green stars are young (usually by saturated X-ray flux), blue stars are both young and of low proper motion, red stars were previously published. The dotted line indicates 1% variability, which is common among M dwarfs. Note that the scale is different than in Jao et al. (2011).

the most luminous in the entire sample; this is a well-known problem with using the ROSAT All-Sky Surveys for X-ray detections, and a main motivation for using the more sensitive GALEX observations. (There is no corresponding trend in  $\frac{L_x}{L_{bol}}$ , as the luminosities of the stars are decreasing at the same rate.)

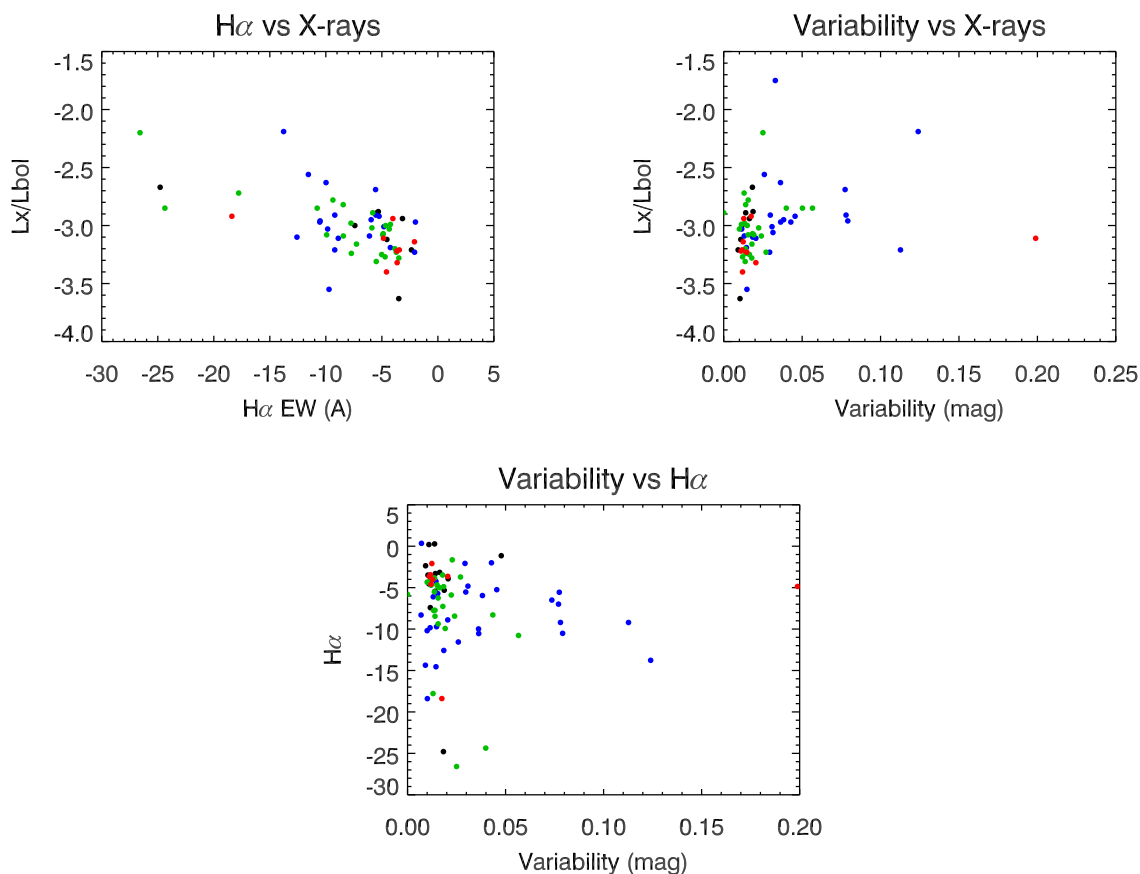


Figure 5.31: Intercomparisons between H $\alpha$  EW,  $L_X/L_{bol}$ , and relative variability. Note only a slight correlation between H $\alpha$  and  $\log(L_X/L_{bol})$ . Black points are normal low-proper-motion stars, green stars are young (usually by saturated X-ray flux), blue stars are both young and of low proper motion, red stars were previously published.

The gravity-sensitive parameters (the Na I index and K I EW) are unfortunately weak parameters at our spectral resolution, as they are measured using spectra only meant for spectral typing. The Na I line is contaminated by telluric features, and I do not feel comfortable attempting to rank stars in age by their appearance below the main sequence locus (Figure 5.34) although any star that does is probably younger than AB Dor age (125 Myr). The K I 7700Å line is free of telluric contamination, and its EW shows similar trends with

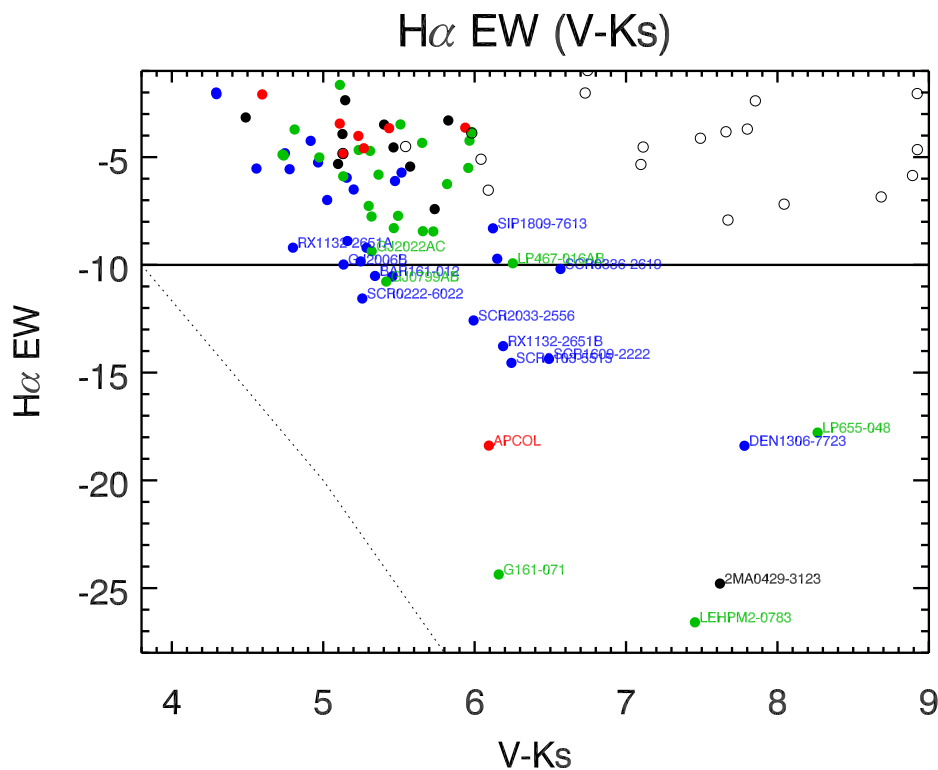


Figure 5.32: The  $H\alpha$  EW of all stars, plotted against  $V - K_s$  color. Black points are normal low-proper-motion stars, green stars are young (usually by saturated X-ray flux), blue stars are both young and of low proper motion, red stars were previously published. The dashed line is (roughly) the dividing line between Classical T Tauri stars to the lower left and older stars to the right, as defined in White & Basri (2003); the solid line at  $H\alpha = -10$  is my dividing line for large  $H\alpha$  emission in Table 5.15. None of the stars (even known young stars like RX 1132-2651AB=TWA 8AB) are potential Classical T Tauri stars.

color (Figure 5.35), but again I do not feel comfortable ranking stars by age given the low precision of the K I EW measurements ( $0.2\text{\AA}$ ).

### X-ray luminosity as a function of distance

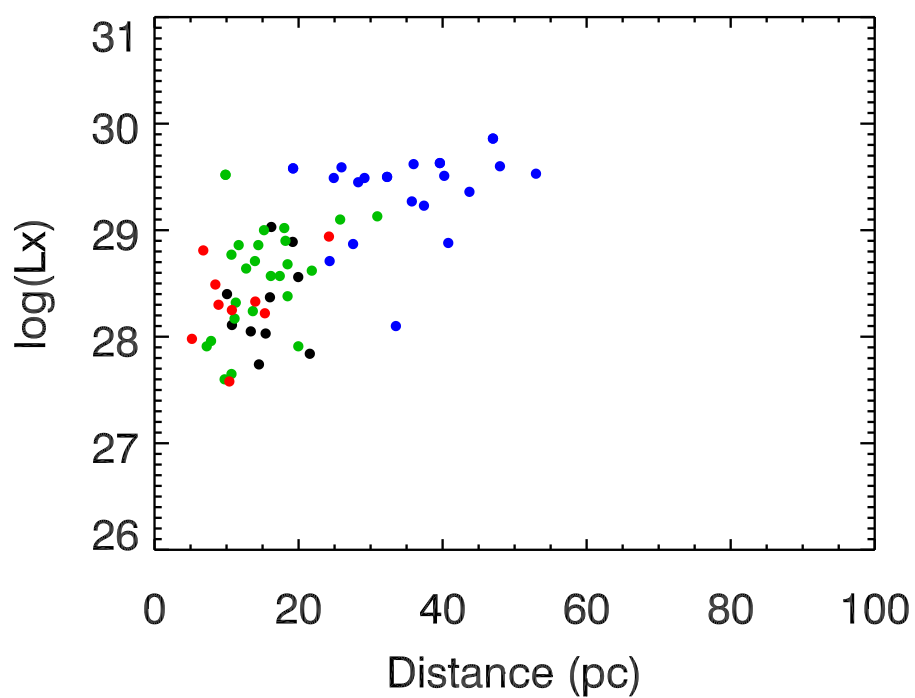


Figure 5.33: As demonstrated in this diagram of distance versus  $L_X$ , the reason there are no X-ray detections past roughly 55 pc is that the stars are simply too faint to be detected. (There is no corresponding trend in  $\frac{L_X}{L_{bol}}$ , as the luminosities of the stars are decreasing at the same rate.) This also implies that the maximum  $L_X$  for M dwarfs is  $\sim 10^{30}$  ergs  $s^{-1}$ .





Finally, there are the oddball systems that cannot be explained. G 165-008AB matches Tuc-Hor in terms of properties, but is almost exactly on the opposite side of the sky from the rest of the Tuc-Hor members. Similarly, SCR 0103-5515, 2MA 0123-6921 and SCR 0336-2610 are all good matches for TW Hya in several ways, but are in the wrong part of the sky, far from the location of all known TW Hydra members (clustered around 12h RA,  $-30^{\circ}$  DEC). There are other possible associations they could belong to (Tuc-Hor or the other 30 Myr old associations in Torres et al. (2008) in every case), but they are far too luminous to be members; each one would have to be at least an unresolved triple for their components to lie along a 30 Myr old isochrone. Then there are the unmatched objects, like LEHPM 2-0783. Some may be close binaries, which would account for both luminosity and X-ray flux. Others, like LP 932-083, which have every youthful property except a match to an association, are harder to explain.

## 5.6 Systems Worthy of Note

In RA order. See also Table 5.10 for details on the various binary systems. (see Table 5.10)

**NLTT 372** ( $M_V=11.30$ ,  $V - K_s=5.15$ ) aka LP 404-32

This system came to our attention as reference star #9 of the G 131-026AB field. It is, with LHS 1749-REF4 in Costa et al. (2005), one of two nearby stars discovered in the reference field of another system. The error on the distance is large enough ( $85.8 \pm 10.6$  pc) that I do not definitely claim the star is overluminous, although its expected distance from CCD photometry is  $47.4 \pm 7.47$  pc, which we should be easily able to measure. It should

be noted that NLTT 372 is close enough to the ROSAT X-ray source I have attributed to G 131-026AB, that it might actually be the (or an additional) source of the X-rays.

**G 131-026AB** ( $M_V=12.19$ ,  $V - K_s=5.51$ ) aka LP 404-33, LTT 10045

Gershberg et al. (1999) note it as a flare star, though it is not listed in the GCVS (Samus et al. 2012). Beuzit et al. (2004) splits it into two components, separation  $0.111''$  @  $169.9^\circ$  and  $\Delta K=0.46$  (see Table 5.10). They suspect the system components are fast rotators and that an accurate mass determination will require an astrometric orbit. Unfortunately, we see no sign of an astrometric perturbation in our 11-year dataset, despite the (expected) orbital period of 4 years.

When properly deblended according to Beuzit et al. (2004), this system appears to be composed of normal main sequence stars. It has no kinematic matches to any known association.

**SCR 0017-6645** ( $M_V=9.43$ ,  $V - K_s=4.75$ ) (from TINYMO)

Appears to be a member of the  $\beta$  Pic association. Its HR diagram position is consistent with  $\beta$  Pic (although, like SCR 2010-2801AB, more luminous), its kinematics are a potential match for  $\beta$  Pic, and it displays signs of slightly lower gravity than a main-sequence star (like BD-21 01074A) and unusually large variability. The one factor it does *not* have is significant  $H\alpha$  emission.

**GJ 2006AB** ( $M_V=10.24$ ,  $V - K_s=4.78$  (A),  $M_V=10.70$ ,  $V - K_s=5.13$  (B)) aka LDS 18AB, WDS J00279-3235AB.

This binary system (see Table 5.10) was not included in CNS3p (Gliese & Jahreiß 1991)

but was included by [Gliese & Jahreiß \(1979\)](#). [Jao et al. \(2003\)](#) reported that at least one component is a long-term variable; we now find that both targets are highly variable, though this may be partially due to the exceptional faintness of the available reference stars.

Based on its kinematics, its location on the color-magnitude diagram (Figure [5.28](#)), and its gravity index, this system appears to be a member of the  $\beta$  Pic association, in which case its radial velocity should be roughly  $+8 \text{ km s}^{-1}$ . This system is one of the few that is less luminous than the current  $\beta$  Pic isochrone. This system is also a kinematic match for the Castor Moving Group, but is far too luminous to be a member.

We see evidence of orbital motion between these two stars despite their  $17.9''$  separation in the form of differential proper motion:  $\Delta\mu_{RA\cos(DEC)} = -1.39 \pm 0.10 \text{ mas yr}^{-1}$   
 $\Delta\mu_{DEC} = -1.70 \pm 0.10 \text{ mas yr}^{-1}$ .

**SCR 0103-5515** ( $M_V=12.10$ ,  $V - K_s=6.24$ ) (from TINYMO)

Like 2MA 0123-6921 and SCR 0336-2610, this system appears to be a member of TW Hydra by kinematics, HR Diagram position and possibly gravity measurement, but given its position in space it cannot be. It is most definitely young (although it has no X-ray flux, possibly a result of its distance). It also matches the kinematics of Tuc-Hor (and AB Dor) but would have to be a higher-order multiple to match their isochrones on the HR Diagram.

**LP 467-016AB** ( $M_V=12.76$ ,  $V - K_s=6.25$ ) aka L 1157-047, RX 0111+1526

This system was identified as young by [Montes et al. \(2001\)](#). [Mochnecki et al. \(2002\)](#) give  $H\alpha$  EW =  $-7.0\text{\AA}$  and  $v\sin i=20 \text{ km s}^{-1}$ , [Mohanty & Basri \(2003\)](#) give  $H\alpha$  EW =  $-6.8\text{\AA}$  and  $v\sin i=15.2 \text{ km s}^{-1}$ . [Beuzit et al. \(2004\)](#) separated it into two components (see Table [5.10](#))

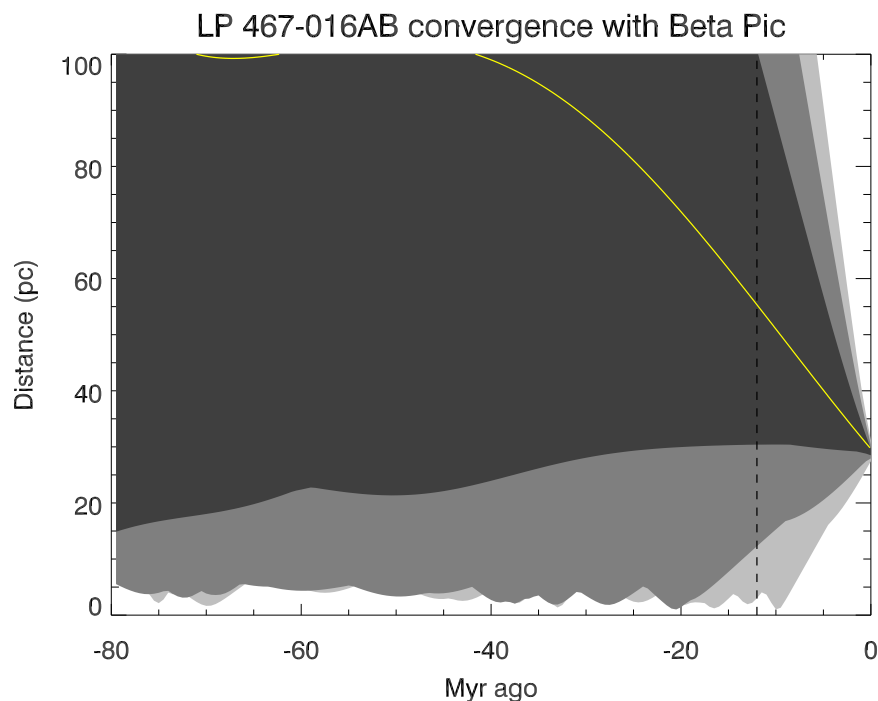


Figure 5.36: Plot of the separation between LP 467-016AB and the  $\beta$  Pic association (represented by the star  $\beta$  Pic and the association UVW velocity from [Torres et al. 2008](#)) as a function of time, going backwards into the past (leftward). The plot shows the result of 6000 sets of UVW velocities within  $1\sigma$  (dark gray),  $2\sigma$  (medium gray), and  $3\sigma$  (light gray) error bounds. LP 467-016AB does not seem to reasonably converge with  $\beta$  Pic 12 Myr ago, assuming a separation of  $<5$  pc counts as necessary for convergence.

with a separation of  $0.409''$  @  $147.2^\circ$  and  $\Delta K = 0.69$ .

This system appears to be a member of  $\beta$  Pic by its kinematics, deblended HR Diagram position, and Na I gravity index. The published radial velocity for the system,  $+4 \pm 0.1$  km  $s^{-1}$  ([Montes et al. 2001](#)), is consistent with  $\beta$  Pic as well.

Unfortunately, attempting a kinematic traceback with the Galactic potential (Figure [5.36](#)) shows that LP 467-016AB does not realistically converge with the location of  $\beta$  Pic (the star) 12 Myr in the past except at the  $3\text{-}\sigma$  level, which suggests it may not be a member.

**2MA 0123-6921** ( $M_V = 16.00$ ,  $V - K_s = 7.80$ ) (from TINYMO)

Like SCR 0103-5515 and SCR 0336-2610, this system is a kinematic and HR Diagram match (we have no spectrum to measure its  $H\alpha$  or gravity features) for the TW Hydra association, but it is on the wrong side of the sky from all known members. It is most definitely young – it plots as more overluminous than TWA 27. It is also kinematically consistent with Tuc-Hor (and AB Dor) but would have to be a higher-order multiple to match either of them on the HR Diagram.

**GJ 2022ABC** ( $M_V=11.50$ ,  $V - K_s=5.32$  (AC),  $M_V=13.44$ ,  $V - K_s=5.82$  (B)) aka G 269-153, RBS 0195 and LEHPM 1-1519.

This system was not included in CNS3p (Gliese & Jahreiß 1991), but was included in Gliese & Jahreiß (1979). It is a hierarchical triple (see Table 5.10) composed of a wide (37.8'') companion (B) to a close (1.8'') nearly-equal-luminosity pair (AC) with a delta magnitude of roughly  $\Delta V=0.08$  (Figure 5.37). where B is actually the least luminous component (to preserve the historical order, we continue to refer to it as 'B'). The C component was first published in Jao et al. (2003), and later recovered by Daemgen et al. (2007); they estimate a distance of  $12.6\pm 2.3$  pc and note that the system seems young. The AC component was re-identified in TINYMO though it has larger than  $0.18'' \text{ yr}^{-1}$  proper motion.

X-ray emission is associated with the AC close binary, and largely on that basis, Shkolnik et al. (2009) estimated an age of 40-300 Myr for AC, and 60-300 Myr for B. We find all three components match the kinematics of the AB Dor association, with best-fit  $RV=+18 \text{ km s}^{-1}$ . They also match the AB Dor isochrone, though as the AB Dor isochrone lies along the high-metallicity end of the main sequence, these stars may be on the main sequence.

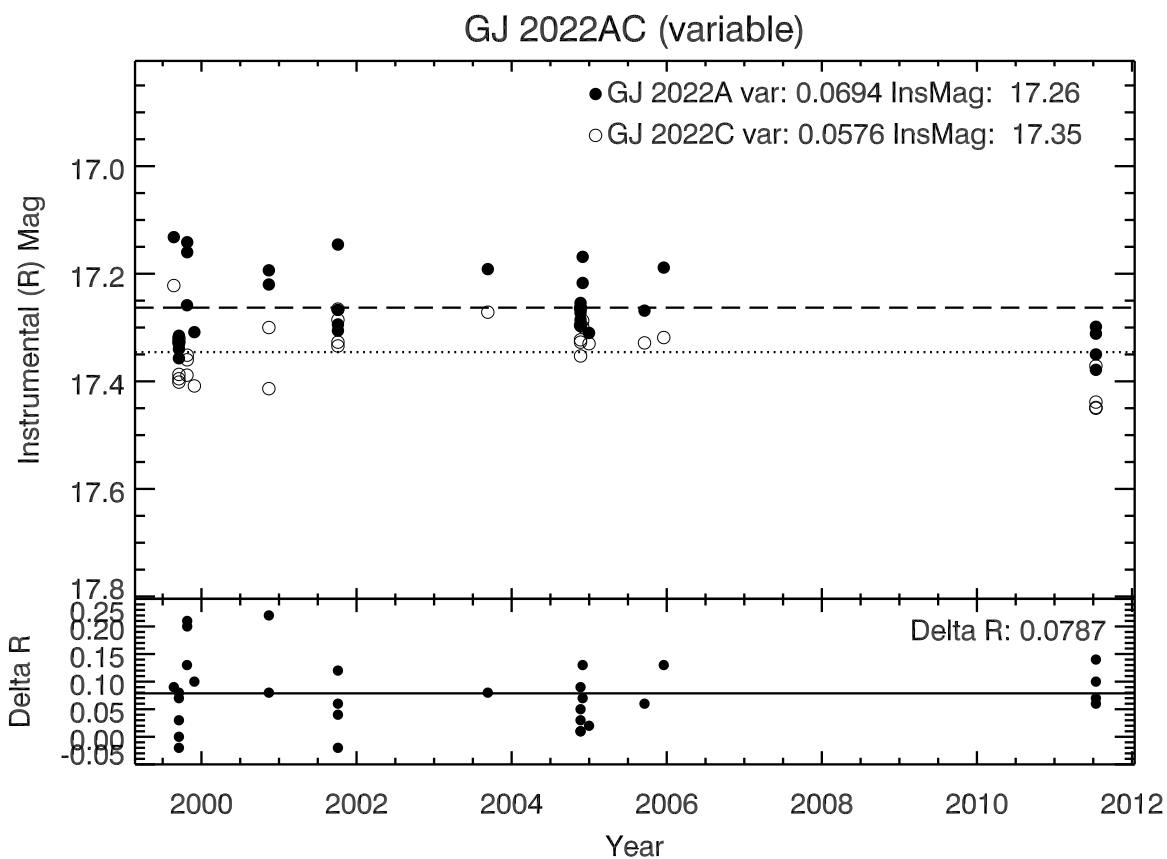


Figure 5.37: The variability of GJ 2022A and C. Given the proximity of the two components, our relative variability is unusually high, and probably contaminated by the other star's PSF.

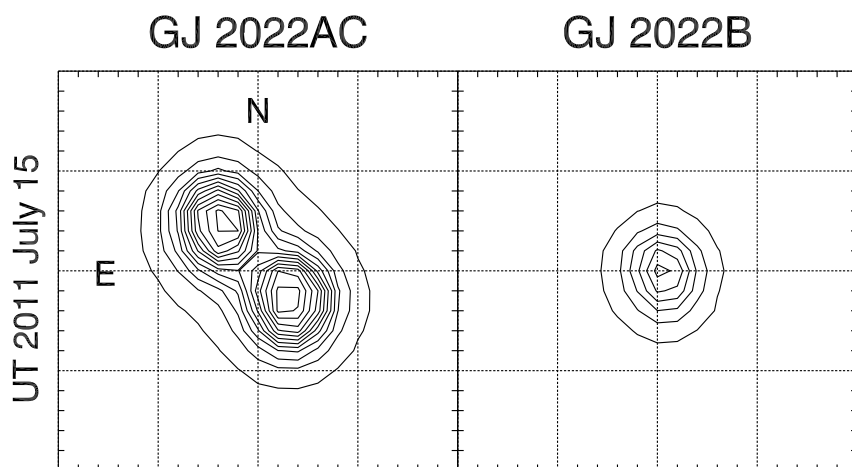


Figure 5.38: Contour plot of GJ 2022A (South) and C (North) on 2011 JULY 15. GJ 2022B (37.8'' distant) is also plotted as an example single-star PSF, with the same contour intervals. Grid lines are 2.05'' apart (5 pixels at the CTIO 0.9m).

The A and C components are close enough to each other (Figure 5.38) that their astrometry is contaminated, and C is often a saddle point on the PSF of A. They are separable on only 31 frames from 14 nights spanning 11.83 years; a separate reduction of all three components yields

1. GJ2022A:  $\pi = 40.91 \pm 5.64$  mas,  $\mu = 210.5 \pm 1.3$  mas yr<sup>-1</sup> @  $126.5 \pm 0.71^\circ$
2. GJ2022B:  $\pi = 42.12 \pm 3.60$  mas,  $\mu = 206.2 \pm 0.8$  mas yr<sup>-1</sup> @  $127.4 \pm 0.46^\circ$
3. GJ2022C:  $\pi = 46.96 \pm 5.31$  mas,  $\mu = 200.6 \pm 1.2$  mas yr<sup>-1</sup> @  $126.8 \pm 0.71^\circ$

This implies a mean parallax of  $43.05 \pm 2.63$  mas ( $23.2 \pm 1.4$  pc), which is consistent with our main reduction of B in Table 5.8 using 66 frames ( $38.80 \pm 2.13$  mas,  $25.8 \pm 1.4$ ) at the  $1.3\sigma$  level. Formally, we are using the parallax of the B component alone as our system parallax, but we do quote the individual proper motions of A and C in Table 5.14

We see tentative signs of the A-C orbit in terms of differential proper motion of the components,  $\Delta\mu_{RA \cos(DEC)} = -8.25 \pm 2.86$  mas yr<sup>-1</sup>,  $\Delta\mu_{DEC} = 5.61 \pm 2.38$  mas yr<sup>-1</sup>. We also see tentative signs of the A-B orbit in differential proper motions:  $\Delta\mu_{RA \cos(DEC)} = -4.91 \pm 1.71$  mas yr<sup>-1</sup>,  $\Delta\mu_{DEC} = -4.18 \pm 1.38$  mas yr<sup>-1</sup>. This amounts to very little orbital motion: on our first epoch (1998 AUGUST 23) A and C were  $1.8''$  @  $46^\circ$  apart, on our last epoch (2011 JULY 14) A and C were  $2.0''$  @  $43^\circ$  apart.

**L 173-019** ( $M_V = 12.33$ ,  $V - K_s = 5.13$ ) (from TINYMO)

This star was included in the NLTT catalog with  $\mu = 0.190''$  yr<sup>-1</sup>, but we find a smaller proper motion of  $\mu = 0.124''$  yr<sup>-1</sup>. It was identified with a distance of 8.3 pc by 11 plate

distance relations. It was put on the parallax and photometry observing lists immediately, where it was found to be  $7.8 \pm 1.2$  pc away by 12 CCD distance relations, and eventually at  $8.2 \pm 0.2$  pc by trigonometric parallax (to be presented in Henry et al., in prep). It appears to be a single main-sequence star.

**LHS 1358** ( $M_V=12.65$ ,  $V - K_s=5.41$ ) aka G 159-046

This system was classified as a UV Ceti flare star by Gershberg et al. (1999) and in the X-ray active sample of Fleming (1998), and a parallax was originally published by RECONS in Riedel et al. (2010). Mochnecki et al. (2002) reports  $vsini < 20$  km s<sup>-1</sup>. The system was also identified as a possible Hyades supercluster member in Eggen (1985, 1993) and Montes et al. (2001). We reproduce that kinematic assignment with our data, though we consider it spurious, as the star must be at least two tidal radii (10 pc) from the Hyades proper (45 pc) and therefore unbound.

**LP 993-115 (A)/LP 993-116AB (BC)** ( $M_V=12.12$ ,  $V - K_s=5.11$  (A),  $M_V=12.43$ ,  $V - K_s=5.49$  (BC))

The A component is also known as LTT 1339, CD-44 836A and is otherwise previously unnoted. The BC component (see Table 5.10) is also known as L 369-044, LTT 1341, CD-44 836B and RBS 353, and is  $44.8''$  from A at  $60.9^\circ$ . Bergfors et al. (2010) resolved the B component (which is noticeably closer than A by CCD photometric distance estimate, Table 5.9, because it is a binary) into two stars with a separation of  $0.257 \pm 0.001''$  @  $214.6 \pm 0.3^\circ$ ,  $\Delta z' 1.12 \pm 0.07$  mag.

We have independent astrometry for the A and BC components (a weighted mean parallax

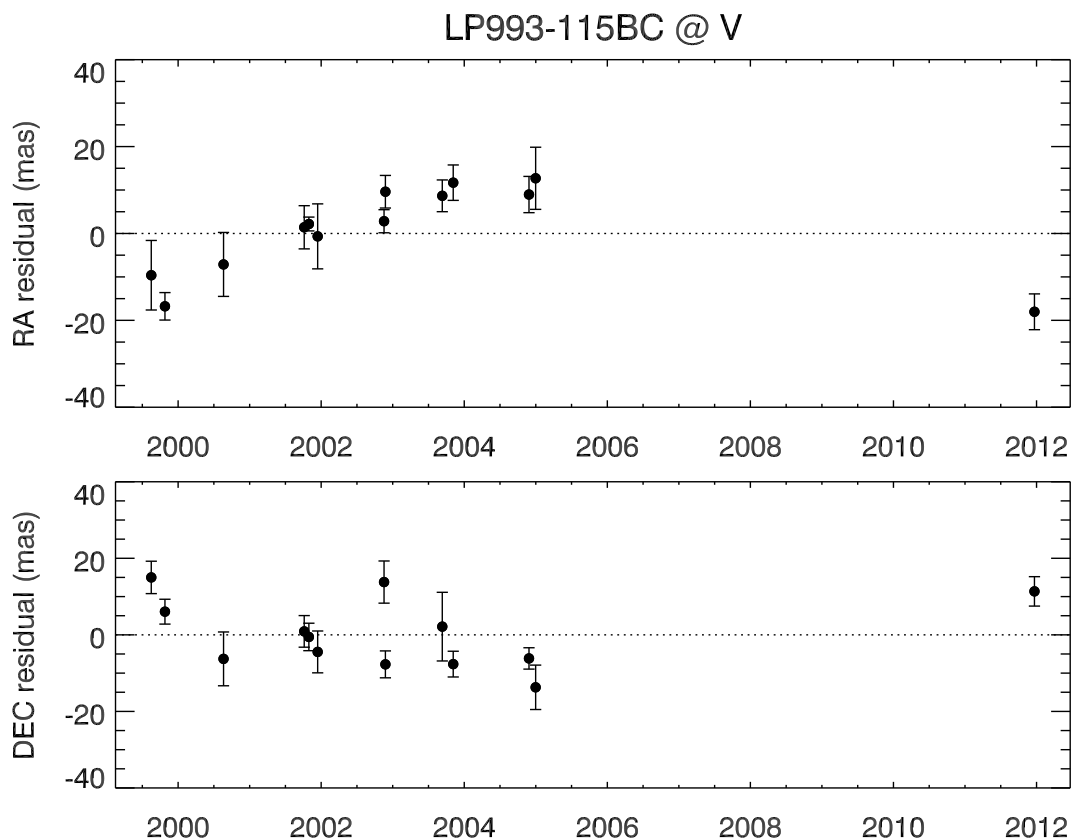


Figure 5.39: Nightly mean residuals of the LP 993-115BC (LP 993-116AB) parallax fit (after the parallax and proper motion have been removed) show a clear astrometric perturbation in both RA and DEC axes. This system is a known binary, but the orbit has not wrapped, and our orbit fit does not converge.

is given in Table [5.14](#)). With one night of astrometry in 2011 (six years after the previous epochs) we now see the astrometric orbital motion of the BC pair (Figure [5.39](#)), although our attempt to fit an orbit did not converge, and the astrometry in Table [5.8](#) was calculated without compensating for orbital motion. We find noticeable differential proper motion ( $\Delta\mu_{RA\cos(DEC)} = -11.58 \pm 0.37 \text{ mas yr}^{-1}$ ,  $\Delta\mu_{DEC} = -21.10 \pm 0.57 \text{ mas yr}^{-1}$ ) for the A and BC components over 12.4 years.

**2MA 0236-5203** ( $M_V=9.28$ ,  $V - K_s=4.56$ ) aka GSC8056-0482

This system was identified in [Zuckerman & Song \(2004\)](#) as a Tuc-Hor member. The star is more luminous than my  $\beta$  Pic isochrone, but its kinematics are not consistent with membership in  $\beta$  Pic or Tuc-Hor. The most plausible membership with a known association is with AB Dor, but the star is far too luminous and would need to be a multiple. The star is too hot for the Na I gravity index or K I EW to say anything about its youth.

**2MA 0254-5108AB** ( $M_V=9.21$ ,  $V - K_s=4.30$  (A),  $M_V=13.93$ ,  $V - K_s=6.36$  (B))

This binary system, with a separation of  $15.3''@ 80.2^\circ$  (see Table [5.10](#)), has the largest  $\Delta V$  (4.72) of any resolved system under consideration here; the astrometry for the B component therefore suffers due to its low SNR. The B component will be the reddest known member of Tuc-Hor with a parallax, if confirmed.

The preliminary trigonometric distances are discrepant at the  $1.9\sigma$  level, which may be caused by the low signal on B, or (alternately) taken as evidence that these are two separate members of Tuc-Hor serendipitously aligned on the sky. Assuming they are a bound system (and with the weighted mean system parallax), the A component is only marginally consistent with Tuc-Hor membership, and would need to be an equal-luminosity binary to fit the Tuc-Hor isochrone. Currently, the agreement with Tuc-Hor (for both components) actually improves if the parallaxes are *NOT* combined, and the two components are treated as separate star systems.

The system shares a single ROSAT X-ray detection; the value for the A component is likely more reflective of the real  $L_X/L_{bol}$ . There are no indications of orbital motion of the components.

**SCR 0336-2619** ( $M_V=13.22$ ,  $V - K_s=6.57$ ) (from TINYMO)

This system is definitely young. By kinematics, HR Diagram position and gravity features, it is a member of the TW Hydra association, but it is in the wrong part of the sky to be a genuine member. It is also kinematically consistent with being an  $\epsilon$  Cha member (for which it is unreasonably underluminous) or a Columba member (for which it is unreasonably overluminous).

**G 007-034** ( $M_V=13.16$ ,  $V - K_s=5.66$ ) aka LTT 11392

Gershberg et al. (1999) cite this star as a UV Ceti flare star. Zickgraf et al. (2005) find no Li EW ( $< 0.00006\text{\AA}$ ), and no measurable vsini. This system appears to be a member of AB Dor: the kinematics match, the HR diagram position is correct for AB Dor (or a high-metallicity main sequence star), and the gravity index indicates it has lower surface gravity than a main-sequence star. It lies in the same part of the diagram as another new suspected AB Dor member, GJ 2022B. There is no sign of multiplicity, in agreement with Law et al. (2008).

**2MA 0429-3123** ( $M_V=16.45$ ,  $V - K_s=7.62$ ) (from TINYMO)

Kinematics are a potential match for the Castor moving group, which would be consistent with the star's main-sequence position on the HR diagram.

**G 039-029AB** ( $M_V=12.04$ ,  $V - K_s=5.23$ ) aka LTT 11472

This system is a known flare star that was resolved into two components (see Table 5.10), separation  $0.54''$  @  $299^\circ$ , by Beuzit et al. (2004); the separation had increased to  $0.87''$  @  $301^\circ$  by Daemgen et al. (2007). Shkolnik et al. (2009) estimate the age as 60-300 Myr (no

youth indicators). [Gizis et al. \(2002\)](#) find it to be a rapid rotator at  $v \sin i = 30 \text{ km s}^{-1}$ , though they did not notice the binary and the lines may have been broadened artificially by its SB nature. Regardless, both components are main sequence stars.

**LP 476-207ABC** ( $M_V=9.55$ ,  $V - K_s=5.16$ ) aka HIP 23418

This system is a known  $\beta$  Pic member as noted in [Song et al. \(2003\)](#) with a radial velocity of  $18.4 \pm 3.0 \text{ km s}^{-1}$  and a cluster distance estimate of 36 pc. The poor *HIPPARCOS* parallax ( $30.12 \pm 9.56 \text{ mas}$  or  $33.2 \pm 10.5 \text{ pc}$ , compared to our  $40.67 \pm 2.12$  or  $24.5 \pm 1.3 \text{ pc}$ ) is probably due to incorrect coordinates in the Hipparcos Input Catalog, compounded by the close binary.

The system is a triple (see Table [5.10](#)) where the AC-B separation is  $0.97''$  with  $\Delta K=0.9$ , while AC is an SB2 binary with a period of  $\sim 12$  days discovered by [Henry et al. \(1997\)](#) (later recovered by [Delfosse et al. 1999](#) and [Balega et al. 2002](#)). [Messina et al. \(2010\)](#) find a rotation period of  $P=6.42 \pm 0.04$  days, though it is not clear which component of the system they refer to; their value may be confused by the presence of the SB2. [Scholz et al. \(2007\)](#) cites  $v \sin i = 7.67 \pm 2.08 \text{ km s}^{-1}$  for A, and  $v \sin i = 21.00 \pm 4.36 \text{ km s}^{-1}$  for B, apparently at odds with the idea of double lines being mistaken for rotational broadening. Finally, [Mentuch et al. \(2008\)](#) find  $\text{Li EW} = 0.020 \pm 0.021 \text{ \AA}$  (N) =  $0.020 \pm 0.022 \text{ \AA}$  (S)

**BD-21 01074ABC** ( $M_V=8.99$ ,  $V - K_s=4.29$  (A),  $M_V=9.66$ ,  $V - K_s=4.97$  (BC)) aka STEPHKM1-546/STEPHKM1-545, RBS 620

This is a visual double (A-BC) where the B component is itself a close binary (DON 93 in WDS) (see Table [5.10](#)). It is a known member of the  $\beta$  Pic association ([Torres et al. 2008](#)). [da Silva et al. \(2009\)](#) give  $\text{Li EW} = 0.020 \text{ \AA}$  for both A and BC, and estimate the

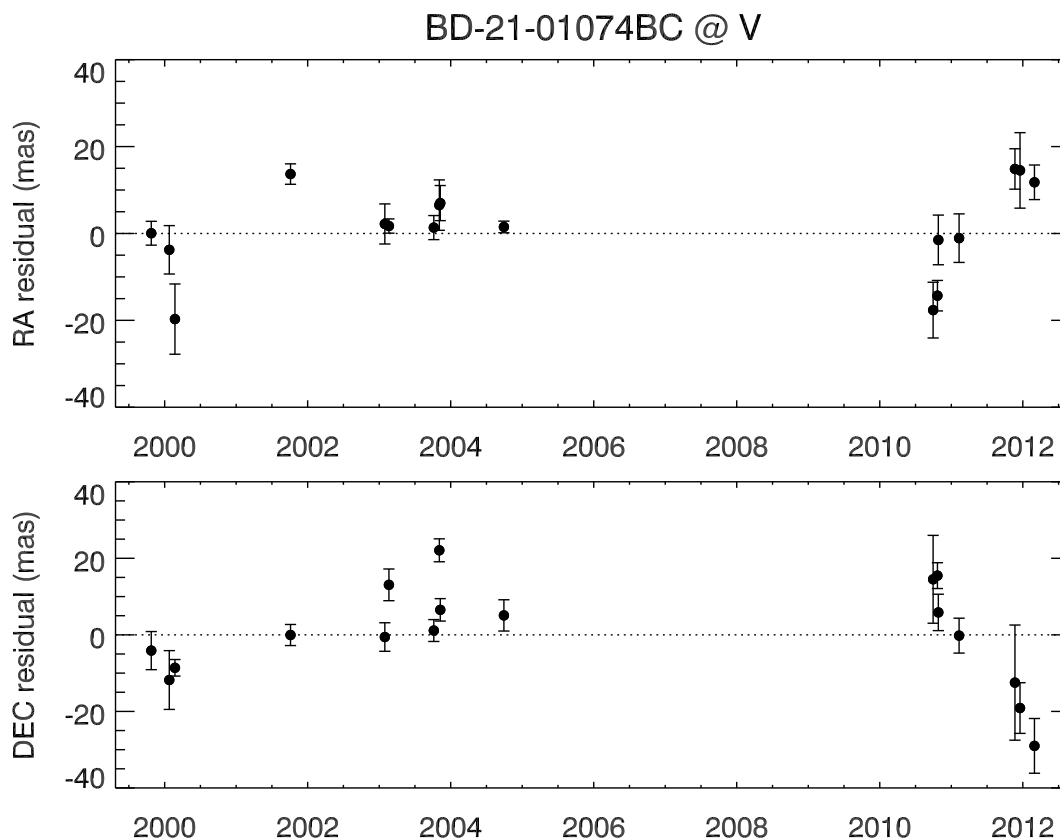


Figure 5.40: Nightly mean residuals of the parallax fit (after the parallax and proper motion have been removed) show a clear astrometric perturbation in both RA and DEC axes. This system is a known binary, but the orbit has not wrapped, and our orbit fit does not converge.

distance as 20pc. As the A component is extremely bright and was not originally targeted for parallax measurement, the weighted mean parallax in Table 5.14 is dominated by the contribution from the BC component. We see some signs of an astrometric perturbation in the BC residuals (Figure 5.40), as well as elongation of the BC PSF (Figure 5.41). WDS lists the most recent BC separation (2010) as  $0.8''$ , with  $\Delta mag=1.19$ , which I assume to be  $\Delta V$ .

Messina et al. (2010) find  $P_{rot}=13.3\pm 0.2$  days for (apparently) the A component. There is

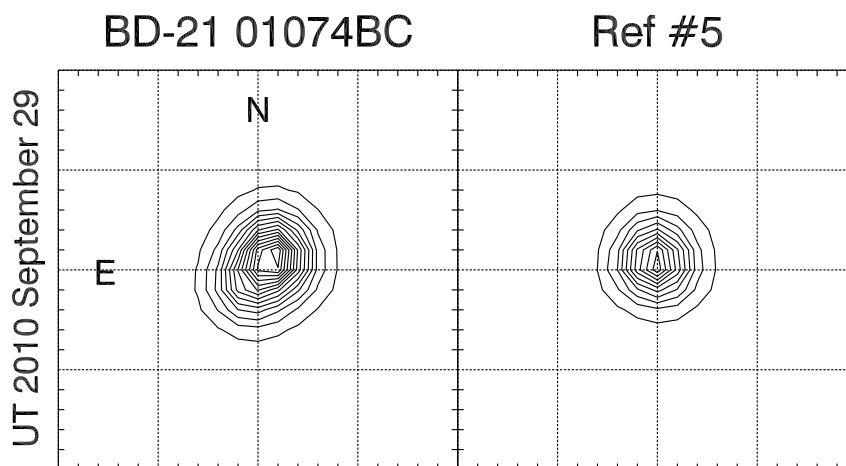


Figure 5.41: Contour plot of BD-21 01074BC on 2010 SEPTEMBER 29; the SE elongation is probably the C component, despite WDS claiming the position angle is  $321^\circ$  (we see the opposite). The nearest reference star (#5) is plotted as a representative single-star PSF, with  $4\times$  smaller contour intervals. BD-21 01074A is saturated on this frame and not shown. Grid lines are  $2.05''$  apart, 5 pixels at the CTIO 0.9m.

measurable differential proper motion between the two resolved components:  $\Delta\mu_{RA\cos DEC}=23.86\pm0.31$  mas yr $^{-1}$ ,  $\Delta\mu_{DEC}=24.38\pm0.49$  mas yr $^{-1}$ . This may have more to do with the BC orbital motion.

**HD 271076** ( $M_V=9.69$ ,  $V - K_s=4.31$ ) (from TINYMO)

This star lies in front of the Large Magellanic Cloud. [Westerlund et al. \(1981\)](#) reasonably suspected it was a supergiant in the LMC. At a distance of  $21.6\pm1.2$  pc, it is clearly a foreground star and a member of the Solar Neighborhood.

**L 449-001AB** ( $M_V=11.35$ ,  $V - K_s=5.13$ ) aka RBS 636 (from TINYMO, though not low proper motion)

[Janson et al. \(2008\)](#) call it an active star following [Scholz et al. \(2005\)](#), and find no companion with Spectral Differential Imaging. An astrometric companion with a  $\sim 2$  year period

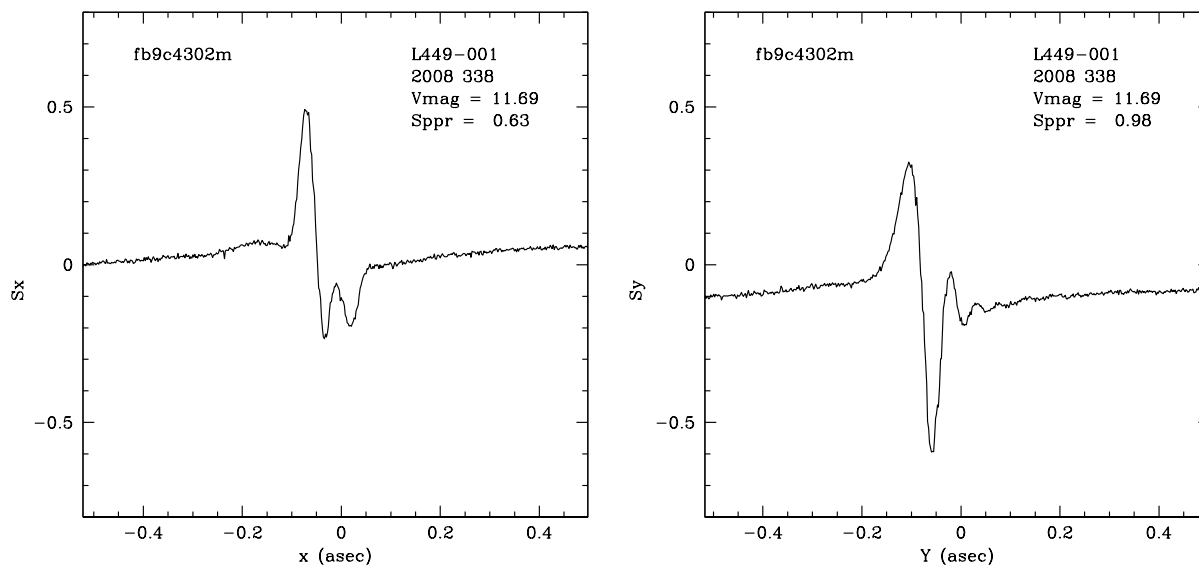


Figure 5.42: The X-axis (left) and Y-axis (right) Hubble Space Telescope Fine Guidance Sensor preliminary results for L 449-001AB. The X-axis “S-Curve” of the Fine Guidance Sensor shows a second dip to the right of the main one, revealing a companion (compare to the curve of SCR 0533-4257AB, Figure 5.45). The companion is not readily resolved in the Y-axis S curve. Figure by Ed Nelan.

(see Table 5.10) is visible in the data (Figure 5.43); the astrometry published in Table 5.8 has been computed with the orbit removed. This system was on the HST Cycle 16 FGS proposal, and was resolved into two stars (Figure 5.42) with  $\Delta V \approx \Delta FGS = 1.1$  mag. While the system appears to be comprised of main sequence stars, its kinematics agree with the Ursa Major moving group.

**SCR 0529-3239** ( $M_V=11.86$ ,  $V - K_s=5.47$ ) (from TINYMO)

The system was found to be an X-ray bright star in Riaz et al. (2006), and is apparently single. It is kinematically consistent with the  $\beta$  Pic (12 Myr) association, although its HR diagram position is somewhat underluminous.

**SCR 0533-4257AB** ( $M_V=12.57$ ,  $V - K_s=5.46$ ) (from TINYMO)

This system was noted by Riaz et al. (2006) as an X-ray emitting star, appears to be a binary at  $10.07 \pm 0.17$  pc. As part of my X-ray bright sample, it was included in the

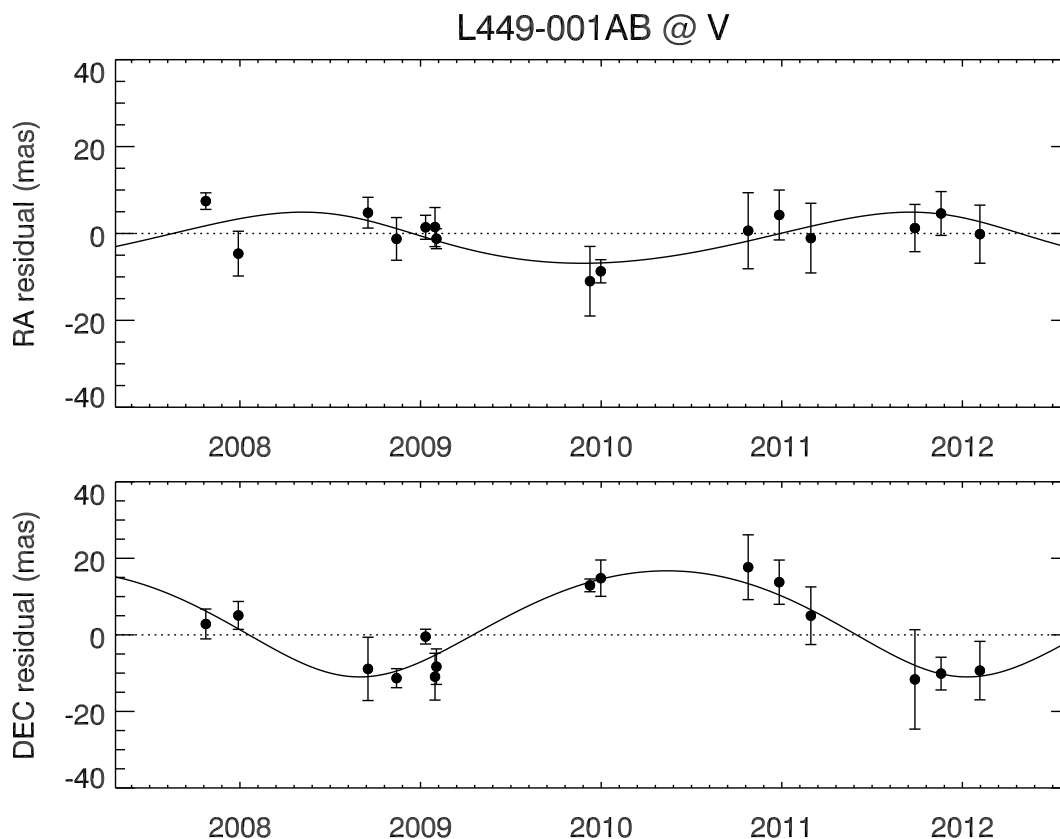


Figure 5.43: Nightly mean residuals of the parallax fit (after the parallax and proper motion have been removed) show a clear astrometric perturbation in both RA and DEC axes. This system has been resolved by HST-FGS and our orbit has wrapped.

FGS Cycle 16B proposal, where it was resolved (Figure 5.45) into a close binary (see Table 5.10) with a 56 mas separation and  $\Delta FGS=0.7$  mag, which implies a projected separation between the components of 0.56 AU, and hence its X-ray flux is not due to the components' interactions. The measured parallax of the system has varied greatly as the orbital motion (Figure 5.44) was mapped. At one point, the preliminary distance was 12 pc away; it may yet be within 10 pc of the Sun, which would make the lowest proper motion nearby star ( $35.5 \pm 1.4$  mas yr<sup>-1</sup>) within 10 pc, slower-moving than SCR 2049-4012 at  $\mu=64.6 \pm 1.4$  mas yr<sup>-1</sup>. The large position angle error in Table 5.8 is due to this small proper motion; the

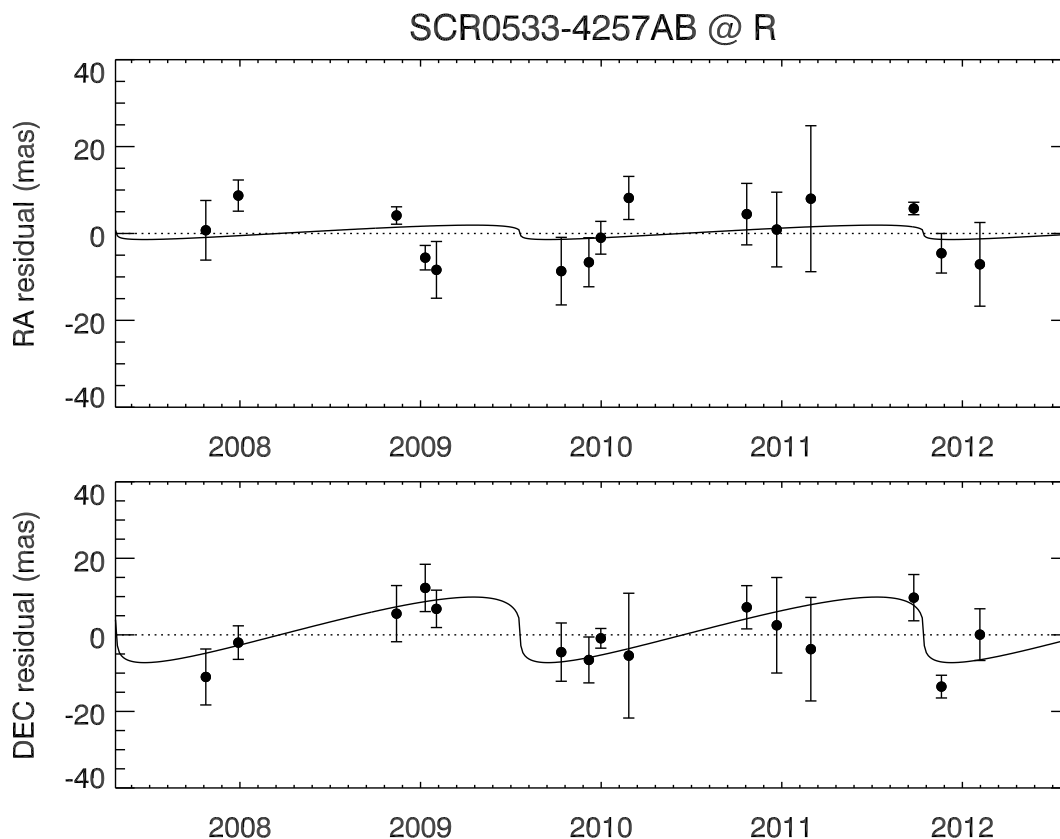


Figure 5.44: Nightly mean residuals of the parallax fit (after the parallax and proper motion have been removed) show an astrometric perturbation in both RA and DEC axes. This system has been resolved by HST-FGS, but the orbit is too messy to cleanly extract from our dataset, and we do not believe the current orbit.

proper motion errors themselves are no worse than for other stars on the program. The astrometry of this target was calculated with the most recent fitted orbit removed.

Given the X-ray emission, the system is probably young; with its combined colors it is an M3.5V star. The kinematics of the system (without radial velocity) suggest it may be a barely pre-main-sequence member of the 200 Myr old Castor moving group, which is consistent with Na I gravity measurements and HR diagram positions indistinguishable from a main-sequence star. Without a radial velocity or a measurement of the star's chemical

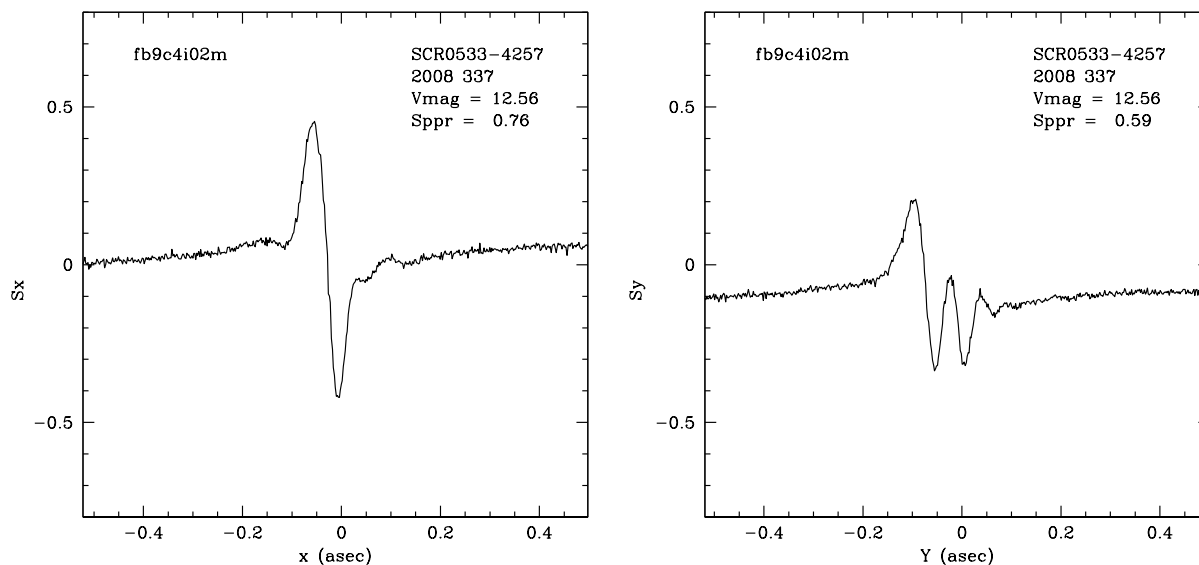


Figure 5.45: The X-axis (left) and Y-axis (right) Hubble Space Telescope Fine Guidance Sensor preliminary results for SCR 0533-4257AB. The Y-axis “S-curve” of the Fine Guidance Sensor shows a second dip to the right of the main one (compare to the Y-axis curve of L 449-001AB, Figure 5.42), revealing a companion. The companion is also resolved in the X-axis S curve, though it is not visibly apparent. Figure by Ed Nelan.

abundances, this identification is merely speculative.

**G 099-049** ( $M_V=12.73$ ,  $V - K_s=5.27$ ) aka LTT 17897, PLX 1383.02

By kinematics, this system is consistent with membership in the Hyades cluster, according to both Montes et al. (2001) and my analysis; however, at only  $5.19 \pm 0.03$  pc from the Sun, it’s a minimum of 40 pc (4 tidal radii) from the Hyades cluster.

**SCR 0613-2742AB** ( $M_V=9.98$ ,  $V - K_s=5.16$ ) (from TINYMO)

This system is the lowest-proper-motion ( $10.7 \pm 0.7$  mas yr<sup>-1</sup>) nearby star ( $29.2 \pm 0.8$  pc) in TINYMO, my thesis, and all of CTIOPI, with a transverse velocity of  $1.5$  km s<sup>-1</sup>. It was identified by Riaz et al. (2006) as X-ray bright. As with SCR 0533-4257AB, the enormous error on the position angle in Table 5.8 is the result of this small proper motion, which is barely distinguishable from zero.

This system was included in the FGS Cycle 16 proposal, where it was resolved (Figure

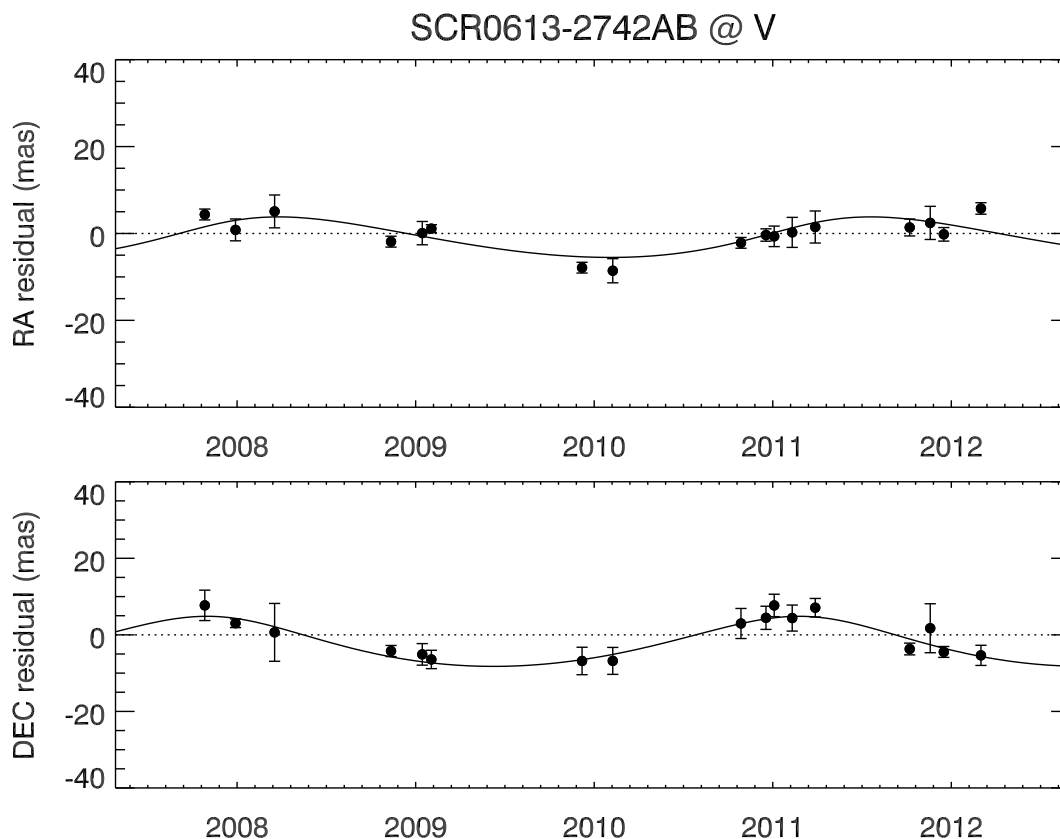


Figure 5.46: Nightly mean residuals of the parallax fit (after the parallax and proper motion have been removed) show a clear astrometric perturbation in both RA and DEC axes. We have resolved this binary with FGS, but the orbit seems to be stuck in a false minimum.

[5.47](#)) into a binary (see Table [5.10](#)) with a separation of 92.5 mas and  $\Delta V \approx \Delta FGS=0.6$ .

More recently, the orbital motion of the system has begun showing up in our astrometric residuals (Figure [5.46](#)); it has a period of at least 4 years; we believe the current “wrapped” orbit is incorrect, as the current period produces an anomalously high system mass. The astrometry published in Table [5.8](#) has been computed with the orbit removed.

This system’s kinematics and isochrone position are consistent with membership in the  $\beta$  Pic Association, with a best-fit radial velocity of  $+21.5 \text{ km s}^{-1}$ , and deblended color-magnitude positions that also lie along the  $\beta$  Pic isochrone. The gravity features (Figure

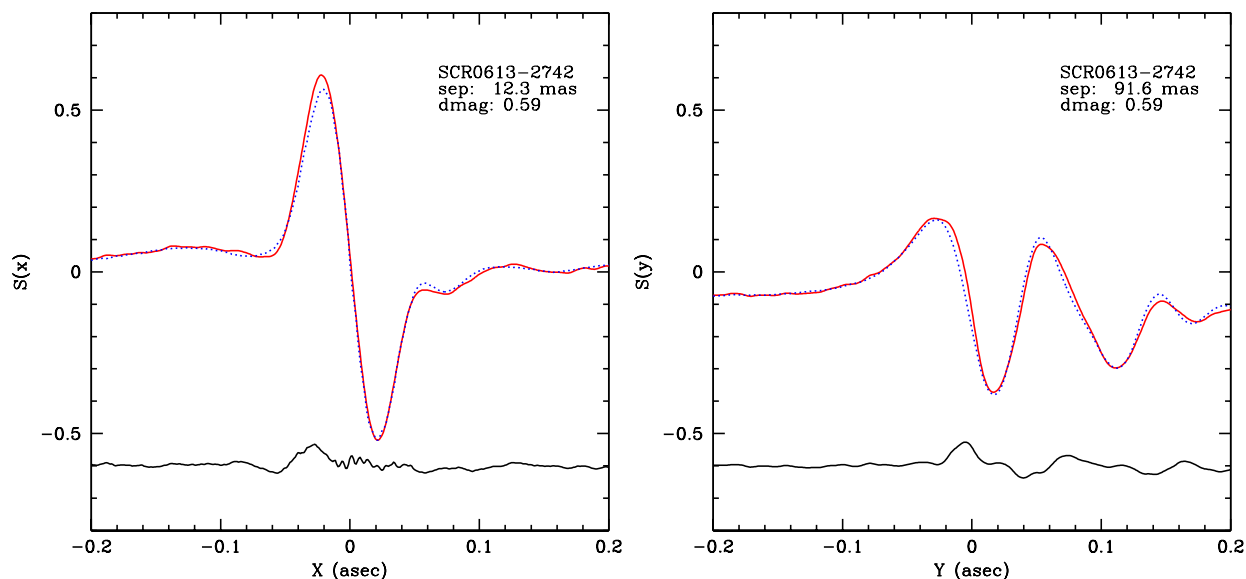


Figure 5.47: The X-axis (left) and Y-axis (right) Hubble Space Telescope Fine Guidance Sensor results for SCR 0613-2742AB. The Y-axis “S-curve” of the Fine Guidance Sensor shows a second dip to the right of the main one (compare to the axes of L 449-001AB, Figure 5.42 and SCR 0533-4257AB, Figure 5.45), revealing a companion. The companion is also barely resolved at  $\pm 12$  mas (near the limit of FGS’s capabilities) in the X-axis, though this is not visibly apparent, and carries a sign ambiguity. Figure by Ed Nelan.

5.35) indicate this system is lower-gravity than a main-sequence star, and roughly equivalent to the EW of BD-21 1074BC, which is a known binary member of  $\beta$  Pic.

**L 034-026** ( $M_V=11.17$ ,  $V - K_s=4.73$ )

The SIMBAD astrophysical database lists it as a pre-main-sequence star as of 03 MAY 2012, but offers no reason why. Torres et al. (2006) note a  $v_{\text{ sini}}$  of  $8.1 \text{ km s}^{-1}$ . The star’s position is along the high-metallicity envelope of the main sequence. A published radial velocity ( $1 \text{ km s}^{-1}$ , no error) from Torres et al. (2006) puts its space velocity near the Ursa Major moving group, but I cannot offer any further evidence of membership, as Ursa Major stars are indistinguishable from main-sequence stars in terms of gravity and HR diagram position.

**SCR 0757-7114** ( $M_V=10.74$ ,  $V - K_s=5.04$ ) (from TINYMO)

This system is overluminous by 2 magnitudes, plotting near the  $\beta$  Pic isochrone on an HR diagram, yet shows no other signs of youth – in fact, it is one of very few stars under consideration with  $H\alpha$  *absorption*. Thus, the star’s elevation on the HR diagram is most likely due to unresolved multiplicity.

**G 041-014ABC** ( $M_V=11.77$ ,  $V - K_s=5.23$ ) aka LHS 6158, LTT 12352, RBS 0732

This hierarchical system (AB-C separation  $0.62''$ ,  $\Delta K=0.5$ ; AB is a 7.6 day SB2, see Table 5.10) was described in Delfosse et al. (1999). The large error on the radial velocity from Gizis et al. (2002) ( $-6.4 \pm 19.0$  km s $^{-1}$ ) appears to produce a false kinematic agreement with the Ursa Major moving group and the Castor moving group.

**G 161-071** ( $M_V=13.04$ ,  $V - K_s=6.16$ ) aka WT 1683

This star is very active in  $H\alpha$  and X-rays, has a low surface gravity by the Na I index, and is clearly pre-main-sequence as seen in Figure 5.28. Its kinematics are consistent with Argus, but it is too luminous to be a member unless it’s a nearly-equal luminosity binary. There are no trustworthy signs of perturbation in the residuals of G 161-071, yet. If it *is* a binary member of Argus, the B component will be the reddest known member of the association with a parallax.

**SCR 1012-3124AB** ( $M_V=9.85$ ,  $V - K_s=5.52$ ) (from TINYMO)

This system is a close  $\sim 1''$  binary (Figure 5.48, Table 5.10). There are a few epochs where the B component (to the east of the A component) can be seen, but for the most part the two components are blended. Unlike other cases (GJ 2022AC, SIP 1110-3731ABC)

where frames have been discarded when both components cannot be centroided, I have not thrown out any frames in the astrometric reduction, or made any attempt to measure the parallax of the B component. As with the reduction of LHS 1955A in Riedel et al. (2010), there is a concern that I am not uniformly centroiding on the A component, particularly in this case where the system appears to be young and the B component may occasionally be brighter. Nevertheless, the reduction appears clean: the parallax errors are normal, there is no apparent astrometric perturbation – all residuals after parallax and proper motion were removed are within 40 mas of zero (and show no sign that the B component ( $\sim 1000$  mas away) was ever accidentally centroided), and the parallax has remained consistently 15–20 mas over time.

The system appears to be a member of the TW Hydra association by kinematics, HR diagram position, and Na I gravity index. While it lies slightly outside the spatial limits of the TW Hydra association (as defined in Torres et al. 2008), the mismatch is not nearly as bad as for SCR 0103-5515, 2MA 0123-6921 or SCR 0336-2619, so I am more inclined to treat this as a genuine member. As with those stars (and TWA 27), there are no noticeable X-rays, which may be a distance effect. Alternately, this system is kinematically consistent with  $\beta$  Pic, Columba, and Castor, but it is too luminous for any of those associations.

**SIP 1110-3731ABC=TWA003ABC** ( $M_V=9.07$ ,  $V - K_s=5.29$ ) aka HEN 3-600 (from TINYMO)

This system was one of the first potential members of the TW Hya association (de la Reza et al. 1989), and has for some time been considered the closest genuine member<sup>20</sup>. Zuckerman & Song

<sup>20</sup>TWA 22AB, at  $17.5 \pm 0.2$  pc, is now widely believed to be a nonmember (Mamajek 2005; Teixeira et al.

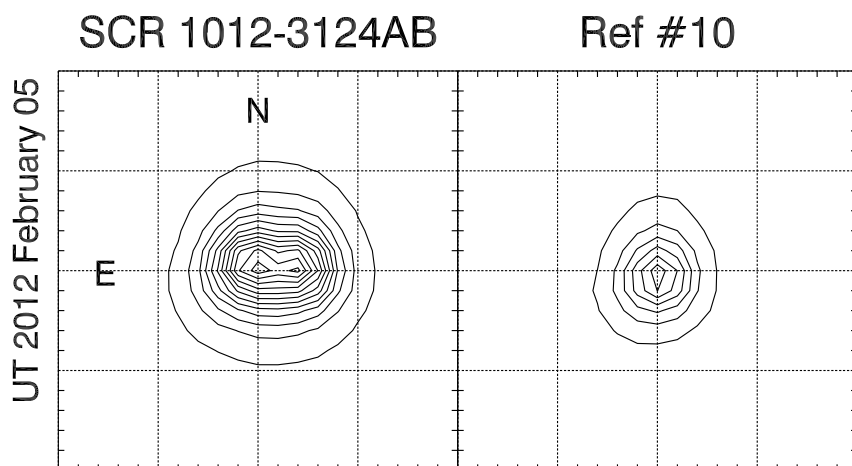


Figure 5.48: Positions of SCR 1012-3124A (E) and B (W) on a rare night where they are resolved. Reference star #10 is also plotted for a comparison of a single-star PSF from the same night, with the same contour intervals. Grid lines are  $2.05''$  apart, or 5 pixels at the CTIO 0.9m.

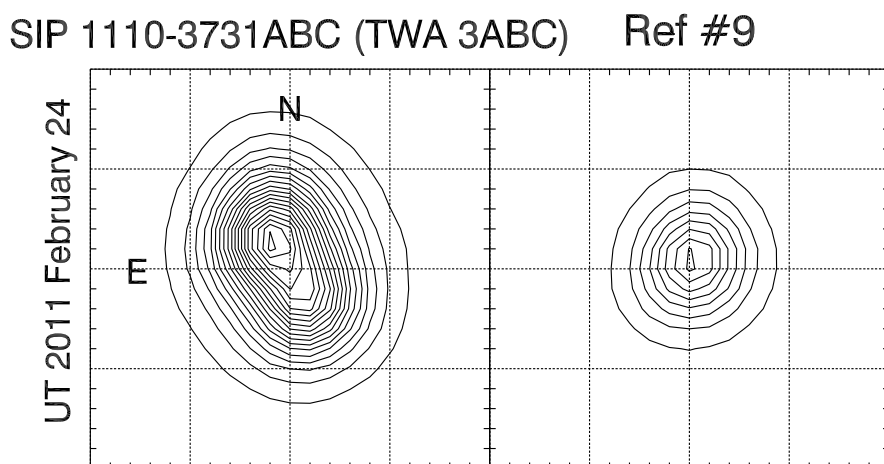


Figure 5.49: Positions of TWA 3 AC (N) and B (S) on 2011 FEBRUARY 24. TWA 3B often appears as an elongation of the TWA 3AC PSF, making reduction difficult. Reference star #9 is also shown as an example single-star PSF, with the same contour intervals. Grid lines are  $2.05''$  apart, or 5 pixels at the CTIO 0.9m.

(2004), Webb et al. (1999) claim that this system is a triple (see Table 5.10) where A is a spectroscopic binary (presumably SB2; with no other information given we assume  $\Delta V = \Delta K = 0$ , which makes B the actual brightest component) but we see no signs of the third component. As the visual components of the system (see Table 5.10) are separated by  $1.2''$  (Figure 5.49) and nearly equal magnitude (Figure 5.50), many frames where seeing rendered the two stars indistinguishable had to be thrown out, and most of the SExtractor output had to be manually edited to correctly identify the B component. The resulting parallaxes in Table 5.8 are poor and show signs of contamination, and the measured variability is probably unreliable. Nevertheless, the combined weighted mean result ( $39.6 \pm 3.8$  pc) is close to the expected distance to the system (42 pc) based on kinematics in Zuckerman & Song (2004). The astrometry also confirms each star is a potential member of the TW Hydra association, though only TWA 3B has a published radial velocity consistent with the predicted best-fit value.

We see minimal signs of orbital motion in the form of differential proper motion between the two components, and the errors (and contamination of the astrometry) are quite apparent in our poor relative proper motions:  $\Delta\mu_{RA \cos DEC} = 20.16 \pm 10.92$  mas yr<sup>-1</sup>,  $\Delta\mu_{DEC} = 34.93 \pm 12.13$  mas yr<sup>-1</sup>. The separation of the two components as measured on our images on 02 APRIL 2012 is  $1.16'' @ 210.2^\circ$ . This agrees with WDS.

**RX 1132-2651AB=TWA 008AB** ( $M_V=8.87$ ,  $V - K_s=4.80$  (B),  $M_V=11.84$ ,  $V - K_s=6.19$  (B)) aka V0550 Hya/V0549 Hya, RBS 994

Both components of this system were discovered by Webb et al. (1999), and recovered (2009), and probably  $\beta$  Pic instead.

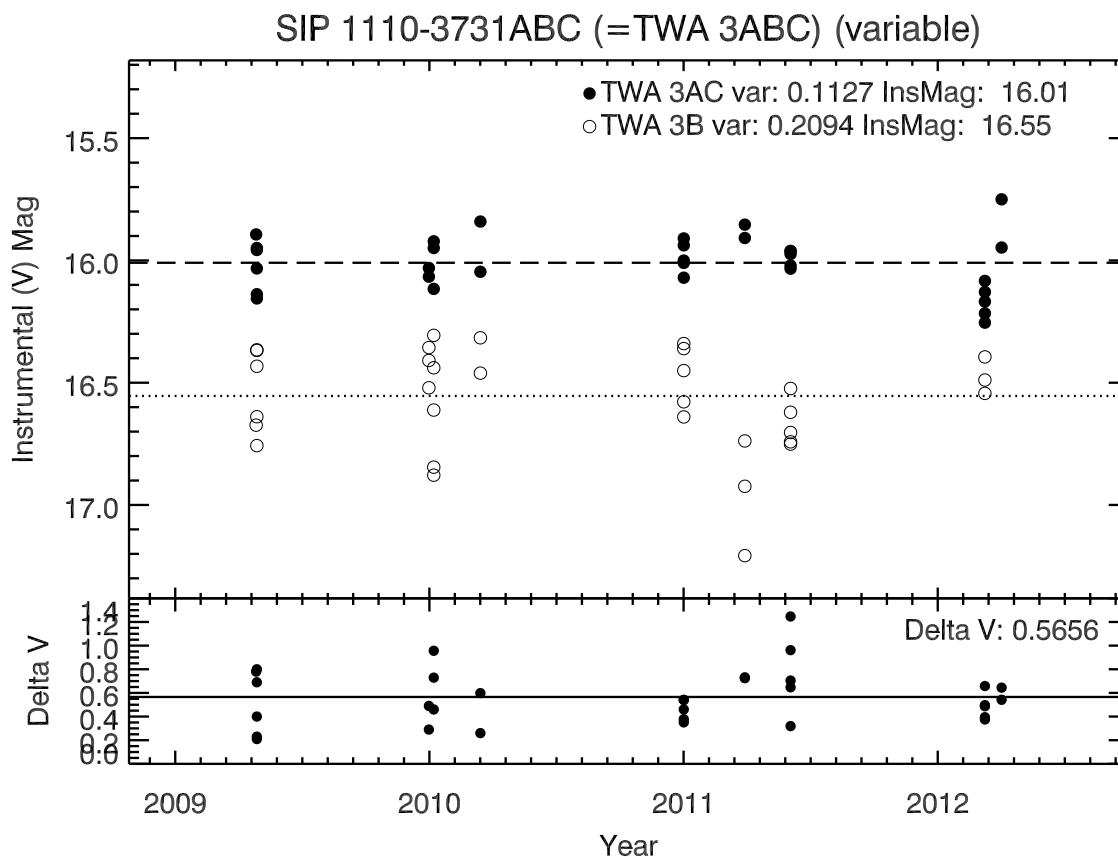


Figure 5.50: The variability of TWA 3 AC and B. Given the spatial proximity of the stars and the contamination of their PSFs, I doubt the nightly spread in instrumental magnitudes is accurate.

by RECONS in [Jao et al. \(2003\)](#) (as RXJ1132-264). The two components (see [Table 5.10](#)) are separated by  $13.1''$  @  $184.7^\circ$ . We present independent distances to both the A and B components, and a combined system parallax in [Table 5.14](#). As expected, our kinematic, isochronal, and gravity diagnostics all agree the system is a member of TW Hya. We see evidence of orbital motion in terms of differential proper motion of the components:  $\Delta\mu_{RA\cos DEC} = -0.24 \pm 0.09$  mas yr $^{-1}$ ,  $\Delta\mu_{DEC} = -3.40 \pm 0.14$  mas yr $^{-1}$ . There is only one ROSAT point for the system, so the  $L_x$  and  $L_x/L_{bol}$  measurements are for the entire system (and should really refer to the system's combined flux).

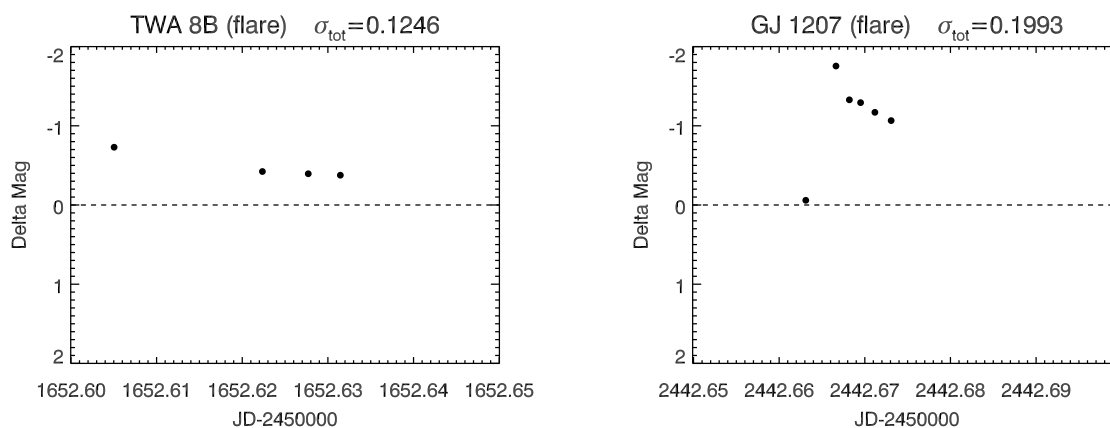


Figure 5.51: Two large partial flares observed in CTIOPI; Note the timescale of the observations; each was observed for less than an hour. We observed the peak of the GJ 1207 flare from 2002 JUNE 17 (which rose in less than 5 minutes), but not the TWA 8B flare from 2000 APRIL 18. Given that each was observed for less than an hour, it is difficult to tell which had a higher peak, was longer-lasting, or had more total energy. The  $\sigma_{tot}$  scatter values are highly biased by these flare events. The zero point of the delta magnitudes were set by all the other reference stars in the astrometric solution.

In addition, as noted in [Jao et al. \(2003\)](#), we have observed part of a flare on the B component in our variability data. It is reproduced in [Figure 5.51](#).

### **2MA 1207-3239AB=TWA 027AB** ( $M_V=16.35$ , $V - K_s=8.01$ )

Discovered by [Gizis et al. \(2002\)](#), this TW Hya member is an M8 brown dwarf with an even lower-mass companion ([Chauvin et al. 2004](#)) with separation  $0.8''$  @  $126^\circ$  (see [Table 5.10](#)). A CTIOPI parallax was published in [Gizis et al. \(2007\)](#), followed by others in [Biller & Close \(2007\)](#) and [Ducourant et al. \(2008\)](#). I confirm its membership in TW Hydra based on our available kinematics, and note the published radial velocity is also consistent with TW Hydra membership.

As I have no spectra to measure, I cannot remark on its  $H\alpha$  emission or Na I indices. It does not appear in the ROSAT catalogs, as expected for a star of its distance and low

bolometric luminosity.

**DEN 1306-7723** ( $M_V=12.42$ ,  $V - K_s=7.78$ ) (from TINYMO)

This system is the most overluminous in my sample; it is most definitely not a giant, but the measured distance ( $107\pm 16$  pc) puts it beyond the range where CTIOPI can get a useful result; for this reason it was dropped from the program, and will likely never be published anywhere apart from this dissertation. It is a known member of the Chamaeleon II Dark Cloud (distance  $\sim 160$  pc), which implies our measured distance may be wrong (especially considering how comparatively large the correction to absolute is, plus the possibility that the rest of the reference field is in Chamaeleon II<sup>21</sup> as well).

Reference star #15 ( $32.1''$  @  $4.6^\circ$ ) is the more famous Chamaeleon II member 2MASS J13065744-7723415 (Spezzi et al. 2008), which appears to be at the same distance, with the following parameters:

- DEN 1306-7723:  $\pi=9.27\pm 1.41$  mas,  $\mu=16.8\pm 2.7$  mas,  $P.A.=265.0\pm 14.27$
- 2MASS J13065744-7723415:  $\pi=9.74\pm 1.51$  mas,  $\mu=13.4\pm 2.9$  mas,  $P.A.=253.6\pm 21.79$

This star is the most variable non-Mira I have seen, with relative variability in  $I$  band of 0.445 mag. If SIMBAD's spectral type (K5) is correct, it may be heavily self-reddened and still accreting, as it has the same  $I$  magnitude as the M4.5Ve star DEN 1306-7723. The stars have overlapping  $\pi$  and  $\mu$  vectors, and a projected separation of 5000 AU (if 160 pc away) or 3500 AU (if 107 pc away), which might make them plausibly members of the same star system, with 2MASS J13065744-7723415 as the system primary (see Table 5.10). In that

---

<sup>21</sup>Reference star #15 was not included in the astrometric solution of DEN 1306-7723.

case, the weighted mean system parallax is  $9.49 \pm 1.03$  mas ( $105 \pm 11$  pc), and this would be the first RECONS example of a companion discovered through parallax.

**LHS 2729** ( $M_V=12.16$ ,  $V - K_s=5.11$ ) aka L 617-035, LP 855-010, LTT 05161

Gershberg et al. (1999) calls this system a flare star. König et al. (2003) find that it is a foreground object and not a TW Hya member despite similar sky location. We find no reason to suspect that this star is young. This system was first published in Riedel et al. (2010).

**G 165-008AB** ( $M_V=10.74$ ,  $V - K_s=5.30$ ) aka DG CVn, LP 323-158, RBS 1280

This system is a known flare star, and was identified as young by Montes et al. (2001). It was resolved into two components (see Table 5.10) by Beuzit et al. (2004) separated by  $0.17''$  @  $253.3^\circ$ , with  $\Delta K = 0.16$  mag, and remarked therein as a magnetically active X-ray source. The system is identified as an ultra-fast rotator in both Delfosse et al. (1998) ( $v_{\text{sini}} = 50 \text{ km s}^{-1}$ ) and Gizis et al. (2002) ( $v_{\text{sini}} = 80 \text{ km s}^{-1}$ ), though neither knew about its binary nature. This system is the most northerly parallax target CTIOPI has attempted, at DEC= +29. The astrometry therefore suffers from the effects of perpetual high airmass, and we cannot see any evidence of orbital motion in the large scatter of the parallax residuals.

Both components of the system are clearly overluminous when deblended (see Figure 5.28), lying somewhere between the  $\beta$  Pic isochrone and the AB Dor isochrone/Main Sequence. Its kinematics are consistent with both Tuc-Hor or  $\epsilon$  Cha, with Tuc-Hor being the better match, and its position on our Na I index gravity plot (Figure 5.34) is also consistent with it being a member of Tuc-Hor.

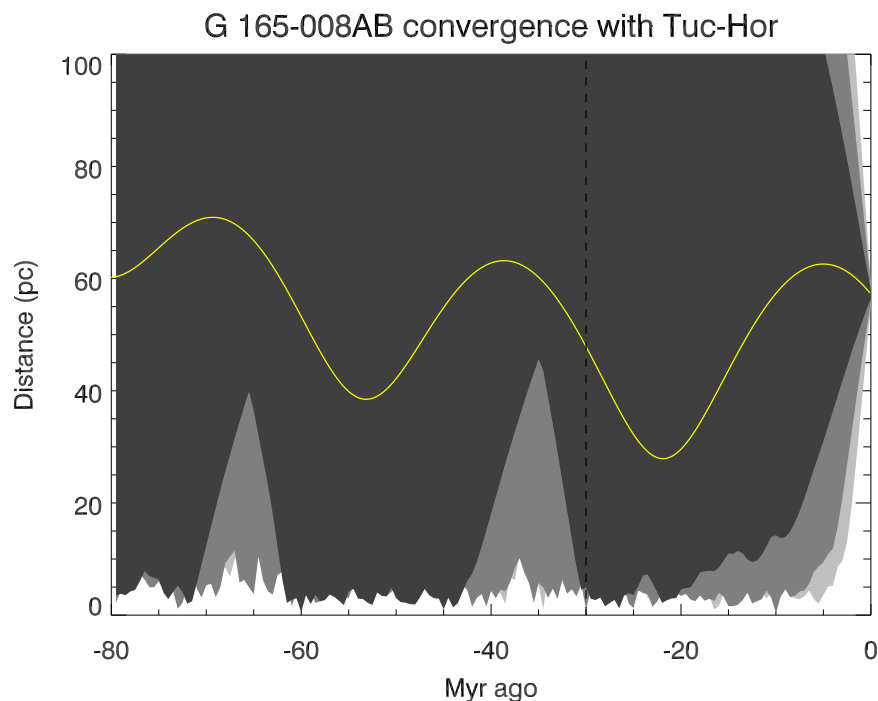


Figure 5.52: Plot of the separation between G 165-008AB and the Tuc-Hor association (represented by HD 2884 and the UVW velocity in Torres et al. 2008) as a function of time, going backwards into the past (leftward). The plot shows the result of 6000 sets of UVW velocities within  $1\sigma$  (dark gray),  $2\sigma$  (medium gray), and  $3\sigma$  (light gray) error bounds, while the current path is traced in yellow. G 165-008AB converges to within 5 pc of with Tuc-Hor at the  $1\sigma$  level between 10-30 Myr ago.

There are some serious counter-indications to its membership in Tuc-Hor, however. Montes et al. (2001) publishes a radial velocity of  $+4.0 \pm 0.1$  km s<sup>-1</sup> for this star, which is inconsistent with Tuc-Hor. Its spatial location is also wrong. Most of the Tuc-Hor association is  $\sim 50$  pc away and between 17h-07h RA (Torres et al. 2008; Zuckerman et al. 2011), but G 165-008AB is less than 20 pc from the Sun at 13h RA, which places it  $\sim 70$  pc from the rest of the group, although kinematic traceback with a Galactic potential puts it believably within Tuc-Hor 20-30 Myr ago, as shown in Figure 5.52.

While a greater physical extent makes sense for an older cluster, G 165-008AB is well

outside the space distribution of Tuc-Hor defined in Torres et al. (2008). Either Tuc-Hor is much larger (part of a larger complex of 30 Myr old clouds, as suggested by Torres et al. 2008, who combine Tuc-Hor, Columba, and Carina) or G 165-008AB is something else entirely.

**SCR 1425-4113** ( $M_V=8.55$ ,  $V - K_s=5.03$ ) (from TINYMO)

This system is consistent, via kinematics, HR diagram position (over 4 magnitudes above the main sequence), and Na I gravity index, with the TW Hydra association. Like SCR 1012-3124AB, it is outside the spatial bounds of the TW Hydra association as published in Torres et al. (2008), but it is close enough to be considered a potential member. While SCR 1425-4113 lies above the TW Hydra isochrone in Figure 5.28 if it is a binary, it may yet be a member. The system is also consistent with being a member of the  $\beta$  Pic and Castor associations, but is too overluminous for either even if it were a binary.

**SCR 1609-2222** ( $M_V=10.36$ ,  $V - K_s=6.49$ ) (from TINYMO)

This system, like DEN 1306-7723, is too far away for CTIOPI to obtain a useful parallax result, and has been dropped from the program. By sky location, it may be a member of the Upper Scorpius region of the Sco-Cen star forming region, which suggests our distance may be approximately correct (if useless, with a 42% error), and the star really is less than 10 Myr old.

**GJ 2122AB** ( $M_V=9.04$ ,  $V - K_s=3.95$ ) aka HIP 82021, HD 150848, CD-38 11189

This system was found to be a binary in Heintz (1987) (at the CTIO 0.9m, at the time outfitted with photographic plates) with separation  $0.59''$  and  $\Delta mag=2.0$  (see Table 5.10); it also shows up as an astrometric binary (Figure 5.53) in our data. Wei-Chun Jao's most

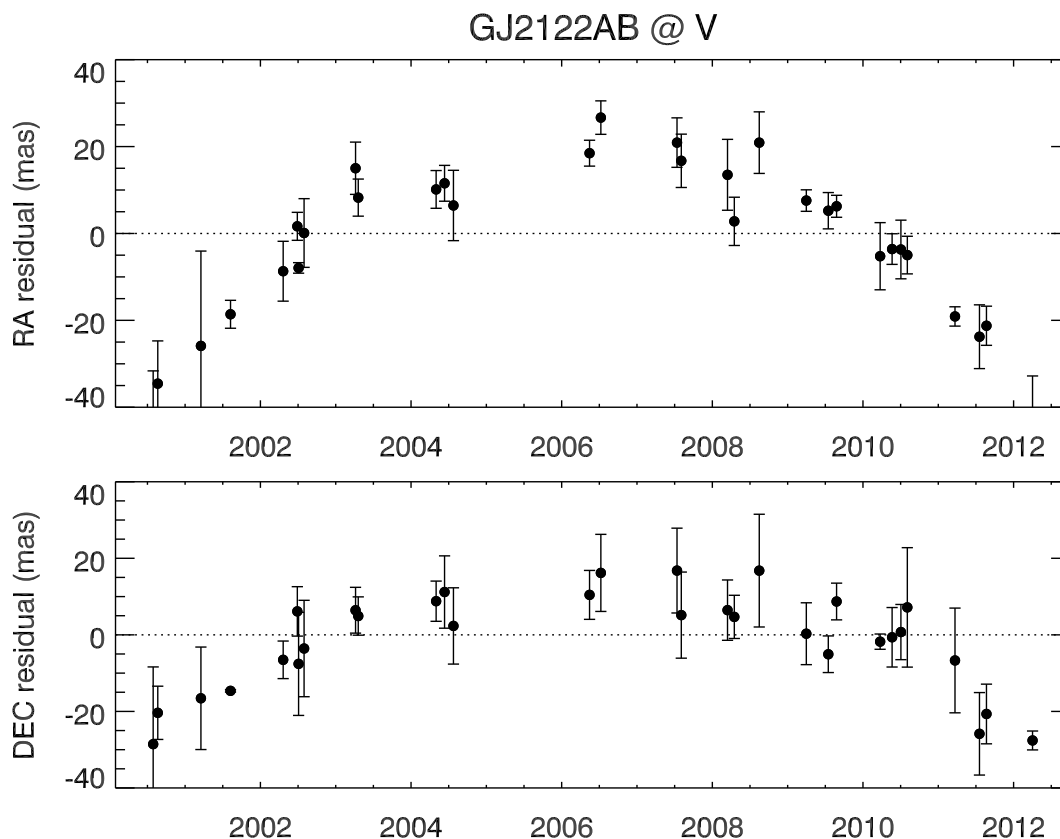


Figure 5.53: Nightly mean residuals of the fit (after the parallax and proper motion have been removed) show a clear astrometric perturbation. This is a well-known binary, but its orbit has not wrapped in our data, nor does our orbital fit converge.

recent attempt to fit an orbit failed; the astrometry in Table 5.8 is thus calculated from data where the astrometric perturbation has been left in.

The binary is HIP 82021, but a bad position (off by  $19''$ , more than the scale of the astrometer grating) in the Hipparcos Input Catalog (Turon et al. 1993) leads to an enormous parallax error, and it was omitted from both official *HIPPARCOS* catalogs. Fabricius & Makarov (2000) re-reduced the *HIPPARCOS* data to get an answer of poor quality ( $71.3 \pm 14.8$  mas,  $14.0 \pm 2.9$  pc) and again blame the pointing error. Our parallax result ( $74.87 \pm 1.71$ ,  $13.4 \pm 0.3$  pc) agrees with Fabricius & Makarov (2000).

**SCR 2036-3607** ( $M_V=10.61$ ,  $V - K_s=4.49$ ) (from TINYMO)

This star was identified as an X-ray bright object in Riaz et al. (2006) and Torres et al. (2006), and erroneously listed by Fruscione (1996) (and for some time, SIMBAD) as a possible blazar. Given  $V=11.66$ , it would have been one of the brightest blazars in the sky, but it is actually a normal main-sequence star  $16.2\pm 0.4$  pc away. It is somewhat more distant than either its plate-based ( $12.0\pm 3.7$  pc) or CCD-based ( $14.2\pm 2.2$  pc) distances predicted, but it is within their errors and does not seem to be young. On the other hand, its kinematics are consistent with the Ursa Major moving group, and confirmed by a radial velocity from Torres et al. (2006). Kinematic backtracking using a Galactic potential (§2.4.2) shows that it is consistent to within  $2\text{-}\sigma$  with a 300 or 600 Myr old Ursa Major moving group (Figure 5.54) assuming a distance of  $< 5$  pc is convergence. Still, we have no measure of its chemical composition to confirm it as a member of Ursa Major.

**GJ 1207** ( $M_V=12.51$ ,  $V - K_s=5.13$ ) aka G 019-007, LHS 3255, L 988-042, LP 686-027, LTT 06767

This star (the first star ever observed by CTIOPI) was identified as a flare star in Gershberg et al. (1999). As reported in Henry et al. (2006), a flare was seen in our astrometric data on UT 2002 June 17. It is reproduced in Figure 5.51. This is a main sequence system. A weighted mean of the YPC parallax and our result is given in Table 5.14.

**GJ 1224** ( $M_V=14.01$ ,  $V - K_s=5.65$ ) aka G 154-044, L 920-026, LHS 3359  
Lee et al. (2010) find slight evidence of variability over a period of an hour; our time-series relative variability is 0.01 mag, normal for field M dwarfs. Jenkins et al. (2009) published

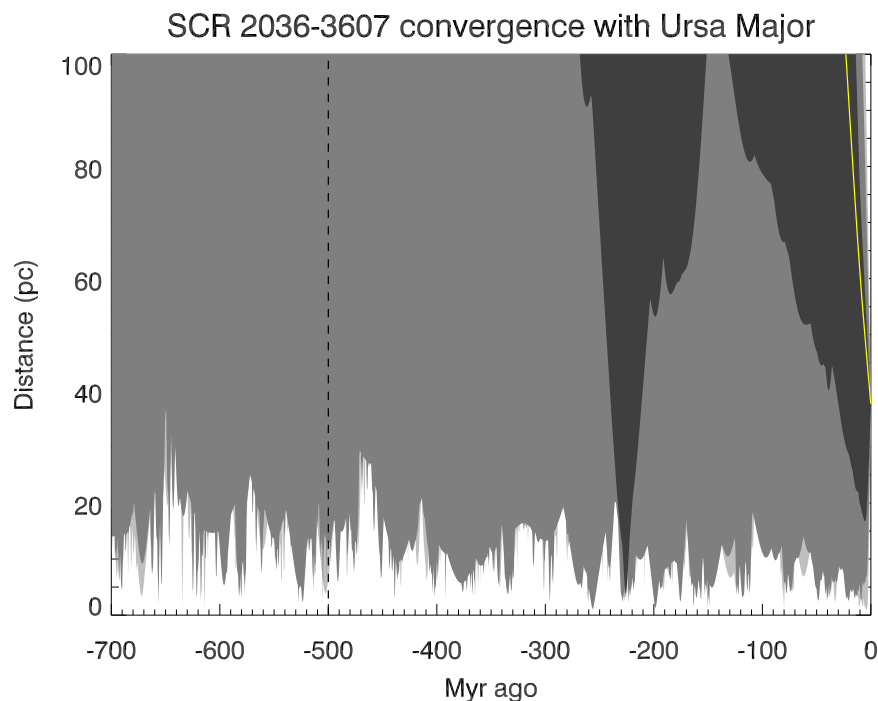


Figure 5.54: Plot of the separation between SCR 2036-3607 and the Ursa Major moving group (represented by Mizar A and the UVW velocity from [King et al. 2003](#)) as a function of time, going backwards into the past (leftward), based on kinematic calculations using a Galactic potential. The plot shows the result of 6000 sets of UVW velocities chosen within  $1\sigma$  (dark gray),  $2\sigma$  (medium gray), and  $3\sigma$  (light gray) error bounds. SCR 2036-3607 is consistent with a 300 or 600 Myr old Ursa Major Moving Group at the  $2\sigma$  level, assuming a pass of less than 5 pc is grounds for convergence.

$vsini < 5.6 \text{ km s}^{-1}$ , while [Reiners et al. \(2009\)](#) finds  $vsini < 3 \text{ km s}^{-1}$ . This is a main-sequence system.

**G 141-029** ( $M_V=12.36$ ,  $V - K_s=5.31$ ) aka V0816 HER, LTT 15516, LP 510-015

The system was identified as a flare star in [Gershberg et al. \(1999\)](#); apart from this there is no evidence of youth or multiplicity.

**SCR 2010-2801AB** ( $M_V=9.58$ ,  $V - K_s=5.25$ ) (from TINYMO)

This system was also discovered by [Riaz et al. \(2006\)](#). [Bergfors et al. \(2010\)](#) found a

companion  $0.61'' @ 280.4^\circ$ , (see Table 5.10) and found  $\Delta i' = 0.80 \pm 0.04$ ,  $\Delta z' = 0.75 \pm 0.03$ .

The deblending in Johnson/2MASS  $\Delta V = 1.2$  and  $\Delta K_s = 0.6$  are estimates.

Kinematics are consistent with membership in  $\beta$  Pic, as is the Na I gravity index. The HR diagram position, regardless of the estimated  $\Delta mag$ , is too luminous for  $\beta$  Pic, which raises questions about whether the parallax is correct, or if SCR 2010-2801AB is genuinely younger still. It is worth noting that several other tentative members of  $\beta$  Pic are almost equally as overluminous (SCR 0017-6645, BAR 161-012, LP 476-207BC (also a guess), SCR 2033-2556) and it may be my isochrone curve that is wrong.

**LEHPM 2-0783** ( $M_V=16.13$ ,  $V - K_s=7.45$ ) aka SIP 2019-5816

Identified as young by Riaz et al. (2006). Its isochronal position is indicative of youth, but its Na I gravity index (Figure 5.34) is not, nor do its kinematics potentially match any known association. This system may merely be an unresolved multiple system. This is the reddest star system ( $V - K_s=7.45$ ) with X-rays in this sample.

**SCR 2033-2556** ( $M_V=11.82$ ,  $V - K_s=5.99$ ) (from TINYMO)

This system is young by its HR diagram position, Na I gravity index, and kinematics. By kinematics, this system may be a member of the  $\beta$  Pic association, but like SCR 2010-2801AB, it is too luminous. It is potentially a binary.

**GJ 0803 (A) /GJ 0799AB (BC)** ( $M_V=10.39$ ,  $V - K_s=5.42$  (BC)) aka AU Mic and AT Mic A & B

This is one of the nearest young systems (see Table 5.10) to the Sun, and a prototypical member of the  $\beta$  Pic association (Barrado y Navascués et al. 1999). AU Mic (unobserved

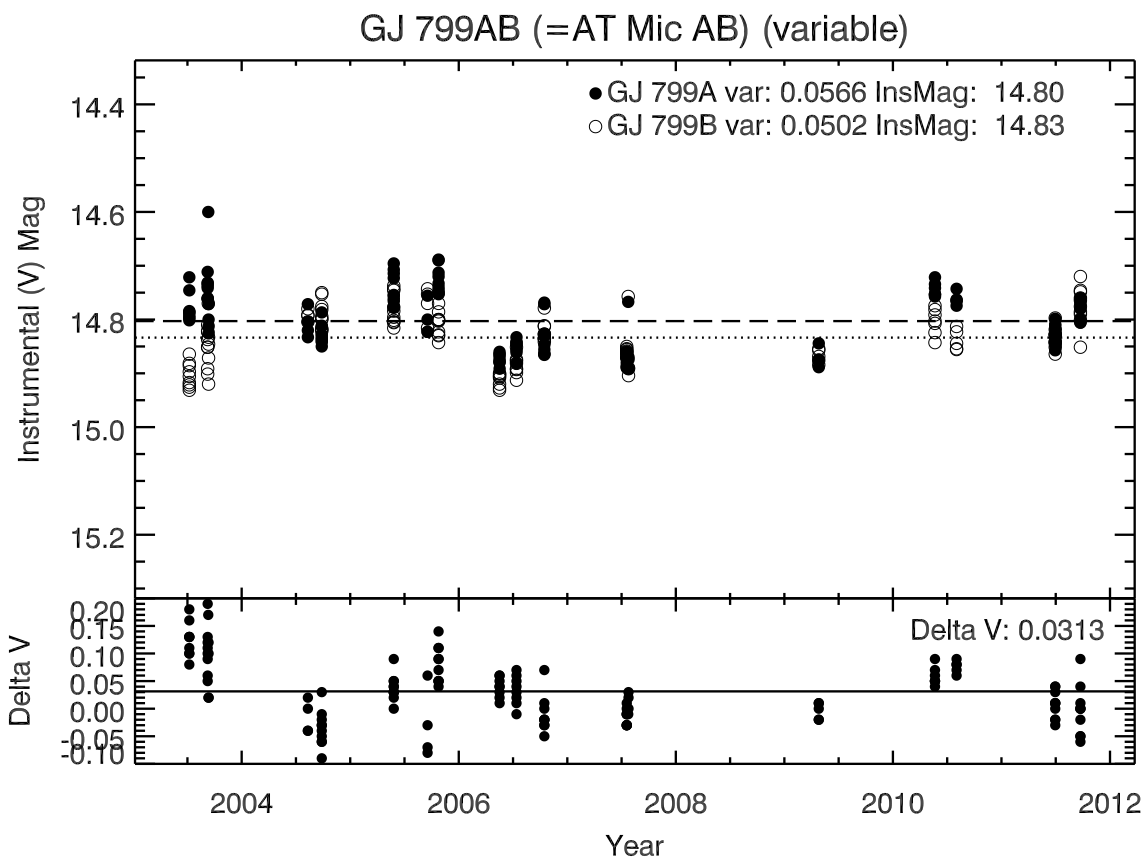


Figure 5.55: The variability of GJ 799A and B. Note that occasionally B is brighter than A.

by CTIOPI) is known to have a dust disk, and several authors note that the AU-AT Mic separation is very large (at least 0.23 pc) and “must be very fragile and will soon be torn apart by third bodies” (Caballero 2009). This system is a well-established member of the 10 parsec sample; with parallaxes from Hipparcos and YPC, our results agree with theirs. A combined system parallax incorporating all known parallax measurements for the system is given in Table 5.14. Interestingly, the variability of the two components – while definitely contaminated by the overlapping PSFs – shows that occasionally the B component is brighter than the A component (Figure 5.55).

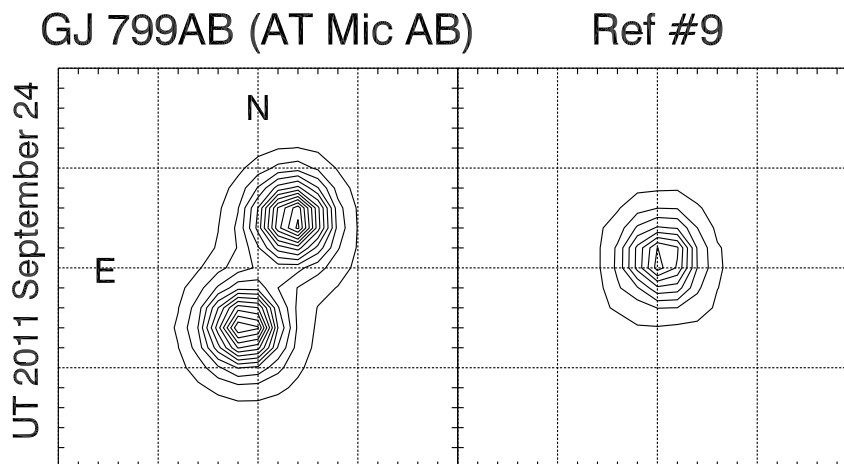


Figure 5.56: GJ 799 A (N) and B (S) on 2011 SEPTEMBER 24. The nearest reference star (# 9) is plotted as an example of a single-star PSF, with  $800\times$  smaller contour intervals. Grid spacings are  $2.05''$ , 5 pixels at the CTIO 0.9m.

We see evidence of orbital motion on these frames in the form of differential proper motion between the two components:  $\Delta\mu_{RA\cos(DEC)} = -66.12 \pm 0.50 \text{ mas yr}^{-1}$ ,  $\Delta\mu_{DEC} = -64.44 \pm 1.99 \text{ mas yr}^{-1}$ . In our first epoch (2003 JULY 09) they were separated by  $2.8''$  @  $171^\circ$ ; in our final epoch (2011 SEPTEMBER 24, Figure 5.56) they were separated by  $2.3''$  @  $156^\circ$ .

**SCR 2049-4012** ( $M_V=13.69$ ,  $V - K_s=5.83$ ) (from TINYMO)

This star was previously known only as BPS CS 22879-0089, an HK emission line candidate in Beers et al. (1996). It was identified as being 10.8 pc away by 11 plate distance relations, subsequently 7.93 pc away by 12 CCD distance relations, and 9.3 pc away by trigonometric parallax. It is the lowest-proper-motion system within 10 pc, and will be published in Henry et al. (in prep).

**LTT 09210 (A)/LP 932-083 (B)** ( $M_V=10.98$ ,  $V - K_s=5.47$  (B)) aka LEHPM 1-5169  
(B)

LP 932-083 (the only component observed by CTIOPI) is the B component in a wide system containing LTT 09210=HIP 112648 ( $217''$  @  $249^\circ$ , see Table 5.10); our parallax ( $26.36 \pm 2.20$  mas,  $37.9 \pm 3.2$  pc) for LP 932-083 agrees with the *HIPPARCOS* parallax ( $24.91 \pm 2.19$  mas,  $40.1 \pm 3.5$  pc) for LTT 09210. LP 932-083 is extremely overluminous (potentially the same age as  $\beta$  Pic), is unusually variable (0.044 mag), and appears has lower surface gravity than a main-sequence star by the Na I line, but it is not a possible match for any known association. According to SIMBAD, there have been no mentions of LTT 09210 or LP 932-083 as young stars.

**GJ 1284AB** ( $M_V=10.23$ ,  $V - K_s=4.81$ ) aka G 273-059, LP 878-087, LTT 09567, HIP 116003 (from TINYMO, though not low proper motion)

This system is a known flare star (Gershberg et al. 1999), and has kinematics consistent with the Columba association, but an overluminosity consistent with it merely being a binary. Torres et al. (2006) found that it *is* an SB2 binary (see Table 5.10). Absent any other information, I have assumed equal luminosities for the components, which make both main-sequence stars. Our gravity indicators also indicate that the stars are both on the main sequence. Torres et al. (2006) published no information about the binary (e.g., a period) that would indicate the separation of the two components, so it is not clear if the X-ray activity is caused by tidal interactions rather than youth.

**BD-13 06242** ( $M_V=8.43$ ,  $V - K_s=3.93$ ) aka RBS 2020

This is a known member of  $\beta$  Pic (Torres et al. 2006), recently added to CTIOPI. The low quality of the astrometric result (still definitely consistent with  $\beta$  Pic) is due to lack of

astrometric data (only 16 frames over 1.03 years), and not any intrinsic property of the star.

**LHS 4016AB** ( $M_V=10.42$ ,  $V - K_s=4.60$ ) aka G 275-106, L 649-024, LTT 09718

This was reported to be a known flare star in Gershberg et al. (1999). No companions were found in Allen & Reid (2008) or Bergfors et al. (2010), but Shkolnik et al. (2010) finds it to be a low mass SB2 (see Table 5.10) with probable orbital period less than 20 days, with a radial velocity of  $+25.30 \pm 0.55$  km s<sup>-1</sup>. As mentioned in Riedel et al. (2010), we have possible signs of a companion with a two-year orbit, so this system may in fact be triple.

## 5.7 Reddened Stars

Apart from the nearby stars and young stars, the TINYMO survey picked up several other stars worthy of some note.

Several reddened stars were picked up in TINYMO; these mostly appear to be members of various subsets of the Sco-Cen star forming region. BD-19 04371 (16:26:23.37 -19:31:35.7), SCR 1627-1925 (16:27:14.03 -19:25:46.7), and SCR 1627-1924 (16:27:14.79 -19:24:16.3) are all in the region of the sky with the Upper Scorpius star forming region, and all appear to be reddened stars of hotter spectral types (Figure 5.57). We have a preliminary parallax for the star SCR 1609-2222 which suggests it may be a member of Upper Scorpius as well.

A few other stars were pre-identified in SIMBAD as members of the Upper Scorpius star forming region, Sco-Oph star forming region, Chamaeleon I dark cloud (CHXR11, 11:03:11.61 -77:21:04.2), or  $\epsilon$  Chamaeleon association/cluster. The only truly unusual set of reddened potential nearby stars were a quartet of reddened objects (which may be K giants; K giants

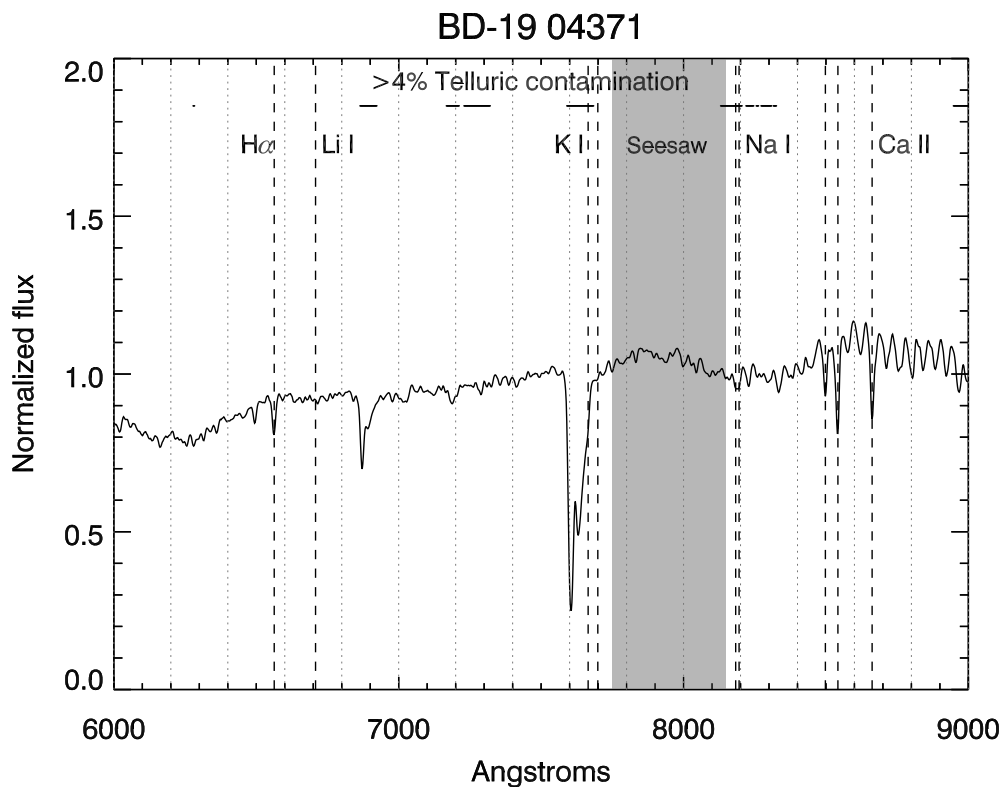


Figure 5.57: CTIO 1.5m spectrum of the reddened K star BD-19 04371 on 2010 SEP 17. The star is an apparent member of the Upper Scorpius star forming region. Its colors are of an M dwarf, but it is missing the strong TiO bands of M dwarfs.

are difficult to distinguish from K dwarfs in our region of spectral coverage):

- CD-58 07828 20:39:19.56 -58:02:29.4  $\mu = 0.036$  @ 099.3°
- CD-61 06505 20:54:02.76 -61:28:25.4  $\mu = 0.002$  @ 010.5°
- SCR 2055-6001 20:55:43.94 -60:01:46.1  $\mu = 0.018$  @ 010.4°
- SCR 2116-5825 21:16:44.72 -58:25:25.2  $\mu = 0.014$  @ 218.1°

There is no known cloud in this location, which is at a high Galactic latitude. It may be that these stars are truly unrelated (their proper motion vectors from SuperCOSMOS appear

different, but are statistically consistent with  $\mu = 0$ ) and all just happen to be reddened, but they are the only concentration of reddened objects I cannot explain.

## 5.8 They Might Be Giants

Table 5.16 contains a list of the new giants and supergiants (confirmed by spectroscopy) discovered in the TINYMO search. The spectral types given in the table were assigned by matching to M dwarf spectra, and identified as giants by Na I index measures of less than 1.02. Accordingly, not much stock should be placed in the spectral types themselves (M dwarf types do not correspond directly to giant or supergiant classifications), although the three giants with  $H\alpha$  emission (denoted by “e” in Table 5.16) do actually seem to have it. Samus et al. (2012) mentions “characteristic late-type emission spectra” in its description of Mira variables, which implies this is a known phenomenon in at least Mira-type giants.

Out of this sample I can identify thirteen new large-amplitude variables (denoted by “var” in Table 5.16) based on either the large errors on their CCD photometry ( $> 0.1$  mag, the error on other known Miras observed by CTIOPI), or  $> 1$  mag discrepancy between their  $R$  magnitudes (SuperCOSMOS and our CCD photometry). These are probably Mira variables, but I have no evidence of either periodicity or the required 2.5 magnitude amplitude required for the GCVS definition of a Mira.

Table 5.16: New giants and supergiants in the TINYMO sample

| Name<br>(1)   | RA<br>(2)   | DEC<br>(3)  | Spectral<br>Type<br>(4) | $B_J$<br>(5) | SuperCOSMOS  |              |                  | $I_{V/N}$<br>(8) | Johnson-Kron-Cousins |             |             | Photometry<br>Nights<br>(12) |
|---------------|-------------|-------------|-------------------------|--------------|--------------|--------------|------------------|------------------|----------------------|-------------|-------------|------------------------------|
|               |             |             |                         |              | $R_1$<br>(6) | $R_2$<br>(7) | $I_{V/N}$<br>(8) |                  | $V$<br>(9)           | $R$<br>(10) | $I$<br>(11) |                              |
| HD270965      | 05 00 40.38 | -71 57 52.9 | K7.0var                 | 13.634       | 13.037       | 12.059       | 11.189           | 11.38±0.02       | 10.62±0.02           | 9.94±0.02   | 2           |                              |
| SCR0537-3344  | 05 37 27.09 | -33 44 18.1 | M6.5                    | 12.786       | 9.216        | 9.705        | 6.470            | ...              | ...                  | ...         | ...         |                              |
| SCR0659-5954  | 06 59 10.94 | -59 54 58.6 | M6.5var                 | 17.009       | 12.583       | 14.850       | 9.653            | ...              | ...                  | ...         | ...         |                              |
| SCR0703-3507  | 07 03 49.64 | -35 07 44.3 | M6.5                    | 16.339       | 13.202       | 13.654       | 9.592            | 15.34±0.02       | 12.80±0.02           | 10.61±0.02  | 1           |                              |
| SCR0705-3534  | 07 05 47.36 | -35 34 25.8 | M6.5                    | 15.407       | 11.401       | 12.064       | 8.599            | 13.95±0.02       | 11.70±0.01           | 9.39±0.01   | 1           |                              |
| SCR0711-3600  | 07 11 03.53 | -36 00 59.7 | CARBON                  | 19.916       | 15.613       | 14.696       | 13.331           | 14.73±0.02       | 12.89±0.02           | 11.44±0.03  | 1           |                              |
| SCR0733-7743  | 07 33 38.27 | -77 43 16.7 | M9.0                    | 14.098       | 10.837       | 11.561       | 7.725            | 13.18±0.04       | 10.76±0.02           | 8.38±0.02   | 1           |                              |
| SCR0747-5412  | 07 47 14.27 | -54 12 02.5 | CARBON                  | 18.172       | 14.102       | 13.404       | 10.102           | 15.50±0.02       | 13.25±0.02           | 11.73±0.02  | 1           |                              |
| SCR0749-6502  | 07 49 05.69 | -65 02 40.0 | K8.0                    | 12.462       | 10.150       | 10.909       | 9.523            | ...              | ...                  | ...         | ...         |                              |
| SCR0753-5150  | 07 53 24.57 | -51 50 22.0 | M9.0                    | 14.121       | 10.952       | 11.513       | 7.672            | 12.66±0.03       | 10.31±0.02           | 7.96±0.05   | 2           |                              |
| SCR0753-6641  | 07 53 49.77 | -66 41 38.3 | K9.0                    | 12.355       | 9.957        | 10.728       | 9.377            | ...              | ...                  | ...         | ...         |                              |
| SCR0805-0743  | 08 05 52.81 | -07 43 05.7 | M9.0                    | 17.496       | 12.944       | 13.261       | 9.737            | ...              | ...                  | ...         | ...         |                              |
| STEPH0097     | 08 14 24.82 | -13 02 22.6 | M6.5                    | 13.972       | 10.822       | 10.544       | 7.196            | 12.69±0.01       | 10.41±0.01           | 8.16±0.01   | 1           |                              |
| SCR0833-6107  | 08 33 27.67 | -61 07 58.4 | M4.5var                 | 15.621       | 14.392       | 15.144       | 10.754           | 13.02±0.01       | 11.90±0.01           | 10.72±0.02  | 1           |                              |
| SCR0857-6734  | 08 57 38.21 | -67 34 10.5 | M5.0                    | 17.394       | 14.808       | 15.142       | 11.483           | ...              | ...                  | ...         | ...         |                              |
| IRA08583-2531 | 09 00 32.06 | -25 43 14.1 | M8.0                    | 14.674       | 11.237       | 11.121       | 7.746            | ...              | ...                  | ...         | ...         |                              |
| SCR0902-7823  | 09 02 35.97 | -78 23 14.7 | M7.5                    | 15.270       | 12.001       | 12.761       | 8.883            | ...              | ...                  | ...         | ...         |                              |
| SCR0910-7214  | 09 10 57.71 | -72 14 52.9 | M5.0                    | 11.356       | 8.643        | 8.650        | 6.293            | 10.31±0.01       | 8.84±0.01            | 7.07±0.01   | 1           |                              |
| SCR0927-8105  | 09 27 04.18 | -81 05 00.7 | M4.5var                 | 15.270       | 11.449       | 12.510       | 7.567            | ...              | ...                  | ...         | ...         |                              |
| SCR0930-8001  | 09 30 06.09 | -80 01 14.4 | M9.0                    | 14.750       | 11.969       | 12.056       | 8.755            | ...              | ...                  | ...         | ...         |                              |
| SCR0932-2806  | 09 32 03.32 | -28 06 27.0 | M9.0                    | 15.824       | 12.105       | 12.318       | 8.898            | ...              | ...                  | ...         | ...         |                              |
| SCR0938-3748  | 09 38 20.24 | -37 48 44.6 | M6.5                    | 13.920       | 10.424       | 10.515       | 7.396            | 12.70±0.02       | 10.45±0.01           | 8.15±0.01   | 1           |                              |
| SCR0945-3430  | 09 45 43.54 | -34 30 18.1 | M4.5var                 | 16.167       | 12.950       | 13.991       | 10.865           | ...              | ...                  | ...         | ...         |                              |
| SCR1044-7543  | 10 44 06.77 | -75 43 42.2 | M2.5                    | 15.119       | 13.211       | 13.389       | 11.593           | ...              | ...                  | ...         | ...         |                              |
| SCR1044-4330  | 10 44 40.73 | -43 30 44.2 | M6.5                    | 15.492       | 13.150       | 13.338       | 10.640           | ...              | ...                  | ...         | ...         |                              |
| SCR1048-7739  | 10 48 26.67 | -77 39 19.1 | M0.0                    | 12.796       | 10.777       | 11.097       | 10.368           | 11.47±0.01       | 10.53±0.01           | 9.64±0.01   | 1           |                              |
| SCR1058-4218  | 10 58 44.39 | -42 18 12.3 | M6.5                    | 16.582       | 13.168       | 13.452       | 10.363           | ...              | ...                  | ...         | ...         |                              |
| SCR1111-4856  | 11 11 28.25 | -48 56 14.3 | M2.5                    | 14.737       | 12.317       | 12.170       | 10.266           | ...              | ...                  | ...         | ...         |                              |
| SCR1138-4338  | 11 38 13.34 | -43 38 04.6 | M9.0                    | 15.960       | 12.741       | 12.909       | 10.502           | ...              | ...                  | ...         | ...         |                              |
| SCR1228-4949  | 12 28 06.16 | -49 49 34.5 | M5.0                    | 15.797       | 13.891       | 13.803       | 10.917           | ...              | ...                  | ...         | ...         |                              |
| STEPH0172     | 12 34 41.61 | -00 14 14.1 | M9.0                    | 14.281       | 10.830       | 11.633       | 7.790            | ...              | ...                  | ...         | ...         |                              |
| SCR1306-4745  | 13 06 42.81 | -47 45 25.7 | M6.5var                 | 14.146       | 11.654       | 13.210       | 9.952            | ...              | ...                  | ...         | ...         |                              |
| SCR1316-5206  | 13 16 42.18 | -52 06 38.3 | M6.5                    | 17.968       | 15.222       | 15.157       | 11.860           | ...              | ...                  | ...         | ...         |                              |
| SCR1317-4643  | 13 17 56.50 | -46 43 54.0 | M9.0var                 | 17.545       | 10.846       | 11.224       | 10.186           | 13.96±0.02       | 12.12±0.01           | 10.02±0.01  | 1           |                              |
| SCR1321-4913  | 13 21 31.72 | -49 13 09.6 | M7.5                    | 17.201       | 14.368       | 14.419       | 10.812           | ...              | ...                  | ...         | ...         |                              |
| SCR1349-7417  | 13 49 16.98 | -74 17 15.4 | M9.0                    | 15.218       | 11.880       | 12.186       | 8.935            | ...              | ...                  | ...         | ...         |                              |
| SCR1358-4910  | 13 58 43.58 | -49 10 52.0 | M7.0                    | 17.619       | 14.464       | 14.580       | 11.093           | 16.14±0.02       | 13.91±0.02           | 11.62±0.02  | 1           |                              |
| SCR1408-3506  | 14 08 36.51 | -35 06 02.3 | M6.5                    | 12.848       | 10.131       | 10.314       | 7.574            | ...              | ...                  | ...         | ...         |                              |
| SCR1424-4427  | 14 24 36.78 | -44 27 05.6 | M7.5                    | 15.875       | 11.799       | 12.448       | 9.312            | ...              | ...                  | ...         | ...         |                              |
| SCR1427-4731  | 14 27 43.90 | -47 31 13.2 | M4.0                    | 15.207       | 13.309       | 13.928       | 10.599           | ...              | ...                  | ...         | ...         |                              |
| SCR1431-4823  | 14 31 28.46 | -48 23 12.1 | M7.0                    | 16.253       | 13.274       | 13.795       | 9.808            | ...              | ...                  | ...         | ...         |                              |
| SCR1439-4506  | 14 39 33.26 | -45 06 42.3 | M4.5                    | 14.880       | 12.616       | 12.781       | 10.703           | ...              | ...                  | ...         | ...         |                              |

*Continued on next page*

Table 5.16 – Continued from previous page

| Name<br>(1)  | RA<br>(2)   | DEC<br>(3)  | Spectral<br>Type<br>(4) | SuperCOSMOS  |              |              |                  |            |             | Johnson-Kron-Cousins |            |     |  | Photometry<br>Nights<br>(12) |
|--------------|-------------|-------------|-------------------------|--------------|--------------|--------------|------------------|------------|-------------|----------------------|------------|-----|--|------------------------------|
|              |             |             |                         | $B_J$<br>(5) | $R_1$<br>(6) | $R_2$<br>(7) | $I_{V,N}$<br>(8) | $V$<br>(9) | $R$<br>(10) | $I$<br>(11)          |            |     |  |                              |
| SCR1440-7837 | 14 40 37.43 | -78 37 11.4 | K8.0                    | 12.182       | 9.718        | 10.407       | 9.090            | 10.75±0.03 | 9.88±0.01   | 9.01±0.01            | 9.01±0.01  | 1   |  |                              |
| SCR1458-4102 | 14 58 23.80 | -41 02 27.9 | M7.0var                 | 13.041       | 9.956        | 9.935        | 6.742            | 11.52±0.24 | 9.37±0.18   | 7.12±0.14            | 7.12±0.14  | 2   |  |                              |
| CD-81-00572  | 15 32 44.68 | -81 43 53.0 | K8.0                    | 11.178       | 8.727        | 9.656        | 8.073            | ...        | ...         | ...                  | ...        | ... |  |                              |
| SCR1534-7237 | 15 34 02.51 | -72 37 11.1 | M6.5                    | 17.739       | 14.704       | 14.865       | 11.198           | 16.03±0.01 | 13.94±0.02  | 11.71±0.02           | 11.71±0.02 | 1   |  |                              |
| SCR1544-1805 | 15 44 44.97 | -18 05 07.1 | M9.0                    | 15.312       | 11.920       | 12.009       | 8.717            | 13.54±0.03 | 11.36±0.01  | 9.09±0.01            | 9.09±0.01  | 1   |  |                              |
| SCR1551-8047 | 15 51 10.25 | -80 47 51.5 | M3.0                    | 14.717       | 12.783       | 12.814       | 11.075           | ...        | ...         | ...                  | ...        | ... |  |                              |
| STEPH0257    | 15 58 20.04 | -06 03 37.4 | M7.0                    | 13.194       | 10.120       | 9.892        | 7.036            | ...        | ...         | ...                  | ...        | ... |  |                              |
| SCR1604-7009 | 16 04 23.14 | -70 09 03.1 | M5.0                    | 13.015       | 10.106       | 9.804        | 7.509            | ...        | ...         | ...                  | ...        | ... |  |                              |
| SCR1612-6858 | 16 12 30.09 | -68 58 52.7 | M6.5                    | 16.653       | 13.026       | 13.811       | 9.984            | ...        | ...         | ...                  | ...        | ... |  |                              |
| SCR1621-6843 | 16 21 18.53 | -68 43 58.4 | M6.5                    | 15.538       | 12.339       | 13.076       | 10.172           | ...        | ...         | ...                  | ...        | ... |  |                              |
| SCR1647-6436 | 16 47 48.35 | -64 36 43.6 | M5.0                    | 16.768       | 13.574       | 13.634       | 10.283           | ...        | ...         | ...                  | ...        | ... |  |                              |
| SCR1654-0055 | 16 54 08.17 | -00 55 04.9 | M9.0                    | 17.488       | 13.788       | 13.767       | 10.534           | ...        | ...         | ...                  | ...        | ... |  |                              |
| SCR1658-6350 | 16 58 12.94 | -63 50 49.3 | M7.5                    | 13.747       | 10.678       | 11.204       | 8.948            | ...        | ...         | ...                  | ...        | ... |  |                              |
| SCR1706-6426 | 17 06 39.02 | -64 26 23.3 | M7.5var                 | 14.429       | 10.999       | 12.059       | 9.407            | ...        | ...         | ...                  | ...        | ... |  |                              |
| SCR1719-6151 | 17 19 09.42 | -61 51 55.7 | M9.0                    | 16.068       | 12.362       | 13.240       | 9.629            | ...        | ...         | ...                  | ...        | ... |  |                              |
| SCR1738-6844 | 17 38 14.51 | -68 44 52.8 | M5.0var                 | 16.196       | 10.905       | 12.576       | 8.949            | ...        | ...         | ...                  | ...        | ... |  |                              |
| SCR1743-4959 | 17 43 35.28 | -49 59 10.6 | M9.0                    | 16.340       | 13.108       | 12.988       | 10.318           | ...        | ...         | ...                  | ...        | ... |  |                              |
| SCR1803-7807 | 18 03 30.88 | -78 07 21.7 | M4.5                    | 14.199       | 12.245       | 12.681       | 9.898            | 13.13±0.01 | 11.71±0.01  | 9.94±0.01            | 9.94±0.01  | 1   |  |                              |
| SCR1807-5839 | 18 07 22.90 | -58 39 59.9 | M4.5                    | 15.194       | 12.749       | 12.970       | 10.303           | ...        | ...         | ...                  | ...        | ... |  |                              |
| SCR1919-2943 | 19 19 23.11 | -29 43 15.0 | M9.0                    | 15.246       | 12.639       | 12.835       | 10.256           | ...        | ...         | ...                  | ...        | ... |  |                              |
| CD-35-13495  | 19 27 08.18 | -35 15 09.6 | M7.5                    | 11.714       | 8.861        | 9.027        | 5.882            | ...        | ...         | ...                  | ...        | ... |  |                              |
| SCR1943-0138 | 19 43 43.06 | -01 38 31.6 | M6.5                    | 16.490       | 13.598       | 13.939       | 10.201           | ...        | ...         | ...                  | ...        | ... |  |                              |
| SCR1944-3414 | 19 44 45.52 | -34 14 41.2 | M9.0                    | 14.682       | 11.679       | 12.568       | 9.024            | ...        | ...         | ...                  | ...        | ... |  |                              |
| CD-45-13476  | 19 53 08.97 | -45 15 15.5 | M7.5                    | 11.755       | 9.495        | 9.099        | 6.669            | 11.57±0.01 | 9.56±0.01   | 7.40±0.01            | 7.40±0.01  | 1   |  |                              |
| SCR1959-1639 | 19 59 35.79 | -16 39 20.3 | M8.0                    | 15.761       | 12.972       | 12.937       | 9.416            | ...        | ...         | ...                  | ...        | ... |  |                              |
| SCR2000-0837 | 20 00 58.33 | -08 37 27.5 | M9.0e                   | 15.924       | 12.496       | 12.639       | 9.330            | 14.49±0.02 | 12.08±0.01  | 9.73±0.01            | 9.73±0.01  | 1   |  |                              |
| SCR2024-2500 | 20 24 15.40 | -25 00 56.8 | M6.5                    | 13.175       | 10.103       | 10.355       | 7.651            | 11.68±0.03 | 9.95±0.02   | 7.92±0.04            | 7.92±0.04  | 2   |  |                              |
| SCR2038-0409 | 20 38 45.49 | -04 09 27.0 | M5.0                    | 17.592       | 14.829       | 14.417       | 10.756           | 16.44±0.04 | 14.01±0.06  | 11.65±0.02           | 11.65±0.02 | 2   |  |                              |
| SCR2107-5734 | 21 07 58.01 | -57 34 17.5 | M7.0var                 | 14.159       | 11.794       | 12.093       | 8.611            | 12.32±0.01 | 10.29±0.01  | 8.08±0.01            | 8.08±0.01  | 1   |  |                              |
| SCR2138-4308 | 21 38 15.11 | -43 08 40.6 | M6.5var                 | 12.787       | 10.655       | 10.096       | 7.462            | 12.20±0.37 | 10.11±0.31  | 7.89±0.21            | 7.89±0.21  | 2   |  |                              |
| CD-24-17228  | 22 34 29.69 | -24 15 17.7 | M6.5                    | 12.664       | 10.033       | 10.084       | 7.226            | 11.23±0.05 | 9.42±0.05   | 7.35±0.06            | 7.35±0.06  | 2   |  |                              |
| SCR2305-3054 | 23 05 14.88 | -30 54 37.1 | M5.0var                 | 12.242       | 9.282        | 9.309        | 7.288            | 11.29±0.52 | 9.74±0.54   | 7.84±0.49            | 7.84±0.49  | 2   |  |                              |

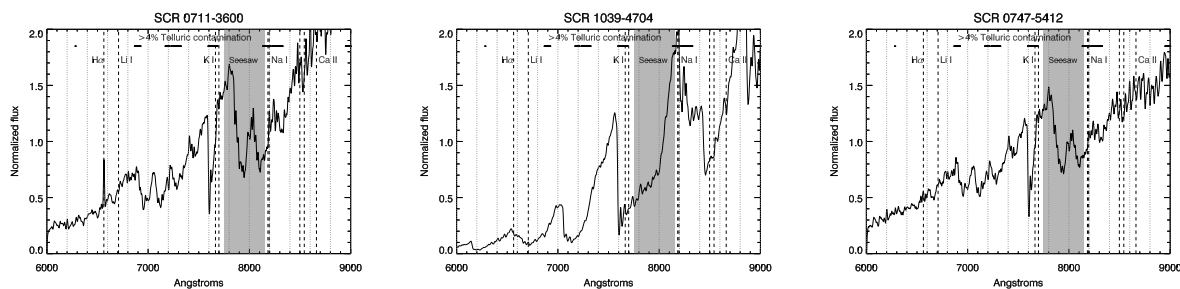


Figure 5.58: CTIO 1.5m spectra of the two new carbon stars (SCR 0711-3600, SCR 0747-5412), both from 2009 SEP 16. The spectrum of a carbon star is unlike an M dwarf or M giant, and contains unusual concentrations of carbon molecules (here, CN bands) rather than TiO or VO bands. SCR 1039-4704, an approximately M7.5III star, is plotted for comparison.

Three carbon stars were observed during data collection. One, IY Hya, was observed on purpose; the other two were new discoveries. I show spectra of the new stars in Figure 5.58. Based on comparisons with spectra in Turnshek et al. (1985), they appear to be genuine C-type stars with CN bands at 6900, 7100, 7500, 7900, and 8100Å.

## CHAPTER 6

### DISCUSSION

The intent of the projects undertaken in this dissertation were twofold. One goal was to identify and classify the population of nearby low proper motion stars in the southern hemisphere, which have been overlooked by most Solar Neighborhood studies in the past; this involved a search of 39.3% of the sky, and detailed followup efforts on candidates with predicted distances  $<15$  pc. The other general goal was to identify new nearby pre-main-sequence stars in known associations based on their kinematics, overluminosity, and spectral features. As outlined in Chapter 5 I have indeed found many new nearby and young stars. With the new RECONS 25 pc Database (§ 3.2) at my disposal, I now have the best possible volume-limited sample available to put my discoveries in context.

#### 6.1 Discoveries of Low Proper Motion Stars

##### *6.1.1 New 25pc statistics*

As a result of my thesis (and TINYMO), I have added 23 new low proper motion star systems to the 25 pc sample. With an additional 58 systems from my two published papers (§5.2, §5.4), I have added a grand total of 81 systems, or 3.9% of all systems known within 25 pc.

My 23 new nearby low-proper-motion stars represent a very different population of stars from known nearby stars. While they are no different in  $M_V$  magnitude (Figure 6.1) from the generic contents of the RECONS 25 pc Database, they comprise a vastly different proper

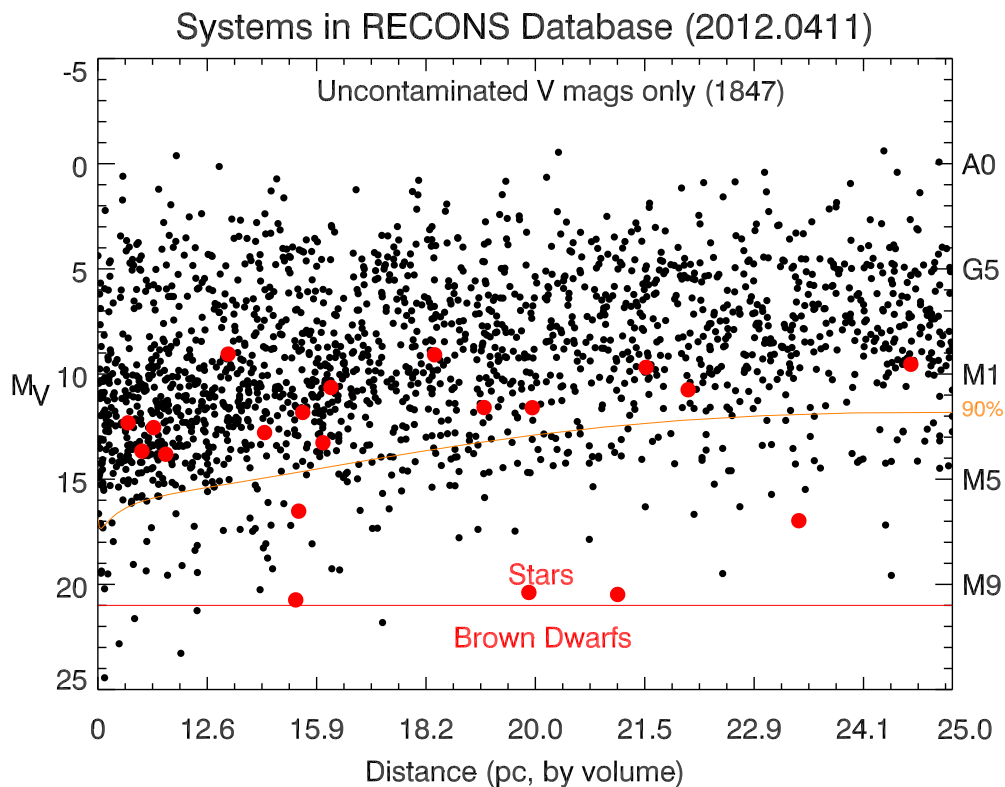


Figure 6.1: A plot of all new low proper motion star systems, as compared to the RECONS 25 pc Database as of 2012 APRIL 11, on an equal-volume scale. Apart from a few stars around the stellar-brown dwarf divide, my sample of stars is small and fairly ordinary. Note that the density of stars is roughly constant for A/F/G/K stars (brighter than  $M_V=9$ ), but very incomplete for M. The curve has been set so that 90% of all known stars lie above the line. Within 10 pc, 90% of all stars are brighter than  $M_V=16$ ; at 25 pc, 90% of known stars are brighter than only  $M_V=12$ .

motion sample (Figure [6.2](#)). This sample of stars is genuinely different from the existing sample of nearby stars.

### 6.1.2 Where are the other low-proper-motion stars?

My sample can be compared to both the model derived in [§ 2.4.3](#) and to actual results from the RECONS 25 pc Database discussed in [§ 3.2](#)

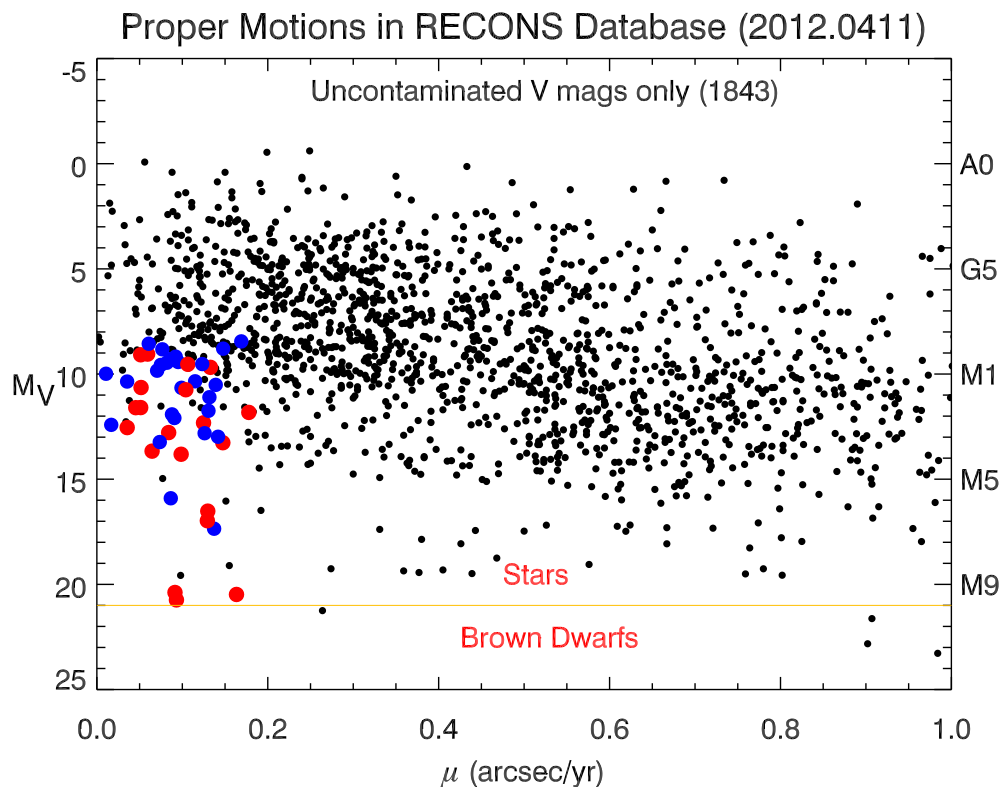


Figure 6.2: The proper motions of the 49 new low proper motion star systems. Red points are within 25 pc, blue points are not. Also note the apparent bimodal distribution of proper motions within the RECONS 25 pc Database as of 2012 APRIL 11: a cluster around  $0.2''\text{yr}^{-1}$ , and another around  $0.5''\text{yr}^{-1}$ , where the density of points increases for  $M_V$  fainter than 10. This is no accident; they correspond to the limits of the NLTT (Luyten 1979b) and LHS (Luyten 1979a) catalogs, respectively. The overall slope of the distribution demonstrates that few A stars have high proper motions (as they are all young, with motions near the local standard of rest), while the fainter M dwarfs are easier to spot at higher proper motions.

One thing that must be taken into account is that my follow-up work focused on stars predicted to be within 15 pc, which not only limits the total number of stars, but also shifts the distribution to substantially higher proper motion. We can extract the # of stellar systems of various proper motions at various distances from the simulated 25 pc sample (Table 6.1) and the real 25 pc sample (Table 6.2):

Table 6.1: Simulated Proper Motions

| Simulated                | <1.3 pc | <5 pc | <10 pc | <15 pc  | <20 pc  | <25 pc  |
|--------------------------|---------|-------|--------|---------|---------|---------|
| <0.04'' yr <sup>-1</sup> | 0.00    | 0.02  | 0.57   | 4.00    | 16.43   | 49.11   |
| <0.18'' yr <sup>-1</sup> | 0.00    | 0.30  | 9.82   | 72.89   | 296.10  | 866.78  |
| <0.30'' yr <sup>-1</sup> | 0.00    | 0.83  | 26.31  | 187.44  | 724.22  | 2000.81 |
| <0.50'' yr <sup>-1</sup> | 0.00    | 2.24  | 66.68  | 432.82  | 1499.49 | 3709.98 |
| <1.00'' yr <sup>-1</sup> | 0.01    | 8.12  | 187.69 | 932.62  | 2613.28 | 5553.67 |
| ALL pm                   | 0.88    | 50.40 | 408.06 | 1377.68 | 3262.67 | 6375.00 |

Derived using  $N=10,000,000$  simulated stars and a density of 6375 stars within 25 pc.

Table 6.2: Real Proper Motions

| Real                     | <1.3 pc | <5 pc | <10 pc | <15 pc | <20 pc | <25 pc |
|--------------------------|---------|-------|--------|--------|--------|--------|
| <0.04'' yr <sup>-1</sup> | 1       | 1     | 1      | 1      | 9      | 18     |
| <0.18'' yr <sup>-1</sup> | 1       | 1     | 3      | 32     | 107    | 240    |
| <0.30'' yr <sup>-1</sup> | 1       | 2     | 12     | 89     | 271    | 576    |
| <0.50'' yr <sup>-1</sup> | 1       | 2     | 37     | 198    | 521    | 1028   |
| <1.00'' yr <sup>-1</sup> | 1       | 11    | 128    | 480    | 1037   | 1719   |
| ALL pm                   | 1       | 51    | 258    | 715    | 1354   | 2067   |

Derived from the RECONS 25 pc database as of 2012 APRIL 11.

There are 2089 systems; only 2067 have listed proper motions. The single system within 1.3 pc moving slower than 0.04'' yr<sup>-1</sup> is the Solar System.

Both tables are cumulative toward the bottom right corner, so as you go down you include all the above columns; as you go right, you include all the columns to the left. Thus, as shown in Figure [2.11](#), 867 of 6375 systems (13.6%) within 25 pc are expected to be moving slower than 0.18'' yr<sup>-1</sup>, but within my 15 pc upper limit, only 73 of 1378 systems (5.3%) should be moving slower than 0.18'' yr<sup>-1</sup>. As TINYMO covered 39.3% of the sky, the maximum number of stars it should have picked up was 29; with 13 already known, there should only be 16 stars remaining to discover.

Ultimately, I do have first parallaxes for 21 new low proper motion systems within 25 pc,

and the first good parallaxes that qualify two more objects (LP 476-207ABC had a parallax that put it outside 25 pc; GJ 2122AB was within 25 pc but with more than 10 mas error) for the RECONS 25 pc database VETTED sample. Of these, only 6 are from the TINYMO survey and within  $2\sigma$  of 15 pc (what we expected to find): L173-019, SCR 2049-4012, SCR 0533-4257, SCR 1214-2345, SCR 0128-1458, 2MA 0429-3123. If we instead consider stars from TINYMO whose trigonometric parallaxes are consistent to  $2\sigma$  with their CCD-based photometric distance estimates (which is what we should expect from our trigonometric parallaxes), we again find six systems from TINYMO that are genuinely main-sequence dwarfs consistent with their photometric distance estimates: L 173-019, SCR 2049-4012, SCR 1214-2345, SCR 0128-1458, SCR 1942-2045, SCR 2036-3607<sup>1</sup>

The discrepancies between the two lists are that SCR 0533-4257 and 2MA 0429-3123 are consistent with being within 15 pc, but are evidently not single, main-sequence stars (SCR 0533-4257 is a known binary, 2MA 0429-3123 may be a member of Argus). Meanwhile, the distances to SCR 1942-2045 and SCR 2036-3607 are consistent with their CCD-based photometric distances (which have larger errors) but are not within  $2\sigma$  of 15 pc by our measured trigonometric parallax. If we include all 8 (6) targets, I have discovered 50% (38%) of the total number of stars left in this parameter space (within 15 pc,  $\mu < 0.18'' \text{ yr}^{-1}$ ).

The remaining 7 (9) systems still hiding in plain sight are probably M dwarfs with  $v - K_s < 4.5$  (M3.0V) or colder than  $v - K_s > 8$  (M7.0V). In particular, analysis of Figure 4.6 shows the cooler stars are simply less common, altogether, in our sample. Supporting this

---

<sup>1</sup>Expanding to systems within  $3\sigma$  of 15 pc by trigonometric parallax adds SCR 1942-2045 and SCR 2036-3607; expanding to  $3\sigma$  discrepancy with the CCD photometric distance estimate adds SCR 0143-0602, 2MA 0936-2610, HD 271076, and (due to poor parallax solutions) Stephenson 164 and SCR 1609-2222.

hypothesis are two additional stars in my thesis sample that meet all the criteria (within 15 pc,  $\mu < 0.18'' \text{ yr}^{-1}$ , in the region of sky searched by TINYMO) but were not found in TINYMO: one (GJ 2122AB,  $V - K_s = 3.95$ ) is too blue; the other (SDSS J1416-3402) is a brown dwarf and too red to have a measured  $V$  magnitude. With these, I have discovered 63% (10 of 16) of the remaining expected 15 pc members. One additional concern is that the requirement of detection on all four plates sometimes puts too stringent a limit on the stars recovered. Several previous nearby star discoveries made by RECONS (e.g. SCR 1845-6357, Hambly et al. 2004) have had missing photometric colors, and not always because they were too faint in  $B_J$ .

Other additional parameters of interest can be pulled from this sample. For instance, the simulation (Table 6.1) only predicts 0.88 stars within 1.3 pc of us (i.e., closer than Proxima Centauri), which might explain why no one has yet been able to find one – the one star in the real sample table is the Sun, at 1 AU. (Table 6.2) Meanwhile, only *one* of the 10,000,000 simulated stars was both closer than 1.3 pc *and* moving less than  $0.18'' \text{ yr}^{-1}$ . We can also verify (roughly) the original reason why proper motions below  $0.2'' \text{ yr}^{-1}$  were ignored: only 9% (296 of 3263) systems within 20 pc are expected to be moving slower than  $0.18'' \text{ yr}^{-1}$ , where Dyson (1917) expected 12.5% moving slower than  $0.2'' \text{ yr}^{-1}$ .

### 6.1.3 Close passes to the Solar System

Without radial velocities it is difficult to determine close passes to the Solar System with any certainty. As an educated guess, however, we can take the stars with the lowest  $V_{tan}$  velocities as being the most likely to have purely radial motion. The most obvious culprit is

SCR 0613-2742AB, the apparent  $\beta$  Pic member. Assuming it really is a member of  $\beta$  Pictoris with the best-fit radial velocity of  $21 \text{ km s}^{-1}$ , its closest approach to the Solar System was 1.3 Myr ago, at a rather healthy distance of 411,000 AU (2 pc). SCR 0533-4257 is a greater threat (assuming, for the moment, that it's a member of Castor, moving at  $14 \text{ km s}^{-1}$ ). Its closest pass would have been 0.6 Myr ago, at a distance of 251,000 AU (1.2 pc).

Bobylev (2010) lists no less than six stars predicted (via a more rigorous Galactic potential analysis) to come closer than either of those stars: GJ 710 (0.21 pc), GJ 551=Proxima Centauri (0.89 pc), GJ 559AB= $\alpha$  Centauri (0.91 pc), GJ 445 (1.06 pc), and GJ 699=Barnard's Star (1.15 pc). Of those stars, the most remarkable is GJ 710, at a current distance of 19.6 pc; the rest are comfortably within 6 pc. GJ 710 will arrive in roughly 1.4 Myr; its proper motion vectors ( $\mu_{RA} = 1.15 \pm 1.66$ ,  $\mu_{DEC} = 1.99 \pm 1.22$ ) are far smaller than any of my stars.

#### 6.1.4 Solar Motion and Solar Siblings

The TINYMO survey probes stellar motion at the level where Solar Motion dominates the apparent proper motion of the star. As seen in Figure 6.3, there is a definite sign of solar reflex motion in the TINYMO sample, at least with the “Good” (apparently normal main-sequence M dwarfs) (green) and “X-ray bright” (blue) subsamples (X-ray flux errors of  $< 25\%$ , and point sources within  $25''$  of the 2MASS point); most of those stars do seem to be converging at the antisolar point.

As for potential solar siblings, they should show up with zero space velocity (no motion relative to the Sun). Using the same kinematics code, I find only one system is consistent with zero motion (zero error, as well; a star would have to match exactly to have stayed

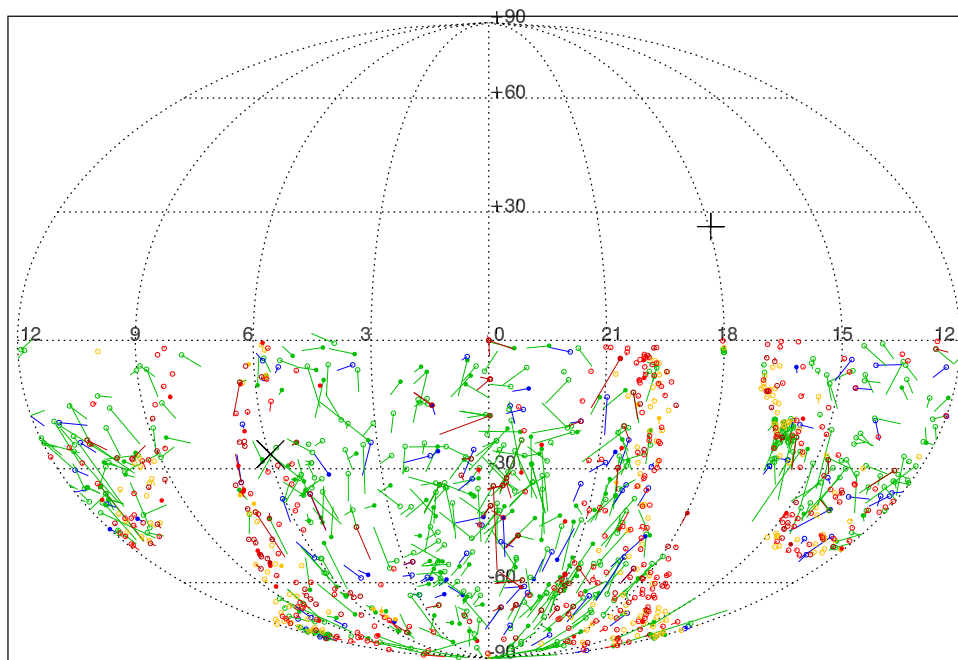


Figure 6.3: The TINYMO sample, plotted with proper motion vectors. The + is the direction of solar motion (according to [Jaschek & Valbousquet 1992](#)), the X is the antisolar point. As expected, a large number (though not all) of the stars have proper motion vectors that converge at the antisolar point. Green stars are apparently normal (“good”), blue stars are X-ray bright, yellow are probable giants, red stars are definite giants or beyond 25 pc by plate photometric distance estimate (and were found by eye).

close enough to the Sun for 4.5 Gyr): SCR 1609-2222. As SCR 1609-2222 is not a plausible main-sequence star (and is in fact more likely a Upper Scorpius member, [§5.6](#)), I conclude there are no solar siblings in my sample.

## 6.2 Discoveries of Young Stars

The most exciting discoveries are the young stars. The list in [Table 5.15](#) outlines what I have been able to determine about the youth of all of those stars. Of course, in nearly all cases I am missing two extremely necessary pieces of information: Lithium equivalent widths and

radial velocities. In both cases I am limited by the low resolution of my available spectra – with  $R \sim 500$  resolving power, I cannot resolve the extremely narrow lithium lines with any confidence. At the same time, though it can and has been done on spectra of this resolution, I have not yet worked out the optimal way to extract radial velocities from my spectra. While I am familiar with cross-correlation and have used it on the spectra (cross-correlation of the [Hinkle et al. 2003](#) atmospheric A-band to the measured A-band as a zeroth-order correction to our wavelength solutions, prior to spectral analysis), no attempt was made to observe spectral standards on a nightly or otherwise regular basis, and I have not gone back to our original data to determine precise times of observation that would allow me to work out a heliocentric correction. A number of attempts were made to get better spectra for the purpose of radial velocities, the most successful of which was the collaboration with Simon Murphy and Carl Melis on AP Col; I did make one successful Gemini-S/PHOENIX proposal in 2010B that got very little data before Phoenix itself was removed from the telescope and the southern hemisphere.

Nevertheless, I feel particularly confident in suggesting the youth and membership of the 25 systems listed in Table [6.3](#).

Table 6.3: Potential Young Systems

| Name                           | J2000 E2000 |             |
|--------------------------------|-------------|-------------|
|                                | RA          | DEC         |
| TW Hydra (8 Myr) – 5 systems   |             |             |
| SCR 1012-3124AB                | 10 12 09.09 | –31 24 45.2 |
| SIP 1110-3731ABC               | 11 10 27.88 | –37 31 52.7 |
| RX 1132-2651AB                 | 11 32 41.16 | –26 52 09.0 |
| 2MA 1207-3239                  | 12 07 33.46 | –39 32 54.0 |
| SCR 1425-4113                  | 14 25 29.13 | –41 13 32.4 |
| Beta Pic (12 Myr) – 12 systems |             |             |
| SCR 0017-6645                  | 00 17 23.53 | –66 45 12.5 |
| GJ 2006AB                      | 00 27 50.24 | –32 33 06.2 |
| BAR 161-012                    | 01 35 13.94 | –07 12 51.8 |
| LP 476-207ABC                  | 05 01 58.81 | +09 58 58.8 |

*Continued on next page*

Table 6.3 – *Continued from previous page*

| Name                         | J2000 E2000 |             |                   |
|------------------------------|-------------|-------------|-------------------|
|                              | RA          | DEC         |                   |
| BD-21 01074ABC               | 05 06 49.92 | −21 35 09.2 | (known)           |
| SCR 0529-3239                | 05 29 44.69 | −32 39 14.2 |                   |
| SCR 0613-2742AB              | 06 13 13.31 | −27 42 05.5 |                   |
| SIP 1809-7613                | 18 09 06.95 | −76 13 23.9 |                   |
| SCR 1816-5844                | 18 16 12.37 | −58 44 05.6 |                   |
| SCR 2033-2556                | 20 33 37.59 | −25 56 52.2 |                   |
| GJ 0799AB                    | 20 41 51.17 | −32 26 07.0 | (known)           |
| BD-13 06424                  | 23 32 30.87 | −12 15 51.4 | (known)           |
| Tuc-Hor (30 Myr) – 1 system  |             |             |                   |
| 2MA 0254-5108AB              | 02 54 33.17 | −51 08 31.4 | (may be separate) |
| Argus (40 Myr) – 4 systems   |             |             |                   |
| AP Col                       | 06 04 52.16 | −34 33 36.0 |                   |
| RX 0413-0139                 | 04 13 26.64 | −01 39 21.2 |                   |
| G 161-071                    | 09 44 54.18 | −12 20 54.4 |                   |
| L 755-019                    | 20 28 43.62 | −11 28 30.8 |                   |
| AB Dor (125 Myr) – 3 systems |             |             |                   |
| GJ 2022ABC                   | 01 24 27.76 | −33 55 08.3 |                   |
| G 007-034                    | 04 17 18.52 | +08 49 22.1 |                   |
| LP 776-025                   | 04 52 24.42 | −16 49 22.2 | (known)           |

This is not to suggest the rest of the stars are not young; for instance, SCR 2010-2801AB is quite possibly young, but the fact that even as an equal-luminosity binary it still lies above the  $\beta$  Pic isochrone makes it difficult to classify it as a member. In fact, the oddballs and stars that lie between the isochrone lines are arguably the most interesting – either my isochrones are wrong (which is possible, given the lack of stars) or I’ve tapped into a large conglomeration of young but unassociated stars. Such wayward young stars have been discussed for years (Mamajek, E.E., private communication, 2011) and raise the specter of continual star formation processes that can spit out single stars at a time<sup>2</sup>, as described in the introduction (§1.4).

<sup>2</sup>In the apparently older cases, these could also be ejected wide companions to stars in associations nowhere near the Earth.

### 6.2.1 *Why there were so many young stars*

One of the most striking things about my sample is the presence of young stars, even those without X-ray flux. The answer appears to be two-fold. First, the TINYMO search (Chapter 4) was carried out with photometric distance estimates, using the assumption that every star was a single, main-sequence object. Young stars, or at least young (and pre-main-sequence) M dwarfs, are significantly brighter than their main-sequence cousins, and therefore appear to be within 25 pc (by photometric distance estimate) even when they are much more distant. They will preferentially scatter into a distance-limited survey like TINYMO.

Beyond that, young stars preferentially have low proper motions, which TINYMO was designed to detect. As discussed in §1.4, the vast clouds of young stars in the Solar Neighborhood are orbiting at essentially the local standard of rest, and the Sun is passing through them at  $20 \text{ km s}^{-1}$ . That kind of tangential velocity drops below  $0.18'' \text{ yr}^{-1}$  at 23.5 pc. I searched that proper motion range, and picked up on that overdensity of young targets. This can be seen in the distribution of tangential velocities in my sample (Figure 6.4), which peaks at  $15\text{-}20 \text{ km s}^{-1}$ .

The velocity peak at  $15\text{-}20 \text{ km s}^{-1}$  is not a velocity selection effect as a result of my  $0.18'' \text{ yr}^{-1}$  proper motion limit. While it is true that stars moving at  $0.18'' \text{ yr}^{-1}$  could have at most  $21 \text{ km s}^{-1}$  tangential velocities if they were within 25 pc, nearly half of my sample of low proper motion stars were *not* within 25 pc, and thus their  $V_{tan}$  was not constrained to  $21 \text{ km s}^{-1}$ . It is also worth noting that the other samples of mostly X-ray bright stars (sections 3 and 4 of Tables in §5.3 and §5.5) had no proper motion constraints on them at

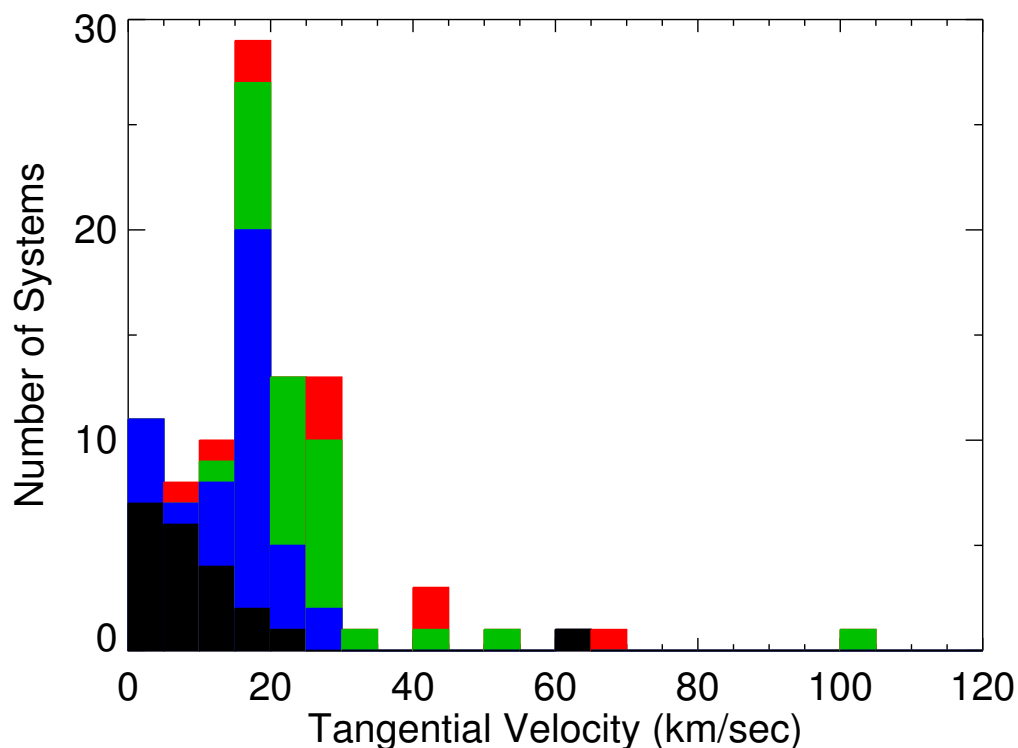


Figure 6.4: The tangential velocity distribution for the 84 stars in my thesis sample. Despite having no overall constraint on  $V_{tan}$ , the distribution peaks at 15-20 km s<sup>-1</sup>. Black=Low Proper Motion, Blue=Low Proper Motion and Young, Green=Young, Red=Previously Published.

all, yet they also contribute to the striking peak in the 15-20 km s<sup>-1</sup> bin.

### 6.2.2 New 25 pc young statistics

At the moment, it is difficult to give exact statistics on the number of young (<125 Myr old) stars within 25 pc. Few authors (Shkolnik et al. 2009, 2011) publish young stars not connected to a known association, so large numbers of such systems (including any systems belonging to as-yet unidentified associations) are likely missing. Nevertheless, we can set lower limits on the population of such young stars, and find that after a quick and non-

exhaustive search of papers (Zuckerman & Song 2004, Torres et al. 2008, Lépine & Simon 2009, Teixeira et al. 2009, Schlieder et al. 2010, Kiss et al. 2011, Desidera et al. 2011, Zuckerman et al. 2011, Riedel et al. 2011, Schlieder et al. 2012a) that there are 38 star systems suspected to have ages less than 125 Myr old and distances within 25 pc of the Solar System (see Table 6.4).

Of these 38 systems, 7 (18%) were first identified by me, either here or in Riedel et al. (2011). With the exception of G 165-008AB and SCR 0757-7114, all of these nearby systems are expected to be members of  $\beta$  Pic, AB Dor, or Argus.

Four of the 38 systems – CD-35 02722, GSC 8894-0426, PM I13143+1320, and TYC 5126-181-1 – have only estimated distances, a fifth – GJ 0714 – has a low-quality YPC parallax. 12 (32%) of the systems have their first parallaxes from CTIOPI, counting the new measurement of LP 476-207ABC that brings its weighted mean parallax within 25 pc. Compared to the RECONS 25 pc Database (2089+5 systems, to accommodate the five that do not yet have parallaxes that would qualify them for membership), 1.8% of all nearby stars are less than 125 Myr (AB Dor age or younger) old. Considering the rough nature of this search and the possibility of further discoveries (GJ 484, a G0V star recently identified by Zuckerman et al. (2011) as an Argus member, is a well-known star with an *HIPPARCOS* parallax) this number must be considered to be a lower limit.

Table 6.4: Young Stars within 25pc

| Name<br>(1)      | J2000<br>RA<br>(2) | J2000<br>DEC<br>(3) | Weighted<br>$\pi$ (mas)<br>(4) | $\pi^a$<br>key<br>(5) | $\mu_{RA \cos DEC}$<br>(mas yr <sup>-1</sup> )<br>(6) | $\mu_{DEC}$<br>(mas yr <sup>-1</sup> )<br>(7) | $\mu$<br>ref.<br>(8) | RV<br>(km s <sup>-1</sup> )<br>(9) | RV<br>(10) | Assoc.<br>(11)       | Assoc.<br>ref<br>(12) |
|------------------|--------------------|---------------------|--------------------------------|-----------------------|---|---|----------------------|------------------------------------|------------|----------------------|-----------------------|
| LP 467-016AB     | 01 11 25.41        | +15 26 21.6         | 45.79±1.78                     | R 1                   | 187.65±0.41   | -120.34±0.41                                  | (this)               | 2.6 ± 1.1                          | Giz02      | BetaPic?             | (this)                |
| HIP 017695       | 03 47 23.34        | -01 58 19.9         | 62.00±2.88                     | V 1                   | 185.53±3.77   | -273.48±3.95                                  | vLe07                |                                    |            | ABDor                | Zuc04                 |
| HD 025457        | 04 02 36.74        | -00 16 08.1         | 53.11±0.32                     | YV 2                  | 149.04±0.42   | -253.02±0.43                                  | vLe07                | 18.3 ± 0.4                         | GCMRV      | ABDor                | Zuc04                 |
| G 007-034        | 04 17 18.52        | +08 49 22.1         | 73.27±1.27                     | R 1                   | 127.45±0.46   | -374.10±0.46                                  | (this)               |                                    |            | ABDor                | (this)                |
| LP 776-025       | 04 52 24.42        | -16 49 22.2         | 69.40±1.70                     | R 1                   | 117.65±1.57   | -214.90±1.57                                  | (this)               |                                    |            | ABDor                | Tor08                 |
| CD-56 01032B     | 04 53 30.54        | -55 51 31.7         | 90.02±1.98                     | V 1                   | 132.85±4.25   | 73.93±3.75                                    | ASCC3                | 30.0                               | Tor06      | ABDor                | Tor08                 |
| CD-56 01032A     | 04 53 31.21        | -55 51 37.1         | 90.02±1.98                     | V 1                   | 134.53±2.39   | 72.68±2.03                                    | vLe07                | 29.0                               | Tor06      | ABDor                | Tor08                 |
| LP 476-207ABC    | 05 01 58.81        | +09 58 58.8         | 40.18±2.07                     | V R 2                 | 26.88±0.99  | -102.91±1.02                                  | (this)               | 14.7 ± 3.7                         | Giz02      | BetaPic              | Zuc04                 |
| BD-21 01074BC    | 05 06 49.47        | -21 35 03.9         | 51.98±1.30                     | RR 2                  | 24.25±0.28  | -44.50±0.27                                   | (this)               | 23.7 ± 1.7                         | Giz02      | BetaPic              | Tor08                 |
| BD-21 01074A     | 05 06 49.92        | -21 35 09.2         | 51.98±1.30                     | RR 2                  | 47.89±0.36  | -18.45±0.37                                   | (this)               | 21.2 ± 0.9                         | Giz02      | BetaPic              | Tor08                 |
| HD 035650        | 05 24 30.17        | -38 58 10.8         | 55.55±0.92                     | V 1                   | 44.25±0.67  | -59.51±1.13                                   | vLe07                | 31.9 ± 0.3                         | Tor06      | ABDor                | Zuc04                 |
| AB Dor ABC       | 05 28 44.83        | -65 26 54.9         | 65.93±0.57                     | V 1                   | 33.16±0.39  | 150.83±0.73                                   | vLe07                | 28.0 ± 1.0                         | Mon01      | ABDor                | Zuc04                 |
| SCR 0529-3239    | 05 29 44.69        | -32 39 14.2         | 41.13±1.72                     | R 1                   | 25.31±1.25  | 1.20±1.19                                     | (this)               |                                    |            | BetaPic              | (this)                |
| $\beta$ Pic      | 05 47 17.09        | -51 03 59.4         | 51.44±0.12                     | V 1                   | 4.65±0.11   | 83.10±0.15                                    | vLe07                | 20.0                               | GCMRV      | BetaPic              | Zuc04                 |
| AP Col           | 06 04 52.16        | -34 33 36.0         | 118.41±0.94                    | R 1                   | 26.58±0.29  | 341.00±0.29                                   | (this)               | 22.4 ± 0.3                         | Rie11      | Argus                | Rie11                 |
| CD-35 02722      | 06 09 19.21        | -35 49 31.1         | (41.67±99.99) <sup>a</sup>     | 0                     | -3.83±1.41  | -58.70±1.45                                   | ASCC3                | 31.4 ± 0.4                         | Tor06      | ABDor                | Tor08                 |
| HD 045270        | 06 22 30.94        | -60 13 07.1         | 42.05±0.27                     | V 1                   | -11.29±0.35   | 64.24±0.30                                    | vLe07                | 32.0                               | Tor06      | ABDor                | Zuc04                 |
| GSC 8894-0426    | 06 25 56.11        | -60 03 27.4         | (43.48±99.99) <sup>a</sup>     | 0                     | 19.8 ±14.7  | 107.1 ±14.7                                   | PPMXL                |                                    |            | ABDor                | Zuc04                 |
| AK Pic AB        | 06 38 00.37        | -61 32 00.2         | 46.96±0.81                     | V 1                   | -47.84±1.04   | 72.73±0.87                                    | vLe07                | 32.3 ± 0.3                         | GCMRV      | ABDor                | Zuc04                 |
| CD-61 01439      | 06 39 50.02        | -61 28 41.5         | 44.74±0.91                     | V 1                   | -27.92±1.00   | 75.34±1.13                                    | vLe07                | 31.7                               | Tor06      | ABDor                | Zuc04                 |
| V0372 Pup AB     | 07 28 51.37        | -30 14 48.5         | 63.72±1.76                     | V 1                   | -130.08±1.36  | -131.55±1.73                                  | vLe07                | 28.1                               | Tor06      | ABDor                | Zuc04                 |
| SCR 0757-7114    | 07 57 32.55        | -71 14 53.8         | 45.25±1.96                     | R 1                   | 104.05±1.73   | -0.89±1.75                                    | (this)               |                                    |            | Argus                | (this)                |
| G 161-071        | 09 44 54.18        | -12 20 54.4         | 71.73±1.36                     | R 1                   | -321.97±0.42  | 40.93±0.42                                    | (this)               |                                    |            | BetaPic              | Sch12a                |
| DK Leo           | 10 14 19.18        | +21 04 29.6         | 43.32±1.80                     | V 1                   | -144.06±1.90  | -154.79±1.10                                  | vLe07                | 14.8 ± 2.1                         | Tei09      | BetaPic <sup>b</sup> | Tei09                 |
| TWA 022AB        | 10 17 26.89        | -53 54 26.5         | 57.00±0.70                     | T 1                   | -175.8 ± 0.8  | -21.3 ± 0.8                                   | Tei09                | 9.1 ± 0.6                          | GCMRV      | ABDor <sup>b</sup>   | Tor08                 |
| GJ 0393          | 10 28 55.55        | +00 50 27.6         | 140.27±2.04                    | YV 2                  | -603.75±1.90  | -728.94±2.04                                  | vLe07                | -0.2                               | GCMRV      | Argus                | Zuc11                 |
| GJ 0448          | 11 49 03.58        | +14 34 19.4         | 90.81±0.51                     | YV 2                  | -497.68±0.87  | -114.67±0.44                                  | vLe07                | -6.3 ± 0.6                         | Mon01      | ABDor                | Zuc04                 |
| PX Vir           | 13 03 49.65        | -05 09 42.5         | 46.10±0.81                     | V 1                   | -191.13±0.86  | -218.73±0.68                                  | vLe07                |                                    |            | ABDor                | Sch12a                |
| PM II 13143+1320 | 13 14 20.39        | +13 20 01.2         | (49.75±99.99) <sup>a</sup>     | 0                     | -244 ±  | -186 ±  | Lep05                |                                    |            | ABDor                | Sch12a                |
| G 165-008AB      | 13 31 46.63        | +29 16 36.5         | 55.51±2.38                     | R 1                   | -218.43±0.75  | -141.20±0.76                                  | (this)               | -7.5 ± 6.5                         | Giz02      | Tuc-Hor              | (this)                |
| GJ 0714          | 18 30 12.01        | -58 16 27.5         | 69.30±15.00                    | Y 1                   | -25.3 ± 2.2   | -446.7 ± 2.3                                  | Tych2                | -3.0 ± 5.3                         | GCMRV      | ABDor                | Sch10                 |
| TYC 5126-181-1   | 18 52 12.65        | -07 13 32.7         | (48.07±99.99) <sup>a</sup>     | 0                     | 67.7 ± 2.8  | -250.7 ± 3.1                                  | Tych2                |                                    |            | ABDor                | Sch10                 |
| L 755-019        | 20 28 43.62        | -11 28 30.8         | 54.14±1.92                     | R 1                   | 159.65±0.99   | -91.71±0.93                                   | (this)               |                                    |            | Argus                | (this)                |
| GJ 0799A (N)     | 20 41 51.17        | -32 26 07.0         | 101.46±0.78                    | YV VRR 6              | 294.69±0.45   | -319.20±0.44                                  | (this)               | -3.7 ± 3.0                         | Mon01      | BetaPic              | Zuc04                 |
| GJ 0799B (S)     | 20 41 51.23        | -32 26 09.5         | 101.46±0.78                    | YV VRR 6              | 228.55±0.49   | -393.86±0.48                                  | (this)               | -2.7 ± 3.0                         | Mon01      | BetaPic              | Zuc04                 |
| GJ 0803          | 20 45 09.53        | -31 20 27.2         | 101.46±0.78                    | YV VRR 6              | 279.96±1.26   | -360.61±0.73                                  | vLe07                | -4.5 ± 1.3                         | GCMRV      | BetaPic              | Zuc04                 |
| LO Peg           | 21 31 01.71        | +23 20 07.4         | 40.33±1.05                     | YV 2                  | 133.38±0.97   | -145.24±0.90                                  | vLe07                | -17.4 ± 1.0                        | Mon01      | ABDor                | Zuc04                 |
| GJ 1264AB        | 21 49 05.84        | -72 06 09.0         | 61.29±1.54                     | V 1                   | 297.92±1.42   | -293.49±1.37                                  | vLe07                | -10.7                              | Tor06      | ABDor                | Sch10                 |
| HIP 110526 AB    | 22 23 29.10        | +32 27 33.9         | 64.47±6.49                     | V 1                   | 251.31±5.54   | -212.28±11.32                                 | vLe07                | -24.0 ± 3.0                        | GCMRV      | ABDor                | Zuc04                 |
| WW PsA (A)       | 22 44 57.97        | -33 15 01.7         | 46.94±2.27                     | VR 2                  | 184.76±2.64   | -119.76±2.31                                  | vLe07                | 2.2                                | Tor06      | BetaPic              | Zuc04                 |
| TX PsA (B)       | 22 45 00.05        | -33 15 25.9         | 46.94±2.27                     | VR 2                  | 184.76±2.64   | -119.76±2.31                                  | vLe07                | 2.4                                | Tor06      | BetaPic              | Zuc04                 |
| HIP 114066       | 23 06 04.84        | +63 55 34.4         | 40.81±1.60                     | V 1                   | 171.46±1.59   | -58.55±1.57                                   | vLe07                | -23.5 ± 1.3                        | Mon01      | ABDor                | Zuc04                 |
| HD 224228        | 23 56 10.67        | -39 03 08.4         | 45.52±0.93                     | V 1                   | 206.72±0.51   | -185.07±0.54                                  | vLe07                | 13.1 ± 0.0                         | Tor06      | ABDor                | Zuc04                 |

<sup>a</sup>No parallax; distance uses kinematic estimate. Y= YPC (van Altena et al. 1995), V=HIPPARCOS (van Leeuwen 2007), R=RECONS (Riedel et al. 2011, this dissertation), T= Teixeira et al. 2009. # is number of measures in weighted mean.<sup>b</sup>Disputed membership.

Interestingly, TX PsA=GJ 871.1B=LP 984-092 is on the CTIOPI observing program, but has no associated X-rays in the ROSAT All Sky Survey (Voges et al. 1999). Its current preliminary parallax is included in Table 6.4

### 6.2.3 *The (potential) impact on theory*

The biggest boon to this young star research may indeed be the stars: Within this thesis, we have the reddest suspected members of  $\beta$  Pictoris (possibly LP 467-016B), AB Doradus (GJ 2022B), Tucanae-Horologium (2MA 0254-5108B), TW Hydra (TWA 027AB), and Argus (AP Col, or RX 0413-0139 if it truly is a member). Note that the known members typically “run out” in Figure 5.29, near the location of the fully-convective boundary, leaving very few ultracool dwarfs that could be used to trace the isochrones. This is an observational oversight, not evidence that there are few members of young associations cooler than the fully convective boundary – the reddest previously confirmed member of Tuc-Hor is HIP 3356B (M3.0V); of AB Dor is AB Dor C (M4.0V), and of  $\beta$  Pic, TWA 22 (M5.0V). All except AB Dor C (no photometry) are plotted in the figure. Only TW Hydra (via TWA 26 and TWA 27) has parallaxes of presumed brown dwarf members at the moment.

There are several reasons why we need redder members of these associations. First, I had severe problems trying to compare the spectrum of AP Col to other young M dwarfs, because there simply weren’t any stars comparably red. Second, we would like to understand better the nature of Li depletion in fully convective stars. Consider Figure 5.21, where there are very few stars redder than AP Col; lower-quality data from IC 2391 had to be used to fill in the areas cooler than the lithium depletion boundary. Many of my new sample

of young M dwarfs are cooler than previous association members, and *many* are below the lithium depletion boundary. Third, these stars below the convective limit fill in an area very poorly explored in every association apart from TW Hydra. Such low-mass stars are currently not well described by stellar evolution models, and the discovery of more stars will provide direct observational feedback into those models. Fourth, only eight masses of any quality have been determined for *any* pre-main-sequence M dwarfs (of any mass) less than 10 Myr old (Mathieu et al. 2007, Irwin et al. 2007, Cargile et al. 2008, Çakırlı & Ibanoglu 2010). What few masses we do have for this latter group are offset from predictions by 50-200% (Hillenbrand & White 2004). In fact, models for these stars at ages less than 10 Myr disagree with each other by similar amounts, while Mathieu et al. (2007) find it impossible to test models with currently available data.

Some work has already been done on low-mass members of the more nearby associations: Guirado et al. (2006) claim to have the first such mass determination for the 125 Myr old AB Dor moving group (AB Dor C), Bonnefoy et al. (2009) have measured the ambiguous TW Hydra/ $\beta$  Pic objects TWA 22AB, and Torres et al. (2010) report new masses for YY Gem AB(=Castor EF, GJ 278C<sup>3</sup>) in the Castor moving group (200 Myr). It is worth noting that both Guirado and Bonnefoy fit their dynamical masses to evolutionary models and got ages conspicuously different from those commonly accepted for the associations based on other stars; this has been taken as more evidence for the necessity of new evolutionary models, and more masses to properly characterize their behavior.

---

<sup>3</sup>CNS3p and ARICNS are/were unaware that each of the three optical components of Castor are SB2 binaries.

My thesis work has uncovered several potentially important binaries, including SCR 1012-3124AB (TW Hya), SCR 0613-2742AB ( $\beta$  Pic), SCR 1425-4113 (TW Hya?), and SCR 2010-2801AB ( $\beta$  Pic?), as well as identifying the previously-known LP 467-016AB as a possible  $\beta$  Pic member. All these stars, if followed, could offer more discriminatory power for comparing and refining evolutionary models.

### 6.3 Future Directions

#### 6.3.1 *TINYMO-North*

One obvious next step would be to conduct the TINYMO search in the northern hemisphere. SuperCOSMOS covers the entire sky, and with some minor modifications (including, perhaps, relaxing the 4-plate-detection requirement to 3 plates) one could carry out the survey in northern hemisphere fields. SuperCOSMOS will have one marked disadvantage, though; the northern hemisphere plates do not have quite the epoch spread of southern hemisphere plates, as the Palomar Optical Sky Survey was carried out relatively faster than the southern hemisphere surveys. Proper motion errors will also be higher thanks to a smaller time baseline.

Of course, the same techniques could be used with other sky surveys – UCAC4 is expected to contain Johnson  $BV$  and SDSS  $g'r'i'$  from the AAVSO Photometric All-Sky Survey (APASS) and  $JHK$  from 2MASS. PPMXL contains USNO-B1  $BRI$  photometry and 2MASS  $JHK$ . The availability of WISE and APASS mean that, with 2MASS and other surveys like SDSS, it is now possible to construct proper motions entirely from CCD-based catalogs

(which are far more accurate than photographic plates), which is being done (Scholz et al. 2011). Ultimately, though, TINYMO may not be worthwhile in the face of the impending SuperBLINK survey from Sebastian Lépine.

### 6.3.2 Kinematic Youth Survey

Rather than simply looking for yet more nearby M dwarfs, we can design a survey to specifically look for young stars. Based on the associations as defined in Torres et al. (2008) and the luminosity functions in the RECONS 25 pc Database, I estimate that there should be at least 1500 total members of the associations listed in Torres et al. (2008), of which currently only around 400 are known – nearly all of them brighter than  $V = 12$  and from TYCHO-2. Within the limits of SuperCOSMOS photometry (Appendix A), I should be able to reveal 600 more members. Of course, SuperCOSMOS proper motions are not absolute, and have errors of  $\sim 10$  mas yr $^{-1}$ , but SuperCOSMOS can be used as the input to more precise but cluttered catalogs like USNO-B1 or UCAC4.

Without parallaxes or radial velocities, I will have only RA, DEC and the two-dimensional proper motions to compare to known associations. This will require either using two free parameters to cut a plane through 6D phase space, or a somewhat backwards technique<sup>4</sup> more commonly used by those without recourse to parallaxes.

There are now many sources of data available to confirm youth parameters. Apart from

---

<sup>4</sup>In brief: given a position of a target star (RA, DEC), an association space velocity UVW, and a distance 10 pc, calculate association  $\mu_{RA \cos(DEC)}, \mu_{DEC}$ . Compare the  $\mu_{RA \cos(DEC)}, \mu_{DEC}$  vector *direction* to the stellar target's  $\mu_{RA \cos(DEC)}, \mu_{DEC}$  vector *direction* and confirm a directional match. If it is a directional match, determine the distance such that the association's proper motion vector *magnitude* best matches the target's proper motion vector *magnitude*. Use the distance to determine the absolute magnitude; check if star matches the association's isochrone.

the old and low-sensitivity ROSAT survey, there is now GALEX data with which to measure chromospheric activity. To augment IRAS (usually, non-)detections, there is now the WISE all-sky point source catalog to search for signs of disks, although this will only be useful at very young ages.

Radial velocity precision for confirming membership need not be particularly accurate. 1 km s<sup>-1</sup> is sufficient to distinguish between currently known<sup>5</sup> structures, and probably for identifying most SB1 binaries as well. Appropriate spectra can be obtained with a variety of instruments at national observatories, particularly FLAMINGOS-2 on Gemini-S. The most compelling observations in this case utilize infrared spectroscopy, as the current state-of-the-art in metallicity measurements is in K band (Rojas-Ayala et al. 2012) or H band, (Terrien et al. 2012). Some optical spectra may still be needed, though, as the only substantially strong lithium lines are the doublet at 6708Å (the lines at 26877Å are in strong water absorption, and much weaker than 6708Å).

These future observations that fill in large portions of the members of nearby associations are our best bets for illuminating several astrophysically interesting questions that still remain unanswered:

**What is the true initial mass function (IMF) of these clusters?** The IMFs of nearby star-forming regions have been investigated (e.g., Orion in Hillenbrand 1997, Chamaeleon I in Luhman 2007). It is worth knowing if the IMF of the smaller gas-less associations are the same. There are reasons we should expect they are not, in particular

---

<sup>5</sup>If currently known associations are broken down further into subgroups, or it becomes vitally necessary to make sure all members track back to the same point in space, this will not be the case.

that none of the nearby young associations appear to contain anything more massive than cool B-type stars, while the Orion star forming region produced extremely massive O and hot B-type stars, whose ionizing radiation may have prevented low-mass stars from forming<sup>6</sup>.

**Is AB Dor is related to the Pleiades?** (Luhman et al. 2005; Ortega et al. 2007)

These two configurations of stars have extremely similar kinematics, but very different spatial dispersions, and it has been claimed (Barenfeld et al. 2012) that AB Dor is not a single chemically homogeneous group.

**Are Argus and IC 2391 linked?** Torres et al. (2008) suggest the Argus association is linked to the IC 2391 open cluster, which currently implies an extremely low space density over a huge area at a younger age than the Pleiades/AB Dor, and probably a much larger initial formation region than is normally expected. I was unable to trace AP Col back to IC 2391 in Riedel et al. (2011), which would seem to imply they are either *not* linked, or our standard picture (that Argus is the dissolving remains of IC 2391) is somehow incorrect.

**Are TW Hydra and Lower Centaurus Crux linked?** The TW Hya association has similar kinematics to an older and more distant piece of Sco-Cen called Lower Centaurus Crux; several stars with TWA names are now believed to be members of Lower Centaurus Crux.

**Are Tuc-Hor, Columba, and Carina linked?** Torres et al. (2008) also lists three associations, Tuc-Hor, Columba and Carina, with tentative ages of 30 Myr, overlapping spatial extents and similar UVW velocities; **are they products of a UVW gradient**

---

<sup>6</sup>Notwithstanding that all the O-type stars should be gone from the nearby young associations anyway, it appears that they must have never been there, as low mass star formation apparently took place in quantity. Kinematic surveys for nearby white dwarfs, neutron stars, and black holes may still be interesting.

that will be “filled in” when more young stars are discovered? G 165-008AB, with its location  $\sim 70$  pc from the rest of the stars, suggests that there may indeed be a larger complex of  $\sim 30$  Myr old stars, which supports the idea of a larger star-forming region (or multiple star-forming regions).

### How many young stars are near the Sun?/What is the nearby Galactic Star Formation Rate?

Papers like Zuckerman & Song (2004) and Torres et al. (2008) only focus on the members of moving groups and associations, and for the most part neglect isolated young stars. A full count should include all nearby young stars. A partial answer is given in §6.2.2, but a more thorough study deserves to be done.

#### 6.3.3 *Non-population aspects*

Given that detection of targets and collection of gross properties (photometry, positions, proper motions, parallaxes) will be increasingly well-handled by the upcoming generation of massive survey projects like PanSTARRS, SkyMapper, Gaia, and LSST, the most important thing in both my TINYMO and young star surveys is the study of the additional parameters of youth. There are plenty of stars in my thesis (and in various other papers on the subject of stellar youth) that need more observations to explain what is going on, particularly if we are to solve the giant mess (§1.4.3) that young star memberships seem to be in right now.

Answering the questions will mean further honing my skills and collecting more data on individual targets to determine their radial velocities, lithium, metallicities, gravity, compositions, and masses (should my efforts to follow SCR 0613-2742AB until its orbit wraps in

~2 years succeed) – in short, efforts like [Riedel et al. \(2011\)](#) on larger scales. With continued work and specific answers on specific stars I hope to build up a body of work that will answer these questions, with the goal of finding the true population and characteristics of star formation in our corner of the Galaxy, and to reveal our Solar neighbors hiding in plain sight.

## REFERENCES

- Adams, J. D., Stauffer, J. R., Monet, D. G., Skrutskie, M. F., & Beichman, C. A. 2001, *AJ*, 121, 2053
- Alksnis, A., Balklavs, A., Dzervitis, U., Eglitis, I., Paupers, O., & Pundure, I. 2001, *Baltic Astronomy*, 10, 1
- Allen, P. R., & Reid, I. N. 2008, *AJ*, 135, 2024
- Allers, K. N. et al. 2007, *ApJ*, 657, 511
- Asiain, R., Figueras, F., & Torra, J. 1999, *A&A*, 350, 434
- Aumer, M., & Binney, J. J. 2009, *MNRAS*, 397, 1286
- Backman, D. E., Burgh, S. J., & Henry, T. J., eds. 2001, *Nearby Stars (NStars) Workshop*
- Balega, I. I., Balega, Y. Y., Hofmann, K.-H., Maksimov, A. F., Pluzhnik, E. A., Schertl, D., Shkhagosheva, Z. U., & Weigelt, G. 2002, *A&A*, 385, 87
- Ball, B., & Bromage, G. 1995, in *Lecture Notes in Physics*, Berlin Springer Verlag, Vol. 454, IAU Colloq. 151: Flares and Flashes, ed. J. Greiner, H. W. Duerbeck, & R. E. Gershberg, 67
- Baraffe, I., & Chabrier, G. 2010, *A&A*, 521, A44
- Barenfeld, S. A., Bubar, E. J., Mamajek, E. E., & Young, P. A. 2012, in *American Astronomical Society Meeting Abstracts*, Vol. 219, American Astronomical Society Meeting Abstracts, #151.30
- Barnes, S. A. 2003, *ApJ*, 586, 464

- Barrado y Navascues, D. 1998, *A&A*, 339, 831
- Barrado y Navascués, D., Stauffer, J. R., Song, I., & Caillault, J. 1999, *ApJ*, 520, L123
- Barrado y Navascués, D., Stauffer, J. R., & Jayawardhana, R. 2004, *ApJ*, 614, 386
- Bartlett, J. L., Ianna, P. A., & Begam, M. C. 2009, *PASP*, 121, 365
- Bastian, U., & Röser, S. 1993, *PPM Star Catalogue. Positions and proper motions of 197179 stars south of -2.5 degrees declination for equinox and epoch J2000.0. Vol. III: Zones -00 degrees to -20 degrees. Vol. IV: Zones -30 degrees to -80 degrees.* (Spektrum Akademischer Verlag, Heidelberg (Germany), 1993, 2011 p., ISBN 3-86025-131-7)
- Beers, T. C., Rossi, S., Ulrich, D., & Wilhelm, R. 1996, *AJ*, 112, 1188
- Benedict, G. F. et al. 1999, *AJ*, 118, 1086
- Bergfors, C. et al. 2010, *A&A*, 520, A54
- Bessel, F. W. 1838, *MNRAS*, 4, 152
- Bessell, M. S. 1986, *PASP*, 98, 1303
- . 1990a, *A&AS*, 83, 357
- . 1990b, *PASP*, 102, 1181
- . 2000, *PASP*, 112, 961
- Beuzit, J.-L. et al. 2004, *A&A*, 425, 997
- Biller, B. A., & Close, L. M. 2007, *ApJ*, 669, L41
- Bobylev, V. V. 2010, *Astronomy Letters*, 36, 220
- Boden, A. F., Torres, G., & Latham, D. W. 2006, *ApJ*, 644, 1193
- Boeshaar, P. C. 1976, *The spectral classification of m-dwarf stars* (Columbus: Ohio State

- University, 1976)
- Bonnefoy, M. et al. 2009, *A&A*, 506, 799
- Boss, A. P. et al. 2009, *PASP*, 121, 1218
- Boyd, M. R., Winters, J. G., Henry, T. J., Jao, W.-C., Finch, C. T., Subasavage, J. P., & Hambly, N. C. 2011a, *AJ*, 142, 10
- Boyd, M. R., Henry, T. J., Jao, W.-C., Subasavage, J. P., & Hambly, N. C. 2011b, *AJ*, 142, 92
- Bradshaw, C. F., Fomalont, E. B., & Geldzahler, B. J. 1997, *ApJ*, 484, L55
- Breddels, M. A. et al. 2010, *A&A*, 511, A90
- Bubar, E. J., & King, J. R. 2010, *AJ*, 140, 293
- Çakırlı, Ö., & Ibanoglu, C. 2010, *MNRAS*, 401, 1141
- Caballero, J. A. 2009, *A&A*, 507, 251
- . 2010, *A&A*, 514, A98
- Cannon, A. J., & Pickering, E. C. 1901, *Annals of Harvard College Observatory*, 28, 129
- Cargile, P. A., Stassun, K. G., & Mathieu, R. D. 2008, *ApJ*, 674, 329
- Casagrande, L., Flynn, C., & Bessell, M. 2008, *MNRAS*, 389, 585
- Castro, S., Porto de Mello, G. F., & da Silva, L. 1999, *MNRAS*, 305, 693
- Chauvin, G., Lagrange, A.-M., Dumas, C., Zuckerman, B., Mouillet, D., Song, I., Beuzit, J.-L., & Lowrance, P. 2004, *A&A*, 425, L29
- Copenhagen University Observatory, Royal Greenwich Observatory, & Real Instituto Y Observatorio de La Armada, E. S. F. 1999, in *Carlsberg Meridian Catalogs Number 1-11*

(1999), 0

Costa, E., Méndez, R. A., Jao, W.-C., Henry, T. J., Subasavage, J. P., Brown, M. A., Ianna, P. A., & Bartlett, J. 2005, *AJ*, 130, 337

Costa, E., Méndez, R. A., Jao, W.-C., Henry, T. J., Subasavage, J. P., & Ianna, P. A. 2006, *AJ*, 132, 1234

Cousins, A. W. J. 1980, *South African Astronomical Observatory Circular*, 1, 234

Cushing, M. C. et al. 2011, *ApJ*, 743, 50

Cutri, R. M. et al. 2003, 2MASS All Sky Catalog of point sources. (NASA/IPAC Infrared Science Archive. <http://irsa.ipac.caltech.edu/applications/Gator/>)

da Silva, L., Torres, C. A. O., de La Reza, R., Quast, G. R., Melo, C. H. F., & Sterzik, M. F. 2009, *A&A*, 508, 833

Daemgen, S., Sieglar, N., Reid, I. N., & Close, L. M. 2007, *ApJ*, 654, 558

de Grijs, R., Goodwin, S. P., Kouwenhoven, M. B. N., & Kroupa, P. 2008, *A&A*, 492, 685

de la Reza, R., Torres, C. A. O., Quast, G., Castilho, B. V., & Vieira, G. L. 1989, *ApJ*, 343, L61

Deacon, N. R., Hambly, N. C., & Cooke, J. A. 2005a, *A&A*, 435, 363

Deacon, N. R., Hambly, N. C., Henry, T. J., Subasavage, J. P., Brown, M. A., & Jao, W.-C. 2005b, *AJ*, 129, 409

Deacon, N. R., & Hambly, N. C. 2007, *A&A*, 468, 163

Deacon, N. R., Hambly, N. C., King, R. R., & McCaughrean, M. J. 2009, *MNRAS*, 394, 857

Dehnen, W., & Binney, J. 1998, *MNRAS*, 294, 429

- Delfosse, X., Forveille, T., Perrier, C., & Mayor, M. 1998, *A&A*, 331, 581
- Delfosse, X., Forveille, T., Beuzit, J., Udry, S., Mayor, M., & Perrier, C. 1999, *A&A*, 344, 897
- Desidera, S. et al. 2011, *A&A*, 529, A54
- Dopita, M., Hart, J., McGregor, P., Oates, P., Bloxham, G., & Jones, D. 2007, *Ap&SS*, 310, 255
- Dopita, M. et al. 2010, *Ap&SS*, 327, 245
- Dotter, A., Chaboyer, B., Jevremović, D., Kostov, V., Baron, E., & Ferguson, J. W. 2008, *ApJS*, 178, 89
- Ducourant, C., Teixeira, R., Chauvin, G., Daigne, G., Le Campion, J.-F., Song, I., & Zuckerman, B. 2008, *A&A*, 477, L1
- Dupuy, T. J., & Liu, M. C. 2012, *ApJS*, 201, 19
- Dyson, Sir, F. W. 1917, *MNRAS*, 77, 212
- Eggen, O. J. 1958, *MNRAS*, 118, 65
- . 1965, *The Observatory*, 85, 191
- . 1985, *AJ*, 90, 74
- . 1993, *AJ*, 106, 1885
- Fabricius, C., & Makarov, V. V. 2000, *A&AS*, 144, 45
- Faherty, J. K. et al. 2012, *ApJ*, 752, 56
- Famaey, B., Jorissen, A., Luri, X., Mayor, M., Udry, S., Dejonghe, H., & Turon, C. 2005, *A&A*, 430, 165

- Fernández, D., Figueras, F., & Torra, J. 2008, *A&A*, 480, 735
- Finch, C. T., Henry, T. J., Subasavage, J. P., Jao, W., & Hambly, N. C. 2007, *AJ*, 133, 2898
- Findeisen, K., & Hillenbrand, L. 2010, *AJ*, 139, 1338
- Fitzpatrick, E. L. 1999, *PASP*, 111, 63
- Fleming, T. A. 1998, *ApJ*, 504, 461
- Fruscione, A. 1996, *ApJ*, 459, 509
- Gatewood, G., Han, I., de Jonge, J. K., Reiland, C. T., & Pourbaix, D. 2001, *ApJ*, 549, 1145
- Gatewood, G. 2005, *AJ*, 130, 809
- Gatewood, G., & Coban, L. 2009, *AJ*, 137, 402
- Gershberg, R. E., Katsova, M. M., Lovkaya, M. N., Terebizh, A. V., & Shakhovskaya, N. I. 1999, *A&AS*, 139, 555
- Giclas, H. L., Burnham, Jr., R., & Thomas, N. G. 1979, *Lowell Observatory Bulletin*, 8, 145
- Gies, D. R. et al. 2008, *ApJ*, 682, L117
- Gizis, J. E. 1997, *AJ*, 113, 806
- Gizis, J. E., Reid, I. N., & Hawley, S. L. 2002, *AJ*, 123, 3356
- Gizis, J. E., Jao, W., Subasavage, J. P., & Henry, T. J. 2007, *ApJ*, 669, L45
- Gliese, W. 1957, *Astron. Rechen-Institut, Heidelberg*, 89 Seiten, 8, 1
- . 1969, *Veroeffentlichungen des Astronomischen Rechen-Instituts Heidelberg*, 22, 1
- Gliese, W., & Jahreiß, H. 1979, *Bulletin d'Information du Centre de Donnees Stellaires*, 16, 92
- . 1982, *A&AS*, 47, 471

- . 1991, Preliminary Version of the Third Catalogue of Nearby Stars, Tech. rep.
- Graham, J. A. 1982, *PASP*, 94, 244
- Gray, R. O., Napier, M. G., & Winkler, L. I. 2001, *AJ*, 121, 2148
- Gray, R. O., Corbally, C. J., Garrison, R. F., McFadden, M. T., & Robinson, P. E. 2003, *AJ*, 126, 2048
- Gray, R. O., Corbally, C. J., Garrison, R. F., McFadden, M. T., Bubar, E. J., McGahee, C. E., O'Donoghue, A. A., & Knox, E. R. 2006, *AJ*, 132, 161
- Gregorio-Hetem, J., Lepine, J. R. D., Quast, G. R., Torres, C. A. O., & de La Reza, R. 1992, *AJ*, 103, 549
- Guirado, J. C. et al. 2006, *A&A*, 446, 733
- Haisch, Jr., K. E., Lada, E. A., & Lada, C. J. 2001, *ApJ*, 553, L153
- Haisch, Jr., K. E., Jayawardhana, R., & Alves, J. 2005, *ApJ*, 627, L57
- Hambly, N. C. et al. 2001a, *MNRAS*, 326, 1279
- Hambly, N. C., Irwin, M. J., & MacGillivray, H. T. 2001b, *MNRAS*, 326, 1295
- Hambly, N. C., Davenhall, A. C., Irwin, M. J., & MacGillivray, H. T. 2001c, *MNRAS*, 326, 1315
- Hambly, N. C., Henry, T. J., Subasavage, J. P., Brown, M. A., & Jao, W. 2004, *AJ*, 128, 437
- Hartkopf, W. I., McAlister, H. A., & Franz, O. G. 1989, *AJ*, 98, 1014
- Hawley, S. L., Gizis, J. E., & Reid, I. N. 1996, *AJ*, 112, 2799
- Hayashi, C. 1966, *ARA&A*, 4, 171

- Heintz, W. D. 1987, ApJS, 65, 161
- Henderson, T. 1839, MNRAS, 4, 168
- Henry, T. J., Kirkpatrick, J. D., & Simons, D. A. 1994, AJ, 108, 1437
- Henry, T. J., Ianna, P. A., Kirkpatrick, J. D., & Jahreiss, H. 1997, AJ, 114, 388
- Henry, T. J., Franz, O. G., Wasserman, L. H., Benedict, G. F., Shelus, P. J., Ianna, P. A., Kirkpatrick, J. D., & McCarthy, Jr., D. W. 1999, ApJ, 512, 864
- Henry, T. J., Walkowicz, L. M., Barto, T. C., & Golimowski, D. A. 2002, AJ, 123, 2002
- Henry, T. J., Subasavage, J. P., Brown, M. A., Beaulieu, T. D., Jao, W., & Hambly, N. C. 2004, AJ, 128, 2460
- Henry, T. J., Jao, W., Subasavage, J. P., Beaulieu, T. D., Ianna, P. A., Costa, E., & Méndez, R. A. 2006, AJ, 132, 2360
- Herschel, W. 1783, Royal Society of London Philosophical Transactions Series I, 73, 247
- Hillenbrand, L. A. 1997, AJ, 113, 1733
- Hillenbrand, L. A., & White, R. J. 2004, ApJ, 604, 741
- Hinkle, K. H., Wallace, L., & Livingston, W. 2003, in Bulletin of the American Astronomical Society, Vol. 35, American Astronomical Society Meeting Abstracts, 1260
- Hirshfeld, A. W. 2001, Parallax : the race to measure the cosmos, ed. Hirshfeld, A. W. (New York : W.H. Freeman and Co., c2001. ISBN : 0716737116)
- Høg, E. et al. 2000, A&A, 355, L27
- Holmberg, J., Nordström, B., & Andersen, J. 2009, A&A, 501, 941
- Honeycutt, R. K. 1992, PASP, 104, 435

- Ianna, P. A., Patterson, R. J., & Swain, M. A. 1996, *AJ*, 111, 492
- Irwin, J. et al. 2007, *MNRAS*, 380, 541
- Janson, M., Brandner, W., & Henning, T. 2008, *A&A*, 478, 597
- Jao, W.-C., Henry, T. J., Subasavage, J. P., Bean, J. L., Costa, E., Ianna, P. A., & Méndez, R. A. 2003, *AJ*, 125, 332
- Jao, W., Henry, T. J., Subasavage, J. P., Brown, M. A., Ianna, P. A., Bartlett, J. L., Costa, E., & Méndez, R. A. 2005, *AJ*, 129, 1954
- Jao, W., Henry, T. J., Subasavage, J. P., Winters, J. G., Riedel, A. R., & Ianna, P. A. 2011, *AJ*, 141, 117
- Jaschek, C., & Valbousquet, A. 1992, *A&A*, 255, 124
- Jefferys, W. H., Fitzpatrick, M. J., & McArthur, B. E. 1988, *Celestial Mechanics*, 41, 39
- Jeffries, R. D., & Naylor, T. 2001, in *Astronomical Society of the Pacific Conference Series*, Vol. 243, *From Darkness to Light: Origin and Evolution of Young Stellar Clusters*, ed. T. Montmerle & P. André, 633–+
- Jenkins, J. S., Ramsey, L. W., Jones, H. R. A., Pavlenko, Y., Gallardo, J., Barnes, J. R., & Pinfield, D. J. 2009, *ApJ*, 704, 975
- Johnson, D. R. H., & Soderblom, D. R. 1987, *AJ*, 93, 864
- Johnson, H. L., Mitchell, R. I., Iriarte, B., & Wisniewski, W. Z. 1966, *Communications of the Lunar and Planetary Laboratory*, 4, 99
- Just, A., & Jahreiß, H. 2010, *MNRAS*, 402, 461
- Keenan, P. C., & McNeil, R. C. 1976, *An atlas of spectra of the cooler stars: Types G,K,M,S*,

- and C. Part 1: Introduction and tables (Columbus: Ohio State University Press, 1976)
- Kenyon, S. J., & Hartmann, L. 1995, *ApJS*, 101, 117
- Kharchenko, N. V. 2001, *Kinematika i Fizika Nebesnykh Tel*, 17, 409
- Khrutskaya, E. V., Izmailov, I. S., & Khovrichev, M. Y. 2010, *Astronomy Letters*, 36, 576
- King, J. R., Villarreal, A. R., Soderblom, D. R., Gulliver, A. F., & Adelman, S. J. 2003, *AJ*, 125, 1980
- Kirkpatrick, J. D., Henry, T. J., & McCarthy, Jr., D. W. 1991, *ApJS*, 77, 417
- Kirkpatrick, J. D., Henry, T. J., & Simons, D. A. 1995, *AJ*, 109, 797
- Kirkpatrick, J. D. et al. 1999, *ApJ*, 519, 802
- Kirkpatrick, J. D. et al. 2011, *ApJS*, 197, 19
- Kiss, L. L. et al. 2011, *MNRAS*, 411, 117
- Koen, C., Kilkeny, D., van Wyk, F., Cooper, D., & Marang, F. 2002, *MNRAS*, 334, 20
- König, B., Neuhäuser, R., Guenther, E. W., & Hambaryan, V. 2003, *Astronomische Nachrichten*, 324, 516
- Kron, G. E., Gascoigne, S. C. B., & White, H. S. 1957, *AJ*, 62, 205
- Landolt, A. U. 1992, *AJ*, 104, 340
- . 2007, *AJ*, 133, 2502
- Law, N. M., Hodgkin, S. T., & Mackay, C. D. 2008, *MNRAS*, 384, 150
- Lawson, W. A., Lyo, A., & Bessell, M. S. 2009, *MNRAS*, 400, L29
- Lee, K.-G., Berger, E., & Knapp, G. R. 2010, *ApJ*, 708, 1482
- Leggett, S. K. et al. 2012, *ApJ*, 748, 74

- Lépine, S., Shara, M. M., & Rich, R. M. 2002, *AJ*, 124, 1190
- Lépine, S., & Shara, M. M. 2005, *AJ*, 129, 1483
- Lépine, S., Rich, R. M., & Shara, M. M. 2005, *ApJ*, 633, L121
- Lépine, S., & Simon, M. 2009, *AJ*, 137, 3632
- Lépine, S., & Gaidos, E. 2011, *AJ*, 142, 138
- Lindgren, L. 2007, *Highlights of Astronomy*, 14, 481
- López-Santiago, J., Micela, G., & Montes, D. 2009, *A&A*, 499, 129
- Lucas, P. W. et al. 2010, *MNRAS*, 408, L56
- Luhman, K. L., Stauffer, J. R., & Mamajek, E. E. 2005, *ApJ*, 628, L69
- Luhman, K. L. 2007, *ApJS*, 173, 104
- Lutz, T. E., & Kelker, D. H. 1973, *PASP*, 85, 573
- Luyten, W. J., & Shapley, H. 1930, *Annals of Harvard College Observatory*, 85, 73
- Luyten, W. J. 1957, *A catalogue of 9867 stars in the Southern Hemisphere with proper motions exceeding 0.2" annually.* (Minneapolis, Lund Press, 1957.)
- . 1979a, *LHS catalogue. A catalogue of stars with proper motions exceeding 0.5" annually* (Minneapolis: University of Minnesota, 1979, 2nd ed.)
- . 1979b, *NLTT catalogue. Volume I. +90 to +30. Volume. II. +30 to 0.* (Publ. by Univ. Minnesota, Minneapolis, USA. Vol. I: 282 p., Vol. II: 286 p.)
- Luyten, W. J. 1988, in *IAU Symposium, Vol. 133, Mapping the Sky: Past Heritage and Future Directions*, ed. S. Debarbat, 301
- Lynds, B. T. 1962, *ApJS*, 7, 1

- Lyo, A.-R., Lawson, W. A., & Bessell, M. S. 2004, MNRAS, 355, 363
- Makarov, V. V., & Urban, S. 2000, MNRAS, 317, 289
- Makarov, V. V., Olling, R. P., & Teuben, P. J. 2004, MNRAS, 352, 1199
- Mamajek, E. E., Lawson, W. A., & Feigelson, E. D. 1999, ApJ, 516, L77
- Mamajek, E. E. 2005, ApJ, 634, 1385
- Mamajek, E. E. 2009, in IAU Symposium, Vol. 258, IAU Symposium, ed. E. E. Mamajek, D. R. Soderblom, & R. F. G. Wyse, 375–382
- Martín, E. 2000, in Astronomical Society of the Pacific Conference Series, Vol. 212, From Giant Planets to Cool Stars, ed. C. A. Griffith & M. S. Marley, 38
- Martinache, F., Rojas-Ayala, B., Ireland, M. J., Lloyd, J. P., & Tuthill, P. G. 2009, ApJ, 695, 1183
- Mathieu, R. D., Baraffe, I., Simon, M., Stassun, K. G., & White, R. 2007, Protostars and Planets V, 411
- Mentuch, E., Brandeker, A., van Kerkwijk, M. H., Jayawardhana, R., & Hauschildt, P. H. 2008, ApJ, 689, 1127
- Messina, S., Desidera, S., Turatto, M., Lanzafame, A. C., & Guinan, E. F. 2010, A&A, 520, A15
- Michell, J. 1767, Royal Society of London Philosophical Transactions Series I, 57, 234
- Mihalas, D., & Binney, J. 1981, Galactic astronomy: Structure and kinematics 2nd edition (San Francisco, CA, W. H. Freeman and Co., 1981. 608 p.)
- Mochnecki, S. W. et al. 2002, AJ, 124, 2868

- Mohanty, S., & Basri, G. 2003, *ApJ*, 583, 451
- Monet, D. G. et al. 2003, *AJ*, 125, 984
- Montagnier, G. et al. 2006, *A&A*, 460, L19
- Montes, D., López-Santiago, J., Fernández-Figueroa, M. J., & Gálvez, M. C. 2001, *A&A*, 379, 976
- Morgan, D. H. 1995, in *Astronomical Society of the Pacific Conference Series*, Vol. 84, IAU Colloq. 148: The Future Utilisation of Schmidt Telescopes, ed. J. Chapman, R. Cannon, S. Harrison, & B. Hidayat, 137
- Morgan, W. W., Keenan, P. C., & Kellman, E. 1943, *An atlas of stellar spectra, with an outline of spectral classification* (Chicago, Ill., The University of Chicago press [1943])
- Murphy, S. J., Lawson, W. A., & Bessell, M. S. 2010, *MNRAS*, 406, L50
- Murphy, S. J. 2012, PhD thesis, Mount Stromlo Observatory, Australian National University, Canberra, Australia [murphysj@mso.anu.edu.au](mailto:murphysj@mso.anu.edu.au)
- Nakajima, T., & Morino, J.-I. 2012, *AJ*, 143, 2
- Nidever, D. L., Marcy, G. W., Butler, R. P., Fischer, D. A., & Vogt, S. S. 2002, *ApJS*, 141, 503
- Ortega, V. G., Jilinski, E., de La Reza, R., & Bazzanella, B. 2007, *MNRAS*, 377, 441
- Perryman, M. A. C. et al. 1997, *A&A*, 323, L49
- Pickering, E. C. 1890, *Annals of Harvard College Observatory*, 27, 1
- Platais, I., Melo, C., Mermilliod, J., Kozhurina-Platais, V., Fulbright, J. P., Méndez, R. A., Altmann, M., & Sperauskas, J. 2007, *A&A*, 461, 509

- Platais, I. et al. 2011, MNRAS, 413, 1024
- Pojmanski, G. 1997, Acta Astron., 47, 467
- Pokorny, R. S., Jones, H. R. A., & Hambly, N. C. 2003, A&A, 397, 575
- Porter, J. G. 1892, AJ, 12, 25
- Porto de Mello, G. F., Lyra, W., & Keller, G. R. 2008, A&A, 488, 653
- Pourbaix, D., & Jorissen, A. 2000, A&AS, 145, 161
- Pravdo, S. H., Shaklan, S. B., Henry, T., & Benedict, G. F. 2004, ApJ, 617, 1323
- Raghavan, D. et al. 2010, ApJS, 190, 1
- Ramm, D. J., Pourbaix, D., Hearnshaw, J. B., & Komonjinda, S. 2009, MNRAS, 394, 1695
- Reid, I. N., Cruz, K. L., & Allen, P. R. 2007, AJ, 133, 2825
- Reid, I. N., Cruz, K. L., Kirkpatrick, J. D., Allen, P. R., Mungall, F., Liebert, J., Lowrance, P., & Sweet, A. 2008, AJ, 136, 1290
- Reid, I. N., Hawley, S. L., & Gizis, J. E. 1995, AJ, 110, 1838
- Reid, I. N., & Hawley, S. L. 1999, AJ, 117, 343
- Reiners, A., Basri, G., & Browning, M. 2009, ApJ, 692, 538
- Riaz, B., Gizis, J. E., & Harvin, J. 2006, AJ, 132, 866
- Riedel, A. R. et al. 2010, AJ, 140, 897
- Riedel, A. R., Murphy, S. J., Henry, T. J., Melis, C., Jao, W.-C., & Subasavage, J. P. 2011, AJ, 142, 104
- Robrade, J., Ness, J., & Schmitt, J. H. M. M. 2004, A&A, 413, 317
- Rodriguez, D. R., Bessell, M. S., Zuckerman, B., & Kastner, J. H. 2011, ApJ, 727, 62

- Roeser, S., & Bastian, U. 1988, *A&AS*, 74, 449
- Roeser, S., Demleitner, M., & Schilbach, E. 2010, *AJ*, 139, 2440
- Rojas-Ayala, B., Covey, K. R., Muirhead, P. S., & Lloyd, J. P. 2012, *ApJ*, 748, 93
- Rajo, P. M., & Harrington, J. 2006, *ApJ*, 649, 553
- Röser, S., Bastian, U., & Kuzmin, A. 1994, *A&AS*, 105, 301
- Röser, S., Schilbach, E., Piskunov, A. E., Kharchenko, N. V., & Scholz, R.-D. 2011, *A&A*, 531, A92
- Rucinski, S. M., & Krautter, J. 1983, *A&A*, 121, 217
- Samus, N. N., Durlevich, O. V., & et al. 2012, *VizieR Online Data Catalog*, 1, 2025
- Sandhu, J. S., Bailes, M., Manchester, R. N., Navarro, J., Kulkarni, S. R., & Anderson, S. B. 1997, *ApJ*, 478, L95
- Schisano, E., Covino, E., Alcalá, J. M., Esposito, M., Gandolfi, D., & Guenther, E. W. 2009, *A&A*, 501, 1013
- Schlieder, J. E., Lépine, S., & Simon, M. 2010, *AJ*, 140, 119
- . 2012a, *AJ*, 143, 80
- Schlieder, J. E., Lépine, S., Rice, E., Simon, M., Fielding, D., & Tomasino, R. 2012b, *AJ*, 143, 114
- Scholz, R.-D., Irwin, M., Ibata, R., Jahreiß, H., & Malkov, O. Y. 2000, *A&A*, 353, 958
- Scholz, R.-D., & Meusinger, H. 2002, *MNRAS*, 336, L49
- Scholz, R., Lo Curto, G., Méndez, R. A., Hambaryan, V., Costa, E., Henry, T. J., & Schwöpe, A. D. 2005, *A&A*, 439, 1127

- Scholz, A., Coffey, J., Brandeker, A., & Jayawardhana, R. 2007, *ApJ*, 662, 1254
- Scholz, R.-D., Bihain, G., Schnurr, O., & Storm, J. 2011, *A&A*, 532, L5
- Schönrich, R., Binney, J., & Dehnen, W. 2010, *MNRAS*, 403, 1829
- Shkolnik, E., Liu, M. C., & Reid, I. N. 2009, *ApJ*, 699, 649
- Shkolnik, E. L., Hebb, L., Liu, M. C., Reid, I. N., & Collier Cameron, A. 2010, *ApJ*, 716, 1522
- Shkolnik, E. L., Liu, M. C., Reid, I. N., Dupuy, T., & Weinberger, A. J. 2011, *ApJ*, 727, 6
- Skrutskie, M. F. et al. 2006, *AJ*, 131, 1163
- Slesnick, C. L., Carpenter, J. M., & Hillenbrand, L. A. 2006a, *AJ*, 131, 3016
- Slesnick, C. L., Carpenter, J. M., Hillenbrand, L. A., & Mamajek, E. E. 2006b, *AJ*, 132, 2665
- Smart, R. L., Ioannidis, G., Jones, H. R. A., Bucciarelli, B., & Lattanzi, M. G. 2010, *A&A*, 514, A84
- Smith, B. A., & Terrile, R. J. 1984, *Science*, 226, 1421
- Smith, J. A. et al. 2002, *AJ*, 123, 2121
- Soderblom, D. R., Nelan, E., Benedict, G. F., McArthur, B., Ramirez, I., Spiesman, W., & Jones, B. F. 2005, *AJ*, 129, 1616
- Söderhjelm, S. 1999, *A&A*, 341, 121
- Song, I., Bessell, M. S., & Zuckerman, B. 2002, *ApJ*, 581, L43
- Song, I., Zuckerman, B., & Bessell, M. S. 2003, *ApJ*, 599, 342
- Sozzetti, A., & Desidera, S. 2010, *A&A*, 509, A103

- Spezzi, L. et al. 2008, *ApJ*, 680, 1295
- Stauffer, J. R., Schultz, G., & Kirkpatrick, J. D. 1998, *ApJ*, 499, L199
- Stauffer, J. et al. 2010, *PASP*, 122, 885
- Subasavage, J. P., Henry, T. J., Hambly, N. C., Brown, M. A., & Jao, W. 2005a, *AJ*, 129, 413
- Subasavage, J. P., Henry, T. J., Hambly, N. C., Brown, M. A., Jao, W.-C., & Finch, C. T. 2005b, *AJ*, 130, 1658
- Subasavage, J. P., Jao, W., Henry, T. J., Bergeron, P., Dufour, P., Ianna, P. A., Costa, E., & Méndez, R. A. 2009, *AJ*, 137, 4547
- Teixeira, R., Ducourant, C., Chauvin, G., Krone-Martins, A., Bonnefoy, M., & Song, I. 2009, *A&A*, 503, 281
- Terrien, R. C., Mahadevan, S., Bender, C. F., Deshpande, R., Ramsey, L. W., & Bochanski, J. J. 2012, *ApJ*, 747, L38
- Thackeray, W. G. 1917, *MNRAS*, 77, 204
- Tinney, C. G. 1993, *AJ*, 105, 1169
- . 1996, *MNRAS*, 281, 644
- Torres, C. A. O., Quast, G. R., de La Reza, R., da Silva, L., Melo, C. H. F., & Sterzik, M. 2003, in *Astrophysics and Space Science Library*, Vol. 299, *Open Issues in Local Star Formation*, ed. J. Lépine & J. Gregorio-Hetem, 83
- Torres, C. A. O., Quast, G. R., da Silva, L., de La Reza, R., Melo, C. H. F., & Sterzik, M. 2006, *A&A*, 460, 695

- Torres, C. A. O., Quast, G. R., Melo, C. H. F., & Sterzik, M. F. 2008, *Handbook of Star Forming Regions, Volume II* (ASP Press), 757
- Torres, G., Stefanik, R. P., & Latham, D. W. 1997, *ApJ*, 474, 256
- Torres, G., & Ribas, I. 2002, *ApJ*, 567, 1140
- Torres, G., Andersen, J., & Giménez, A. 2010, *A&A Rev.*, 18, 67
- Turnshek, D. E., Turnshek, D. A., Craine, E. R., & Boeshaar, P. C. 1985, *An atlas of digital spectra of cool stars (Types G, K, M, S and C)*. (Western Research Company, 2030 E. Speedway Suite 213, Tucson, Arizona 85719, USA. 6+17 pp.+75 charts. Price US\$ 30.00 (1985). ISBN 0-934525-00-5.)
- Turon, C. et al. 1993, *Bulletin d'Information du Centre de Données Stellaires*, 43, 5
- Urban, S. E., Corbin, T. E., Wycoff, G. L., Martin, J. C., Jackson, E. S., Zacharias, M. I., & Hall, D. M. 1998, *AJ*, 115, 1212
- van Altena, W. F., Lee, J. T., & Hoffleit, E. D. 1995, *The general catalogue of trigonometric [stellar] parallaxes* (New Haven, CT: Yale University Observatory, (c) 1995, 4th ed., completely revised and enlarged)
- van de Kamp, P. 1969, *PASP*, 81, 5
- . 1981, *Stellar paths: Photographic astrometry with long-focus instruments* (Dordrecht, D. Reidel Publishing Co. (Astrophysics and Space Science Library. Volume 85), 1981. 182 p.)
- van Leeuwen, F., & Evans, D. W. 1998, *A&AS*, 130, 157
- van Leeuwen, F., ed. 2007, *Astrophysics and Space Science Library*, Vol. 350, *Hipparcos*, the

New Reduction of the Raw Data (Astrophysics and Space Science Library)

van Maanen, A. 1915, *ApJ*, 41, 187

Voges, W. et al. 1999, *A&A*, 349, 389

———. 2000, *IAUcirc*, 7432, 1

Vogt, S. S. 1987, *PASP*, 99, 1214

Vogt, S. S. et al. 1994, in *Society of Photo-Optical Instrumentation Engineers (SPIE) Conference Series*, Vol. 2198, *Society of Photo-Optical Instrumentation Engineers (SPIE) Conference Series*, ed. D. L. Crawford & E. R. Craine, 362

Webb, R. A., Zuckerman, B., Platais, I., Patience, J., White, R. J., Schwartz, M. J., & McCarthy, C. 1999, *ApJ*, 512, L63

Weinberger, A. J., Anglada-Escudé, G., & Boss, A. 2011, in *Bulletin of the American Astronomical Society*, Vol. 43, *American Astronomical Society Meeting Abstracts #217*, #340.12

Weis, E. W. 1993, *AJ*, 105, 1962

———. 1996, *AJ*, 112, 2300

Weis, E. W., Lee, J. T., Lee, A. H., Griese, III, J. W., Vincent, J. M., & Uppgren, A. R. 1999, *AJ*, 117, 1037

West, A. A., & Basri, G. 2009, *ApJ*, 693, 1283

West, A. A., Hawley, S. L., Bochanski, J. J., Covey, K. R., Reid, I. N., Dhital, S., Hilton, E. J., & Masuda, M. 2008, *AJ*, 135, 785

Westerlund, B. E., Olander, N., & Hedin, B. 1981, *A&AS*, 43, 267

- White, R. J., & Basri, G. 2003, *ApJ*, 582, 1109
- Wichmann, R., Schmitt, J. H. M. M., & Hubrig, S. 2003, *A&A*, 399, 983
- Winters, J. G., Henry, T. J., Jao, W., Subasavage, J. P., Finch, C. T., & Hambly, N. C. 2011, *AJ*, 141, 21
- Woolley, R., Epps, E. A., Penston, M. J., & Poccock, S. B. 1970, *Royal Observatory Annals*, 5
- Wroblewski, H., & Torres, C. 1989, *A&AS*, 78, 231
- . 1991, *A&AS*, 91, 129
- . 1994, *A&AS*, 105, 179
- Yee, J. C., & Jensen, E. L. N. 2010, *ApJ*, 711, 303
- Zacharias, N. et al. 2010, *AJ*, 139, 2184
- Zacharias, N., Urban, S. E., Zacharias, M. I., Wycoff, G. L., Hall, D. M., Monet, D. G., & Rafferty, T. J. 2004, *AJ*, 127, 3043
- Zickgraf, F.-J., Krautter, J., Reffert, S., Alcalá, J. M., Mujica, R., Covino, E., & Sterzik, M. F. 2005, *A&A*, 433, 151
- Zuckerman, B., & Song, I. 2004, *ARA&A*, 42, 685
- Zuckerman, B., Bessell, M. S., Song, I., & Kim, S. 2006, *ApJ*, 649, L115
- Zuckerman, B., Rhee, J. H., Song, I., & Bessell, M. S. 2011, *ApJ*, 732, 61

## APPENDIX A

## HOW ACCURATE ARE SUPERCOSMOS MAGNITUDES?

The SuperCOSMOS Sky Survey (Hambly et al. 2001a,b,c) is an all-sky survey made by digitizing the Science and Engineering Research Council (SERC) Survey plates taken at Siding Spring Observatory from 1949-2001. All of the plates were digitized on the SuperCOSMOS scanning machine, and then assembled into a complete map of the sky with deep four-colour photometry at every point, with 2MASS cross-matches where possible. The plate sequences used were:

1. SERC-J/EJ, a roughly blue filter taken from 1974-1994, limiting magnitude  $B_J=23$ , 95% completeness threshold magnitude  $B_J=21$ .
2. ESO-R, a first epoch red filter for  $\text{DEC} < -20$ , taken from 1978-1990, limiting magnitude  $R_1=22$ .
3. POSS-I E, a first epoch red filter for  $\text{DEC} > -18^1$ , taken from 1949-1958, limiting magnitude  $R_1=20$ .
4. SERC-ER/AAO-R, second epoch red filters taken from 1984-2000, limiting magnitude  $R_2=22$ .
5. SERC-I, an infrared filter taken from 1978-2001, limiting magnitude  $I=19$ .

The SERC and AAO surveys were taken with the UK 1.2m Schmidt telescope at Siding Spring, Australia; the POSS-I plates were taken at Palomar in California with its 1.2m

---

<sup>1</sup>Declination of the frame centers; Schmidt plates covered huge areas of sky (roughly  $6^\circ$  square) and there is overlap.

Schmidt telescope; and the ESO plates were taken with the 1.0m ESO Schmidt telescope at La Silla, Chile.

We can do a rough comparison of the bandpasses of the plate emulsions used to the Johnson-Kron-Cousins passbands thanks to a table in Morgan (1995) for the plate emulsions used, and a comparison of the bandpasses in Bessell (1986). The IIIa-J blue emulsion (SERC-J & SERC-EJ  $B_J$ ) covers 3950–5400Å, which could be consistent with Johnson  $B$  (3600Å–5400Å, judging by Figure 5 of Bessell 1990b) though not necessarily calibrated in the same fashion. The IIIa-F red emulsion (SERC-ER & AAO-R  $R_2$ , and ESO-R  $R_1$ ) covers 5900–6900Å, which is significantly narrower than the Kron-Cousins  $R$  passband with its long red tail, 5500–9000Å according to Figure 1 of Bessell (1986). The 103a-E red emulsion (POSS-I E  $R_1$ ) is narrower still, covering only 6300–6900Å ( $R_{63E}$  on Figure 1 of Bessell 1986). The IV-N infrared emulsion covers 7150–9000Å, which is very similar to Kron-Cousins  $I$  but somewhat bluer (Figure 1 of Bessell 1986). Morgan (1995) does not list the filters used with those plates; it is thus entirely possible that the ESO-R  $R_1$  photometry are very different from the SERC-ER  $R_2$  plates even though they both used Kodak’s IIIa-F red plates.

Nevertheless, an accurate source of photometry and colors, when properly calibrated, can be used to derive magnitudes in other bandpasses, e.g. SDSS  $u'g'r'i'z'$  to Johnson-Kron-Cousins  $UBVRI$  in Smith et al. (2002). Hambly et al. (2001a,b) claim to have calibrated SuperCOSMOS photometry against various sources (including Bessell 1986, which compares them to Johnson-Kron-Cousins) to get it on a natural  $B_J R_{59F} R_{63E} I_{VN}$  system, but also claim to have compared it to Landolt (1992), TYCHO-2, and GSC-1 colors; all of which are

trying to be on the Johnson-Kron-Cousins system. They claim 0.3 magnitude external errors (that is, compared to other catalogs, which were all Johnson-Kron-Cousins), with color errors of 0.016 or better<sup>2</sup>. On the other hand, RECONS has always treated SuperCOSMOS photometry as a unique (if similar) photometric system: the photometric distance estimators for SuperCOSMOS *BRIJHK* and Johnson-Kron-Cousins *VRIJHK* in § 2.2.5 were developed independently and make no assumptions that they are the same system. Internally, we use  $R_2$  magnitudes in observing lists to help the on-site observer guess at exposure times.

### A.1 Test Data

448 objects in the RECONS 25pc database (11 APRIL 2012) have resolved (e.g., not joint) *BVRI* photometry from Bessell (1990a) and Cousins (source unknown, likely also from Bessell), which we take as standard quality references for Johnson-Kron-Cousins.

As most of the 448 objects in the RECONS 25 pc database are high proper motion stars, SuperCOSMOS photometry was extracted from Nigel Hambly's Secret RECONS high proper motion database used in Hambly et al. (2004), Henry et al. (2004), Subasavage et al. (2005a), Subasavage et al. (2005b), Finch et al. (2007), Boyd et al. (2011a), and Boyd et al. (2011b). That photometry is from the same calibration available at the SuperCOSMOS Science Archive<sup>3</sup> and that was used for TINYMO.

The SuperCOSMOS entries were slid to J2000 E2000 positions, as were the input RECONS 25pc stars; cross-matches were then carried out within  $10''$ . All matches were verified

---

<sup>2</sup>Yes, really.

<sup>3</sup><http://surveys.roe.ac.uk/ssa/index.html> checked 2012 JUL 15.

by comparing  $\mu$  and P.A. Owing to magnitude limits (half the Bessel and Cousins stars were brighter than  $V=6$ ) and the occasional low-proper-motion 25 pc object, only 215 stars had corresponding  $B_J R_1 R_2 I$  photometry.

## A.2 Comparisons

The simplest intercomparison is SuperCOSMOS  $B_J$  versus Johnson  $B$  (etc.). The results are shown in Figure [A.1](#). They are similar, but there are systematic effects.

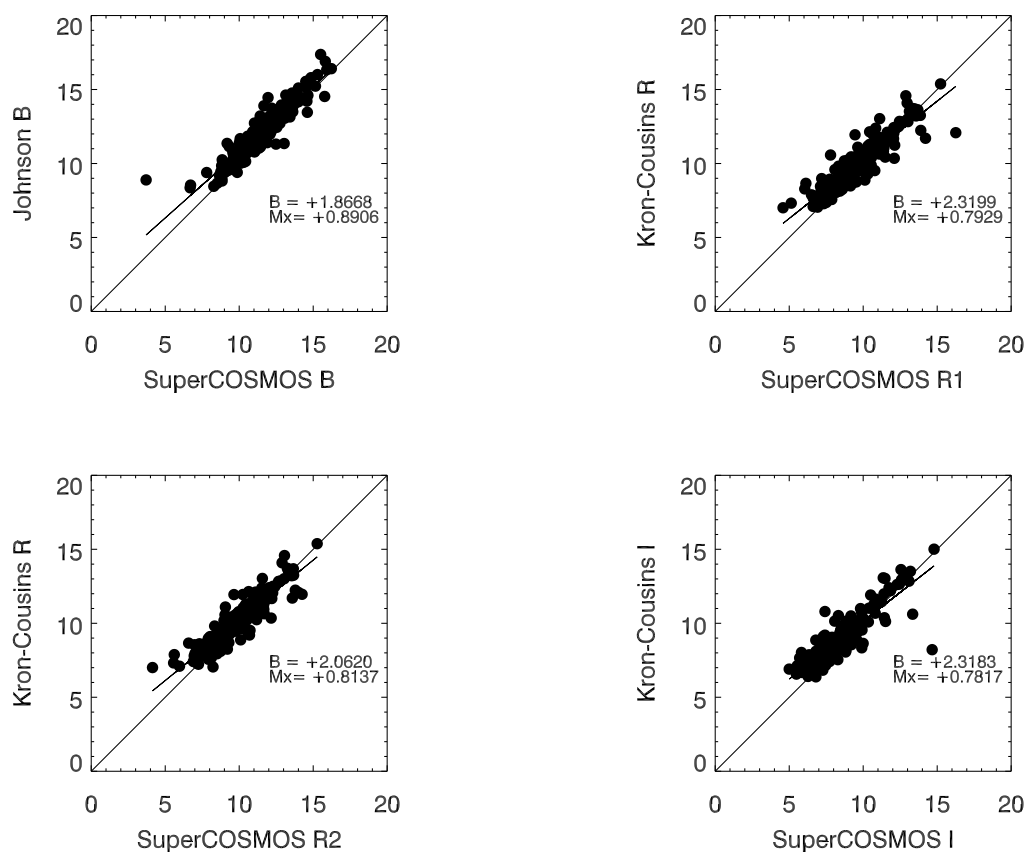


Figure A.1: The four SuperCOSMOS colors plotted against their Johnson-Kron-Cousins counterparts. There appear to be systematic magnitude offsets, represented here as linear corrections of the form  $A=Mx+B$ .

To check for a color term, we plotted the residuals (SuperCOSMOS - Johnson-Kron-Cousins) versus SuperCOSMOS  $B_J$  - SuperCOSMOS  $I$  in Figure A.2. There appears to be no color term, but there is a systematic magnitude offset of  $\sim 0.4$  magnitudes: SuperCOSMOS is nearly always brighter than Johnson-Kron-Cousins. The other notable effect is the scatter in points: standard deviations of  $\sim 0.7$  magnitudes, rather than the 0.3 mag quoted in Hambly et al. (2001b).

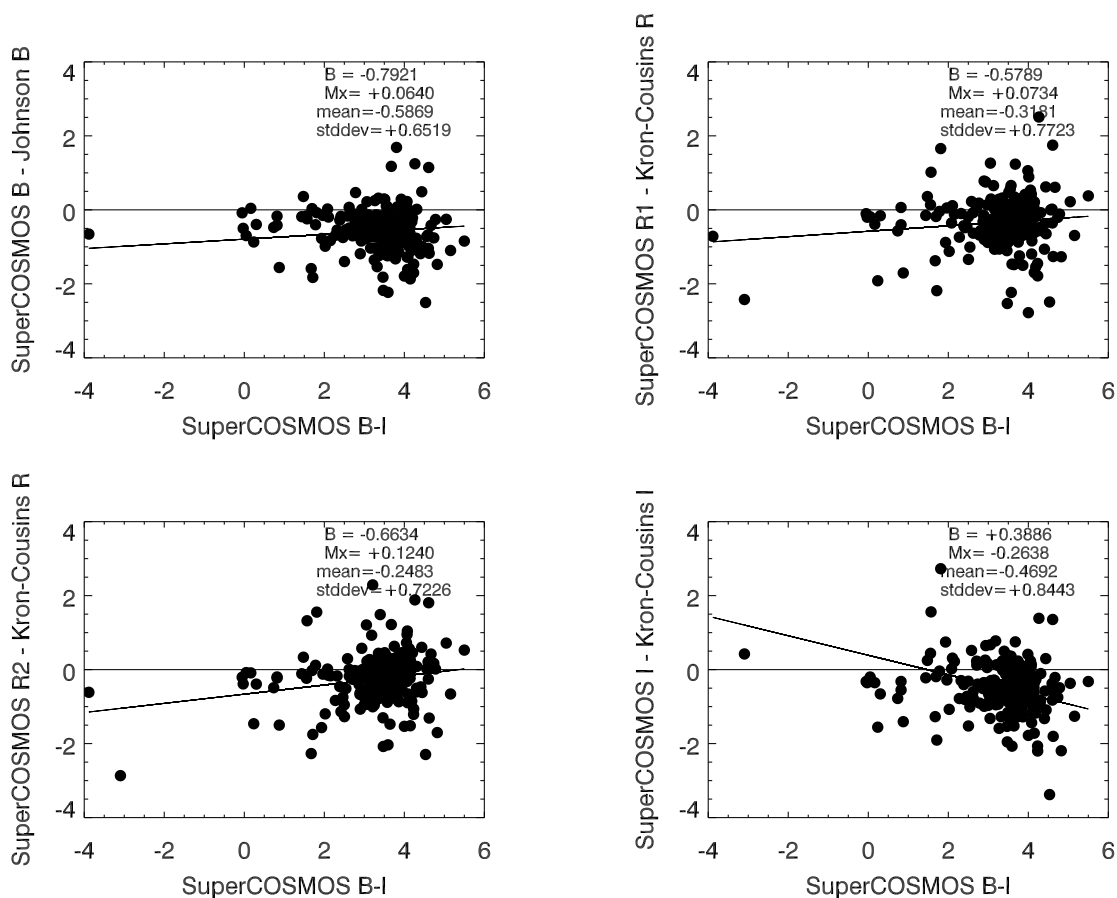


Figure A.2: The residuals of (SuperCOSMOS - Johnson-Kron-Cousins) plotted versus color. The best-fit line describes nothing of value, leaving only the systematic offset of the mean and the large standard deviation.

Comparing color against color (SuperCOSMOS  $B_J - I$  vs Johnson-Kron-Cousins  $B - I$ ) demonstrates no apparent systematics, (Figure A.3) although there is large scatter.

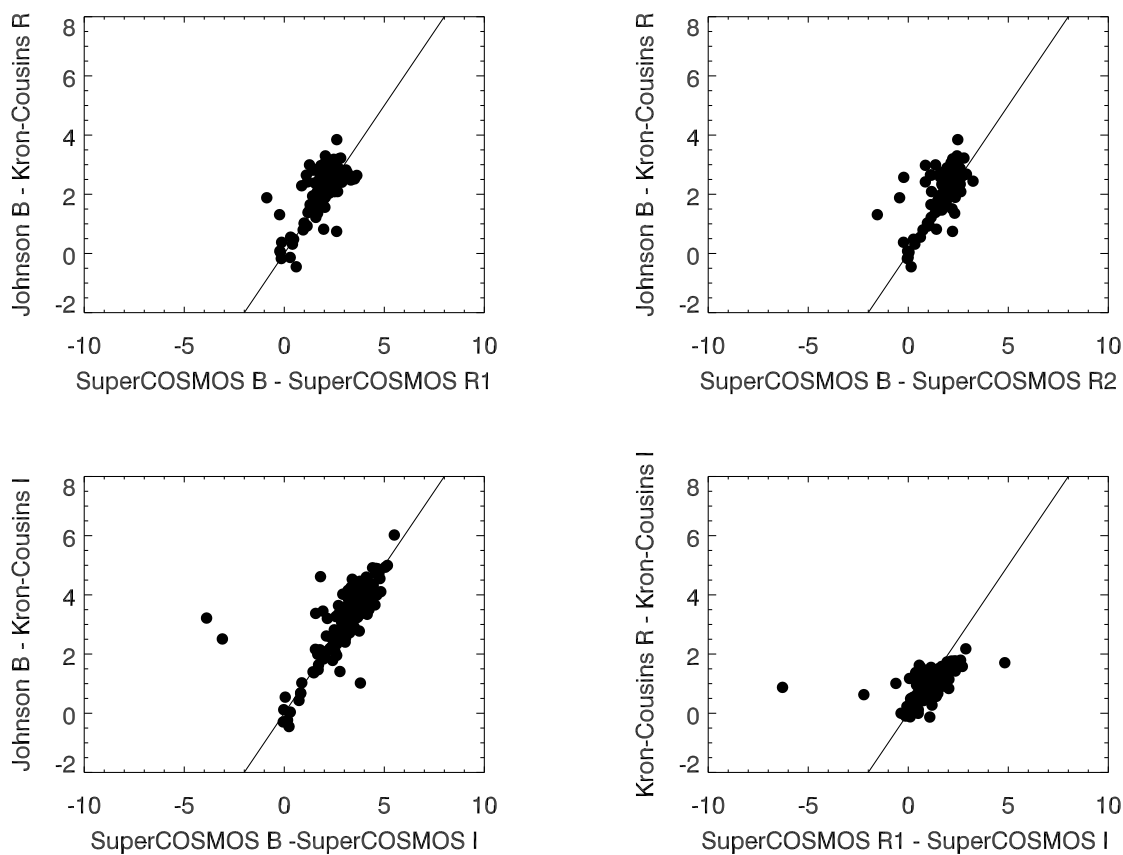


Figure A.3: Color-color plots of SuperCOSMOS colors vs. Johnson-Kron-Cousins colors. No systematics can be seen, although the scatter is fairly large.

### A.3 Conclusions

Hambly et al. (2001b) have never claimed to put their magnitudes on the Johnson-Kron-Cousins system. They used a ‘natural’  $B_J R_{59F} R_{63E} I_{VN}$  system, calibrated by using Johnson-Kron-Cousins photometry transformed to the natural system using transformations in Bessell

(1986) and others.

As for the additional color cuts:  $J - K$  are from 2MASS, and not relevant here.  $R_1 - R_2$  are from SuperCOSMOS, and as shown in Figure A.4 the general scatter is low enough that  $|R_1 - R_2| > 1$  is a  $> 2\sigma$  event.

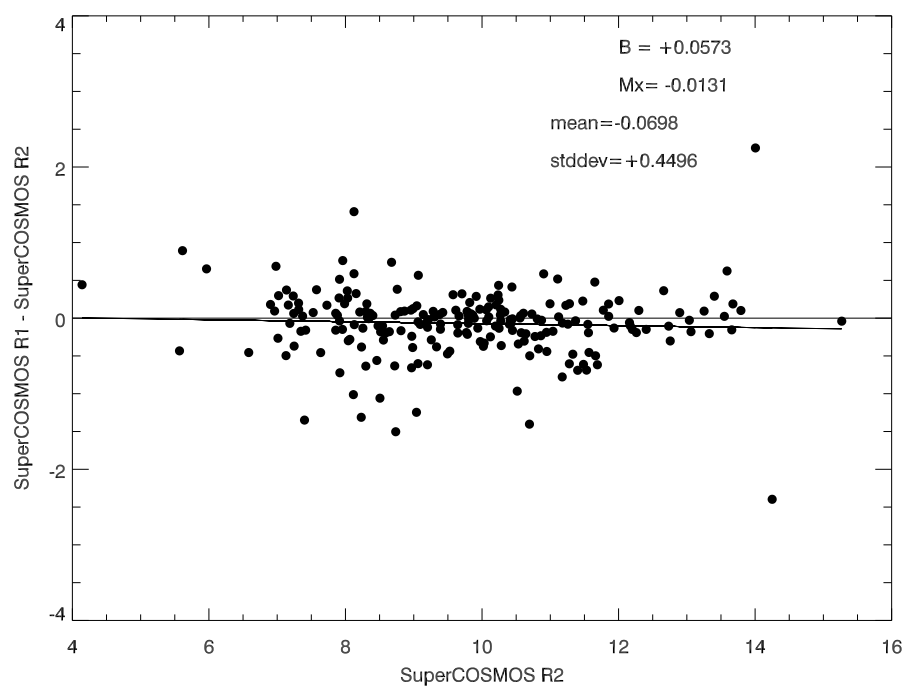


Figure A.4: The residuals of (SuperCOSMOS  $R_1$  - SuperCOSMOS  $R_2$ ) plotted versus magnitude. The mean is 0 (good internal color agreement, as in Hambly et al. (2001b)), and the scatter is only 0.4 mag.

## APPENDIX B

### NEARBY LOW PROPER MOTION STARS FOUND IN TINYMO

The following tables contain all of the potential nearby low-proper-motion ( $< 0.18'' \text{ yr}^{-1}$ ) stars found within the TINYMO survey, including stars not mentioned elsewhere in this dissertation.

The tables are broken into three groups as per §4.1.6:

1. X-ray bright stars, with ROSAT (Voges et al. 1999, 2000) point sources within  $25''$  of the 2MASS point source, and  $< 25\%$  error on the count rate.
2. “Good” and otherwise unremarkable stars. They have no X-rays, normal  $J - K_s$  colors and no spectroscopic indication that they are giants.
3. Probable giants, with  $J - K_s > 1.2$  or significantly discrepant SuperCOSMOS  $R$  magnitudes ( $|R_1 - R_2| > 1$ ), as in §5.8; only systems with  $> 9$  working plate relations are considered.

As most of these stars were never followed up for photometry, spectroscopy or astrometry, many are likely to be as-yet-unnoticed giants, multiples and overluminous pre-main-sequence stars, as per earlier discussions in §4.1.2.

Table B.1: X-ray bright sample

| Name           | RA          | DEC         | $\mu$ | P.A.  | SuperCOSMOS |        |        |        |       | Johnson-Kron-Cousins |       |      |       |      | 2MASS  |        |       |        |       | No. ccd:rel |             | No. ccd:st    |                     | X-ray flux    |                     |               |                     |               |                     |               |                     |               |                     |
|----------------|-------------|-------------|-------|-------|-------------|--------|--------|--------|-------|----------------------|-------|------|-------|------|--------|--------|-------|--------|-------|-------------|-------------|---------------|---------------------|---------------|---------------------|---------------|---------------------|---------------|---------------------|---------------|---------------------|---------------|---------------------|
| (1)            | (2)         | (3)         | (4)   | (5)   | (6)         | (7)    | (8)    | (9)    | (10)  | (11)                 | (12)  | (13) | (14)  | (15) | (16)   | (17)   | (18)  | (19)   | (20)  | (21)        | (22)        | (23)          | (24)                | (25)          | (26)                | (27)          | (28)                | (29)          | (30)                | (31)          | (32)                | (33)          |                     |
| SCR0017-6645   | 00 17 23.52 | -66 45 12.5 | 0.114 | 096.9 | 13.227      | 11.147 | 11.212 | 9.396  | 12.45 | 2                    | 11.37 | 2    | 10.00 | 2    | 8.563  | ±0.021 | 7.928 | ±0.042 | 7.703 | ±0.021      | 11 15.7±4.2 | 12 14.82±2.69 | 2 1.3e-01±3.20e-02  | 12 18.81±4.87 | 1 1.44e-01±2.48e-02 | 12 22.56±3.50 | 1 1.14e-01±2.81e-02 | 12 22.06±2.50 | 1 1.39e-02±3.07e-02 | 12 18.06±2.50 | 1 1.44e-01±2.81e-02 | 12 22.56±3.50 | 1 1.14e-01±2.81e-02 |
| SCR0040-2747   | 00 40 29.29 | -27 47 54.3 | 0.069 | 246.0 | 13.471      | 11.121 | 11.634 | 10.036 | 11.94 | 1                    | 10.98 | 1    | 9.96  | 1    | 8.857  | ±0.023 | 8.163 | ±0.029 | 8.038 | ±0.031      | 11 17.6±5.5 | 12 28.81±4.87 | 1 1.44e-01±2.48e-02 | 12 22.56±3.50 | 1 1.14e-01±2.81e-02 | 12 22.06±2.50 | 1 1.39e-02±3.07e-02 | 12 18.06±2.50 | 1 1.44e-01±2.81e-02 | 12 22.56±3.50 | 1 1.14e-01±2.81e-02 | 12 22.06±2.50 | 1 1.39e-02±3.07e-02 |
| SCR0042-5444   | 00 42 10.10 | -54 44 43.1 | 0.123 | 121.9 | 14.998      | 12.580 | 12.710 | 10.645 | 13.96 | 1                    | 12.78 | 1    | 11.24 | 1    | 9.814  | ±0.024 | 9.203 | ±0.024 | 9.932 | ±0.023      | 11 23.7±6.8 | 12 22.06±2.50 | 1 1.39e-02±3.07e-02 | 12 22.56±3.50 | 1 1.14e-01±2.81e-02 | 12 22.06±2.50 | 1 1.39e-02±3.07e-02 | 12 18.06±2.50 | 1 1.44e-01±2.81e-02 | 12 22.56±3.50 | 1 1.14e-01±2.81e-02 | 12 22.06±2.50 | 1 1.39e-02±3.07e-02 |
| SCR0106-6346   | 01 06 22.67 | -63 46 39.1 | 0.168 | 070.5 | 14.662      | 12.400 | 12.476 | 10.728 | 13.38 | 1                    | 12.18 | 1    | 10.66 | 1    | 9.259  | ±0.022 | 8.643 | ±0.029 | 8.394 | ±0.025      | 11 15.7±4.9 | 12 26.28±4.54 | 1 5.70e-02±1.42e-02 |
| LEHPM1-1481    | 01 22 50.95 | -24 39 50.7 | 0.168 | 136.7 | 15.360      | 13.833 | 13.289 | 11.219 | 14.21 | 1                    | 12.99 | 1    | 11.45 | 1    | 10.084 | ±0.028 | 9.470 | ±0.023 | 9.198 | ±0.026      | 11 16.0±4.6 | 12 26.28±4.54 | 1 5.70e-02±1.42e-02 |
| BAR161-012     | 01 35 13.94 | -07 12 51.8 | 0.118 | 118.6 | 14.043      | 11.833 | 12.030 | 9.746  | 13.42 | 2                    | 12.19 | 2    | 10.57 | 2    | 8.964  | ±0.021 | 8.387 | ±0.027 | 8.078 | ±0.033      | 11 16.0±4.6 | 12 26.28±4.54 | 1 5.70e-02±1.42e-02 |
| SCR0143-0602   | 01 43 45.13 | -06 02 40.1 | 0.060 | 115.5 | 13.700      | 11.285 | 11.558 | 9.496  | 13.01 | 2                    | 11.80 | 2    | 10.25 | 2    | 8.770  | ±0.023 | 8.174 | ±0.034 | 7.912 | ±0.018      | 11 16.2±4.6 | 12 26.28±4.54 | 1 5.70e-02±1.42e-02 |
| SCR0204-5346   | 02 04 53.18 | -53 46 16.3 | 0.099 | 103.1 | 11.607      | 13.914 | 14.114 | 11.921 | 15.18 | 1                    | 13.83 | 1    | 12.09 | 1    | 10.438 | ±0.024 | 9.807 | ±0.022 | 9.563 | ±0.021      | 11 16.2±4.6 | 12 26.28±4.54 | 1 5.70e-02±1.42e-02 |
| SCR0212-5851   | 02 12 58.20 | -58 51 18.2 | 0.103 | 099.7 | 14.576      | 12.294 | 12.640 | 11.181 | 12.92 | 1                    | 11.87 | 1    | 10.61 | 1    | 9.325  | ±0.024 | 8.652 | ±0.055 | 8.440 | ±0.023      | 11 15.9±7.0 | 12 26.28±4.54 | 1 5.70e-02±1.42e-02 |
| SCR0213-4654   | 02 13 30.22 | -46 54 10.5 | 0.053 | 089.0 | 14.766      | 12.006 | 12.735 | 10.797 | 13.66 | 1                    | 12.52 | 1    | 10.95 | 1    | 9.489  | ±0.026 | 8.795 | ±0.049 | 8.599 | ±0.019      | 11 17.7±5.1 | 12 26.28±4.54 | 1 5.70e-02±1.42e-02 |
| SCR0215-0929   | 02 15 58.93 | -09 29 12.2 | 0.104 | 126.5 | 13.368      | 11.380 | 11.231 | 9.501  | 12.18 | 1                    | 11.11 | 1    | 9.78  | 1    | 8.431  | ±0.026 | 7.895 | ±0.029 | 7.546 | ±0.021      | 11 13.1±3.5 | 12 26.28±4.54 | 1 5.70e-02±1.42e-02 |
| SCR0222-6022   | 02 22 44.17 | -60 22 47.6 | 0.149 | 096.2 | 13.796      | 11.464 | 11.692 | 9.533  | 13.36 | 3                    | 12.12 | 3    | 10.52 | 3    | 8.900  | ±0.021 | 8.390 | ±0.042 | 8.102 | ±0.031      | 11 18.5±4.8 | 12 26.28±4.54 | 1 5.70e-02±1.42e-02 |
| SCR0238-3404   | 02 38 52.62 | -34 04 24.7 | 0.113 | 107.5 | 14.619      | 12.050 | 12.543 | 10.735 | 13.65 | 1                    | 12.43 | 1    | 10.81 | 1    | 9.308  | ±0.026 | 8.826 | ±0.029 | 8.396 | ±0.025      | 11 16.5±4.8 | 12 26.28±4.54 | 1 5.70e-02±1.42e-02 |
| SCR0242-3904   | 03 24 04.57 | -39 04 22.7 | 0.096 | 098.9 | 15.112      | 13.144 | 12.944 | 10.272 | 14.14 | 1                    | 12.92 | 1    | 11.34 | 1    | 9.870  | ±0.023 | 9.267 | ±0.029 | 9.029 | ±0.023      | 11 23.7±7.0 | 12 26.28±4.54 | 1 5.70e-02±1.42e-02 |
| RX0413-0139    | 04 13 26.64 | -01 39 21.2 | 0.163 | 094.8 | 14.880      | 11.905 | 12.829 | 10.485 | 13.96 | 2                    | 12.66 | 2    | 10.98 | 2    | 9.375  | ±0.024 | 8.761 | ±0.027 | 8.504 | ±0.021      | 11 16.0±4.7 | 12 26.28±4.54 | 1 5.70e-02±1.42e-02 |
| 2MA0424-0647   | 04 24 42.62 | -06 47 31.4 | 0.149 | 085.1 | 14.486      | 12.190 | 12.291 | 10.165 | 13.95 | 1                    | 12.69 | 1    | 11.08 | 1    | 9.566  | ±0.026 | 8.943 | ±0.022 | 8.632 | ±0.019      | 11 22.7±6.8 | 12 26.28±4.54 | 1 5.70e-02±1.42e-02 |
| SCR0459-0333   | 04 59 58.56 | -03 33 12.2 | 0.090 | 060.0 | 14.948      | 12.721 | 12.594 | 10.601 | 13.97 | 1                    | 12.73 | 1    | 11.26 | 1    | 9.759  | ±0.021 | 9.199 | ±0.026 | 8.906 | ±0.023      | 11 24.0±6.8 | 12 26.28±4.54 | 1 5.70e-02±1.42e-02 |
| SCR0509-4209   | 05 09 03.57 | -42 09 19.9 | 0.061 | 036.3 | 14.465      | 12.078 | 12.236 | 10.270 | 13.77 | 1                    | 12.53 | 1    | 11.04 | 1    | 9.578  | ±0.022 | 8.983 | ±0.022 | 8.758 | ±0.023      | 11 24.8±7.0 | 12 26.28±4.54 | 1 5.70e-02±1.42e-02 |
| 2MA0510-2340A  | 05 10 04.27 | -23 40 40.7 | 0.044 | 111.1 | 13.991      | 11.434 | 11.900 | 10.101 | 13.05 | 1                    | 11.95 | 1    | 10.55 | 1    | 9.241  | ±0.028 | 8.581 | ±0.033 | 8.362 | ±0.023      | 11 20.6±5.5 | 12 26.28±4.54 | 1 5.70e-02±1.42e-02 |
| 2MA0510-2340B  | 05 10 04.88 | -23 40 14.9 | 0.041 | 106.9 | 14.049      | 11.568 | 11.997 | 10.214 | 13.05 | 1                    | 11.95 | 1    | 10.55 | 1    | 9.241  | ±0.028 | 8.581 | ±0.033 | 8.362 | ±0.023      | 11 20.6±5.5 | 12 26.28±4.54 | 1 5.70e-02±1.42e-02 |
| SCR0519-1124AB | 05 19 55.83 | -11 24 56.9 | 0.037 | 128.8 | 15.785      | 13.699 | 13.700 | 11.518 | 14.57 | 1                    | 13.32 | 1    | 11.70 | 1    | 10.103 | ±0.024 | 9.524 | ±0.021 | 9.222 | ±0.021      | 11 24.7±6.7 | 12 26.28±4.54 | 1 5.70e-02±1.42e-02 |
| SCR0524-3622   | 05 24 18.19 | -36 22 02.5 | 0.046 | 098.7 | 14.996      | 12.857 | 12.911 | 11.126 | 13.63 | 1                    | 12.51 | 1    | 11.15 | 1    | 9.795  | ±0.022 | 9.171 | ±0.024 | 8.904 | ±0.019      | 11 21.3±6.3 | 12 26.28±4.54 | 1 5.70e-02±1.42e-02 |
| SCR0529-3239   | 05 29 44.69 | -32 39 14.2 | 0.030 | 084.2 | 14.647      | 12.312 | 13.310 | 10.020 | 13.79 | 1                    | 12.50 | 1    | 10.80 | 1    | 9.215  | ±0.026 | 8.609 | ±0.042 |       |             |             |               |                     |               |                     |               |                     |               |                     |               |                     |               |                     |

Table B.1 – Continued from previous page

| Name         | J2000 E2000 |             |       |       | SuperCOSMOS |        |        |        | Johnson-Kron-Cousins |      |       |      | 2MASS |      |       |             | X-ray flux<br>( $\text{cnt s}^{-1}$ ) |             |       |             |                   |                     |                         |
|--------------|-------------|-------------|-------|-------|-------------|--------|--------|--------|----------------------|------|-------|------|-------|------|-------|-------------|---------------------------------------|-------------|-------|-------------|-------------------|---------------------|-------------------------|
|              | (2)         | (3)         | (4)   | (5)   | (6)         | (7)    | (8)    | (9)    | (10)                 | (11) | (12)  | (13) | (14)  | (15) | (16)  | (17)        |                                       | (18)        | (19)  | (20)        | (21)              | (22)                | (23)                    |
| RX2227-0113  | 22 27 48.84 | -01 13 52.8 | 0.172 | 0.935 | 14.383      | 12.121 | 12.547 | 10.364 | 13.50                | 1    | 12.37 | 1    | 10.87 | 1    | 9.475 | $\pm 0.024$ | 8.781                                 | $\pm 0.071$ | 8.583 | $\pm 0.023$ | 11 19.9 $\pm 5.7$ | 12 20.17 $\pm 3.34$ | 9.43e-02 $\pm 2.29e-02$ |
| SCR2237-2622 | 22 37 14.95 | -26 22 33.3 | 0.145 | 0.962 | 14.574      | 12.151 | 12.467 | 10.360 | 13.35                | 1    | 12.14 | 1    | 10.60 | 1    | 9.164 | $\pm 0.025$ | 8.570                                 | $\pm 0.033$ | 8.314 | $\pm 0.023$ | 11 15.3 $\pm 4.2$ | 12 16.79 $\pm 2.64$ | 2.32e-01 $\pm 3.23e-02$ |
| SCR2328-6802 | 23 28 57.64 | -68 02 33.9 | 0.112 | 1.294 | 14.084      | 11.926 | 12.060 | 10.162 | 13.02                | 1    | 11.95 | 1    | 10.62 | 1    | 9.257 | $\pm 0.023$ | 8.637                                 | $\pm 0.036$ | 8.381 | $\pm 0.023$ | 11 20.0 $\pm 5.4$ | 12 22.12 $\pm 3.71$ | 1.34e-01 $\pm 2.04e-02$ |

Table B.2: Good sample

| Name         | J2000 E2000 |             |       |       | SuperCOSMOS |        |        |        | Johnson-Kron-Cousins |      |       |      | 2MASS |      |                    |                    | X-ray flux<br>( $\text{cnt s}^{-1}$ ) |                    |                   |                     |               |               |               |
|--------------|-------------|-------------|-------|-------|-------------|--------|--------|--------|----------------------|------|-------|------|-------|------|--------------------|--------------------|---------------------------------------|--------------------|-------------------|---------------------|---------------|---------------|---------------|
|              | (2)         | (3)         | (4)   | (5)   | (6)         | (7)    | (8)    | (9)    | (10)                 | (11) | (12)  | (13) | (14)  | (15) | (16)               | (17)               |                                       | (18)               | (19)              | (20)                | (21)          | (22)          | (23)          |
| SCR0002-2148 | 00 02 38.86 | -21 48 33.9 | 0.047 | 332.7 | 16.891      | 14.675 | 14.683 | 12.358 | ...                  | ...  | ...   | ...  | ...   | ...  | 10.514 $\pm 0.019$ | 9.934 $\pm 0.021$  | 9.642 $\pm 0.021$                     | 9.642 $\pm 0.021$  | 11 18.5 $\pm 6.0$ | 0                   | nan $\pm$ nan | 0             | nan $\pm$ nan |
| DEN0004-1709 | 00 04 57.55 | -17 09 37.0 | 0.147 | 0.955 | 17.712      | 15.098 | 15.242 | 10.304 | ...                  | ...  | ...   | ...  | ...   | ...  | 10.997 $\pm 0.022$ | 10.455 $\pm 0.021$ | 10.084 $\pm 0.021$                    | 10.084 $\pm 0.021$ | 11 23.1 $\pm 9.3$ | 0                   | nan $\pm$ nan | 0             | nan $\pm$ nan |
| SCR0006-0705 | 00 06 39.25 | -07 05 35.3 | 0.138 | 313.0 | 15.857      | 12.948 | 13.505 | 10.821 | ...                  | ...  | ...   | ...  | ...   | ...  | 9.831 $\pm 0.026$  | 9.261 $\pm 0.025$  | 9.958 $\pm 0.023$                     | 9.958 $\pm 0.023$  | 11 17.8 $\pm 7.0$ | 0                   | nan $\pm$ nan | 0             | nan $\pm$ nan |
| SCR0012-4406 | 00 12 52.80 | -44 06 27.0 | 0.062 | 081.0 | 15.515      | 13.204 | 13.517 | 11.168 | ...                  | ...  | ...   | ...  | ...   | ...  | 10.146 $\pm 0.024$ | 9.509 $\pm 0.026$  | 9.229 $\pm 0.019$                     | 9.229 $\pm 0.019$  | 11 23.3 $\pm 6.9$ | 0                   | nan $\pm$ nan | 0             | nan $\pm$ nan |
| GIC0004      | 00 15 36.71 | -29 46 00.5 | 0.142 | 127.2 | 15.406      | 12.999 | 13.293 | 11.526 | ...                  | ...  | ...   | ...  | ...   | ...  | 9.775 $\pm 0.022$  | 9.254 $\pm 0.028$  | 8.896 $\pm 0.023$                     | 8.896 $\pm 0.023$  | 11 17.7 $\pm 6.6$ | 0                   | nan $\pm$ nan | 0             | nan $\pm$ nan |
| SCR0019-0554 | 00 19 31.95 | -05 54 40.6 | 0.125 | 124.4 | 17.888      | 15.559 | 15.602 | 12.912 | ...                  | ...  | ...   | ...  | ...   | ...  | 11.171 $\pm 0.021$ | 10.618 $\pm 0.022$ | 10.324 $\pm 0.023$                    | 10.324 $\pm 0.023$ | 11 23.3 $\pm 6.7$ | 0                   | nan $\pm$ nan | 0             | nan $\pm$ nan |
| SCR0021-6351 | 00 21 27.73 | -63 51 08.1 | 0.124 | 120.0 | 18.061      | 15.796 | 15.962 | 12.988 | ...                  | ...  | ...   | ...  | ...   | ...  | 11.021 $\pm 0.024$ | 10.483 $\pm 0.028$ | 10.108 $\pm 0.025$                    | 10.108 $\pm 0.025$ | 11 17.7 $\pm 5.1$ | 0                   | nan $\pm$ nan | 0             | nan $\pm$ nan |
| SCR0024-2522 | 00 24 32.03 | -25 22 52.9 | 0.164 | 143.2 | 14.899      | 12.581 | 12.595 | 11.105 | ...                  | ...  | ...   | ...  | ...   | ...  | 9.836 $\pm 0.024$  | 9.181 $\pm 0.022$  | 8.949 $\pm 0.021$                     | 8.949 $\pm 0.021$  | 11 24.1 $\pm 7.3$ | 0                   | nan $\pm$ nan | 0             | nan $\pm$ nan |
| SCR0027-3639 | 00 27 03.52 | -36 39 35.3 | 0.032 | 267.3 | 14.950      | 12.682 | 13.121 | 11.352 | ...                  | ...  | ...   | ...  | ...   | ...  | 9.977 $\pm 0.026$  | 9.347 $\pm 0.025$  | 9.112 $\pm 0.025$                     | 9.112 $\pm 0.025$  | 11 24.5 $\pm 8.1$ | 0                   | nan $\pm$ nan | 0             | nan $\pm$ nan |
| SCR0027-6157 | 00 27 33.30 | -61 57 17.0 | 0.114 | 122.2 | 16.139      | 13.892 | 14.105 | 11.685 | ...                  | ...  | ...   | ...  | ...   | ...  | 10.327 $\pm 0.026$ | 9.731 $\pm 0.024$  | 9.468 $\pm 0.024$                     | 9.468 $\pm 0.024$  | 11 21.6 $\pm 6.2$ | 0                   | nan $\pm$ nan | 0             | nan $\pm$ nan |
| GIC0009      | 00 28 14.35 | -32 22 55.7 | 0.136 | 114.8 | 16.347      | 14.144 | 14.140 | 11.858 | ...                  | ...  | ...   | ...  | ...   | ...  | 10.121 $\pm 0.022$ | 9.564 $\pm 0.025$  | 9.278 $\pm 0.021$                     | 9.278 $\pm 0.021$  | 11 16.9 $\pm 5.2$ | 0                   | nan $\pm$ nan | 0             | nan $\pm$ nan |
| SCR0030-7202 | 00 30 19.66 | -72 02 17.6 | 0.136 | 143.7 | 14.410      | 11.822 | 12.592 | 11.261 | ...                  | ...  | ...   | ...  | ...   | ...  | 9.673 $\pm 0.024$  | 9.083 $\pm 0.025$  | 8.856 $\pm 0.020$                     | 8.856 $\pm 0.020$  | 11 24.1 $\pm 9.8$ | 0                   | nan $\pm$ nan | 0             | nan $\pm$ nan |
| SCR0031-3606 | 00 31 36.96 | -36 06 50.5 | 0.046 | 295.9 | 13.156      | 10.948 | 10.825 | 9.731  | 11.85                | 1    | 10.81 | 1    | 9.56  | 1    | 8.339 $\pm 0.022$  | 7.676 $\pm 0.026$  | 7.442 $\pm 0.026$                     | 7.442 $\pm 0.026$  | 11 13.4 $\pm 4.9$ | 12 16.83 $\pm 2.73$ | 0             | nan $\pm$ nan |               |
| SCR0033-0342 | 00 33 01.10 | -03 42 57.9 | 0.046 | 111.6 | 15.091      | 12.950 | 12.976 | 11.168 | ...                  | ...  | ...   | ...  | ...   | ...  | 9.974 $\pm 0.023$  | 9.377 $\pm 0.025$  | 9.115 $\pm 0.019$                     | 9.115 $\pm 0.019$  | 11 24.9 $\pm 6.8$ | 0                   | nan $\pm$ nan | 0             | nan $\pm$ nan |
| SCR0033-5116 | 00 33 24.39 | -51 16 43.4 | 0.127 | 122.8 | 15.294      | 12.782 | 13.481 | 11.327 | ...                  | ...  | ...   | ...  | ...   | ...  | 9.861 $\pm 0.023$  | 9.271 $\pm 0.025$  | 9.011 $\pm 0.023$                     | 9.011 $\pm 0.023$  | 11 19.3 $\pm 6.0$ | 0                   | nan $\pm$ nan | 0             | nan $\pm$ nan |
| LP881-2339   | 00 45 28.75 | -27 37 30.0 | 0.180 | 126.7 | 15.565      | 13.102 | 13.496 | 11.121 | ...                  | ...  | ...   | ...  | ...   | ...  | 10.029 $\pm 0.024$ | 9.467 $\pm 0.023$  | 9.180 $\pm 0.021$                     | 9.180 $\pm 0.021$  | 11 22.0 $\pm 6.6$ | 0                   | nan $\pm$ nan | 0             | nan $\pm$ nan |
| HIP003556    | 00 45 35.19 | -51 37 34.0 | 0.109 | 121.7 | 13.336      | 11.851 | 11.194 | 9.737  | ...                  | ...  | ...   | ...  | ...   | ...  | 8.481 $\pm 0.020$  | 7.867 $\pm 0.024$  | 7.623 $\pm 0.021$                     | 7.623 $\pm 0.021$  | 11 14.0 $\pm 4.3$ | 0                   | nan $\pm$ nan | 0             | nan $\pm$ nan |
| SCR0049-6347 | 00 49 35.67 | -63 47 41.6 | 0.124 | 118.0 | 14.063      | 11.631 | 11.913 | 10.304 | ...                  | ...  | ...   | ...  | ...   | ...  | 9.281 $\pm 0.029$  | 8.660 $\pm 0.040$  | 8.427 $\pm 0.027$                     | 8.427 $\pm 0.027$  | 11 21.2 $\pm 5.7$ | 0                   | nan $\pm$ nan | 0             | nan $\pm$ nan |
| SCR0058-7711 | 00 58 13.74 | -77 11 07.6 | 0.088 | 049.1 | 13.951      | 10.882 | 11.832 | 10.526 | ...                  | ...  | ...   | ...  | ...   | ...  | 9.142 $\pm 0.022$  | 8.467 $\pm 0.059$  | 8.332 $\pm 0.034$                     | 8.332 $\pm 0.034$  | 11 19.5 $\pm 6.8$ | 0                   | nan $\pm$ nan | 0             | nan $\pm$ nan |
| SCR0102-6235 | 01 02 43.75 | -62 35 34.5 | 0.099 | 110.0 | 15.207      | 13.167 | 13.180 | 11.073 | ...                  | ...  | ...   | ...  | ...   | ...  | 9.642 $\pm 0.023$  | 9.042 $\pm 0.023$  | 8.802 $\pm 0.022$                     | 8.802 $\pm 0.022$  | 11 17.3 $\pm 5.0$ | 0                   | nan $\pm$ nan | 0             | nan $\pm$ nan |
| SCR0103-5515 | 01 03 35.64 | -55 15 56.2 | 0.120 | 116.2 | 16.682      | 14.420 | 14.611 | 11.987 | 15.48                | 2    | 14.00 | 2    | 12.07 | 2    | 10.162 $\pm 0.023$ | 9.580 $\pm 0.025$  | 9.237 $\pm 0.022$                     | 9.237 $\pm 0.022$  | 11 14.2 $\pm 4.3$ | 0                   | nan $\pm$ nan | 0             | nan $\pm$ nan |
| SCR0104-6858 | 01 04 25.21 | -68 58 37.1 | 0.116 | 077.0 | 15.675      | 13.860 | 13.575 | 11.966 | ...                  | ...  | ...   | ...  | ...   | ...  | 10.352 $\pm 0.028$ | 9.713 $\pm 0.030$  | 9.403 $\pm 0.025$                     | 9.403 $\pm 0.025$  | 11 24.8 $\pm 9.3$ | 0                   | nan $\pm$ nan | 0             | nan $\pm$ nan |
| SCR0112-8312 | 01 12 11.65 | -83 12 28.1 | 0.120 | 140.5 | 14.419      | 12.439 | 12.530 | 11.887 | ...                  | ...  | ...   | ...  | ...   | ...  | 9.602 $\pm 0.027$  | 8.975 $\pm 0.040$  | 8.749 $\pm 0.019$                     | 8.749 $\pm 0.019$  | 11 22.6 $\pm 7.2$ | 0                   | nan $\pm$ nan | 0             | nan $\pm$ nan |
| SCR0112-7046 | 01 12 21.43 | -70 46 31.4 | 0.055 | 063.5 | 15.120      | 13.069 | 13.155 | 11.439 | ...                  | ...  | ...   | ...  | ...   | ...  | 9.801 $\pm 0.024$  | 9.203 $\pm 0.027$  | 8.939 $\pm 0.021$                     | 8.939 $\pm 0.021$  | 11 19.9 $\pm 7.4$ | 0                   | nan $\pm$ nan | 0             | nan $\pm$ nan |
| GIC0038      | 01 13 03.62 | -34 38 18.4 | 0.138 | 119.1 | 16.167      | 13.974 | 14.185 | 12.074 | ...                  | ...  | ...   | ...  | ...   | ...  | 10.413 $\pm 0.023$ | 9.851 $\pm 0.026$  | 9.588 $\pm 0.025$                     | 9.588 $\pm 0.025$  | 11 22.7 $\pm 7.4$ | 0                   | nan $\pm$ nan | 0             | nan $\pm$ nan |
| LP768-141    | 01 13 40.32 | -59 39 34.6 | 0.092 | 084.0 | 15.262      | 13.067 | 13.037 | 11.300 | ...                  | ...  | ...   | ...  | ...   | ...  | 9.953 $\pm 0.024$  | 9.343 $\pm 0.026$  | 9.060 $\pm 0.025$                     | 9.060 $\pm 0.025$  | 11 24.8 $\pm 5.3$ | 0                   | nan $\pm$ nan | 0             | nan $\pm$ nan |
| PS0190       | 01 22 44.04 | -52 47 07.8 | 0.054 | 111.1 | 14.221      | 11.876 | 11.753 | 10.316 | 13.03                | 1    | 11.92 | 1    | 10.49 | 1    | 9.134 $\pm 0.026$  | 8.574 $\pm 0.059$  | 8.282 $\pm 0.027$                     | 8.282 $\pm 0.027$  | 11 18.7 $\pm 6.6$ | 0                   | nan $\pm$ nan | 0             | nan $\pm$ nan |
| SCR0128-1458 | 01 28 39.52 | -14 58 04.2 | 0.049 | 205.8 | 14.404      | 11.489 | 11.935 | 9.729  | 13.60                | 3    | 12.33 | 3    | 10.67 | 3    | 10.561 $\pm 0.024$ | 9.990 $\pm 0.025$  | 9.711 $\pm 0.026$                     | 9.711 $\pm 0.026$  | 11 22.4 $\pm 6.8$ | 0                   | nan $\pm$ nan | 0             | nan $\pm$ nan |
| SCR0130-3329 | 01 30 55.28 | -33 29 04.6 | 0.127 | 094.5 | 17.890      | 15.490 | 15.624 | 13.107 | ...                  | ...  | ...   | ...  | ...   | ...  | 11.292 $\pm 0.024$ | 10.718 $\pm 0.022$ | 10.422 $\pm 0.019$                    | 10.422 $\pm 0.019$ | 11 24.8 $\pm 7.4$ | 0                   | nan $\pm$ nan | 0             | nan $\pm$ nan |
| SCR0131-3545 | 01 31 55.39 | -35 45 44.4 | 0.169 | 161.3 | 15.209      | 12.957 | 13.034 | 11.300 | ...                  | ...  | ...   | ...  | ...   | ...  | 10.014 $\pm 0.026$ | 9.376 $\pm 0.022$  | 9.100 $\pm 0.023$                     | 9.100 $\pm 0.023$  | 11 23.7 $\pm 6.8$ | 0                   | nan $\pm$ nan | 0             | nan $\pm$ nan |
| LP768-141    | 01 35 23.99 | -14 40 42.6 | 0.092 | 084.0 | 15.262      | 13.067 | 13.037 | 11.274 | ...                  | ...  | ...   | ...  | ...   | ...  | 10.016 $\pm 0.025$ | 9.404 $\pm 0.022$  | 9.153 $\pm 0.022$                     | 9.153 $\pm 0.022$  | 11 23.2 $\pm 6.6$ | 0                   | nan $\pm$ nan | 0             | nan $\pm$ nan |
| GIC0138      | 01 35 56.45 | -13 25 47.3 | 0.110 | 109.8 | 14.652      | 12.363 | 12.598 | 10.882 | ...                  | ...  | ...   | ...  | ...   | ...  | 9.664 $\pm 0.023$  | 9.081 $\pm 0.017$  | 8.806 $\pm 0.017$                     | 8.806 $\pm 0.017$  | 11 22.6 $\pm 6.4$ | 0                   | nan $\pm$ nan | 0             | nan $\pm$ nan |
| SCR0137-4558 | 01 37 27.82 | -45 58 26.2 | 0.142 | 106.0 | 18.103      | 15.715 | 15.971 | 13.358 | ...                  | ...  | ...   | ...  | ...   | ...  | 11.106 $\pm 0.024$ | 10.537 $\pm 0.024$ | 10.189 $\pm 0.019$                    | 10.189 $\pm 0.019$ | 11                |                     |               |               |               |

Table B.2 – Continued from previous page

| Name<br>(1)   | RA           |              | DEC             |                 | $\mu$<br>(4) | P.A.<br>(5) | SuperCOSMOS  |              |               | Johnson-Kron-Cousins |             |              | 2MASS            |                  |             | No.<br>K pl.r.el<br>(18) | No.<br>pl.r.el<br>(20) | No.<br>ccd.r.el<br>(21) | No.<br>ccddist<br>(22) | X-ray flux<br>(cnt. s <sup>-1</sup> )<br>(23) |
|---------------|--------------|--------------|-----------------|-----------------|--------------|-------------|--------------|--------------|---------------|----------------------|-------------|--------------|------------------|------------------|-------------|--------------------------|------------------------|-------------------------|------------------------|---|
|               | J2000<br>(2) | E2000<br>(3) | $\alpha$<br>(6) | $\delta$<br>(7) |              |             | $B_J$<br>(8) | $R_I$<br>(9) | $R_2$<br>(10) | $I_V$<br>(11)        | $V$<br>(12) | $I$<br>(13)  | $I_{15}$<br>(14) | $I_{15}$<br>(15) | $J$<br>(16) |                          |                        |                         |                        |   |
| SCR0242-5359A | 02 42 04.05  | -53 59 00.1  | 0.1110          | 099.815         | 935.13       | 694.13      | 748.11       | 347          | ...           | ...                  | ...         | 10.110±0.023 | 9.528±0.026      | 9.287±0.019      | 11          | 20.3±6.2                 | 0                      | nan±nan                 | 3.63e-02±1.21e-02      |   |
| SCR0254-5746  | 02 54 06.31  | -57 46 30.1  | 0.1111          | 093.614         | 637.12       | 846.12      | 634.10       | 600          | ...           | ...                  | ...         | 9.626±0.026  | 9.049±0.022      | 8.830±0.023      | 11          | 23.1±6.3                 | 0                      | nan±nan                 | 6.38e-02±1.80e-02      |   |
| SCR0256-6343  | 02 56 47.09  | -63 43 02.8  | 0.0777          | 086.215         | 146.12       | 815.12      | 996.10       | 676          | ...           | ...                  | ...         | 9.863±0.026  | 9.218±0.025      | 9.012±0.026      | 11          | 23.1±7.4                 | 0                      | nan±nan                 | 4.38e-02±1.80e-02      |   |
| SCR0257-6341  | 02 57 26.83  | -63 41 29.4  | 0.0777          | 090.115         | 699.13       | 336.13      | 426.11       | 223          | ...           | ...                  | ...         | 10.164±0.023 | 9.566±0.024      | 9.332±0.025      | 11          | 24.5±7.1                 | 0                      | nan±nan                 | ...                    |   |
| SCR0302-1911  | 03 02 51.57  | -19 11 49.7  | 0.1110          | 122.216         | 458.13       | 925.14      | 137.11       | 747          | ...           | ...                  | ...         | 10.541±0.024 | 9.976±0.027      | 9.684±0.023      | 11          | 24.8±7.6                 | 0                      | nan±nan                 | ...                    |   |
| SCR0315-5342  | 03 15 23.64  | -53 42 54.0  | 0.0995          | 095.017         | 997.15       | 532.15      | 801.12       | 952          | ...           | ...                  | ...         | 11.280±0.023 | 10.714±0.023     | 10.365±0.019     | 11          | 23.3±6.9                 | 0                      | nan±nan                 | ...                    |   |
| SCR0321-0647  | 03 21 11.66  | -06 47 16.9  | 0.1027          | 179.155         | 570.13       | 566.13      | 601.11       | 647          | ...           | ...                  | ...         | 10.240±0.028 | 9.615±0.029      | 9.350±0.026      | 11          | 24.1±7.3                 | 0                      | nan±nan                 | ...                    |   |
| SCR0328-0537  | 03 28 36.11  | -05 37 36.7  | 0.1267          | 102.015         | 673.13       | 723.13      | 804.11       | 658          | ...           | ...                  | ...         | 10.287±0.023 | 9.733±0.026      | 9.440±0.023      | 11          | 24.1±6.9                 | 0                      | nan±nan                 | 4.36e-02±1.47e-02      |   |
| SCR0336-2619  | 03 36 31.46  | -26 19 57.9  | 0.0877          | 108.517         | 404.14       | 949.15      | 114.22       | 70.33        | 2             | 14.76                | 2           | 10.675±0.023 | 10.134±0.024     | 9.763±0.021      | 11          | 18.2±5.7                 | 12                     | 14.19±2.21              | ...                    |   |
| SCR0342-1914  | 03 42 52.09  | -19 14 02.0  | 0.0381          | 142.618         | 526.16       | 017.16      | 158.13       | 095          | ...           | ...                  | ...         | 11.445±0.024 | 10.889±0.023     | 10.539±0.024     | 11          | 23.4±7.8                 | 0                      | nan±nan                 | ...                    |   |
| SCR0352-1822  | 03 52 45.75  | -18 22 11.1  | 0.1877          | 039.715         | 249.12       | 828.12      | 985.10       | 718          | ...           | ...                  | ...         | 9.841±0.024  | 9.306±0.023      | 9.054±0.024      | 11          | 23.2±7.3                 | 0                      | nan±nan                 | ...                    |   |
| SCR0353-2526  | 03 53 42.35  | -25 27 02.0  | 0.1007          | 196.916         | 395.14       | 229.14      | 194.11       | 809          | ...           | ...                  | ...         | 10.473±0.024 | 9.821±0.022      | 9.518±0.021      | 11          | 21.3±6.1                 | 0                      | nan±nan                 | ...                    |   |
| SCR0405-4011  | 04 05 24.63  | -40 11 38.0  | 0.0949          | 155.915         | 569.12       | 924.13      | 171.10       | 897          | ...           | ...                  | ...         | 10.072±0.026 | 9.460±0.022      | 9.121±0.019      | 11          | 23.2±7.7                 | 0                      | nan±nan                 | ...                    |   |
| SCR0405-4114  | 04 05 39.63  | -40 14 10.4  | 0.0995          | 105.815         | 553.13       | 354.13      | 482.11       | 329          | ...           | ...                  | ...         | 9.818±0.023  | 9.264±0.026      | 8.981±0.021      | 11          | 17.8±5.2                 | 0                      | nan±nan                 | ...                    |   |
| SCR0406-0534  | 04 06 06.88  | -05 34 44.6  | 0.1477          | 168.614         | 565.12       | 064.12      | 304.10       | 110          | ...           | ...                  | ...         | 9.128±0.023  | 8.554±0.024      | 8.304±0.021      | 11          | 16.0±4.7                 | 0                      | nan±nan                 | ...                    |   |
| SCR0409-4435  | 04 09 32.34  | -44 35 39.9  | 0.1115          | 354.215         | 098.12       | 533.12      | 689.10       | 420          | ...           | ...                  | ...         | 9.464±0.024  | 8.912±0.022      | 8.561±0.021      | 11          | 17.1±5.5                 | 0                      | nan±nan                 | ...                    |   |
| SCR0427-2316  | 04 27 35.99  | -23 16 58.7  | 0.0775          | 108.916         | 469.14       | 016.14      | 214.11       | 619          | ...           | ...                  | ...         | 10.473±0.023 | 9.864±0.022      | 9.578±0.019      | 11          | 22.6±7.7                 | 0                      | nan±nan                 | ...                    |   |
| 2MA0429-3123  | 04 29 18.43  | -31 23 56.7  | 0.1299          | 039.018         | 595.16       | 078.16      | 185.12       | 821          | 17.39         | 3                    | 15.50       | 3            | 10.874±0.024     | 10.211±0.024     | 9.770±0.022 | 11                       | 12.4±3.6               | 12                      | 10.56±1.68             | 3.58e-02±1.30e-02                             |
| SCR0432-5741  | 04 32 57.78  | -57 41 45.9  | 0.0884          | 071.315         | 862.13       | 359.13      | 543.11       | 244          | 14.52         | 1                    | 11.51       | 1            | 9.945±0.024      | 9.338±0.022      | 9.072±0.021 | 11                       | 18.2±5.3               | 12                      | 18.42±2.95             | 2.94e-02±9.95e-03                             |
| SCR0448-3539  | 04 48 40.13  | -35 39 22.1  | 0.1501          | 201.416         | 830.14       | 530.14      | 599.12       | 029          | ...           | ...                  | ...         | 10.521±0.026 | 9.990±0.022      | 9.652±0.021      | 11          | 20.1±5.9                 | 0                      | nan±nan                 | ...                    |   |
| SCR0451-2407  | 04 51 16.66  | -24 07 17.1  | 0.0114          | 114.215         | 201.12       | 962.12      | 485.11       | 175          | ...           | ...                  | ...         | 9.826±0.024  | 9.159±0.022      | 8.945±0.021      | 11          | 23.0±7.8                 | 0                      | nan±nan                 | ...                    |   |
| SCR0453-2835B | 04 53 36.05  | -28 35 35.0  | 0.0588          | 100.716         | 184.13       | 745.13      | 943.10       | 961          | ...           | ...                  | ...         | 10.174±0.024 | 9.606±0.024      | 9.301±0.021      | 11          | 21.3±10.3                | 0                      | nan±nan                 | ...                    |   |
| SCR0453-2835A | 04 53 37.57  | -28 35 30.2  | 0.0467          | 076.915         | 689.12       | 548.12      | 537.10       | 362          | ...           | ...                  | ...         | 9.705±0.023  | 9.086±0.024      | 8.811±0.025      | 11          | 20.3±8.8                 | 0                      | nan±nan                 | ...                    |   |
| SCR0453-5836  | 04 53 43.80  | -58 36 24.8  | 0.1233          | 052.814         | 733.12       | 426.12      | 656.10       | 612          | ...           | ...                  | ...         | 9.740±0.021  | 9.174±0.023      | 8.907±0.020      | 11          | 24.5±6.8                 | 0                      | nan±nan                 | 6.28e-02±1.61e-02      |   |
| SCR0455-3212  | 04 55 19.01  | -32 12 23.4  | 0.0628          | 019.177         | 348.14       | 731.15      | 011.11       | 945          | ...           | ...                  | ...         | 10.683±0.027 | 10.102±0.024     | 9.814±0.021      | 11          | 20.5±8.7                 | 0                      | nan±nan                 | ...                    |   |
| HD268899      | 05 00 26.90  | -68 58 48.9  | 0.0288          | 120.013         | 938.12       | 741.12      | 032.11       | 159          | 11.18         | 2                    | 10.49       | 2            | 8.912±0.024      | 8.153±0.023      | 8.047±0.022 | 11                       | 14.5±9.3               | 8                       | 42.43±0.57             | ...   |
| SCR0502-0439  | 05 04 56.63  | -04 39 48.3  | 0.0508          | 303.514         | 589.12       | 389.12      | 540.10       | 823          | ...           | ...                  | ...         | 9.458±0.027  | 8.872±0.023      | 8.607±0.023      | 11          | 19.2±5.8                 | 0                      | nan±nan                 | ...                    |   |
| HD271076      | 05 10 09.69  | -72 36 27.9  | 0.0100          | 094.813         | 495.12       | 479.11      | 753.10       | 186          | 11.36         | 2                    | 10.34       | 2            | 7.888±0.027      | 7.317±0.033      | 7.054±0.016 | 11                       | 7.2±4.3                | 12                      | 14.94±2.31             | 1.37e-02±6.01e-03                             |
| SCR0516-3124  | 05 16 01.19  | -31 24 45.7  | 0.0443          | 101.016         | 652.14       | 221.14      | 495.12       | 220          | ...           | ...                  | ...         | 10.628±0.026 | 10.136±0.024     | 9.791±0.024      | 11          | 23.4±6.8                 | 0                      | nan±nan                 | ...                    |   |
| SCR0516-3516  | 05 16 14.79  | -35 15 06.6  | 0.1527          | 356.716         | 188.13       | 925.14      | 047.12       | 014          | ...           | ...                  | ...         | 10.578±0.024 | 9.894±0.023      | 9.618±0.019      | 11          | 24.5±7.3                 | 0                      | nan±nan                 | ...                    |   |
| SCR0516-7630  | 05 16 24.09  | -36 30 24.0  | 0.0881          | 129.316         | 387.14       | 314.14      | 404.12       | 299          | ...           | ...                  | ...         | 10.544±0.023 | 9.898±0.025      | 9.641±0.021      | 11          | 21.7±7.8                 | 0                      | nan±nan                 | ...                    |   |
| SCR0519-0436  | 05 19 49.41  | -04 36 16.6  | 0.1333          | 257.614         | 881.12       | 861.12      | 940.10       | 756          | ...           | ...                  | ...         | 9.681±0.024  | 9.124±0.025      | 8.849±0.023      | 11          | 21.1±6.0                 | 0                      | nan±nan                 | ...                    |   |
| SCR0522-0066  | 05 22 40.70  | -06 06 23.9  | 0.0399          | 137.115         | 211.12       | 11.21       | 565.13       | 316          | 10.969        | ...                  | ...         | 10.007±0.026 | 9.401±0.023      | 9.133±0.019      | 11          | 23.8±7.2                 | 0                      | nan±nan                 | 1.87e-02±8.60e-03      |   |
| SCR0523-3628  | 05 23 52.70  | -36 28 20.1  | 0.1511          | 064.114         | 513.12       | 287.12      | 430.10       | 882          | ...           | ...                  | ...         | 9.645±0.027  | 9.073±0.030      | 8.819±0.023      | 11          | 24.1±7.1                 | 0                      | nan±nan                 | ...                    |   |
| HD269679      | 05 31 16.12  | -67 54 24.7  | 0.0444          | 066.713         | 385.12       | 513.11      | 857.10       | 044          | ...           | ...                  | ...         | 8.928±0.024  | 8.273±0.038      | 8.085±0.023      | 10          | 16.2±9.4                 | 0                      | nan±nan                 | ...                    |   |
| SCR0531-4323  | 05 31 31.42  | -43 23 04.2  | 0.0447          | 075.916         | 781.14       | 477.14      | 629.10       | 010          | ...           | ...                  | ...         | 10.741±0.023 | 10.132±0.023     | 9.837±0.021      | 11          | 23.9±7.7                 | 0                      | nan±nan                 | ...                    |   |
| 2MA0534-6921  | 05 34 25.90  | -69 21 48.0  | 0.0116          | 060.413         | 916.13       | 032.12      | 186.10       | 531          | 11.00         | 2                    | 10.19       | 2            | 8.308±0.026      | 7.606±0.029      | 7.350±0.029 | 11                       | 7.9±4.7                | 10                      | 24.60±6.36             | ...   |
| SCR0600-3742  | 05 42 37.93  | -08 17 02.7  | 0.0044          | 035.016         | 227.14       | 834.14      | 117.12       | 529          | ...           | ...                  | ...         | 10.295±0.024 | 9.618±0.022      | 9.256±0.021      | 11          | 17.7±10.4                | 0                      | nan±nan                 | ...                    |   |
| SCR0603-0827  | 05 43 37.09  | -08 27 48.4  | 0.0115          | 356.615         | 051.13       | 723.13      | 872.11       | 329          | ...           | ...                  | ...         | 10.443±0.024 | 9.841±0.023      | 9.569±0.021      | 9           | 23.5±15.9                | 0                      | nan±nan                 | ...                    |   |
| SCR0544-0406  | 05 44 27.15  | -04 06 01.4  | 0.0804          | 216.515         | 896.13       | 895.14      | 295.11       | 341          | ...           | ...                  | ...         | 10.291±0.022 | 9.723±0.023      | 9.443±0.023      | 11          | 22.7±8.6                 | 0                      | nan±nan                 | ...                    |   |
| SCR0546-0844  | 05 46 03.30  | -08 44 22.0  | 0.0044          | 267.915         | 208.13       | 496.13      | 638.11       | 165          | ...           | ...                  | ...         | 10.081±0.024 | 9.468±0.023      | 9.173±0.020      | 11          | 23.2±7.4                 | 0                      | nan±nan                 | 3.84e-02±1.11e-02      |   |
| SCR0546-0440  | 05 46 08.19  | -04 40 11.8  | 0.0599          | 053.916         | 076.14       | 044.14      | 287.11       | 605          | ...           | ...                  | ...         | 10.366±0.026 | 9.774±0.024      | 9.451±0.021      | 11          | 21.6±6.8                 | 0                      | nan±nan                 | 1.75e-02±8.02e-03      |   |
| SCR0551-5306  | 05 51 01.45  | -53 06 15.0  | 0.1200          | 161.113         | 997.11       | 963.12      | 344.10       | 435          | ...           | ...                  | ...         | 9.532±0.024  | 8.860±0.029      | 8.655±0.021      | 11          | 24.3±7.3                 | 0                      | nan±nan                 | ...                    |   |
| SCR0600-3742  | 06 00 47.23  | -37 42 19.5  | 0.1288          | 310.414         | 870.12       | 446.12      | 576.10       | 527          | ...           | ...                  | ...         | 9.693±0.024  | 9.111±0.028      | 8.806±0.019      | 11          | 22.5±6.5                 | 0                      | nan±nan                 | ...                    |   |
| SCR0603-3722  | 06 03 12.31  | -37 22 42.7  | 0.1222          | 166.116         | 637.14       | 236.14      | 415.11       | 935          | ...           | ...                  | ...         | 10.453±0.022 | 9.903±0.022      | 9.614±0.021      | 11          | 20.7±6.0                 | 0                      | nan±nan                 | 3.10e-02±8.09e-03      |   |
| SCR0605-5254  | 06 05 25.22  | -52 54 58.7  | 0.1116          | 040.815         | 104.12       | 939.13      | 084.11       | 174          | ...           | ...                  | ...         | 9.953±0.026  | 9.393±0.022      | 9.128±0.023      | 11          | 24.5±6.8                 | 0                      | nan±nan                 | 2.25e-02±8.00e-03      |   |
| SCR0605-5718  | 06 05 50.03  | -57 18 11.5  | 0.0444          | 143.316         | 968.14       | 572.14      | 790.12       | 559          | ...           | ...                  | ...         | 10.678±0.024 | 10.064±0.022     | 9.760±0.023      | 11          | 19.8±6.9                 | 0                      | nan±nan                 | ...                    |   |
| SCR0606-6359  | 06 06 22.46  | -63 59 01.3  | 0.0393          | 041.015         | 419.13       | 008.13      | 146.11       | 308          | ...           | ...                  | ...         | 9.934±0.029  | 9.306±0.031      | 9.005±0.026      | 11          | 20.4±5.9                 | 0                      | nan±nan                 | ...                    |   |
| SCR0608-5703  | 06 08 36.09  | -57 03 40.2  | 0.1500          | 017.617         | 368.15       | 062.15      | 305.12       | 836          | ...           | ...                  | ...         | 11.015±0.022 | 10.470±0.021     | 10.130±0.021     | 11          | 22.9±7.2                 | 0                      | nan±nan                 | ...                    |   |
| SCR0623-0938  | 06 23 38.47  | -09 38 51.7  | 0.0554          | 280.215         | 054.12       | 507.12      | 804.10       | 575          | ...           | ...                  | ...         | 9.819±0.026  | 9.295±0.031      | 8.947±0.024      | 11          | 23.8±7.5                 | 0                      | nan±nan                 | 3.37e-02±9.19e-03      |   |
| SCR0630-1923  | 06 30 01.87  | -19 23 06.4  | 0.0119          | 190.015         | 685.13       | 547.13      | 690.11       | 416          | ...           | ...                  | ...         | 10.092±0.020 | 9.530±0.022      | 9.254±0.021      | 11          | 21.4±6.1                 | 0                      | nan±nan                 | ...                    |   |
| SCR0702-3320A | 07 02 33.32  | -33 20 34.8  | 0.1455          | 338.915         | 300.13       | 046.13      | 349.11       | 187          | ...           | ...                  | ...         | 10.054±0.024 | 9.479±0.023      | 9.170±0.021      | 11          | 23.7±6.6                 | 0                      | nan±nan                 | 4.33e-02±1.28e-02      |   |
| SCR0716-4118  | 07 16 42.04  | -41 18 05.6  | 0.1607          | 129.714         | 604          |             |              |              |               |                      |             |              |                  |                  |             |                          |                        |                         |                        |   |

Table B.2 – Continued from previous page

| Name<br>(1)    | RA           |              | DEC             |                 | $\mu$<br>( $'', \text{yr}^{-1}$ ) | P.A.         |              | SuperCOSMOS  |                  | Johnson-Kron-Cousins |                   | J<br>(16)    | H<br>(17)    | K<br>pl.r.el<br>(18) | No.<br>pl.r.el<br>(19) | No.<br>ccd.r.el<br>(21) | ccddist<br>(pc)<br>(22) | X-ray flux<br>( $\text{cnt. s}^{-1}$ )<br>(23) |                   |                   |
|----------------|--------------|--------------|-----------------|-----------------|-----------------------------------|--------------|--------------|--------------|------------------|----------------------|-------------------|--------------|--------------|----------------------|------------------------|-------------------------|-------------------------|--|-------------------|-------------------|
|                | J2000<br>(2) | E2000<br>(3) | $\alpha$<br>(4) | $\delta$<br>(5) |                                   | $B_J$<br>(6) | $R_I$<br>(7) | $R_2$<br>(8) | $I_{V,N}$<br>(9) | V<br>nobs<br>(10)    | I<br>nobs<br>(11) |              |              |                      |                        |                         |                         |  | J<br>nobs<br>(12) | K<br>nobs<br>(13) |
| SCR0937-6754   | 09 37 33.65  | -67 54 40.4  | 0.033           | 290.617         | 688.15                            | 383.15       | 572.12       | 12.71        | ...              | ...                  | ...               | 10.976±0.023 | 10.337±0.024 | 10.112±0.019         | 11                     | 20.3±5.9                | 0                       | nan±nan  | ±                 |                   |
| SCR1005-7137   | 10 05 25.48  | -71 37 28.4  | 0.004           | 257.414         | 708.12                            | 582.12       | 680.10       | 9.950        | ...              | ...                  | ...               | 9.724±0.026  | 9.046±0.025  | 8.802±0.021          | 11                     | 21.8±6.4                | 0                       | nan±nan  | ±                 |                   |
| SCR1006-1246   | 10 06 52.97  | -12 46 54.4  | 0.111           | 166.915         | 688.13                            | 211.13       | 406.10       | 9.909        | ...              | ...                  | ...               | 9.749±0.023  | 9.229±0.026  | 8.902±0.019          | 11                     | 17.3±5.7                | 0                       | nan±nan  | ±                 |                   |
| SCR1007-2014   | 10 07 54.77  | -20 14 29.4  | 0.136           | 188.017         | 699.15                            | 316.15       | 662.12       | 7.79         | ...              | ...                  | ...               | 11.167±0.023 | 10.559±0.024 | 10.221±0.027         | 11                     | 21.8±6.6                | 0                       | nan±nan  | ±                 |                   |
| SCR1011-2725   | 10 11 14.20  | -27 25 26.5  | 0.004           | 666.117         | 348.15                            | 204.15       | 164.12       | 8.67         | ...              | ...                  | ...               | 10.956±0.023 | 10.419±0.024 | 10.120±0.023         | 11                     | 23.0±7.7                | 0                       | nan±nan  | ±                 |                   |
| SCR1012-3124AB | 10 12 09.08  | -31 24 45.2  | 0.065           | 258.414         | 674.12                            | 305.12       | 439.10       | 9.906        | 13.51            | 2                    | 12.20             | 2            | 10.51        | 2                    | 11.8±4.0               | 12                      | 10.56±1.63              | 0  | nan±nan           | ±                 |
| SCR1014-7040   | 10 14 37.32  | -70 40 43.0  | 0.140           | 255.214         | 708.12                            | 552.12       | 712.10       | 6.995        | ...              | ...                  | ...               | 9.499±0.022  | 8.877±0.044  | 8.615±0.019          | 11                     | 18.5±5.1                | 0                       | nan±nan  | ±                 |                   |
| SCR1028-2830   | 10 28 45.80  | -28 30 37.0  | 0.058           | 254.517         | 667.15                            | 292.15       | 448.12       | 8.005        | ...              | ...                  | ...               | 10.953±0.027 | 10.410±0.026 | 10.026±0.024         | 11                     | 19.6±5.8                | 0                       | nan±nan  | ±                 |                   |
| SCR1040-7812   | 10 40 49.66  | -78 12 50.0  | 0.010           | 222.513         | 593.12                            | 100.12       | 245.11       | 10.67        | ...              | ...                  | ...               | 9.320±0.024  | 8.590±0.044  | 8.365±0.021          | 11                     | 20.2±10.4               | 0                       | nan±nan  | ±                 |                   |
| SCR1046-7719   | 10 46 57.39  | -77 19 52.0  | 0.008           | 326.114         | 370.12                            | 607.12       | 615.12       | 13.36        | ...              | ...                  | ...               | 9.802±0.024  | 9.093±0.021  | 8.870±0.019          | 9                      | 19.5±11.1               | 0                       | nan±nan  | ±                 |                   |
| SCR1050-7727   | 10 50 23.54  | -77 27 42.6  | 0.005           | 266.013         | 945.12                            | 205.12       | 138.11       | 6.37         | ...              | ...                  | ...               | 9.414±0.023  | 8.666±0.047  | 8.459±0.021          | 9                      | 16.6±9.2                | 0                       | nan±nan  | ±                 |                   |
| SCR1053-7735   | 10 53 37.50  | -77 35 27.3  | 0.035           | 303.813         | 920.12                            | 269.12       | 527.11       | 5.62         | ...              | ...                  | ...               | 9.498±0.023  | 8.820±0.024  | 8.580±0.019          | 10                     | 19.6±11.2               | 0                       | nan±nan  | ±                 |                   |
| SCR1054-1507   | 10 54 25.04  | -15 07 06.9  | 0.122           | 239.517         | 458.15                            | 192.15       | 137.12       | 8.53         | ...              | ...                  | ...               | 11.097±0.026 | 10.573±0.024 | 10.256±0.021         | 11                     | 24.5±7.3                | 0                       | nan±nan  | ±                 |                   |
| SCR1055-4607   | 10 55 25.56  | -46 07 08.2  | 0.129           | 262.215         | 746.13                            | 175.13       | 367.10       | 8.61         | ...              | ...                  | ...               | 10.023±0.024 | 9.463±0.027  | 9.174±0.019          | 11                     | 22.4±8.5                | 0                       | nan±nan  | ±                 |                   |
| SCR1058-7702   | 10 58 01.55  | -77 02 38.9  | 0.012           | 114.215         | 667.13                            | 574.13       | 512.12       | 9.61         | ...              | ...                  | ...               | 10.460±0.023 | 9.791±0.024  | 9.519±0.023          | 9                      | 24.6±14.9               | 0                       | nan±nan  | ±                 |                   |
| SCR1058-2346   | 10 58 50.53  | -23 46 20.7  | 0.100           | 242.416         | 640.14                            | 417.14       | 360.11       | 6.41         | ...              | ...                  | ...               | 10.302±0.028 | 9.712±0.022  | 9.430±0.023          | 11                     | 18.4±6.2                | 0                       | nan±nan  | ±                 |                   |
| SCR1058-7558   | 10 58 54.82  | -75 58 19.5  | 0.014           | 294.817         | 686.15                            | 479.15       | 799.13       | 4.62         | ...              | ...                  | ...               | 11.142±0.023 | 10.450±0.024 | 10.190±0.021         | 11                     | 20.4±10.2               | 0                       | nan±nan  | ±                 |                   |
| SCR1059-7745   | 10 59 20.98  | -77 45 02.6  | 0.008           | 333.916         | 103.14                            | 472.14       | 405.13       | 8.84         | ...              | ...                  | ...               | 11.003±0.022 | 10.272±0.023 | 10.002±0.023         | 9                      | 23.7±14.2               | 0                       | nan±nan  | ±                 |                   |
| SCR1103-7648   | 11 03 04.98  | -76 48 47.8  | 0.038           | 218.016         | 239.14                            | 565.14       | 710.13       | 4.04         | ...              | ...                  | ...               | 10.648±0.027 | 10.056±0.023 | 9.780±0.027          | 11                     | 24.2±15.6               | 0                       | nan±nan  | ±                 |                   |
| CHXR11         | 11 03 11.61  | -77 21 04.2  | 0.013           | 209.512         | 738.11                            | 075.11       | 203.10       | 40.88        | 11.46            | 1                    | 10.52             | 1            | 9.58         | 1                    | 10.2±6.4               | 12                      | 16.65±5.21              | 0  | nan±nan           | ±                 |
| SCR1103-7659   | 11 03 14.11  | -76 59 27.9  | 0.003           | 027.614         | 982.13                            | 241.13       | 111.12       | 4.74         | ...              | ...                  | ...               | 10.157±0.023 | 9.416±0.023  | 9.186±0.023          | 10                     | 23.4±14.7               | 0                       | nan±nan  | ±                 |                   |
| UVCHA          | 11 05 52.61  | -76 18 25.6  | 0.011           | 282.415         | 174.13                            | 208.13       | 367.12       | 8.07         | ...              | ...                  | ...               | 10.312±0.024 | 9.593±0.023  | 9.339±0.019          | 9                      | 20.8±11.8               | 0                       | nan±nan  | ±                 |                   |
| ISO-CHA199     | 11 07 20.41  | -77 29 40.4  | 0.013           | 271.617         | 349.16                            | 152.16       | 241.15       | 25.4         | ...              | ...                  | ...               | 11.134±0.024 | 10.547±0.023 | 10.259±0.021         | 9                      | 23.1±22.4               | 0                       | nan±nan  | ±                 |                   |
| SCR1107-3605   | 11 07 41.07  | -36 05 58.8  | 0.085           | 150.814         | 245.12                            | 124.12       | 197.10       | 5.86         | ...              | ...                  | ...               | 9.584±0.026  | 8.918±0.034  | 8.660±0.019          | 11                     | 23.9±6.6                | 0                       | nan±nan  | ±                 |                   |
| SCR1107-3607   | 11 07 42.80  | -36 07 37.9  | 0.097           | 149.015         | 269.13                            | 157.13       | 193.11       | 1.88         | ...              | ...                  | ...               | 9.988±0.027  | 9.360±0.022  | 9.112±0.025          | 11                     | 22.9±6.3                | 0                       | nan±nan  | ±                 |                   |
| RXJ108-7519A   | 11 08 53.27  | -75 19 37.4  | 0.018           | 299.614         | 481.12                            | 666.12       | 435.11       | 3.17         | ...              | ...                  | ...               | 9.737±0.027  | 9.030±0.049  | 8.800±0.024          | 11                     | 23.8±10.2               | 0                       | nan±nan  | ±                 |                   |
| DEN1109-2414   | 11 09 53.28  | -24 14 59.4  | 0.095           | 034.715         | 963.13                            | 539.13       | 725.11       | 2.03         | ...              | ...                  | ...               | 10.144±0.020 | 9.602±0.022  | 9.260±0.021          | 11                     | 21.3±7.2                | 0                       | nan±nan  | ±                 |                   |
| SCR1112-7445   | 11 12 31.18  | -74 45 26.8  | 0.032           | 303.916         | 712.12                            | 557.14       | 695.12       | 8.66         | ...              | ...                  | ...               | 10.848±0.026 | 10.050±0.026 | 9.840±0.019          | 11                     | 22.9±11.3               | 0                       | nan±nan  | ±                 |                   |
| SCR1118-7643   | 11 18 33.80  | -76 43 04.2  | 0.007           | 280.518         | 077.16                            | 117.16       | 329.13       | 6.95         | ...              | ...                  | ...               | 11.336±0.032 | 10.783±0.030 | 10.418±0.027         | 11                     | 21.0±9.7                | 0                       | nan±nan  | ±                 |                   |
| SCR1121-3845   | 11 21 05.49  | -38 45 35.5  | 0.064           | 255.413         | 889.11                            | 263.11       | 744.10       | 4.04         | ...              | ...                  | ...               | 9.999±0.034  | 8.334±0.033  | 8.053±0.029          | 11                     | 16.3±3.8                | 0                       | nan±nan  | ±                 |                   |
| SCR1124-7554   | 11 24 29.81  | -75 54 23.7  | 0.019           | 325.017         | 872.15                            | 608.15       | 837.13       | 4.10         | ...              | ...                  | ...               | 10.931±0.024 | 10.202±0.023 | 9.884±0.021          | 11                     | 15.5±8.0                | 0                       | nan±nan  | ±                 |                   |
| SCR1126-3824   | 11 26 51.34  | -38 24 55.3  | 0.052           | 249.815         | 531.13                            | 676.13       | 826.11       | 5.36         | ...              | ...                  | ...               | 10.017±0.026 | 9.362±0.023  | 9.118±0.021          | 11                     | 19.3±6.2                | 0                       | nan±nan  | ±                 |                   |
| RXJ132-3019    | 11 32 18.31  | -30 19 51.8  | 0.086           | 251.215         | 298.12                            | 710.12       | 682.10       | 11.17        | ...              | ...                  | ...               | 9.641±0.024  | 9.030±0.023  | 8.765±0.021          | 11                     | 19.9±9.2                | 0                       | nan±nan  | ±                 |                   |
| SCR1133-7622   | 11 33 23.28  | -76 22 09.2  | 0.026           | 248.616         | 628.14                            | 728.14       | 921.12       | 8.39         | ...              | ...                  | ...               | 10.594±0.022 | 9.999±0.025  | 9.714±0.023          | 11                     | 20.0±10.7               | 0                       | nan±nan  | ±                 |                   |
| SCR1138-3455   | 11 38 30.10  | -34 55 35.5  | 0.133           | 338.814         | 486.12                            | 327.12       | 502.10       | 9.18         | ...              | ...                  | ...               | 9.593±0.024  | 9.017±0.023  | 8.778±0.021          | 11                     | 22.9±7.2                | 0                       | nan±nan  | ±                 |                   |
| SCR1146-4528   | 11 46 21.91  | -45 28 35.5  | 0.077           | 201.716         | 793.14                            | 172.14       | 363.11       | 3.94         | ...              | ...                  | ...               | 10.606±0.024 | 10.001±0.022 | 9.762±0.023          | 11                     | 23.0±6.9                | 0                       | nan±nan  | ±                 |                   |
| 2MA1149-3809   | 11 49 25.92  | -38 09 27.8  | 0.046           | 019.818         | 124.15                            | 845.15       | 963.12       | 8.51         | ...              | ...                  | ...               | 11.124±0.029 | 10.503±0.023 | 10.180±0.025         | 11                     | 19.1±5.8                | 0                       | nan±nan  | ±                 |                   |
| SCR1149-0219   | 11 49 30.25  | -02 19 27.2  | 0.104           | 124.415         | 213.12                            | 900.13       | 017.10       | 8.23         | ...              | ...                  | ...               | 9.874±0.023  | 9.282±0.022  | 9.017±0.021          | 11                     | 22.7±6.6                | 0                       | nan±nan  | ±                 |                   |
| SCR1153-7902   | 11 53 34.46  | -79 02 33.1  | 0.024           | 253.116         | 140.14                            | 252.14       | 316.10       | 9.91         | ...              | ...                  | ...               | 10.304±0.024 | 9.636±0.022  | 9.403±0.023          | 11                     | 18.9±7.1                | 0                       | nan±nan  | ±                 |                   |
| SCR1154-0206   | 11 54 56.93  | -02 06 09.2  | 0.099           | 297.114         | 668.12                            | 139.12       | 357.10       | 7.15         | ...              | ...                  | ...               | 9.547±0.022  | 8.957±0.024  | 8.685±0.021          | 11                     | 21.3±5.8                | 0                       | nan±nan  | ±                 |                   |
| SCR1155-7819   | 11 55 04.93  | -78 19 02.8  | 0.036           | 233.116         | 786.14                            | 797.14       | 846.12       | 3.41         | ...              | ...                  | ...               | 10.691±0.023 | 10.096±0.021 | 9.808±0.021          | 11                     | 21.5±5.5                | 0                       | nan±nan  | ±                 |                   |
| LP851-410      | 11 58 19.78  | -22 40 59.7  | 0.125           | 229.314         | 085.11                            | 930.12       | 023.10       | 13.37        | ...              | ...                  | ...               | 9.330±0.022  | 8.677±0.031  | 8.425±0.021          | 11                     | 21.1±5.7                | 0                       | nan±nan  | ±                 |                   |
| SCR1200-7848   | 12 00 01.11  | -78 48 28.8  | 0.036           | 231.716         | 356.14                            | 259.14       | 415.12       | 3.13         | ...              | ...                  | ...               | 10.590±0.021 | 9.948±0.025  | 9.689±0.025          | 11                     | 22.8±8.1                | 0                       | nan±nan  | ±                 |                   |
| SCR1200-1731   | 12 00 01.60  | -17 31 30.8  | 0.088           | 238.914         | 827.12                            | 828.12       | 772.10       | 8.56         | ...              | ...                  | ...               | 9.403±0.026  | 8.687±0.044  | 8.465±0.031          | 11                     | 15.3±4.8                | 0                       | nan±nan  | ±                 |                   |
| SCR1202-3328   | 12 02 37.99  | -33 28 40.3  | 0.065           | 241.216         | 742.14                            | 370.14       | 665.12       | 2.21         | ...              | ...                  | ...               | 10.686±0.023 | 10.123±0.023 | 9.847±0.019          | 11                     | 23.3±6.7                | 0                       | nan±nan  | ±                 |                   |
| 2MA1207-3247   | 12 07 27.38  | -32 47 00.3  | 0.070           | 236.013         | 406.11                            | 164.11       | 288.10       | 9.501        | ...              | ...                  | ...               | 8.618±0.029  | 8.025±0.044  | 7.751±0.031          | 11                     | 15.6±4.1                | 0                       | nan±nan  | ±                 |                   |
| SCR1209-7505   | 12 09 29.99  | -75 05 40.1  | 0.059           | 272.214         | 831.12                            | 829.13       | 074.11       | 2.74         | ...              | ...                  | ...               | 9.911±0.023  | 9.243±0.023  | 9.011±0.023          | 11                     | 23.4±7.9                | 0                       | nan±nan  | ±                 |                   |
| SCR1212-7822   | 12 12 22.85  | -78 22 03.9  | 0.036           | 248.417         | 447.15                            | 339.15       | 494.12       | 8.51         | ...              | ...                  | ...               | 10.835±0.024 | 10.283±0.025 | 9.949±0.021          | 11                     | 18.5±6.3                | 0                       | nan±nan  | ±                 |                   |
| SCR1217-3644   | 12 17 47.46  | -36 44 50.3  | 0.119           | 115.313         | 504.11                            | 108.11       | 310.10       | 9.681        | ...              | ...                  | ...               | 8.675±0.024  | 8.063±0.033  | 7.828±0.024          | 11                     | 16.0±4.2                | 0                       | nan±nan  | ±                 |                   |
| SCR1218-0609   | 12 18 41.88  | -06 09 12.3  | 0.103           | 117.815         | 896.13                            | 334.13       | 714.11       | 3.74         | ...              | ...                  | ...               | 10.117±0.024 | 9.579±0.026  | 9.280±0.021          | 11                     | 21.1±6.1                | 0                       | nan±nan  | ±                 |                   |
| SCR1219-7420   | 12 19 53.56  | -74 20 09.3  | 0.028           | 240.515         | 843.14                            | 034.13       | 870.12       | 1.83         | ...              | ...                  | ...               | 10.438±0.026 | 9.775±0.025  | 9.545±0.021          | 11                     | 24.9±10.3               | 0                       | nan±nan  | ±                 |                   |
| SCR1221-5004   | 12 21 29.06  | -50 04 08.7  | 0.102           | 282.815         | 885.13                            | 521.13       | 530.11       | 3.06         | ...              | ...                  | ...               | 10.117±0.022 | 9.499±0.023  | 9.235±0.018          | 11                     | 21.2±6.1                | 0                       | nan±nan  | ±                 |                   |
| SCR1225-2814   | 12 25 46.98  | -28 14 03.8  | 0.019           | 119.218         | 281.14                            | 255.14       | 421.11       | 6.26         | ...              | ...                  | ...               | 10.427±0.024 | 9.654±0.022  | 9.409±0.021          | 11                     | 15.6±8.0                | 0                       | nan±nan  | ±                 |                   |
| SCR1226-3316   | 12 26 51.35  | -33 16 12.5  | 0.059           | 238.417         | 140.15                            | 169.15       | 371.12       | 7.06         | ...              | ...                  | ...               | 10.691±0.024 | 10.122±0.028 | 9.78                 |                        |                         |                         |  |                   |                   |

Table B.2 – Continued from previous page

| Name          | RA<br>(2)   | DEC<br>(3)  | $\mu$<br>(4) | P.A.<br>(5) | SuperCOSMOS |        |        | $I_{V,N}$ | $I_{R,N}$ | $I_{B,N}$ | $I_{G,N}$ | $I_{R,nobs}$ | $I_{B,nobs}$ | $I_{G,nobs}$ | $J$<br>(16)  | $H$<br>(17)  | $K$<br>(18) | No. p.l.r.el<br>(19) | No. p.l.r.el<br>(20) | No. ccd.rel<br>(21) | ccddist<br>(pc)<br>(22) | X-ray flux<br>( $\text{cnt. s}^{-1}$ )<br>(23) |
|---------------|-------------|-------------|--------------|-------------|-------------|--------|--------|-----------|-----------|-----------|-----------|--------------|--------------|--------------|--------------|--------------|-------------|----------------------|----------------------|---------------------|-------------------------|--|
| SRI1306-3728  | 13 06 18.21 | -34 28 56.9 | 0.046        | 217.7       | 16.548      | 14.451 | 14.496 | 12.193    | ...       | ...       | ...       | ...          | ...          | 10.503±0.024 | 9.898±0.022  | 9.632±0.020  | 11          | 20.5±6.4             | 0                    | nan±nan             | ±                       |  |
| 2MA1306-7730  | 13 06 38.83 | -37 30 35.3 | 0.020        | 226.0       | 17.803      | 15.854 | 15.765 | 13.355    | ...       | ...       | ...       | ...          | ...          | 11.493±0.024 | 10.788±0.022 | 10.409±0.020 | 11          | 25.0±8.9             | 0                    | nan±nan             | ±                       |  |
| 2MA1306-7723  | 13 06 56.56 | -37 29 05.5 | 0.019        | 244.9       | 18.368      | 16.067 | 16.227 | 13.237    | 17.58     | 1         | 13.51     | 1            | ...          | 10.951±0.023 | 10.225±0.025 | 9.798±0.025  | 11          | 12.5±4.3             | 12                   | 10.44±1.75          | ±                       |  |
| SRI1316-0858  | 13 16 40.54 | -08 58 25.6 | 0.093        | 226.3       | 15.661      | 13.187 | 13.192 | 10.848    | ...       | ...       | ...       | ...          | ...          | 10.043±0.024 | 9.500±0.024  | 9.199±0.021  | 11          | 24.1±8.7             | 0                    | nan±nan             | ±                       |  |
| SRI1321-0543  | 13 21 14.46 | -05 43 31.4 | 0.126        | 236.4       | 14.744      | 12.643 | 12.909 | 11.060    | ...       | ...       | ...       | ...          | ...          | 9.793±0.024  | 9.178±0.024  | 8.851±0.021  | 11          | 21.9±6.8             | 0                    | nan±nan             | ±                       |  |
| SRI1325-0454  | 13 25 28.93 | -04 54 15.1 | 0.178        | 148.2       | 16.219      | 13.892 | 14.145 | 12.090    | ...       | ...       | ...       | ...          | ...          | 10.479±0.026 | 9.869±0.023  | 9.589±0.021  | 11          | 22.9±7.3             | 0                    | nan±nan             | ±                       |  |
| SRI1333-4739  | 13 33 07.60 | -47 39 24.3 | 0.032        | 212.9       | 15.749      | 13.372 | 13.631 | 11.203    | ...       | ...       | ...       | ...          | ...          | 9.982±0.022  | 9.389±0.026  | 9.122±0.021  | 11          | 19.3±5.8             | 0                    | nan±nan             | ±                       |  |
| SRI1344-4020A | 13 44 25.47 | -40 20 15.2 | 0.180        | 070.1       | 12.999      | 10.533 | 10.821 | 8.751     | ...       | ...       | ...       | ...          | ...          | 9.589±0.024  | 9.038±0.025  | 8.756±0.021  | 5           | 31.9±13.5            | 0                    | nan±nan             | ±                       |  |
| SRI1344-4020B | 13 44 25.47 | -40 20 15.2 | 0.180        | 070.1       | 12.999      | 10.533 | 10.821 | 8.751     | ...       | ...       | ...       | ...          | ...          | 9.453±0.024  | 8.867±0.046  | 8.632±0.024  | 6           | 31.4±12.6            | 0                    | nan±nan             | ±                       |  |
| SRI1344-4020C | 13 44 27.56 | -40 18 40.0 | 0.176        | 068.4       | 16.000      | 13.390 | 13.553 | 11.257    | ...       | ...       | ...       | ...          | ...          | 10.249±0.022 | 9.723±0.023  | 9.426±0.021  | 11          | 24.9±8.2             | 0                    | nan±nan             | ±                       |  |
| SRI1349-1832  | 13 49 54.97 | -18 32 09.2 | 0.133        | 224.5       | 15.985      | 13.843 | 14.078 | 12.039    | ...       | ...       | ...       | ...          | ...          | 10.365±0.022 | 9.790±0.023  | 9.533±0.021  | 11          | 23.1±7.9             | 0                    | nan±nan             | ±                       |  |
| SRI1358-0046  | 13 58 21.64 | -00 46 26.3 | 0.114        | 232.0       | 17.093      | 14.765 | 14.863 | 12.272    | ...       | ...       | ...       | ...          | ...          | 10.808±0.024 | 10.240±0.023 | 9.941±0.021  | 11          | 23.0±6.9             | 0                    | nan±nan             | ±                       |  |
| SRI1409-2403  | 14 09 58.97 | -24 03 37.7 | 0.091        | 275.4       | 14.676      | 12.171 | 12.168 | 10.510    | ...       | ...       | ...       | ...          | ...          | 9.434±0.030  | 8.853±0.046  | 8.604±0.022  | 11          | 20.6±5.6             | 0                    | nan±nan             | ±                       |  |
| SRI1410-2234  | 14 10 27.92 | -22 34 23.3 | 0.174        | 257.1       | 15.278      | 13.066 | 13.174 | 11.583    | ...       | ...       | ...       | ...          | ...          | 10.084±0.024 | 9.393±0.025  | 9.175±0.019  | 11          | 23.7±8.3             | 0                    | nan±nan             | ±                       |  |
| SRI1428-3825  | 14 28 05.21 | -38 25 35.3 | 0.031        | 271.6       | 14.402      | 12.197 | 12.243 | 10.635    | ...       | ...       | ...       | ...          | ...          | 9.341±0.026  | 8.758±0.042  | 8.480±0.026  | 11          | 19.1±5.6             | 0                    | nan±nan             | ±                       |  |
| SRI1433-1100  | 14 33 30.44 | -11 00 20.4 | 0.128        | 267.2       | 14.551      | 12.244 | 12.566 | 10.865    | ...       | ...       | ...       | ...          | ...          | 9.810±0.024  | 9.197±0.024  | 8.943±0.021  | 11          | 24.2±6.4             | 0                    | nan±nan             | ±                       |  |
| SRI1438-3941  | 14 38 36.26 | -39 41 06.3 | 0.164        | 214.5       | 14.104      | 11.808 | 11.991 | 10.437    | ...       | ...       | ...       | ...          | ...          | 9.403±0.024  | 8.726±0.026  | 8.517±0.021  | 11          | 22.4±6.2             | 0                    | nan±nan             | ±                       |  |
| SRI1444-0424  | 14 44 28.11 | -04 24 07.9 | 0.150        | 131.0       | 14.868      | 12.641 | 12.713 | 10.970    | ...       | ...       | ...       | ...          | ...          | 9.728±0.029  | 9.122±0.027  | 8.865±0.026  | 11          | 22.1±6.2             | 0                    | nan±nan             | ±                       |  |
| SRI1514-0958  | 15 14 16.90 | -09 58 38.8 | 0.152        | 220.4       | 15.305      | 13.353 | 13.367 | 11.216    | ...       | ...       | ...       | ...          | ...          | 9.665±0.029  | 9.087±0.026  | 8.780±0.023  | 11          | 16.2±5.0             | 0                    | nan±nan             | ±                       |  |
| SRI1519-1707  | 15 19 46.83 | -17 07 25.2 | 0.018        | 219.4       | 14.765      | 13.051 | 12.742 | 11.237    | ...       | ...       | ...       | ...          | ...          | 9.873±0.023  | 9.204±0.024  | 8.985±0.023  | 11          | 24.7±8.2             | 0                    | nan±nan             | ±                       |  |
| SRI1550-0756  | 15 20 45.45 | -07 56 13.7 | 0.137        | 210.2       | 16.068      | 13.880 | 13.982 | 11.857    | ...       | ...       | ...       | ...          | ...          | 10.346±0.026 | 9.781±0.026  | 9.435±0.023  | 11          | 21.8±6.5             | 0                    | nan±nan             | ±                       |  |
| SRI1555-0655  | 15 35 07.56 | -06 55 22.1 | 0.022        | 206.1       | 16.287      | 14.137 | 14.543 | 12.031    | ...       | ...       | ...       | ...          | ...          | 10.571±0.026 | 9.949±0.027  | 9.705±0.023  | 11          | 23.4±7.2             | 0                    | nan±nan             | ±                       |  |
| SRI1543-2556  | 15 43 43.79 | -25 56 04.9 | 0.053        | 212.5       | 15.664      | 13.547 | 13.592 | 11.661    | ...       | ...       | ...       | ...          | ...          | 10.273±0.023 | 9.631±0.022  | 9.384±0.021  | 11          | 24.3±7.2             | 0                    | nan±nan             | ±                       |  |
| BPS0329-0045  | 15 45 47.54 | -03 13 06.8 | 0.030        | 202.9       | 14.828      | 12.562 | 12.888 | 11.210    | ...       | ...       | ...       | ...          | ...          | 9.689±0.026  | 9.005±0.023  | 8.771±0.023  | 11          | 19.5±7.0             | 0                    | nan±nan             | ±                       |  |
| SRI1546-2751  | 15 45 41.88 | -05 15 31.8 | 0.029        | 201.7       | 16.532      | 14.362 | 14.508 | 12.500    | ...       | ...       | ...       | ...          | ...          | 10.501±0.023 | 9.860±0.024  | 9.599±0.022  | 11          | 19.8±8.6             | 0                    | nan±nan             | ±                       |  |
| SRI1546-2726A | 15 46 29.97 | -27 26 11.7 | 0.079        | 166.4       | 16.046      | 13.693 | 13.779 | 11.733    | ...       | ...       | ...       | ...          | ...          | 10.266±0.023 | 9.708±0.025  | 9.447±0.023  | 11          | 22.6±6.4             | 0                    | nan±nan             | ±                       |  |
| SRI1546-2726B | 15 46 40.65 | -27 26 41.7 | 0.164        | 200.4       | 15.210      | 13.131 | 13.535 | 11.866    | ...       | ...       | ...       | ...          | ...          | 10.082±0.026 | 9.506±0.023  | 9.231±0.023  | 11          | 23.4±10.4            | 0                    | nan±nan             | ±                       |  |
| SRI1546-2262B | 15 46 41.67 | -22 26 33.8 | 0.172        | 203.2       | 17.092      | 14.988 | 15.208 | 13.192    | ...       | ...       | ...       | ...          | ...          | 11.330±0.024 | 10.737±0.022 | 10.439±0.019 | 11          | 32.0±13.0            | 0                    | nan±nan             | ±                       |  |
| SRI1546-1935  | 15 46 56.70 | -19 31 32.0 | 0.115        | 262.0       | 14.387      | 12.422 | 12.451 | 10.690    | ...       | ...       | ...       | ...          | ...          | 9.353±0.026  | 8.700±0.026  | 8.472±0.023  | 11          | 18.1±5.7             | 0                    | nan±nan             | ±                       |  |
| SRI1547-2751  | 15 47 29.83 | -27 55 12.2 | 0.107        | 083.8       | 14.200      | 12.144 | 12.191 | 10.322    | ...       | ...       | ...       | ...          | ...          | 9.308±0.026  | 8.715±0.038  | 8.473±0.025  | 11          | 20.3±5.5             | 0                    | nan±nan             | ±                       |  |
| RX1550-2312   | 15 50 04.99 | -23 11 53.8 | 0.061        | 184.7       | 14.867      | 12.881 | 12.842 | 11.237    | ...       | ...       | ...       | ...          | ...          | 9.885±0.024  | 9.215±0.023  | 8.930±0.023  | 11          | 22.9±7.5             | 0                    | nan±nan             | ±                       |  |
| SRI1550-2226  | 15 50 21.14 | -22 26 37.1 | 0.035        | 197.5       | 16.209      | 14.225 | 14.464 | 12.534    | ...       | ...       | ...       | ...          | ...          | 10.645±0.026 | 9.964±0.031  | 9.633±0.024  | 11          | 22.7±10.5            | 0                    | nan±nan             | ±                       |  |
| SRI1553-2315  | 15 53 58.77 | -23 15 43.7 | 0.032        | 184.0       | 17.116      | 15.029 | 15.098 | 12.719    | ...       | ...       | ...       | ...          | ...          | 11.070±0.022 | 10.395±0.024 | 10.086±0.021 | 11          | 24.5±9.5             | 0                    | nan±nan             | ±                       |  |
| SRI1554-2217  | 15 54 34.14 | -22 17 15.6 | 0.030        | 179.9       | 18.400      | 16.196 | 16.302 | 13.808    | ...       | ...       | ...       | ...          | ...          | 11.617±0.022 | 10.984±0.024 | 10.665±0.019 | 11          | 24.2±9.6             | 0                    | nan±nan             | ±                       |  |
| SRI1556-2016  | 15 56 25.12 | -20 16 16.0 | 0.024        | 174.8       | 17.675      | 15.453 | 15.604 | 13.147    | ...       | ...       | ...       | ...          | ...          | 10.820±0.023 | 10.173±0.022 | 9.857±0.023  | 11          | 16.1±7.2             | 0                    | nan±nan             | ±                       |  |
| RX1556-2338   | 15 56 27.62 | -23 38 52.1 | 0.030        | 194.9       | 15.336      | 13.062 | 13.253 | 11.250    | ...       | ...       | ...       | ...          | ...          | 10.087±0.023 | 9.389±0.023  | 9.111±0.026  | 11          | 22.7±6.2             | 0                    | nan±nan             | ±                       |  |
| SRI1556-1950  | 15 56 47.69 | -19 50 07.7 | 0.034        | 169.4       | 14.720      | 12.656 | 12.825 | 11.492    | ...       | ...       | ...       | ...          | ...          | 9.902±0.021  | 9.168±0.025  | 8.946±0.025  | 11          | 23.7±10.1            | 0                    | nan±nan             | ±                       |  |
| SRI1603-1805  | 15 59 18.39 | -22 10 43.1 | 0.023        | 196.1       | 17.529      | 15.313 | 15.547 | 12.963    | ...       | ...       | ...       | ...          | ...          | 11.044±0.025 | 10.341±0.021 | 10.073±0.023 | 11          | 20.1±6.8             | 0                    | nan±nan             | ±                       |  |
| USCOCT05      | 15 59 50.51 | -19 44 37.4 | 0.035        | 191.7       | 17.348      | 15.131 | 15.210 | 12.972    | ...       | ...       | ...       | ...          | ...          | 11.172±0.023 | 10.445±0.026 | 10.170±0.021 | 11          | 24.3±8.5             | 0                    | nan±nan             | ±                       |  |
| SRI1559-1830  | 15 59 58.87 | -18 30 03.7 | 0.032        | 186.3       | 17.300      | 15.233 | 15.264 | 13.074    | ...       | ...       | ...       | ...          | ...          | 11.135±0.024 | 10.489±0.027 | 10.211±0.021 | 11          | 23.4±9.3             | 0                    | nan±nan             | ±                       |  |
| 2MA1601-2222  | 16 01 10.38 | -22 22 27.6 | 0.041        | 197.2       | 16.657      | 14.597 | 14.840 | 12.520    | ...       | ...       | ...       | ...          | ...          | 10.739±0.024 | 10.023±0.022 | 9.758±0.023  | 11          | 21.1±7.8             | 0                    | nan±nan             | ±                       |  |
| SRI1603-2234  | 16 03 14.91 | -22 34 45.5 | 0.029        | 198.3       | 18.533      | 16.304 | 16.399 | 13.872    | ...       | ...       | ...       | ...          | ...          | 11.674±0.023 | 10.999±0.025 | 10.702±0.022 | 11          | 23.9±9.3             | 0                    | nan±nan             | ±                       |  |
| SRI1603-1805  | 16 03 50.08 | -18 05 46.0 | 0.026        | 178.0       | 18.312      | 15.957 | 16.081 | 13.664    | ...       | ...       | ...       | ...          | ...          | 11.489±0.021 | 10.842±0.025 | 10.499±0.022 | 11          | 22.5±8.8             | 0                    | nan±nan             | ±                       |  |
| 2MA1605-2035  | 16 05 02.14 | -20 35 07.1 | 0.032        | 176.3       | 15.813      | 13.521 | 13.706 | 11.808    | ...       | ...       | ...       | ...          | ...          | 10.440±0.024 | 9.659±0.025  | 9.447±0.026  | 11          | 24.4±7.5             | 0                    | nan±nan             | ±                       |  |
| SRI1606-2212  | 16 06 13.31 | -22 12 53.8 | 0.042        | 179.0       | 16.248      | 14.019 | 14.140 | 11.872    | ...       | ...       | ...       | ...          | ...          | 10.520±0.024 | 9.867±0.023  | 9.586±0.021  | 11          | 23.3±6.6             | 0                    | nan±nan             | ±                       |  |
| 2MA1606-2052  | 16 06 28.98 | -20 52 16.8 | 0.028        | 183.1       | 17.961      | 15.689 | 15.742 | 13.207    | ...       | ...       | ...       | ...          | ...          | 11.013±0.023 | 10.402±0.026 | 10.002±0.021 | 11          | 17.1±6.4             | 0                    | nan±nan             | ±                       |  |
| SRI1606-2727  | 16 06 38.04 | -27 27 55.4 | 0.033        | 174.0       | 16.712      | 14.239 | 14.555 | 12.055    | ...       | ...       | ...       | ...          | ...          | 10.708±0.026 | 10.014±0.024 | 9.758±0.024  | 11          | 22.8±6.7             | 0                    | nan±nan             | ±                       |  |
| SRI1607-2825  | 16 07 41.05 | -28 25 03.9 | 0.144        | 220.7       | 15.621      | 13.410 | 13.373 | 11.167    | ...       | ...       | ...       | ...          | ...          | 9.983±0.023  | 9.407±0.022  | 9.124±0.019  | 11          | 21.0±5.9             | 0                    | nan±nan             | ±                       |  |
| 2MA1607-2036  | 16 07 44.49 | -20 36 03.1 | 0.032        | 171.1       | 15.848      | 13.847 | 13.815 | 11.628    | ...       | ...       | ...       | ...          | ...          | 10.076±0.023 | 9.343±0.024  | 9.077±0.021  | 11          | 17.1±5.4             | 0                    | nan±nan             | ±                       |  |
| SRI1609-2222A | 16 09 31.63 | -22 22 05.7 | 0.022        | 179.0       | 17.122      | 14.979 | 15.036 | 12.434    | 15.99     | 1         | 12.49     | 1            | ...          | 10.498±0.028 | 9.842±0.027  | 9.499±0.021  | 11          | 15.0±4.9             | 12                   | 13.15±2.12          | ±                       |  |
| LH1609-2229A  | 16 09 31.65 | -22 29 22.4 | 0.021        | 167.4       | 15.254      | 13.249 | 13.218 | 11.435    | ...       | ...       | ...       | ...          | ...          | 10.143±0.028 | 9.383±0.023  | 9.148±0.021  | 11          | 23.6±7.3             | 0                    | nan±nan             | ±                       |  |
| SRI1610-2728  | 16 10 03.11 | -27 28 05.6 | 0.032        | 166.4       | 16.725      | 14.739 | 14.905 | 12.720    | ...       | ...       | ...       | ...          | ...          | 10.773±0.023 | 10.141±0.021 | 9.837±0.023  | 11          | 21.9±9.2             | 0                    |                     |                         |  |

Table B.2 – Continued from previous page

| Name<br>(1)   | RA           |              | DEC          |              | $\mu$<br>( $''_{yr^{-1}}$ ) (4) | P.A.<br>° (5) | SuperCOSMOS  |              |             | Johnson-Kron-Cousins |             |             | 2MASS       |               |             | No.<br>No. pltr.rel<br>(19) | No. ccd,rel<br>(21) | No. ccd,ist<br>(22) | X-ray flux<br>( $cnt\ s^{-1}$ )<br>(23) |             |              |              |   |
|---------------|--------------|--------------|--------------|--------------|---------------------------------|---------------|--------------|--------------|-------------|----------------------|-------------|-------------|-------------|---------------|-------------|-----------------------------|---------------------|---------------------|---|-------------|--------------|--------------|---|
|               | J2000<br>(2) | E2000<br>(3) | $B_J$<br>(6) | $R_1$<br>(7) |                                 |               | $R_2$<br>(8) | $I_V$<br>(9) | $V$<br>(10) | $I$<br>(11)          | $J$<br>(12) | $H$<br>(13) | $I$<br>(14) | $I_s$<br>(15) | $J$<br>(16) |                             |                     |                     |   | $H$<br>(17) | $K$<br>(18)  |              |   |
| SCR1614-2340  | 16 14 52.69  | -23 08 02.6  | 0.016        | 174.2        | 16.345                          | 14.051        | 14.069       | 11.805       | ...         | ...                  | ...         | 10.569      | ±0.026      | 9.884         | ±0.026      | 9.603                       | ±0.021              | 11                  | 23.9 ± 6.8                              | 0           | nan ± nan    | ±            |   |
| SCR1616-2440  | 16 16 47.95  | -24 04 28.3  | 0.026        | 166.3        | 17.585                          | 15.493        | 15.538       | 13.839       | ...         | ...                  | ...         | 11.312      | ±0.023      | 10.539        | ±0.026      | 10.264                      | ±0.024              | 11                  | 24.6 ± 16.6                             | 0           | nan ± nan    | ±            |   |
| SCR1617-2450  | 16 17 26.15  | -24 50 59.3  | 0.028        | 174.6        | 17.057                          | 15.190        | 15.205       | 13.863       | ...         | ...                  | ...         | 10.912      | ±0.024      | 10.135        | ±0.023      | 9.852                       | ±0.024              | 11                  | 21.8 ± 18.7                             | 0           | nan ± nan    | ±            |   |
| SCR1617-2421  | 16 17 27.69  | -24 21 02.6  | 0.032        | 170.7        | 17.921                          | 16.008        | 16.095       | 13.986       | ...         | ...                  | ...         | 11.329      | ±0.023      | 10.661        | ±0.022      | 10.296                      | ±0.021              | 11                  | 21.3 ± 14.0                             | 0           | nan ± nan    | ±            |   |
| SCR1618-2328  | 16 18 09.91  | -23 28 54.9  | 0.025        | 171.8        | 17.381                          | 15.117        | 15.330       | 13.524       | ...         | ...                  | ...         | 11.135      | ±0.024      | 10.404        | ±0.024      | 10.097                      | ±0.021              | 11                  | 22.7 ± 13.8                             | 0           | nan ± nan    | ±            |   |
| SCR1620-2123  | 16 20 36.41  | -21 23 12.1  | 0.033        | 190.4        | 16.876                          | 14.768        | 14.893       | 12.878       | ...         | ...                  | ...         | 10.942      | ±0.022      | 10.307        | ±0.022      | 10.016                      | ±0.021              | 11                  | 24.7 ± 10.4                             | 0           | nan ± nan    | ±            |   |
| BD-19-04371   | 16 26 23.37  | -19 31 35.7  | 0.010        | 053.3        | 11.835                          | 10.062        | 10.74        | 9.943        | 10.61       | 1                    | 8.90        | 1           | 7.561       | ±0.021        | 6.899       | ±0.044                      | 6.647               | ±0.017              | 10                                      | 8.2 ± 5.5   | 12           | 14.64 ± 4.55 | ± |
| SCR1627-1925A | 16 27 03.60  | -19 11 48.8  | 0.014        | 140.5        | 14.340                          | 12.544        | 12.571       | 11.954       | ...         | ...                  | ...         | 8.927       | ±0.022      | 9.021         | ±0.022      | 8.802                       | ±0.019              | 10                  | 20.8 ± 12.8                             | 0           | nan ± nan    | ±            |   |
| SCR1627-1925B | 16 27 14.03  | -19 25 46.7  | 0.012        | 130.7        | 14.108                          | 12.603        | 12.584       | 11.447       | 12.85       | 1                    | 10.67       | 1           | 8.927       | ±0.027        | 8.299       | ±0.042                      | 7.933               | ±0.027              | 11                                      | 12.2 ± 8.6  | 12           | 15.66 ± 6.18 | ± |
| SCR1628-1905  | 16 28 04.24  | -19 05 35.0  | 0.052        | 134.3        | 13.435                          | 11.886        | 12.130       | 11.515       | ...         | ...                  | ...         | 9.300       | ±0.027      | 8.621         | ±0.027      | 8.338                       | ±0.040              | 11                  | 16.1 ± 10.7                             | 0           | nan ± nan    | ±            |   |
| SCR1628-1815  | 16 28 15.85  | -18 15 16.9  | 0.010        | 112.5        | 13.789                          | 11.806        | 12.368       | 11.686       | ...         | ...                  | ...         | 9.146       | ±0.027      | 8.460         | ±0.036      | 8.265                       | ±0.017              | 9                   | 15.5 ± 9.7                              | 0           | nan ± nan    | ±            |   |
| SCR1628-1842  | 16 28 36.74  | -18 14 13.5  | 0.014        | 141.0        | 14.363                          | 12.823        | 13.023       | 12.316       | ...         | ...                  | ...         | 9.330       | ±0.023      | 8.589         | ±0.042      | 8.380                       | ±0.023              | 11                  | 17.6 ± 11.8                             | 0           | nan ± nan    | ±            |   |
| SCR1629-1835  | 16 29 02.02  | -18 35 04.6  | 0.013        | 184.7        | 14.342                          | 12.920        | 13.005       | 12.391       | ...         | ...                  | ...         | 10.005      | ±0.023      | 9.266         | ±0.024      | 9.083                       | ±0.025              | 10                  | 24.9 ± 16.4                             | 0           | nan ± nan    | ±            |   |
| SCR1629-1835  | 16 29 02.02  | -18 35 04.6  | 0.013        | 184.7        | 14.342                          | 12.920        | 13.005       | 12.391       | ...         | ...                  | ...         | 9.984       | ±0.024      | 9.309         | ±0.022      | 9.127                       | ±0.024              | 10                  | 22.6 ± 14.1                             | 0           | nan ± nan    | ±            |   |
| SCR1629-1815  | 16 29 18.07  | -18 15 26.2  | 0.008        | 126.7        | 13.636                          | 12.937        | 13.024       | 12.419       | ...         | ...                  | ...         | 10.169      | ±0.022      | 9.498         | ±0.026      | 9.337                       | ±0.025              | 9                   | 24.9 ± 16.5                             | 0           | nan ± nan    | ±            |   |
| SCR1656-0722  | 16 56 42.52  | -07 22 18.9  | 0.042        | 187.1        | 13.692                          | 11.688        | 12.618       | 11.469       | ...         | ...                  | ...         | 9.490       | ±0.023      | 8.790         | ±0.044      | 8.578                       | ±0.023              | 10                  | 20.4 ± 11.3                             | 0           | nan ± nan    | ±            |   |
| SCR1658-0537  | 16 58 34.11  | -05 37 12.0  | 0.012        | 108.5        | 14.305                          | 12.492        | 12.539       | 11.784       | ...         | ...                  | ...         | 9.742       | ±0.030      | 9.017         | ±0.044      | 8.798                       | ±0.025              | 11                  | 24.1 ± 14.0                             | 0           | nan ± nan    | ±            |   |
| SCR1708-6936  | 17 08 08.82  | -69 36 18.7  | 0.107        | 210.8        | 13.931                          | 11.813        | 11.975       | 10.185       | ...         | ...                  | ...         | 9.058       | ±0.021      | 8.420         | ±0.027      | 8.204                       | ±0.021              | 11                  | 17.6 ± 5.0                              | 0           | nan ± nan    | ±            |   |
| SCR1718-6945  | 17 18 15.01  | -69 45 45.7  | 0.050        | 198.6        | 15.493                          | 13.286        | 13.462       | 11.499       | ...         | ...                  | ...         | 10.185      | ±0.023      | 9.544         | ±0.025      | 9.306                       | ±0.021              | 11                  | 24.2 ± 7.0                              | 0           | nan ± nan    | ±            |   |
| SCR1725-1925A | 17 25 13.80  | -80 34 59.0  | 0.120        | 141.5        | 13.456                          | 11.053        | 11.365       | 10.070       | ...         | ...                  | ...         | 8.669       | ±0.021      | 8.078         | ±0.038      | 7.850                       | ±0.029              | 11                  | 15.8 ± 5.5                              | 0           | nan ± nan    | ±            |   |
| SCR1800-0241  | 18 00 17.57  | -02 41 59.7  | 0.006        | 074.7        | 15.388                          | 13.757        | 13.726       | 12.676       | ...         | ...                  | ...         | 10.329      | ±0.023      | 9.563         | ±0.024      | 9.337                       | ±0.025              | 11                  | 24.5 ± 16.5                             | 0           | nan ± nan    | ±            |   |
| SCR1800-0246  | 18 00 22.12  | -02 46 27.4  | 0.009        | 042.5        | 15.004                          | 13.391        | 13.038       | 12.108       | ...         | ...                  | ...         | 9.846       | ±0.021      | 9.087         | ±0.024      | 8.873                       | ±0.023              | 11                  | 20.2 ± 13.2                             | 0           | nan ± nan    | ±            |   |
| SCR1800-0244  | 18 00 27.10  | -02 44 07.7  | 0.014        | 282.9        | 15.659                          | 13.599        | 14.031       | 12.921       | ...         | ...                  | ...         | 10.478      | ±0.023      | 9.705         | ±0.024      | 9.467                       | ±0.023              | 11                  | 24.6 ± 17.3                             | 0           | nan ± nan    | ±            |   |
| SCR1800-0216  | 18 00 59.81  | -02 16 32.0  | 0.022        | 093.3        | 13.714                          | 12.624        | 12.722       | 11.621       | ...         | ...                  | ...         | 9.428       | ±0.022      | 8.744         | ±0.033      | 8.574                       | ±0.021              | 10                  | 19.1 ± 11.7                             | 0           | nan ± nan    | ±            |   |
| SCR1801-0214  | 18 01 36.04  | -02 14 56.5  | 0.020        | 042.6        | 12.907                          | 11.809        | 11.831       | 10.206       | 11.81       | 1                    | 10.01       | 1           | 8.615       | ±0.032        | 7.897       | ±0.042                      | 7.721               | ±0.029              | 11                                      | 14.4 ± 7.1  | 12           | 22.03 ± 7.08 | ± |
| SCR1801-0201  | 18 01 59.67  | -02 01 18.1  | 0.006        | 065.4        | 14.772                          | 13.507        | 13.20        | 12.555       | ...         | ...                  | ...         | 10.256      | ±0.026      | 9.564         | ±0.022      | 9.368                       | ±0.021              | 9                   | 24.6 ± 14.2                             | 0           | nan ± nan    | ±            |   |
| SCR1805-5704  | 18 05 06.94  | -57 04 30.8  | 0.066        | 157.1        | 14.300                          | 12.382        | 12.504       | 10.645       | ...         | ...                  | ...         | 9.564       | ±0.024      | 8.881         | ±0.059      | 8.630                       | ±0.020              | 11                  | 21.6 ± 6.4                              | 0           | nan ± nan    | ±            |   |
| SPI1809-7613  | 18 09 06.94  | -76 13 23.9  | 0.156        | 175.5        | 16.229                          | 13.919        | 14.016       | 11.511       | 2           | 13.62                | 2           | 9.817       | ±0.021      | 9.275         | ±0.021      | 8.989                       | ±0.021              | 11                  | 13.7 ± 4.2                              | 12          | 11.97 ± 1.90 | ±            |   |
| SCR1809-5430  | 18 09 29.70  | -54 30 53.3  | 0.113        | 175.5        | 16.188                          | 13.857        | 13.948       | 11.452       | ...         | ...                  | ...         | 9.996       | ±0.024      | 9.405         | ±0.022      | 9.117                       | ±0.023              | 11                  | 16.3 ± 4.8                              | 0           | nan ± nan    | ±            |   |
| SCR1812-7009  | 18 12 59.74  | -07 09 07.2  | 0.070        | 035.3        | 13.994                          | 11.743        | 11.916       | 10.178       | ...         | ...                  | ...         | 9.258       | ±0.029      | 8.534         | ±0.034      | 8.346                       | ±0.021              | 11                  | 20.2 ± 5.4                              | 0           | nan ± nan    | ±            |   |
| SCR1816-6830  | 18 16 12.37  | -68 34 05.6  | 0.097        | 192.5        | 13.161                          | 11.205        | 11.501       | 9.854        | 12.75       | 1                    | 10.05       | 1           | 8.599       | ±0.024        | 7.964       | ±0.059                      | 7.699               | ±0.016              | 11                                      | 14.7 ± 5.1  | 12           | 12.54 ± 1.96 | ± |
| SCR1816-6305  | 18 16 50.87  | -63 05 19.8  | 0.125        | 251.2        | 13.894                          | 11.651        | 11.929       | 10.048       | ...         | ...                  | ...         | 9.281       | ±0.024      | 8.614         | ±0.031      | 8.389                       | ±0.029              | 11                  | 21.6 ± 5.9                              | 0           | nan ± nan    | ±            |   |
| SCR1827-6528  | 18 27 06.84  | -65 28 18.8  | 0.083        | 336.4        | 14.644                          | 12.526        | 12.628       | 11.057       | ...         | ...                  | ...         | 9.740       | ±0.020      | 9.159         | ±0.025      | 8.912                       | ±0.023              | 11                  | 24.3 ± 7.6                              | 0           | nan ± nan    | ±            |   |
| SCR1829-8026  | 18 29 09.61  | -80 26 44.1  | 0.062        | 204.1        | 15.400                          | 13.512        | 13.575       | 11.678       | ...         | ...                  | ...         | 10.184      | ±0.023      | 9.551         | ±0.021      | 9.315                       | ±0.023              | 11                  | 24.1 ± 8.2                              | 0           | nan ± nan    | ±            |   |
| SCR1842-5554A | 18 42 06.95  | -55 54 25.5  | 0.085        | 161.0        | 14.536                          | 12.220        | 12.215       | 10.799       | ...         | ...                  | ...         | 9.488       | ±0.024      | 8.825         | ±0.025      | 8.584                       | ±0.020              | 11                  | 20.5 ± 6.5                              | 0           | nan ± nan    | ±            |   |
| SCR1856-6922  | 18 56 04.37  | -69 22 00.3  | 0.114        | 177.2        | 13.513                          | 11.038        | 11.125       | 9.182        | ...         | ...                  | ...         | 8.531       | ±0.023      | 7.944         | ±0.029      | 7.698                       | ±0.016              | 11                  | 15.2 ± 4.4                              | 0           | nan ± nan    | ±            |   |
| SCR1856-6630  | 18 56 11.11  | -66 30 57.0  | 0.166        | 220.6        | 15.452                          | 13.056        | 13.178       | 11.378       | ...         | ...                  | ...         | 9.963       | ±0.023      | 9.387         | ±0.025      | 9.113                       | ±0.023              | 11                  | 21.8 ± 6.4                              | 0           | nan ± nan    | ±            |   |
| SCR1906-6830  | 19 06 14.90  | -68 34 35.1  | 0.115        | 149.0        | 16.975                          | 14.713        | 14.854       | 12.083       | ...         | ...                  | ...         | 10.531      | ±0.021      | 9.973         | ±0.020      | 9.688                       | ±0.020              | 11                  | 19.0 ± 5.8                              | 0           | nan ± nan    | ±            |   |
| RX1924-3442   | 19 24 34.95  | -34 42 39.4  | 0.101        | 153.2        | 15.069                          | 12.802        | 12.910       | 10.546       | ...         | ...                  | ...         | 9.670       | ±0.023      | 9.058         | ±0.026      | 8.785                       | ±0.025              | 11                  | 19.9 ± 6.4                              | 0           | nan ± nan    | ±            |   |
| SCR1926-5331  | 19 26 00.75  | -53 31 26.9  | 0.102        | 159.6        | 14.949                          | 12.727        | 12.864       | 10.829       | ...         | ...                  | ...         | 9.595       | ±0.027      | 8.983         | ±0.023      | 8.684                       | ±0.019              | 11                  | 18.2 ± 5.0                              | 0           | nan ± nan    | ±            |   |
| WT0651        | 19 28 38.94  | -63 38 07.6  | 0.176        | 157.1        | 16.383                          | 13.934        | 14.019       | 11.847       | ...         | ...                  | ...         | 10.438      | ±0.021      | 9.863         | ±0.023      | 9.591                       | ±0.019              | 11                  | 23.0 ± 6.5                              | 0           | nan ± nan    | ±            |   |
| SCR1929-2932  | 19 29 10.67  | -29 32 11.6  | 0.022        | 331.9        | 14.927                          | 12.749        | 12.756       | 10.918       | ...         | ...                  | ...         | 9.708       | ±0.024      | 9.082         | ±0.024      | 8.833                       | ±0.023              | 11                  | 21.0 ± 5.8                              | 0           | nan ± nan    | ±            |   |
| SCR1938-2416  | 19 38 36.90  | -24 16 58.6  | 0.085        | 032.0        | 14.340                          | 12.056        | 12.151       | 10.554       | ...         | ...                  | ...         | 9.329       | ±0.021      | 8.767         | ±0.023      | 8.511                       | ±0.021              | 11                  | 20.2 ± 5.7                              | 0           | nan ± nan    | ±            |   |
| SCR1942-0620  | 19 42 21.20  | -06 20 24.0  | 0.167        | 157.9        | 16.407                          | 14.385        | 14.383       | 12.192       | ...         | ...                  | ...         | 10.575      | ±0.026      | 9.985         | ±0.023      | 9.706                       | ±0.024              | 11                  | 23.2 ± 7.2                              | 0           | nan ± nan    | ±            |   |
| SCR1942-6359  | 19 42 21.65  | -63 59 06.2  | 0.174        | 179.6        | 15.095                          | 12.863        | 12.949       | 11.066       | ...         | ...                  | ...         | 9.704       | ±0.021      | 9.122         | ±0.023      | 8.857                       | ±0.022              | 11                  | 19.7 ± 5.6                              | 0           | nan ± nan    | ±            |   |
| SCR1945-0815  | 19 45 50.83  | -08 15 04.6  | 0.028        | 160.2        | 17.552                          | 15.444        | 15.468       | 13.259       | ...         | ...                  | ...         | 11.225      | ±0.027      | 10.534        | ±0.022      | 10.237                      | ±0.019              | 11                  | 23.4 ± 9.7                              | 0           | nan ± nan    | ±            |   |
| SCR1950-4327  | 19 50 19.99  | -43 27 02.6  | 0.175        | 135.2        | 15.886                          | 13.641        | 13.745       | 11.486       | ...         | ...                  | ...         | 10.197      | ±0.024      | 9.596         | ±0.028      | 9.301                       | ±0.021              | 11                  | 21.4 ± 6.0                              | 0           | nan ± nan    | ±            |   |
| SCR1952-7735  | 19 52 27.03  | -77 35 28.3  | 0.112        | 145.2        | 14.819                          | 12.729        | 12.818       | 10.904       | ...         | ...                  | ...         | 9.641       | ±0.023      | 9.027         | ±0.034      | 8.768                       | ±0.023              | 11                  | 20.1 ± 5.7                              | 0           | nan ± nan    | ±            |   |
| SCR1953-4611  | 19 53 27.71  | -46 11 32.2  | 0.100        | 018.0        | 16.147                          | 13.730        | 13.846       | 11.407       | ...         | ...                  | ...         | 10.308      | ±0.023      | 9.759         | ±0.022      | 9.440                       | ±0.019              | 11                  | 23.1 ± 7.5                              | 0           | nan ± nan    | ±            |   |
| SCR1953-0707  | 19 53 31.70  | -07 07 00.2  | 0.062        | 126.4        | 16.856                          | 15.070        | 14.982       | 12.822       | ...         | ...                  | ...         | 10.815      | ±0.023      | 10.200        |             |                             |                     |                     |   |             |              |              |   |

Table B.2 – Continued from previous page

| Name<br>(1)  | RA           |              | DEC          |              | $\mu$<br>( $'_{yr^{-1}}$ )<br>(4) | P.A.<br>( $^{\circ}$ )<br>(5) | SuperCOSMOS  |                 |                  | Johnson-Kron-Cousins |                  |             | 2MASS       |             |                   | No.<br>No. pldst<br>(20) (21) | No.<br>No. ccdist<br>(22) | X-ray flux<br>( $cnt\ s^{-1}$ )<br>(23) |             |                   |
|--------------|--------------|--------------|--------------|--------------|-----------------------------------|-------------------------------|--------------|-----------------|------------------|----------------------|------------------|-------------|-------------|-------------|-------------------|-------------------------------|---------------------------|---|-------------|-------------------|
|              | J2000<br>(2) | E2000<br>(3) | $B_J$<br>(6) | $R_1$<br>(7) |                                   |                               | $R_2$<br>(8) | $I_{VN}$<br>(9) | $V$ nobs<br>(10) | $R$ nobs<br>(11)     | $I$ nobs<br>(12) | $J$<br>(13) | $H$<br>(14) | $K$<br>(15) | $K$ pldst<br>(16) |                               |                           |   | $H$<br>(17) | $K$ pldst<br>(18) |
| SCR2046-2829 | 20 46 51.24  | -28 29 13.4  | 0.132        | 110.7        | 15.220                            | 12.875                        | 13.098       | 10.995          | ...              | ...                  | ...              | ...         | ...         | ...         | ...               | ...                           | ...                       | ...                                     | ...         | ...               |
| SCR2049-4012 | 20 49 09.94  | -40 12 06.2  | 0.064        | 260.6        | 14.587                            | 11.850                        | 12.023       | 9.374           | 13.53            | 3                    | 12.12            | 3           | 10.31       | 3           | 8.596             | 0.032                         | 9.244                     | 0.024                                   | 9.041       | 0.021             |
| SCR2053-6223 | 20 53 55.50  | -62 23 57.4  | 0.032        | 117.0        | 15.429                            | 13.028                        | 13.272       | 11.598          | 13.81            | 1                    | 12.61            | 1           | 11.04       | 1           | 8.596             | 0.032                         | 9.244                     | 0.024                                   | 9.041       | 0.021             |
| CD-61-06505  | 20 54 02.76  | -61 28 25.8  | 0.002        | 010.5        | 12.765                            | 10.827                        | 11.073       | 9.945           | 10.79            | 2                    | 10.01            | 2           | 9.29        | 2           | 8.256             | 0.020                         | 7.577                     | 0.047                                   | 7.334       | 0.024             |
| SCR2055-6001 | 20 55 43.94  | -60 01 46.2  | 0.018        | 010.4        | 12.486                            | 10.433                        | 10.507       | 9.419           | 10.49            | 2                    | 9.68             | 2           | 8.94        | 2           | 7.848             | 0.021                         | 7.136                     | 0.049                                   | 6.920       | 0.029             |
| SCR2056-1301 | 20 56 11.82  | -13 01 42.9  | 0.179        | 182.4        | 16.006                            | 12.912                        | 13.732       | 11.330          | ...              | ...                  | ...              | ...         | ...         | ...         | ...               | ...                           | ...                       | ...                                     | ...         | ...               |
| SCR2107-7056 | 21 07 22.48  | -70 56 12.6  | 0.101        | 155.9        | 14.796                            | 12.669                        | 12.953       | 10.976          | ...              | ...                  | ...              | ...         | ...         | ...         | ...               | ...                           | ...                       | ...                                     | ...         | ...               |
| SCR2108-4244 | 21 08 38.26  | -42 44 54.1  | 0.098        | 158.3        | 15.512                            | 13.580                        | 13.754       | 11.202          | ...              | ...                  | ...              | ...         | ...         | ...         | ...               | ...                           | ...                       | ...                                     | ...         | ...               |
| SCR2112-8128 | 21 12 15.97  | -81 28 45.2  | 0.122        | 149.8        | 17.147                            | 15.188                        | 15.270       | 12.716          | ...              | ...                  | ...              | ...         | ...         | ...         | ...               | ...                           | ...                       | ...                                     | ...         | ...               |
| SCR2112-6318 | 21 12 17.01  | -63 18 10.4  | 0.147        | 211.4        | 17.540                            | 15.296                        | 15.440       | 12.763          | ...              | ...                  | ...              | ...         | ...         | ...         | ...               | ...                           | ...                       | ...                                     | ...         | ...               |
| SCR2116-6005 | 21 16 55.29  | -60 05 12.4  | 0.113        | 156.4        | 16.012                            | 13.972                        | 13.917       | 11.985          | ...              | ...                  | ...              | ...         | ...         | ...         | ...               | ...                           | ...                       | ...                                     | ...         | ...               |
| SCR2142-4422 | 21 16 44.72  | -44 22 42.7  | 0.014        | 218.1        | 12.470                            | 10.514                        | 10.700       | 9.639           | 10.55            | 2                    | 9.78             | 2           | 9.08        | 2           | 8.028             | 0.021                         | 7.252                     | 0.026                                   | 7.035       | 0.018             |
| SCR2143-0147 | 21 16 44.72  | -44 22 42.7  | 0.014        | 218.1        | 12.470                            | 10.514                        | 10.700       | 9.639           | 10.55            | 2                    | 9.78             | 2           | 9.08        | 2           | 8.028             | 0.021                         | 7.252                     | 0.026                                   | 7.035       | 0.018             |
| SCR2143-0147 | 21 16 44.72  | -44 22 42.7  | 0.014        | 218.1        | 12.470                            | 10.514                        | 10.700       | 9.639           | 10.55            | 2                    | 9.78             | 2           | 9.08        | 2           | 8.028             | 0.021                         | 7.252                     | 0.026                                   | 7.035       | 0.018             |
| SCR2143-0147 | 21 16 44.72  | -44 22 42.7  | 0.014        | 218.1        | 12.470                            | 10.514                        | 10.700       | 9.639           | 10.55            | 2                    | 9.78             | 2           | 9.08        | 2           | 8.028             | 0.021                         | 7.252                     | 0.026                                   | 7.035       | 0.018             |
| SCR2143-0147 | 21 16 44.72  | -44 22 42.7  | 0.014        | 218.1        | 12.470                            | 10.514                        | 10.700       | 9.639           | 10.55            | 2                    | 9.78             | 2           | 9.08        | 2           | 8.028             | 0.021                         | 7.252                     | 0.026                                   | 7.035       | 0.018             |
| SCR2143-0147 | 21 16 44.72  | -44 22 42.7  | 0.014        | 218.1        | 12.470                            | 10.514                        | 10.700       | 9.639           | 10.55            | 2                    | 9.78             | 2           | 9.08        | 2           | 8.028             | 0.021                         | 7.252                     | 0.026                                   | 7.035       | 0.018             |
| SCR2143-0147 | 21 16 44.72  | -44 22 42.7  | 0.014        | 218.1        | 12.470                            | 10.514                        | 10.700       | 9.639           | 10.55            | 2                    | 9.78             | 2           | 9.08        | 2           | 8.028             | 0.021                         | 7.252                     | 0.026                                   | 7.035       | 0.018             |
| SCR2143-0147 | 21 16 44.72  | -44 22 42.7  | 0.014        | 218.1        | 12.470                            | 10.514                        | 10.700       | 9.639           | 10.55            | 2                    | 9.78             | 2           | 9.08        | 2           | 8.028             | 0.021                         | 7.252                     | 0.026                                   | 7.035       | 0.018             |
| SCR2143-0147 | 21 16 44.72  | -44 22 42.7  | 0.014        | 218.1        | 12.470                            | 10.514                        | 10.700       | 9.639           | 10.55            | 2                    | 9.78             | 2           | 9.08        | 2           | 8.028             | 0.021                         | 7.252                     | 0.026                                   | 7.035       | 0.018             |
| SCR2143-0147 | 21 16 44.72  | -44 22 42.7  | 0.014        | 218.1        | 12.470                            | 10.514                        | 10.700       | 9.639           | 10.55            | 2                    | 9.78             | 2           | 9.08        | 2           | 8.028             | 0.021                         | 7.252                     | 0.026                                   | 7.035       | 0.018             |
| SCR2143-0147 | 21 16 44.72  | -44 22 42.7  | 0.014        | 218.1        | 12.470                            | 10.514                        | 10.700       | 9.639           | 10.55            | 2                    | 9.78             | 2           | 9.08        | 2           | 8.028             | 0.021                         | 7.252                     | 0.026                                   | 7.035       | 0.018             |
| SCR2143-0147 | 21 16 44.72  | -44 22 42.7  | 0.014        | 218.1        | 12.470                            | 10.514                        | 10.700       | 9.639           | 10.55            | 2                    | 9.78             | 2           | 9.08        | 2           | 8.028             | 0.021                         | 7.252                     | 0.026                                   | 7.035       | 0.018             |
| SCR2143-0147 | 21 16 44.72  | -44 22 42.7  | 0.014        | 218.1        | 12.470                            | 10.514                        | 10.700       | 9.639           | 10.55            | 2                    | 9.78             | 2           | 9.08        | 2           | 8.028             | 0.021                         | 7.252                     | 0.026                                   | 7.035       | 0.018             |
| SCR2143-0147 | 21 16 44.72  | -44 22 42.7  | 0.014        | 218.1        | 12.470                            | 10.514                        | 10.700       | 9.639           | 10.55            | 2                    | 9.78             | 2           | 9.08        | 2           | 8.028             | 0.021                         | 7.252                     | 0.026                                   | 7.035       | 0.018             |
| SCR2143-0147 | 21 16 44.72  | -44 22 42.7  | 0.014        | 218.1        | 12.470                            | 10.514                        | 10.700       | 9.639           | 10.55            | 2                    | 9.78             | 2           | 9.08        | 2           | 8.028             | 0.021                         | 7.252                     | 0.026                                   | 7.035       | 0.018             |
| SCR2143-0147 | 21 16 44.72  | -44 22 42.7  | 0.014        | 218.1        | 12.470                            | 10.514                        | 10.700       | 9.639           | 10.55            | 2                    | 9.78             | 2           | 9.08        | 2           | 8.028             | 0.021                         | 7.252                     | 0.026                                   | 7.035       | 0.018             |
| SCR2143-0147 | 21 16 44.72  | -44 22 42.7  | 0.014        | 218.1        | 12.470                            | 10.514                        | 10.700       | 9.639           | 10.55            | 2                    | 9.78             | 2           | 9.08        | 2           | 8.028             | 0.021                         | 7.252                     | 0.026                                   | 7.035       | 0.018             |
| SCR2143-0147 | 21 16 44.72  | -44 22 42.7  | 0.014        | 218.1        | 12.470                            | 10.514                        | 10.700       | 9.639           | 10.55            | 2                    | 9.78             | 2           | 9.08        | 2           | 8.028             | 0.021                         | 7.252                     | 0.026                                   | 7.035       | 0.018             |
| SCR2143-0147 | 21 16 44.72  | -44 22 42.7  | 0.014        | 218.1        | 12.470                            | 10.514                        | 10.700       | 9.639           | 10.55            | 2                    | 9.78             | 2           | 9.08        | 2           | 8.028             | 0.021                         | 7.252                     | 0.026                                   | 7.035       | 0.018             |
| SCR2143-0147 | 21 16 44.72  | -44 22 42.7  | 0.014        | 218.1        | 12.470                            | 10.514                        | 10.700       | 9.639           | 10.55            | 2                    | 9.78             | 2           | 9.08        | 2           | 8.028             | 0.021                         | 7.252                     | 0.026                                   | 7.035       | 0.018             |
| SCR2143-0147 | 21 16 44.72  | -44 22 42.7  | 0.014        | 218.1        | 12.470                            | 10.514                        | 10.700       | 9.639           | 10.55            | 2                    | 9.78             | 2           | 9.08        | 2           | 8.028             | 0.021                         | 7.252                     | 0.026                                   | 7.035       | 0.018             |
| SCR2143-0147 | 21 16 44.72  | -44 22 42.7  | 0.014        | 218.1        | 12.470                            | 10.514                        | 10.700       | 9.639           | 10.55            | 2                    | 9.78             | 2           | 9.08        | 2           | 8.028             | 0.021                         | 7.252                     | 0.026                                   | 7.035       | 0.018             |
| SCR2143-0147 | 21 16 44.72  | -44 22 42.7  | 0.014        | 218.1        | 12.470                            | 10.514                        | 10.700       | 9.639           | 10.55            | 2                    | 9.78             | 2           | 9.08        | 2           | 8.028             | 0.021                         | 7.252                     | 0.026                                   | 7.035       | 0.018             |
| SCR2143-0147 | 21 16 44.72  | -44 22 42.7  | 0.014        | 218.1        | 12.470                            | 10.514                        | 10.700       | 9.639           | 10.55            | 2                    | 9.78             | 2           | 9.08        | 2           | 8.028             | 0.021                         | 7.252                     | 0.026                                   | 7.035       | 0.018             |
| SCR2143-0147 | 21 16 44.72  | -44 22 42.7  | 0.014        | 218.1        | 12.470                            | 10.514                        | 10.700       | 9.639           | 10.55            | 2                    | 9.78             | 2           | 9.08        | 2           | 8.028             | 0.021                         | 7.252                     | 0.026                                   | 7.035       | 0.018             |
| SCR2143-0147 | 21 16 44.72  | -44 22 42.7  | 0.014        | 218.1        | 12.470                            | 10.514                        | 10.700       | 9.639           | 10.55            | 2                    | 9.78             | 2           | 9.08        | 2           | 8.028             | 0.021                         | 7.252                     | 0.026                                   | 7.035       | 0.018             |
| SCR2143-0147 | 21 16 44.72  | -44 22 42.7  | 0.014        | 218.1        | 12.470                            | 10.514                        | 10.700       | 9.639           | 10.55            | 2                    | 9.78             | 2           | 9.08        | 2           | 8.028             | 0.021                         | 7.252                     | 0.026                                   | 7.035       | 0.018             |
| SCR2143-0147 | 21 16 44.72  | -44 22 42.7  | 0.014        | 218.1        | 12.470                            | 10.514                        | 10.700       | 9.639           | 10.55            | 2                    | 9.78             | 2           | 9.08        | 2           | 8.028             | 0.021                         | 7.252                     | 0.026                                   | 7.035       | 0.018             |
| SCR2143-0147 | 21 16 44.72  | -44 22 42.7  | 0.014        | 218.1        | 12.470                            | 10.514                        | 10.700       | 9.639           | 10.55            | 2                    | 9.78             | 2           | 9.08        | 2           | 8.028             | 0.021                         | 7.252                     | 0.026                                   | 7.035       | 0.018             |
| SCR2143-0147 | 21 16 44.72  | -44 22 42.7  | 0.014        | 218.1        | 12.470                            | 10.514                        | 10.700       | 9.639           | 10.55            | 2                    | 9.78             | 2           | 9.08        | 2           | 8.028             | 0.021                         | 7.252                     | 0.026                                   | 7.035       | 0.018             |
| SCR2143-0147 | 21 16 44.72  | -44 22 42.7  | 0.014        | 218.1        | 12.470                            | 10.514                        | 10.700       | 9.639           | 10.55            | 2                    | 9.78             | 2           | 9.08        | 2           | 8.028             | 0.021                         | 7.252                     | 0.026                                   | 7.035       | 0.018             |
| SCR2143-0147 | 21 16 44.72  | -44 22 42.7  | 0.014        | 218.1        | 12.470                            | 10.514                        | 10.700       | 9.639           | 10.55            | 2                    | 9.78             | 2           | 9.08        | 2           | 8.028             | 0.021                         | 7.252                     | 0.026                                   | 7.035       | 0.018             |
| SCR2143-0147 | 21 16 44.72  | -44 22 42.7  | 0.014        | 218.1        | 12.470                            | 10.514                        | 10.700       | 9.639           | 10.55            | 2                    | 9.78             | 2           | 9.08        | 2           | 8.028             | 0.021                         | 7.252                     | 0.026                                   | 7.035       | 0.018             |
| SCR2143-0147 | 21 16 44.72  | -44 22 42.7  | 0.014        | 218.1        | 12.470                            | 10.514                        | 10.700       | 9.639           | 10.55            | 2                    | 9.78             | 2           | 9.08        | 2           | 8.028             | 0.021                         | 7.252                     | 0.026                                   | 7.035       | 0.018             |
| SCR2143-0147 | 21 16 44.72  | -44 22 42.7  | 0.014        | 218.1        | 12.470                            | 10.514                        | 10.700       | 9.639           | 10.55            | 2                    | 9.78             | 2           | 9.08        | 2           | 8.028             | 0.021                         | 7.252                     | 0.026                                   | 7.035       | 0.018             |
| SCR2143-0147 | 21 16 44.72  | -44 22 42.7  | 0.014        | 218.1        | 12.470                            | 10.514                        | 10.700       | 9.639           | 10.55            | 2                    | 9.78             | 2           | 9.08        | 2           | 8.028             | 0.021                         | 7.252                     | 0.026                                   | 7.035       | 0.018             |
| SCR2143-0147 | 21 16 44.72  | -44 22 42.7  | 0.014        | 218.1        | 12.470                            | 10.514                        | 10.700       | 9.639           | 10.55            | 2                    | 9.78             | 2           | 9.08        | 2           | 8.028             | 0.021                         | 7.252                     | 0.026                                   | 7.035       | 0.018             |
| SCR2143-0147 | 21 16 44.72  | -44 22 42.7  | 0.014        | 218.1        | 12.470                            | 10.514                        | 10.700       | 9.639           | 10.55            | 2                    | 9.78             | 2           | 9.08        | 2           | 8.028             | 0.021                         | 7.252                     | 0.026                                   | 7.035       | 0.018             |
| SCR2143-0147 | 21 16 44.72  | -44 22 42.7  | 0.014        | 218.1        | 12.470                            | 10.514                        | 10.700       | 9.639           | 10.55            | 2                    | 9.78             | 2           | 9.08        | 2           | 8.028             | 0.021                         | 7.252                     | 0.026                                   | 7.035       | 0.018             |
| SCR2143-0147 | 21 16 44.72  | -44 22 42.7  | 0.014        | 218.1        | 12.470                            | 10.514                        | 10.700       | 9.639           | 10.55            | 2                    | 9.78             | 2           | 9.08        | 2           | 8.028             | 0.021                         | 7.252                     | 0.026                                   | 7.035       | 0.018             |
| SCR2143-0147 | 21 16 44.72  | -44 22 42.7  | 0.014        | 218.1        | 12.470                            | 10.514                        | 10.700       | 9.639           | 10.55            | 2                    | 9.78             | 2           | 9.08        | 2           | 8.028             | 0.021                         | 7.252                     | 0.026                                   | 7.035       | 0.018             |
| SCR2143-0147 | 21 16 44.72  | -44 22 42.7  | 0.014        | 218.1        | 12.470                            | 10.514                        | 10.700       | 9.639           | 10.55            | 2                    | 9.78             | 2           | 9.08        | 2           | 8.028             | 0.021                         | 7.252                     | 0.026                                   | 7.035       | 0.018             |
| SCR2143-0147 | 21 16 44.72  | -44 22 42.7  | 0.014        | 218.1        | 12.470                            | 10.514                        | 10.700       | 9.639           | 10.55            | 2                    | 9.78             | 2           | 9.08        | 2           | 8.028             | 0.021                         | 7.252                     | 0.026                                   | 7.035       | 0.018             |
| SCR2143-0147 | 21 16 44.72  | -44 22 42.7  | 0.014        | 218.1        | 12.470                            | 10.514                        | 10.700       | 9.639           | 10.55            | 2                    | 9.78             | 2           |             |             |                   |                               |                           |   |             |                   |

## APPENDIX C

### GAL\_UVWXYZ

The following routine is a heavily modified version of the IDL GAL\_UVW routine by W. Landsman (2000). The key differences are that where the original GAL\_UVW routine returns only the UVW velocities given proper inputs, my routine incorporates the errors on UVW (as given in Johnson & Soderblom 1987) as well as the XYZ positions and their errors. The errors have been tested by comparing them to a version that uses Monte Carlo; they are functionally identical except that this version runs hundreds of times faster.

Additionally, I have changed the system to right-handed coordinates where U points toward the Galactic center, and updated the LSR velocities with values from Aumer & Binney (2009).

```

pro gal_uvxyz, u, uerr, v, verr, w, werr, x, xerr, y, yerr, z, zerr, $
  LSR = lsr, ra=ra, raerr=raerr, dec=dec, decerr=decerr,$
  pmra_ = pmra, pmraerr= pmraerr, pmdec=pmdec, pmdecerr=pmdecerr, $
  vrad_ = vrad, vraderr=vraderr, plx_ = plx, plxerr=plxerr
;+
; NAME:
;   GAL_UVW
; PURPOSE:
;   Calculate the Galactic space velocity (U,V,W) of star
; EXPLANATION:
;   Calculates the Galactic space velocity U, V, W of star given its
;   (1) coordinates, (2) proper motion, (3) distance (or parallax), and
;   (4) radial velocity.
; CALLING SEQUENCE:
;   GAL_UVWXYZ, U, Uerr, V, Verr, W, Werr, [/LSR, RA=, RAERR=, DEC=, DECERR=, PMRA= ,
;   PMRAerr=, PMDEC=, PMDECerr=, VRAD=, VRADerr=, PLX=, PLXerr= ]
; OUTPUT PARAMETERS:
;   U - Velocity (km/s) positive toward the Galactic center
;   V - Velocity (km/s) positive in the direction of Galactic rotation
;   W - Velocity (km/s) positive toward the North Galactic Pole
; REQUIRED INPUT KEYWORDS:
;   User must supply a position, proper motion, radial velocity and distance
;   (or parallax). Either scalars or vectors can be supplied.
;   (1) Position:
;   RA - Right Ascension in *Degrees*
;   Dec - Declination in *Degrees*
;   (2) Proper Motion
;   PMRA = Proper motion in RA in arc units (typically milli-arcseconds/yr)
;   PMDEC = Proper motion in Declination (typically mas/yr)
;   (3) Radial Velocity
;   VRAD = radial velocity in km/s
;   (4) Distance or Parallax
;   PLX - parallax with same distance units as proper motion measurements
;   typically milliarcseconds (mas)
; OPTIONAL INPUT KEYWORD:
;   /LSR - If this keyword is set, then the output velocities will be

```

**Code 2:** The IDL code. Tested with IDL 7.0.

```

;       corrected for the solar motion (U,V,W)_Sun = (11.10,+12.24,
;       +7.25) (Schoenrich, Binney & Dehnen, 2010).
;
; EXAMPLE:
; (1) Compute the U,V,W coordinates for the halo star HD 6755.
;     Use values from Hipparcos catalog, and correct to the LSR
;     ra = ten(1,9,42.3)*15.   & dec = ten(61,32,49.5)
;     pmra = 627.89 & pmdec = 77.84   ;mas/yr
;     dis = 144   & vrad = -321.4
;     gal_uvW,u,v,w,ra=ra,dec=dec,pmra=pmra,pmdec=pmdec,vrad=vrad,dis=dis,/lsr
;     ==> u=154 v = -493 w = 97   ;km/s
;
; (2) Use the Hipparcos Input and Output Catalog IDL databases (see
;     http://idlastro.gsfc.nasa.gov/ftp/zdbase/) to obtain space velocities
;     for all stars within 10 pc with radial velocities > 10 km/s
;
;     dbopen,'hipparcos,hic'   ;Need Hipparcos output and input catalogs
;     list = dbfind('plx>100,vrad>10')   ;Plx > 100 mas, Vrad > 10 km/s
;     dbext,list,'pmra,pmdec,vrad,ra,dec,plx',pmra,pmdec,vrad,ra,dec,plx
;     ra = ra*15.   ;Need right ascension in degrees
;     GAL_UVW,u,v,w,ra=ra,dec=dec,pmra=pmra,pmdec=pmdec,vrad=vrad,plx = plx
;     forprint,u,v,w   ;Display results
;
; METHOD:
; Follows the general outline of Johnson & Soderblom (1987, AJ, 93,864)
; except that the J2000 transformation matrix to Galactic
; coordinates is taken from the introduction to the Hipparcos catalog.
; REVISION HISTORY:
; Written, W. Landsman   December 2000
;
;-
if N_Params() EQ 0 then begin
  print,'Syntax - GAL_UVW, U, V, W, [/LSR, RA=, DEC=, PMRA= ,PMDEC=, VRAD='
  print,'   Distance=, PLX='
  print,'   U, V, W - output Galactic space velocities (km/s)'
  return
endif

Nra = N_elements(ra)
if (nra EQ 0) or (N_elements(dec) EQ 0) then message, $
  'ERROR - The RA, Dec (J2000) position keywords must be supplied (degrees)'
if (N_elements(vrad) LT Nra) then message, $
  'ERROR - A Radial Velocity (km/s) must be supplied for each star'
if (N_elements(pmra) LT Nra) or (N_elements(pmdec) LT Nra) then message, $
  'ERROR - A proper motion must be supplied for each star'
if N_elements(distance) GT 0 then begin
  nbad = where(distance LE 0, Nbad)
  if Nbad GT 0 then message,'ERROR - All distances must be > 0'
  plx = 1/distance   ;Parallax in milli-arcseconds
endif else begin
  if N_elements(plx) EQ 0 then message, $
    'ERROR - Either a parallax or distance must be specified'
  nbad = where(plx LE 0.0, Nbad)
  if Nbad GT 0 then message,'ERROR - Parallaxes must be > 0'
endif

cosd = cos(dec/!radeg)
sind = sin(dec/!radeg)
cosa = cos(ra/!RADEG)
sina = sin(ra/!RADEG)

u = fltarr(Nra) & v = u & w = u
uerr = fltarr(Nra) & verr = uerr & werr = uerr
x = fltarr(Nra) & y = x & z = x
xerr = fltarr(Nra) & yerr = xerr & zerr = xerr

uerr = fltarr(Nra) & verr = uerr & werr = uerr

k = 4.74047   ;Equivalent of 1 A.U./yr in km/s
t = [ [-0.0548755604, +0.4941094279, -0.8676661490], $
      [-0.8734370902, -0.4448296300, -0.1980763734], $
      [-0.4838350155, +0.7469822445, +0.4559837762] ]

for i = 0,Nra -1 do begin
;print,i
a = [ [cosa[i]*cosd[i],sina[i]*cosd[i],sind[i] ], [-sina[i], cosa[i], 0], $
      [-cosa[i]*sind[i],-sina[i]*sind[i],cosd[i]] ]
b = t#a

; From Johnson & Soderblom 1987
pos1 = [cosd[i]*cosa[i],cosd[i]*sina[i],sind[i]]
starpos = (t#pos1)

x[i]= 1/plx*starpos[0]
y[i]= 1/plx*starpos[1]
z[i]= 1/plx*starpos[2]

```

```

starpos2=[starpos[0]^2,starpos[1]^2,starpos[2]^2]
pos2= [(cosd*(-sina)*raerr)^2+((-sind)*cosa*decerr)^2,(cosd*cosa*raerr)^2+((-sind)*sina*decerr)^2,(cosd*decerr)^2]
c=[[t[0,0]^2,t[1,0]^2,t[2,0]^2],[t[0,1]^2,t[1,1]^2,t[2,1]^2],[t[0,2]^2,t[1,2]^2,t[2,2]^2]]
poserror= plxerr^2/plx^4*starpos2 + 1/plx^2*c#pos2
xerr[i]=sqrt(poserror[0])
yerr[i]=sqrt(poserror[1])
zerr[i]=sqrt(poserror[2])

vec = [vrad[i], k*pmra[i]/plx[i], k*pmdec[i]/plx[i] ]
starvel = b#vec
if keyword_set(lsr) then starvel = starvel + [11.10,12.24,7.25]
u[i] = starvel[0]
v[i] = starvel[1]
w[i] = starvel[2]

; Ci,j = Bi,j^2
c=[[b[0,0]^2,b[1,0]^2,b[2,0]^2],[b[0,1]^2,b[1,1]^2,b[2,1]^2],[b[0,2]^2,b[1,2]^2,b[2,2]^2]]
d=[vraderr[i]^2. ,(k/plx[i])^2.*(pmraerr[i]^2+(pmra[i]*plxerr[i]/plx[i])^2.), $
(k/plx[i])^2.*(pmdecerr[i]^2+(pmdec[i]*plxerr[i]/plx[i])^2.)]
vecerror = c#d+2*pmra[i]*pmdec[i]*k^2*plxerr[i]^2/plx[i]^4*[[b[1,0]*b[2,0]],[b[1,1]*b[2,1]],[b[1,2]*b[2,2]]]
uerr[i]=sqrt(vecerror[0])
verr[i]=sqrt(vecerror[1])
werr[i]=sqrt(vecerror[2])

;print,x[i],y[i],z[i],xerr[i],yerr[i],zerr[i],u[i],v[i],w[i],uerr[i],verr[i],werr[i]

endfor

sz = size(ra)
if sz(0) EQ 0 then begin
  u = u[0] & v = v[0] & w = w[0]
  uerr = uerr[0] & verr = verr[0] & werr = werr[0]
  x = x[0] & y = y[0] & z = z[0]
  xerr = xerr[0] & yerr = yerr[0] & zerr = zerr[0]
endif

return
end

```